Role of herpes simplex virus 1 protein ICP47 in antigen presentation and pathogenesis

Thilaga Velusamy

January 2019

A thesis submitted for the degree of Doctor of Philosophy of
The Australian National University

Declaration

This thesis contains no material, which has been accepted for the award of any other degree or diploma in any university. To the best of the author's knowledge, it contains no material previously published or written by another person, except where due reference is made in the text.

Thilaga Velusamy

January 2019

Acknowledgments

This research is supported by an Australian Government Research Training Program (RTP) Scholarship.

My PhD journey would not have happened without the help and support of a great number of people, whom I would like to acknowledge here.

First and foremost, I am deeply grateful to Prof David Tscharke for providing excellent academic supervision and endless support during the course of my PhD studies. I am also grateful for your financial support while writing my thesis. As busy as you are, you always made the time to meet me and provided brilliant suggestions on experimental designs, assay developments, presentation strategies, scientific writing and so on. Your creative and analytical mind truly inspired me, learning from you made me grow as a scientist.

My sincere thanks also go to the members of my PhD advisory committee, Dr Peter Kerr and Dr Alexander Maier. They generously gave their time during our panel meetings by offering me valuable advice and constructive criticisms, which helped me towards improving my work. I would like to express my gratitude to Dr Terry Neeman for providing excellent advice on statistical analysis.

I am very grateful to our collaborators Prof Anthony Purcell and Dr Nathan Croft for lending me their expertise and welcoming to work in their group. Special thanks to Nathan, for your fine teaching and guidance with the mass spectrometry experiments, for meticulously reading my thesis chapters and providing very useful feedback.

To Dr Tiffany Russell and Ms Tijana Stefanovic, thanks for teaching me cell culture, virology and mouse work in my early days of PhD. Tiffany, I admire your intellect, dedication and hard work. Thanks for providing the starter for this project work.

My sincere thanks to Mr Stewart Smith, for sharing his admirable scientific knowledge - both old school and contemporary, for helping me out in large-scale infection experiments and for creating a pleasant cheerful work environment. More than all thanks for being so supportive and injecting sanity into my lab-life during the past few years.

Thanks, Mr Yeu-Yang (Ryan) Tseng for answering my never-ending questions on statistical analysis and for your friendship throughout this journey. Thanks, must also go to all the

members of the Tscharke lab, for making my life at work more enjoyable. I am thankful to Mr Matthew Witney, Dr Anjali Gowripalan, Ms Grace Patricia, Dr Tiffany Russell, Mr Stewart Smith, Ms Sarita Dhounchak, Ms Jessica Garrett, Ms Sherin and Mr Navneet Singh, for kindly providing critical feedback and for proofreading this work.

My heartfelt appreciation extends to the animal service staff, for their tireless effort in ensuring the smooth running of the facility, which made the work in this thesis achievable. To Dr Harpreet Vohra and Mr Michael Devoy, thanks for your warm welcoming nature, excellent training and advice on using the flow cytometry facility. I extend my thanks to all academic and professional staffs at the John Curtin School of Medical Research and Research School of Biology, who helped me directly or indirectly during my PhD.

Finally, yet importantly, I would like to thank my family and friends. I thank my wonderful friend Sarita, for being there during my ups and downs, keeping me sane and for bringing together our weekend writing squad. To Yasmin, Nick and Tironi, I admire your dedication and thanks for showing up every weekend with great enthusiasm. I hope you all finish your degrees with flying colours. Naz, from you, I learned how to be strong and I sorely missed you.

Appa and Amma, thank you! If I had not had your endless support and unconditional love, perhaps getting here would have been unachievable for me. Words are in dearth to jot down my gratitude to my beloved husband and son. Thank you for unending sacrifice, patience, love and support over the last few years. This thesis is almost as much yours as it is mine.

Abstract

The herpes simplex virus (HSV) immunomodulatory protein, ICP47, conceals infected cells from $CD8^+$ T cells by inhibiting the presentation of peptides on MHC class I (MHC I). The mechanism by which ICP47 exerts this function is by binding to the transporter associated with antigen processing (TAP) protein, blocking peptide transport and loading onto MHC I molecules in the ER. The earliest studies of ICP47 supported by biochemical and *in vitro* observations noted marked species specificity with human but not mouse TAP being inhibited by this protein. However, later work demonstrated that ICP47 could contribute to HSV-1 neurovirulence in mice. The discordance between biochemical and *in vivo* data leaves our understanding of ICP47 and its role in evading $CD8^+$ T cells incomplete. Data from our laboratory suggested that ICP47 is likely to be expressed during the establishment and maintenance of HSV-1 latency, however, its exact function during these stages of infection is unknown. Therefore, in this study, we sought to re-visit the discrepancies discussed above and investigate the role of ICP47 during HSV-1 infection. We utilised different strains of HSV and mice, as well as an alternate infection model and unique methods to quantify the effect of ICP47 on levels of antigen presentation.

In our mouse model, where HSV-1 is confined to the peripheral nervous system, deletion of ICP47 from HSV-1 KOS did not alter lesion development, virus load, spread or reactivation. Likewise, latency was unaffected by ICP47 deficiency as determined using a sensitive Cre-marking mouse model. Further observations from the Cre-marking mouse model revealed that unlike the ICP47 promoter inserted in an ectopic locus, native promoters did not induce additional neuronal marking by Cre beyond lytic infection. We evaluated the reasons behind the difference in marking using newly generated recombinant viruses. Subsequent flank infection of ROSA26R mice with these viruses showed that the local genomic context is also important for regulation of gene expression.

By contrast to our *in vivo* pathogenesis data, we were able to show that ICP47 does inhibit antigen presentation significantly on HSV-infected mouse cells using *in vitro* antigen presentation assays. However, in mouse cells, antigen presentation was ablated by 44%, compared to an 85% reduction in human cells. As $CD8^+$ T cells have been shown to recognize very few peptide-MHC I complexes on the surface of target cells, it is important to consider the efficiency at which ICP47 inhibits human and mouse TAP. Therefore, we used mass spectrometry to identify and quantify MHC I bound peptides derived from

HSV-1 during viral infection. We found that more peptide sequences were presented on mouse cells infected with ICP47 null virus compared to those infected with wild-type virus. We quantified the presentation of 14 of these peptides and the contribution of ICP47 to this process in human and mouse cells. We found that ICP47 almost entirely blocks human TAP-mediated peptide presentation, though the degree of inhibition was somewhat peptide-specific. Conversely, the effect of ICP47 on mouse TAP was far less profound, resulting in only up to five-fold reduction in MHC-peptide abundance. In conclusion, this study shows that despite significant inhibition of antigen presentation in mouse cells, ICP47 may not be an effective immune modulator in mice and suggests a need for re-evaluation of suitable mouse models.

Abbreviations

ABC	Antibody Binding Capacity
ACRF	Australian Cancer Research Foundation
ADCC	Antibody-Dependent Cellular Cytotoxicity
ALR	Absent in melanoma 2-Like Receptor
amol	Attamole
ANOVA	Analysis of variance
ANU	Australian National University
APC	Antigen Presenting Cell
ANN	Artificial Neural Network
BGH	Bovine Growth Hormone
Cas9	CRISPR associated protein 9
CAT	Chloramphenicol Acetyltransferase
CD8	Cluster of Differentiation 8
CLR	C-type Lectin Receptor
CMC	Carboxymethyl cellulose
CMV	Cytomegalovirus
CMV IE	CMV Immediate-Early
CNS	Central Nervous System
CO_2	Carbon dioxide
CoREST	Corepressor of REST
CRISPR	Clustered Regularly Spaced Palindromic Repeats
CTCF	CCCTC-binding factor
C-terminus	Carboxyl terminus
CV	Column Volume
CHX	Cycloheximide
CXCL	chemokine (C-X-C motif) Ligand
CXCR	chemokine (C-X-C motif) Receptor
CHR	Cycloheximide reversal
D0	Dulbecco's modified Eagle medium without foetal bovine serum
D10	Dulbecco's modified Eagle medium with 10% foetal bovine serum
D2	Dulbecco's modified Eagle medium with 2% foetal bovine serum
DC	Dendritic Cell
dpi	days post-infection
DMEM	Dulbecco's Modified Eagle Medium
DMF	N, N Dimethylformamide
DMSO	Dimethyl sulfoxide
DNA	Deoxyribonucleic acid
dNTP	deoxynucleotide triphosphate
DRG	Dorsal Root Ganglia

E	Early
EBV	Epstein-Barr Virus
EDTA	Ethylenediaminetetraacetic acid
eGFP	enhanced Green Fluorescent Protein
ER	Endoplasmic Reticulum
ERAP	ER Aminopeptidase
Egr1	Early growth response protein 1
FBS	Foetal Bovine Serum
FITC	Fluorescein isothiocyanate
fmole	femtomole
g	g-force
gB	glycoprotein B
GABP	GA-Binding Protein
GDNF	Glial cell-Derived Neurotrophic Factor
gRNA	guide RNA
gzmB	granzyme B
HCF	Host Cell Factor
HCl	Hydrochloric acid
HCMV	Human Cytomegalovirus
HDAC	Histone deacetylase
HE	Herpes Encephalitis
HEPES	4-(2-hydroxyethyl)-1-piperazine-1-ethane sulfonic acid
HIV	Human Immunodeficiency Virus
HLA	Human Leukocyte Antigen
HPLC	High Performance Liquid Chromatography
HSK	Herpes Stromal Keratitis
HSV-1	Herpes Simplex Virus type 1
HSV-2	Herpes Simplex Virus type 2
IC_{50}	Half maximal Inhibitory Concentration
ICP	Infected Cell Protein
ICS	Intracellular Cytokine Staining
IE	Immediate Early
IFN	Interferon
IgG	Immunoglobulin G
IL	Interleukin
iNOS	inducible Nitric Oxide Synthase
IRES	Internal Ribosomal Entry Site
IRF	Interferon Regulatory Factor
IRL	Internal Repeat Long
IRS	Internal Repeat Short
iRT	indexed Retention Time

JNK	c-Jun N-terminal Kinase
Kbp	Kilo base pair
kDa	kilo Dalton
lacZ	Gene encoding β-galactosidase
LAT	Latency Associated Transcript
LB	Luria-Bertani media
LB-agar	Luria Bertani Agar
LC	Liquid Chromatography
LSD1	Lysine Specific Demethylase 1
M	Molar
m/z	mass-to-charge ratio
M0	Minimum Essential Medium without foetal bovine serum
M10	Minimum Essential Medium with 10% foetal bovine serum
M2	Minimum Essential Medium with 2% foetal bovine serum
MCMV	Murine Cytomegalovirus
MEM	Minimum Essential Medium
MFI	Mean Fluorescence Intensity
mg	Milligram
MHC	Major Histocompatibility Complex
min	Minute
miRNA	micro RNA
mL	milli Litre
mM	milli Molar
MRM	Multiple Reaction Monitoring
mRNA	messenger RNA
MS	Mass Spectrometry
mTORC1	mammalian Target Of Rapamycin Complex 1
MOI	Multiplicity Of Infection
MVA	Modified Vaccinia virus Ankara
n	number of samples
NBD	Nucleotide-Binding Domain
NEB	New England Biolabs
NFIII	Nuclear Factor III
ng	nanogram
NGF	Nerve Growth Factor
NK	Natural Killer
NLR	Nucleotide-binding oligomerization domain-Like Receptor
nm	Nanometre
NMR	Nuclear Magnetic Resonance
N-terminus	Amino terminus
OBP	Origin Binding Protein

OCT	Octamer Binding Protein
OriL	Origin of Replication in the Long region of the HSV-1 genome
OriS	Origin of Replication in the Short region of the HSV-1 genome
p	probability value
PAMP	Pathogen-Associated Molecular Patterns
PBS	Phosphate-Buffered Saline
PCR	Polymerase Chain Reaction
PE	Phycoerythrin
PFA	Paraformaldehyde
pfu	plaque forming units
PI3-K	Phosphatidyl Inositol 3-Kinase
pMHC	peptide-Major Histocompatibility Complex
pmole	picomole
PMT	Photomultiplier tube
PNS	Peripheral Nervous System
PRC	Polycomb Repressor Complex
PRR	Pattern Recognition Receptor
RANTES	Regulated on Activation, Normal T cell Expressed and Secreted
REST	Repressor Element-1 Silencing Transcription factor
RFLP	Restriction Fragment Length Polymorphism
RIG	Retinoic acid-Inducible Gene
RLR	Retinoic acid-inducible gene-I-Like Receptor
RNA	Ribonucleic acid
ROSA26R	B6.129S4-Gt(ROSA)26Sor$^{tm1So/J}$
rpm	revolutions per minute
SABC	Specific Antibody-Binding Capacity
SD	Standard Deviation
SDS	Sodium Dodecyl Sulphate
sec	second
SEM	Standard Error of the Mean
sgRNA	single guide RNA
SMM	Stabilised Matrix Method
spCas9	*Streptococcus pyogenes* CRISPR associated protein 9
Sp1	Stimulator protein 1
STAT	Signal Transducer and Activator of Transcription
SV40	Simian virus 40
TAP	Transporter associated antigen processing
TCR	T Cell Receptor
TG	Trigeminal Ganglia
Th	T helper
TLR	Toll-Like Receptors

TMD	Transmembrane Domain
TNF	Tumour Necrosis Factor
TrkA	Tropomysin kinase A receptor
TRL	Terminal Repeat Long
TRS	Terminal Repeat Short
T_{RM}	resident memory T cell
UL	Unique Long
US	Unique Short
UTR	Untranslated region
UV	Ultra Violet
v/v	volume/volume
VACV	Vaccinia Virus
VHS	Virion Host Shutoff
VIC	VP16-Inducing Complex
VZV	Varicella Zoster Virus
w/v	weight/volume
X-Gal	5-bromo-4-chloro-indolyl-β-D-galactopyranoside
α	alpha
β	beta
β-gal	beta-galactopyranoside
γ	gamma
γ1	Leaky late
γ2	True late
Δ	deletion
μg	microgram
μM	micro Molar
°C	Degree centigrade
μL	micro Litre

Amino acids

A	Alanine
R	Arginine
N	Asparagine
D	Aspartate
C	Cysteine
E	Glutamate
Q	Glutamine
G	Glycine
H	Histidine
I	Isoleucine

L	Leucine
K	Lysine
M	Methionine
F	Phenylalanine
P	Proline
S	Serine
T	Threonine
W	Tryptophan
Y	Tyrosine
V	Valine

Table of Contents

List of Tables

List of Figures

Chapter 1
Introduction

1 Introduction

1.1 Herpes simplex virus

Herpesviruses are abundant ancient viruses that co-existed with their hosts for millions of years. Common attributes of these viruses include: a) a large double-stranded DNA genome, which comprises terminal and internal reiterated sequences, b) the establishment of a long-term relationship with the host via generation of latent reservoirs in specific cell types in immunocompetent hosts and c) enveloped virions of 100 to 300 nm in size, which consist of an icosahedral nucleocapsid surrounding the core and an unstructured layer of tegument proteins beneath the lipid bilayer envelop. The family Herpesviridae comprises three subfamilies alphaherpesvirinae, betaherpesvirinae and gammaherpesvirinae. The key characteristic of alphaherpesvirinae is that they establish a lifelong latent reservoir in primary sensory neurons and its members infect a wide range of hosts, including mammals, birds and reptiles (Davison, 2010). The alpha herpesviruses, such as type 1 herpes simplex virus (HSV-1), type 2 herpes simplex virus (HSV-2) and varicella zoster virus (VZV) are among the most highly successful human pathogens. They occur worldwide and infect a majority of the population, across all age brackets. Availability of a protective vaccine against VZV along with nationwide childhood vaccination programs have greatly reduced the incidence of VZV disease in both developed and developing countries (Seward et al., 2002; Oxman et al., 2005; Seward and Jumaan, 2007; Sheridan et al., 2017; Fu et al., 2017). Furthermore, reactivation of VZV, which typically occurs in older adults and clinically manifests as herpes zoster or shingles, can be limited by, Zostavax, a live attenuated herpes zoster vaccine. This has been shown to reduce the incidence of shingles from 51.3 % in people aged over 60 years (Oxman et al., 2005). However, for HSV-1 and 2 no such licensed vaccines are available yet. Globally, 67% of people under the age of 50 are estimated to be seropositive for HSV-1 (Looker et al., 2015a) and 11.3% are seropositive for HSV-2 (Looker et al., 2015b). Most seropositive individuals experience episodic viral shedding, which aids in viral transmission, with a small proportion also showing symptoms of recurrent HSV disease (Kaufman et al., 2005; Ramchandani et al., 2016). Lack of a preventative or therapeutic vaccine for HSV and high incidence of disease imposes an enormous global public health burden.

1.2 HSV disease

HSV-1 and 2 cause a spectrum of clinical disease from mild mucocutaneous lesions, such as oral herpes, to severe systemic manifestations like neonatal herpes. The majority of initial HSV-1 infections occur during childhood and present as a local ulcerative lesion often associated with fever. The oro-mucosal HSV infection allows virions to enter and establish latency in neurons of the trigeminal ganglia (TG). HSV-1 reactivation in the ophthalmic branch of the TG may lead to herpetic eye diseases, such as herpes epithelial keratitis and herpes stromal keratitis (HSK) (Shimeld et al., 1990a, 1990b; Rowe et al., 2013). With frequent recurrences of HSK, active viral replication together with potent immune response in the cornea, may eventually lead to irreversible corneal scarring and blindness (Darougar et al., 1985; Babu et al., 1996; Thomas et al., 1997; Gangappa et al., 1999; Deshpande et al., 2001; Jiang et al., 2015). Globally, 40,000 people are estimated to have severe visual impairment or blindness as a result of HSV-1 infection (Farooq and Shukla, 2012). Additionally, it costs approximately 17.7 million USD per annum to treat HSV related eye diseases in the United States alone (Lairson et al., 2003). It is typically thought that Genital herpes is caused by HSV-2 infection in the genital mucosa. However, recent studies demonstrate an increased incidence of genital herpes disease caused by HSV-1, which may be attributed to an alteration in sexual practices among young adults and a reduction in exposure to HSV-1 during early childhood (Looker et al., 2015a, 2017). Genital herpes is one of the most common sexually transmittable diseases globally and has also been implicated in increases in both the acquisition and sexual transmission of human immunodeficiency virus (HIV) (Nahmias et al., 1990; McClelland et al., 2002; Corey et al., 2004; Looker et al., 2015b). Apart from mucosal infections, HSV-1 is able to mediate cutaneous infections in other body parts. For example, eczema herpeticum in individuals with atopic dermatitis (Wollenberg et al., 2003) and herpes gladiatorum among young athletes involved in contact sports (Selling and Kibrick, 1964; Becker et al., 1988; Anderson, 2003) are well recognized HSV-1 diseases.

In rare instances, HSV-1 can lead to more debilitating diseases. When the virus spreads trans-synaptically from the peripheral nervous system (PNS) to the central nervous system (CNS), it can lead to herpes encephalitis (HE) (Zarafonetis and Smadel, 1944; Esiri, 1982; Kramer and Enquist, 2013). HSV is the leading cause of sporadic fatal encephalitis especially in western countries (Hjalmarsson et al., 2007; Mailles et al., 2009; Trung et al.,

2012; Boucher et al., 2017). Despite the frequency of HE is being low (1 case in 1,000,000 annually), the mortality rate is very high if there is a failure in the administration of antiviral drugs. Even with rapid treatment, the long-term outlook after a HE incidence is poor (Utley et al., 1997; Whitley, 2006; Jouan et al., 2015). Similar to HE, neonatal herpes is a rare but serious incapacitating HSV disease of infants (Kimberlin, 2004). Such infection occurs from exposure to HSV-1 or HSV-2 in the genital tract of an infected mother. Globally, 10 cases of neonatal infection per 100,000 live births are recorded each year (Looker et al., 2017). Although the exact cost involved in the diagnosis, treatment and long-term disability care is not known, because a large proportion of the global population is harbouring HSV, these diseases are a significant economic burden (Stanberry et al., 2000; Fisman et al., 2002).

1.3 HSV-1 genome

HSV-1 is a large double-stranded DNA virus. The 152 kbp genome of this virus consists of long (UL) and short (US) unique regions, each flanked by inverted repeat regions (Figure 1.1). In addition, a short repeat region of approximately 400 bp is present at each terminus of the genome and exists as an inverted repeat at the junction between long and short regions (McGeoch et al., 1985, 1986, 1988; Perry and McGeoch, 1988; Wadsworth et al., 1975). The genome also accommodates two functional origins of replications with OriL located within the UL region and two identical copies of OriS present in short repeat regions (Stow, 1982). The HSV-1 genome has 84 single copy open reading frames in total and the majority of the protein-coding genes are located in the unique region of the genome (Rajcáni et al., 2004). The genes ICP0, ICP34.5 and the latency-associated transcripts (LATs) are located in the repeat regions and therefore, maintained as two copies within the genome. Several non-coding RNA transcripts are expressed in the HSV-1 genome both in the unique and the repeat region. The virus expresses 27 mature microRNAs of which the majority of them are proximal to or within the LAT locus, however, some can be found throughout the genome (Jurak et al., 2010; Piedade and Azevedo-Pereira, 2016).

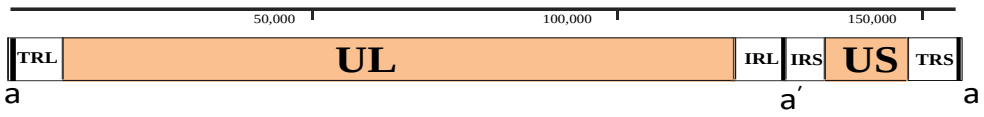

Figure 1.1 Schematic representation of the HSV genome. UL denotes unique long sequence, US denotes unique short sequence, TRL and IRL are inverted repeat sequences flanking UL, TRS and IRS are inverted repeat sequences flanking US and a and a′ represents short inverted repeats.

1.4 Experimental mouse models of HSV-1 infection

Animal species such as mice, rabbits, rats, guinea pigs, cotton rats, owl monkeys and rhesus macaques have been utilized in experimental model systems to understand different aspects of the human disease (Kollias et al., 2015a). Of these species, mice and rabbits are commonly used as models of HSV-1 latency, reactivation and recurrence. Both species have specific advantages and disadvantages. Spontaneous reactivation is attainable in rabbits infected with specific strains of HSV-1, whereas mouse models do not display efficient reactivation (Shimeld et al., 1990b; Hill et al., 2012). Limited availability of inbred strains and transgenic animals in addition to the expensive housing make rabbit models a less preferred choice. Mouse models are predominantly used in HSV research due to the availability of inbred and useful transgenic strains, extensive genetic and immunological characterisation and a myriad of useful molecular reagents available for research. HSV-1 reproducibly establishes latency in mice and reactivation can be induced by various means. Nevertheless, the susceptibility outcome of infection in mouse model varies based on the virus strain, infection dose, host genetics, the age of the animal and the route of infection. Several infection models have been used for HSV-1 infection such as corneal scarification (Stulting et al., 1985), footpad inoculation (Cook and Stevens, 1973a), lip infection (Kastrukoff et al., 1982), the zosteriform model (Blyth et al., 1984), as well as intranasal (Kern et al., 1986), intracerebral, intraperitoneal and intravenous infection (Zawatzky et al., 1982). Each of these infection models has strengths and limitations, pertaining to the experimental system as a whole.

Although most HSV-1 strains can grow efficiently in cultured cells, as well as peripheral infection sites and neural tissues in mice, they exhibit differences in the severity of symptoms (Dix et al., 1983). Typically, HSV infection and replication occurs in cells at the primary infection site and in primary sensory neurons that innervate the corresponding dermatome. The symptoms are generally self-limiting, however, in some cases, depending on the virus strain, route of infection and mouse strain, the virus can invade CNS leading to debilitating disease. In this thesis, the term "neurovirulence" is referred to the ability of the virus to cause neurologic disease due to the invasion of the CNS after a peripheral infection. Among widely used laboratory passaged HSV-1 strains, McKrae, SC16 and 17 syn+ are highly neurovirulent; F and RE are mildly virulent compared to KOS, which is a non-neurovirulent strain (Dix et al., 1983; Stevens et al., 1987b; Kollias et al., 2015b). Even

two HSV-1 strains from same source individual, KOS63 and KOS79, showed dramatic difference in virulence after footpad and intra-cerebral infection of BALB/c mice; KOS79 is a highly neuroinvasive and neurovirulent strain compared to KOS63 (Dix et al., 1983). A recent study has demonstrated that KOS79 and KOS63 are genetically distinct, providing a possible explanation for the difference in virulence (Bowen et al., 2016). Viral genes, including UL34.5 (Bolovan et al., 1994), thymidine kinase (Gordon et al., 1984), ribonuclease reductase (Cameron et al., 1988), US12 (Goldsmith et al., 1998), and US3 protein kinase (Kurachi et al., 1993) have all been linked to neurovirulence.

Besides virus strain variability, the host's genetic background and the infection route also influence the virulence. For example, in C57BL/6 mouse, HSV-1 McKrae appears to replicate in the brain and brainstem, following a corneal infection, however, such neurovirulence does not occur after an intra-vaginal infection. However, infected BALB/b mice display enhanced viral replication in the brain after both corneal and intra-vaginal infection routes (Wang et al., 2013a). Another study performed by Cavellero and colleagues demonstrated that with the same level of inoculum, corneal scarification of BALB/c mice with HSV strain SC16 resulted in severe morbidity and mortality compared to lip injection. Whilst in the same study, corneal scarification with HSV-1 KOS caused epithelial lesions but had no effect on the survival of mice (Cavallero et al., 2014). HSV-1 KOS is generally considered non-neurovirulent. However, in BALB/c mice, hind footpad inoculation of HSV-1 KOS resulted in paralysis of more than 80% of mice by 14 days after infection (Orr et al., 2005). Of the commonly used mouse strains, C57BL/6 mice limits virus spread in the periphery, restricts virion entry into the CNS (Metcalf and Michaelis, 1984; Sprecher and Becker, 1987; Kastrukoff et al., 2012a) and allows efficient establishment of latency in the peripheral sensory neurons (Cavallero et al., 2014; Price and Schmitz, 1978). On the other hand, CBA, Swiss-Webster, BALB/c and A/J mice are more susceptible to severe, acute infection in peripheral tissues, and can succumb more easily to encephalitis driven by virulent HSV-1 strains (Kastrukoff et al., 1982, 2012a; Metcalf and Michaelis, 1984). Host immunity, governed by $CD8^+$ T cells, $CD4^+$ T cells and cytotoxic natural killer (NK) cells, plays a major role in determining the susceptibility of a mouse to HSV infection (Simmons and Tscharke, 1992; Leib et al., 1999; Kastrukoff et al., 2010, 2015; Sheridan et al., 2009).

Often the selection of a model depends on the question to be addressed by the proposed research (reviewed in Simmons et al., 1992). Some infection routes bear little resemblance

to the human HSV-1 infection, however, they are useful to study specific aspects of HSV-1 pathogenesis. For example, intracranial infection of mice provides insight into the role of a selected viral gene in CNS infection (Dix et al., 1983). However, to study the natural history of infection and pathogenesis of HSV-1 disease, it is important to consider whether the route of inoculation is natural and faithfully represent human infection.

1.5 Overview of HSV-1 infection

HSV-1 infection can be categorised into three distinct stages: primary infection, latency, and reactivation (reviewed in Whitley and Roizman, 2001) (Figure 1.2). The primary infection occurs when HSV-1 is transmitted from an infected individual to the uninfected host by direct exposure of virus to the abraded skin or mucosal surface. A majority of the primary infections are sub-clinical and therefore unrecognised (Lafferty et al., 1987; Fillet, 2002; Brady and Bernstein, 2004). However, in some cases, the infected individual develops vesiculo-ulcerative lesions and other clinical symptoms, which typically subside within 10-14 days (Greenberg, 1996; Whitley et al., 1998; Simmons, 2002; Stoopler et al., 2003). Following initial infection, the virus enters sensory nerve endings that innervate the infection site and virions are transported to the neuronal nuclei through retrograde axonal transport (Goodpasture and Teague, 1923; Goodpasture, 1925; Cook and Stevens, 1973b). The progeny virus from the ganglion also undergoes anterograde transportation via the axons to the periphery (Walz et al., 1974; Norgren et al., 1992; Penfold et al., 1994). This process continues until viral replication is terminated by the cell-mediated immune response (Simmons and Tscharke, 1992; Koelle et al., 1994a, 1994b, 1998; Manickan and Rouse, 1995). Despite the elimination of replicating virus, the viral genome is sequestered in the nucleus of some primary sensory neurons for the life of the host. This non-replicative state is known as latency. From the quiescent state, HSV-1 reactivates in the ganglia periodically. This results in the generation of new infectious virions, which can be transported along the axons and released from nerve endings to the skin or mucosa. Viral replication at the epidermal cells can then result in discrete shedding episodes, which are commonly subclinical but in some cases present as recrudescent disease, characterised by visible ulcers and vesicles (Spruance, 1984; Darougar et al., 1985; Kameyama et al., 1988; Scott et al., 1997; Rowe et al., 2013; Ramchandani et al., 2016). Asymptomatic shedding is thought to be a potential risk for transmission of the virus (Koelle, 2000). Each of the

stages of HSV-1 infection, including primary infection, latency and reactivation are elaborated at the cellular and molecular level in the following sections.

1.5.1 Lytic infection in epithelium and neurons

Initial HSV-1 infection occurs mainly through epithelial cells or mucosal surfaces (Whitley and Roizman, 2001). Immediately following infection, HSV DNA attains a circular form in the nucleus of the host cell (Strang and Stow, 2005) and becomes associated with histones (Kent et al., 2004). It was established in cell culture that HSV follows a temporal cascade of gene expression and based on this, HSV genes are chronologically grouped as immediate early (IE), early (E) and late (L) genes (Honess and Roizman, 1974, 1975). A general consensus is that the initiation of transcription of viral genes requires VP16-inducing complex (VIC) (Post et al., 1981; Campbell et al., 1984; Triezenberg et al., 1988; Sadowski et al., 1988). VIC is a multi-protein transactivation complex comprising viral tegument protein VP16 and two cellular proteins, including host cell factor (HCF) and octamer binding transcription factor (OCT-1) (Wysocka and Herr, 2003). VIC binds to VP16-responsive element (TAATGARAT) in the promoter region of IE genes. This interaction initiates the viral gene expression cascade by inducing the expression of IE genes (O'Hare, 1993). Having noted this main paradigm, models using HSV-1 mutants lacking VP16 transcription activation function suggest that VIC-independent gene transcription pathways may also exist (Ace et al., 1989; Tal-Singer et al., 1999).

There are five IE gene products, of which, ICP0, ICP4, ICP22 and ICP27 are involved in controlling the initiation of gene expression at the transcriptional or post-transcriptional levels (Honess and Roizman, 1974, 1975). The last IE protein, ICP47, has not been shown to take part in transcription regulation, but it participates in immune evasion (Honess and Roizman, 1974, 1975; York et al., 1994). IE protein synthesis is followed by the expression of early genes, which mainly encode enzymes essential for replication of viral DNA, and transactivation of late gene expression. While late gene products are largely structural proteins of virions, some of them are also involved in virion assembly and egress. Late genes are further classified as leaky late and true late genes, where the latter are expressed strictly after the viral DNA replication. Collectively, these genes are referred to as "lytic genes" since they are expressed abundantly during lytic infection both at the peripheral infection site as well as in neurons.

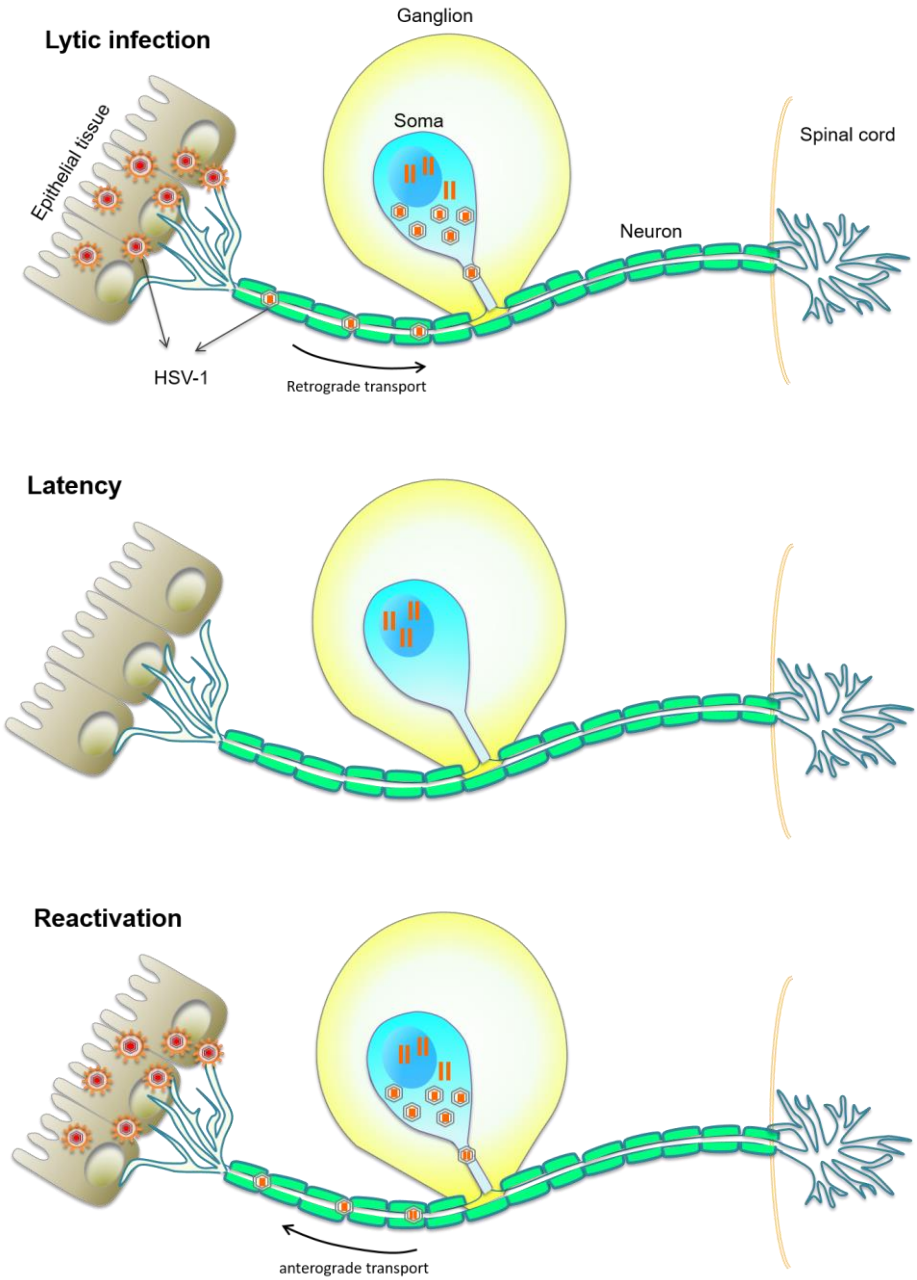

Figure 1.2 Overview of HSV-1 infection. Initial HSV-1 infection typically occurs at the periphery, where the virus enters via damaged epithelium and starts replicating. Some virions enter the nerve endings, innervating the infection site, and travel in a retrograde manner to the neuronal cell bodies or soma. The virus replicates in epithelial cells and neurons resulting in the production of progeny virus. This phase is known as "lytic infection". Some viruses persist in neuronal nuclei in the form of non-integrating genomes, during which infectious virus is absent. This stage is termed "latency". Latency is disrupted sporadically with the production of infectious virus particles in neurons, which travel in an

anterograde direction, along the axon to the periphery. This phase is known as "reactivation".

1.5.2 Establishment and maintenance of latency in sensory neurons

While in some infected neurons, HSV enters lytic infection, others retain viral genomes as circular, non-replicating episomes in the nucleus (Stevens and Cook, 1971a; Cook et al., 1974; Efstathiou et al., 1986a; Mellerick and Fraser', 1987; Simmons et al., 1992b). Studies by Efstathiou's group demonstrated that lytic gene expression takes place in a majority of neurons prior to the establishment of latency (Proença et al., 2008, 2011, 2016). This suggests that the establishment of latency is not compromised by the expression of lytic genes. Latency is characterised by the absolute lack of infectious virus, however, viral transcripts can be still found at this stage. The most abundant of these transcripts are the so called "latency-associated transcripts" (LATs) which are non-coding overlapping transcripts of 1.5 and 2.0 Kbp in size (Stevens et al., 1987b; Spivack et al., 1991). Various genetic mutants have been generated to understand the role of LATs in the establishment and maintenance of latency. Currently all evidence suggest that LATs are not essential for the establishment of latency (Javier et al., 1988; Steiner et al., 1989, 1989). However, these transcripts were shown to promote and maintain latency presumably by the suppression of viral lytic gene expression via post-transcriptional or epigenetic mechanisms (Chen et al., 1997; Garber et al., 1997; Wang et al., 2005a; Umbach et al., 2008; Cliffe et al., 2009). Other functions associated with LAT expression include aiding reactivation (Leib et al., 1989; Hill et al., 1990; Perng et al., 1994a; Chen et al., 1997; Watson et al., 2018), protection from neuronal cell death (Bloom, 2004) including apoptosis (Perng, 2000; Ahmed et al., 2002; Branco and Fraser, 2005) and protection from $CD8^+$ T-cell killing (Chentoufi et al., 2011; Jiang et al., 2011). At least six miRNAs transcribed from the LAT locus were also reported to be present in significant amounts in the ganglia of latently infected mice (Du et al., 2015; Umbach et al., 2008). The exact role of these miRNAs is still being investigated and is suspected to interfere with lytic gene expression (Umbach et al., 2008; Tang et al., 2008, 2009).

The lytic transcripts are found at relatively low levels during latency and can only be detected using highly sensitive techniques. Whilst earlier studies reported on the expression of a few specific lytic transcripts in latently infected ganglia (Deatly et al., 1987; Gordon et al., 1988; Feldman et al., 2002a; Maillet et al., 2006; Kramer and Coen, 1995), contemporary studies at the single neuron level have further illuminated the dynamics of gene expression

during latency. The single-cell transcriptome analysis by Ma and colleagues showed that at a given time, genes from at-least one kinetic class were expressed in two-thirds of neurons while a third remained transcriptionally silent (Ma et al., 2014). Later, an investigation by Russell and Tscharke showed that representative HSV-1 promoters of each kinetic class of the temporal cascade can be expressed prior to, during and after the establishment of latency (Russell and Tscharke, 2016). However, whether the expression of lytic genes during latency is a result of abortive replication or residual gene expression is not yet clear, nor is the significance of such gene expression. Moreover, factors that trigger HSV-1 to enter the latent state are yet to be fully defined. It appears that a complex interplay of viral and cellular factors determines the switch between productive and latent infection. Four important pathways that may lead to the establishment of latency are discussed below:

a) Failure to initiate productive infection due to lack of formation of the VIC in neurons has been proposed as an underlying mechanism behind the establishment of latency. In neurons the formation of this complex may be hindered due to insufficient transport of VP16 from axonal terminus to neuronal nucleus (Hafezi et al., 2012), sequestration of HCF in cytoplasm (Kristie et al., 1999) or the inhibition of OCT-1 from binding to IE promoters by other cellular proteins (Latchman, 1999). It was suggested that such failure to form VP16 induced complex could restrict the activation of IE gene expression (Efstathiou and Preston, 2005; Thompson et al., 2009). The evidence that VP16 is dispensable for latency establishment also supports this hypothesis (Steiner et al., 1990).

b) Epigenetic regulation of viral gene expression is a key characteristic of HSV latency. The naked viral DNA associates with histones immediately after being released from virion capsid into the nucleus (Cereghini and Yaniv, 1984). Histones associate with the HSV genome at the lytic stage and in latency. However, during productive infection, the lytic gene promoters are sparsely associated with histones and are enriched with active euchromatin markers, such as activating tri-methylation of lysine 4 of H3 (H3K4me3) and acetylation of lysines 9 and 14 of H3 (H3K9ac and H3K14ac, respectively) (Herrera and Triezenberg, 2004; Kent et al., 2004). Conversely, the latent genome is characterised by ordered nucleosomes (Deshmane and Fraser, 1989). During latency, lytic gene promoters are associated with histones containing silencing heterochromatin markers such as H3K9me2, whereas, at LAT promoter, histones

mainly accumulate euchromatin markers (Kubat et al., 2004; Wang et al., 2005b). This is consistent with the accumulation of LAT mRNA during latency and its ability to promote repressing heterochromatin markers on the HSV genome (Cliffe et al., 2009). Furthermore, emerging evidence suggests that the HSV genome is separated into transcriptionally active and repressed domains. For example, CCCTC and CTCCC motifs that bind CTCF (CCCTC binding factor) proteins are clustered throughout the HSV-1 genome (Amelio et al., 2006). In the dorsal root ganglia (DRG) and TG of mice, CTCF proteins were found to be enriched on CTCF clusters during latency (Amelio et al., 2006; Ertel et al., 2012) and application of reactivation stimuli significantly diminished CTCF proteins from those clusters (Ertel et al., 2012). In addition, CTCF motifs clustered around the LAT promoter/enhancer region block the extension of enhancer activity to ICP0 expression, thus functioning like an insulator (Amelio et al., 2006; Chen et al., 2007). Such partitioning of the genome into active and repressed regions emphasises the role of epigenetic regulation in the switch between lytic and latent infection. Chromatin repressor complexes such as REST/CoREST/LSD1/HDAC complex (Roizman, 2011) and polycomb repressor complexes were also suggested to be involved in the control of latency (Kwiatkowski et al., 2009; Cliffe et al., 2013a).

c) Neuronal intrinsic factors such as neuronal subtypes, growth factors and neuron-specific signalling pathways also influence the establishment of latency. In mice, HSV-1 specifically establishes latency in A5+ neurons, which are the nociceptive neurons that express a marker identified by the A5 monoclonal antibody (Margolis et al., 2007; Yang et al., 2000). A5+ neurons constitute only 11% of the neurons in the TG. *In vitro*, A5+ neurons are non-permissive for productive replication whereas KH10+ neurons, another subtype that express KH10 marker, readily allowed HSV-1 lytic infection (Bertke et al., 2011). A5+ neurons respond to nerve growth factor (NGF) and express the NGF receptor called tropomysin kinase receptor (TrkA), whereas, KH10+ neurons respond to a glial cell-derived neurotrophic factor (GNDF) (Bennett et al., 1998). Furthermore, TrkA receptor blockade allowed rapid reactivation of the virus (Camarena et al., 2010). Similarly, suppression of mammalian target of rapamycin complex 1 (mTORC1) kinase, which acts downstream of NGF-TrkA-mediated phosphatidylinositol 3-kinase (PI3-K)/Akt signalling pathway also leads to the reactivation of the virus (Kobayashi et al., 2012). Although these data suggest that the

NGF signalling pathways contribute to the establishment of latency, the exact mechanisms remain to be explored. Neuron-specific microRNA, miR138, targets ICP0 directly downregulating its expression and consequently the expression of other lytic genes. An HSV-1 lacking the miR138 target site showed enhanced virulence in mice and the TG of these mice showed increased lytic gene expression both during and after the establishment of latency (Pan et al., 2014). Together, these studies indicate the importance of neuronal factors in the control of latency.

d) Latency can be established efficiently in immunodeficient mice lacking T and B lymphocytes, gamma interferon (IFNγ) or NK cells as in immunocompetent mice (Ellison et al., 2000). Thus, host immunity is not required for establishment of HSV latency. However, components of both innate (Kodukula et al., 1999; Liu et al., 2001; Nandakumar et al., 2008) and adaptive immune system (Ghiasi et al., 2000; Manickan and Rouse, 1995; Simmons et al., 1992a) are vital for limiting productive infection and may help to maintain the virus in the latent state. The role of the host immune system during different stages of HSV infection will be discussed in detail in the later sections.

1.5.3 Reactivation and productive infection

From latency, HSV periodically re-enters the lytic phase of infection to form the infectious virus. This process is known as reactivation. Many physiological stress factors can trigger reactivation (Margolis et al., 1992; Cunningham et al., 2006; Wilson and Mohr, 2012a). In humans, reactivation may lead to painful recrudescent lesions or can result in asymptomatic recurrent shedding, leading to transmission of the virus (Scott et al., 1997; Wagner and Bloom, 1997). The molecular mechanisms behind latency and reactivation have been studied using animal models (mouse, rat, guinea pigs and rabbit) and *in vitro* cultured neurons (Wagner and Bloom, 1997). In mice, reactivation is most commonly studied using explanted ganglia (Sawtell and Thompson, 2004; Stevens and Cook, 1971b). Other methods used to induce reactivation in mice include depletion of NGF, axotomy, heat shock, UV irradiation and application of systemic stimuli using pharmacological agents (Blyth et al., 1976; Halford et al., 1996; Hill et al., 1978; Sawtell and Thompson, 1992; Wilcox and Johnson, 1987) Such stress stimuli can activate the c-Jun N-terminal kinase (JNK) signalling pathway, which then mediates the phosphorylation of histone 3 on lytic promoters, allowing the expression of previously repressed lytic genes (Cliffe et al., 2015). The initial phase of reactivation involving transcription and translation of viral genes has

been termed animation (Kim et al., 2012a). It has been suggested that at the early phase of animation, transcription of lytic genes from the repressed state depends neither on VP16 nor on a temporal gene expression cascade. In this case, genes from all kinetic classes are expressed independently of protein synthesis (Tal-Singer et al., 1997; Thompson and Sawtell, 2006; Du et al., 2011; Kim et al., 2012a). At the later stage of animation, gene expression resembles the orderly cascade that occurs during acute infection of cultured cells (Kim et al., 2012a). This is followed by DNA replication, packaging of virions and anterograde transport of virion components via axons to the peripheral tissues resulting in productive infection (Wilson and Mohr, 2012b). Although not required for animation, lack of viral genes such as VP16 or ICP0 can result in inefficient reactivation, where the provision of either of these in *trans* can trigger successful reactivation (Halford and Schaffer, 2001; Thompson et al., 2009). In the rabbit ocular infection model, spontaneous shedding of the virus was reduced in a LAT mutant-infected sample compared to wild-type virus, suggesting a role for LAT in reactivation (Perng et al., 1994b). In addition to viral gene products, the host immune system can also influence reactivation. Stress stimuli induce glucocorticoid and interleukin (IL)-6 levels and greatly reduces the number of IFNγ producing immune cells, including macrophages, NK cells and $CD8^+$ T cells in latently infected ganglia (Noisakran et al., 1998; Cantin et al., 1999; Freeman et al., 2007a; Huang et al., 2011). Such compromise in immune functions might ultimately lead to the complete reactivation of the virus.

Studies have shown that only a subset of neurons undergo productive reactivation in a latently infected ganglion. Bertke et al. using dissociated adult mouse TG neurons demonstrated that certain neuronal subtypes are non-permissive for productive infection. For instance, HSV-1 preferentially establishes latency in A5+ neurons due to their inability to support viral gene expression and productive infection (Bertke et al., 2011). Besides neuronal heterogeneity, other factors such as the amount of viral genomes in a latently infected neuron also determines the efficiency of reactivation. Using *in vivo* hyperthermia induced reactivation model, Sawtell and Thompson showed that on average, only 1–3 neurons per TG reactivate (Sawtell and Thompson, 1992) and that the probability of reactivation is correlated to the number of neurons containing the latent genome as well as the number of copies of viral DNA present in those neurons (Sawtell, 1997; Proença et al., 2016). Even though multiple copies of viral genome can enter a single neuronal cell, all are not equally capable of entering into productive infection (Kobiler et al., 2010). The main

take home from these studies is that the virus and its host neuron together can impose a significant degree of control over HSV-1 lifecycle.

1.6 An overview of the immune system

The immune system enables the host to recognise and effectively eliminate invading pathogens, minimise damage to self and establish an immunological memory to protect from re-infection. The mammalian immune system has a variety of mechanisms to defend against invading pathogens. Broadly, the host immune response is composed of two arms: the innate and the adaptive. However, in practice, the two components are integrated, with both contributing to shaping the immune response to infection. Here, I provide a general overview of the immune system to help understand the specifics of an immune response to HSV-1 infection outlined in section 1.7.

1.6.1 Innate immunity

The innate immune system is important for rapidly detecting incoming pathogens and is essential for activating adaptive immune cells. Host cells at the infection site, both immune and non-immune, are equipped with pattern recognition receptors (PRRs) that recognise pathogen-associated molecular patterns (PAMPs), which are conserved motifs derived from pathogens (reviewed by Kawai and Akira, 2009). PRRs such as Toll-like receptors (TLRs) and C-type lectin receptors (CLRs) are located in the cell membrane or membranes of the endosomes and lysosomes. Other PRRs, including NOD-like receptors (NLRs), retinoic acid-inducible gene- (RIG-) I-like receptors (RLRs) and AIM2-like receptor (ALR) reside in intracellular compartments (Ting et al., 2008; Yoneyama and Fujita, 2008; Gray et al., 2016). Examples of PAMPs include bacterial lipopolysaccharides, peptidoglycans, mannose-rich oligosaccharides, flagellin and pathogen-derived nucleic acid components, such as DNA and single or double-stranded RNA (Janeway, 1989). The stimulation of PRRs by appropriate PAMPs results in signal transduction leading to the synthesis and secretion of type I interferon (IFN), pro-inflammatory cytokines and chemokines. The type I IFNs act in a cell-intrinsic way, inducing expression of hundreds of genes that together interfere with every stage of viral replication cycle and sensitises cells for apoptosis (reviewed by Stetson and Medzhitov, 2006). The cytokines and chemokines further recruit and activate innate immune cells, such as macrophages, neutrophils, dendritic cells (DCs), mast cells, basophils, eosinophils and NK cells. Together, the innate immune cells perform two main functions. One is to directly eliminate invading pathogens by phagocytosis,

production of type II interferon, secretion of anti-microbial components and induction of apoptosis (reviewed by Medzhitov, 2007). The other function is to promote antigen-specific adaptive immunity by presenting processed antigens derived from pathogens to T and B cells, whilst concurrently providing necessary signals for their activation.

1.6.2 Adaptive immunity

The adaptive immune system is equipped with two arms: humoral immunity and cell mediated immunity. The humoral immunity is responsible for the production of antibodies by B cells (Mitchell and Miller, 1968; Nossal et al., 1968; Roitt et al., 1969; Ryser and Vassalli, 1974) and the cell-mediated immunity, in which T cells, specifically $CD4^+$ and $CD8^+$ subsets (Roitt et al., 1969; Bevan, 1977; Zinkernagel, 1982), play a central role. Although temporally delayed, the adaptive immune system protects the host from pathogens through more specific responses than innate immunity. This is facilitated by the presence of unique receptors on the surface of adaptive immune cells. The specific recognition of foreign antigens by B cells and T cells is mediated by the B cell receptors (BCRs) and T cell receptors (TCRs), respectively. The diverse repertoire of receptors is generated in each individual through genetic recombination and other additional mechanisms (Petrie, 1995). This allows adaptive immune cells to recognise almost any pathogenic invasion in a specific manner.

Mature, naïve B and T cells circulate through peripheral lymphoid organs, such as lymph nodes and spleen, where an adaptive immune response is elicited if these cells meet their corresponding antigens. The B cell receptors can directly recognise free antigens, which can be derived from proteins or carbohydrates. B cells also recognise antigens presented by professional antigen presenting cells (APCs) with the help of $CD4^+$ T cells (Tony and Parker, 1985). Following antigen engagement and activation, B cells expand and differentiate to plasma cells that synthesise antibodies, and long-term memory B cells. By binding to specific epitopes, antibodies can confer viral immunity in four ways: bind to and neutralise pathogens, opsonise pathogens leading to their elimination, activation of the complement system and mediation of antibody-dependent cell-mediated cytotoxicity (reviewed by LeBien and Tedder, 2008).

Unlike with B cells, TCRs recognise peptides derived from foreign antigens only when they are presented on the surface of cells by special host glycoproteins called major

histocompatibility complex (MHC) molecules. $CD8^+$ T cells recognise peptides presented in the context of MHC I whilst $CD4^+$ T cells recognise peptides presented by MHC II (Reinherz et al., 1999; Babbitt et al., 2005; Wucherpfennig, 2010). APCs such as DCs and macrophages that take up the antigen from peripheral tissues reach the lymph node or spleen via the lymph or blood, respectively. In these lymphoid organs, APCs present antigen to the naïve T cells. This process is initiated by the binding of a cell adhesion molecule called CD2 expressed on APCs, to an integrin protein called lymphocyte function associated antigen-3 (LFA-3) expressed on T cells. Another T cell integrin, namely LFA-1, synergistically binds to the intercellular adhesion molecules ICAM-1 and ICAM-2 on APCs. These transient interactions provide an opportunity for the TCR to sample peptide-MHC (pMHC) molecules on APCs. Recognition of a specific pMHC complex by the TCR stabilises the association between the T cell and the APC and provides the primary signal for T cell activation (Dustin, 1987; Staunton et al., 1989; Simmons, 1995; Dustin et al., 1997). The second signal for activation is provided by ligation of the co-stimulatory molecule, CD28, on T cells to CD80/CD86 on APCs. The third signal is driven by the cytokine IL-2, produced by T cells as a result of the pMHC-TCR interaction. After these early activation events, several subsequent co-stimulatory signals complete the activation process and aid in the survival, proliferation and differentiation of T cells. The activation of naïve T cells by APCs is also known as "priming" (reviewed by Smith-Garvin et al., 2009).

Depending on the cytokine environment, naïve $CD4^+$ T cells can differentiate into different subsets, including $CD4^+$ T helper (Th1 or Th2) cells, Th17 cells, regulatory T cells (Tregs) and follicular T cells (Tfh) (reviewed in O'Garra, 1998; Zhu and Paul, 2008). The differentiated T cell subsets, in turn, secrete different cytokines and chemokines that determine their immune response. $CD4^+$ T cells are important for coordinating immune responses against a variety of pathogens, boosting antibody production, enhancing and maintaining responses of $CD8^+$ T cells, regulating macrophage function, and manipulating general immune responses (Sakaguchi et al., 1995; Abbas et al., 1996; Asano et al., 1996; Breitfeld et al., 2000; Schaerli et al., 2000). After activation, naïve $CD8^+$ T cells function as effector cells that are capable of recognising and killing the infected cells by secretion of cytolytic granules and cytokines (Lowin et al., 1994; Guidotti et al., 1996; Slifka et al., 1999; Harty et al., 2000; Trapani and Smyth, 2002). The primed $CD8^+$ T cells travel from the lymphoid tissues to the infection sites with the help of infection-associated cell adhesion molecules (ICAMs) expressed on the blood vessels and several other chemotactic factors

(reviewed by von Andrian and Mackay, 2000). At the infection site, the activated $CD8^+$ T cells bind transiently via cell adhesion receptors such as LFA-1 to their respective ligands (ICAMs) on the infected target cell (Anikeeva et al., 2005). This interaction facilitates the recognition of the specific pMHC by the TCR and subsequent release of effector molecules. Activation and effector function of $CD8^+$ T cells is depicted in Figure 1.3 and Figure 1.4.

A key feature of the adaptive immune system is the development of memory B and T cells. Memory B cells are derived from naïve B cells that have undergone $CD4^+$ T cell-dependent antigen stimulation (Jacob et al., 1991). After re-exposure to even low dose antigens, memory B cells proliferate and differentiate to plasma cells, which produce large quantities of high-affinity antibody (reviewed by McHeyzer-Williams and McHeyzer-Williams, 2005). Unlike B cells, in the case of $CD4^+$ and $CD8^+$ T cells, memory cells are derived from effector T cells. After pathogen elimination during primary infection, most effector T cells die, however, a small number of cells survive to become long-lived memory T cells. The memory T cell class comprises different sub-populations. This includes circulating memory T cells, which enter the lymph node and recirculate into the blood, and the tissue-resident memory T (TRM) cells, which are locally confined at the site of previous pathogen encounter (Sallusto et al., 1999; Masopust, 2001; Reinhardt et al., 2001; Mueller and Mackay, 2016). Owing to clonal expansion during primary infection, relatively large numbers of antigen-specific memory T cells persist in immune individuals (reviewed by Ahmed and Gray, 1996). Furthermore, these memory cells can undergo rapid expansion and exhibit accelerated effector functions. Thus, once immunological memory has been created in an individual, either because of primary pathogen encounter or by immunisation, adaptive immunity ensures that the individual is protected against future challenges with the same pathogen. Whilst in normal settings, memory $CD8^+$ T cells become quiescent without losing the effector capacity, during chronic viral infections and cancer, long-term antigenic stimulation can result in functional exhaustion of $CD8^+$ T cell function (Hashimoto et al., 2018). $CD8^+$ T cell exhaustion is typically characterized by gradual loss of IL-2, IFNγ, TNFα and granzyme expression, acquisition of inhibitory receptors such as programmed cell death protein 1 (PD-1), and production of immunosuppressive cytokines such as IL10 (Wherry, 2011). Ultimately, this can result in $CD8^+$ T cell control of infections and cancer.

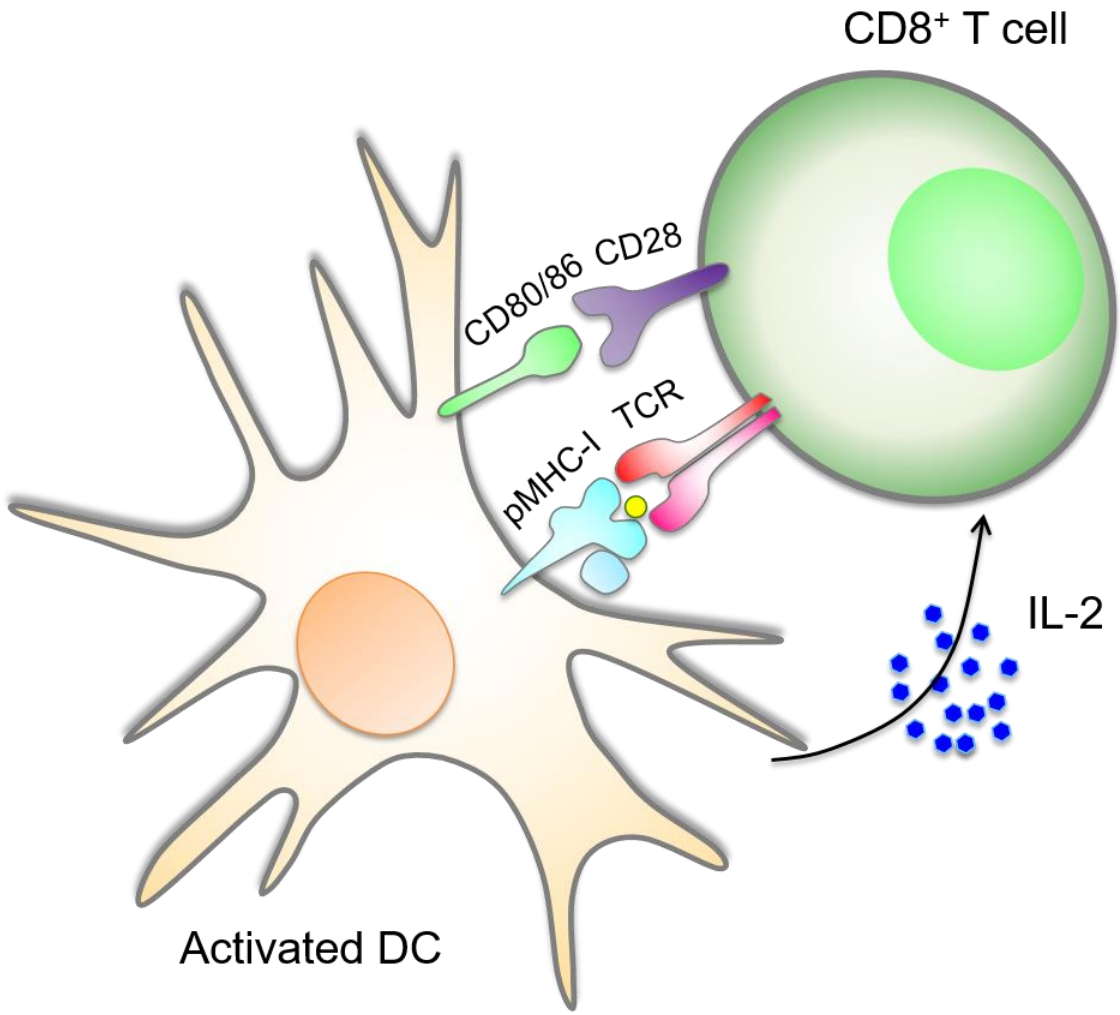

Figure 1.3 CD8$^+$ T cell priming. For activation, it is important that the pMHC-I complexes on APCs are recognised by the cognate TCR on the naïve CD8$^+$ T cells. To become fully activated, additional, antigen-independent stimulation by APCs is essential. This stimulation occurs as a result of binding of co-stimulatory molecules such as CD80 or CD86 on APCs to the receptor, CD28, on CD8$^+$ T cells. Further, the initial TCR – pMHC-I interaction stimulates APCs to secrete cytokines such as IL-2 and type I IFNs that drive robust CD8$^+$ T cell activation, proliferation and functioning. Adapted from Thaiss et al., 2011.

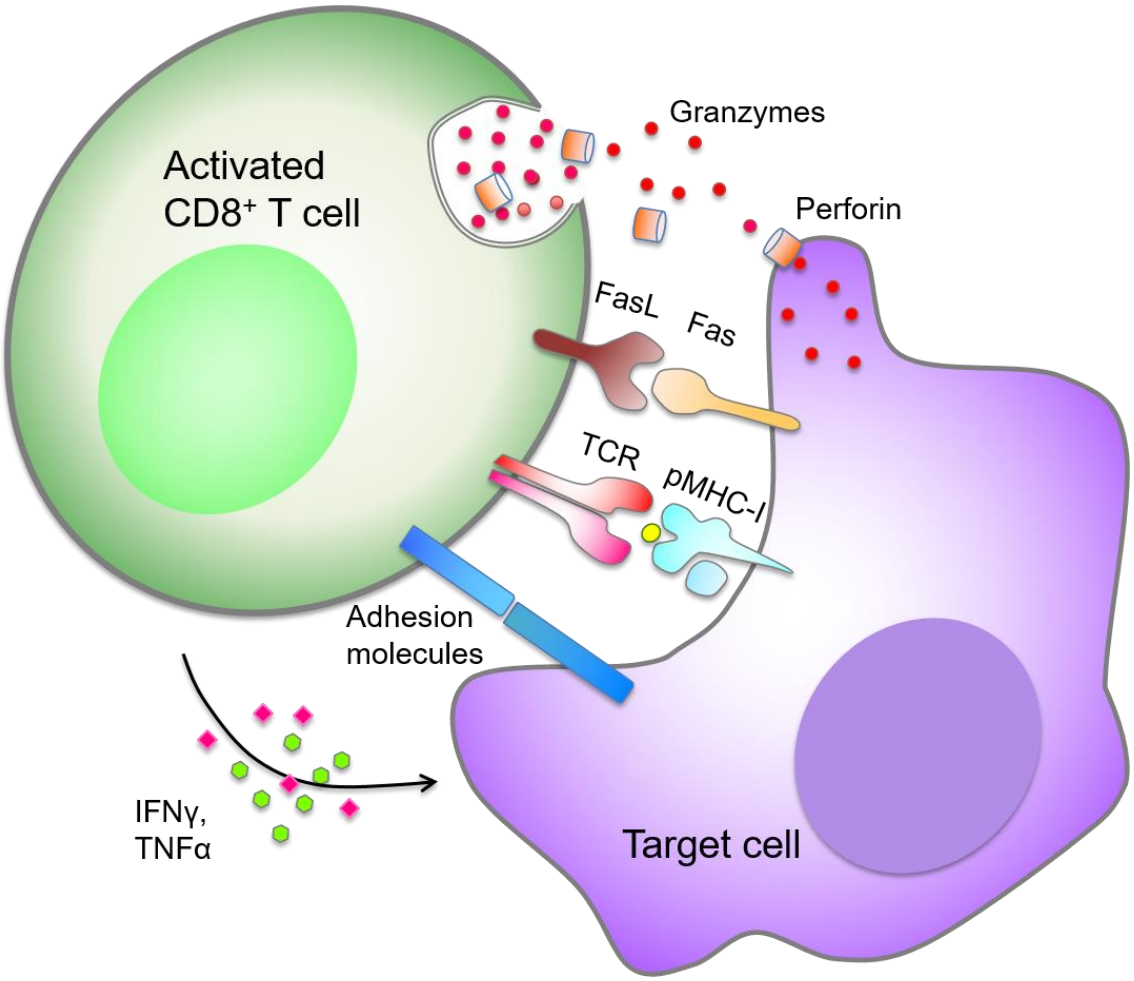

Figure 1.4 Functioning of activated CD8$^+$ T cells. After recognising pMHC-I on target cells, CD8$^+$ T cells use various mechanisms to deliver effector molecules. First, CD8$^+$ T cells secrete cytokines such as IFNγ and tumour necrosis factor α (TNFα), which have anti-viral and anti-microbial properties. Second, CD8$^+$ T cells produce and secrete cytolytic granules that contain perforin and granzymes. Whilst perforins form pores on the target cell membrane, granzymes use these pores to enter the target cells. Granzymes are serine proteases that cleave cytoplasmic proteins and ultimately trigger the apoptotic pathway. Finally, CD8$^+$ T cells express FasL, the ligands that bind to Fas receptors expressed on the surface of target cells. The Fas-FasL interaction leads to downstream signalling that activates caspase-mediated apoptotic cell death pathway. Adapted from Barry and Bleackley, 2002.

1.6.3 Antigen presentation to CD8$^+$ T cells

1.6.3.1 MHC I

The major function of MHC I molecules is to display a large number of antigenic peptides on the cell surface. Any given TCR specifically recognises a unique combination of a peptide and the surrounding α chain residues of MHC I (Garboczi et al., 2010; Rudolph et al., 2006). The canonical MHC I molecules are heterodimeric glycoproteins composed of a heavy α chain and a light β chain (Madden, 1995) (Figure 1.5). The extracellular portion of the heavy chain is folded into three-immunoglobulin domains, termed α1-α3. The interface between the α1 and α2 forms a shallow peptide-binding groove (Figure 1.5) (Garrett et al., 1989; Matsumura et al., 1992; Madden, 1995). At both ends of the groove are clusters of conserved amino acid residues, which form hydrogen bonds with the residues at the amino (N) and carboxy (C) termini of peptides. The peptides are anchored to so-called peptide binding pockets interspaced along the groove. Complementary binding occurs between the side chains of amino acids at a particular position in a peptide, known as anchor residues, and the specialised pockets of MHC I. The main anchor residues are often placed in the second and the last position from the N-terminus of the peptide (Fremont et al., 1992; Madden, 1995). This interaction restricts the length of the peptides that bind MHC I to 8-10 residues. However, peptides longer than 10 amino acids are sometimes accommodated in this region. In this case, the peptides bulge out of the groove due to kinks in the middle section of the peptide backbone (Guo et al., 1992; Chen et al., 1994; Urban et al., 1994; Tynan et al., 2005). The amino acid residues that line the peptide-binding groove of MHC I in the α1 and α2 domains are highly variable (Madden, 1995). The α3 domain of heavy chain, as well as the β chain of MHC I, also known as β-2 microglobulin, are relatively conserved. These domains provide support and stability to the MHC I molecule. Furthermore, trans-membrane helices of the heavy chain anchor the MHC I molecule in the membrane (Figure 1.5).

MHC I is polygenic. In humans, the genes that encode the classical MHC I are called human leukocyte antigen (HLA) genes. There are three MHC I α chain genes in humans, which encode the HLA-A, -B and -C molecules, respectively (Degli-Esposti et al., 1992; Horton et al., 2008). In mice, these genes are known as H-2 -K, -D and -L (Ozato et al., 1980). Each MHC I allele is polymorphic, and the anchor residues are different for every

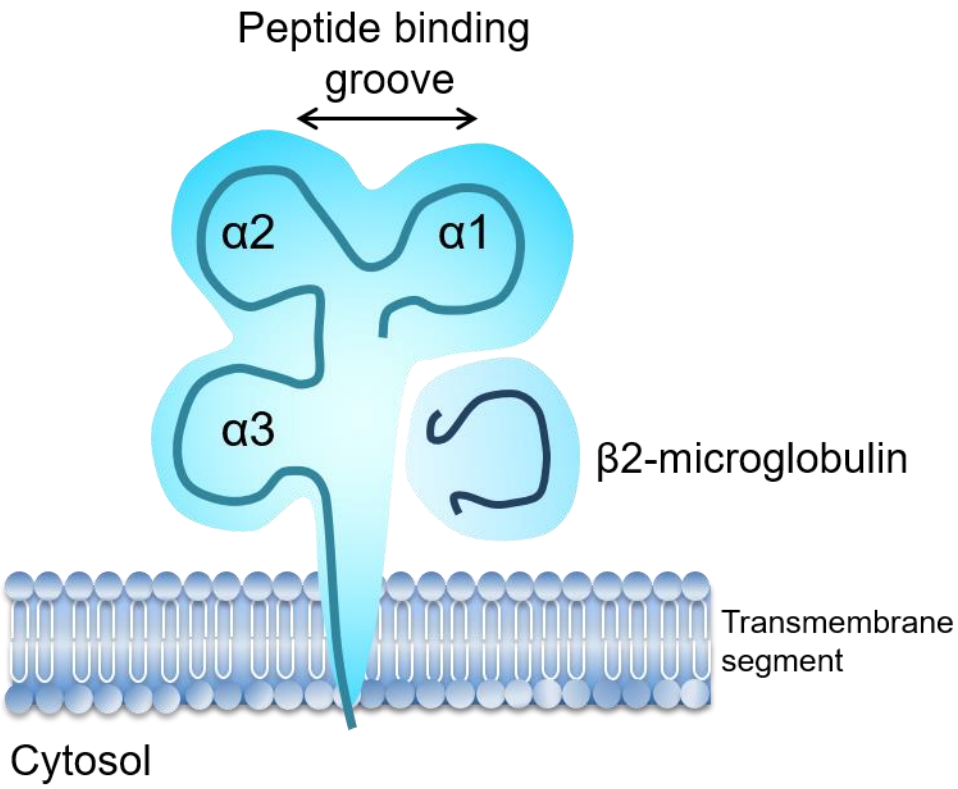

Figure 1.5 Diagrammatic representation of MHC I. MHC I is comprised of a heavy α chain and a light non-covalently bound β-2 microglobulin. The heavy chain forms three immunoglobulin domains α1, α2 and α3. The α1 and α2 domains interact with peptide via the peptide-binding groove. The α3 contains the transmembrane region that binds the whole MHC I to the membrane. Adapted from Mak and Jett, 2014.

allele. The polygenic and polymorphic nature of this system contributes to the high variability of peptides presented by MHC I (Lawlor et al., 1990).

1.6.3.2 Antigen processing and generation of peptides

The majority of the peptides that bind MHC I are generated due to proteolytic degradation of proteins or polypeptides, which occurs as a part of the cellular protein turnover machinery. Unwanted proteins, such as misfolded or damaged proteins and defective ribosomal products (DRiPs), form the major source of the peptides (Watts, 1997; Yewdell, 2007; Apcher et al., 2011; Bassani-Sternberg et al., 2015). DRiPs are thought to be generated as a result of *a)* pre-mature termination of transcription or translation, *b)* use of an alternate reading frame, *c)* delay or failure in the assembly of polypeptides into a protein complex or *d)* alterations in ubiquitin modification (reviewed by Yewdell, 2011). The source proteins of antigenic peptides may be self-proteins expressed at abnormal levels in cancer cells or foreign peptides derived from intracellular pathogens following infection. Recently, interest has been drawn to spliced peptides, where two peptide fragments generated by proteolytic degradation are re-ligated to form a new peptide sequence suitable for presentation by MHC I (Spivack et al., 1991; Vigneron et al., 2004; Liepe et al., 2016).

A bulk of these peptide precursors are then degraded by cellular proteasomes (reviewed in Goldberg and Rock, 1992; Pamer and Cresswell, 1998; Rock and Goldberg, 1999) (Figure 1.6). The 26S proteasome is a highly sophisticated, multi-catalytic protease composed of a 20S catalytic core that is capped at each end by the 19S regulatory complex (Walz et al., 1998). The 20S catalytic core is comprised of four symmetrical hetero-heptameric rings. The two outer rings are composed of α-subunits whilst the inner rings are composed of β-subunits, each containing seven similar subunits. The β-subunits act as a proteolytic chamber in which the catalytic activity is restricted to the inside of the core. Although proteasomes can sometimes act on substrates in a ubiquitin-independent manner (Grune et al., 2003), peptide precursors tagged with a poly-ubiquitin chain serve as the principal substrate (Ciechanover, 1998). It is the 19S complex that recognises the ubiquitin-tagged protein substrates and unfolds them for entry into the core catalytic chamber. Here, the β-subunits mediate proteolytic cleavage at specific sites, which results in a heterogeneous population of peptides ranging from 4-30 amino acids. Isoforms of the proteasome, called immunoproteasomes, are generated when cells are exposed to immunomodulatory cytokines, particularly IFNγ (Cerundolo et al., 1995). These immunoproteasomes have

specialised catalytic subunits with altered cleavage properties for efficient antigen processing and generation of diverse peptide repertoires for MHC I presentation (reviewed by McCarthy and Weinberg, 2015). Some proteasome cleaved products can be transported directly into the endoplasmic reticulum (ER) without further processing. Whereas, longer peptides are further trimmed by other peptidases such as cytosolic aminopeptidase, thimet oligopeptidase (TOP) and leucine aminopeptidase in the cytoplasm before entering into ER (Beninga et al., 1998; Mo et al., 1999; Portaro et al., 1999). The N-terminally extended peptide intermediates that enter ER are processed by the ER amino-peptidases, ERAP-1 and ERAP-2, to yield the final peptides for MHC I presentation (Serwold et al., 2002).

1.6.3.3 MHC I-mediated antigen presentation

The pathway that involves the processing and presentation of endogenous antigen is called the classical or direct MHC I presentation pathway (Figure 1.6) and it takes place in all nucleated cells. In this pathway, the peptides generated in the cytosol are transported into the lumen of the ER in order for antigen presentation to continue. This process is facilitated by the transporter associated with antigen processing (TAP), a member of the ATP binding cassette family of transporters (reviewed by Townsend and Trowsdale, 1993) (Figure 1.6). The TAP complex is a heterodimeric complex consisting of TAP1 and TAP2 (Figure 1.7). Each of these subunits contains a cytosolic nuclear binding domain (NBD), a transmembrane domain (TMD) and an N-terminal transmembrane domain (TMD0) (Schmitt and Tampé, 2002). The binding of peptide and ATP to the NBD at the cytosolic interface induces dimerization of NBDs. This is followed by a conformational switch of TMDs that enables movement of peptides from the cytoplasm into the ER (Oldham et al., 2016a). The influx of peptide into the ER results in ATP hydrolysis, which resets the TAP complex back to the pre-translocation state.

MHC I proteins are synthesised on membrane-bound ribosomes and delivered into the ER, where their assembly and folding is aided by the peptide loading complex (PLC) (Figure 1.6). The PLC is a macromolecular assemblage of different protein subunits comprising TAP, the MHC I heterodimer, the oxidoreductase ERp57, and ER-resident chaperones, such as tapasin and calreticulin, that co-ordinate loading of peptides onto the peptide receptive MHC I (Cresswell et al., 1999; Ortmann et al., 1997; Sadasivan et al., 1996; Blees et al., 2017) (Figure 1.6). The peptide loaded MHC I molecules dissociate from the PLC followed by exit from ER perhaps with the help of transport receptors (Spiliotis et al.,

2000). Subsequently, the stable pMHC-I complexes are translocated to the cell surface via the Golgi apparatus. MHC I molecules devoid of peptides or that bind low-affinity peptides often fail to reach the cell surface (Ljunggren et al., 1990). Thus, only peptides of reasonable affinity for MHC I get displayed for presentation. The ER is also the site of initiation of post-translational glycosylation of MHC I. The most prominent glycans on MHC I are N-linked. N-glycosylations play a role in proper folding and trafficking of these proteins to cell surface in addition to the assembly of peptide-MHC I complex (Barbosa et al., 1987; Ryan and Cobb, 2012). Initially, the N-glycans on MHC I are susceptible to release by endoglycosidase H (endo H) digestion. However, as the pMHC-I moves through the Golgi, the glycoproteins undergo extensive processing giving rise to complex glycans that are resistant to endo H cleavage. The resistance of MHC I to endo H is often used as evidence of passage through the Golgi apparatus (Townsend et al., 1989; York et al., 1994).

Another pathway exists where exogenous antigens are internalised by cells and presented on MHC I. This is referred to as the cross-presentation pathway (reviewed by Huang et al., 1996; Heath and Carbone, 2001; Rock and Shen, 2005; Cresswell et al., 2005; Basta and Alatery, 2007, 2007; Neefjes et al., 2011; Joffre et al., 2012). The major cell types that cross-present antigens to the TCR are the professional APCs, which mainly consist of specific subsets of DCs. These cells have the ability to take up the antigen from extracellular milieu through various processes, including phagocytosis, endocytosis and macropinocytosis (reviewed by Blum et al., 2013). Phagocytosis is a regulated process that helps internalise particulate antigens, apoptotic or necrotic cells, and pathogens via phagosomes (Shen et al., 1997). Endocytosis, on the other hand, captures membrane components and solubilised macromolecules in endosomes. During macropinocytosis, macromolecules, extracellular materials and pathogens are captured in large quantities within vesicles known as pinosomes, which eventually fuse with lysosomes (Norbury et al., 1995). The internalised antigens may access the cytosol through the vesicular compartments, where they are processed by proteasomes and the resultant peptides enter the TAP-mediated antigen presentation pathway. However, antigen processing and peptide loading can also occur in the endocytic compartment independent of TAP. This idea is further supported by the detection of MHC I molecules in phagosomes and endosomes (Ackerman et al., 2003; Guermonprez et al., 2003). Cross-presentation is essential for the initiation of a $CD8^+$ T cell response against pathogens that do not infect DCs.

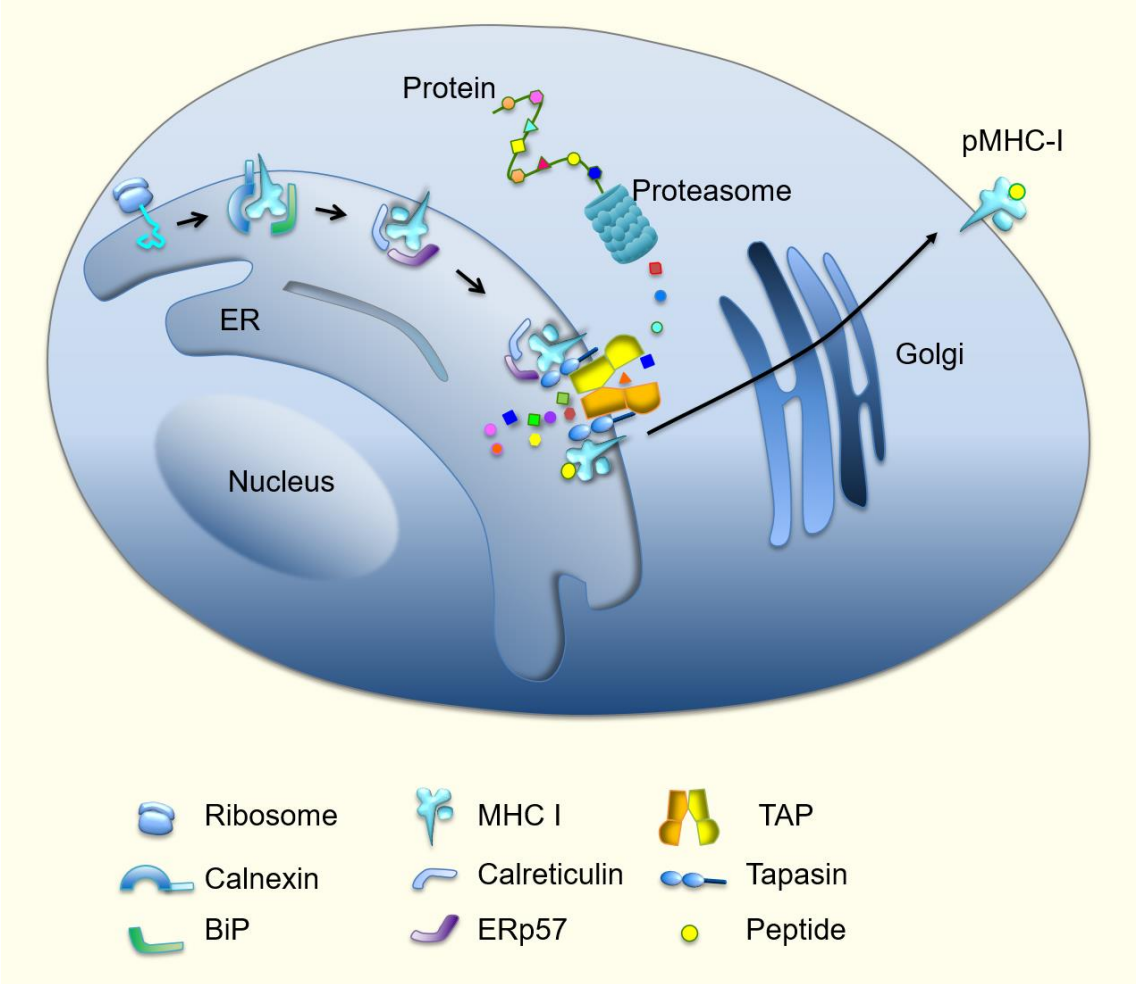

Figure 1.6 Schematic representation of classical MHC I antigen presentation pathway. The nascent heavy chain and β-2 microglobulin of MHC I are delivered into the ER lumen during protein synthesis via ribosomes. In the ER, the MHC I components fold and assemble together with the help of chaperone molecules calnexin, calreticulin, BiP and ERp57. Concurrently, the peptides generated by proteasomal degradation in the cytosol are transported into ER lumen by TAP. These peptides are loaded on the empty MHC I by the peptide loading complex, which includes TAP, tapasin, calreticulin, ERp57 and MHC I. Subsequently, the peptide-MHC I complexes are translocated to the surface of cells via the Golgi apparatus. Adapted from Schölz and Tampé, 2005.

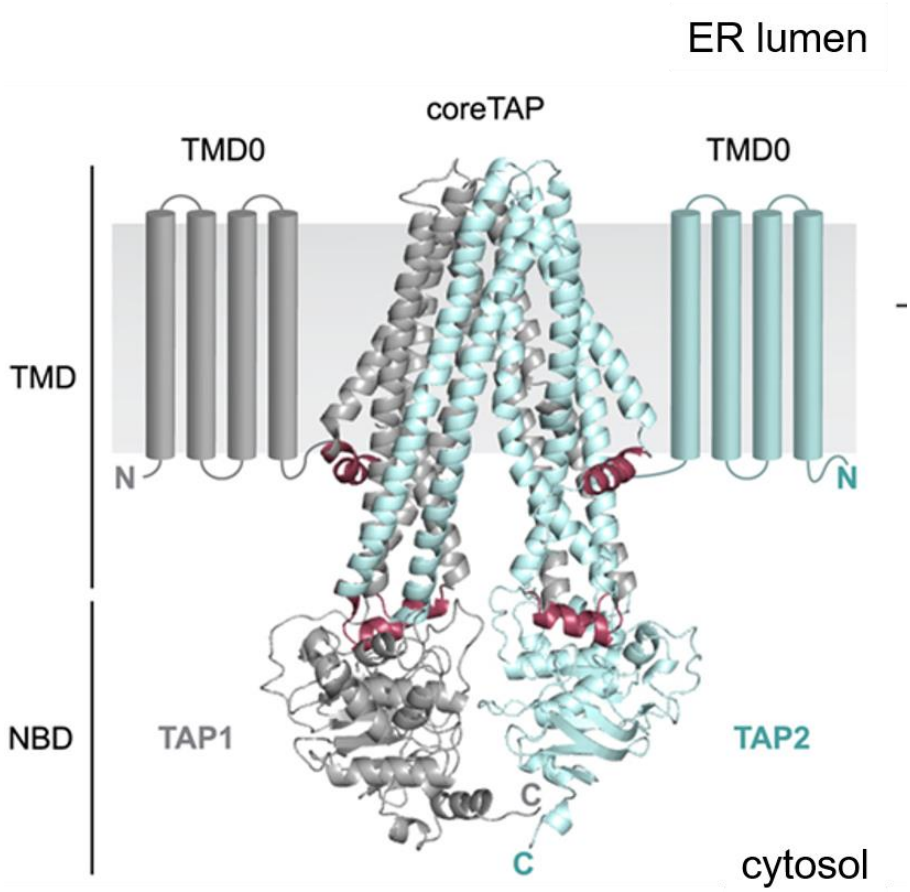

Figure 1.7 Structural model of TAP. TAP is a heterodimeric subunit complex made up of TAP1 and TAP2. Each subunit is comprised of a transmembrane domain (TMD) and a nuclear binding domain (NBD). The N-terminal four transmembrane helix bundle of TMD is referred to as TMD0. A TAP complex without TMD0, called core TAP, is sufficient for translocation of peptides into ER. Modified from Lehnert and Tampé, 2017.

1.7 Immune response to HSV-1 infection

With the overview of the innate and adaptive immune system outlined above, the following sections focus on detailed review of the immune response against HSV-1 infection, with a particular focus on the $CD8^+$ T cell-mediated immunity and the ability of HSV-1 to evade detection by $CD8^+$ T cells.

1.7.1 Innate immune cells

The immune recognition of HSV-1 infection begins at the level of infected epithelial cells and neurons (Sato and Iwasaki, 2004; Jin et al., 2007; Lucinda et al., 2017). PRRs are strategically placed at multiple cellular locations to maximize the chance for recognition of a viral infection. For example, TLR2 recognises the infecting viral particles at the cell surface (Kurt-Jones et al., 2004), TLR9 interacts with viral DNA released via endosomes in the cytoplasm (Krug et al., 2004), cytosolic viral DNA is also recognised by receptors such as DNA-dependent activator of interferon regulatory factor (DAI) (Takaoka et al., 2007), interferon gamma inducible protein 16 (IFI16) (Conrady et al., 2010), RNA polymerase III and retinoic inducible gene RIG-I (Chiu et al., 2009); and finally, transcription intermediates such as double-stranded RNA are recognised by melanoma associated differentiation gene 5 (MDA5) in the cytoplasm (Melchjorsen et al., 2010) and TLR3 in the endosome (Zhou et al., 2009; Lafaille et al., 2012). In fact, it has been demonstrated that a deficiency in TLR2, TLR9 or TLR3 leads to severe consequences during HSV infection (Kurt-Jones et al., 2004; Lima et al., 2010; Mørk et al., 2015; Zhou et al., 2009). Following cellular recognition of PAMPs, cells activate the type I and type III interferon pathways which drive production of pro-inflammatory cytokines. Consequently, circulating immune cells, including γδ T cells, macrophages, NK cells and DCs are recruited to the epithelial and ganglionic infection sites where they infiltrate and then become further activated by inflammatory signals (Liu et al., 1996; Donaghy et al., 2009; Melchjorsen et al., 2010; Shimeld, 1995; Lucinda et al., 2017). These immune cells can directly function as effector cells by releasing anti-viral molecules, as well as orchestrate an anti-viral response by recruiting the adaptive immune components to the infection site.

Macrophages are multifunctional; they can phagocytise virus particles and infected cells, present processed antigen to adaptive immune cells (Unanue, 1984; Ramirez and Sigal, 2002) and release anti-viral cytokines (Scieux, 1997; Kodukula et al., 1999). Additionally,

they are intrinsically resistant to HSV infection (Hirsch et al., 1970; Stevens and Cook, 1971a; Lopez and Dudas, 1979), and provide extrinsic resistance by releasing anti-viral factors, which inhibit viral replication in other infected cells (Morahan et al., 1980; Benencia and Courreges, 1999). In particular, within the TG of HSV-1 infected mice, infiltrating macrophages secrete anti-viral factors such as TNFα, regulated on activation normal T cell expressed and secreted (RANTES), IL-12 and inducible nitric oxide synthase (iNOS) (Kodukula et al., 1999; Melchjorsen et al., 2002; Mott et al., 2007). In line with this, depletion of macrophages, TNFα or inhibition of nitric oxide production favours early viral replication in HSV-1 infected mice (Benencia and Courreges, 1999; Kodukula et al., 1999), although the kinetics of virus control is comparable between the macrophage-depleted mice and wild-type mice (Sciammas et al., 1997; Kodukula et al., 1999; Cheng et al., 2000). In addition, macrophages do not affect HSV-1 latency, as determined by the level of LAT expression in latently infected mice (Mott et al., 2007). These findings suggest that macrophages are involved in controlling initial viral replication but do not contribute to the clearance of the infectious virus.

DCs, that are tissue-resident or tissue infiltrating, can detect HSV-1 invasion through PRRs and inflammatory cytokines secreted at the site of infection. Activated DCs secrete type-I interferon and release cytokines such as IL-12, IL-15 and IL-18. These cytokines, specifically IL-12 and IL-15, have been shown to play a role in NK cell activation (Ferlazzo et al., 2004). For instance, DCs were critical for optimal IFNγ production by an NK cell subset in the popliteal lymph node of mice following footpad infection with HSV-1 (Kassim et al., 2009). In addition, corneal resident dendritic cells recruited circulating NK cells to the site of infection (Frank et al., 2012). Besides boosting the innate immune response via NK cells, DCs are efficient APCs due to their elevated expression of major histocompatibility complex (MHC I and II) and co-stimulatory molecules. Together these help to prime naïve T cells and secrete IL-12, which leads to the activation and differentiation of $CD4^+$ T cells and $CD8^+$ T cells (Banchereau and Steinman, 1998; Sato and Iwasaki, 2004; Henry et al., 2008).

DCs are heterogeneous in their phenotype, location and function. For example, epidermal Langerhans cells (LCs) are located in the basal epidermal layer of skin and are among the first immune cells to encounter HSV. Depletion of LCs in mice enhances viral replication in the skin suggesting that these cells provide local immunity to HSV-1 (Sprecher and

Becker, 1989). HSV-1 counteracts this process by inducing apoptotic cell death of infected LCs (Bosnjak et al., 2005a). Curiously, in further studies, these cells were shown to neither participate directly in presenting antigen to $CD8^+$ T cells (Allan et al., 2003) nor deliver HSV-1 antigens from the peripheral infection site to lymphoid organs for priming as determined using cutaneous infection model (Whitney et al., 2017). Nevertheless, in lymph nodes HSV-1-derived peptides are presented to naïve $CD8^+$ T cells specifically by the lymph-node resident $CD8\alpha^+$ DCs in the initial stages of acute cutaneous infection in mice (Allan et al., 2003; Jirmo et al., 2009) and predominantly by the migratory dermal $CD103^+$ DCs during the later stages (Bedoui et al., 2009). Kim and colleagues (2015) made similar observations in human *in situ* models. Using the human foreskin explant and HSV-1 infected penile skin biopsy models, they showed that HSV infected LCs undergo apoptosis and migrate to the dermal layer, where the dermal DCs take up the infected LCs, suggesting the possibility that the dermal DCs might relay HSV antigens from the infection site for antigen presentation (Kim et al., 2015). While the lymph-node resident DCs were the main APCs during cutaneous infection of mice, Lee et al., showed using vaginal infection model that, in addition to lymph nodes resident $CD8\alpha^+$ DCs, migratory DCs, but not Langerhans cells, also present antigen and contribute to the priming of $CD8^+$ and $CD4^+$ T cells (Lee et al., 2009). Another subset of DCs, known as plasmacytoid dendritic cells (pDCs), are also capable of secreting high amounts of type I IFNs and respond against HSV-1 infection in a TLR9-dependent manner (Lund et al., 2003; Krug et al., 2004; Sato et al., 2006). However, the participation of pDCs in antigen presentation was shown to be unlikely in a vaginal infection model (Lee et al., 2009). Together, these studies indicate that different DC subsets display a differential role in priming of $CD8^+$ T cells and overall, DCs play a predominant role in linking the innate and adaptive immune system to primary HSV infection.

NK cells are heterogeneous in their expression of cell surface receptors, phenotypic markers and their cytolytic activity. It is well established that NK cells can become activated directly after being exposed to interferons (IFN α, β or γ) or interleukins such as IL-12, IL-15 and IL-18 (Biron et al., 1984; Biron, 1997; Ahmad et al., 2000). In addition to cytokine-mediated recognition, NK cells also employ receptor-mediated detection of pathogens, such as in the context of murine cytomegalovirus (MCMV) infection. NK cells use two kinds of receptors: activating receptors which induce cytolysis after engaging an

appropriate ligand on virus-infected cells (Diefenbach and Raulet, 2001) and inhibitory receptors which recognise MHC I on the cell surface to provide a protective signal and suppress the cytolytic activity of NK cells (Kärre et al., 1986; Storkus et al., 1987). Use of such receptors for recognising HSV infected cells is under-explored. Analysis of NK cell recognition of HSV infected cells at the clonal level indicated that both activating and inhibitory receptors might be involved (Pietra et al., 2000). HSV (type 1 and 2) infection down-modulates the MHC I on the cell surface using an infected cell protein (ICP) 47 (York et al., 1994; Hill et al., 1995). In particular, an NK cell clone bearing an inhibitory receptor was able to lyse ICP47 expressing cells *in vitro* (Huard and Früh, 2000) suggesting that the loss of inhibitory signal stimulated the NK cell cytolytic activity. Conversely, in another study, neither infection with an ICP47 deletion virus nor the blocking of inhibitory receptors on NK cells abolished the killing of HSV-1 infected target cells (Chisholm et al., 2007). The effects of down-modulation of MHC I on NK cell recognition of HSV-1 infected cells, therefore, remains unresolved. Regardless, earlier reports have documented that human patients lacking NK cell activity become extremely susceptible to HSV infection (Lopez et al., 1983; Biron et al., 1989) highlighting the important protective role of NK cells. These cells perform their anti-viral cytolytic function by releasing IFNγ, cytotoxic granules containing perforin and several granzymes, tumour necrosis factor and other cytokines upon recognition of viral invasion (Smyth et al., 2005). Besides the cytolysis of infected cells, emerging evidence indicates that NK cells might be involved in linking innate and adaptive immunity. In HSV-2-induced lesions in humans, the activated NK cells were shown to be in contact with plasmacytoid DCs (Donaghy et al., 2009) and they also formed an immunological synapse with $CD4^+$ T cells (Kim et al., 2012b). The up-regulation of TLR-2 and MHC II on NK cells upon stimulation with HSV antigens *in vitro* suggests that NK cells may also serve as APCs (Kim et al., 2012b). The functional significance of such interaction between DCs, NK cells and T cells remain to be elucidated.

1.7.2 Adaptive immune cells

The initial infiltration of innate immune components is later replaced by adaptive immune cells, which are essential for complete clearance of the infectious virus. All arms of the adaptive immune system, including B cells, $CD4^+$ T cells and $CD8^+$ T cells have been shown to infiltrate the infection sites (Liu et al., 1996) and function against acute HSV infection (Minagawa et al., 1988).

1.7.2.1 Humoral immunity against HSV infection

Many earlier studies using mouse models tested the efficacy of passive immunisation with HSV-specific antibodies in controlling primary HSV disease. Following flank infection of BALB/c mice, passive immunisation with a high dose of neutralising antibody prevented the formation of secondary skin lesions, indicating that the antibody neutralised the extracellular virus released from nerve endings (Simmons and Nash, 1985). Similarly, passive immunisation of mice prior to HSV-1 infection by corneal scarification significantly reduced the herpetic eye disease and the incidence of mortality (Shimeld et al., 1990a). Studies in B cell-deficient mice also support a role for humoral immunity against HSV infection. Beland and colleagues (1999) demonstrated that B cell-deficient, but not control mice (C57BL/6), developed encephalomyelitis due to viral spread to the CNS after intra-peritoneal injection of HSV-1 strain KOS. Further, the survival of HSV-1 infected B cell-deficient mice was improved after administration of HSV-specific hyper immune serum (Beland et al., 1999). These studies emphasise that neutralising antibody ameliorates disease in experimentally infected mice, possibly by limiting the spread of the virus at early stages of infection. Even though these experiments reveal the value of immunisation, the functional role of B cells in natural infection is not well defined.

Other mouse studies, however, challenge the significance of antibody-mediated protection against HSV infection. Dudley et al. (2000) observed that, although there is a slight delay, B-cell deficient μMT mice clear HSV-2 infection efficiently as their immunocompetent counterparts after vaginal infection. Furthermore, prior immunisation of wild-type mice did not provide adequate resistance against HSV-2 in the absence of T cells (Dudley et al., 2000). In another study, intranasal immunisation of mice with recombinant vaccinia virus expressing HSV glycoproteins gB or gD failed to prevent primary vaginal epithelial infection with HSV-1. This was despite the induction of a high titre of antigen-specific antibodies (Kuklin et al., 1998). Furthermore, depletion of $CD4^+$ T cell in these immune mice leads to increased viral replication in the vaginal tract (Kuklin et al., 1998).

The role of B cells in control of human HSV infection has been the subject of extensive investigation. Compelling evidence of the protective function of antibodies comes from neonatal infection, where the transfer of maternal antibodies to neonates reduces the risk of acquiring neonatal herpes. For example, trans-placental transfer of neutralising antibody from mother to infants provides a various degree of protection against neonatal herpes

disease, including complete neutralisation of the virus in some infants (Yeager et al., 1980; Brown et al., 1991, 1997). Furthermore, a recent study demonstrated that virus-specific maternal antibodies can infiltrate and persist in uninfected human foetal TG and are capable of protecting neonates from fatal HSV infection (Jiang et al., 2017). In adults, HSV-1 infection elicits humoral immune responses, with neutralising antibodies against viral glycoproteins, gB and gD, being detected (Bravo et al., 1996; McClements et al., 1997; Wang et al., 2016). However, the recombinant glycoprotein subunit vaccines failed large-scale human clinical trials and interestingly, levels of neutralising antibody did not correlate with the disease outcome (Corey et al., 1999). It appears that antibodies play a supporting role rather than providing primary protection against HSV disease.

Together, the above findings indicate that antibodies are potentially useful in controlling the early spread of the virus and protect against lethal viral challenge, likely by neutralising the free virus. However, antibody responses alone are not sufficient to provide complete protection against acute as well as recurrent HSV infection. Instead, a vigorous T cell response is required.

1.7.2.2 Cell-mediated immunity against HSV-1

The evidence that T cells contribute significantly to the defense against HSV infection came from early studies utilising congenitally athymic nude mice, which lack both their $CD4^+$ T cells and their $CD8^+$ T cells. Athymic mice in a BALB/c genetic background typically die as a result of HSV-1 infection, irrespective of the route of infection (Nagafuchi et al., 1979; Kapoor et al., 1982; Metcalf and Michaelis, 1984). Passive transfer of splenocytes from previously infected mice to HSV-infected athymic mice protected these mice from mortality (Nagafuchi et al., 1979). However, depletion of T cells from the splenocytes prior to transfer, or infusion with HSV-1 specific antibody, did not provide resistance against HSV-1 in the athymic mice (Nagafuchi et al., 1979). Additionally, compared to immunocompetent mice, athymic mice had significantly more infectious virus at the peripheral infection site, ganglia, spinal cord and brain, demonstrating a progressive spread of the virus to the CNS which resulted in the death of the animal (Walz et al., 1976; Kapoor et al., 1982). The above reports in mice indicate that T cells are indispensable for the control of HSV infection. Subsequent studies showed that a large number of $CD4^+$ T cells and $CD8^+$ T cells infiltrate infection sites during both the initial HSV-1 infection (Liu et al., 1996) and reactivation (Shimeld et al., 1996a, 1996b) in mice. Similarly, in humans,

both HSV-2 specific $CD4^+$ T cells and $CD8^+$ T cells have been isolated from genital lesions (Koelle et al., 1994a, 1994b, 1998; Posavad et al., 2000; Hosken et al., 2006). The relative importance of each of these subsets has been argued, with some proposing that $CD4^+$ T cells play a primary role in anti-HSV immunity (Kuklin et al., 1998; Manickan and Rouse, 1995; Ghiasi et al., 2000; Milligan et al., 2005; Mott et al., 2016), whilst others favour the importance of $CD8^+$ T cells (Simmons and Tscharke, 1992; Koelle et al., 1998; Posavad et al., 2000; Khanna et al., 2003a). Despite these incongruities, various groups have demonstrated that the effector activity of at least one of the T cell subsets, whether $CD4^+$ or $CD8^+$ T cells, are strictly required and sufficient to clear infectious virions from the epithelial, mucosal and neural mouse tissues (Nash et al., 1987; Ghiasi et al., 2000; van Lint et al., 2004a; Johnson et al., 2008a).

The functionality of $CD4^+$ T cells during acute infection is critical for the development of an effective adaptive immune response. $CD4^+$ T cells are the predominant source of IFNγ, which has been shown to suppress HSV-2 replication in mucosal epithelial tissues (Iijima et al., 2008). In addition to this, $CD4^+$ T cells secrete chemokines, such as CXCL9 and CXCL10, at the local infected tissue (Nakanishi et al., 2009). Through IFNγ, CXCL9 and CXCL10, $CD4^+$ T cells enable the migration of effector $CD8^+$ T cells to the site of infection (Nakanishi et al., 2009). By secreting IL-2 and enhancing the provision of co-stimulatory signals by DCs, $CD4^+$ T cells assist $CD8^+$ T cells in activating, expanding and mounting a response against infection (Smith et al., 2004; Wilson and Livingstone, 2008). Consistently, HSV-1 infected $CD4^+$ T cell-deficient mice contained less virus-specific $CD8^+$ T cells. However, the remaining $CD8^+$ T cells were fully functional, producing perforin and granzyme B at levels equivalent to wild-type mice (Rajasagi et al., 2009; Frank et al., 2010). As a result, the $CD4^+$ T cell depleted mice were able to clear HSV-1 and maintain latency similar to that of the infected wild-type mice (Frank et al., 2010). This suggests that $CD8^+$ T cells can function efficiently in the absence of $CD4^+$ T cells. Despite the lack of evidence suggesting $CD4^+$ T cells do not play a direct role in the establishment and maintenance of latency, they reside in the TG, next to neurons expressing LATs (van Velzen et al., 2013a) and help prevent $CD8^+$ T cells from functional exhaustion (Frank et al., 2010).

The role of $CD8^+$ T cells during both the acute HSV-1 infection and the latency are elaborated below.

1.7.3 How do CD8+ T cells recognise and respond to HSV-1 infection?

$CD8^+$ T cells play a predominant role in eliminating actively replicating HSV-1 virions by initiating a series of steps, which precede the mounting of an effective immune response. It appears that within hours of infection, migratory DCs acquire HSV antigens from the site of infection and reach the draining lymph nodes, where antigens are delivered to resident DCs. These cells then present the viral peptides in the context of MHC I to circulating naïve $CD8^+$ T cells (Mueller et al., 2002; Bosnjak et al., 2005a; Jirmo et al., 2009). The different DC subtypes that might be involved in cross-presentation of HSV-1 peptides to $CD8^+$ T cells are described in Section 1.7.1. After optimal priming, $CD8^+$ T cells undergo rapid clonal expansion and gain effector functions within the lymph node (Coles et al., 2002). The mobilisation of activated effector cells from the lymph node to infection sites is likely to depend on chemokines, such as CXCL9 and CXCL10, that operate through the CXCR3 receptor on $CD8^+$ T cells (Araki-Sasaki et al., 2006; Thapa et al., 2008; Nakanishi et al., 2009). Consistent with this, CXCL9 and CXCL10 levels were shown to be elevated in the neural and epithelial tissue of mice, after infection with HSV-2 (Thapa et al., 2008). The activated effector $CD8^+$ T cells leave the lymphoid organs and reach the infected epithelial and neural tissues within 5 days of HSV-1 infection in mice (van Lint et al., 2004a; Lang and Nikolich-Zugich, 2005).

At the infection site, when the TCR on infiltrating effector $CD8^+$ T cells re-engages with the pMHC presented on the infected cells, $CD8^+$ T cells are usually stimulated to secrete effector molecules such as IFNγ, TNFα and lytic granules containing perforin and granzymes (Harty et al., 2000; Lucinda et al., 2017). Smith et al. (1994) suggested that an antiviral mechanism that is common to both $CD4^+$ and $CD8^+$ T cells, such as IFNγ, is primarily responsible for curtailing viral replication. Consistent with this hypothesis, antibody-mediated neutralisation of IFNγ after HSV-1 infection in mice resulted in increased viral replication in the skin and delayed virus clearance (Smith et al., 1994). Concordantly, one study previously suggested that IFNγ also enhanced antigen presentation on virus-infected cells, improving the chance of recognition by $CD8^+$ T cells (Wallach et al., 1982). Alternatively, Dobbs et al. offer a more complex interpretation to Smith et al. (1994), suggesting that IFNγ alone cannot provide complete protection against replicating virus, but requires the function of perforin and granzymes (Dobbs et al., 2005). Perforin is secreted to bind and oligomerize on the plasma membrane of infected cells,

resulting in the formation of cell membrane pores, through which granzymes enter, leading to the fragmentation of cellular proteins triggering apoptotic cell death pathway (Trapani and Smyth, 2002). Granzymes belong to the serine protease family and are capable of inducing apoptosis (reviewed by Trapani, 2001). There are five types of granzymes in human and eight in mice. Granzyme -A and -B are shown to be primarily involved during HSV infection. Granzyme A induces apoptosis in a caspase-independent manner by cleaving single-stranded DNA and by hydrolysing histone proteins (Zhang et al., 2001; Fan et al., 2003; Lee et al., 2016). Granzyme A can also induce apoptosis by activating IL-1β, which can function as a positive mediator of cell death (Irmler et al., 1995). Granzyme B induces caspase-dependent apoptotic pathway (Metkar et al., 2003) and it is the predominant type of granzyme expressed by HSV-1 specific $CD8^+$ T cells that infiltrate the infection sites during lytic phase (van Lint et al., 2004a). Adoptive transfer of antigen-specific $CD8^+$ T cells from TCR transgenic mice to HSV-2 infected recipient mice resulted in efficient control of viral replication, whereas, transfer of antigen-specific $CD8^+$ T cells deficient in IFNγ or perforin resulted in impaired resolution of genital infection (Dobbs et al., 2005).

After the elimination of the infectious virus, a distinct population of memory $CD8^+$ T cells, termed $CD8^+$ T_{RM} cells, establish residence at antigen-challenged peripheral skin tissues (Ariotti et al., 2012; Gebhardt et al., 2009, 2011; Zhu et al., 2007, 2013a). Ariotti and colleagues used intra-vital imaging to understand the function of these epidermal $CD8^+$ T_{RM} cells in mice challenged by intra-epidermal injection with a $gB_{498\text{-}505}$ epitope-encoding DNA vaccine and exposed to a transfer of $gB_{498\text{-}505}$ epitope-specific $CD8^+$ T cells (Ariotti et al., 2012). They found that the $CD8^+$ T_{RM} cells possess a dendritic-shaped morphology and steady-state slow migration compared to effector $CD8^+$ T cells in the epidermis of HSV infected mice (Ariotti et al., 2012). Whether the morphology and migration of $CD8^+$ T_{RM} cells in ganglia are similar to that of the epidermis is not known. Interestingly, when they used a mouse model in which only a small fraction of epidermal cells were allowed to express $gB_{498\text{-}505}$ epitope, the $CD8^+$ T_{RM} cells were capable of recognising these antigen presenting cells and attain morphological configuration of effector $CD8^+$ T cells (Ariotti et al., 2012). Further, transcriptome analysis of these cells showed that HSV challenge can rapidly induce IFNγ expression, which subsequently up-regulates expression of antiviral transcripts in the neighbouring skin cells (Ariotti et al., 2014). Further, these virus-specific

skin-resident $CD8^+$ T cells was shown to be capable of providing protection against local re-infection with HSV-1 (Gebhardt et al., 2009). From the above data, it is evident that the $CD8^+$ T cells patrol both the ganglia and skin during latency and can rapidly attain an effector state upon cognate antigen recognition. Subsequent secretion of IFNγ may also induce a tissue-wide pathogen alert, activate innate immune cells and stimulate further recruitment of circulating memory T cells.

Consistent with the results obtained from mouse models, Zhu and colleagues have shown that $CD8^+$ T cells may be crucial for controlling recurrent HSV-2 infections in the human female genital tract. They analysed biopsies taken at regular intervals from human patients who experienced recurrent genital lesions and demonstrated that $CD8^+$ T cells, both antigen-specific and non-specific cells, infiltrate infected tissues in large numbers during productive HSV-2 infection (Zhu et al., 2007). The $CD8^+$ T cells isolated from these recurrent lesions were functional as they induced cytolytic killing of the target cells (Zhu et al., 2007). In addition, after complete resolution of the recurrent lesions, a long-term residence of $CD8^+$ T cells was observed at the dermal-epidermal junctions (Zhu et al., 2007). Later they demonstrated that these $CD8^+$ T cells, at the site of previous reactivation, expressed genes involved in $CD8^+$ T cell activation and produced perforin as shown by immunofluorescent staining (Zhu et al., 2013a). In biopsies displaying asymptomatic viral shedding, $CD8^+$ T cells containing perforin granules were found clustered around HSV-2 infected cells (Zhu et al., 2013a). Furthermore, an inverse correlation was drawn between the duration of viral shedding and $CD8^+$ T cell density in the human genital tract, suggesting that the $CD8^+$ T cells established during prior infection at peripheral site are a major factor in control and containment of infection, as well as the severity of reactivation (Schiffer et al., 2010). The long-term persistence of virus-specific $CD8^+$ T cells in dermal-epidermal junctions of recurrent infection site and their physical interaction with the HSV-2 infected cells imply that $CD8^+$ T cells may provide surveillance at the cutaneous infection site during latency and are equipped to contain the virus shedding from nerve endings during reactivation.

1.7.4 Role of $CD8^+$ T cells in maintaining HSV latency

Investigations using mouse models led to findings related to the significance of $CD8^+$ T cells during latent infection in the ganglia. In C57BL/6 mouse model, a large fraction of HSV-1-specific $CD8^+$ T cells recognizes a single epitope $gB_{498\text{-}505}$, while the remainder of the cells recognise at least 18

sub-dominant epitopes in varying frequency (St Leger et al., 2011). Khanna and colleagues showed that a stable population of HSV-1 specific $CD8^+$ T cells existed proximally to latently infected neurons (Khanna et al., 2003a). These $CD8^+$ T cells had an activated phenotype, as indicated by expression of markers for recent (CD69) and memory (CD44) activation, as well as granzyme B expression (Khanna et al., 2003a; van Lint et al., 2005; Verjans et al., 2007). This subset of virus-specific non-migrating $CD8^+$ T cells is distinguished from circulating memory cells by the expression of CD103 (also known as integrin αE) and persist in the ganglia and the skin long after the establishment of latency (Gebhardt et al., 2009; Himmelein et al., 2011). In addition, many HSV-1 specific $CD8^+$ T cells persist in a functional state during latent infection as indicated by IFN-γ production and presence of lytic granules (Khanna et al., 2003b; Knickelbein et al., 2008; Mackay et al., 2012). In addition to mice, similar observations have been reported following examination of latently infected human trigeminal ganglion (Theil et al., 2003; Verjans et al., 2007; van Velzen et al., 2013b) and other human cranial ganglia such as geniculate and vestibular ganglia, where HSV-1 can establish latency (Arbusow et al., 2010). Furthermore, it was observed that neurons are not lost due to $CD8^+$ T cell-mediated cytolysis nor reactivation despite the presence of functional $CD8^+$ T cells in latent ganglia (Pereira et al., 2000; Decman et al., 2005; Knickelbein et al., 2008). Mice lacking granzyme B or perforin show an exacerbation of reactivation in the latently infected TG, as illustrated by a dramatic increase in viral genome copy number. Regardless, these mice cleared the infectious virus with the same kinetics as the wild-type mice (Knickelbein et al., 2008). Additionally, using immunostaining, it was shown that granzyme B-containing $CD8^+$ T cells are juxtaposed to latently infected neurons that lack activated caspases (Knickelbein et al., 2008). Together these observations imply that granzyme B and perforin participate in controlling viral replication in ganglia using a caspase-independent, non-cytolytic mechanism. In another study, Pereira and colleagues found that granzyme A can restrict the inter-neuronal spread of virus without inducing cytolysis (Pereira et al., 2000). However, the participation of granzyme A after the establishment of latency has not been shown. Collectively, the above studies imply that both lytic granules and IFNγ released from $CD8^+$ T cells act synergistically to rapidly eliminate the infectious virus and possibly, help maintain latency.

Although there is no direct evidence to show that ganglia-resident $CD8^+$ T cells help maintain latency and prevent full-blown reactivation, the following data from mouse studies support this hypothesis. Antibody-mediated depletion of $CD8^+$ T cells or depletion of IFNγ in explant cultured

TG of mice resulted in enhanced reactivation of the virus (Liu et al., 2000, 2001). Other work has also shown that $CD8^+$ T cell depletion of mice harbouring latent HSV-1 resulted in increased HSV-1 DNA load and protein synthesis in the latently infected ganglia compared to untreated mice (Freeman et al., 2007b; Hoshino et al., 2007). Upon reactivation, the ganglion resident $CD8^+$ T cells were capable of proliferation. This was evidenced by explanting latently infected DRG from $gB_{498-505}$ epitope specific TCR transgenic mice to under the kidney capsule of naïve syngeneic recipients (Mackay et al., 2012). Moreover, TRM cells are also capable of secreting multiple effector molecules upon reactivation of the virus (Mackay et al., 2012). The ability of TRM cells to proliferate and secrete effector molecules suggests that upon reactivation of the virus in the ganglia, these cells are capable of mounting a rapid local response. While gB-specific cells retained their function, some have speculated that $CD8^+$ T cells specific to sub-dominant epitopes undergo functional exhaustion in ganglia during latency (Treat et al., 2017). This idea is based on studies that showed increased PD1 expression on gB-non-specific $CD8^+$ T cells and IL-10-mediated inhibition of proliferation of subdominant $CD8^+$ T cells in mouse TG (Jeon et al., 2013; St Leger et al., 2013). Currently, there is no apparent explanation for the difference in the functionality of gB-specific and -non-specific $CD8^+$ T cells.

1.7.5 Do neurons present HSV antigens to $CD8^+$ T cells?

For many years the nervous system was thought to be functionally immune-privileged, displaying a complete lack or delayed infiltration of immune cells (Barker and Billingham, 1977; Lampson, 1995). However, this perception is no longer widely held. It is now well documented that $CD8^+$ T cells can enter the CNS or PNS upon viral infection of neurons and in a range of autoimmune CNS diseases, $CD8^+$ T cells are involved in mediating neuronal destruction (Babbe et al., 2000; Zhang et al., 2008; Aye et al., 2009; Varadkar et al., 2014). $CD8^+$ T cell-mediated neuronal destruction depends on interactions with MHC I molecules, which have been recently found on neuronal cells. For example, experiments performed on mouse hippocampal neurons showed that electrically-silenced neurons of the CNS can express MHC I on the cell surface in the presence of pro-inflammatory cytokine IFNγ (Neumann et al., 1995). Concurrently, Pereira and colleagues, using northern blot analysis and *in situ* hybridization, found that the MHC I transcripts were up-regulated in neurons of the PNS during acute HSV-1 infection of mice (Pereira et al., 1994; Pereira and Simmons, 1999). However, these transcripts were undetectable during HSV-1 latency (Pereira et al., 1994). Furthermore, mice infected intra-cranially with mouse hepatitis virus (MHV), but not sham-infected mice, displayed expression of MHC I proteins in neurons,

oligodendrocytes and microglia (Redwine et al., 2001). While the above studies indicate that MHC I is expressed in neurons only during injury or infection, later investigations using more sensitive techniques to detect mRNA and protein have demonstrated that MHC I is present in normal healthy neurons of both the developing and adult nervous system (Corriveau et al., 1998; Huh et al., 2000; Elmer and McAllister, 2012; Ma et al., 2014; Tyler and Boulanger, 2014). Indeed, MHC I molecules are crucial for synaptic plasticity, memory and learning (Tyler and Boulanger, 2014). However, the immune function of MHC I in neurons have yet to be explored in detail.

Although direct evidence to show the participation of neurons in presenting antigen to $CD8^+$ T cells is lacking, there are sufficient data to suggest that cognate antigen recognition by $CD8^+$ T cells occurs in the nervous system. A number of studies demonstrated that $CD8^+$ T cells are essential for clearing neurotropic viruses, such as HSV (Nash et al., 1987; Simmons, 1989; Simmons and Tscharke, 1992), murine cytomegalovirus (Cheeran et al., 2005), West Nile virus (Shrestha and Diamond, 2004; Shrestha et al., 2006) and mouse hepatitis virus (MacNamara et al., 2005) from the nervous system (CNS or PNS) during acute infection. Moreover, it has been demonstrated that $CD8^+$ T cells form and maintain a stable contact with infected neurons until the infected cells are subsequently destroyed (Khanna et al., 2003a; Chevalier et al., 2011). Notably, during HSV-1 latency, virus-specific $CD8^+$ T cells reside long-term in the ganglia in an activated state forming an immunological synapse with neurons containing latent genomes (Khanna et al., 2003a; Theil et al., 2003; Verjans et al., 2007; Gebhardt et al., 2009). The reason for the lack of MHC I transcripts during latency in earlier studies (Pereira and Simmons, 1999) could be due to the method employed and the sensitivity of detection. This is contrasted by acute infection where inflammatory cytokines could have driven up-regulation of MHC I expression to a detectable level. Together, the MHC I expression in healthy neurons and preferential presence of $CD8^+$ T cells in ganglia, suggests that these neurons not only express surface MHC I, but, may also present virus-specific epitopes to $CD8^+$ T cells. Only a small number of pMHC-I is thought to be required for a $CD8^+$ T cell to respond (Sykulev et al., 1996), hence determining if there is even a low-level synthesis of MHC I would be of paramount importance to understanding elements of neuronal HSV-1 infection.

1.8 Immune evasion by HSV

HSV is remarkable in its ability to subvert both the innate and the adaptive immune system by interfering with several anti-viral pathways.

HSV evades host innate sensing of viral PAMPs at a very early stage of infection. For example, HSV-1 US3 protein kinase reduces TLR3 expression, which ultimately results in reduced type I IFN response (Peri et al., 2008). HSV-1 immediate early protein ICP0 was shown to reduce the levels of myeloid differentiation primary response protein (MyD88) and MyD88-adapter like (MAL) protein, which are involved in TLR2 mediated inflammatory response (van Lint et al., 2010). The virion host shut-off (vhs) protein counteracts the cytosolic DNA-sensing pathway by degrading the transcripts of a key DNA sensor called cyclic GMP-AMP synthase (cGAS) (Su and Zheng, 2017). Other HSV proteins, ICP27 and vhs, induce global shut-off of host protein synthesis by inducing degradation of cellular mRNA or by repressing transcription and splicing (Smiley, 2004). Proteins including, ICP0, ICP27, vhs, US3, VP16 and UL36, interfere with type I and type II interferon anti-viral pathways (reviewed by Paladino and Mossman, 2009; Su et al., 2016). Additionally, ICP0 was shown to interfere with the synthesis of interferon-stimulated genes (ISG) by blocking interferon regulatory factors, IRF3 and IRF7 (Lin et al., 2004). Finally, ICP27 was shown to dampen interferon secretion by interfering with activation of IRF3 and signal transducer and activator of transcription 1 (STAT1) (Melchjorsen et al., 2006; Johnson et al., 2008b).

HSV has the capacity to inhibit apoptosis, a critical innate immune mechanism that limits viral replication and spread. The HSV-1 proteins US3 protein kinase and glycoprotein J inhibit Fas- or caspase-dependent apoptotic pathway, both of which are utilised by $CD8^+$ T cells to kill virus-infected cells (Jerome et al., 1999). Additionally, other HSV proteins such as ICP4, ICP27, ICP24, glycoprotein D and UL14 are shown to be involved in protection of infected cells against apoptosis. Anti-apoptotic function of LATs has been demonstrated both in cultured cells and *in vivo* animal studies (Perng, 2000; Henderson et al., 2002; Branco and Fraser, 2005). Necroptosis is an alternate cell death pathway to apoptosis that can be activated by TNF family death receptors, Toll-like receptors and interferon receptors (Nailwal and Chan, 2019). HSV-1 protein ICP6 interacts with caspase 8 and supresses necroptosis in human cells (Guo et al., 2015). In mouse cells, HSV-1 lacking ICP6 failed to trigger necroptosis indicating that ICP6-mediated evasion of necroptosis is

specific to human cells (Huang et al., 2015; Wang et al., 2014). The exact mechanism behind this species specificity is not clear.

HSV-1 proteins can also specifically dampen the adaptive immune response. For example, glycoproteins gE and gI form heterodimeric receptor complexes and bind the Fc portion of the IgG antibody (FcγR) (Johnson et al., 1988). Such interactions between FcγR and the HSV antibody subsequently blocks complement activation and NK cell-mediated antibody-dependent cellular cytotoxicity (ADCC), thereby increasing the severity of the disease (Lubinski et al., 2011). HSV being a large DNA virus encodes 84 unique proteins during productive infection, which will generate a large number of peptides for presentation to $CD8^+$ T cells. This will render the infected cells more susceptible to elimination by the virus-specific $CD8^+$ T cells. As a countermeasure, HSV has evolved various evasion mechanisms that can hamper different processes that elicit a $CD8^+$ T cell response. For example, when HSV-1 penetrates $CD8^+$ T cells following contact with infected fibroblast cells, the viral proteins can alter tyrosine phosphorylation equilibrium and negatively regulate TCR signalling (Sloan et al., 2006). An early-late protein, ICP34.5 is capable of inhibiting type I IFN production in DCs and also can suppress DC maturation, leading to attenuation of $CD4^+$ T cell activation (Jin et al., 2009). As $CD8^+$ T cells play a prominent role in clearing replicating virus, HSV has co-evolved mechanisms to evade $CD8^+$ T cell recognition using ICP47, a viral protein that abrogates the MHC I antigen presentation pathway (York et al., 1994; Früh et al., 1995; Hill et al., 1995). The next section will focus on ICP47, its mechanism of action and will address some caveats in the previous *in vitro* and *in vivo* studies in determining the functional significance of ICP47.

1.8.1 Infected cell protein 47

To escape from $CD8^+$ T cells, HSV utilises an efficient strategy driven by the ICP47 protein, which is able to bind the peptide binding site of TAP and prevent the formation of peptide-MHC complex in the lumen of the endoplasmic reticulum (ER) (York et al., 1994; Früh et al., 1995; Hill et al., 1995; Ahn et al., 1996) (Figure 1.8). ICP47 is a relatively small protein, comprising 88 amino acids with a minimal active site mapped to the amino terminus (amino acid position 3-34) of the protein (Galocha et al., 1997; Neumann et al., 1997). It was demonstrated that ICP47 by itself is not transported into ER lumen, but binds to TAP with higher affinity than peptide substrates (Tomazin et al., 1996). For

effective ICP47 functioning, binding to the TMD domains of both the subunits of TAP is required (York et al., 1994; Hill et al., 1995).

Beinert and colleagues found that the protein did not attain a specific conformation in solution, but in a lipid environment a more refined α-helical conformation was noticed (Beinert et al., 1997). Later, Aisenbrey and colleagues resolved the structure of ICP47 using solid-state nuclear magnetic resonance (NMR) spectroscopy and found that ICP47 attains helix-loop-helix conformation (Aisenbrey et al., 2006). The structure of ICP47 was further refined using cryo-electron microscopy by Oldham and colleagues (2016) (Figure 1.9). According to their model, at the peptide receptive stage, TAP is in an inverted "V" shaped conformation with the N-terminus of TMDs close to each other and NBD domains placed apart. When bound to TAP, ICP47 attains a hairpin-like structure with the two helices running anti-parallel to each other connected by a linker. The N-terminal part of ICP47 was found to form physical contacts with the inner surface of the TMD of TAP1 and TAP2 (Oldham et al., 2016a). A short conserved motif "$_{50}$PLL$_{52}$" within the middle part of ICP47 is needed for the freezing of TAP in the inactive state (Matschulla et al., 2017). This specific interaction between ICP47 and TAP holds the transporter in an inactive state that is incapable of binding and transporting peptides. In contrast, the conserved C-terminal part of ICP47 was shown to be required for the stability of ICP47 (Herbring et al., 2016). When associated with TAP, ICP47 attains a stable conformation, which blocks the binding and translocation of peptides into ER lumen (Oldham et al., 2016a).

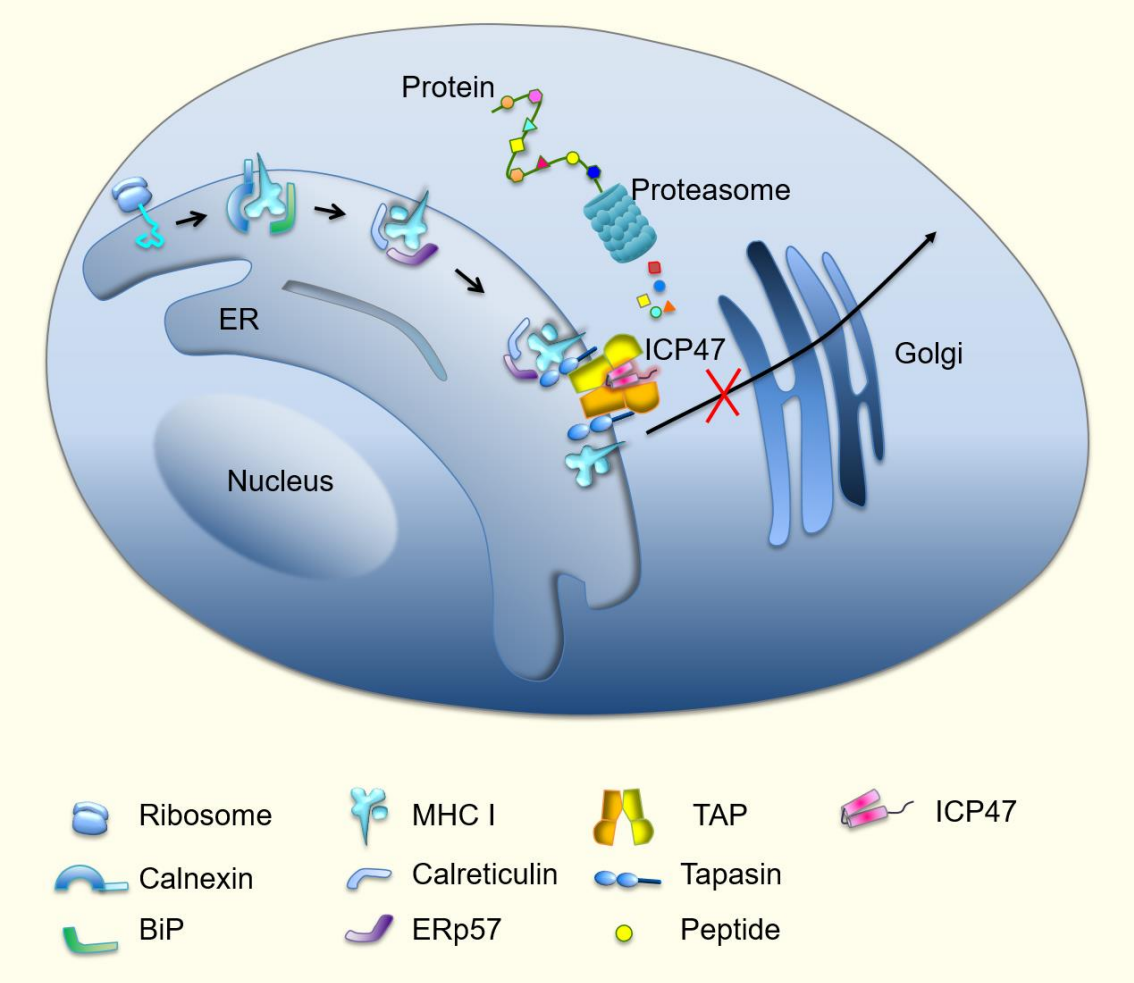

Figure 1.8 ICP47 targets and blocks TAP-mediated antigen presentation pathway. The HSV-1 protein ICP47 binds, with high affinity, to TAP1 and TAP2 on the cytosolic side of the ER membrane and blocks the transport of peptides into the ER lumen. Interaction of ICP47 with TAP ultimately results in the blockade of TAP-mediated presentation of peptides on the cell surface. Adapted from Schölz and Tampé, 2005.

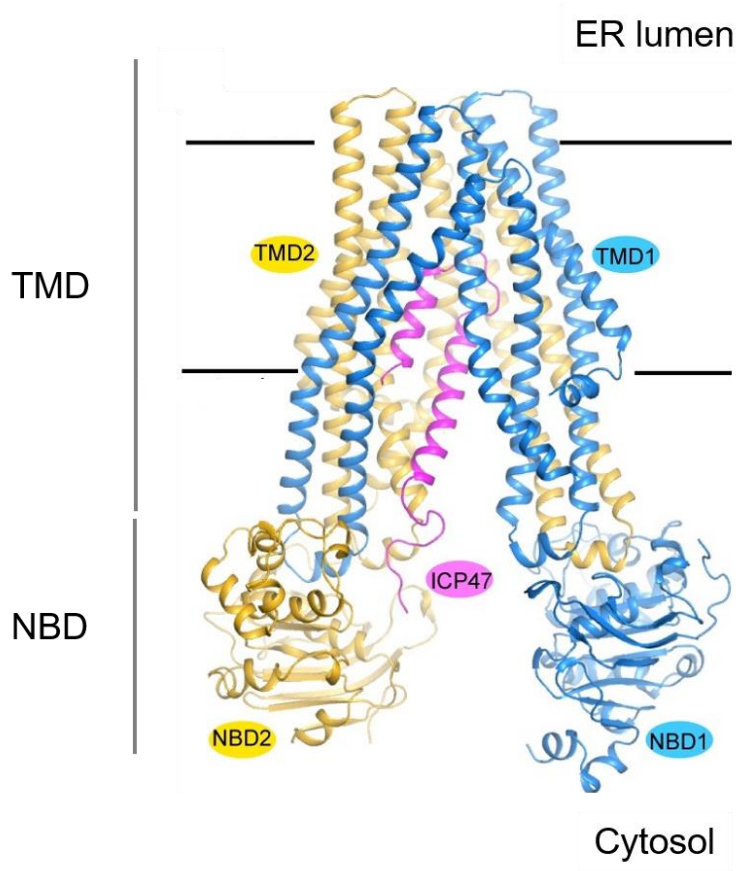

Figure 1.9 Structure of ICP47-TAP complex. The ribbon structure shown in blue represents TAP1 and in yellow represents TAP2. The transmembrane and nucleotide binding domains in TAP1 and TAP2 are labelled. ICP47 bound to TAP is shown in magenta. Modified from Oldham et al., 2016.

In past murine models of HSV-1 infection, most experiments were performed using deletion viruses containing mutations in one or more genes in addition to ICP47. For instance, intra-peritoneal injection of an ICP47 deletion mutant that also lacks US9, US10, US11 and US12, showed that viral replication was not significantly different to the virulent parent strain, Patton, various organs tested, including brain tissues. However, despite normal replication, there was a delayed invasion into the spinal cord and brain (Nishiyama et al., 1993). Similarly, when HSV-1 strain F, containing a deletion of ICP47 and a part of the US11 gene, was introduced in the cornea (Meignier et al., 1988) or injected intravenously (Burgos et al., 2006), the virus displayed a significant reduction in virulence in the CNS. Furthermore, the titre of the deletion virus was recovered to wild-type levels in TAP-deficient mice, indicating a specific function which is provided by the TAP-ICP47 interaction (Burgos et al., 2006). Unlike above studies, Goldsmith and colleagues (1998) generated a single gene deletion mutant with a deletion of just ICP47 sparing the neighbouring genes in neurovirulent strain F. With this virus, they tested the effect of ICP47 on viral pathogenesis using an ocular mouse model. Although viral replication was unaltered in the cornea of the infected mice, they found a reduction in neurovirulence in the absence of ICP47. Furthermore, depletion of $CD8^+$ T cells in mice rescued the virulence phenotype when mice were infected with the ICP47 deletion mutant, suggesting that ICP47 has a role in combating the $CD8^+$ T cell-mediated protection to HSV (Goldsmith et al., 1998). Although these findings are consistent with the above studies, it is not clear if this dampened neurovirulence of the ICP47 mutant is exclusively due to its inability to block antigen presentation to $CD8^+$ T cells. Given that HSV infection commonly occurs via damaged skin or mucous membranes, the virus becomes restricted to dermatomes and therefore, to the peripheral nervous system in an immunocompetent host. Using models that invariably cause encephalitis in mice cannot exemplify a typical HSV disease. Such infection models are not well suited to investigate the function of ICP47 during latency. Moreover, the impact of ICP47 on resistance to $CD8^+$ T cell recognition has not been tested in other infection models or using non-neuroinvasive HSV-1 strains.

An important yet unresolved dispute while using HSV mouse models is the species-specific binding of ICP47 to TAP. Evidence from biochemical studies indicates that ICP47 binds to human TAP with 100 fold more affinity compared to murine TAP (Ahn et al., 1996; Tomazin et al., 1996; Jugovic et al., 1998). Cytotoxic T cell killing assays further supported this as ICP47 inhibited the recognition of human cells but not mouse cells by HSV-specific

$CD8^+$ T cells (York et al., 1994). Subsequently, this led some researchers to argue that ICP47 is entirely non-functional in mice. The *in vivo* and biochemical data are difficult to reconcile, and this leaves our understanding of ICP47 and its role in evading $CD8^+$ T cells incomplete. Additionally, spontaneous reactivation and viral shedding are rare in mice (Tullo et al., 1982; Shimeld et al., 1990b) but occur periodically in humans. This has been attributed to the poor binding of ICP47 to mouse TAP (Liu et al., 2000; Leger and Hendricks, 2011). Attempts were made to mimic the function of ICP47 by using recombinant HSV with human cytomegalovirus (HCMV) US11 or murine cytomegalovirus (MCMV) m152, whose expression inhibits MHC I -mediated antigen presentation efficiently in mice (Wiertz et al., 1996; Ziegler et al., 2000; Orr et al., 2005). It was shown that infection of BALB/c mice with the above recombinant HSV showed an increase in viral replication in the spinal cord and enhanced disease progression. The phenotype was reversed in TAP-deficient mice or in mice depleted of $CD8^+$ T cells (Orr et al., 2005). In the relatively HSV-resistant mouse strain C57BL/6, ocular infection with recombinant HSV-1 expressing HCMV US11 or MCMV m152, but not the control virus, increased the frequency of reactivation in TG. This was shown using an *in vitro* explant reactivation model and *in vivo* reactivation model via UV irradiation (Orr et al., 2007). Consistently, depletion of $CD8^+$ T cells induced the reactivation of control virus similar to that of the recombinant HSV-1 (Orr et al., 2007). However, these experiments are not always simple to interpret as they involve the use of non-HSV genes and promoters. Nonetheless, these studies by Orr and colleagues reinforce the idea that $CD8^+$ T cells may provide immune surveillance during latency.

1.9 Cre-reporter mouse model

The spatiotemporal evaluation of HSV-1 gene expression during latency proved to be challenging to researchers for decades. In recent years, the development of single cell-based detection systems has engendered a significant shift in the understanding of gene expression during latency (Ma et al., 2014). While, single-cell transcriptome analysis provides a snap-shot of transcriptional events at a given time, tracking of lytic gene expression in neurons from initial infection to throughout the life of the animal has only recently become possible due to the ROSA26R reporter mouse model (Russell and Tscharke, 2016).

ROSA26R transgenic mice contain the *lacZ* reporter gene under the control of the ROSA promoter (Figure 1.10). However, the synthesis of a *lacZ* gene product is muted by the presence of a loxP-flanked stop element between the reporter gene and the ROSA promoter (Soriano, 1999). The expression of Cre recombinase induces removal of the stop element by recombination between loxP-sites and allows the synthesis of β-galactosidase enzyme (Figure 1.10). In the event of this recombination, the cell is permanently marked by β-galactosidase, which can be visualised at a later time point by staining with a chromogenic substrate such as X-Gal. By infecting ROSA26R reporter mice with recombinant HSV-1, which contains Cre recombinase under the control of a selected HSV-1 promoter, the transcriptional history of that promoter can be studied at any time during the life of the mouse. This tracking method depends on the activation of the selected viral promoter, which when occurs, leads to Cre-mediated recombination taking place and driving constitutive reporter gene expression.

Recombinant HSV-1, engineered to express Cre from the cytomegalovirus IE (CMV IE) promoter, triggers Cre expression in every infected cell regardless of its fate leading to the permanent marking of that cell (Arthur et al., 2001; Proença et al., 2008; Wakim et al., 2008). While the CMV IE promoter marks all neurons, it had been noted from previous studies that native HSV-1 promoters are regulated such that only a proportion of the infected neurons are marked by β-galactosidase expression during lytic infection (Proença et al., 2008; Russell and Tscharke, 2016). Further, using this model, Russell and Tscharke (2016) found that lytic gene expression also occurs during and after the establishment of latency. They generated HSV-1 expressing Cre under the control of ICP0, ICP47, ICP6 or gB promoters. By infecting ROSA26R mice with these recombinant viruses, they made several interesting findings. First, Cre-mediated marking by lytic promoters occurred beyond the initial lytic infection, indicating that the virus spread after the peak of acute infection. Secondly, the lytic promoters ICP47, ICP6 and gB, were active during latency suggesting the possibility that these proteins might be expressed during latency. Finally, the ICP47 promoter, unlike other lytic promoters tested, was active during the establishment phase of latency. The authors suggested that ICP47 might be involved in promoting neuronal survival.

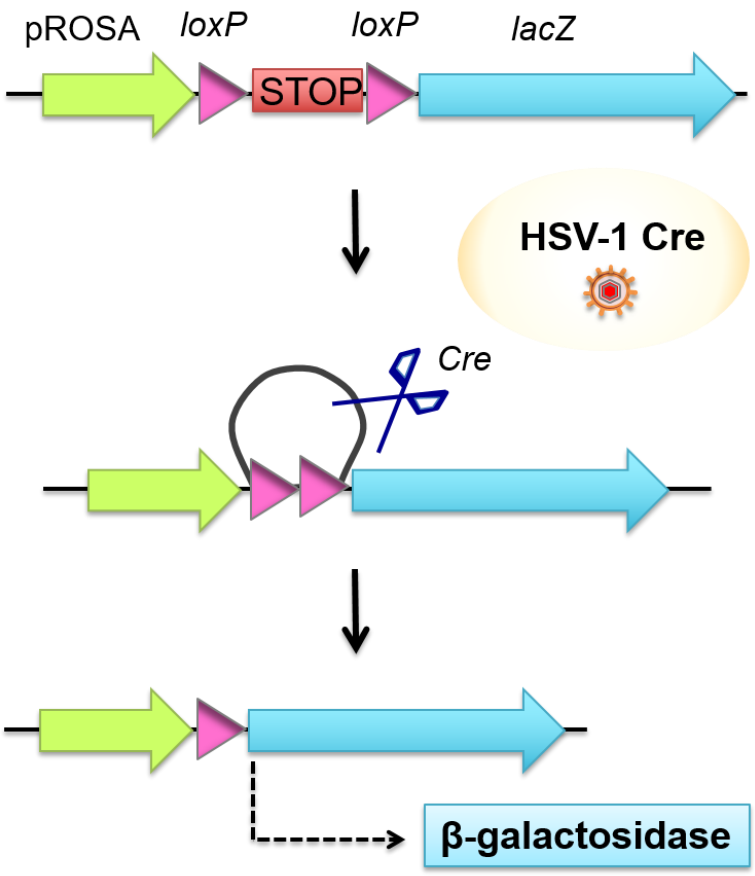

Figure 1.10 Schematic diagram of ROSA26R/Cre reporter mouse model. The ROSA26R reporter constructs consists of a ROSA promoter, which drives a loxP flanked coding sequence of the *lacZ* gene. Following Cre-mediated recombination between the two loxP sites, the stop element gets excised and the ROSA promoter can now constitutively drive the expression of the *lacZ* gene leading to the synthesis of β-galactosidase. ROSA26 mice infected with recombinant HSV-1 that express Cre display permanent β-galactosidase synthesis in infected cells in which Cre is expressed. These cells can be tracked later by staining the tissue using X-Gal.

1.10 Aims of this thesis

The ability of HSV-1 to modulate $CD8^+$ T cell recognition is of clinical significance in human recrudescent disease. Equally, the ability of the host to recognise and respond to HSV-1 infection is of paramount importance to control the primary infection and reactivation. Over the past two decades, our knowledge on the $CD8^+$ T cell immunity to HSV-1 infection has substantially increased with the use of mouse models. However, there is still a discrepancy in the HSV-1 field on the functionality of the immunomodulatory protein ICP47 in mice. On the one hand, *in vitro* assays and biochemical studies suggest a poor inhibition of mouse TAP by ICP47, but on the other, *in vivo* mouse studies suggests that ICP47 enhances HSV-1 neurovirulence in mice. The overall aim of my PhD study was to improve our understanding of the role of ICP47 by bridging the current gap between the available *in vitro* biochemical data and the *in vivo* pathogenesis data.

The first aim of the thesis was to investigate the role of ICP47 during different facets of HSV-1 infection in mice. For this, I generated ICP47 mutant and appropriate control viruses and analysed the ability of ICP47 to inhibit antigen presentation in mouse cells by an *in vitro* flow cytometry-based assay. Then, I assessed the influence of ICP47 on viral pathogenesis, establishment of latency, stability of latency and reactivation of the virus in mice using a zosteriform infection model (Chapter 3). The results from this chapter lead to the subsequent aims of this thesis.

The second aim was to investigate the basis of the difference in Cre-mediated neuronal marking by the ICP47 promoter when placed in different regions of HSV-1 genome using ROSA Cre reporter mouse model (Chapter 4).

The third aim was to assess the efficiency at which ICP47 block antigen presentation in human cells and mouse cells by an absolute quantification of MHC I bound peptides presented on cells infected with wild-type virus or ICP47 null mutant (Chapter 5).

Chapter 2
Materials and Methods

2 Materials and Methods

2.2 Materials

2.2.1 Media, buffers, and solvents

2.2.1.1 Cell culture media

Dulbecco's Modified Eagle Medium (DMEM)	Dulbecco's Modified Eagle Medium (DMEM); high glucose with phenol red (Invitrogen™); was supplemented with 2 mM L-glutamine. Heat inactivated foetal bovine serum (FBS) was added at a concentration of 2% v/v (D2) or 10% v/v (D10). Media without FBS was referred to as D0.
Minimum essential medium (MEM)	MEM with phenol red (Invitrogen™) was supplemented with 4 mM L-glutamine, 5mM HEPES buffer (Invitrogen™) and 50 μM β-mercaptoethanol. Heat-inactivated FBS was added at a concentration of 2% v/v (M2) or 10% v/v (M10). Media without FBS was referred to as M0.
Foetal bovine serum (FBS)	
CMC-MEM	0.4% (w/v) Carboxymethyl cellulose in M2.

2.2.1.2 Media for bacterial culture

Luria Bertani (LB) media	10 g/L Tryptone (Bacto), 5 g/L yeast extract (Bacto), 10 g/L sodium chloride (Merck) in deionised water.
LB agar	1.5% (w/v) Agar (Bacto) in liquid LB media.

2.2.1.3 Buffers and solutions

FBS-PBS	PBS (Sigma Aldrich) supplemented with 2% (v/v) FBS.
Red cell lysis buffer	0.14 mM Ammonium chloride (Sigma Aldrich) and 19 mM Trizma base (Sigma Aldrich) in deionised water, pH 7.2. The buffer was sterilised by autoclaving and stored at 4°C.

RSB buffer	10 mM Trizma base, 10 mM potassium chloride (Sigma Aldrich) and 1.5 mM magnesium chloride (Ajax FineChem) in deionised water.
0.5 M EDTA	0.5 M Ethylenediaminetetraaceticacid (EDTA) (Sigma-Aldrich) in deionised water, pH adjusted to 8.0 with sodium hydroxide pellets.
Tris-Acetate-EDTA (TAE) buffer	40 mM Trizma base (Sigma-Aldrich), 20 mM glacial acetic acid (Univar) and 1 mM EDTA in deionised water.
Tris-EDTA (TE) buffer	10 mM Trizma base and 1 mM EDTA in deionised water.
Crystal violet solution	0.1% (w/v) of crystal violet (Sigma Aldrich) and 15% (v/v) ethanol in deionised water.
Avertin	12.5 mg/mL 2, 2, 2 – tribromoethanol (Sigma Aldrich) and 2.5% (v/v) 2-methyl-butanol dissolved in sterile water and filter sterilised. Stored in the dark at 4°C for no more than 14 days.
Fixative for DRG	2% (v/v) Paraformaldehyde (PFA) (COM) and 0.5% glutaraldehyde (Sigma Aldrich) in PBS.
X-Gal permeabilisation buffer	2 mM Magnesium chloride, 0.01% (w/v) sodium deoxycholate (Sigma-Aldrich), 0.02% (v/v) IGEPAL® CA-630 (Octyl phenoxy poly (ethyleneoxy) ethanol) (Sigma-Aldrich), 5 mM potassium ferrocyanide (Sigma-Aldrich) and 5 mM potassium ferricyanide (Sigma-Aldrich) in deionised water.
X-Gal staining solution	X-Gal permeabilisation buffer with 1 mg/mL 5-bromo-4-chloro-indolyl-β-D-galactopyranoside (X-Gal).
50% Glycerol	50% (w/v) Glycerol (Sigma-Aldrich) in PBS.
Trioxsalen	1 μg/μL Trioxsalen (Sigma-Aldrich) in PBS.
6× DNA gel loading buffer	50% (w/v) Glycerol, 0.25% (w/v) Bromophenol blue (Merck) and 0.25% (w/v) xylene cyanol (Sigma-Aldrich) in deionised water.
Saponin	5% (w/v) Saponin (Fluka) in deionised water.

2.2.1.4 Buffers and solutions used for mass spectrometry

DPM crosslinker	40 mM Dimethyl pimelimidate (Sigma D8388) in Triethanolamine (0.2 M, pH 8.2). The pH of the solution was adjusted to 8.3 using NaOH.
1× Lysis buffer	0.5% (v/v) IGEPAL CA-630 from Sigma, 50 mM Tris-HCl (pH 8.0), 150 mM sodium chloride, cOmplete™ protease inhibitor cocktail (Sigma-Aldrich) in Milli-Q water.
Wash buffer 1	0.005% (v/v) NP-40, 50 mM Tris-HCl (pH 8.0), 150 mM sodium chloride, 5 mM EDTA, 100 µM phenyl methyl sulfonyl fluoride (stored at -20°C as 0.1 M stock in absolute ethanol), 1 µg/mL pepstatin A (stored at -20°C as 1 mg/mL in isopropanol) and Milli-Q water. The buffer was freshly prepared and stored on ice.
Wash buffer 2	50 mM Tris-HCl (pH 8.0), 150 mM sodium chloride in Milli-Q water. The buffer was freshly prepared and stored on ice.
Wash buffer 3	50 mM Tris-HCl (pH 8.0), 450 mM sodium chloride in Milli-Q water. Freshly made and stored on ice.
Wash buffer 4	50 mM Tris-HCl (pH 8.0) in Milli-Q water. The buffer was freshly made and stored on ice.
Elution buffer	10% (v/v) Acetic acid (Sigma ACS grade) in Milli-Q water.
HPLC fractionation buffer A	0.1% (w/v) Trifluoroacetic acid (Sigma-Aldrich) in Milli-Q water.
HPLC fractionation buffer B	0.1% (w/w) Trifluoroacetic acid and 80% (v/v) acetonitrile (Sigma-Aldrich) in Milli-Q water.
Borate buffer pH 8	50 mM Boric acid, 50 mM potassium chloride and 3.97 mM sodium hydroxide in Milli-Q water. Filter sterilized through a 0.22 µm syringe filter.
Citrate buffer pH 3.0	0.1 M Citrate (Sigma-Aldrich), pH 3.0. Filter sterilized through a 0.22 µm syringe filter.
MS buffer A	0.1% (v/v) Formic acid (Sigma-Aldrich) in Milli-Q water.
MS buffer B	95% (v/v) Acetonitrile (Sigma-Aldrich) and 0.1% (v/v) formic acid in Milli-Q water.

2.2.2 Antibodies

The antibodies used for this study are listed in Table 2.1.

Table 2.1 Summary of the antibodies used in this thesis

Antibody	Species	Clone	Source
Anti-mouse-H-2K^b	Mouse	Y-3	Purcell lab*
Anti-mouse-H-2D^b	Mouse	28-14-8S	Purcell lab*
Anti-mouse-CD8α-Phycoerythrin	Rat	53.6.7	Biolegend®
Anti-mouse-IFNγ-Allophycocyanin	Rat	XMG1.2	Biolegend®
Anti-mouse-SIINFEKL bound to H-2K^b-Allophycocyanin	Mouse	25-D1.16	Biolegend®
Fluorescein isothiocyanate (FITC) - conjugated goat anti-mouse F(ab)$_2$ (Polyclonal)	Goat	---	Agilent Dako
Anti-MVA hyperimmune serum	Rabbit	---	Institute of Medical and Veterinary Science, South Australia#

*Antibody produced in-house in the Purcell laboratory, Monash University, Victoria

#The hyperimmune serum was generated by immunising rabbit at three weekly intervals with 10^7 focal forming units of VACV strain MVA. The serum was collected two weeks after the last immunisation at Institute of Medical and Veterinary Science, South Australia#

--- Not applicable.

2.2.3 Chemicals and Reagents

DNA markers (100 bp and 1.0 Kbp)	New England Biolabs
1 Kbp DNA extension ladder	Invitrogen™
UltraPure Agarose	Life Technologies
BigDye terminator for Sanger sequencing	Biomolecular resource facility, John Curtin School of Medical Research
5× reaction buffer for Sanger sequencing	Biomolecular resource facility, John Curtin School of Medical Research

Deoxyribonucleotide triphosphate (dNTP) mix (10 mM)	Bioline
10 μg/mL Proteinase K	Roche
Cycloheximide	100 mg/mL cycloheximide (Sigma-Aldrich).
Actinomycin D	20 mg/mL in methanol (Life Technologies).
Ampicillin	100 μg/L in deionised water (Sigma-Aldrich).
Kanamycin	50 μg/L in deionised water (Sigma-Aldrich).
Penicillin Streptomycin (Pen Strep)	100× concentrated solution contains 5000 units/mL of penicillin and 5000 μg/mL of streptomycin. (Thermo Fisher Scientific).
Sodium dodecyl sulfate	20% (w/v) in deionised water (Sigma-Aldrich).
0.4% (v/v) Trypan blue solution	Invitrogen™
Phenol – chloroform – isoamyl alcohol mixture (25:24:1)	Sigma-Aldrich

2.2.4 Plasmids

The plasmids generated in this study and the parent vectors are listed in the Table 2.2. The CRISPR Cas-9/guide plasmids and homology directed repair (HDR) templates were used for the generation of recombinant HSV-1.

Table 2.2 Summary of plasmids used in this thesis

Plasmid	Description	Viruses
px330 icp47	A plasmid with Cas-9/guide sequence targeting ICP47 gene.	HSV-1 Ka47Δ HSV-1 GKa47Δ HSV-1 Ka47inΔ
px330 icp47del	A plasmid with Cas-9/guide sequence targeting ICP47 region in HSV-1 Ka47Δ.	HSV-1 Ka47R HSV-1 GKa47R
pxUL26/7	A plasmid with Cas-9/guide sequence targeting intergenic region between UL26 and UL27 genes.	HSV-1 Ka47rescue HSV-1 UL27-pa47min

Plasmid	Description	Viruses
pxUL3/4	A plasmid with Cas-9/guide sequence targeting intergenic region between UL3 and UL4 genes.	HSV-1 UL3-pa47 HSV-1 UL3-pa47ΔoriS
pUC ICP47del	ICP47 deletion region and left homology arm amplified from HSV-1 Ka47Δ and cloned into the unique HindIII site of RF_CP47_HIII. Used as homology-directed repair (HDR) template.	HSV-1 GKa47Δ
pT CMV IE eGFP Cre	DNA template to amplify EGFP Cre BGH PolyA fusion gene for cloning (Russell et al., 2015).	HSV-1 Ka47inΔ
pICP47 eGFPCrePolyA	eGFP Cre BGH PolyA and ICP47 left homology arm cloned into the unique HindIII site of RF_CP47_HIII. Used as HDR template.	HSV-1 Ka47inΔ
pU26/7 pI47	A plasmid containing ICP47 promoter without oriS flanked by UL26 and UL27 region of HSV-1 KOS (Tiffany Russell, unpublished).	Plasmid: pUL26\7 pICP47eGC BGH PolyA
pUL26/27 ICP47 SV40 PolyA	This plasmid was constructed in two steps. First, the ICP47 coding sequence was amplified from HSV-1 KOS genomic DNA and cloned into the unique SpeI site of pU26/7 pI47. Then, the sequence corresponding to SV40 PolyA signal was amplified from pT CMV IE eGFP Cre and cloned into the unique EcoRV site downstream of the ICP47 coding sequence. Used as HDR template.	HSV-1 Ka47rescue
pUL26/7 pICP47eGC BGH PolyA	eGFP Cre BGH PolyA amplified from pT CMV IE eGFP Cre and cloned into NotI site of pU26/7 pI47. Used as HDR template.	HSV-1 UL27-pa47min
mnpICP47 eGC	A plasmid containing eGFP Cre BGH PolyA placed under the full-length ICP47 promoter with mutated oriS site flanked by right and left homology arms from UL3-UL4 region. Used as HDR template. Synthesised by GenScript.	HSV-1 UL3-pa47ΔoriS
npICP47 eGC	A plasmid containing eGFP Cre BGH PolyA placed under the full-length ICP47 promoter flanked by right and left homology arms from UL3-UL4 region. Used as HDR template. Synthesised by GenScript.	HSV-1 UL3-pa47

2.2.5 Oligodeoxynucleotides

The oligonucleotides listed in Table 2.3 were synthesized by Sigma-Aldrich.

Table 2.3 Summary of oligonucleotides used in this thesis

Oligo	Sequence 5′ to 3′	Use
ICP47 Seq Fwd	CAGAGACTCGGGTGATGGTCG	To amplify the ICP47 coding region.
ICP47R2	GTTGCGTGGACCGCTTC	To amplify HSV-1 KOS or HSV-1 Ka47Δ.
ICP47mR	GGGCCCTGAAGCTTTGAC	Specific reverse primer to screen for recombinant HSV-1 Ka47Δ.
ICP47wR	GCCCTGGAAATGGCGGAC	Specific reverse primer to screen for HSV-1 KOS.
ICP47wR2	TGTCGTGGGCCCTGGAAA	Specific reverse primer to screen for HSV-1 KOS.
ICP47revRP	GGAAAAGCATGTCGTGGGCTCTA	Specific reverse primer to screen for Ka47R.
47_EGFPCreBGH_FP*	GGAAGGTGTCCGCCAAAGAACTAGCTGCTATTGTCTT	To amplify EGFP Cre BGH PolyA signal from pT CMV eGFP Cre plasmid for the construction of the plasmid, pICP47eGFPCrePolyA.
rf47_egfpcre RP*	TCGGGGGGGAAAAGCTATGGTGAGCAAGGGCGAG	
LF_FP infusion*	TGATTACGCCAAGCTTGGTCCGCGGGCAACATCAC	Forward primer to amplify left homology arm from ICP47 region for the construction of the plasmid, pICP47eGFPCrePolyA.
LFpBII_EGFPCreBGH_RP*	TAGCAGCTAGTTCTTTGGCGGACACCTTCCTGGACAA	
icp47 LF seq FP	CAACATGGCCCCTGTAGCCG	To confirm the insertion site in HSV-1 Ka47inΔ.
Cre Lf Seq	CACGACCAAGTGACAGCAAT	

Oligo	Sequence 5′ to 3′	Use
Cre Rf Seq	TGGCAATTTCGGCTATACGT	Sequencing primer that binds the Cre coding sequence.
BGH Seq Fwd	AAGCCTTCGACGTGGAGG	Sequencing primer.
pUS12UL26_27 infusion F*	GAAAGATATCGCGGCCTCAACGGGTTACCGGATTAC	Primers to amplify the ICP47 coding sequence for the construction of the plasmid, pUL26/27 ICP47 SV40 PolyA.
pUS12UL26_27 infusion R*	GGCACTAGTGCGGCCATGTCGTGGGCCCTGGAAATG	
SV40 F*	TTGTTGGGTACCAGCCAGACATGATAAGATACATTG	Forward primer to amplify SV40 PolyA signal.
SV40 R*	CCCGGCTGTGATAGAACTTGTTTATTGCAGC	Reverse primer to amplify SV40 PolyA signal.
ICP47F	GTTCTTCGATGTGCCACACC	PCR primer used to screen for HSV-1 Ka47rescue. It was paired with ICP47wR2.
UL26inF	AGGCGGGTAGCTTTACAATGCAAAAG	PCR primers used to plaque purify HSV-1 Ka47rescue and UL27-pa47min.
UL27R	AAGTTCCCAACAAAGACGGTGACG	
UL4 Seq Rev	CGTCGTCAACACCAACATCA	Primer pair to confirm the insertion site in HSV-1 UL3-pa47 and HSV-1 UL3-pa47ΔoriS.
BGHr	CTGTGCCTTCTAGTTGCCAG	
UL3_Seq_Fwd	GCCGTCAAGAACTGTTATCC	Primer pair to confirm the insertion site in HSV-1 UL3-pa47 and HSV-1 UL3-pa47ΔoriS
pICP47_Seq_Rev	ACGCCGGGACCAACGGG	
ptracer UL3 Lf	TTACACGCGATCTTCGGACG	Primer pair used to plaque purify HSV-1 UL3-pa47 and HSV-1 UL3-pa47ΔoriS.
ptracer UL4 Rf	CGCGGACACCATTTACATCA	
Seq_RevpEGFPN1	CTCGACCAGGATGGGCAC	Sequencing primer that binds the eGFP coding sequence.

Oligo	Sequence 5′ to 3′	Use
ICP47 seq2	CGCACTTCGCCCTAATAAT	Sequencing primer that binds the ICP47 promoter region.
Tomato_BGH_rev*	CGCCCTTGCTCACCATGCGGCCGCACTAGTG	Primers to amplify eGFP Cre BGH PolyA for the construction of the plasmid pUL27-pa47min.
UL7pICP47eGC inf*	AGATATCGCGGCCGCTGCTATTGTCTTCCCAATCC	
HSVgB_p4	GAGTACGGCGGCTCCTTCCGAT	Used with pICP47_Seq_Rev for screening HSV-1 UL27-pa47min.
M13 Rev+	CAGGAAACAGCTATGAC	Used with an appropriate guide oligo for the screening of the corresponding *CRISPR* associated protein 9 (Cas9)/guide sequence containing plasmid.

*Oligos used for generating PCR fragments compatible for In-Fusion cloning. The underlined nucleotides are complementary to a linearised vector end or an adjacent PCR fragment.

2.2.6 Cell lines

All cell lines were handled in a class II biosafety cabinet and maintained in a humidified incubator at 37°C and 5% CO_2. All cell lines used in this study were sub-cultured twice a week. Table 2.4 provides the list of cell lines used for this study.

Table 2.4 Summary of cell lines used in this thesis

Cell line	Origin	Media	Used for
Veros	African green monkey kidney epithelial cells	M10	*a.* Purification of recombinant HSV-1 *b.* Plaque assay *c.* Preparation of HSV-1 stocks *d.* Cycloheximide reversal assay
293A	Primary human embryonic kidney cells transformed with human adenovirus 5 DNA	D10	Generation of recombinant HSV-1
MC57G	A cell line derived from Methylcholanthrene induced fibrosarcoma in C57BL/6J mice	D10	*a.* Quantification of surface H-2K^b using QIFIKIT *b.* *In vitro* antigen presentation assay *c.* Mass spectrometry based discovery and quantification of MHC I bound peptides
293KbC2	293A cells that stably express H-2 K^b under cytomegalovirus promoter (Tscharke et al., 2005)	D10	*a.* Quantification of surface H-2K^b using QIFIKIT *b.* *In vitro* antigen presentation assay *c.* Mass spectrometry based discovery and quantification of MHC I bound peptides
293DbA5	293A cells that stably express H-2 K^b under cytomegalovirus promoter (Tscharke et al., 2005)		Quantification of surface H-2K^b using QIFIKIT
BHK-21	Syrian gold hamster kidney fibroblast	M10	Preparation of MVA stocks and plaque assay

2.2.7 Viruses

The wild-type HSV-1 strain KOS used throughout this thesis was a gift from Dr. F. R. Carbone (University of Melbourne, Australia). The recombinant HSV-1s were generated on the background HSV-1 strain KOS. Recombinant vaccinia viruses and recombinant HSV-1 viruses used in this study are listed in Table 2.5 and Table 2.6.

Table 2.5 Summary of recombinant HSV-1 made for this study

Virus	Description
HSV-1 Ka47Δ	HSV-1 ICP47 null mutant generated by introducing a stop codon downstream of the ICP47 translation initiation site in HSV-1 KOS.
HSV-1 Ka47R	Revertant of HSV-1 Ka47Δ, capable of encoding functional ICP47.
HSV-1 Ka47inΔ	HSV-1 ICP47 null mutant generated by inserting eGFP Cre in place of ICP47 gene in HSV-1 KOS. The native ICP47 promoter drives the expression of the fusion gene.
HSV-1 Ka47rescue	Rescuant of Ka47inΔ that encodes functional ICP47. ICP47 coding sequence placed downstream of the modified ICP47 promoter (without oriS) was inserted into the intergenic region between UL3 and UL4 genes. The virus was generated using HSV-1 Ka47inΔ as the background.
HSV-1 GKa47Δ	HSV-1 ICP47 null mutant generated by introducing a stop codon downstream of the ICP47 translation initiation site in HSV-1 pCMV IE eGFP Cre.
HSV-1 GKa47R	Revertant of HSV-1 GKa47Δ that encodes functional ICP47.
HSV-1 UL27-pa47min	HSV-1 that expresses eGFP-Cre fusion gene under the control of a minimal ICP47 promoter without oriS. The reporter cassette was inserted into the intergenic region between the UL26 and UL27 genes.
HSV-1 UL3-pa47	HSV-1 that expresses eGFP-Cre fusion gene under the control of a full-length ICP47 promoter. The reporter cassette was inserted into the intergenic region between the UL3 and UL4 genes.
HSV-1 UL3-pa47ΔoriS	HSV-1 that expresses eGFP-Cre fusion gene under the control of a full-length ICP47 promoter. The reporter cassette was inserted into the intergenic region between the UL3 and UL4 genes. The oriS site in the full-length ICP47 promoter was modified to stop the function of the ectopic oriS.

Table 2.6 Recombinant viruses already available for this study

Virus	Description	Reference
HSV-1 pCMV IE eGFP Cre	HSV-1 expressing eGFP-Cre fusion gene driven by CMV IE promoter.	Ma et al., 2014
HSV-1 UL3-pa47min	HSV-1 expressing eGFP-Cre fusion gene driven by the modified ICP47 promoter (without oriS). Originally, this virus was referred to as HSV-1 pICP47_eGC.	Russell and Tscharke, 2016
MVA ES mini OVA*	MVA with the ER-targeted $OVA_{257-264}$ mini gene inserted in the TK locus and driven by VACV p7.5 promoter.	Generated by YC Wong in Tscharke Lab
MVA mini OVA*	MVA with the $OVA_{257-264}$ mini gene inserted in the TK locus and driven by VACV p7.5 promoter.	Generated by YC Wong in Tscharke Lab
MVA mini Flu PR8 PB1F2(62-70)*	MVA with the PR8 $PB1F2_{62-70}$ mini gene inserted in the TK locus and driven by VACV p7.5 promoter.	Generated in Tscharke Lab

*Modified Vaccinia virus Ankara (MVA) is an attenuated vaccinia virus derived from the parental strain chorioallantois vaccinia virus Ankara (CVA) by multiple laboratory passages in chicken embryo fibroblast.

2.2.8 Mice

Six weeks old pathogen-free female C57BL/6 mice or B6.129S4-Gt(ROSA)26Sor^{tm1So}/J (ROSA26R; Soriano, 1999) mice were obtained from the Australian Phenomics Facility (Canberra, Australia). ROSA26R mice were a kind gift from Dr. F. R. Carbone (University of Melbourne, Australia), housed and bred at the Australian Phenomics Facility. Mice were housed and all experiments were conducted according to the ethical requirements under approvals A2014/025 and A2017/39 from the Australian National University Animal Ethics and Experimental Committee.

2.3 Methods

2.3.1 Polymerase chain reaction (PCR)

Standard *Taq* Polymerase (NEB) was used for performing colony PCR and screening for isolation of recombinant virus. Phusion® High fidelity DNA polymerase (NEB) was used for the amplification of DNA fragments for molecular cloning and amplification of recombinant viral DNA for sequencing. PCR was performed using Eppendorf Mastercycler or ABI Veriti 96-well thermocycler. PCR was set up according to manufacturer's protocol in a volume of 20 µL or 50 µL on ice.

PCR using *Taq* polymerase (NEB) was performed in a reaction mix consisting of 1× ThermoPol buffer, 200 µM dNTPs, 0.2 µM each of forward primer and reverse primer, an appropriate amount of DNA template and 1 unit of *Taq* polymerase enzyme in sterile deionised water. The PCR conditions were as follows: initial denaturation at 95°C for 30 sec, 30 cycles of denaturation (95°C, 15 sec), annealing (appropriate temperature for the primer pair, 30 sec), extension (68°C, 1 minute/kb), and the final extension at 68°C for 5 minutes. The reaction was placed on hold at 16°C until subsequent use.

PCR using Phusion® High fidelity DNA polymerase (NEB) was done using 1 unit of the enzyme, 1× Phusion GC buffer, 200 µM dNTPs, and 0.5 µM each of forward primer and reverse primer, 3% (v/v) DMSO and approximately 10 ng of DNA template in sterile deionised water. The thermocycling condition for PCR included initial denaturation at 98°C for 30 sec, 30 cycles of denaturation (98°C, 10 sec) followed by annealing (appropriate temperature for the primer pair, 30 sec) then extension (72°C, 15 sec/kb). The final extension was performed at 72°C for 10 minutes. Again, the reaction was placed on hold at 16°C until subsequent use.

2.3.1.1 Preparation of DNA template for PCR

The DNA template for colony PCR generally came from a small portion of a recently transformed bacterial colony that was resuspended in 10 µL of deionized water and boiled at 95°C for 5 minutes. After heat treatment, the cell debris was pelleted using a microcentrifuge and 2 µL of the clear supernatant was used for conducting PCR.

For screening of plaque picks during the isolation of recombinant virus (see section 2.3.5.4), DNA template was prepared from virus grown in Vero cells in a 96-well plate. Briefly, Vero cells were inoculated with the virus from a plaque pick and allowed to grow for 48 hours at 37°C and 5% CO_2. The inoculum was removed, and the cells were washed with PBS. To each well, 100 µL of 10 µg/mL of proteinase K in 1× ThermoPol PCR buffer was added, the plate was freeze-thawed once and then, incubated at 56°C for 20 minutes. Proteinase K was heat inactivated by incubating the plate at 85°C for 15 minutes. Subsequently, for PCR screening 2 µL of the DNA preparation was used as a template. Extraction of viral DNA from seed stock was performed as described previously by mixing 10 µL of seed stock with 1 µg/mL proteinase K in 1× ThermoPol PCR buffer, incubating at 56°C for 20 minutes followed by heat killing proteinase K at 85°C for 15 minutes. For PCR, 10 µL of this solution was used as a template. In some cases, purified plasmid DNA or viral genomic DNA were used as a template for PCR.

2.3.2 DNA sequencing

Automated Sanger sequencing was carried out to confirm and verify the desired modification introduced into the plasmid DNA or viral genomic DNA. The sequencing reaction was performed in a volume of 20 µL and contained 1 µL of Big Dye Terminator, 3.2 pmol of the sequencing primer, 1× sequencing buffer and an appropriate amount of DNA template. Generally, 200 ng of plasmid or 10 ng of PCR amplified product was used for sequencing. The thermocycling conditions for PCR were:

Step	Temperature	Duration	Cycle
Initial denaturation	94°C	5 min	1
Denaturation	96°C	10 sec	30
Annealing	50°C	5 sec	
Extension	60°C	4 min	
Hold	4°C		

The sequencing reaction was subjected to ethanol/sodium acetate precipitation and air-drying prior to submission for sequencing to ACRF Biomolecular Resource Facility, ANU. The sequencing data was analysed using CLC Main Workbench (version 7.6.2).

2.3.3 Restriction enzyme digestion

Restriction enzyme digestion was carried out to *a)* produce linearised plasmids for cloning (section 2.3.4.1), *b)* produce linearised plasmids for the generation of HDR template (section 2.3.5.1) and for the restriction digestion analysis of genomic DNA of the recombinant HSV-1 (section 2.3.7.2). Restriction digestion reactions were carried out using NEB restriction enzymes and corresponding reagents according to the manufacturer's instructions.

2.3.4 Molecular cloning and bacterial transformation

2.3.4.1 Ligation cloning

Linear double-stranded DNA fragments were obtained either by annealing of complementary oligonucleotides (section 2.3.5.2) or by PCR amplification. The resulting products were cloned into vectors previously linearised by restriction digestion reaction. The purified DNA fragments containing complementary overhanging sequences were ligated together using NEB ligase enzyme according to the manufacturer's protocol.

2.3.4.2 In-Fusion cloning

The In-Fusion cloning system involves the insertion of multiple DNA fragments into a linearised vector based on a 15 bp homologous overlapping segments in the adjacent fragments. This facilitates directional cloning of multiple fragments into the desired vector. The inserts used in this thesis were generated by PCR amplification using viral DNA or plasmid DNA as a template and high-fidelity DNA polymerase. The backbone vector was linearised by restriction enzyme digestion at a unique recognition site. The purified DNA fragments were subsequently cloned using the In-Fusion PCR cloning kit (Clontech) according to the manufacturer's protocol. Briefly, a 10 μL reaction mix consisting of 5× In-Fusion HD enzyme premix, linearized vector, purified PCR fragments and deionised water was incubated at 50ºC for 15 minutes, before being cooled on ice and transformed into α-select gold competent cells (Bioline) or One Shot™ Stbl3™ chemically competent *E. coli* cells (Invitrogen™) cells.

2.3.4.3 Transformation and plasmid isolation

For purification of plasmids after cloning competent *E. coli* cells were transformed using the manufacturer's protocol. Briefly, an appropriate amount of plasmid, ligation mix or In-Fusion PCR reaction was added to a vial of competent cells. After gentle mixing, the

transformation mix was incubated on ice for 30 minutes, followed by 45 sec of heat shock at 42ºC in a water bath. The tube was then immediately cooled on ice for 2 minutes with the subsequent addition of 1 mL of pre-warmed LB media. The tubes were incubated for a further 60 minutes in a shaking incubator set to 37ºC and 250 rpm. For each transformation, 100 µL of the transformed cells was inoculated onto agar plates by spreading and the plates were incubated overnight at 37°C. The following day, individual colonies were screened by colony PCR. The correct clone was cultured in 5 mL of LB broth overnight at 37°C in a shaking incubator. Following this, plasmid DNA was extracted using the AxyPrep plasmid miniprep kit (Axygen Biosciences). The sequence of the DNA insert was verified by Sanger sequencing (section 2.3.2).

2.3.5 Generation of recombinant HSV-1

To study the role of ICP47 during HSV-1 infection and to study the activation of the ICP47 promoter during latency establishment and maintenance, nine recombinant HSV-1 were generated in this study (Table 2.5). The steps involved in the construction of the recombinant viruses are: *a)* the generation of homology-directed repair (HDR) templates that incorporated the desired modification or contained an insert, *b)* the generation of plasmids that could express Cas9 protein and an appropriate guide RNA *c)* the co-transfection of HDR template and CRISPR Cas9 plasmids into 293A cells, iv) infection of transfected cells at a low plaque forming units (pfu)/cell) with an appropriate HSV-1 parent virus that could serve as the backbone of the recombinant virus and v) isolation of the recombinant virus.

2.3.5.1 Generation of HDR template

For the construction of HSV-1 Ka47Δ, HSV-1 Ka47R and HSV-1 GKa47R, long single-stranded oligo dideoxynucleotides (ssODN) were used as the repair templates. These oligos incorporated modification of a few nucleotides in the ICP47 coding sequence. Regions composed of 75 bp DNA arms, which flanked the nucleotide modification site, helped to direct the homology-based repair of the HSV-1 genome. The sequence information of the ssODNs used in this study can be found in Table 2.7. Instead of using ssODN, for the construction of HSV-1 GKa47Δ linearized plasmid pUC ICP47del was used. This plasmid contained appropriate nucleotide modifications in the ICP47 coding sequence flanked by DNA homologous to sequences flanking the desired modification site in the HSV-1

genome. Similarly, for the construction of recombinants HSV-1 Ka47inΔ, HSV-1 Ka47rescue, HSV-1 UL27-pa47min, HSV-1 UL3-pa47 and HSV-1 UL3-pa47ΔoriS, linearised plasmid DNA was used as the HDR template (See Table 2.2).

Table 2.7 List of ssODNs used for the construction of recombinant HSV-1

Name	Sequence 5′ to 3′	Virus
*cp47	ttattgatctcatcgcgtacgtcggcgtacgtcctgggcccaacccgcatgttgtcc aggaaggtgtccgcca**cgtcaAAGCTT**cagggcccacgacatgcttttcc ccccgacgagcaggaagcggtccacgcaacggtcgccgccggtcgcctcgacg	HSV-1 Ka47Δ
#rev_cp_47	ttattgatctcatcgcgtacgtcggcgtacgtcctgggcccaacccgcatgttgtcc aggaaggtgtccgccatt**T**CT**A**GAgcccacgacatgcttttcccgacgagc aggaagcggtccacgcaacggtcgccgccggtcgcctcgacgagggcgtt	HSV-1 Ka47R HSV-1 GKa47R

*The nucleotide substitutions compared to wild-type HSV-1 KOS sequence are shown in bold.

#The restriction enzyme recognition sites introduced for verification of the recombinants are shown in uppercase letters.

2.3.5.2 The CRISPR-Cas9 plasmid

Single expression vector, pX330-U6-Chimeric_BB-CBh-hSpCas9 (Addgene plasmid # 42230, a gift from Feng Zhang), that has both a chimeric single guide RNA driven by the U6 promoter and a human-codon optimised spCas9 gene driven by the CBh promoter was used as backbone for the construction of all the recombinant viruses described in this thesis (Cong et al., 2013). The guide DNA sequences for construction of various CRISPR-Cas9 plasmids used in this study are listed in Table 2.8. For guide RNA plasmid construction, the protocol described by Ran et al. (2013) was followed. Briefly, the nucleotide sequence of 20 bases located 5′ to an NGG motif was chosen in close proximity to the desired genome modification site. A guanine residue was appended at the 5′ end of the guide sequence if not already present. The complementary guide DNA oligos (Sigma) were designed such that the annealed oligos have overhangs compatible for cloning into the backbone vector. The oligo pairs were mixed at the equimolar ratio and annealed by incubating at 95°C for 5 minutes, followed by slow cooling at room temperature. The annealed oligo was cloned into the px330 vector, which had been previously linearised using BbsI. The ligated vector was transformed into One Shot™ Stbl3™ chemically

competent *E. coli* as per the manufacturer's instruction. The clones were selected using 100 μg/mL ampicillin-containing LB media and screened for the presence of insert by colony PCR. The inserted guide DNA sequence was further verified by Sanger sequencing.

Table 2.8 Guide DNA sequences used to induce double-stranded break at the target region of the HSV-1 genome

Name of the oligo	Sequence	Target location	Plasmid
sgRNA_icp47 top	CACCGGAAGGTGTCC GCCATTTCC	ICP47 region in HSV-1 KOS	px330 icp47
sgRNA_icp47 bottom	AAACGGAAATGGCG GACACCTTCC		
sgRNA_icp47 r top	CACCGTCCGCCACGT CAAAGCTTC	ICP47 region in HSV-1 Ka47Δ	px330 icp47del
sgRNA_icp47 r bottom	AAACGAAGCTTTGAC GTGGCGGAC		
px330UL26\7 T	CACCTTTGTCACGGG AAAGGAAAG	Intergenic region between the UL26 and UL27 genes in HSV-1 KOS	pxUL26/27
px330UL26\7 B	AAACCTTTCCTTTCCC GTGACAAA		
pxul3\4F	CACCTGGTTGTTTGT TGTCTTTAA	Intergenic region between the UL3 and UL4 genes in HSV-1 KOS	pxUL3/4
pxul3\4R	TTAAAGACAACAAAC AACCACAAA		

2.3.5.3 Transfection and infection

The day before transfection, 293A cells were seeded on to a 6-well plate and incubated at 37°C and 5% CO_2. The monolayer of cells in each well was transfected with a total of 3 μg of DNA comprising an equimolar amount of the HDR template and the CRISPR-Cas9 plasmid. Transfection was carried out using Lipofectamine 2000 (Invitrogen™) according to the manufacturer's instructions. Transfected cells were incubated for 5 hours at 37°C and 5% CO_2. Subsequently, the transfected cells were infected with 0.01 pfu/cell of HSV-1 in a volume of 1 mL of D0. After two hours of incubation, the inoculum was removed and replaced with fresh D2 after which the cells were incubated to allow recombination and

virus replication. After 72 hours, the cells and supernatants were collected and stored at -80°C until further use.

2.3.5.4 Isolation of recombinant virus

Five-fold dilutions of the above-harvested transfection/infection mix were made, and appropriate dilutions were used to infect confluent Vero cells in a 6-well plate. After 2 hours of incubation at 37°C and 5% CO_2, the virus inoculum was removed, and cells were overlayed with 2 mL of CMC-MEM. The plate was incubated for 48 hours at 37°C and 5% CO_2. The individual plaques were marked and 10 µl of cells with the medium from this marked region was aspirated using a micropipette and transferred to 500 µL of D2. This virus inoculum is referred to as "plaque pick". The plaque picks were then subjected to three freeze-thaw cycles before infecting individual wells of a 96-well plate with confluent Vero cells. A range of PCR primers were used to confirm the presence of the recombinant virus and detect the parental virus. Multiple rounds of plaque purification were carried out until the stock was free of the parental virus. The genome modification and insertion sites were verified by Sanger sequencing (section 2.3.2) and restriction fragment length polymorphism (RFLP) analysis (section 2.3.7.2).

2.3.5.5 Preparation of HSV-1 stocks

For the preparation of seed stock, the virus from the purified plaque was added to a 25 cm^2 flask with confluent Vero cells. The virus was allowed to grow for 72 hours followed by a collection of both the adherent cells and the supernatant with the help of a cell scraper (BD Biosciences). The infected cells were centrifuged at 524 g for 10 minutes at 4°C. The supernatant was discarded, and the cell pellet was resuspended in 500 µl of M2, which formed the seed stock. After freeze-thawing three times, 100 µl of the seed stock was inoculated into a T75 flask containing confluent Vero cells and incubated at 37°C and 5% CO_2. After 72 hours, the infected cells were collected with the culture medium with the aid of a cell scraper (BD Biosciences). The cell suspension was centrifuged for 10 minutes at 524 g. The supernatant was collected and subjected to ultracentrifugation for 90 minutes at 12,000 rpm and 4°C. In this step, the centrifugation was performed in Beckmann Coulter Optima™ L-90K ultracentrifuge using the SW32Ti rotor. Subsequently, the supernatant was discarded, and the pellet was resuspended in M2. This became the supernatant virus. The cell-associated virus was harvested by resuspending the cell pellet in M0, sonicating the

cells thrice for 20 sec each, followed by centrifugation at 524 g for 5 minutes. This step was repeated an additional time and the supernatants from the two rounds of centrifugation were pooled to obtain the cell-associated virus. The cell-associated virus and the supernatant virus were then pooled, mixed by pipetting and used as the master stock. For working stock, the confluent Vero cells in five T175 flasks were inoculated with 0.01 pfu/cell of master stock and incubated at 37°C and 5% CO_2 for 72 hours. After this, the stock was prepared following the same procedure as the master stock. The centrifugation was performed using Beckmann coulter AllegraX-15R benchtop centrifuge unless specified otherwise.

2.3.6 Plaque assay

Plaque assays were used to estimate the virus titre (Russell, 1962) of the newly prepared stocks, samples from the growth curve and tissue homogenates. For virus stocks, 10-fold dilutions of the stock were prepared in duplicate in M0. The culture media from 6-well plate containing confluent Vero cells was removed and replaced with 500 µL of the inoculum from the appropriate viral dilutions. The plates were incubated at 37ºC and 5% CO_2 for 90 minutes with rocking every 15 minutes to allow even spread of the inoculum. After the incubation step, the inoculum was removed and replaced with 2 mL of CMC-MEM. The plates were incubated at 37ºC and 5% CO_2 for 48 hours. To visualise the plaques, the culture medium was removed, and 1 mL of crystal violet staining solution was added to each well. After 10 minutes, the staining solution was removed and the number of plaque forming units was enumerated under the microscope. The virus titre was calculated based on the average number of plaques formed in an appropriate dilution between duplicates. When the values differed more than two-fold between the duplicates or dilutions within a replicate, the outcome was rejected, and the assay was repeated. For tissue homogenates, 10-fold dilutions were prepared as described previously and the assay was conducted without duplicates. In this case, less than two-fold difference between the dilutions was tolerated and the titre was calculated appropriately. The virus titre is presented as a number of pfu per mL or per mouse.

2.3.7 Characterisation of newly constructed recombinant viruses

The newly generated recombinant viruses were compared with their parent virus or unmodified KOS for their ability to grow in cell culture and its virulence in mice. Further, to test if the recombination affected the overall structure of the HSV-1 genome, an RFLP

analysis was performed. The revertant and rescuant viruses serve as a control for any unintended random mutation that could occur during the virus purification process.

2.3.7.1 Multi-step growth assay

The growth characteristics of the newly constructed recombinant HSV-1 were determined by infecting Vero cells at 0.01 pfu/cell in a 6-well tissue culture plate and incubated at 37ºC and 5% CO_2. The infections were carried out in triplicates. After 1 hour, the inoculum was removed, and the cells were washed with 2 mL of warm FBS-PBS twice to remove the un-adsorbed virus. Then, 2 mL of warm M2 was added to each well. This point was considered as 0 hours post-infection (hpi). At this time, the cells were immediately scraped into the media using cell lifters (Corning Costar), harvested and stored at -80ºC. The remaining plates were incubated at 37ºC and 5% CO_2. At 6, 24, 48 and 72 hpi, the cells and the supernatant were harvested together using cell-lifters. The samples from all five time points after infection were subjected to three freeze-thaw cycles before determining the virus titre.

2.3.7.2 Isolation of HSV-1 genomic DNA and RFLP analysis

Confluent Vero cells in a T175 flask were infected with wild-type or recombinant HSV-1 at 0.1 pfu/cell and incubated at 37ºC and 5% CO_2 for 24 hours or until full cytopathic effect (CPE) was observed. The cells were harvested along with the media with the aid of a cell scraper (BD Biosciences) and centrifuged at 524 g for 10 minutes at 4ºC (Beckmann coulter AllegraX-15R). The supernatant was separated and stored on ice until further processing. The cell pellet was resuspended in 10 mL of cold RSB buffer and incubated for 10 minutes on ice. The lysate was centrifuged at 524 g for 10 minutes at 4ºC. The supernatant was collected and stored on ice. The pellet was lysed again as described above. All of the supernatants were pooled and subjected to centrifugation at 12, 000 rpm for 90 minutes at 4ºC (Beckmann Coulter Optima™ LE-90K Ultracentrifuge, SW32Ti rotor). The supernatant was discarded, and the pellet was resuspended in TE buffer containing 50 μg/mL proteinase K and 0.5% (w/v) SDS. After 5 minutes of incubation at room temperature, an equal volume of phenol:chloroform (24:1 mixture) was added to the aqueous mixture and mixed gently. The mixture was then centrifuged at 13,523 g for 10 minutes using Eppendorf 5454 Benchtop Centrifuge. The aqueous phase was separated and subjected to phenol: chloroform extraction twice more. Finally, the aqueous phase, containing the DNA, was treated with 0.1 volume of 3 M sodium acetate and three

volumes of 100% (v/v) ethanol. The DNA was isolated by centrifugation at 13,523 g for 20 minutes and washed using 70% (v/v) ethanol. After drying, the DNA was resuspended in TE buffer.

The genome structure of newly generated recombinant viruses was compared with the wild-type or the parent virus by performing restriction enzyme digestion of the purified genomic DNA. The DNA fragments were then analysed by agarose gel electrophoresis.

2.3.8 Cycloheximide reversal assay

Vero cells grown to confluency in a 24-well plate were pre-treated with 100 μg/mL of cycloheximide in M2 for 1 hour at 37ºC and 5% CO_2. Later, the media was removed, and the cells were infected with wild-type or recombinant HSV-1 at 5 pfu/cell in M0 with added cycloheximide. The virus was adsorbed for 1 hour at 37ºC. Then, the inoculum was removed and replaced with fresh M2 containing cycloheximide. The plate was incubated for 6 hours at 37ºC and 5% CO_2. The media containing cycloheximide was then removed and the cells were washed with media containing actinomycin D at a concentration of 5 μg/mL. The infection was allowed to proceed in the presence of actinomycin D for a further 4 hours, after which, the cells were washed with PBS and harvested by trypsinisation. Similarly, control samples were prepared for each virus by following the above steps in the absence of cycloheximide and actinomycin D. After neutralisation of trypsin, the cells were transferred to individual wells of a 96-well plate (U bottomed plate, Falcon) and centrifuged at 524 g (Beckmann coulter AllegraX-15R) for 5 minutes at 4ºC. The cell pellets were resuspended in 150 μL of PBS and centrifuged again. Then, the cells were fixed using 50 μL of 1% (v/v) PFA (in PBS) for 20 minutes and washed three times with FBS-PBS. To wash the cells, the cell pellets were dislodged by gentle vortexing, followed by addition of 150 μL of FBS-PBS to each well and centrifugation at 931 g (Beckmann coulter AllegraX-15R) for 3 minutes. Subsequently, the cells were resuspended in an appropriate volume of FBS-PBS and analysed by flow cytometry.

2.3.9 Functional verification of genome modification in the newly generated recombinant viruses

The function of ICP47 in various recombinant viruses generated in this study was tested using the following two assays.

2.3.9.1 Quantitative analysis of MHC I using QIFIKIT

To assess the effect of ICP47 on the cell surface expression of H-2K^b, 10^6 MC57G, 293KbC2 or 293DbA5 cells were infected with the wild-type HSV-1 (strain KOS), ICP47 null mutant (HSV-1 Ka47Δ) or revertant (HSV-1 Ka47R) at 5 pfu/cell in 200 µL D0. Uninfected cells were used as a control. The infection was carried out in a 4 mL tube (Sarstedt). For infection, the cells were first incubated at 37ºC water bath for 3 minutes with intermittent shaking. Then the tubes were transferred to 37ºC shaking incubator at 250 rpm. After 30 minutes, the cells were transferred to a 15 mL tube containing 9.75 mL of pre-warmed D2 and incubated at 37ºC and 5% CO_2 in a MACSmix™ tube rotator. After 5.5 hours of incubation, the cells were harvested by centrifugation at 524 g (Beckmann coulter AllegraX-15R) and 4ºC for 5 minutes. The cells were washed using FBS-PBS, transferred to individual wells of a 96-well U-bottom tissue culture plate (BD Biosciences). Afterward, 50 µL of anti-H-2K^b (Y-3 clone) diluted to a concentration of 200 µg/mL was added to the wells and the plate was incubated for 30 minutes at 4ºC. The cells were then washed three times by resuspending in FBS-PBS and centrifuging at 524 g (Beckmann coulter AllegraX-15R), 5 minutes, 4ºC, followed by staining with a saturating concentration of FITC-conjugated goat anti-mouse F(ab)$_2$ fragments provided in the QIFIKIT® (Dako, Glostrup, Denmark). After incubating for 45 minutes at 4ºC in dark, the cells were washed using PBS thrice and fixed using 1% (v/v) PFA. At this stage, the calibration beads provided were washed using FBS-PBS and stained using the FITC-conjugated antibody as per the manufacturer's instructions. The cells and the beads were washed using FBS-PBS at least three times and analysed for FITC flourescence using flow cytometer. The photomultiplier tube (PMT) voltages were set up according to the manufacturer's instruction. The calibration beads consist of five populations, each coated with a defined number of antibody binding sites per bead (Figure 2.1 A). The fluorescence data from each of the five-bead populations were used for the construction of the standard calibration curve by relating the mean fluorescence intensity to the antibody binding capacity (ABC) of the beads (Figure 2.1 B). The mean fluorescent intensity (MFI) of samples was interpolated on to the standard curve to obtain the ABC of the samples (Figure 2.2). The actual number of H-2K^b molecules was calculated by subtracting the ABC of negative control from the ABC of the desired sample.

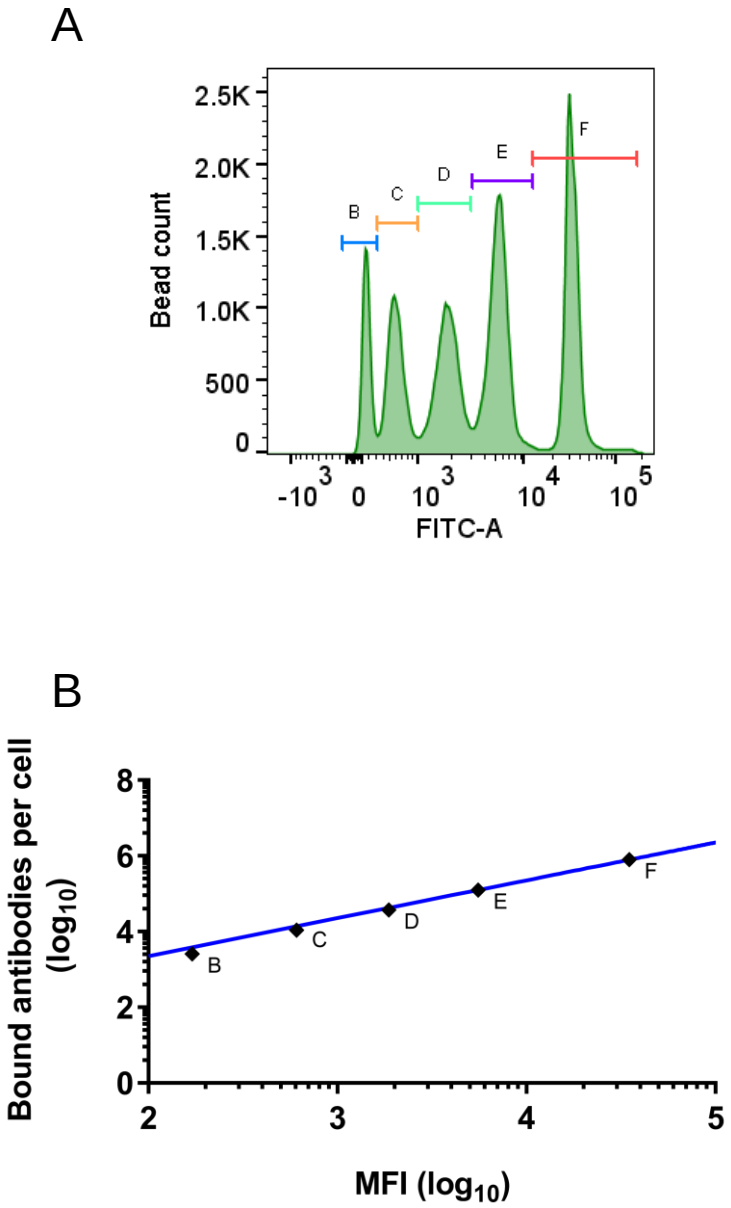

Figure 2.1 Generation of a standard curve using QIFIKIT calibration beads. (A) Calibration bead populations (B to F) were gated to obtain MFI. A different population of beads shown in the figure bind to a specified amount of antibody also known as antibody binding capacity (ABC) (B) A linear regression curve was plotted using the MFI and the corresponding ABC of different bead populations.

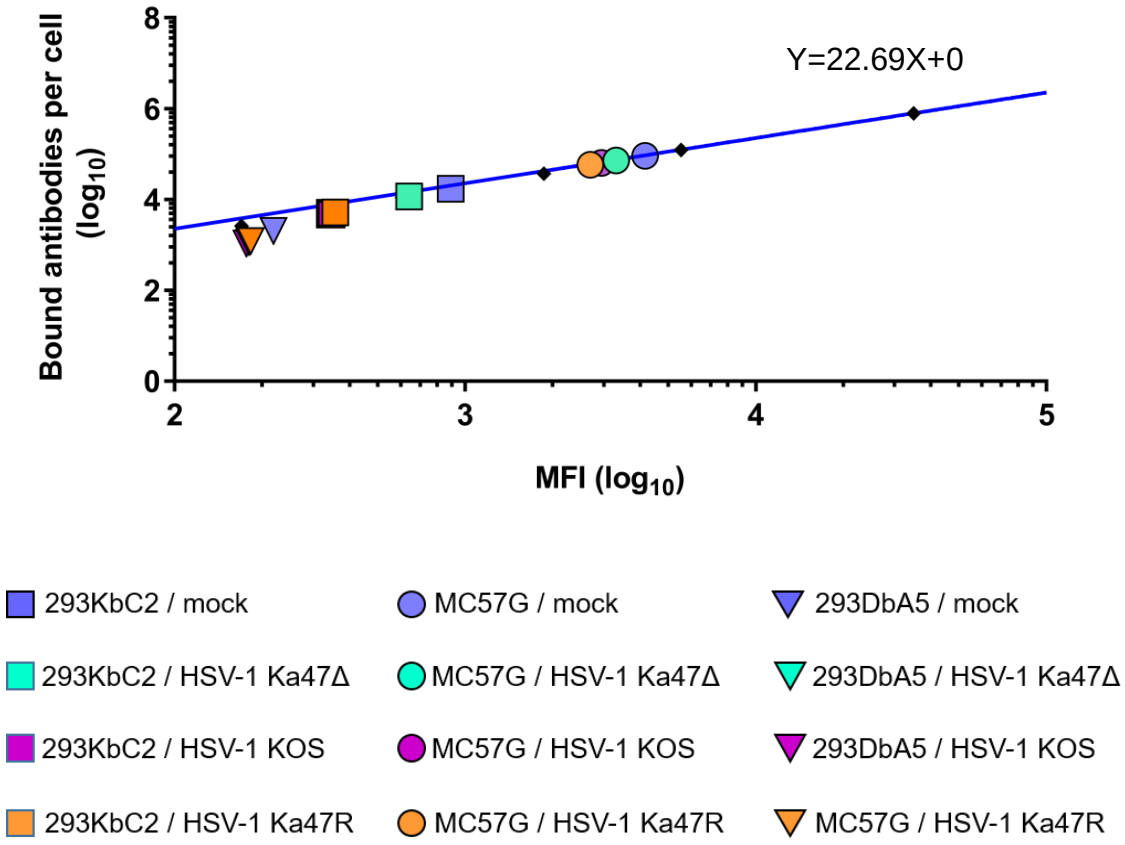

Figure 2.2. Computation of total cell surface H-2K^b molecules using the calibration curve. Mock-treated or infected cells were incubated with anti- H-2K^b antibody, followed by staining with the FITC-conjugated secondary antibody. The ABC of each sample was obtained by interpolating the MFI into the standard curve constructed using QIFIKIT calibration beads.

2.3.9.2 Flow cytometry-based antigen presentation assay

293KbC2 or MC57G cells were infected with 10 pfu/cell of HSV-1 KOS, HSV-1 Ka47Δ, HSV-1 Ka47R, HSV-1 Ka47inΔ, HSV-1 Ka47rescue, HSV-1 GKa47Δ or HSV-1 GKa47R. Briefly, 3 to 6 × 10^6 cells were added to appropriate tubes. This was followed by addition of the virus in an appropriate volume of D0. Uninfected cells were used as a control. The tubes were incubated at 37ºC in a water bath for 3 minutes with intermittent shaking. The tubes were then transferred to 37ºC shaking incubator at 250 rpm. After 30 minutes, the cells were shifted to a 15 mL tube containing 9.5 mL of pre-warmed D2 and incubated at 37ºC and 5% CO_2 for 2.5 hours in a MACSmix™ tube rotator. The cells were pelleted by centrifugation at 524 g for 5 minutes and resuspended in D0. An appropriate number of cells was transferred to 15 mL tube for infection with MVA mini OVA, MVA ES mini OVA or MVA mini Flu. Cells not infected with HSV-1 were separated into 5 tubes for infection with MVA mini OVA, MVA ES mini OVA or MVA mini Flu, incubating with 10^{-7} mM OVA (SIINFEKL) peptide or to serve as an uninfected control. Infection with MVA was performed at 10 pfu/cell. The treatments were performed in a total volume of 500 µL of D0. The tubes were incubated at 37ºC water bath for 3 mins with intermittent shaking, followed by incubating for 30 minutes in 37ºC shaking incubator (250 rpm). After incubation, 9.5 mL of warm D2 was added to each tube and incubated at 37ºC and 5% CO_2 in the MACSmix™ tube rotator. After 5.5 hours of incubation, the cells were pelleted by centrifugation at 524 g for 5 minutes. The cells were resuspended in 150 µL of cold FBS-PBS and transferred to individual wells of a U-bottomed 96-well plate (BD Biosciences). The cell pellets obtained after centrifugation at 524 g for 5 minutes were resuspended in cold FBS-PBS. This washing step was repeated one more time before staining the cells using 50 µL of allophycocyanin-conjugated monoclonal antibody specific to H-2K^b/SIINFEKL complex (clone 25D.1.16) at a 1/200 dilution in cold FBS-PBS. The cells were incubated for 1 hour on ice followed by 3 wash steps as described above. They were then fixed using 50 µL of 1% (v/v) PFA (in PBS) for 20 minutes at room temperature and subsequently washed twice using cold FBS-PBS. Finally, the cells were resuspended in cold FBS-PBS and the fluorescence was measured using flow cytometry. Uninfected cells, uninfected cells pulsed with SIINFEKL peptide and cells infected with HSV-1 or MVA alone were used as controls. 293KbC2 is a stably transfected clone of 293A, a human embryonic kidney cell line (Tscharke et al., 2005). This cell line was used to validate recombinant HSV-1 ICP47 null mutants by testing their function, which is to inhibit TAP

mediated antigen presentation. The species specificity of ICP47 was assessed by comparing the level of K^b-SIINFEKL complex between 293KbC2 and MC57G. A diagrammatic representation of this assay is displayed in Figure 3.5.

2.3.10 *In vivo* analysis of HSV-1 infection using a mouse model

2.3.10.1 HSV-1 infection model and pathogenesis

Female C57BL/6 mice aged 8 weeks or more were inoculated with HSV-1 using a flank infection model (Russell et al., 2015). In brief, mice were anesthetized using Avertin (1, 1, 1-tribromoethanol in 2-methyl-2-butanol) at 250 mg per kilogram weight of mice, fur was clipped and depilated from upper to lower midline on the left flank. A 25 mm^2 area was marked, using the tip of the spleen as a landmark for tattooing. The marked area was tattooed using a round shader needle immediately after dipping in 10^8 pfu/mL virus stock. After removing the excess inoculum, the mice were wrapped in tissue and monitored throughout the anaesthesia to manage potential complications such as hypothermia. Following infection, the progress of the HSV-1 induced skin lesion was monitored from the day when the primary lesion appeared until resolution. Additionally, mice were examined for signs of generalised systemic illness based on posture, activity and fur texture and scored according to the criteria provided in Table 2.9. Grades 0, 1, and 2 were given a score of 0, 1 and 2 respectively. The scores from different criteria were summed to obtain a total score. A total score of less than 3 was considered mild, 3 to 5 was considered moderate and a score of 6 was considered to be indicative of severe clinical symptoms.

Table 2.9 Scoring criteria for systemic illness

Criteria	Grade 0	Grade 1	Grade 2
Posture	Normal	Hunching noted only at rest	Severe hunching impairs movement
Activity	Normal	Mild to moderately decreased	Stationary unless stimulated
Fur texture	Normal	Mild to moderate ruffling	Severe ruffling/poor grooming

2.3.10.2 Assessment of virus growth in mice

Amounts of virus from skin and DRG were quantified using plaque assay. For this, skin tissue that was 0.8 cm wide from upper to lower midline of the infected dermatome was excised in 800 µL of D2. Similarly, DRG from spinal levels T5 to L1 were collected. After harvesting, the tissues were frozen using dry ice and stored at -80ºC until further processing. The tissues were later homogenised using a 1 mL tissue grinder. The amount of virus in the homogenates was determined using a plaque assay (see section 2.3.6) and plotted as pfu/mouse.

2.3.10.3 Analysis of reactivation competence

Reactivation of HSV-1 can be induced in latently infected ganglia by removing them from mice and culturing as explant in D2 (Price and Schmitz, 1978). For assessing the reactivation efficiency between the wild-type HSV-1 (strain KOS), HSV-1 Ka47Δ or HSV-1 Ka47R, mice were tattoo-infected at least 30 days prior to performing the reactivation assay. Once latency was established (>30 days post-infection), mice were culled and their DRG corresponding to thoracic level T4 to T13 and lumbar level L1 to L3 were excised. The DRGs were placed individually in each well of a 96-well plate (U bottomed, BD) containing 100 µL of M10 with Pen-Strep. The explanted DRG were cultured for 5 days in the culture media at 37ºC and 5% CO_2, homogenized and the homogenates were assessed for the presence of the infectious virus on Vero cell monolayers. Differences in percentage of reactivation were compared on the level of individual mice, or at the spinal level.

In other experiments, where the ability of the recombinant viruses to reactivate from latency was tested, DRG were excised from thoracic level T4 to T13 and lumbar level L1 to L3 of the latently infected mice. The harvested tissues were pooled per mouse in D2 and cultured for five days at 37ºC and 5% CO_2. After this culture period, the DRG were homogenised using a 1 mL tissue grinder. The homogenate was assessed for infectious virus by inoculating the Vero cells in a 6-well plate and incubated at 37ºC and 5% CO_2 for two days. For the recombinant viruses that experessed eGFP, the plaques were tested for the expression of GFP by fluorescence microscopy (Olympus CKX41).

2.3.10.4 Intracellular cytokine staining for IFNγ

The $CD8^+$ T cell response following infection in mice was measured using the intracellular cytokine staining (ICS) assay. The technique used in this study involved *ex vivo* stimulation of splenocytes using synthetic peptides in the presence of Brefeldin A and antibody staining for CD8 and IFNγ followed by analysis using flow cytometry (Flesch et al., 2012).

Previously infected mice were euthanized using CO_2 and their spleens were collected in 1 mL of D10 and stored on ice until further processing. Splenocytes were prepared by crushing the spleens using plungers from 1 mL syringes and passing them through cell strainers using PBS. The isolated splenocytes were pelleted by centrifugation at 524 g for 5 minutes (Beckman coulter AllegraX-15R) and resuspended in 5 mL of red cell lysis buffer. After incubating for 3 minutes, the reaction was stopped by adding 30 mL of PBS. The cells were centrifuged at 524 g at 4ºC for 5 minutes (Beckman coulter AllegraX-15R). The cell pellet was resuspended in 5 mL of D10. After staining with trypan blue solution, viable splenocytes were enumerated using haemocytometer. The number of splenocytes in each sample was adjusted to 10^7 cells/mL using D10. From this, 100 µL of cells were transferred to each well of a 96-well plate (U-bottom, BD Biosciences) for ICS assay. To the cells, 100 µL of 0.2 µM synthetic peptide (in D0) or 100 µL of D0 (control) was added and incubated for 1 hour at 37ºC and 5% CO_2. Afterward, 20 µL of 50 µg/mL Brefeldin A was added to each well and incubated for further 3 hours. The cells were then spun down at 524 g at 4ºC for 5 minutes (Beckman coulter AllegraX-15R) and resuspended in 50 µL of anti-CD8α-PE clone 53-6.7 at a 1/150 dilution in FBS-PBS. The staining was done in dark for 30 minutes on the ice after which the cells were washed three times by resuspending in PBS. After washing, the cells were fixed using 1% (v/v) PFA (in PBS) for 20 minutes at room temperature followed by washing thrice using FBS-PBS. Next, for intracellular staining, the cells were resuspended in 50 µL of anti-IFNγ-APC diluted 1/200 in FBS-PBS containing 0.25% (w/v) saponin, and then incubated at 4°C overnight. The following day, the cells were washed thrice using FBS-PBS and analysed by flow cytometry. The magnitude of peptide-specific responses was reported as a percentage of $IFN\gamma^+$ of $CD8^+$ cells. The gating strategy can be seen in Figure 2.3.

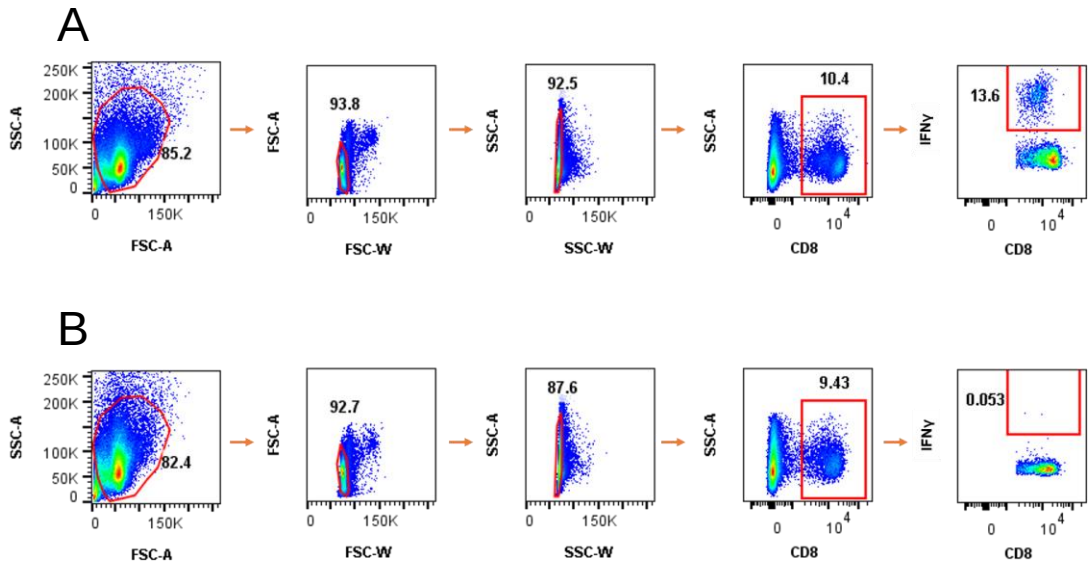

Figure 2.3 Gating strategy to identify HSV-1 specific CD8$^+$ T cells. Splenocytes from C57BL/6 mice previously infected with HSV-1 KOS were treated exogenously with HSV-1 $gB_{498\text{-}505}$ synthetic peptide (A) or left untreated (B). Then, the cells were stained for surface expression of CD8α and intracellular expression of IFNγ. The events were first selected according to the forward scatter (FSC) and side scatter (SSC) parameters. Then, doublet exclusion was performed using width and area parameters of FSC and then SSC accordingly. The singlet events were then gated using CD8α × SSC (area) to detect CD8$^+$ T cell events. Finally, IFNγ$^+$ events were gated from the CD8$^+$ T cell events on a CD8 × IFNγ plot.

2.3.11 X-Gal staining of DRG

ROSA26R mice were infected with a recombinant HSV-1 that expresses Cre recombinase. Mice were euthanized using CO_2 at 5, 10, 20, 40 and 100 days after infection. DRG ipsilateral to the site of infection from T4 to L1 were excised and added to individual wells of a 96-well plate (U bottomed, BS) containing 50 µL of fixative (2% (v/v) PFA and 0.5% (v/v) Glutaraldehyde in PBS). DRG were incubated in the fixative for at least 1 hour on ice. After this, they were washed twice using 200 µL of cold PBS. PBS was later replaced with 50 µL of X-Gal permeabilisation buffer and incubated for 15 minutes on ice. The permeabilisation buffer was then replaced with 50 µL of X-Gal staining solution (1 mg/mL X-Gal) and the plate was incubated overnight at 4ºC. The following day, the X-Gal staining solution was removed, the DRG were rinsed twice using PBS and then, stored in 50% (w/v) glycerol. Prior to imaging, the DRG were whole mounted on microscopic slides using glycerol as a mounting medium and photographed using an Olympus CKX41 microscope.

2.3.12 Mass spectrometry-based peptide identification and quantification

2.3.12.1 HSV-1 infection of in vitro cultured cells for mass spectrometry

Cells (2×10^8 or 5×10^7) were grown in D10 in T175 flasks to confluency. The cells were trypsinized and infected at 5 pfu/cell with HSV-1 KOS, Ka47Δ or Ka47R in D0. First, cells were mixed with the appropriate virus in a 15 mL round bottom polypropylene tubes in a total volume of 2 mL and incubated in 37°C shaking incubator at 250 rpm for 30 minutes. Later, the contents were transferred to a 50 mL tube containing 38 mL of pre-warmed D2 and incubated at 37°C with continuous rotation using MACSmix™ tube rotator for 5 hours and 30 minutes. After infecting the cells for a total of 6 hours, viable cells were counted post-staining with trypan blue. The cells were then centrifuged at 524 g for 5 minutes and the resultant cell pellets were washed using 10 mL of cold PBS. For peptide discovery, the cell pellet was resuspended in 1 µL/mL of Trioxsalen and UV inactivated for 20 minutes on ice with intermittent mixing every 5 minutes (Fischer et al., 2007; Schneider et al., 2015). The virus-inactivated cells were resuspended in 10 mL of cold PBS, transferred to a 15 mL tube and centrifuged at 524 g for 5 minutes. The supernatant was removed, and the resultant cell pellet was snap frozen using dry-ice ethanol bath and stored in a freezer at -80°C until lysis.

2.3.12.2 Solubilising AQUA peptides

AQUA peptides were solubilised in 100% (v/v) DMSO to a concentration of 5 mM. The volume of DMSO added to each peptide was calculated based on *a)* the molecular weight of each peptide and *b)* the synthesised weight of the respective peptide as indicated by the manufacturer. Since the purity of the peptides were less than 100%, the exact concentration of the solubilised peptides was subsequently determined using a Direct Detect® spectrophotometer (EMD Millipore) following the manufacturer's instruction. Based on this data, the peptides were diluted to 5 pmoles/μL using MS buffer A.

2.3.12.3 Generation of cell lysate

For cell lysis, 1 mL of ice-cold 2× concentrated lysis buffer was added to the frozen cell pellet and mixed gently to disrupt the pellet. Then, 2 mL of 2× concentrated lysis buffer and 2 mL of Milli-Q water were added to the resuspended pellet and mixed end-over-end for 1 hour at 4ºC with gentle rotation. The lysate was centrifuged (Beckman coulter AllegraX-15R) at 3724 g for 10 minutes at 4°C. The supernatant was transferred to three 2 mL polypropylene (Eppendorf) tubes and centrifuged for a further 10 minutes at 15,871 g at 4°C. Cleared lysates were collected and stored on ice prior to immunoprecipitation with protein A-crosslinked MHC-specific antibodies.

2.3.12.4 Preparation of cross-linked immunoaffinity column

Poly-prep Chromatography column (BioRad) was first conditioned for crosslinking by incubating the column with 10 mL of 10% (v/v) acetic acid for 20 minutes. The column was rinsed once again with 10% (v/v) acetic acid and finally rinsed with Milli-Q water to remove traces of acetic acid before air-drying. Protein A sepharose was supplied as 50% slurry in 20% (v/v) ethanol. The slurry was thoroughly mixed before transferring to the capped column. The protein A sepharose was rinsed and equilibrated with 10 column volumes (CV) of PBS to remove ethanol. Antibody diluted with PBS was mixed with the resin at a concentration of 10 mg antibody to 1 mL protein A in a 50 mL tube. The mixture was incubated for 1 hour at 4°C with gentle rotation, then transferred back to the column. Any unbound antibody was removed by washing the column with 10 CV of borate buffer, followed by equilibrating the resin with 10 CV of 0.2 M Triethanolamine, pH 8.0. The bound antibody was cross-linked to protein A sepharose using 40 mM DMP cross-linker for 1 hour at room temperature. Cross-linking was terminated by the addition of ice-cold

0.2 M Tris, pH 8. The column was then washed using 10 CV 0.1 M citrate buffer, pH 3 followed by 10 CV borate buffer. The column containing antibody cross-linked to protein A sepharose was then stored at 4°C in PBS prior to use. The cross-linked antibody was used within 4 days of preparation.

2.3.12.5 Immunoaffinity purification of peptide-MHC I complexes

Immunoaffinity purification of pMHC-I was carried out as specified by Dudek et al. (2016). For each sample, 1.5 mg of antibody cross-linked protein A sepharose slurry was transferred to a clean poly-prep column. The affinity column was equilibrated with 10 CV of Wash buffer 1. The cell lysate was initially passed through a pre-column containing protein A sepharose without the cross-linked antibody to remove any contaminants that non-specifically bind to protein A. The flow-through from this pre-column was dripped directly onto an immunoaffinity column containing anti-H-2K^b covalently bound to protein A sepharose. To maximise the binding of pMHC I to the antibody, the lysate was mixed with the slurry and incubated for 5 minutes. The lysate was then allowed to pass through the column by gravity flow, collected, and then passed over a second time. Flow-through from this second pass was dripped directly onto an anti-H-2D^b column. After resuspension and 5 minutes incubation, the flowthrough was collected by gravity flow and passed again through the anti-H-2D^b column. Two mL of the final flowthrough from the anti-H-2D^b column was collected and stored for proteomics analysis. Each immunoaffinity column was then washed using 20 CV of a sequential series of buffers from Wash buffer 1 to Wash buffer 4, in order to remove unbound material, detergent, non-specifically bound components and salt, respectively. Finally, antibody-bound pMHC-I was eluted using 2 mL (5 CV) of 10% (v/v) acetic acid from both the columns separately. For MRM-MS peptide quantification experiments, 50 fmoles of AQUA peptides were added to the eluate at this stage.

2.3.12.6 HPLC Purification, fractionation and concentration of peptides

The above acid eluate, containing peptides, MHC I heavy chain and β-microglobulin, was fractionated using reverse-phase high-performance liquid chromatography (HPLC) using a C18 column (Chromolith high-resolution RP-18 endcapped, Merck) on an ÄKTAmicro HPLC system (GE Healthcare). The mobile phase buffer system used in the column consisted of HPLC fractionation buffer A and HPLC fractionation buffer B at a flow rate

of 1 mL/min. The peptides were separated across a gradient of HPLC fractionation buffer B from 2% to 45% over the course of 20 minutes. This process separates the peptides from free MHC I heavy chain and β-2 microglobulin. Peptide fractions (500 µL) were collected in LoBind Eppendorf tubes, vacuum concentrated and pooled via a concatenation strategy to reduce the complexity of any given pool. Specifically, pool 1 consisted of fractions A3, A4, A8, A12, B15; pool 2 consisted of A5, A9, A13, B14; pool 3 consisted of A6, A10, A14, B13; and pool 4 consisted of A7, A11, and A15. The pooled fractions were vacuum concentrated using a Labconco Centrivac concentrator (Thermo Fisher Scientific) and equalised to a final volume of 12 µL using MS buffer A. Custom synthesised standard indexed retention time (iRT) peptide mix was added to pooled fractions, followed by sonication for 10 minutes and centrifugation at 15,871 g for 10 minutes (Escher et al., 2012). 10 µL of the supernatant was transferred to mass spectrometer autosampler vials and stored at 4°C until analysis. For targeted MS analysis, iRT peptides were not included but the pooled fraction was sonicated and centrifuged as described above before transferring to the mass spec vials.

2.3.12.7 LC-MS/MS and peptide identification

For the identification of MHC I restricted HSV-1 peptides, a Q Exactive™ hybrid quadrupole-Orbitrap MS (Thermo Scientific) coupled to UltiMate 3000 RSLCnano HPLC (Thermo Scientific) was used. Each sample was loaded by an autosampler via a trap column (100 µm × 2 cm NanoViper PepMap100 (Thermo Scientific) at a flow rate of 15 µL/min in MS buffer A on to the analytical nanocolumn (75 µm × 50 cm PepMap100 C18 3 mm, 100 Aº; Thermo Scientific). Peptides were separated by liquid chromatography using an increasing linear concentration gradient of MS buffer B at 250 nL/min flow rate for 90 minutes. Up to 12 MS/MS most intense spectra were acquired per cycle with dynamic exclusion at the level of MS1 for 15 seconds to exclude re-sequencing of the exact same peptide and improve the repertoire of peptides identified.

2.3.12.8 Optimisation of MRM transition conditions

To improve the efficiency of detection of target peptides using MRM-MS, the MS acquisition parameters such as collision energy need to be optimised for selected MRM transitions. For initial selection of precursor ions, collision energy (CE) and the fragment ions, 500 fmoles of each AQUA peptide was loaded onto a SCIEX QTRAP® 6500 mass

spectrometer as a mixture and operated in enhanced MS mode followed by enhanced product ion scan with an m/z ranging from 80 to 1000. The dominant precursor ion and its corresponding predicted collision energy (calculated by the QTRAP instrument) for each AQUA peptide were determined from the LC-MS/MS analysis. A set of 6 to 9 of the most intense product ions was then selected for MRM transitions. A targeted MRM method was then used to refine the collision energy for each individual MRM transition by injecting 500 fmoles of each AQUA peptide. MRM ion pairs corresponding to the 5 most intense peaks were selected for creating an optimised MRM method. For each transition pair, three CE values, in 4 eV increments, above or below the previously assigned (predicted) values were used to refine the analysis in order to obtain an optimal CE per transition per peptide (Lange et al., 2008; Sherwood et al., 2009). Finally, the MRM assay was validated in the triple-quadruple instrument SCIEX QTRAP® 6500. For determining the optimal concentration of AQUA peptides to add to the endogenous sample, a series of 10-fold dilutions of the pooled peptide mix were made and injected from 500 fmoles down to 5 amoles into the SCIEX QTRAP® 6500 instrument. A standard curve was constructed for each peptide by plotting the peptide concentration against its sum peak area (Figure 5.13). From this analysis, 50 fmoles for each deemed within a suitable linear range of detection. The final MRM assay method (Table 5.2) included a transition list of each precursor m/z and its corresponding selected product ions and associated collision energy values; matching transition m/z values were also incorporated for the unlabelled (i.e. non-isotopic) peptides.

2.3.12.9 Estimation of peptide copies

The area under each MRM transition peak was calculated using Skyline Targeted Mass Spec Environment application (MacCoss Lab Software) (MacLean et al., 2010; Schilling et al., 2012). The area of all MRM transitions for a peptide was combined to obtain the sum peak area. The estimated copy number of a detected endogenous peptide was calculated by taking the ratio between the peak areas of the peptide with that of its corresponding AQUA peptide. It was then possible to determine the amount of endogenous peptide detected by multiplying the ratio by that of the moles of AQUA peptide spiked into the sample (i.e. 50 fmoles of AQUA, or $5x10^{-14}$ moles). Moles were converted to molecules by multiplying by Avogadro's number, and then dividing the number of molecules by the total number of cells for the sample arrives at a copy number for the peptide. The following equation summarises this:

$$Copies\ per\ cell = \frac{\frac{Sum\ peak\ area_{endogenous}}{Sum\ peak\ area_{AQUA}} \times Moles_{AQUA} \times 6.022 \times 10^{23}}{Total\ number\ of\ cells}$$

2.3.13 Statistical analysis

Statistical comparisons were made using GraphPad Prism 7 for Windows (version 7.04). For comparison of means of two groups, two-tailed unpaired t-test was performed. For comparison of means of more than two groups one-way or two-way ANOVA was used with an appropriate multiple comparisons post-hoc test. In all cases, p value less that 0.05 was considered statistically significant.

Chapter 3
Effect of ICP47 during HSV-1 infection in mice

3 Effect of ICP47 during HSV-1 infection in mice

3.1 Introduction

The HSV-1 protein ICP47 targets the MHC I antigen presentation pathway by interfering with the TAP-mediated transport of peptides into the ER lumen (York et al., 1994; Früh et al., 1995). The high affinity binding of ICP47 to the inner surface of the TAP1 and TAP2 transmembrane helices, precludes peptide binding and freezes TAP in an inactive conformation, thus inhibiting the peptide transport into the ER lumen (Oldham et al., 2016a). The lack of peptides in the ER lumen lead to a substantial reduction in the surface MHC I expression and presentation of HSV-1 peptides (York et al., 1994). As a consequence, HSV infected human cells show a remarkable level of resistance to $CD8^+$ T cell-mediated specific lysis *in vitro* (York et al., 1994). Interestingly, while this holds true for human cells, mouse cells are susceptible to $CD8^+$ T cell killing (York et al., 1994; Jugovic et al., 1998). In addition, earlier biochemical studies proposed that ICP47 does not function in mice because a competitive binding assay conducted using insect microsomes demonstrated that ICP47 had 100-fold lower binding affinity towards murine TAP compared to human TAP (Ahn et al., 1996; Tomazin et al., 1996). The biochemical analysis was performed in buffered salt solution in ambient conditions. So, these solutions lack various biological components present in the cytoplasmic milieu that can have significant effects on the binding behavior of peptides and proteins. Further, by resolving the structure of ICP47-TAP complex, Oldham et al. (2016) showed that the inactive, closed conformation of TAP1/TAP2 complex induced as a result of stable binding of ICP47 is the critical reason for blocking of peptide transport, rather than competitive inhibition. Thus, an assay that directly quantifies the antigen presentation on HSV-1 infected cells might overcome the difficulties associated with the biochemical assay and improve our understanding of species specificity of ICP47.

Even though the aforementioned *in vitro* studies cast doubt over the relevance of using mouse models in studying the $CD8^+$ T cell immunity to HSV infection, other *in vivo* studies have shown that ICP47 enhances the neurovirulence of HSV-1 in mice (Goldsmith et al., 1998; Burgos et al., 2006). Due to the inherent low-level antigen-presenting capacity of neurons, the authors postulated that even a modest inhibition of TAP function by ICP47 is sufficient to affect $CD8^+$ T cell recognition of infected neurons. This study reveals an apparent discrepancy between the data obtained from the *in vitro* assay system and the

biologically relevant *in vivo* model. However, these studies used models that permit the virus to enter the central nervous system (CNS) and induce encephalitis-mediated mortality in most of the infected mice. Accordingly, the neurovirulence model is not conducive to study the establishment of latency and reactivation, which are typical of natural HSV infection.

It is well understood both from human and mouse studies that acute HSV-1 infection elicits a large $CD8^+$ T cell response (Posavad et al., 1997; Koelle et al., 1998; Hosken et al., 2006). This response is important in acute infection as depletion of $CD8^+$ T cells in mice led to prolonged HSV-1 replication and delayed viral clearance in neurons after the initial primary infection (Simmons and Tscharke, 1992). Besides curtailing the acute infection, $CD8^+$ T cells containing markers for functional activation were observed in close proximity to the latently infected neurons suggesting that they may play a role in immune surveillance in ganglia during latency (Khanna et al., 2003a; Theil et al., 2003; Verjans et al., 2007). Incidentally, ICP47 promoter was found to be active in a subset of neurons long after the clearance of infectious virus (Ma et al., 2014; Russell and Tscharke, 2016). The above observations prompted us to ask, if $CD8^+$ T cells have a role in latency as well as in acute infection, then what is the consequence of expression of ICP47 and $CD8^+$ T cell evasion during HSV infection? Therefore, we thought it would be timely to revisit the discrepancy between the biochemical and *in vivo* data and re-examine the role of ICP47 using a model where the virus is contained to the PNS as is similar of natural HSV-1 infection.

To investigate the impact of ICP47 during HSV infection we a) generated a new set of ICP47 null mutants in the HSV-1 strain KOS background, b) developed an assay to measure directly the ICP47-mediated inhibition of antigen presentation in a human and a mouse cell line, c) examined *in vivo* role of ICP47 using a flank model of HSV-1 infection in C57BL/6 mouse strain and d) used ROSA26R reporter mouse system to track the influence of ICP47 upon HSV-1 latency. HSV-1 KOS was selected because it can infect and establish latency in neurons without the demise of mice. Also, since $CD8^+$ T cell-mediated response to HSV-1 has been thoroughly examined in C57BL/6 mice in the past, by utilizing this mouse model, we could better understand the impact of ICP47 mediated evasion from $CD8^+$ T cells. With these new set of tools, we set out to study the consequence of inhibition of MHC I mediated antigen presentation by ICP47 on HSV-1 pathogenesis, latency, and reactivation in mice.

3.2 Results

3.2.1 Generation and verification of recombinant ICP47 null mutant and revertant viruses

A recombinant ICP47 null virus containing nucleotide sequence modifications that would prevent the synthesis of ICP47 and an appropriate revertant virus were generated using CRISPR-Cas9 genome editing technology. Given the possibility that the selection marker may interfere with the expression of neighbouring open reading frames (ORFs), any alterations in the viral genome were kept to a minimum. The steps taken to generate recombinant HSV-1 are described in detail in the methods section and the modifications introduced in the genome are shown diagrammatically in Figure 3.1. Amino acid residues 3 to 34 on the N-terminal of ICP47 are sufficient and critical for the inhibition of TAP function (Galocha et al., 1997; Neumann et al., 1997). To generate an ICP47 null mutant virus, we introduced a stop codon and a restriction enzyme recognition sequence after the sixth codon of ICP47, such that it would abruptly curtail the translation of a full-length protein (Figure 3.1). The sequence modification at this position of ICP47 gene means that the *cis*-regulatory elements of the neighbouring and overlapping ORFs will not be disrupted. The resultant ICP47 null mutant virus was named as HSV-1 Ka47Δ. The mutation of ICP47 in Ka47Δ was then repaired in the revertant virus Ka47R so that the virus could synthesize a functional ICP47 (Figure 3.1). For ease of screening and verification, a restriction enzyme recognition site was introduced by silent substitution mutation in the genome of the revertant virus.

The sequence modifications in the recombinant viruses, Ka47Δ and Ka47R, were confirmed by sequencing of the corresponding DNA fragment (data not shown) and by analysing the whole genome using restriction fragment length polymorphism (Figure 3.2). While the modification to the HSV-1 genome was kept to a minimum, the *in vitro* growth characteristics of the engineered viruses were monitored to evaluate the impact of gene modification on the virus replication. Multi-step growth analysis was performed in Vero cells over 72 hours and found that the growth kinetics of the recombinant viruses HSV-1 Ka47Δ and HSV-1 Ka47R is like that of the HSV-1 KOS (Figure 3.3). This suggests that the virus replication was unaffected by either nucleotide modification or loss of ICP47 function.

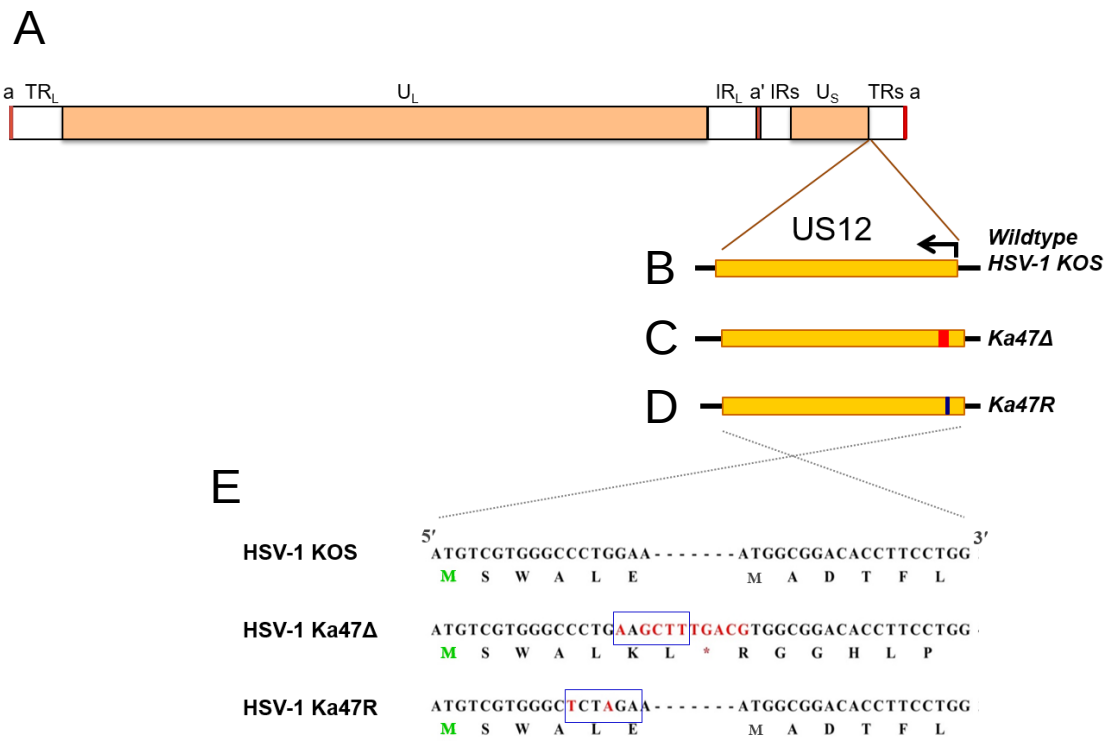

Figure 3.1 Schematic representation of recombinant HSV-1 with modification in the ICP47 coding sequence. (A) Diagram of the HSV-1 genome with the location of unique and repeat regions shown. (B), (C) and (D) Diagram indicates the region of nucleotide modification in the US12 coding sequence. In HSV-1 Ka47Δ, a stop codon was introduced upstream of AUG start codon shown in red bar and in HSV-1 Ka47R, the blue bar represents silent substitutions used to create a restriction enzyme recognition site. (E) Sequence alignment between HSV-1 KOS, HSV-1 Ka47Δ and HSV-1 Ka47R is shown. The modified nucleotides are indicated in red and the gaps are shown in hyphens. The blue boxes represent the HindIII recognition sequence in Ka47Δ and XbaI recognition sequence in Ka47R. Amino acid sequence translation is provided immediately below the nucleotide sequence. The asterisk symbol in the amino acid sequence of Ka47Δ represents the stop codon.

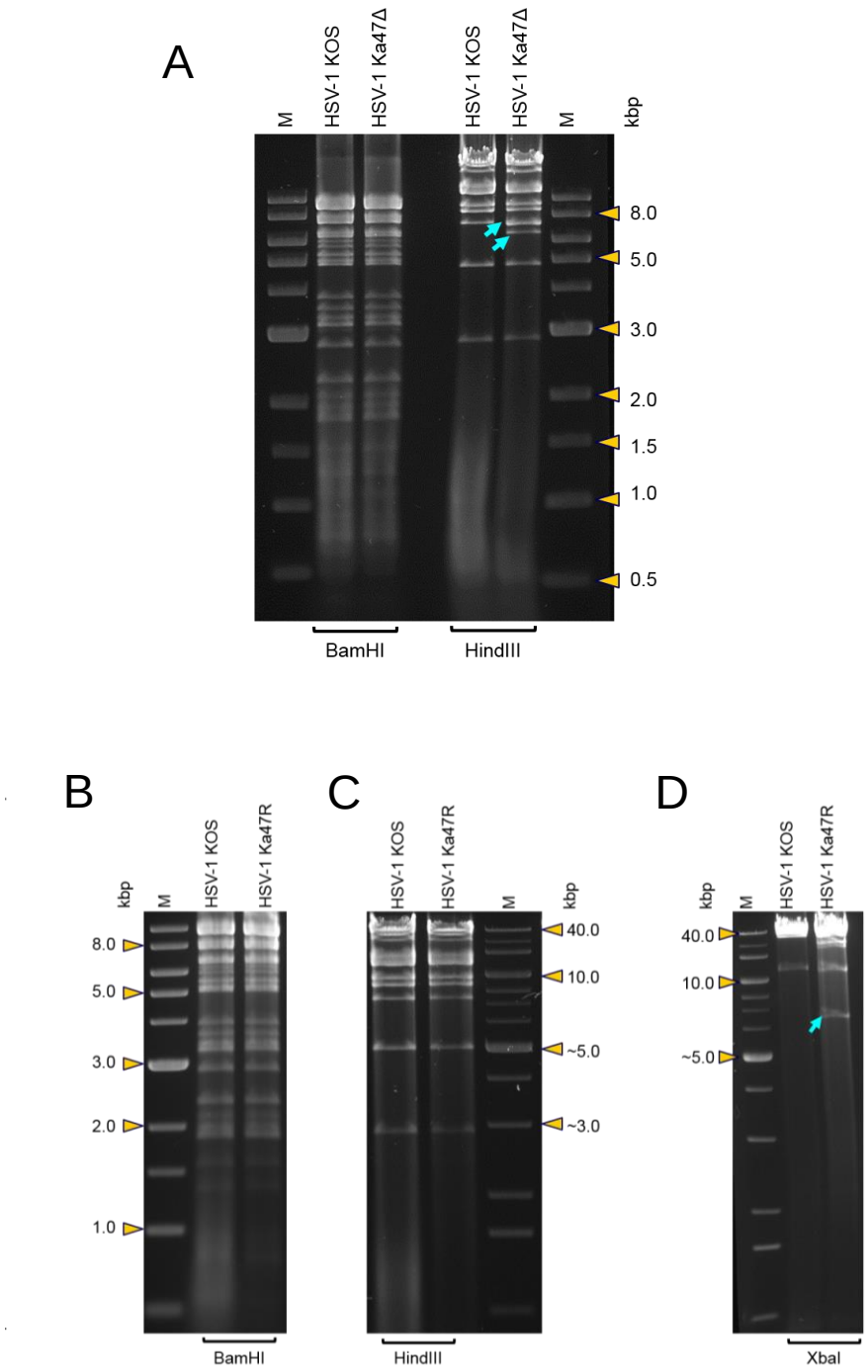

Figure 3.2 Characterisation of the recombinant viruses by RFLP analysis. (A) The genome of wild-type HSV-1 (strain KOS) and HSV-1 Ka47Δ were analysed by restriction digestion using enzymes BamHI or HindIII. (B) The wild-type HSV-1 and HSV-1 Ka47R DNA were analysed by restriction digestion using enzymes BamHI, HindIII or XbaI. Blue arrows in (A) and (D) indicate the characteristic DNA fragments that were obtained with the recombinant viruses but not with wild-type HSV-1. Yellow arrowheads indicate sizes of the relevant fragments of molecular markers.

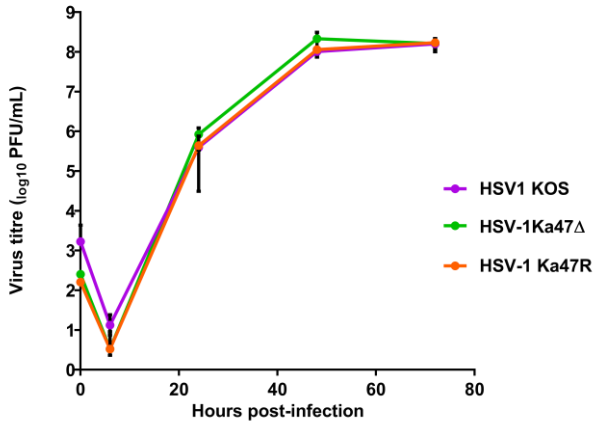

Figure 3.3 ICP47 does not affect virus replication *in vitro*. Vero cells were infected with the wild-type HSV-1, Ka47Δ or Ka47R at 0.01 pfu/cell. After adsorption for 1 hour, the media containing virus inoculum was removed and replaced with 2 mL of serum containing culture media. The virus was then harvested in the culture medium at indicated time points and virus titre was determined using a plaque assay on Vero monolayers. Data are from triplicate measurements and are expressed as mean ± standard deviation (SD) (error bars). In some cases, the error bars are obscured by the symbols.

3.2.2 Deletion of ICP47 has a major effect on down-regulation of MHC I in human, but not mouse cells

As ICP47 interferes with TAP-mediated peptide transport and prevents the translocation of fully assembled pMHC-I complexes to the cell surface, it has been reported that ICP47 down-modulates the overall surface MHC I in HSV-1 infected cells (York et al., 1994; Ahn et al., 1997). To functionally validate the ICP47 null mutant and the revertant viruses, the number of surface MHC I molecules were quantified on the infected cell surface using a flow-cytometry based indirect immunofluorescence assay. The assay was performed on 293KbC2 cells, a human fibroblast cell line that stably expresses mouse H-2K^b (Tscharke et al., 2005) and MC57G cells, a mouse fibroblast cell line derived initially from the C57BL/6 strain. These cell lines allowed us to quantify MHC I H-2K^b here, and later measure antigen presentation (see section 3.2.3). Briefly, quantification was done after infecting the cells with 5 pfu/cell of the recombinant or wild-type HSV-1 for 6 hours, followed by incubation with the anti-H-2K^b antibody (clone Y3) and then stained with F(ab')$_2$ fragment of FITC-conjugated goat anti-mouse antibody. Computation of total surface H-2K^b molecules is described in the methods section 2.3.9.1 and represented in Figure 2.2. Compared to the wild-type virus and the revertant viruses, the ability of Ka47Δ to induce down-regulation of MHC I was substantially attenuated in 293KbC2 cells (Figure 3.4 A, C & E). These data are consistent with our understanding since Ka47Δ does not produce ICP47, whereas a functional ICP47 protein is made from the revertant HSV-1 Ka47R. In MC57G cells, infection with ICP47 null mutant showed a slight increase in the level of MHC I compared to the wild-type and the revertant control, but the difference was not statistically significant (Figure 3.4 B, C & D). Together, our data show that ICP47 down-modulates surface MHC I in human but not in mouse cells, which is indeed consistent with previous findings. Because a substantial number of MHC I were detected on the surface of infected mouse cells, it appears as though ICP47 does not inhibit mouse TAP. However, measurement of the level of surface MHC I does not discriminate between the pMHC-I complexes that are newly assembled after infection and the pre-existing stable pMHC-I on the cell surface. Given that *a)* only about half of the K^b-bound peptides that reach the cell surface are stably presented for more than 20 hours (Su and Miller, 2001), and *b)* ICP47 has relatively weak binding affinity towards mouse TAP (Tomazin et al., 1998), it is possible that the impact of ICP47 on mouse TAP was not shown in its entirety using this assay. Thus, a more sensitive assay that measures the pMHC-I assembled after HSV-1 infection is required.

Figure 3.4 ICP47 down-regulates the surface MHC I on human cells but not on mouse cells. The 293KbC2 cells and MC57G cells were infected with 5 pfu/cell of appropriate HSV-1 for 6 hours followed by incubation with the anti-H-2K^b antibody (clone Y3). The cells were subsequently stained using the FITC conjugated goat anti-mouse secondary antibody and then analysed by flow-cytometry. The histograms show the fluorescence level on 293KbC2 (A) or MC57G cells (B) infected by the HSV-1 KOS, Ka47Δ or Ka47R. In the same flow cytometry experiment, calibration beads from the QIFIKIT were stained separately with the secondary antibody to calculate the specific antigen binding capacity (SABC), which reflects the absolute numbers of MHC I on the cell surface. (C) The data shown in the bar graph denotes the number of surface H-2K^b molecules per cell in MC57G and 293KbC2 cells under different conditions. The data from four independent experiments are shown. Error bars represent the mean ± SEM. (D and E) The scatter plots show the level of H-2K^b relative to mock-treated samples of MC57G (D) and 293KbC2 (E) cell lines. Data from four independent experiments are shown. Error bars represent the mean ± SD. The statistical significance was calculated using one-way ANOVA with Tukey's multiple comparison post-test. $^{**}p < 0.01$.

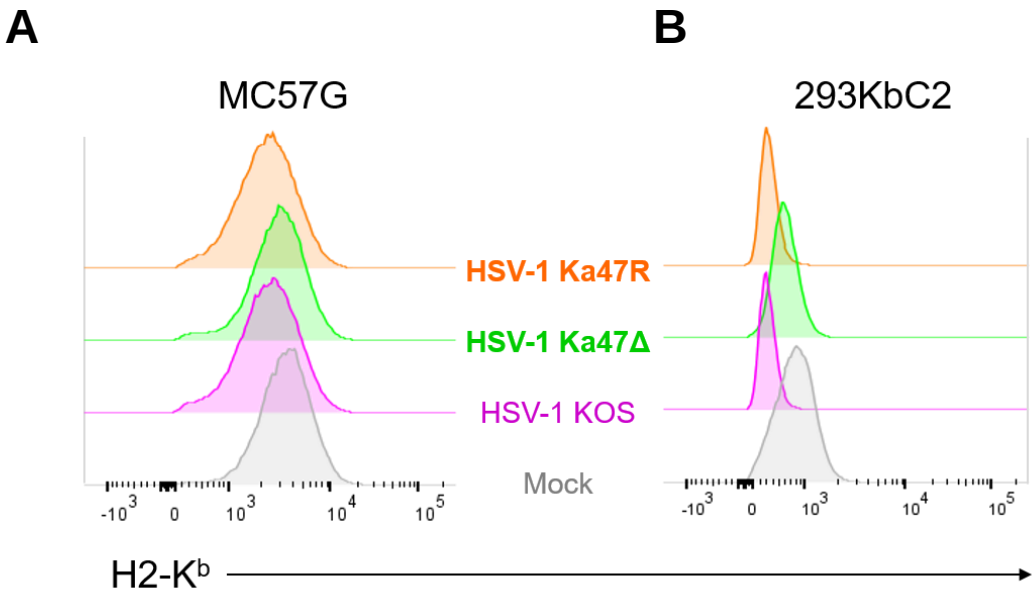
A
B
MC57G
293KbC2
HSV-1 Ka47R
HSV-1 Ka47Δ
HSV-1 KOS
Mock
H2-Kb

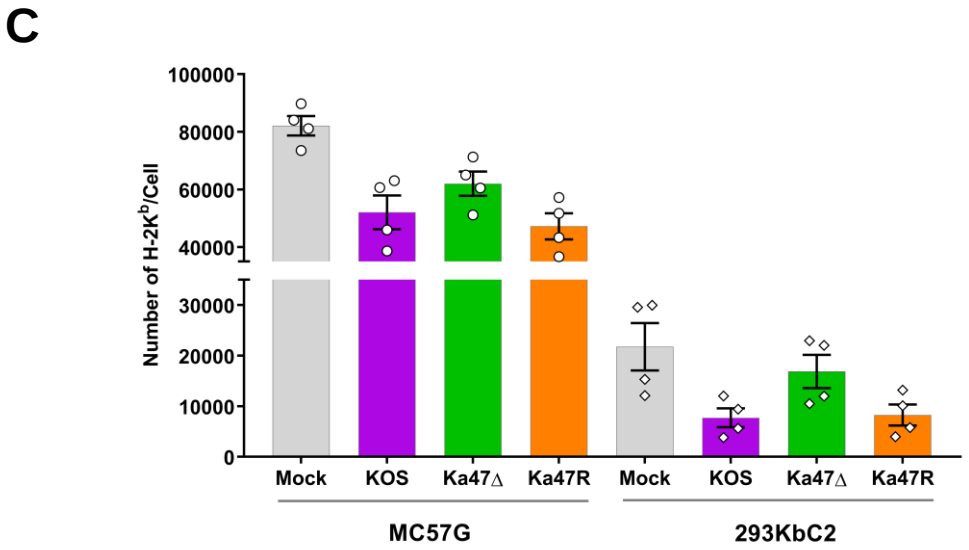
C
Number of H-2Kb/Cell
Mock
KOS
Ka47Δ
Ka47R
MC57G
293KbC2

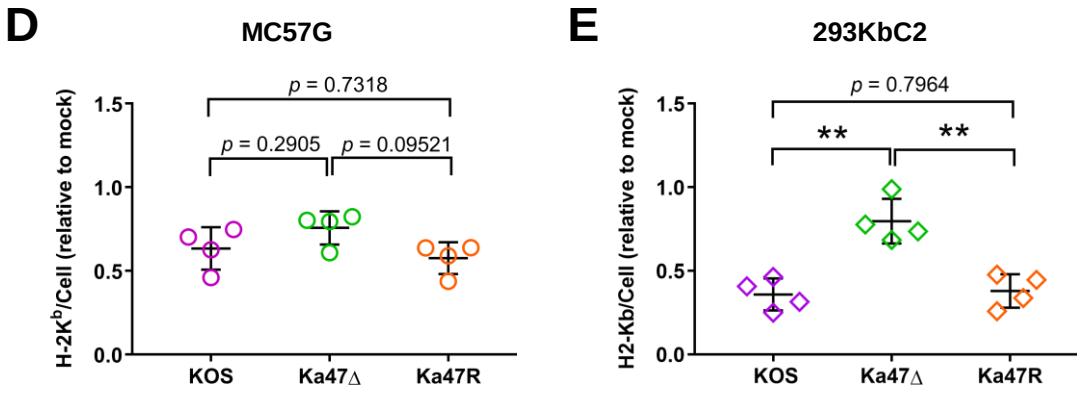
D
MC57G
H-2Kb/Cell (relative to mock)
p = 0.7318
p = 0.2905
p = 0.09521
KOS
Ka47Δ
Ka47R
E
293KbC2
H2-Kb/Cell (relative to mock)
p = 0.7964
**
**

3.2.3 ICP47 can inhibit TAP mediated antigen presentation effectively in mouse cells

To measure the presentation of pMHC-I newly made at the time of infection, we designed a novel antigen presentation assay (see materials and methods, section 2.3.9.2) (Figure 3.5). In this assay, the surface K^b-SIINFEKL complex was measured after super-infection of the HSV-1 infected cells with recombinant vaccinia virus (strain MVA) expressing ovalbumin peptide SIINFEKL, termed MVA mini OVA (Figure 3.5). The cells were infected with HSV-1 for three hours before infection by MVA mini OVA to ensure that ICP47 will be present when the SIINFEKL peptide is first translated. As a positive control, MVA ES mini OVA expressing SIINFEKL peptide fused with ER targeting signal was used for infection instead of MVA mini OVA. The SIINFEKL peptide produced by this virus will bypass TAP mediated translocation and directly enter the ER lumen, hence evading ICP47 influence on TAP. Recombinant MVA expressing influenza A virus (IAV) strain PR8 $PB1F2_{62\text{-}70}$ peptide, termed MVA mini Flu, was used as a negative control since the antibody used in this assay cannot detect MHC I K^b – $PB1F2_{62\text{-}70}$ peptide complex.

When 293KbC2 cells were infected with HSV-1 wild-type virus or revertant control and then super-infected with MVA mini OVA, the level of detection of H-$2K^b$–SIINFEKL complexes on the cell surface was similar to that of the cells super-infected with MVA mini Flu (Figure 3.6). In contrast, when the cells were infected with Ka47Δ and then MVA mini OVA, the surface K^b–SIINFEKL complexes were at a similar level to that of the Ka47Δ infected cells superinfected with MVA ES mini OVA (Figure 3.6). These data confirmed the presence of functional ICP47 in Ka47R and the lack of ICP47 in Ka47Δ. Expressing the data from our antigen presentation assay as fold increase in MFI over negative control allowed direct comparison of levels of K^b–SIINFEKL across viruses and cell types. Comparisons were made between the cells infected with HSV-1 KOS, Ka47 Δ and Ka47R, each superinfected with MVA mini OVA. In 293KbC2 cells, antigen presentation was significantly higher in the absence of ICP47 compared to the cells containing the functional protein (Figure 3.8 A). These data suggest that ICP47 significantly blocks the presentation of newly generated pMHC-I complex in human cells.

Interestingly, the level of antigen presentation in MC57G samples infected with HSV-1 KOS or Ka47R and MVA mini OVA was significantly lower compared to the ICP47 null virus and MVA mini OVA-infected cells (Figure 3.7 and Figure 3.8 B). This data

demonstrates that ICP47 can certainly impair antigen presentation in mouse cells. However, the level of MHC I K^b–SIINFEKL on HSV-1 KOS or Ka47R infected cells appeared considerably higher than the negative control (Figure 3.7 and Figure 3.8 B). Therefore, a direct comparison of the degree of inhibition exhibited by ICP47 between 293KbC2 and MC57G cell lines was made (Figure 3.8 C&D). The results show that the presence of ICP47 caused a significant reduction in the surface MHC I K^b–SIINFEKL complex in 293KbC2 cells compared to the mouse cells (Figure 3.8 C). However, no significant difference was observed between 293KbC2 and MC57G cells infected with Ka47Δ and MVA mini OVA (Figure 3.8 D).

Together, the above findings demonstrate that ICP47 can function in mouse cells, although to a lesser extent compared to human cells. These data suggest that the direct biochemical comparison of ICP47 binding to human and mouse TAP exaggerated the species difference and as a result, the potential impact of ICP47 in mice was underestimated. This later has borne out in the *in vivo* mouse studies.

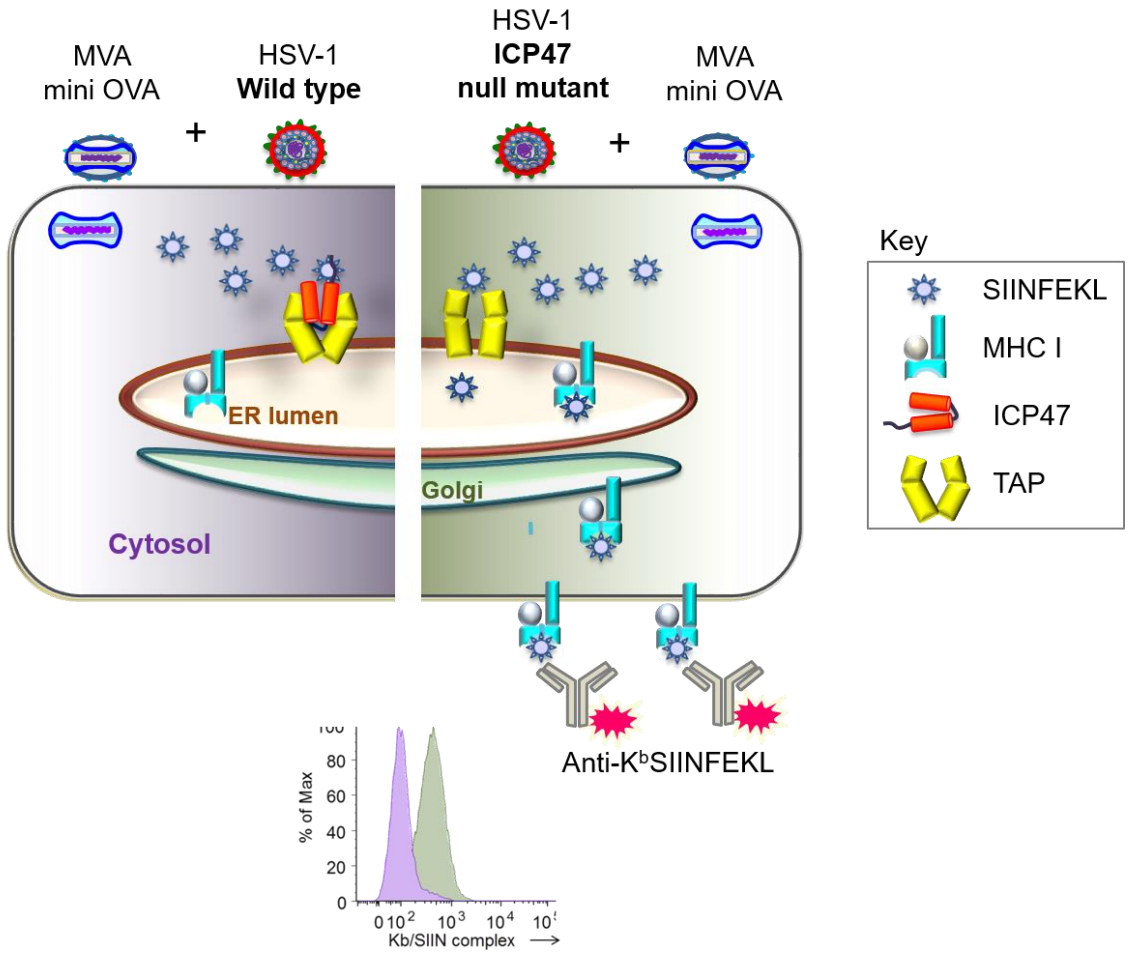

Figure 3.5 Diagrammatic representation of the antigen presentation assay to measure the inhibition of antigen presentation by ICP47. 293KbC2 or MC57G cells were infected with wild-type HSV-1, ICP47 null mutant or revertant virus at 10 pfu/cell for three hours, followed by infection of HSV-1 infected cells with MVA expressing mini OVA at 10 pfu/cell. After 6 hours, the cells were fixed and then stained using 25D.1.16 antibody. Fluorescence was later analysed using flow cytometry. Infection of a cell with wild-type HSV-1 would result in the synthesis of ICP47, which was expected to block TAP. During subsequent infection with MVA mini OVA, SIINFEKL peptides will be produced and in the absence of TAP function the peptides are expected to remain in the cytoplasm. This, in turn, will prevent the presentation of MHC I K^b-SIINFEKL complex on the cell surface. Conversely, the HSV-1 ICP47 null mutant will not be able to block the antigen presentation, which will be detected by specific antibody staining.

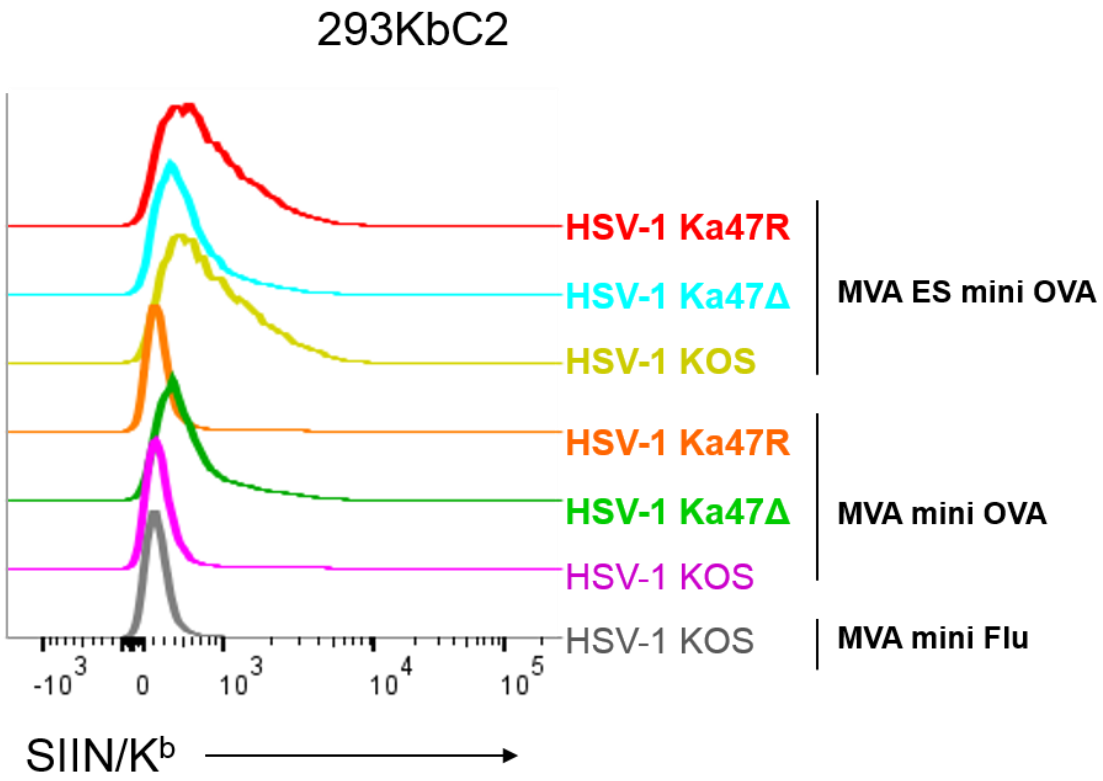

Figure 3.6 ICP47 blocks antigen presentation on human cells. The human cell line 293KbC2 was infected with HSV-1 KOS, Ka47Δ or Ka47R at 10 pfu/cell. After incubation for 3 hours, the cells were superinfected with MVA expressing OVA peptide SIINFEKL tagged to ER targeting signal (MVA ES mini OVA), MVA expressing SIINFEKL without the ER targeting signal (MVA mini OVA) or MVA expressing IAV PR8 PB1F2$_{62\text{-}70}$ (MVA mini Flu) at 10 pfu/cell for 6 hours. Then the cells surface expression of K^b-SIINFEKL complex was analysed using flow cytometry as described previously. The histograms show the level of fluorescence detected due to staining by APC conjugated antibody (clone 25D.1.16) as a measure of H-2K^b-SIINFEKL complex. The data are representative of five independent experiments.

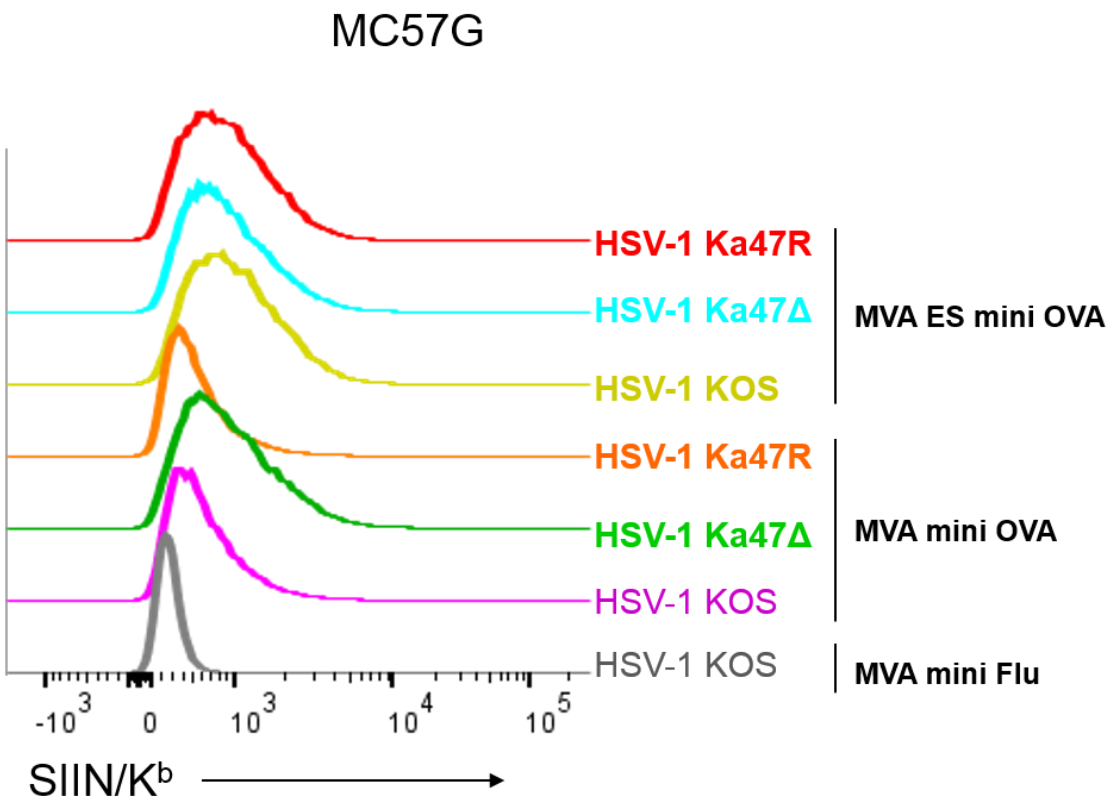

Figure 3.7 ICP47 blocks antigen presentation on mouse cells. The mouse cell line MC57G was infected with HSV-1 KOS, Ka47Δ or Ka47R at 10 pfu/cell. After incubation for 3 hours, the cells were superinfected with MVA expressing OVA peptide SIINFEKL tagged to ER-targeting signal sequence (MVA ES mini OVA), MVA expressing SIINFEKL without the targeting sequence (MVA mini OVA) or MVA expressing IAV PR8 $PB1F2_{62\text{-}70}$ (MVA mini Flu) at 10 pfu/cell for 6 hours. The cells surface expression of K^b-SIINFEKL complex was then analysed using flow cytometry as described previously. The histograms show the level of fluorescence detected due to staining by APC conjugated antibody (clone 25D.1.16) as a measure of H-$2K^b$-SIINFEKL complex. The data are representative of 4 independent experiments.

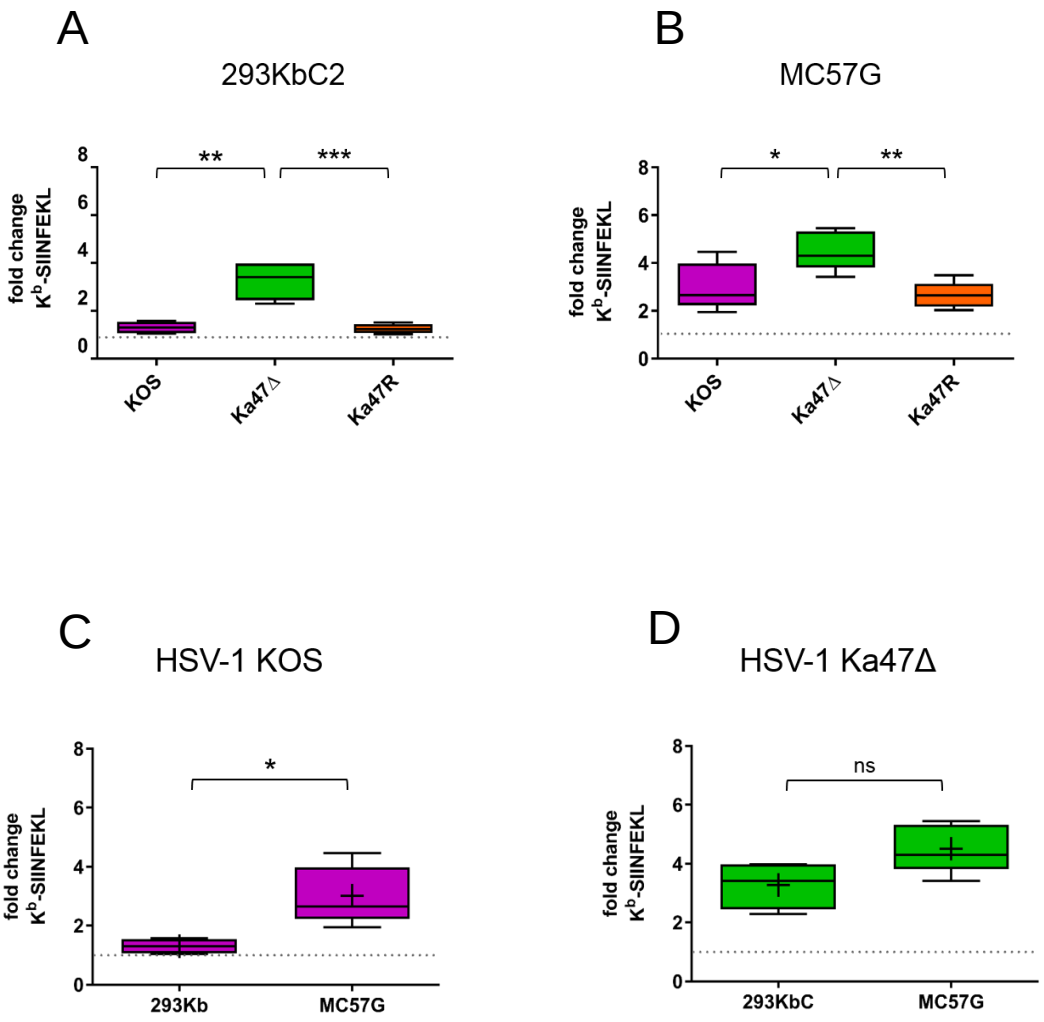

Figure 3.8 Quantification of cell surface expression of K^b-SIINFEKL complex in HSV-1 infected 293KbC2 and MC57G cells. (A) 293KbC2 and (B) MC57G cells were assessed for the cell surface expression of K^b-SIINFEKL complex using an antigen presentation assay. The cells were infected with HSV-1 KOS, Ka47Δ or Ka47R and superinfected with MVA mini OVA as described previously. The cells infected with HSV-1 KOS and superinfected with MVA mini Flu was used as the negative control. The fold change in mean fluorescence intensity (MFI) relative to the negative control is shown for indicated cell lines as a box-and-whisker plot. Statistical significance was calculated by comparing means using one-way ANOVA with Tukey's multiple comparisons test (***p<0.001, **p<0.01, *p<0.05). C and D show a comparison of K^b-SIINFEKL presentation between the human cell line (293KbC2) and the mouse cell line (MC57G) for indicated viruses. Box plots show the median (horizontal line) and the interquartile range; whiskers indicate the minimum and maximum values. The dashed line shows the baseline of detection. Statistical significance was calculated by comparing means using unpaired t-test with Welch's correction (***p<0.001, **p<0.01, *p<0.05) and ns indicates that the data are not significantly different. Error bars represent standard deviation (n = 4 to 5).

3.2.4 Does inhibition of antigen presentation by ICP47 affect HSV-1 infection in mice?

Our antigen presentation assay revealed that ICP47 inhibit TAP-mediated peptide presentation in mouse cells. However, the biological implication of this inhibition in mice *in vivo* during HSV infection is not fully known. To investigate the role of ICP47 during different stages of HSV-1 infection, we compared the viral pathogenesis, establishment of latency, stability of latency and reactivation of ICP47 null mutant viruses using a mouse flank infection model.

The zosteriform model otherwise called the flank infection model typically involves scarification of depilated skin on the mouse flank, followed by infection using a defined amount of virus (Blyth et al., 1984; Simmons and Nash, 1984). As the virus is unable to penetrate intact skin, a productive infection necessitates physical trauma induced to the skin (Blyth et al., 1984). Instead of scarifying the skin, we introduce the virus by tattooing it on the mouse flank (Russell and Tscharke, 2016). Our modified method leaves no visible mark on the skin immediately after tattooing and a lesion starts developing as early as two days post infection at the site of initial infection. After infection of the skin, the virus travels to the sensory neurons of the dorsal root ganglia (DRG), where it undergoes brief replication and spread before returning to the skin of the same neurodermatome. As a result, approximately four days after inoculation of the virus, a series of secondary lesions develop which progresses to a vesicular ulcerous band in the corresponding dermatome (Figure 3.9). The appearance of the lesion is similar to that typical of herpes zoster, hence the name "zosteriform" being used to describe the model.

Flank infection models have been previously utilised to show the critical importance of $CD8^+$ T cell immunity to HSV-1 infection by curtailing acute infection of the nervous system (Simmons and Nash, 1984; Simmons and Tscharke, 1992). Furthermore, employing a flank infection model to track promoter activation in ROSA26R mice has previously provided novel insights into the promoter activity that occurs during latency and a better understanding of the fate of neurons after lytic infection (Proença et al., 2008, 2011; Russell and Tscharke, 2016).

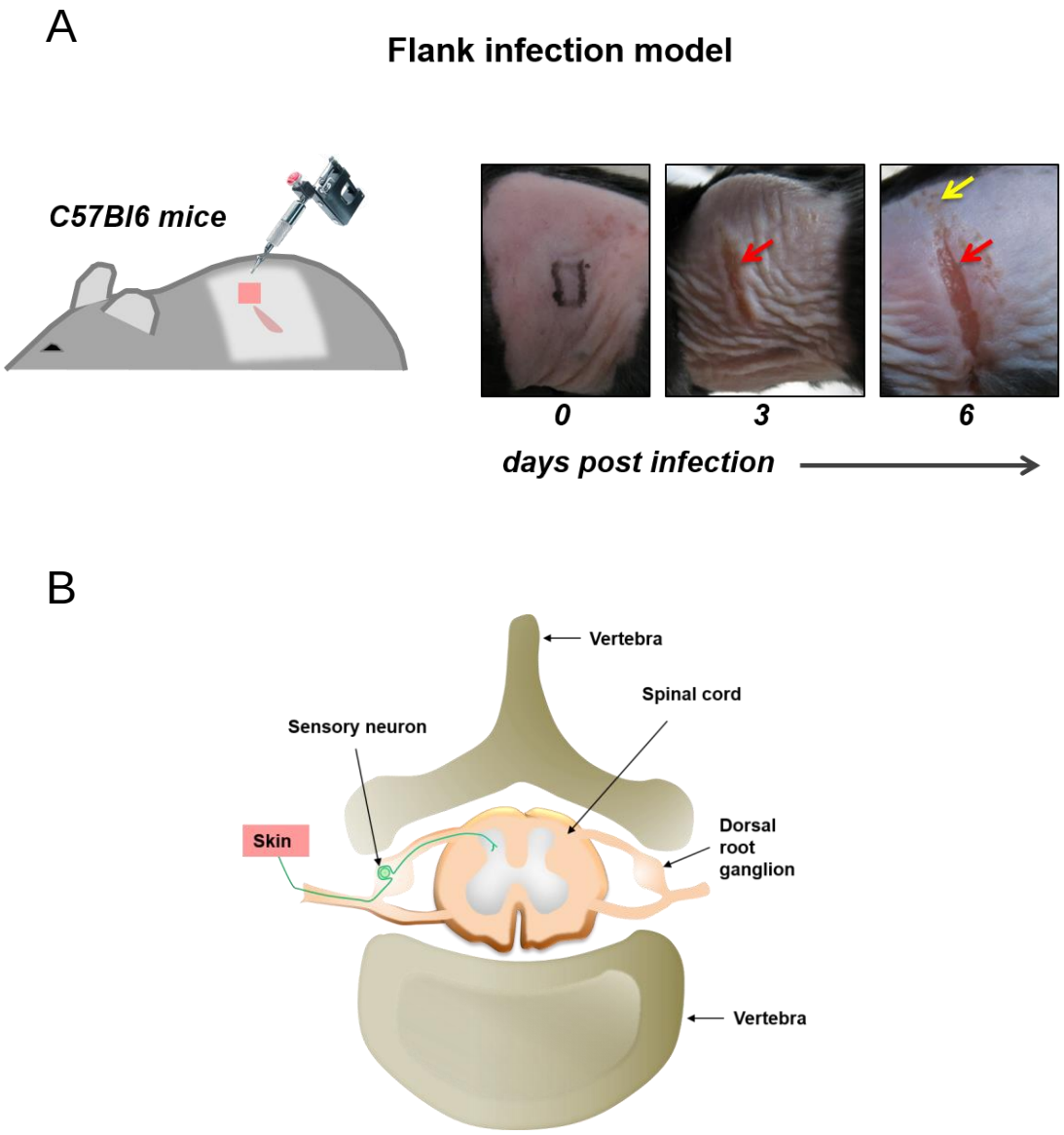

Figure 3.9. Flank infection model. The virus was tattoo infected on to the skin of mice. The virus replicates in the skin and some virus enters the innervating nerve fibres, and travels in a retrograde direction to the neuronal cell body in the DRG. The virus after replicating in the DRG travels back in the anterograde direction to the skin resulting in the secondary skin lesion. (A) The tip of the spleen visualised through the skin is used to position the site of tattoo infection. The progression of the infection-induced lesion is shown. A primary lesion begins to appear from two days and the secondary lesion starts to emerge from four days after infection. Red arrows indicate the primary lesion and the yellow arrow shows the secondary lesion on designated days after infection. (B) The diagrammatic representation of the anatomical location of dorsal root ganglion.

3.2.4.1 Severity and resolution of lesions are independent of ICP47 expression

The flank infection model is ideal for tracking the progression of infection by measuring virus titre in the primary and secondary infection sites on the skin and the ganglia in addition to monitoring skin lesion size. Age and sex-matched mice were infected with wild-type HSV-1, ICP47 null mutant (Ka47Δ) or the revertant (Ka47R) virus. A zosteriform lesion was observed on all mice infected in all groups between days four and five after infection, and the lesions resolved in all infected groups by day 14. As shown in (Figure 3.10 A), the lesion size was comparable between the ICP47 null mutant and the control viruses. Mice never progressed beyond a clinical score of three (see materials and methods, Table 2.9) and remained healthy throughout the experiment.

3.2.4.2 ICP47 does not alter virus replication in mice

It had been previously shown using a flank infection model that the level of infectious virus is at its peak four days post infection and replication is curtailed after seven days of infection in both the skin and the DRG of HSV-1 infected mice (Speck and Simmons, 1998; van Lint et al., 2004a). Coinciding with the cessation of virus replication, activated $CD8^+$ T cells infiltrate both the initial infection site and DRG as early as five days after infection on the flank of mice (van Lint et al., 2005).

Infection of mice with the ICP47 null virus, in theory, allows increased antigen presentation, which might lead to more rapid and efficient clearance of the infectious virus by HSV specific $CD8^+$ T cells. We tested this hypothesis by measuring the levels of infectious virus in the homogenates of skin and DRG of mice at four and six days after infection using plaque assay (Figure 3.10 B & C). No difference in virus titre was expected on day 4, but on day 6 a decrease in virus titre was expected for Ka47Δ-infected mice, based on the kinetics of $CD8^+$ T cell infiltration at the infection site. However, the amount of virus in skin and DRG were similar among cohorts of mice infected with wild-type, ICP47 null mutant (Ka47Δ) and the revertant (Ka47R) virus at the two time points. These findings show that the loss of ICP47 function neither affects virus replication in infected tissues in mice nor supports early clearance of the virus.

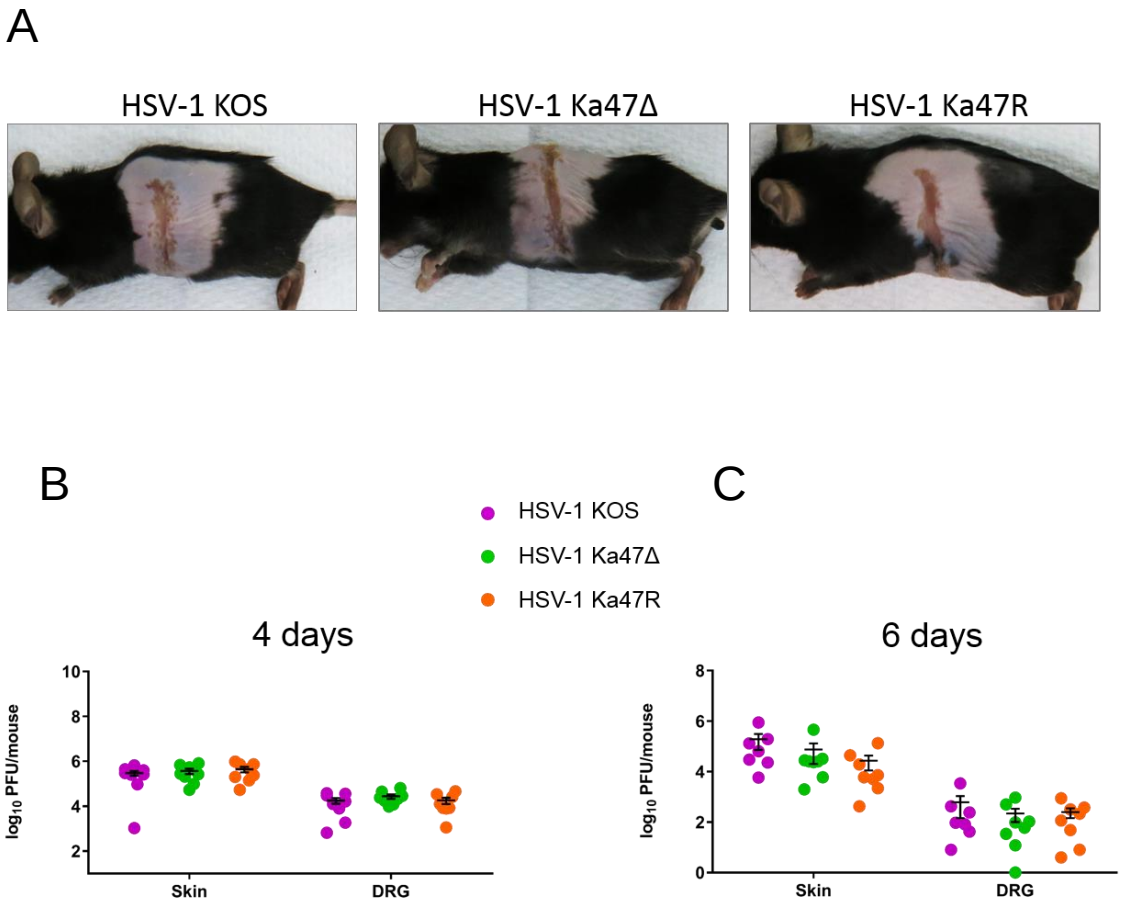

Figure 3.10 ICP47 does not affect the severity of skin lesion or virus replication in mice. (A) Groups of mice were tattoo infected with HSV-1 KOS, HSV-1 Ka47Δ or HSV-1 Ka47R and lesion development was monitored over several days until resolved. Shown are the representative images of skin lesion taken seven days post-infection. (B and D) In another experiment, the virus titre in skin and DRG was measured four days after infection (B) and six days after infection (C). The data shown are pooled from two independent experiments with n=3-4 for each group. Each symbol represents the virus titre in one mouse and the error bars represent mean ± SEM. The means of virus titre were compared between the groups using one-way ANOVA with Tukey's multiple comparison post-test. No statistically significant differences were found between the three viruses at any time or site.

3.2.4.3 ICP47 does not affect the size of CD8$^+$ T cell response in mice infected with HSV-1

Considering that CD8$^+$ T cell response is vital for the clearance of the acute HSV-1 infection, we examined whether lack of ICP47 mediated inhibition of antigen presentation can influence the total HSV-1 specific CD8$^+$ T cell response. The $gB_{498\text{-}505}$ peptide-specific CD8$^+$ T cell accumulation in the spleen was monitored from 5 days to 9 days after flank infection of C57BL/6 mice with HSV-1 strain KOS. Consistent to previous studies (Coles et al., 2002), we found that the proportion of $gB_{498\text{-}505}$ peptide-specific CD8$^+$ T cells in spleen reached a maximum on 8 days after infection and fell considerably afterward (Figure 3.11 A). Next, the size of splenic CD8$^+$ T cell response to the immunogenic HSV-1 peptides $gB_{498\text{-}505}$, $RR1_{822\text{-}829}$, $ICP8_{171\text{-}178}$ and $UL28_{629\text{-}637}$ was determined 7 days after infection with HSV-1 KOS, Ka47Δ or Ka47R (Figure 3.11 B). No statistically significant difference was observed between the groups of mice infected with the virus lacking ICP47 and the control viruses suggesting that ICP47 does not hinder the generation of CD8$^+$ T cell responses to HSV infection in mice.

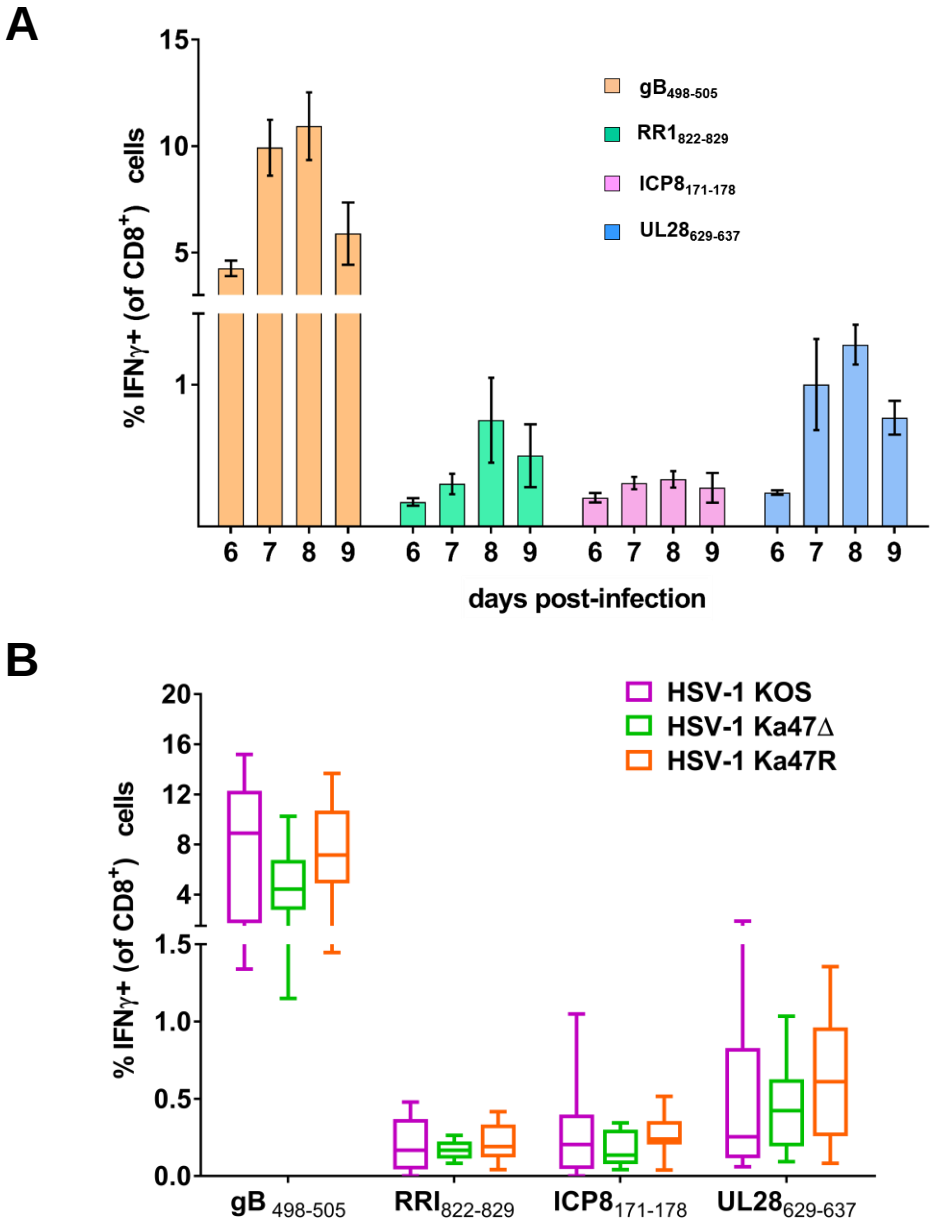

Figure 3.11 Peptide-specific CD8$^+$ T cell response to HSV-1 infection is not increased in the absence of the TAP-inhibitor, ICP47. (A) Groups of 5 mice were infected with HSV-1 KOS. On indicated days after infection, splenocytes were dispersed into single cell suspension and stimulated using immunogenic HSV-1 peptides for 4 hours, followed by surface staining for CD8$^+$ T cells and intracellular staining for IFNγ. Bars represent the mean ± SEM percentage of CD8$^+$ T cells that secrete IFNγ (B) Groups of three mice were infected with HSV-1 KOS, HSV-1 Ka47Δ or HSV-1 Ka47R. The percentage of IFNγ$^+$ CD8$^+$ T cells in spleen after stimulation by immunogenic HSV-1 peptides on day 7 post-infection is shown. The experiment was repeated four times and the pooled data are shown in box and whiskers plot. Box plots show the median (horizontal line) and the interquartile range; whiskers indicate the minimum and maximum values. The means were compared by two-way ANOVA and Tukey's multiple comparison post-test. The difference between the groups was not statistically significant.

3.2.4.4 Does ICP47 affect the establishment or maintenance of latency in mice?

Previously, Russell and Tscharke (2016) had found that the number of neurons marked by ICP47 promoter increased swiftly from 10 to 20 days after infection. Further, a continued increase in the marking from 20 to 100 days was observed, which suggests that some neurons had experienced ICP47 expression during the establishment of latency and during latency (Russell and Tscharke, 2016). Further, our finding that ICP47 can reduce antigen presentation in mouse cells has opened questions such as a) whether the ICP47 expression in neurons promotes the establishment of latency?, b) whether ICP47 expression helps in the spread of the virus?, c) does ICP47 affect the stability of latency?, and d) what is the fate of neurons that do not express ICP47? To answer the above questions, I generated two sets of Cre expressing ICP47 null mutant and control viruses, which were used to infect ROSA26R reporter mouse followed by analysis of neuronal marking.

3.2.4.4.1 Generation and characterisation of Cre recombinase encoding ICP47 null mutant and control viruses

To study the overall effect of ICP47 on infected neurons, an ICP47 null mutant was constructed on the HSV-1 pC_eGC background, which is a recombinant virus that expresses an eGFP-Cre fusion gene driven by a CMV IE promoter in UL3-UL4 region (Ma et al., 2014; Russell and Tscharke, 2016). The resultant virus was named HSV-1 GKa47Δ. A revertant virus, called HSV-1 GKa47R, capable of expressing ICP47 was later generated from HSV-1 GKa47Δ. Therefore, both HSV-1 GKa47Δ and GKa47R can express Cre controlled by the CMV IE promoter (Figure 3.12). The strategy used for generating the above viruses was identical to that used for constructing Ka47Δ and Ka47R, respectively (see section 3.2.1).

To investigate the effect of ICP47 on the fate of those neurons that express ICP47, a null virus encoding an eGFP-Cre fusion protein under the control of the native ICP47 promoter was generated by replacing the ICP47 coding sequence with eGFP-Cre. This virus was named Ka47inΔ. The ICP47 gene was rescued in Ka47inΔ background by inserting an ICP47 gene cassette into the intergenic region between UL26 and UL27 and the resultant virus was named HSV-1 Ka47rescue. In Ka47rescue, a minimal ICP47 promoter previously characterised by Russell and Tscharke (2016) was used to control the expression of ICP47. This modification in the ICP47 promoter was shown not to affect the kinetic class or gene expression in the previous study (Russell and Tscharke, 2016). Of

note, Ka47rescue also expresses eGFP-Cre from ICP47 regions similar to the parent virus Ka47inΔ. Schematic representation of ICP47 insertion-deletion mutant and the control rescuant virus is shown in Figure 3.14 A&B. The Cre-expressing recombinant HSV-1 viruses generated for this chapter is listed in Table 3.1.

The genomic structure of all recombinants was confirmed by PCR and restriction enzyme digestion analysis as shown in Figure 3.13 and Figure 3.15. The sequence modification introduced in the recombinants did not affect their replication and growth kinetics *in vitro* (Figure 3.16). The recombinant viruses were functionally characterised by using the antigen presentation assay described in section 3.2.3. Our antigen presentation assay showed that in 293KbC2 cells, GKa47Δ and Ka47inΔ allowed the presentation of SIINFEKL from MVA mini OVA to a level similar to that of presentation from MVA ES mini OVA (Figure 3.17 A&B) suggesting that these recombinant viruses do not express functional ICP47. In contrast, the revertant GKa47R and the rescuant Ka47rescue inhibited the presentation to levels similar to that of the wild-type virus (Figure 3.17 A&B), confirming the expression of functional ICP47 in these cells.

In mice, the amount of viruses found in the skin and DRG during the acute phase of infection were comparable between the recombinant viruses and the wild-type strain KOS (Figure 3.18 A&B). Likewise, the lesion induced by flank infection was resolved in both recombinant and the parent viruses almost at a similar rate (data not shown). An explant reactivation assay indicated that all recombinant viruses generated in this study were able to reactivate from latency (Figure 3.19). These data suggest that the recombinant viruses are phenotypically similar to the wild-type virus, confirming the previous observation that ICP47 deficiency does not affect the replication and pathogenesis of the virus *in vivo*.

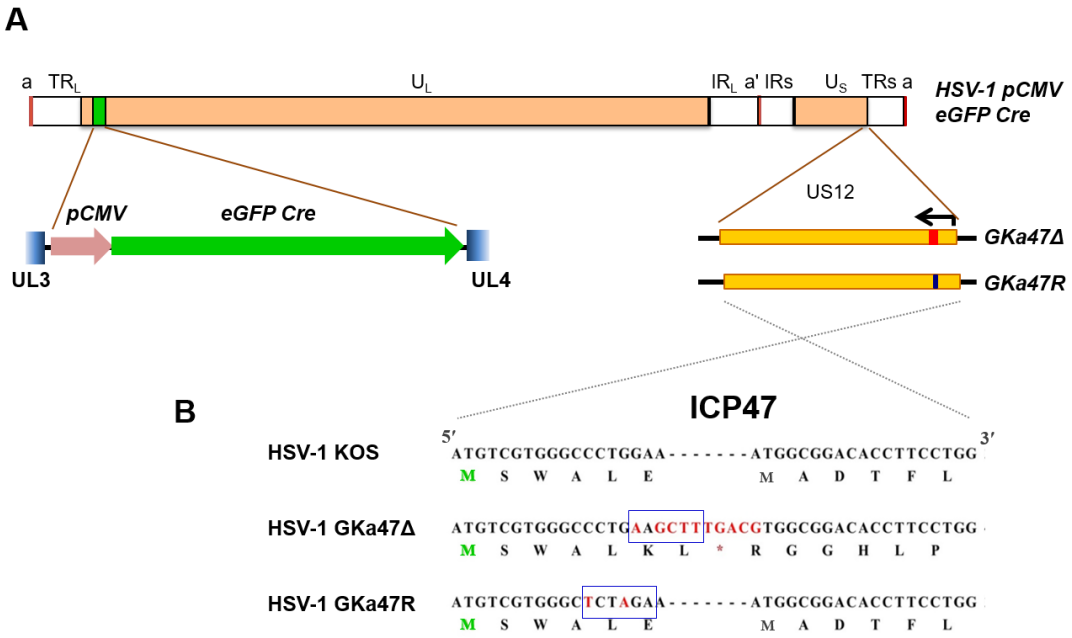

Figure 3.12 Schematic representation of ICP47 null mutant and revertant viruses that express eGFP-Cre driven by the constitutive CMV IE promoter. (A) Diagram of HSV-1 pCMV eGFP-Cre genome with the location of eGFP-Cre expression cassette in the UL segment is indicated. The position of US12 gene in the US segment of the genome is also indicated in the diagram. The arrow points to the orientation of the gene. In HSV-1 GKa47Δ, a stop codon was introduced upstream of AUG start codon shown in red bar and in HSV-1 GKa47R, the blue bar represents silent substitutions used to create a restriction enzyme recognition site. These modifications are the same as made on the wild-type KOS to generate Ka47Δ and Ka47R. (B) Sequence alignment of a relevant ICP47 region of HSV-1 KOS, HSV-1 GKa47Δ and HSV-1 GKa47R is shown. The modified nucleotides are indicated in red, and the gaps are shown in dashes. HindIII recognition sequence in GKa47Δ and XbaI recognition sequence in GKa47R are represented by the blue boxes. Amino acid sequence translation is provided immediately below the nucleotide sequence. Here, the asterisk symbol represents the stop codon.

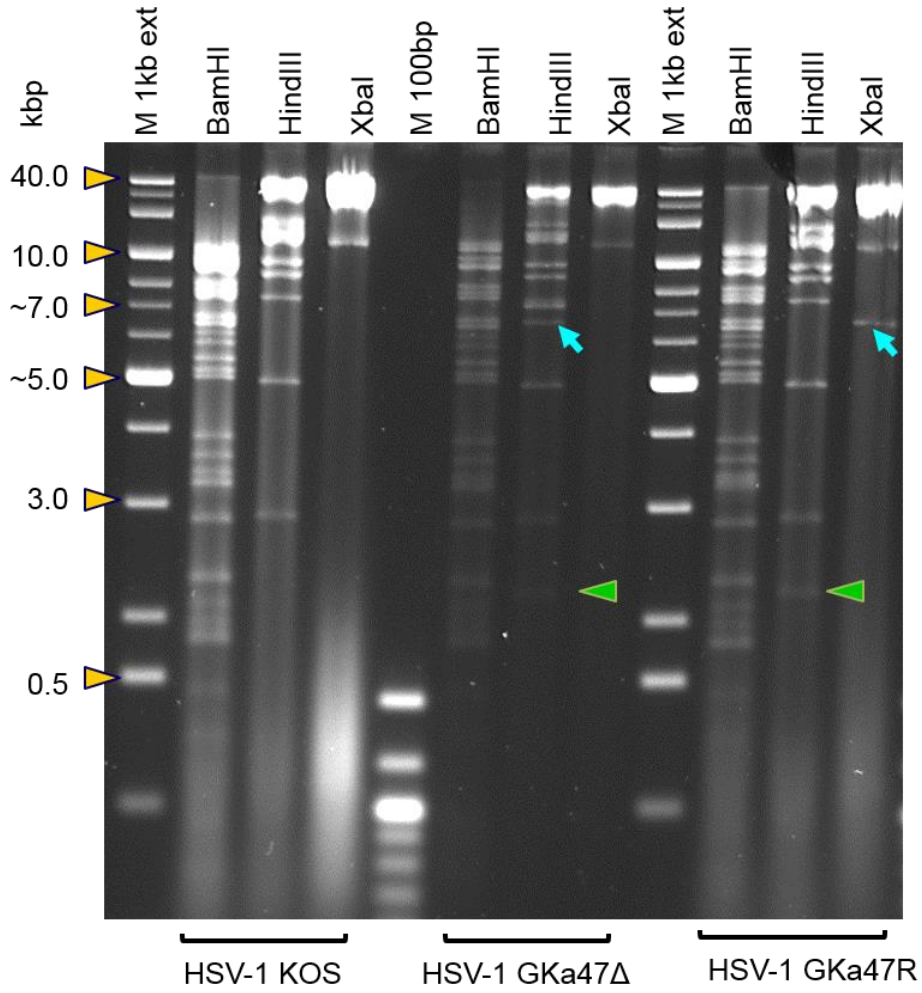

Figure 3.13 Characterisation of the recombinant viruses by RFLP analysis. The genome of wild-type HSV-1 (strain KOS), HSV-1 GKa47Δ and GKa47R were analysed by restriction digestion using enzymes BamHI, HindIII and XbaI. Blue arrows indicate the characteristic DNA fragments that were obtained due to the introduction of recognition sites for HindIII or XbaI in the genome of the recombinant viruses but not in the wild-type HSV-1. Green arrowheads indicate the DNA fragment generated from the cleavage of the pCMV IE eGFP-Cre cassette. Yellow arrowheads indicate sizes of the relevant fragment of the molecular markers.

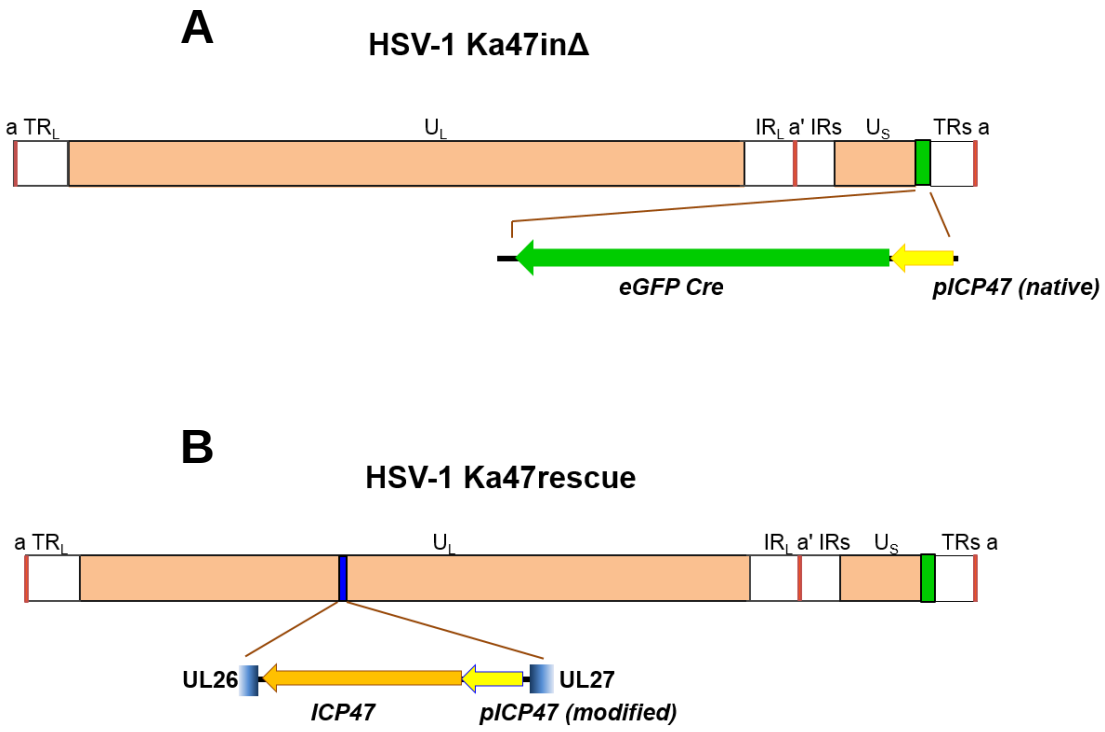

Figure 3.14 Schematic overview of recombinant ICP47 null mutant and rescuant viruses expressing eGFP-Cre controlled by the ICP47 promoter. (A) The depiction of the ICP47 null mutant is shown. The top line represents the prototypic arrangement of the HSV genome, with the green line representing the region of eGFP Cre polyA cassette inserted into the genome. Shown below is the expanded genomic region showing the location of insertion of the fusion gene. In the Ka47inΔ, the first 19 bp from the 5′ region of the ICP47 coding sequence was deleted and replaced by eGFP-Cre fusion gene with BGH polyA termination signal. (B) The depiction of the ICP47 rescuant virus is shown. The top line represents the HSV-1 Ka47rescue genome with the location of eGFP-Cre fusion gene indicated by the green line and the position of rescued ICP47 gene indicated by the blue line. Shown below is the expanded region of the ICP47 gene cassette containing ICP47 coding sequence followed by SV40 polyA termination signal controlled by the modified ICP47 promoter.

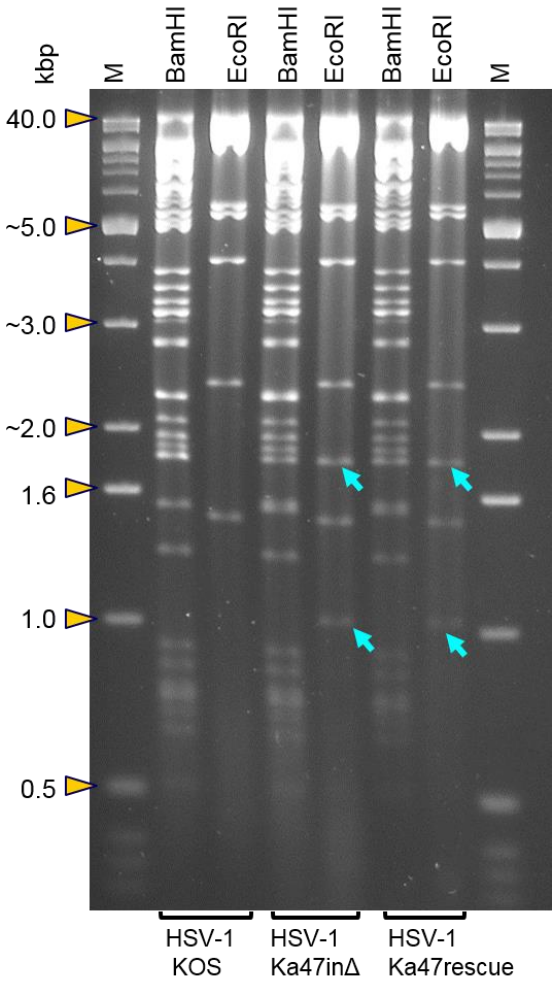

Figure 3.15 Analysis of genomic DNA from the recombinant viruses HSV-1 Ka47inΔ and HSV-1 Ka47rescue by RFLP. DNA from the recombinant viruses was isolated and digested with BamHI or EcoRI and electrophoresed on an agarose gel. There are two EcoRI recognition sequences in the eGFP Cre polyA cassette. Blue arrows indicate the characteristic DNA fragments that were obtained after restriction digestion with EcoRI. Yellow arrowheads indicate sizes of the relevant fragment of the molecular markers.

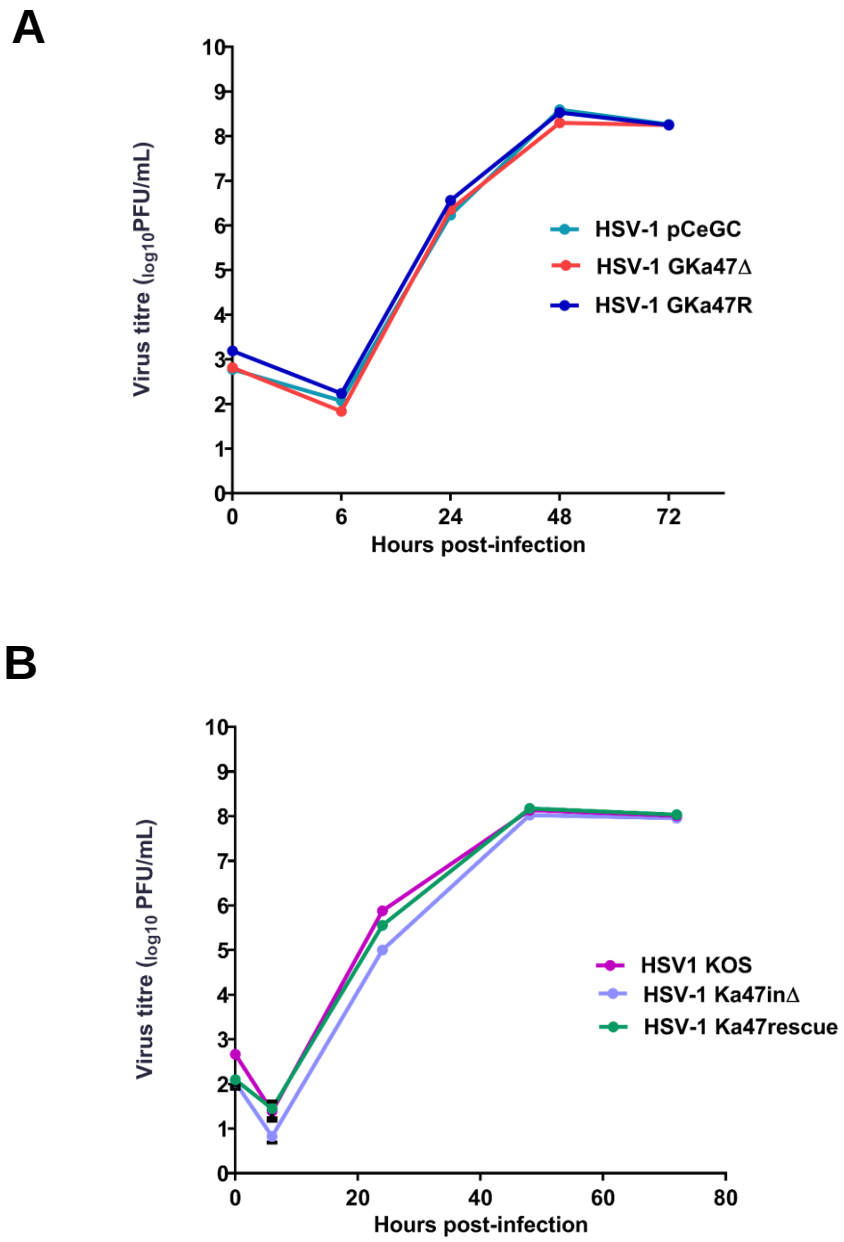

Figure 3.16 *In vitro* growth properties of parental and recombinant viruses. Vero cells were infected with the indicated viruses at 0.01 pfu/cell. After adsorption for 1 hour, the virus inoculum was removed and replaced with FBS-containing medium. The cells were then harvested in the culture medium at indicated time points and virus titre was determined by plaque assay. Comparisons were made between the recombinant viruses and their respective parental viruses. Data are from triplicate measurements and are expressed as mean ± SD (error bars). In some cases, the error bars are obscured by symbols showing means.

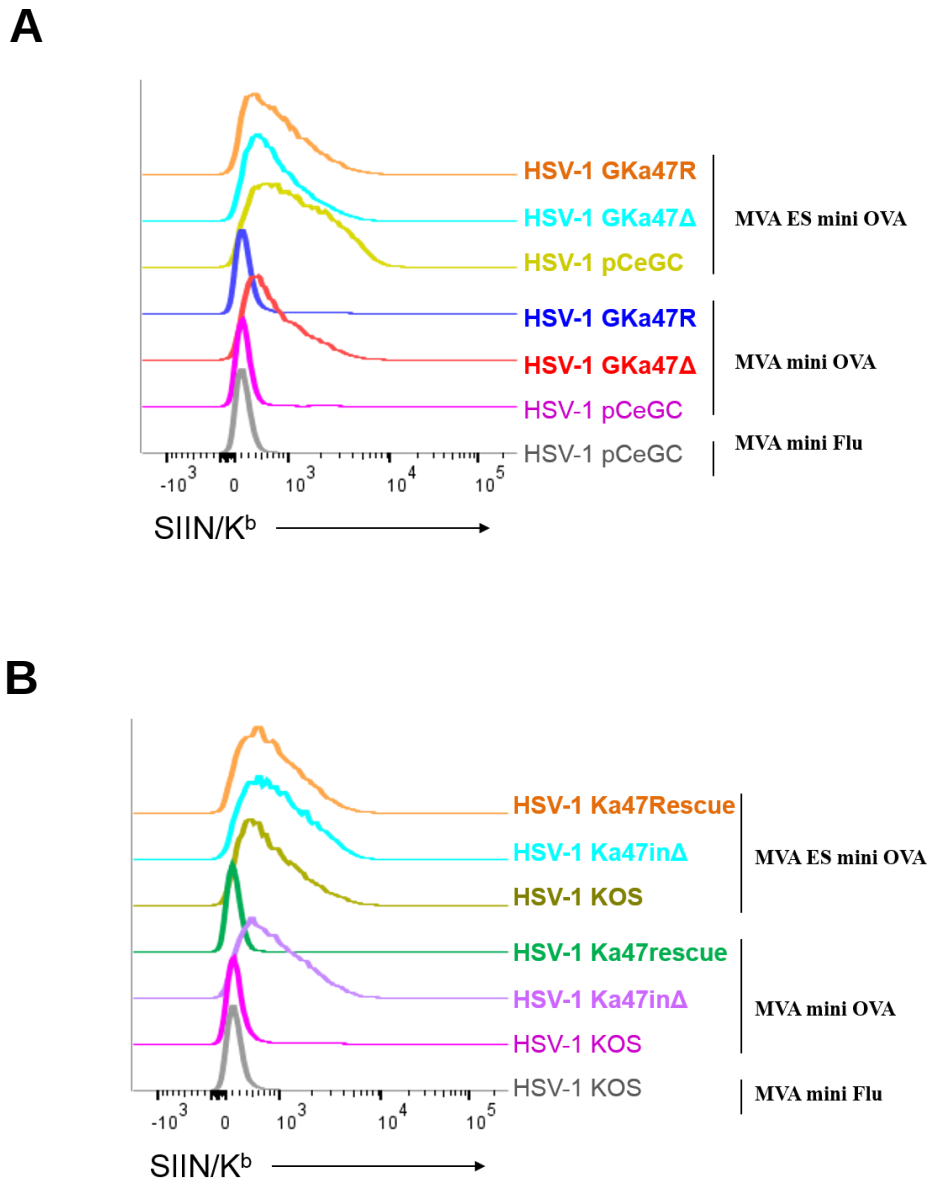

Figure 3.17 Verification of recombinant viruses using antigen presentation assay. The human cell line 293KbC2 was infected with the wild-type HSV-1 or indicated recombinant viruses at 10 pfu/cell. After incubation for 3 hours, the cells were superinfected with MVA expressing OVA peptide SIINFEKL tagged to ER-targeting signal sequence (MVA ES mini OVA), MVA expressing SIINFEKL without the targeting sequence (MVA mini OVA) or MVA expressing Flu peptide (MVA mini Flu) at 10 pfu/cell for 6 hours. Then the cells surface expression of K^b-SIINFEKL complex was analysed using flow-cytometry. (A and B) Histograms of K^b-SIINFEKL complex detected by APC conjugated primary anti- K^b-SIINFEKL –mAb (clone 25D.1.16) on infected cells is shown.

Table 3.1 List of recombinant HSV-1 to assess the influence of ICP47 using ROSA26R/Cre reporter system

Recombinant HSV-1	ICP47		Promoter driving eGFP-Cre	Location of eGFP-Cre
	+/−	*Location*		
GKa47Δ	−	NA	CMV IE	Between UL3 and UL4
GKa47R	+	Native position	CMV IE	Between UL3 and UL4
Ka47inΔ	−	NA	Native ICP47 promoter	ICP47 gene locus
Ka47rescue	+	Between UL26 and UL27	Native ICP47 promoter	ICP47 gene locus

Note:
+ ICP47 gene encode a functional protein
− ICP47 gene does not encode a functional protein
NA – Not applicable

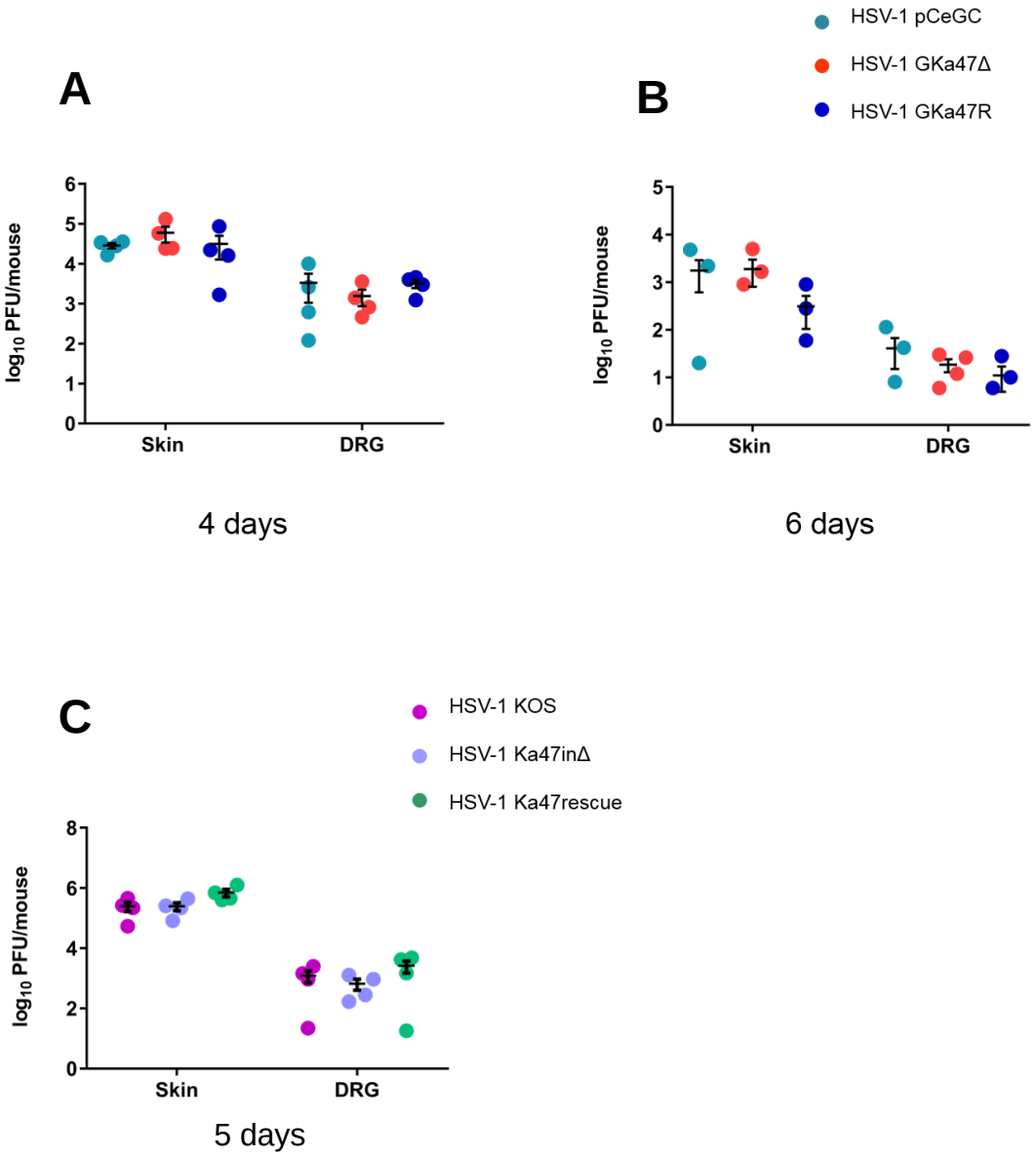

Figure 3.18 *In vivo* growth characteristics of Cre expressing ICP47 null mutant and control viruses. To test the *in vivo* growth characteristics of recombinant viruses, groups of mice were infected with the indicated viruses and virus titres were determined from skin and DRG by plaque assay. The amount of virus found in skin and DRG were comparable between mice infected with HSV-1 pCeGC, HSV-1 GKa47Δ and HSV-1 GKa47R both after 4 days (A) and after 6 days (B) of infection. Similarly, comparison of the average virus titre after 5 days of infection between mice infected with wild-type (KOS), HSV-1 Ka47inΔ, HSV-1 Ka47rescue shows no statistically significant difference (C). Each symbol represents virus titre in a single mouse and error bars represent mean ± SEM for 4 mice per time point. The means were tested by one-way ANOVA with Tukey's multiple comparisons post-test and no groups were found to be statistically significant.

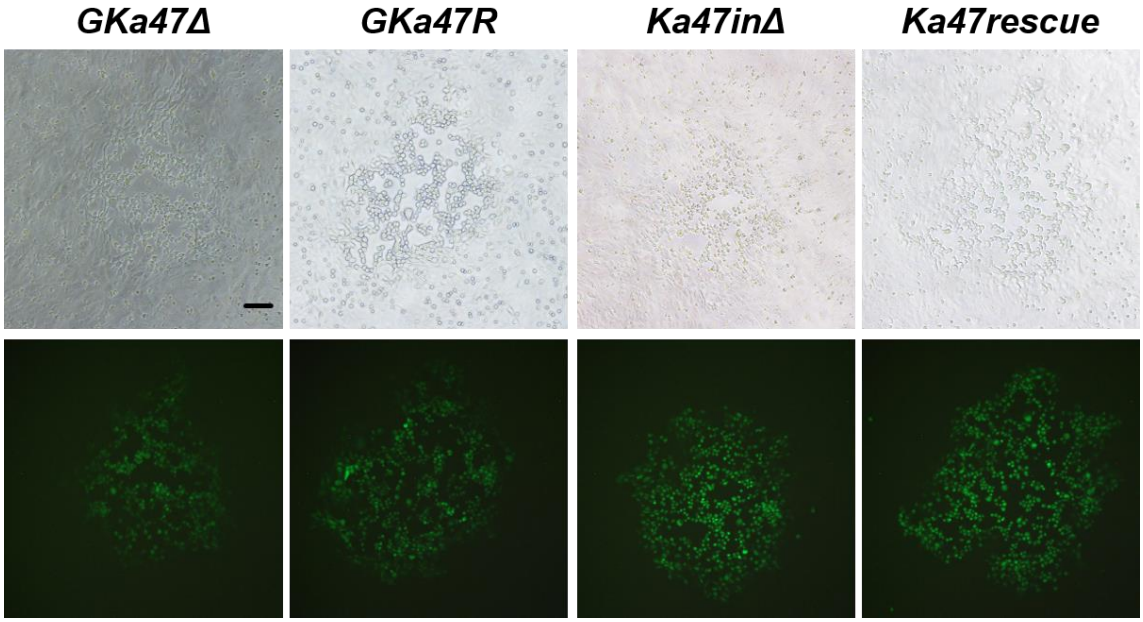

Figure 3.19 Reactivation of Cre expressing ICP47 null mutant and control viruses in explanted DRG. Mice infected with the GKa47Δ, GKa47R, Ka47inΔ or HSV-1 Ka47rescue were euthanised 50 days after infection. DRG from spinal levels T5 to L1 were excised and incubated in culture media at 37ºC with 5% CO_2 for 5 days. The DRG were then homogenised and assessed for infectious virus on Vero cell monolayers. After two days, the plaques were examined by fluorescence microscopy for eGFP expression. Representative plaques formed by recombinant viruses after *ex vivo* reactivation are shown. The top row shows photomicrographs taken using phase-contrast microscopy and the bottom row shows the detection of eGFP by fluorescent microscopy. The images were captured at 100× magnification. The scale bar (150 μm) is shown in the top left photomicrograph.

3.2.4.4.2 ICP47 does not affect establishment and maintenance of latency in mice

The influence of ICP47 on HSV-1 latency was studied using the ROSA26R reporter mouse system so that the frequency of cell marking in the presence or absence of ICP47 could be compared. For this, cohorts of ROSA26R mice were infected with GKa47Δ and GKa47R. DRG from spinal level T5 to L1 were excised at different time points after infection, stained using X-Gal after which the number of neurons producing β-galactosidase were counted as a measure of historic CMV IE promoter activation. No difference in the number of β-gal positive neurons was observed when DRG from GKa47Δ and GKa47R infected mice were examined 5, 10, 20, 40 and 100 days after infection (Figure 3.20 A). Similar to marking by the parent virus HSV-1 pC_eGC virus (Russell, 2015; Ma et al., 2014), infection by GKa47Δ and GKa47R, resulted in the number of β-galactosidase positive neurons rising from 5 day to 10 days post-infection (dpi) followed by a rapid fall until 20 days and thereafter, being numerical stability in both the null mutant and in the revertant viruses. The comparable level of marking during lytic infection (5 and 10 dpi) by viruses lacking ICP47 and control viruses is consistent with the similar level of virus titre observed in DRG on four and six days after infection. Further, the comparable number of neurons marked on days 20, 40 and 100 after infection suggests that ICP47 does not play a significant role during the establishment or maintenance of latency.

In our infection model, the virus is tattooed on the flank of mice, which allows the virus primarily to infect the neurons innervating the same dermatome. However, during subsequent rounds of replication, the virus spreads to spinal ganglia not directly innervating the initial infection site (Simmons and Nash, 1984; Speck and Simmons, 1991). Based on the enumeration of β-gal positive neurons in DRG across the spinal levels using ROSA26R mouse model, Russell and Tscharke (2016) have shown that the virus spreads to multiple DRGs along the spine after the peak of acute infection and during the establishment phase of latency (10 to 20 days). In the current study, infection of ROSA26R mice with GKa47Δ or HSV-1 GKa47R showed that a similar number of DRG experienced Cre mediated β-gal marking at different times examined (Figure 3.20 B). This finding implies that the loss of ICP47 has no effect on the virus spread to DRG distal to those that directly innervate the cutaneous site of infection.

Based on the assumption that ICP47 can be expressed in some neurons during the establishment of latency (Russell and Tscharke, 2016), we examined the fate of those neurons by employing ICP47 null mutant and rescuant viruses in which the ICP47 promoter controls Cre expression. ROSA26R mice were infected with HSV-1 Ka47inΔ or HSV-1 Ka47rescue and their DRG were examined for β-gal expression on 5, 10, 20, 40 and 100 days after infection. The results presented in Figure 3.21 A show that the number of neurons marked was similar between the null virus and the control viruses at all time points examined, except on day 10 after infection. Further, the number of DRG with marked neurons was comparable between the viruses (Figure 3.21 B). The lack of difference in the number of neurons marked on days 20, 40 and 100 suggests that ICP47 expression neither influences the ability of HSV-1 to establish and maintain latency nor affects the survival of infected neurons.

On day 10, the number of neurons marked by Ka47inΔ was significantly lower than the marking by the control virus Ka47rescue. By analysing virus titre, we found a similar reduction in infectious virus in the DRG from 4 to 6 days of infection by the ICP47 null mutant (Ka47Δ or GKa47Δ) and control viruses (wild-type, Ka47R or GKa47R) (Figure 3.10 B, C and Figure 3.17). Similar titres on day 6 indicate that the virus is cleared at the same pace regardless of the presence of ICP47. Consistent with this, the difference in the amount of infectious virus detected on 5 dpi by the wild-type, Ka47inΔ or Ka47rescue is not statistically significant. Further, a similar level of β-gal marking of neurons observed from 20 to 100 days post-infection indicates that the lack of ICP47 does not impair the ability of the virus to enter latency. Since, viral gene expression can occur beyond acute infection in neurons (Steiner et al., 1990; Margolis et al., 1992; Kramer et al., 1998; Russell and Tscharke, 2016), our result cannot rule out the possibility that ICP47 prolongs virus activity at the molecular level or perhaps increase the survival of the neurons until 10 days after infection. However, these possibilities were not explored further in this thesis.

In contrast to the previous finding by Russell and Tscharke (2016), the ICP47 promoter in our study did not induce additional β-gal marking during the establishment phase. Instead, the numbers dropped from 5 to 20 days after infection and then remained stable during latency. The basis of this difference is examined in detail and the results are presented in the next chapter. Collectively, the data from ROSA26R reporter mice infected with the

different Cre expressing ICP47 null mutants suggest that the lack of ICP47 did not affect the spread of the virus in the ganglia or across the spinal levels. Further, ICP47 deficiency neither impacted the establishment of latency nor the stability of latency.

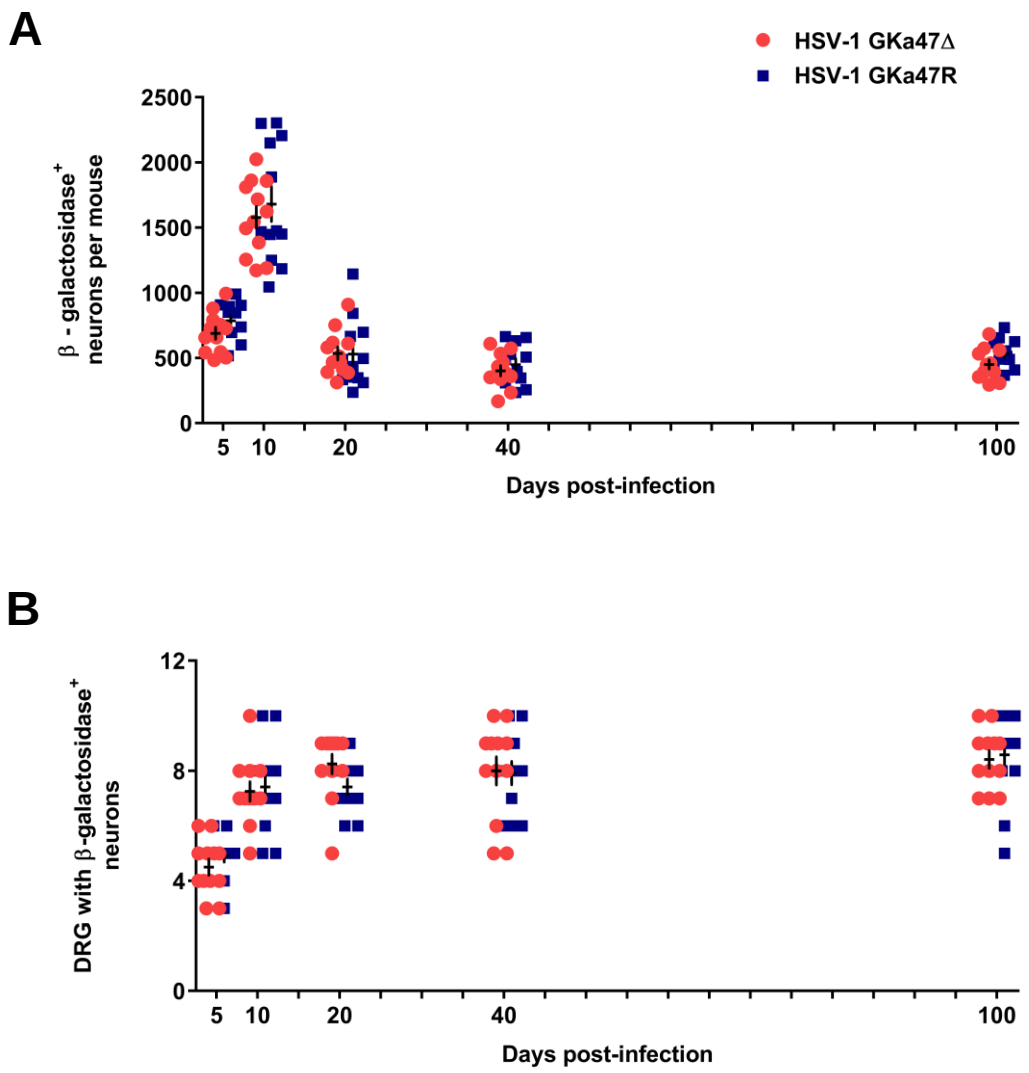

Figure 3.20 Historical marking of neurons by CMV IE promoter activation reveals that ICP47 does not affect the establishment of latency or the stability of latency. Groups of ROSA26R mice were infected with GKa47Δ or GKa47R on the flank. DRG from T5 to L1 were excised from each mouse on 5, 10, 20, 40- and 100-days post-infection, DRG were stained with X-Gal, mounted intact and large blue cells were counted. (A) The graph shows the number of neuronal cells marked by X-Gal staining per mouse. (B) The graph shows the number of DRG containing at least one β-gal synthesising neuron per mouse. Each symbol represents a mouse and bars represent mean ± SEM. Data shown are pooled from two experiments. The comparison of cell marking or spread of the virus between the viruses GKa47Δ and GKa47R was not significantly different based on two-way ANOVA and Sidak's multiple comparisons test.

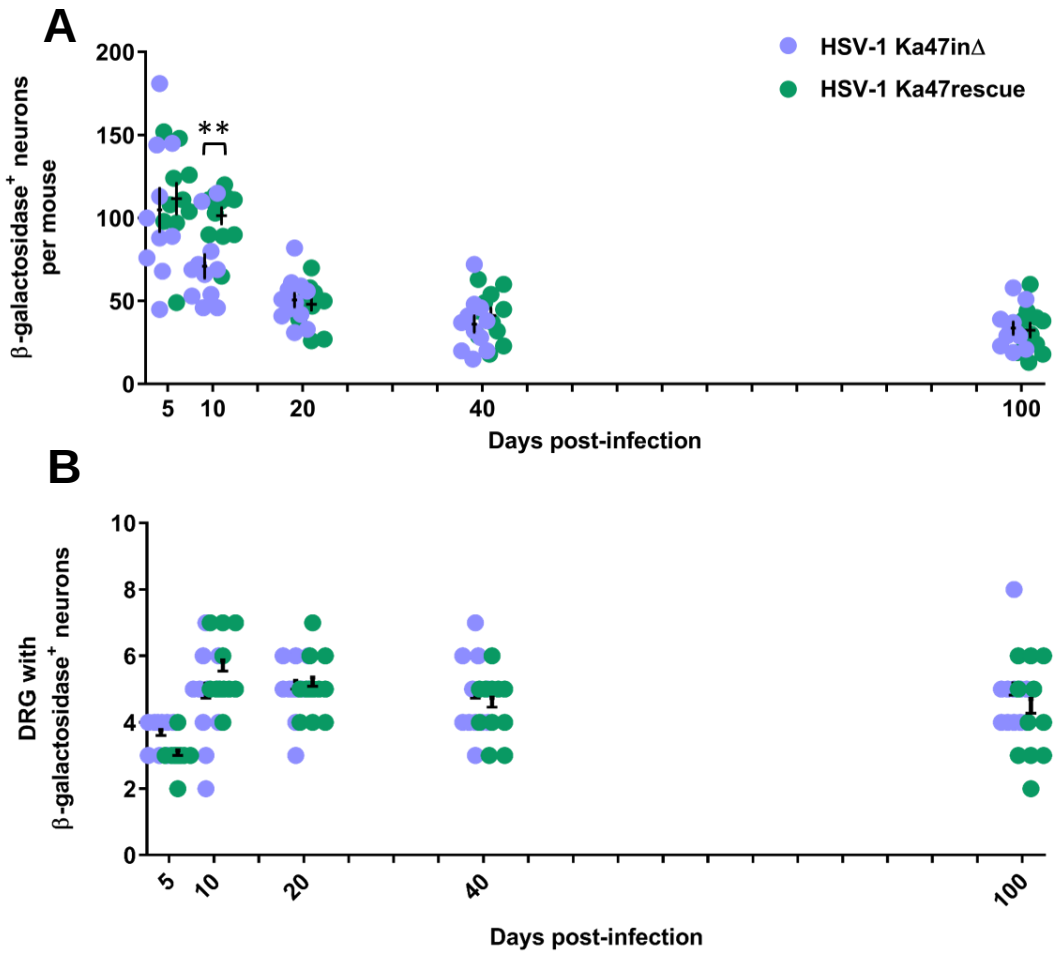

Figure 3.21 Historical marking of neurons by HSV-1 ICP47 promoter activation reveals that ICP47 does not affect the establishment of latency or the stability of latency. Groups of ROSA26R mice were infected with HSV-1 Ka47inΔ or HSV-1 Ka47rescue on the flank. DRG from T5 to L1 were excised from each mouse on 5, 10, 20, 40- and 100-days post infection. DRG were stained with X-Gal, mounted intact and large blue cells were counted. (A) The graph shows the number of neuronal cells marked by X-Gal staining per mouse. (B) The graph shows the number of DRG containing at least one β-gal synthesising neuron per mouse. Data shown are pooled from two experiments. Each symbol represents a mouse and bars represent mean ± SEM. Statistical significance was calculated by comparing means using two-way ANOVA and Sidak's multiple comparison test (**$p<0.01$). Except for day 10, the number of β-gal marked neurons was not different at other time points between the groups. The spread of the virus between DRG across spinal level was not significantly different.

3.2.4.5 Reactivation ability of the virus is not affected by the loss of ICP47 function of the virus

Co-localization of activated HSV-specific effector memory $CD8^+$ T cells and latently infected neurons has been reported both in human (Theil et al., 2003; Verjans et al., 2007) and in mouse studies (Shimeld et al., 1990b; Simmons and Tscharke, 1992; Khanna et al., 2003a). Mackay and colleagues have shown that $CD8^+$ T cells retained in the ganglia of HSV-1 infected mice are actively involved in recognition of latently infected cells and respond by the production of granzyme B (Mackay et al., 2012). Convincingly, the addition of HSV-specific $CD8^+$ T cells to cell suspension of latently infected mouse ganglia prevented reactivation of the virus in an MHC I-dependent manner (Khanna et al., 2003a; Orr et al., 2007). These studies indicate a possible protective role of $CD8^+$ T cells during latency. However, it is not yet clear whether the inhibition of MHC I-mediated antigen presentation by ICP47 contributes to the reactivation of the virus in mice. Therefore, the role of ICP47 in reactivation from latently infected sensory neurons was explored in this project using an explant reactivation assay (see materials and methods, section 2.3.10.3).

In this assay, DRG from thoracic level 4 (T4) to lumbar level 3 (L3) were excised from latently infected mouse, explant cultured *in vitro* for 5 days and then assayed for infectious virus. We found that the percentage of ganglia with reactivated virus from each mouse and percentage of ganglia with the reactivated virus from individual spinal level was comparable amongst groups of mice infected with HSV-1 KOS, Ka47Δ or Ka47R (Figure 3.22 A and B). These data show that ICP47 did not alter reactivation ability of the virus nor curtail the reactivation in the absence of ICP47 in an *ex vivo* condition.

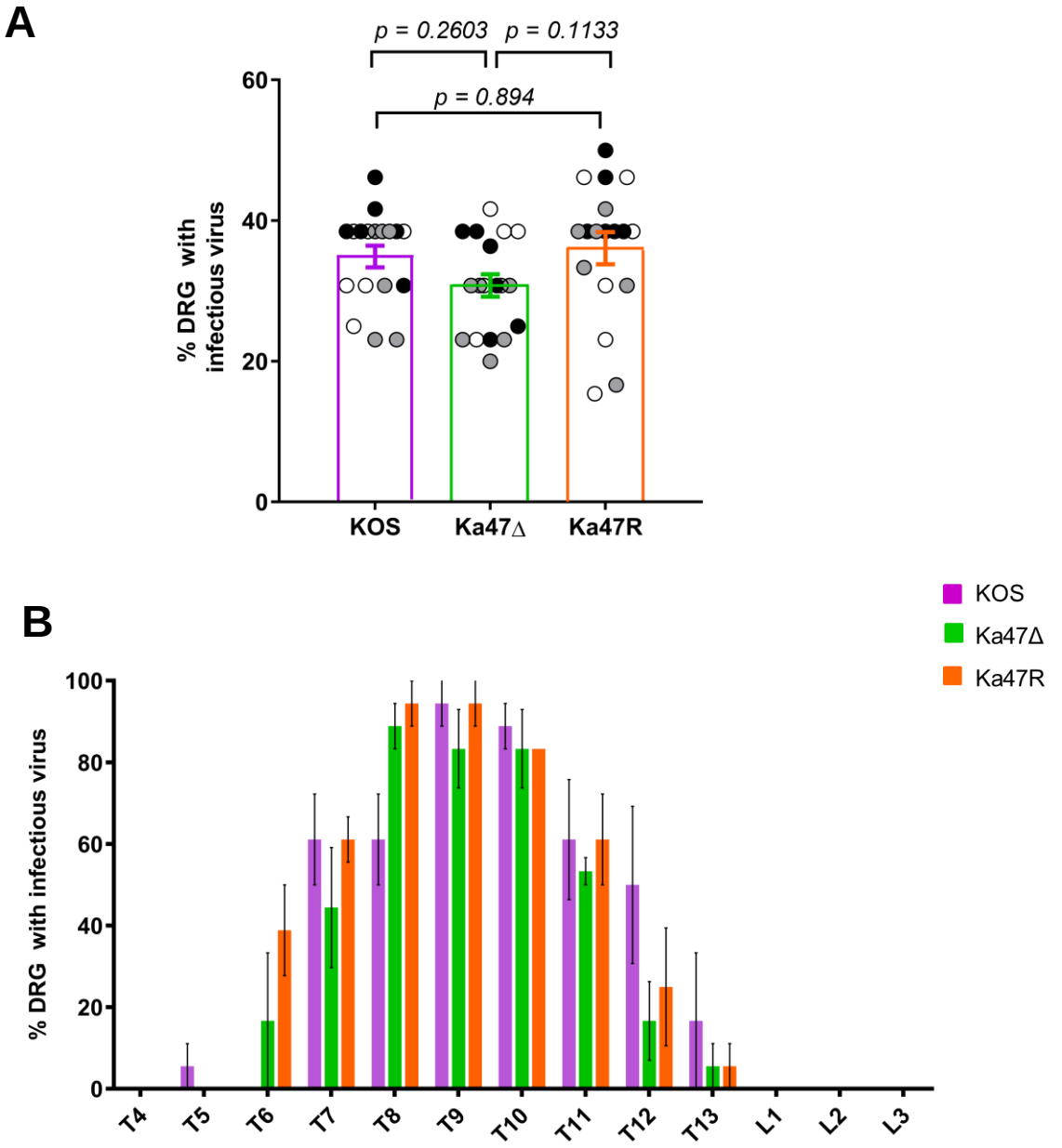

Figure 3.22 ICP47 does not influence reactivation of HSV-1 from DRG of mice. Groups of six mice were infected on the flank with HSV-1 KOS, HSV-1 Ka47Δ or HSV-1 Ka47R. DRG from spinal levels T4 to L3 were excised after 30 days of infection. Reactivation was induced *in vitro* by explant culture as described in methods section. (A) Percentage of DRG with the infectious virus was calculated from each mouse. Data were pooled from 3 independent experiments. Each symbol represents a mouse and data from different experiments are color-coded. The error bar represents mean ± SEM. Ordinary one-way ANOVA with Tukey's multiple comparisons test was used to analyse the statistical difference amongst the groups. (B) Percentage of DRG with the infectious virus was calculated for each spinal level (T4 to L3). The data from 3 experiments are plotted. The error bar represents mean ± SEM. The difference between the viruses is not statistically significant according to one-way ANOVA and Newman-Keuls multiple comparisons test

3.3 Discussion

HSV, compared to other herpesviruses, has an advantage as a model virus as it can productively infect mice and therefore understanding the *in vivo* significance of TAP inhibition by ICP47, at least in principle is possible. Previous *in vivo* findings suggest that inhibition of TAP by ICP47 is critical for virus spreading from PNS to CNS (Goldsmith et al., 1998; Burgos et al., 2006). However, the role of ICP47 in mouse models apparently contradicted *in vitro* studies that demonstrated the lack of ICP47 functioning in mouse cells (Ahn et al., 1996; Tomazin et al., 1996; Jugovic et al., 1998; Berger et al., 2000; Easterfield et al., 2001; Radosevich et al., 2003). Here, we attempted to resolve the disparity between the *in vitro* and *in vivo* findings by using new assays and infection models in conjunction with alternate virus strain and mouse strain. In the discussion that follows, we attempted to derive a global insight into the relevance of ICP47 during different stages of HSV-1 infection in mice.

Consistent with published data, in our study the ability of HSV-1 to down-modulate total surface MHC I was seen in infected human cells but not in mouse cells. While down-modulation of total surface MHC I reflects the function of ICP47 on suppressing antigen presentation, the full extent of inhibition in mouse cells may have been underestimated due to the persistence of baseline pMHC-I that were present pre-infection. Therefore, ICP47 mediated inhibition of presentation in mouse cells might not be revealed by merely determining surface MHC I levels. Using a super-infection-based antigen presentation assay, we were able to expose the influence of ICP47 on the presentation of newly synthesised peptides. We found that in human and mouse cells infected with wild-type HSV-1, followed by infection with SIINFEKL expressing MVA, the level of H-2K^b-SIINFEKL complexes on the cell surface was significantly reduced compared with cells infected with Ka47Δ. While in human cells, ICP47 showed inhibition of antigen presentation to near background levels, in mouse cells there was significant, but relatively reduced inhibition. Nevertheless, our antigen presentation assay indicates that ICP47 functions in mouse cells and it might be sufficient for evasion of CD8$^+$ T cells by HSV-1 in neuronal cells that inherently express less MHC I in an *in vivo* setting as has been suggested previously (Corriveau et al., 1998; Redwine et al., 2001).

While ICP47 was shown to enhance the neurovirulence in a lethal encephalitis model (Goldsmith et al., 1998; Burgos et al., 2006), whether this outcome is due to the defect in

the generation of HSV-1 specific $CD8^+$ T cells was not tested. Our finding demonstrates that the magnitude of the $CD8^+$ T cell response mounted against HSV-1 during acute infection is similar irrespective of ICP47. Similarly, Orr and colleagues (2005) found that footpad infection with recombinant HSV-1 viruses expressing potent inhibitors of antigen presentation, despite inducing neurological disease, did not alter the size of the $CD8^+$ T cell response. This suggests that the total virus-specific $CD8^+$ T cell response during lytic infection is unaltered in spite of an efficient inhibition of antigen presentation. The above data fit with the idea that the initial priming of naïve $CD8^+$ T cells in the lymphoid organs occur mainly through the cross-presentation of HSV-1 antigens by uninfected CD8α+ DCs (Bosnjak et al., 2005a; Bedoui et al., 2009; Whitney et al., 2017).

Another scenario where ICP47-mediated inhibition of antigen presentation would be of relevance is in infected cells that are targets for activated $CD8^+$ T cells. Transcription of ICP47 begins soon after infection in the human fibroblast cells and mouse neuronal culture (Harkness et al., 2014). The kinetics of its expression raises the possibility that ICP47 plays an essential role in favouring the survival of HSV infected cells against the $CD8^+$ T cell response leading to the better establishment of initial infection. The *in vivo* experiments described in this chapter show that following flank infection of C57BL/6 mice with HSV-1, lack of ICP47 resulted in no difference in the virus replication in the skin and DRG on four and six days after infection. Others have also made a similar observation in corneal epithelia using the corneal scarification model (Goldsmith et al., 1998). The lack of measurable difference in viral replication in the skin could be due to other more dominant or redundant immune responses. Accordingly, $CD4^+$ T cells and IFNγ have been shown to be critical for the elimination of infectious virus in mice (Smith et al., 1994; Manickan et al., 1995). IFNγ expression by epidermal cells and infiltrating immune cells can partially overcome ICP47 mediated down-regulation of MHC I, increasing their prospect of being recognised by activated $CD8^+$ T cells (Mikloska et al., 1996; Radosevich et al., 2003). Therefore, it can be argued that TAP inhibition by ICP47 is unlikely to have a significant impact on virus replication in the skin in an immunocompetent host. However, in the peripheral sensory neurons, $CD8^+$ T cells have a significant role in curtailing virus replication with limited neuronal cell death (Simmons and Tscharke, 1992). Additionally, Orr and colleagues found that inhibition of antigen presentation by m152 provided a replication advantage to HSV-1 in the eye and TG of mice during acute infection,

suggesting that effective inhibition of antigen presentation would result in improved viral fitness in the nervous system. Therefore, a possible explanation for the comparable level of infectious virus in the infected tissues could be that ICP47 does not reduce the antigen presentation sufficiently during acute infection to impact the visibility of infected cells to $CD8^+$ T cells.

HSV-1 replication at the peripheral site is not a prerequisite for the establishment of neuronal latency in mice (Efstathiou et al., 1989). Likewise, virus lacking immediate early genes, including ICP47, can enter latency in mouse neurons (Meignier et al., 1988; Nishiyama et al., 1993). HSV-1 DNA can be detected as early as 8 hours post-infection (Wakim et al., 2008) and the infectious virus can be recovered by 32 hours in sensory ganglia of mice following infection with HSV-1 (Kramer et al., 1998). However, it takes a few days for the HSV-1 specific $CD8^+$ T cells to be primed, expand and appear at the infection site (Coles et al., 2002). Given the rapidity at which the virus travels from the skin to the sensory neurons, it is unlikely that $CD8^+$ T cells can prevent the establishment of latency during HSV-1 infection. Consistent with these data, we found that similar to wild-type and revertant viruses, ICP47 null mutant viruses establish latency in all infected mice infected as measured by their ability to reactivate after 30 days of infection.

From mouse studies, it is apparent that stable latency in the absence of any productive infection is established many days after the detection of infectious virus, typically 28 to 34 days after the initial infection (Miller et al., 1998). During this latency establishment phase, some neurons tolerate lytic gene expression and virus spread (Lachmann et al., 1999; Arthur et al., 2001; Feldman et al., 2002a; Proença et al., 2008, 2011; Russell and Tscharke, 2016). As a consequence, viral antigens will be present in at least a proportion of these neurons at this time. Moreover, virus infection in neural tissues induces the expression of MHC I and various other components of the antigen processing pathway (Neumann et al., 1995; Pereira and Simmons, 1999; Kimura and Griffin, 2000; Chevalier et al., 2011). Additionally, mouse studies suggest ongoing stimulation of $CD8^+$ T cells in ganglia well beyond the termination of lytic infection (Cantin et al., 1995; Khanna et al., 2003a). With the absence of professional APCs in the ganglia during latency, neurons are considered to be responsible for presenting viral antigens to $CD8^+$ T cells (van Lint et al., 2005). Taken together, the above observations suggest that neurons present antigen during and after the establishment of latency. We hypothesised that the primary function of ICP47 might not

be to ensure the establishment of latency *per se,* but it may help seed a larger latent pool by decreasing the ability of the $CD8^+$ T cells to respond against infected neurons. In theory, an HSV-1 virus lacking ICP47 would permit presentation of an increased number of viral epitopes on neurons, hence increasing the chances of their elimination by $CD8^+$ T cells. This effect could be reflected by a reduction in the number of neurons entering latency. On the contrary, in our study ICP47 did not impact the number of neurons marked by CMV IE promoter or HSV-1 ICP47 promoter activity during the latency establishment phase. Similarly, the latency of ICP47 null mutant and control viruses was stably maintained as indicated by the similar level of marking at different times examined during latency. In this study, we based our assumptions on our data that showed ICP47 can block antigen presentation in mouse fibroblast cells and predicted that ICP47 influences latency. However, we lack knowledge of the abundance of peptide epitopes presented on HSV-1 infected mouse cells. $CD8^+$ T cells are highly sensitive in sensing low-levels of cognate antigen presentation, at least under ideal conditions *in vitro* (Valitutti et al., 1995; Purbhoo et al., 2004; Hogan et al., 2014). Hence, if the antigen presentation in neurons was not completely inhibited by ICP47 during the latency establishment phase, then infected-neurons will still be eliminated by $CD8^+$ T cells, leading to a similar number of marked neurons. If this proves not to be the case, different factors will need to be considered, such as whether immunogenic antigens are abundantly expressed in neurons for presentation after lytic infection and whether the spatial and temporal expression of ICP47 coincides with or precedes the expression of antigenic proteins.

Another explanation for the lack of difference in a number of β-gal+ neurons between ICP47 null virus and control viruses is that $CD8^+$ T cells may control HSV replication by using non-cytolytic mechanisms in neurons. In that case, the removal of ICP47 will not have any effect on the maintenance of latently infected neurons. Antiviral cytokines produced by $CD8^+$ T cells, such as IFNγ or TNFα, can stimulate intracellular pathways that inhibit the expression of essential viral genes required for viral replication (Decman et al., 2005). Similarly, in the TG of infected mice, granzyme B was able to curtail virus reactivation without inducing caspase-mediated apoptotic cell death. Instead, the control of virus replication was thought to be due to granzyme B mediated-degradation of ICP4, an immediate early gene essential for the expression of early genes (Knickelbein et al., 2008). Consistently, in human cadaveric TG, $CD8^+$ T cells containing granzyme B were clustered close to neurons expressing LAT and showed limited neuronal destruction (Verjans et al.,

2007). In addition, a large body of evidence indicates that LATs, which are the most abundant viral transcripts made during latency, interfere with apoptotic pathways directly or by blocking granzyme B from activating caspase-3 (Ahmed et al., 2002; Henderson et al., 2002; Branco and Fraser, 2005; Jiang et al., 2011). Perhaps if the $CD8^+$ T cells implement one or more of these mechanisms to protect neurons presenting HSV peptides, then lack of ICP47 will not have any visible effect on the number of neurons after the establishment of latency. Although such a complicated explanation cannot be excluded, the incomplete TAP inhibition by ICP47 or redundancy in immune control is the most plausible explanation for the data presented in this thesis.

Goldsmith and colleagues found that the deletion of ICP47 resulted in the reduced spread of the virus to the CNS following ocular infection of BALB/c mice in a $CD8^+$ T cell-dependent manner suggesting that ICP47 enhances neurovirulence in mice by inhibiting TAP-mediated peptide transport (Goldsmith et al., 1998). The capacity of the virus to enter the CNS depends on multiple factors that often act in combination (Kollias et al., 2015a). First, the genetic composition of the virus is critical in determining the severity of infection (Dix et al., 1983; Bergström et al., 1990). Second, genetic and immunological factors of a mouse strain may determine the resistance to CNS infection (Kastrukoff et al., 2012b). Third, the route of infection also determines the ease of travel of the virus to the CNS (Simmons and La Vista, 1989; Wang et al., 2013b). In a susceptible mouse model, ocular infection, intranasal inoculation or lip injection of virulent HSV can readily permit CNS infection, where the virus travels via the olfactory or trigeminal route (Esiri, 1982; Esiri and Tomlinson, 1984; Menendez and Carr, 2017). A recent study showed that following corneal scarification of C57BL/6 mice with a neurovirulent HSV-1, the virus travelled via trigeminal ganglia to the olfactory bulb (OB) and established latency. More importantly, IFNγ producing HSV-1 specific $CD8^+$ T cells were found in the OB of the infected mice during latency suggesting that $CD8^+$ T cells could be relevant in preventing virus dissemination to the CNS (Menendez and Carr, 2017). In the flank infection model, the virus first infects the DRG that directly innervate the site of infection followed by spread to adjacent DRG likely via inter-neuronal synapse formed in the spinal column (Lachmann et al., 1999; Speck and Simmons, 1991). CNS infection was not expected to be infected in our mouse model, which employs C57BL/6 mice and the avirulent HSV-1 (KOS) strain (Thompson et al., 1986; Goel et al., 2002). However, given that $CD8^+$ T cells can access sites such as spinal cord (Lang and Nikolich-Zugich, 2005; Lundberg et al., 2008), we

predicted that these cells would curtail the spread of the virus to adjacent spinal DRG that are not innervating the site of infection in the absence of ICP47. However, our experiment using the ROSA26R Cre model shows that this was not the case. Instead, both the ICP47 null mutants and the control viruses showed a comparable level of marking at all the examined time points at neuron level and at the level of DRG implying that ICP47 does not influence the spread of the virus.

Only a fraction of latently infected neurons in a ganglion express ICP47 at a detectable level at any given time (Ma et al., 2014; Russell and Tscharke, 2016), therefore it is not expected that ICP47 would completely block antigen presentation in ganglia during latency. Therefore, the antigenic stimulation and activation of memory $CD8^+$ T cells seen by others are not surprising. In terms of their function, an inverse correlation was established between the number of ganglionic $CD8^+$ T cells and the rate of reactivation (Hoshino et al., 2007). Consistently others have shown that the depletion of $CD8^+$ T cells from ganglia favours HSV-1 reactivation and supplementing ganglionic cultures with activated $CD8^+$ T cells reduced the reactivation efficiency (Liu et al., 2000; Decman et al., 2005; Sheridan et al., 2009). Presence of armed $CD8^+$ T cells in ganglia means that they may be able to reduce the probability of reactivation when it occurs at molecular level even before viral DNA replication is initiated and infectious virus is assembled. In the face of the change in gene expression cascade during reactivation (Tal-Singer et al., 1997), the removal of ICP47 was thought to enhance the probability of antigen recognition by ganglionic virus-specific $CD8^+$ T cells resulting in the termination of reactivation. In our study, ICP47 showed no influence on the reactivating ability of the virus using our explant reactivation model. However, when Orr and colleagues infected C57BL/6 mice with recombinant HSV-1 expressing MCMV glycoprotein gp40 (gene m152) or HCMV US11, $CD8^+$ T cell control of HSV-1 reactivation was impaired as demonstrated by the frequent recovery of infectious virus from the eyes and ganglia of UV exposed mice (Orr et al., 2007). MCMV gp40 interferes with the transport of pMHC-I to cell surface by retention in the ER and Golgi compartments (Pinto and Hill, 2005; Janßen et al., 2016), whereas HCMV US11 directs newly synthesised MHC I molecules from ER to cytosol where they undergo proteosomal degradation (Wiertz et al., 1996). The mechanism by which these two proteins down-regulate MHC I differ from that of ICP47 is not known, however, they function relatively efficiently in a mouse model. While it is convincing that $CD8^+$ T cells can inhibit

reactivation, it appears that ICP47 does not provide an absolute blockade of antigen presentation and therefore, there is no effect on reactivation.

Where we failed to find a phenotype for our ICP47 null virus during different stages of HSV-1 infection, there was a significant decrease in the number of neurons marked by Cre on day 10 in Ka47inΔ-infected ROSA26R mice compared to Ka47rescue-infected mice. A similar but statistically insignificant trend was observed for the number of DRG with Cre marked neurons on this time point. It is possible that this difference was not apparent when CMV IE promoter induced Cre marking as it drives Cre expression in an extensive number of neurons in DRG of mice (i.e., in most of the live infected neurons). Comparatively, more marked neurons in Ka47rescue-infected mice allude to the association of ICP47 with survival of infected neurons. However, such an interpretation remains speculative because the difference in number of Cre marked neurons between the two viruses vanished on day 20 and the numbers remained stable until 100 days after infection. This suggests that the additionally marked neurons on day 10 did not continue to survive until the establishment of latency. If ICP47 enhances neuronal survival during lytic infection, it may result in the production of more infectious virus in DRG. Although the virus titre in DRG was similar on days 4, 5 or 6, and disease resolution occurred at a similar rate, it is possible that a small amount of infectious virus is present beyond this time in neurons expressing ICP47. Virus titre and viral genome copy number should be determined for an extended time in future studies in the DRG of infected mice to elucidate if ICP47 enhances survival of infected neurons and consequently results in an increase in the amount of infectious virus.

Overall, our *in vivo* study using mouse model showed that ICP47 does not affect lytic infection, establishment and maintenance of latency or reactivation of the virus. Our new *in vitro* antigen presentation assay demonstrated that the inhibition of antigen presentation by ICP47 is less efficient in mouse cells compared to human cells, which is consistent with other published *in vitro* findings. Together, the above findings suggest that the lack of discernible phenotype for ICP47 in our mouse model is most likely due to the partial inhibition of MHC I mediated antigen presentation by ICP47 in mice. However, the question remains, "how much peptide presentation is inhibited by ICP47 in human than mouse?" The abundance of HSV peptides in infected human and mouse cells is explored in chapter 5.

Chapter 4
Characterisation of ICP47 promoter using ROSA26R Cre reporter mouse system

4 Characterisation of ICP47 promoter using ROSA26R/Cre reporter mouse system

4.1 Introduction

Recombinant HSV-1 has been used extensively as a research tool. For this purpose, genes from a variety of sources have been inserted into viral genomic regions non-essential for virus growth in culture and virulence in mice. Typically, a viral promoter 5′ to the inserted sequence, another HSV-1 promoter or a heterologous promoter is used to control the expression of inserted genes. Of the insertion sites, the intergenic regions between UL3 and UL4, UL26 and UL27, and UL50 and UL51 have been previously confirmed as suitable for reporter gene expression without altering the efficiency of viral replication in cell culture and in mice (Balliet et al., 2007; Morimoto et al., 2009; Russell et al., 2015). In particular, the UL3-UL4 locus had often been utilised by others to generate recombinant viruses and insertion at this site does not impair viral replication *in vitro* or *in vivo* nor does it affect the establishment and maintenance of latency (Baines and Roizman, 1991; Cocchi et al., 1998; Menotti et al., 2002; Tanaka et al., 2003, 2004; Taylor et al., 2007; Morimoto et al., 2009; Bedadala et al., 2014; Miyagawa et al., 2015; Russell et al., 2015). Further, insertion at this location is not thought to affect the expression of adjacent genes as UL3 and UL4 are both orientated towards the intergenic region, and no *cis*-elements have been mapped to this region (Morimoto et al., 2009). Russell and Tscharke (2016) utilised the intergenic region between UL3 and UL4 to introduce various HSV-1 lytic gene promoters to drive the expression of Cre. Testing these viruses in the previously described ROSA26R/Cre reporter system revealed that the promoters of lytic genes (ICP47, ICP6 and gB) induced a detectable level of Cre expression in a subset of neurons during latency. In particular, ICP47 promoter induced Cre activity in a significant proportion of neurons during the establishment of latency (Russell and Tscharke, 2016). However, this seems not to be the case for the ICP47 promoter at the native location (Figure 3.21). Intriguingly, after the lytic phase, Cre activity driven by native ICP47 promoter in HSV-1 Ka47inΔ and Ka47rescue viruses differed drastically from Cre activation by ICP47 promoter in HSV-1 pICP47_eGC, used in the previous study (Russell and Tscharke, 2016). The recombinant virus HSV-1 pICP47_eGC will be referred to as HSV-1 UL3-pa47min in this thesis.

In the experiment shown in Figure 3.21, UL3-pa47min was included for direct comparison, but not shown in the figure with an intension to highlight the role of ICP47. All viruses are

now shown in Figure 4.1. In brief, the following observations were made. First, the neuronal marking driven by all three viruses was comparable during lytic infection (5 dpi). Further in a previous study Russell (2015) confirmed that the strength of the native ICP47 promoter was not significantly different to the ectopic version in UL3-pa47min as demonstrated by the similar amount of Cre and ICP47 transcripts found during lytic infection in mice infected with HSV-1 UL3-pa47min (Russell, 2015). Second, while the Cre mediated marking of neurons was similar during lytic infection between HSV-1 Ka47inΔ or Ka47rescue and HSV-1 UL3-pa47min, it appeared to be differentially regulated between these viruses especially during the latency establishment and latency. Unlike HSV-1 UL3-pa47min, the viruses generated in this study (HSV-1 Ka47inΔ and Ka47rescue) did not mark new neurons beyond lytic infection, instead the number of labeled neurons dropped and ultimately became stable as latency established (Figure 4.1 A). Finally, the number of DRG with β-gal marked neurons increased from 5 to 100 days in UL3-pa47min-infected mice, however, no new marking was visualised beyond ten days in mice infected with Ka47inΔ or Ka47rescue (Figure 4.1 B). So far, it remains undetermined whether the lack of β-gal staining means no Cre activity or insufficient Cre expression to mediate the genetic recombination, but it is clear that the activity of the promoter driving Cre differs between these viruses.

Two main differences between the viruses used in the current and the previous study could account for the differential Cre marking during latency. Firstly, while in the present study eGFP-Cre fusion gene is driven from the native ICP47 location, Russell and Tscharke (2016) introduced an eGFP-Cre fusion gene cassette in the intergenic region between the genes UL3 and UL4 (Figure 4.2). Although the reporter gene expression from UL3-UL4 locus and the native locus are similar during acute infection in mice, the possibility that the UL3-UL4 locus might be relatively permissive for gene expression during latency cannot be ruled out. Likewise, it is possible that the insertion of a transgene cassette into the ICP47 locus, which is located close to the TRS, might have affected the promoter activation during latency. Second, the promoter that Russell and Tscharke used differed from the native ICP47 promoter having a 62 bp deletion to remove the origin of replication (oriS), and the omission of the 5' untranslated region and an intron that occurs between the ICP47 promoter and coding sequence (Figure 4.3). Potential regulatory elements that likely occur in this missing region are reviewed below.

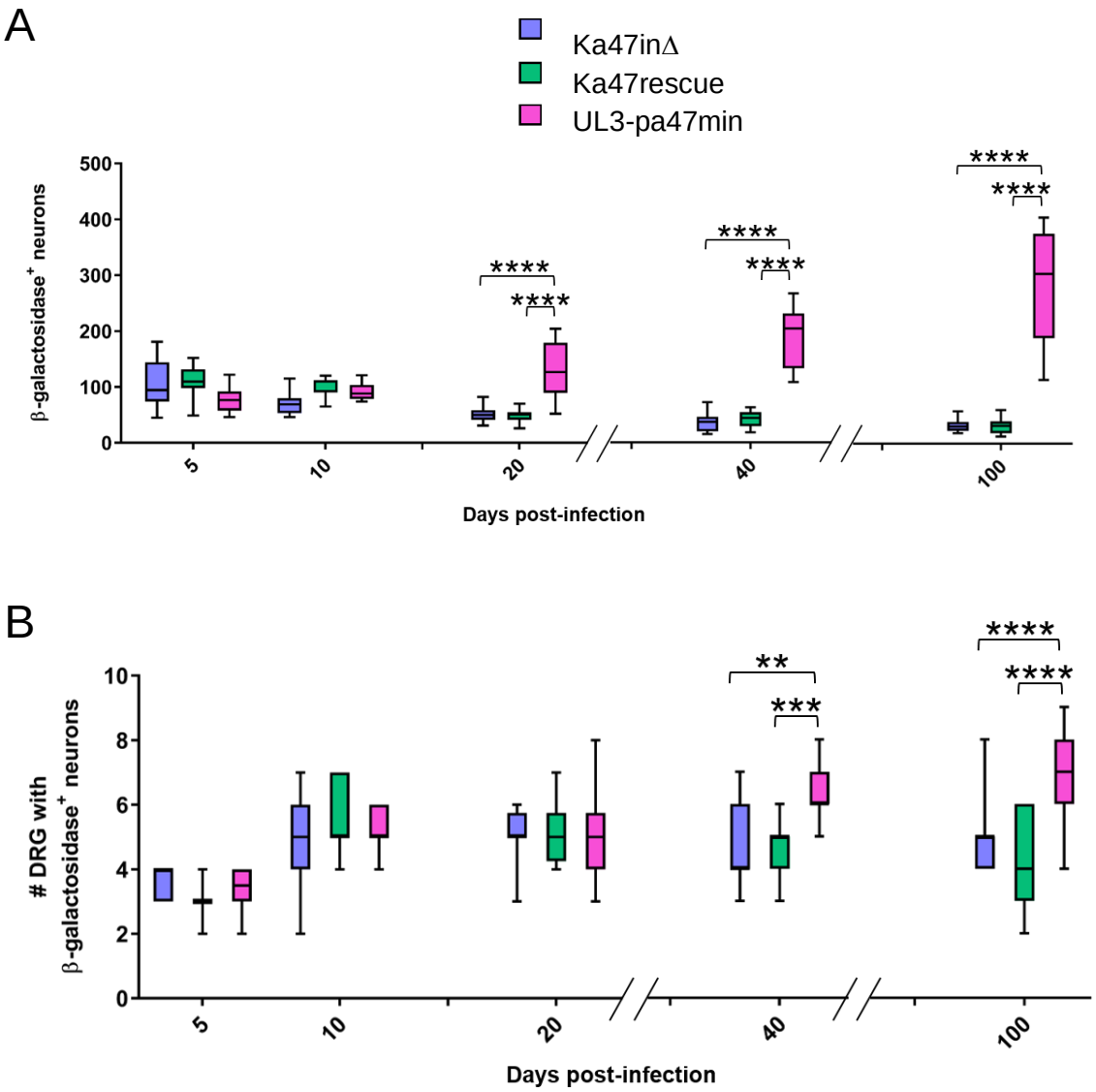

Figure 4.1 Comparison of β-gal marking of neurons by the ICP47 promoter in HSV-1 UL3-pa47min, HSV-1 Ka47inΔ and HSV-1 Ka47rescue. The transcriptional history of the ICP47 promoter was analysed in ROSA26R mice in the previous chapter and compared to another virus, UL3-pa47min, here. (A) Data represent the number of neurons marked by β-gal in ROSA26R mice infected with HSV-1 UL3-pa47min, HSV-1 Ka47inΔ and HSV-1 Ka47rescue on different days after infection. (B) Data represent the number of DRG containing at least one β-gal+ cell per mouse previously infected with HSV-1 UL3-pa47min, HSV-1 Ka47inΔ or HSV-1 Ka47rescue at different days after infection. (A&B) The data shown are pooled from 3 independent experiments with overlapping time points. Box plots show the median (horizontal line) and the interquartile range; whiskers indicate the minimum and maximal values. Means were compared using two-way ANOVA combined with Bonferroni's multiple comparisons post-test (**p<0.01, ***p<0.001, ***p<0.0001).

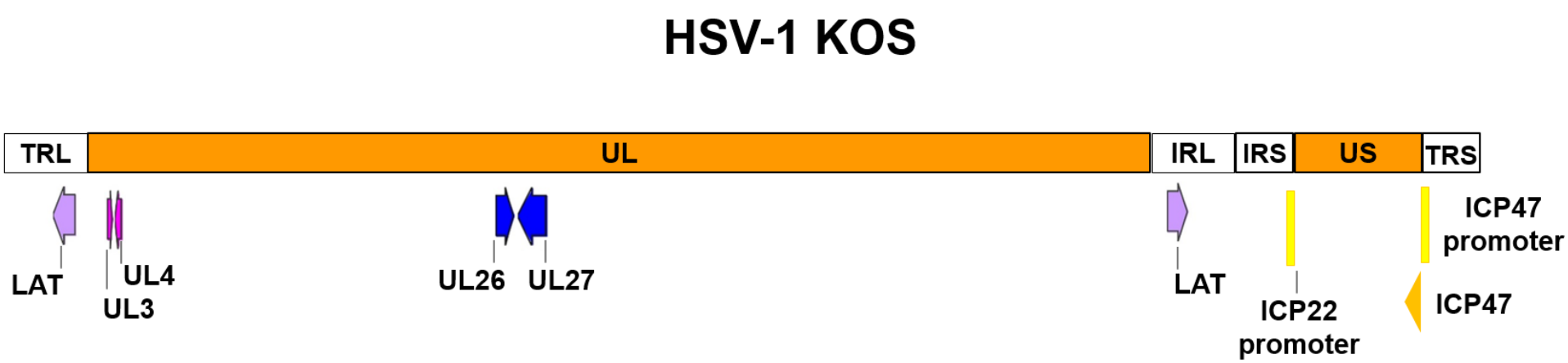

Figure 4.2 Location of the reporter gene insertion and position of ICP47 in the HSV-1 genome. Two loci commonly used for heterologous gene expression in HSV-1 are the intergenic region between the genes UL3 and UL4 and between UL26 and UL27. A diagrammatic representation of the HSV-1 genome with unique regions and repeat regions is shown above. Below, the locations of relevant genes are annotated. Arrows in magenta indicate the location and orientation of UL3 and UL4 genes. Blue arrows indicate the location and orientation of UL26 and UL27 genes. Yellow lines flanking the unique short (US) region indicate ICP47 promoter on the right and ICP22 promoter on the left. The ICP47 promoter is in the terminal repeat TRS, and pICP22 is in the internal (inverted) repeat IRS, which makes these promoter sequences similar. The orange arrowhead represents the location and orientation of ICP47 gene in the US region of the HSV-1 genome. Being in the repeat region, the LAT gene is duplicated (purple arrows), located proximal to either end of the UL segment.

4.1.1 The ICP47 locus contains several cis-acting regulatory proteins binding motifs

The regulation of HSV-1 IE gene expression during lytic infection is well-studied *in vitro*. In order to define the *cis*-acting elements that mediate IE gene expression, promoter regions were cloned upstream of a reporter gene whose activity was then assessed following transfection of the various constructs into infected cells. It is well-established that all immediate early genes possess in their promoter region a reiterated *cis*-acting inducible element, with consensus sequence 5′ TAATGARAT 3′, that is bound by the Oct-1/VP16/HCF-1 transactivation complex (Mackem and Roizman, 1982; Gaffney et al., 1985; Preston et al., 1988; Roizman et al., 1988; Hagmann et al., 1995). Binding of VP16 transactivation complexes induces IE gene transcription by interacting with various host transcription factors and RNA polymerase II (Batterson and Roizman, 1983; Campbell et al., 1984). The regulatory domains of IE gene promoters also contain TATA box and binding sites for other cellular transcription factors such as stimulator protein 1 (Sp1), a member of the zinc finger/krupple family proteins, and GABP binding factors (Jones and Tjian, 1985). Together, these binding sites form the basis for the "core IE promoter," and have been shown to up-regulate IE gene transcription in cell culture. However, although these regulatory elements are required for efficient virus replication, they were demonstrated to be dispensable for the establishment of HSV latency or reactivation in mice (Davido and Leib, 1996). The above *cis*-acting regulatory elements in the core promoter are preserved in the modified ICP47 promoter used in the previous study.

Of note, the promoter of the IE genes, ICP47 and ICP22, are situated in the repeat sequences that flank the unique short region of the HSV genome, hence they have identical nucleotide sequences (Barklie et al., 1977; Murchie and Mcgeoch, 1982; Gelman and Silverstein, 1987). Several transcription factors and *cis*-acting elements that potentially regulate ICP22 gene expression were also discovered in the regions flanking the core promoter. Since the ICP47 promoter region is identical to that of ICP22, it is reasonable to assume that binding of the regulatory factors to these *cis* elements is likely to influence the expression of ICP47. Greco and colleagues evaluated the 5′-untranslated region (UTR) of ICP22 mRNA for the presence of regulatory element using mutants with progressive deletions within that region and *in vitro* chloramphenicol acetyltransferase (CAT) assays. They found that the region within the first exon of ICP22 mRNA is sufficient to induce high-level CAT activity (cis-element is localised in the 5′ UTR but not in the intron) (Greco

et al., 1994). Later, Gelman and Silverstein found a region downstream of the ICP22/47 core promoter that represses gene expression significantly from the basal level (Gelman and Silverstein, 1987). Despite the knowledge of possible regulatory elements located downstream of the ICP22/47 promoter, it is unclear under what conditions the regulatory proteins bind and control the promoter activity. Likewise, the regulatory proteins that bind to this region are unknown. Another study conducted by Bedadala and colleagues discovered the presence of five copies of the early growth response (Egr1) transcription factor binding element to the intron of the ICP22 gene (Bedadala et al., 2007). Egr-1 is a multifunctional zinc finger DNA binding protein involved in regulating inflammation, cell proliferation and apoptosis (Virolle et al., 2003; Cho et al., 2006; Yu et al., 2007). HSV-1 infection induces Egr-1 expression in epithelial cells after which Egr1 is recruited to the ICP22 promoter (Bedadala et al., 2011). How Egr-1 regulates the ICP22 promoter, and the consequence of Egr-1 activity is controversial, with studies divided as to whether Egr-1 positively or negatively regulates IE gene expression (Tatarowicz et al., 1997; Bedadala et al., 2007; Chen et al., 2008; Yao et al., 2012; Hsia, 2013). Additionally, while Egr1 is expressed in the nervous system, whether and how this protein controls gene expression in HSV-1 infected neurons is currently unknown (Beckmann and Wilce, 1997). Importantly, the Egr-1 binding element and the 5′ UTR are located in the region of the promoter that is absent from the ICP47 promoter used in the previous study by Russell and Tscharke (2016). Although much of the above information has been inferred based on *in vitro* systems using neuronal or non-neuronal cell lines, their relevance to ICP47 expression in the context of the viral genome in latently infected neurons *in vivo* is yet to be established.

A further complication of this part of the HSV-1 genome is that the HSV-1 oriS region resides within a 90-bp sequence in the ICP22/47 promoter. The UL9 encoded origin binding protein (OBP) binds specific regions of oriS, and this sequence-specific binding of OBP is essential for activation of oriS mediated DNA replication (Elias et al., 1990; Wong and Schaffer, 1991; Nguyen-Huynh and Schaffer, 1998). While some of the cis-acting elements in the ICP22/47 promoter region were shown to strongly influence the origin function of oriS (Wong and Schaffer, 1991), a 62 bp deletion of the minimal OBP binding region in oriS only had a mild effect on gene expression in cell culture (Nguyen-Huynh and Schaffer, 1998). Summers and Leib drove a luciferase gene by ICP22/47 promoter with an intact OBP binding site or the promoter lacking this site. Although the deletion did not affect virus pathogenesis, virus replication or reactivation in mice, they found that the

removal of OBP binding site increased ICP47 promoter activity by two- to three-fold in cell culture indicating the likeliness of repressor function associated with this site (Summers and Leib, 2002). However, whether this OBP binding site has any repressor elements and whether they would inhibit gene expression during latency is not known. This literature is summarised in a map of the region up-stream of ICP47 (Figure 4.3).

Using the ROSA26R/Cre reporter system, it was found that HSV-1 promoters of genes whose products are of immunological relevance were active in a subpopulation of neurons during the establishment of latency and also during latency (Russell and Tscharke, 2016). Nevertheless, there appears to be a discrepancy in the activation status of the ICP47 promoter based upon either the position of the genome from where the expression cassette was placed or the promoter sequence and the potential regulatory elements present in the regions flanking the promoter. Given the potential scope of this reporter system to unravel the host and the viral factors contributing to the latency establishment and long-term stability of latency, we aimed to address the reason behind differential gene expression observed between the two studies. Therefore in this study, we set out to generate new recombinant viruses. The design of the promoters used to drive Cre in the newly constructed recombinant viruses are described in the following section.

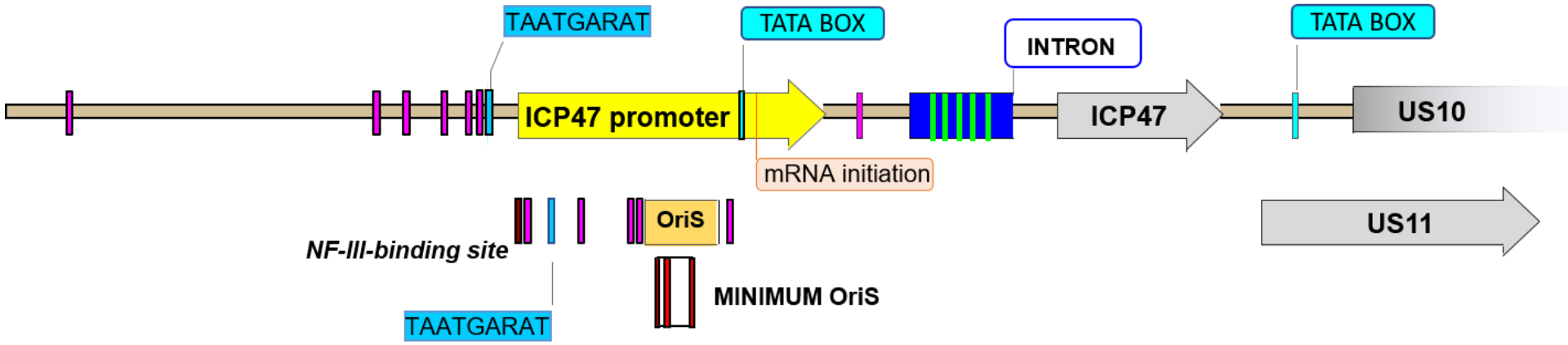

Figure 4.3 Schematic of the HSV-1 genome expanded showing the *cis*-acting regulatory elements in the ICP47 promoter region. Location and orientation of region coding for ICP47, US11 and US10 (partial) are shown in grey arrows. The minimal promoter required for ICP47 expression and its orientation is indicated by the yellow arrow. The ICP47 promoter includes a copy of the oriS shown as orange box and the minimum oriS site of 62 bp is shown as a white box. In UL3-pa47min, the promoter used to drive Cre expression is the minimal promoter shown in yellow arrow without the minimum oriS site. The three red lines in the oriS site indicate the box I, box II and box III to which the OBP bind. The ICP47 transcription initiation site is located 19 bp downstream of the TATA box shown in the orange line. An intron is located 5′ to the ICP47 coding region and 3′ to the promoter indicated by the blue box. The TATA box and the VP16 inducing complex binding motif (TAATGARAT) are shown as dark blue and light blue lines, respectively. The pink lines represent the sp1 binding motifs, which span the ICP47 promoter. Located within intron, indicated as green lines, are the reiterated Egr1 binding motifs. NFIII-binding site is indicated as dark red line situated 5′ to the ICP47 promoter.

4.2 Results

4.2.1 Design of recombinant HSV-1 viruses that express Cre under the ICP47 promoter

We generated three recombinant viruses, UL27-pa47min, UL3-pa47 and UL3-pa47ΔoriS, that each expresses an eGFP-Cre fusion gene driven by different version of the ICP47 promoter, from one of the two different ectopic locations.

The three promoters include:

a) pa47min, a minimal ICP47 promoter without oriS used by Russell and Tscharke (Figure 4.4)

b) pa47, a complete promoter comprising 869 bp nucleotide sequence upstream of ICP47 translation initiation codon, with no deletion or modification (Figure 4.4). The promoter pa47 includes the previously annotated ICP47 minimal promoter (Gelman and Silverstein, 1987), intron, 5′ UTR and the oriS site.

c) pa47ΔoriS, a promoter comprising an 869 bp nucleotide sequence upstream of the ICP47 translation initiation codon with dinucleotide substitutions in OBP-binding site to disrupt the oriS function (Figure 4.4). Three defined sites of significant sequence homology called boxes I, II and III are located in the oriS site to which the OBP specifically interact (Elias and Lehman, 1988; Elias et al., 1990; Martin et al., 1991). The binding sites in each of these boxes were further narrowed down to 3 dinucleotides (Hernandez et al., 1991). OBP in collaboration with the single-stranded DNA binding protein (ICP8) bind these oriS sites resulting in an unwinding of supercoiled DNA and subsequently lead to activation of the replication process (Lee and Lehman, 1997; Makhov et al., 2003). Hernandez and colleagues showed that dinucleotide substitution mutation in any of these boxes cause a reduction in oriS-directed DNA replication and when all three sites were substituted simultaneously, the replication of an oriS containing plasmid was abolished entirely (Hernandez et al., 1991). Similar dinucleotide substitutions were made in the oriS site of pa47ΔoriS.

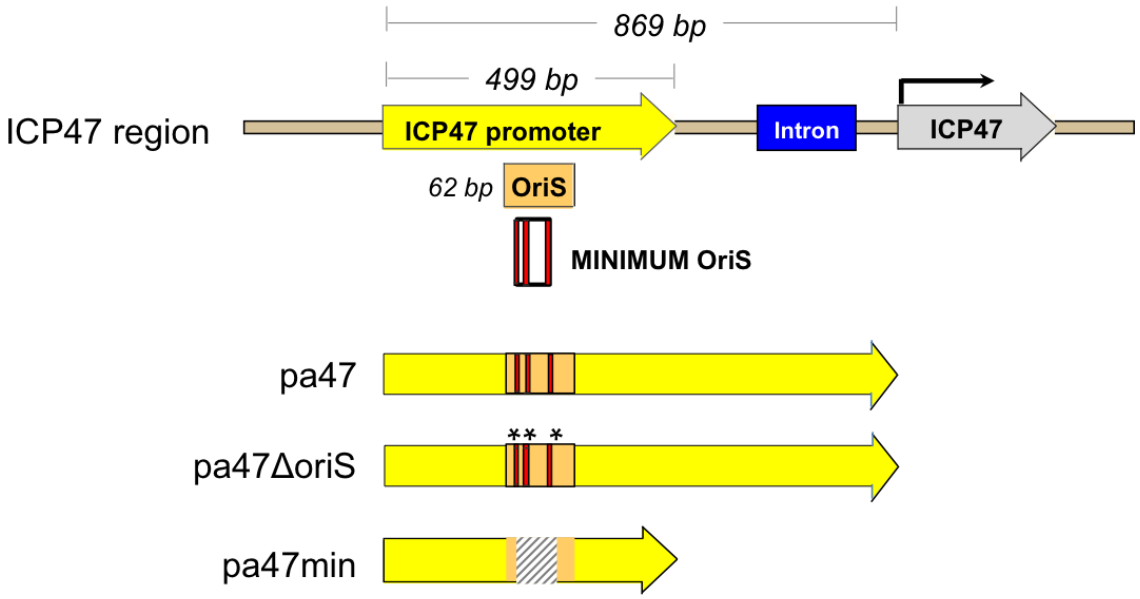

Figure 4.4 Design of ICP47 promoters to drive Cre expression from different loci. The orientation and relative location of minimal ICP47 promoter (yellow arrow), oriS region (orange and white boxes), intron region (blue box) and ICP47 gene (grey arrow) are depicted in the top stacks. The minimal promoter sequence is 499 bp. The distance from the start of the minimal promoter to the translation start site is 869 bp, which is referred to as "full-length ICP47 promoter" or "pa47". To eliminate oriS function from the ectopic full-length ICP47 promoter, dinucleotide substitutions were created in box I, box II and box III of minimal oriS site. This promoter is referred to as "pa47ΔoriS" and the asterisks indicate the location of substitution mutations. The promoter "pa47min" used by Russell and Tscharke (2016) is the minimal ICP47 promoter without oriS site. Removal of oriS from ICP47 promoter is indicated as a rectangular box with diagonal stripes.

To test whether the neighbouring cis-elements are involved in regulating the minimal ICP47 promoter, two viruses were constructed. They are HSV-1 UL3-pa47 and HSV-1 UL3-pa47ΔoriS, in which the promoters, pa47 and pa47ΔoriS, respectively, were inserted between UL3 and UL4 genes. To study the role of insertion loci in gene expression, activity of the original ICP47 promoter (pa47min) used by Russell and Tscharke (2016) was tested in the intergenic region between UL26 and UL27 by generating recombinant HSV-1 UL27-pa47min. The viruses used in this chapter are described in Table 4.1. The following sections describe the generation and characterisation of each of these viruses.

Table 4.1 List of recombinant HSV-1 viruses engineered to express eGFP-Cre controlled by the ICP47 promoter.

Recombinant HSV-1	Insertion locus	Promoter	Reference
Ka47inΔ	ICP47	Native ICP47 promoter	Chapter 3, section 3.2.4.4.1 and Figure 3.14
Ka47rescue	ICP47	Native ICP47 promoter	Chapter 3, section 3.2.4.3.1 and Figure 3.14
UL3-pa47min	Intergenic region between UL3 and UL4	pa47min	Russell and Tscharke, 2016
UL27-pa47min	Intergenic region between UL26 and UL27	Pa47min	Chapter 4, section 4.2.2 and Figure 4.5
UL3-pa47	Intergenic region between UL3 and UL4	pa47	Chapter 4, section 4.2.3 and Figure 4.7
UL3-pa47ΔoriS	Intergenic region between UL3 and UL4	pa47ΔoriS	Chapter 4, section 4.2.3 and Figure 4.7

4.2.2 Generation of HSV-1 UL27-pa47min

One of the variables that could have contributed to the differential gene expression observed during latency is the insertion position of the gene cassette in the genome. In the previous study when the modified promoter pa47min driving Tdtomato reporter gene was

inserted into the intergenic region between UL26 and UL27, gene expression in DRG during lytic infection was comparable to that observed with HSV-1 UL3-pa47min (Russell and Tscharke, 2016). Therefore, it was concluded that the location of gene expression does not influence the promoter activity. However, activation of the ICP47 promoter during latency establishment and latency was not tested in the UL26-UL27 region. This locus has been used previously by others for heterologous gene expression and found that gene insertion in this locus does not affect the viral replication *in vivo* or the latent viral genome load (Balliet et al., 2007; Russell et al., 2015). To seek understanding of the influence of gene expression locus on promoter activation after lytic infection, recombinant HSV-1 viruses that express the eGFP-Cre fusion gene under the control of the pa47min were engineered by inserting the transgene construct in the intergenic region between the genes UL26 and UL27. If pa47min could promote Cre-induced β-gal marking of neurons during latency establishment and latency from the UL26-UL27 locus (similar to pa47min in the UL3-UL4 locus), we could infer that the position of insertion may not be the underlying cause of the differential marking. For the generation of the virus, I employed CRISPR-Cas9 genome editing techniques and transfection-infection methods as described in materials and methods (section 2.3.5). The double-stranded break was introduced in the intergenic region between UL26 and UL27 using Cas9-expressing plasmid, px330_ul26/7, containing the appropriate guide sequence. To direct the homology-mediated repair mechanisms, a linearised plasmid containing gene cassette comprising pa47min upstream of eGFP-Cre fusion gene was inserted between flanking regions homologous to the region of insertion in HSV-1 genome. The gene cassette was introduced such that transcription of the fusion gene occurred in the same orientation as that of the UL27 gene. The resultant recombinant virus was called UL27-pa47min (Figure 4.5 A). An RFLP analysis demonstrated that UL27-pa47min displayed an expected pattern of DNA fragments (Figure 4.5 B). PCR amplification and sequencing confirmed the site of insertion of the expression cassette and orientation. Further, no difference was observed in the *in vitro* growth properties of the recombinant virus (Figure 4.6).

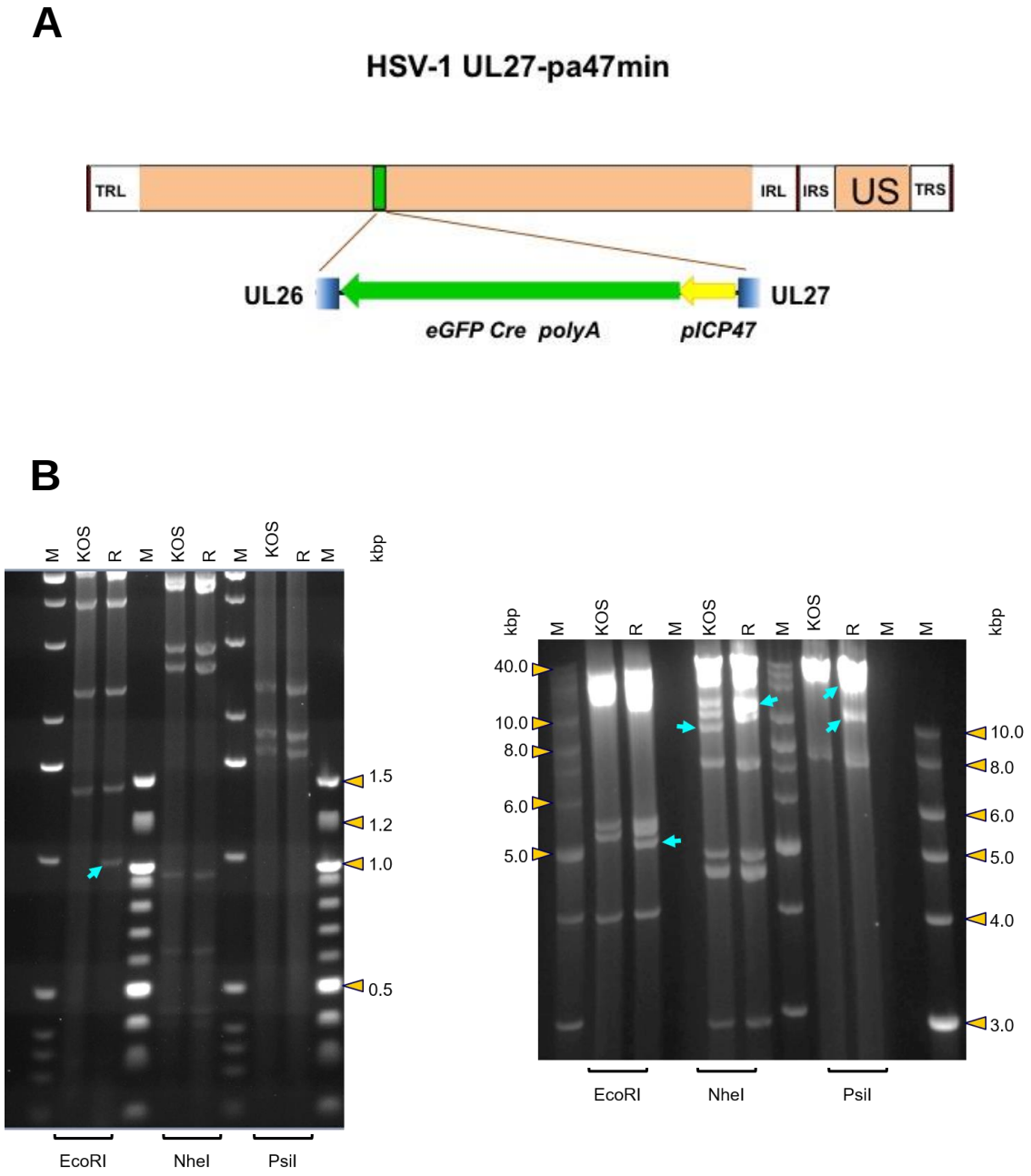

Figure 4.5 Construction of recombinant HSV-1 UL27-pa47min. (A) Diagram of the HSV-1 genome showing the typical arrangement of the unique and repeat regions. The green line represents the location of pa47min eGFP Cre cassette in the HSV-1 genome. Below is the expanded region showing the orientation of the inserted cassette. (B) RFLP analysis of the genome of the recombinant virus is shown. The viral genome was isolated from infected Vero cells and digested using restriction enzymes EcoRI, NheI or PsiI. The two images show the resolution of smaller DNA fragments (left) and larger fragments (right). The image on the left was captured first and after further electrophoresis to resolve the larger DNA fragments, the image on the right was taken. The blue arrows indicate the specific DNA fragments obtained because of modification introduced in the recombinant virus and sizes of the resultant fragments match the *in-silico* prediction. The yellow arrowheads point to the size of relevant fragments of molecular marker.

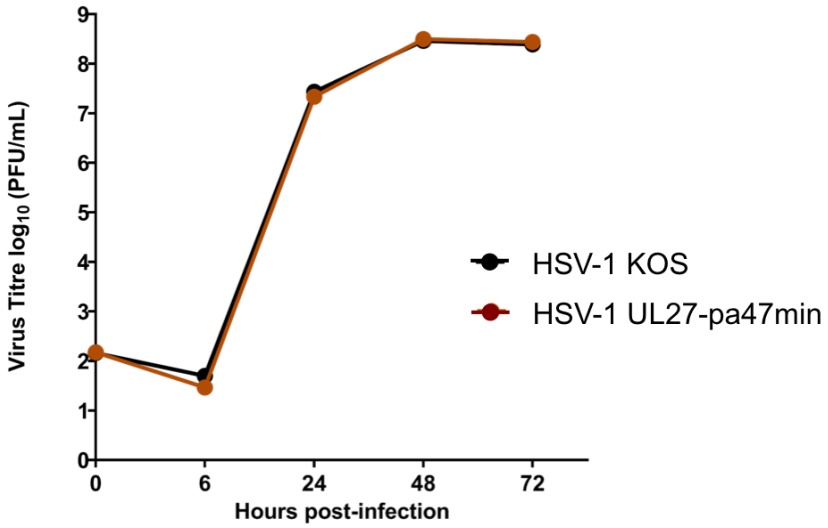

Figure 4.6 Multi-step replication kinetics of KOS and recombinant UL27-pa47min in Vero cells. Multi-step growth assay was performed as described in chapter 2 and viral titre was determined using a plaque assay at indicated time points. The experiment was conducted in triplicate. The error bars represent mean ± SEM, which bars are obscured by the symbols.

4.2.3 Generation of UL3-pa47 and UL3-pa47ΔoriS

To examine if the regulatory elements that reside in the region flanking ICP47 promoter or the oriS site are responsible for influencing marking of neurons during latency, two recombinant viruses, HSV-1 UL3-pa47 and HSV-1 UL3-pa47ΔoriS, were generated. In these viruses, a full-length copy of the ICP47 promoter was utilised to drive expression of an eGFP-Cre fusion gene located from the UL3-UL4 locus (see Figure 4.4 and Table 4.1). The ICP47 promoter driving eGFP-Cre fusion gene in UL3-pa47ΔoriS is similar to that of UL3-pa47 except for dinucleotide substitutions generated to disrupt the function of oriS (Figure 4.4). The rationale for constructing the UL3-pa47ΔoriS virus was to control for anomalies that may be introduced by adding an extra oriS sequence into the HSV-1 genome. The gene cassette in both viruses was inserted between the UL3 and UL4 genes, with the orientation of the reporter cassette same as that of UL3 (Figure 4.7 A&B). The design of these viruses is similar to the HSV-1 UL3-pa47min used by Russell and Tscharke (2016).

Restriction enzyme digestion using ScaI demonstrated that both UL3-pa47 and HSV-1 UL3-pa47ΔoriS displayed similar DNA fragment arrays to that of the wild-type virus (Figure 4.8 A). This result was expected due to the absence of the ScaI site in the inserted gene cassette. Furthermore, the position and orientation of insertion of the reporter cassette were also confirmed by PCR amplification followed by sequence verification (Figure 4.8 B). We examined whether introducing reporter gene cassette and additional oriS into viral genome affect viral replication, using a multiple-step growth analysis (Figure 4.9). Wild-type KOS virus and the recombinant viruses (HSV-1 UL3-pa47 and HSV-1 UL3-pa47ΔoriS) showed similar growth efficiencies and kinetics, suggesting that the virus replication was unaffected in these recombinant viruses.

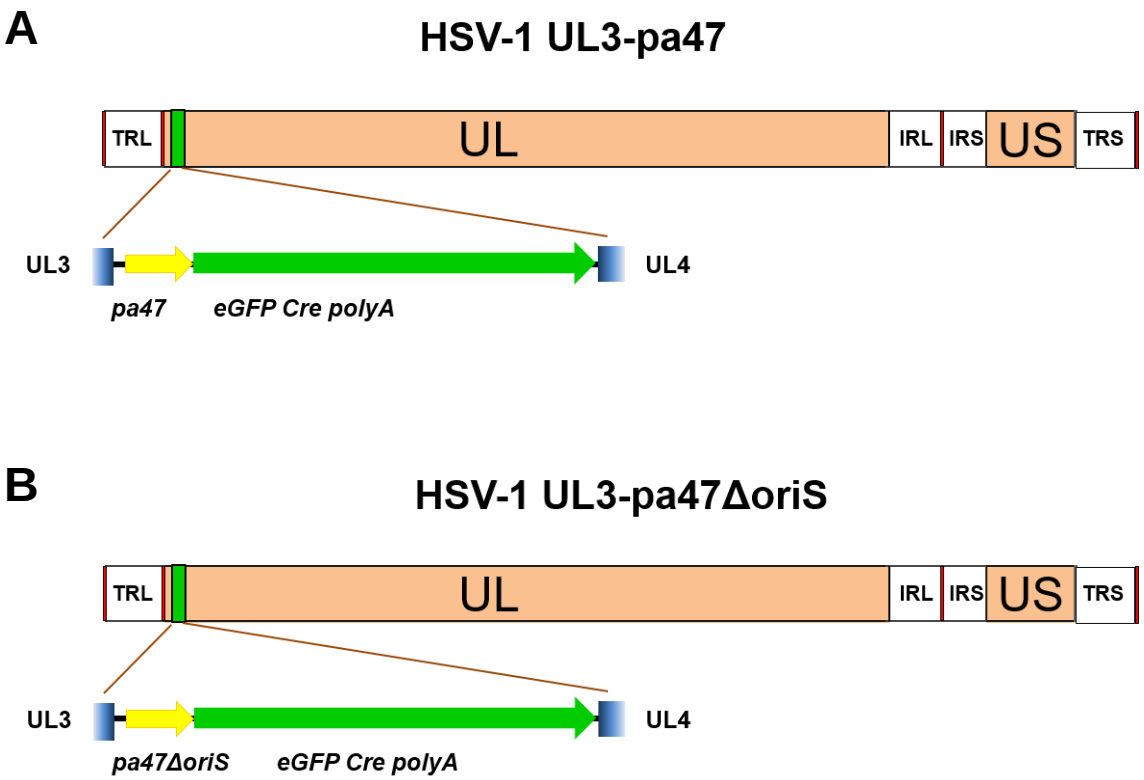

Figure 4.7 Schematic representation of the HSV-1 UL3-pa47 and HSV-1 UL3-pa47ΔoriS genomes. Diagrams of HSV-1 genomes showing the typical arrangement of the unique and the repeat regions. The green line represents the region of insertion of the (A) pa47- and (B) pa47ΔoriS- eGFP Cre cassette in the HSV-1 genome. The expanded region highlights the orientation of the inserted cassette and the flanking region.

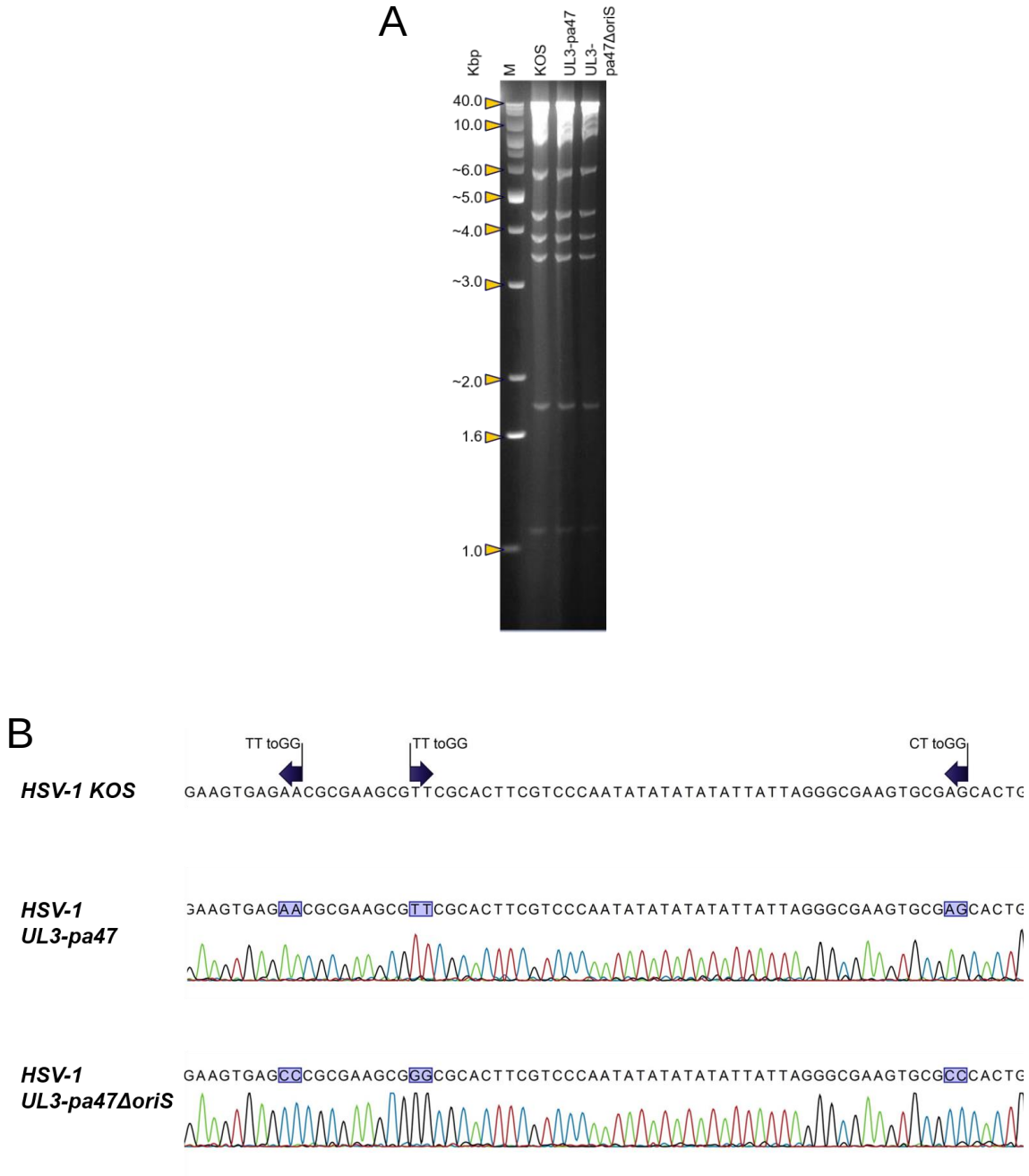

Figure 4.8 Analysis of recombinant HSV-1 UL3-pa47 and HSV-1 UL3-pa47ΔoriS sequences by whole genome digestion and Sanger sequencing. (A) Viral DNA isolated from wild-type and the recombinant HSV-1 viruses were digested using ScaI, and the fragments were separated using agarose gel electrophoresis. The yellow arrowheads to the left of the gel image indicate the position of relevant marker fragments (in kbp). (B) The nucleotide sequence data of the oriS region of the wild-type strain KOS and the recombinant viruses are shown. The position of the dinucleotide substitutions made in UL3-pa47ΔoriS is highlighted in the image.

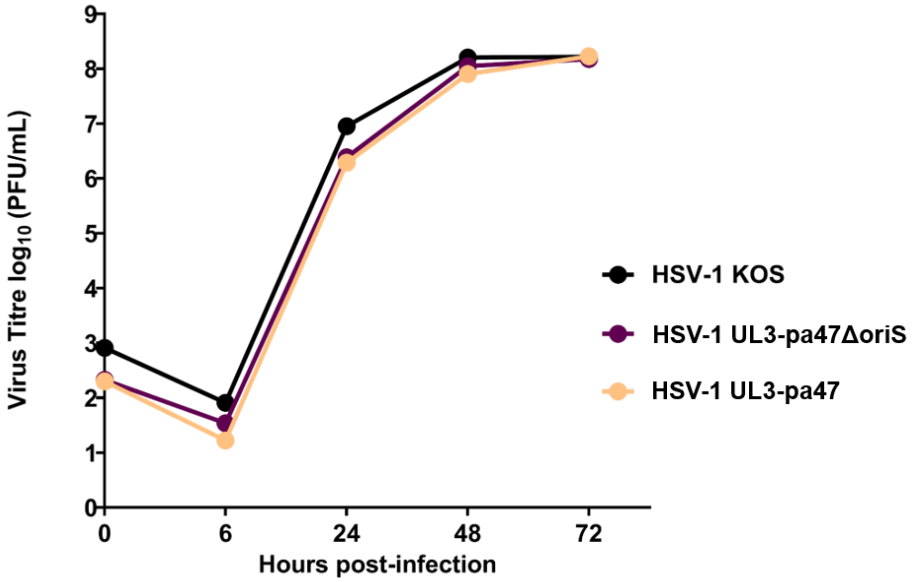

Figure 4.9 Multi-step replication kinetics of KOS, HSV-1 UL3-pa47 and HSV-1 UL3-pa47ΔoriS viruses in Vero cells. Monolayers of Vero cells were infected at 0.01 pfu/cell and multi-step growth curves were performed as described earlier (see section 2.3.7.1). The amount of virus in infected cells was determined using plaque assays at the indicated time points. The experiment was conducted in triplicate. The results are shown as mean pfu/mL ± SEM. The error bars are obscured by the symbols.

4.2.4 Replication of the recombinant viruses is not impaired in the skin and DRG

To determine if insertion of the reporter gene cassettes altered virus replication in mice, groups of mice were infected with 1×10^8 PFU/mL of wild-type or recombinant viruses, HSV-1 UL3-pa47 or HSV-1 UL3-pa47ΔoriS, on the left flank (see methods section 2.3.10.1). After five days, 8 mm wide skin tissue sample, running from the dorsal to ventral mid-line surrounding the infection site, was surgically recovered and snap frozen. Additionally, ipsilateral DRG from spinal levels T5 to L1 were collected and snap frozen. The tissues were thawed and homogenised in culture media, and the amount of virus was determined using a plaque assay. The average virus titre in the skin and DRG was comparable between the wild-type and UL27-pa47min virus suggesting that insertion of pa47min eGFP Cre cassette into UL26 and UL27 intergenic region did not affect virus growth *in vivo* (Figure 4.10 A). Similarly, the difference in mean virus titre between the wild-type HSV-1 KOS and the recombinants, HSV-1 UL3-pa47 or HSV-1 UL3-pa47ΔoriS, was not statistically significant (Figure 4.10 B). These results suggest that all three viruses have wild-type replication *in vivo*.

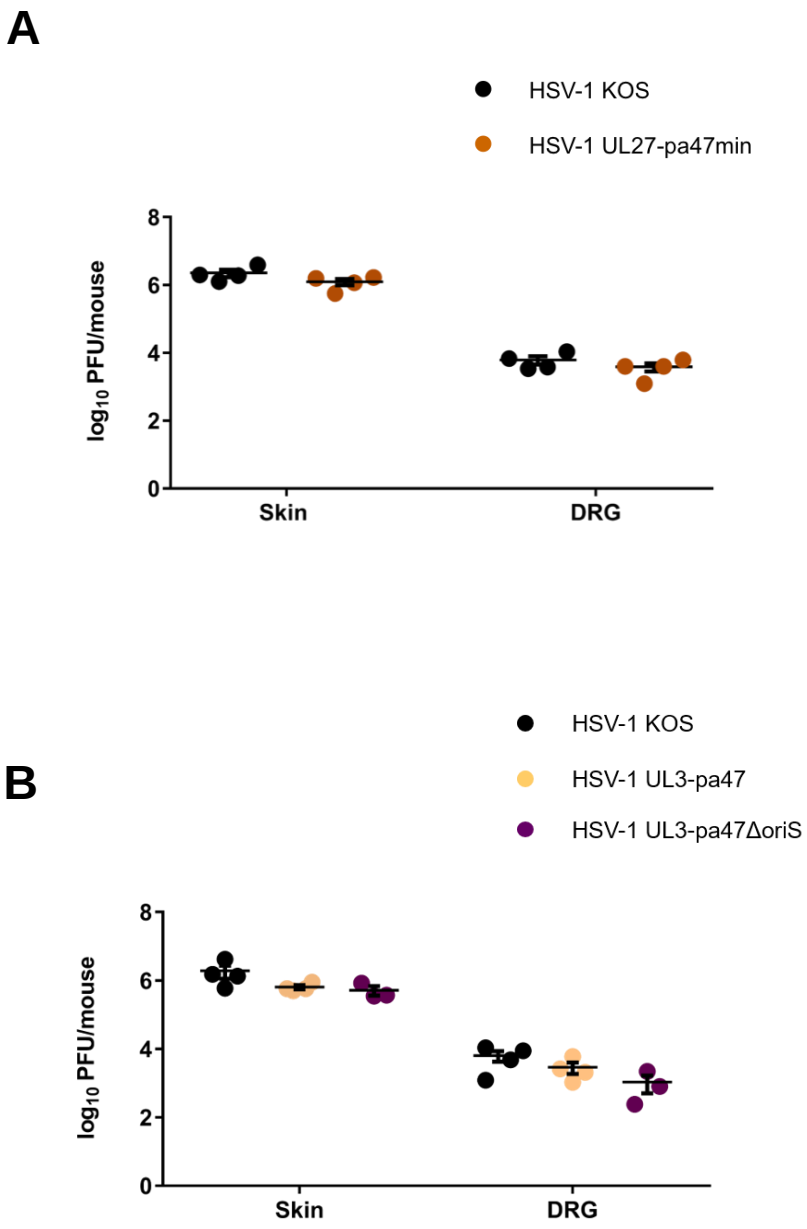

Figure 4.10 Growth analysis of HSV-1 KOS and recombinant viruses, HSV-1 UL27-pa47min, HSV-1 UL3-pa47 and HSV-1 UL3-pa47ΔoriS, in mice. Mice were infected on the left flank by tattooing. Five days after infection, the skin and DRG were collected, homogenised and virus titre determined using plaque assay. (A) Amounts of KOS and UL27-pa47min in skin and DRG of mice are shown. The mean titres of the two viruses were not significantly different in both tissue types as assessed by unpaired t-test. (B) Virus titre of KOS, UL3-pa47, and UL3-pa47ΔoriS in skin and DRG of mice are shown. The means of the recombinant viruses were compared to the wild-type virus using one-way ANOVA with Dunnet's multiple comparisons post-test. The differences were not statistically significant. The error bars in both graphs represent mean ± SEM.

4.2.5 ICP47 follows the IE class of gene expression regardless of location or the promoter sequence

ICP47 falls under the immediate-early (IE) category in the gene expression cascade and is expressed as early as one hour after infection (Harkness et al., 2014). Hence, in our recombinant viruses, eGFP expression was expected to follow the same IE kinetic class. To test whether in our recombinant viruses the reporter gene was expressed as an IE gene, we used an assay based on cycloheximide and actinomycin D (see section 2.3.8). Expression of IE genes does not require prior viral protein synthesis, but the E and L genes need IE proteins for their expression (Honess and Roizman, 1974). Addition of cycloheximide (CHX) to the culture media blocks the *de novo* protein synthesis in cells. Therefore, in the presence of CHX, only IE mRNA will be made and accumulate in infected cells. These IE mRNAs can then be translated to protein if the inhibition enacted by CHX is released. Replacing CHX by actinomycin D (AD) leads to a loss of further transcription and therefore blocks the synthesis of E and L gene products. The final outcome is that the only viral proteins that are made will be IE gene products. This CHX reversal (CHR) assay is commonly used to identify a promoter belonging to the IE class (Honess and Roizman, 1974; Barklie et al., 1977).

Monolayers of Vero cells pre-treated with CHX were infected with wild-type virus or recombinant viruses expressing eGFP-Cre fusion gene controlled by various HSV-1 promoters. A control with no drug treatment was included for each infection. The viruses, HSV-1 pICP0_eGC and HSV-1 gB_eGC, generated and tested by Russell and Tscharke (2016), were used here as control viruses. Expression of eGFP was noted in all the samples that were not treated with CHX or AD irrespective of the kinetic class of the promoter (Figure 4.11). Following the CHR process, reporter gene expression was observed in cells infected with HSV-1 pICP0_eGC, HSV-1 UL3-pa47min, HSV-1 Ka47inΔ, Ka47rescue, UL27-pa47min, UL3-pa47 and UL3-pa47ΔoriS. Whereas in cells infected with the HSV-1 gB_eGC virus, in which the leaky-late gB promoter drive eGFP-Cre, we could not detect eGFP, confirming that CHX and AD were active. These results suggest that the ICP47 promoter functions as an IE promoter regardless of the region from which it is expressed or the alterations in the promoter sequence. This was true for all recombinant viruses studied in this chapter. However, we can separate the promoters into two distinct classes on the basis of GFP-positive cell proportion. In one group, including pICP0_eGC, Ka47rescue and Ka47inΔ, eGFP accumulated equally well in the presence or absence of

CHX. In the other group, which includes UL3-pa47min, UL27-pa47min, UL3-pa47 and UL3-pa47ΔoriS, eGFP expressing cells were proportionately reduced from two to three-fold in CHX treated cells compared to untreated cells. These data suggest that when the ICP47 promoter is situated at an ectopic location it functions differently to the native promoter, specifically it is less active under strict IE conditions *in vitro*.

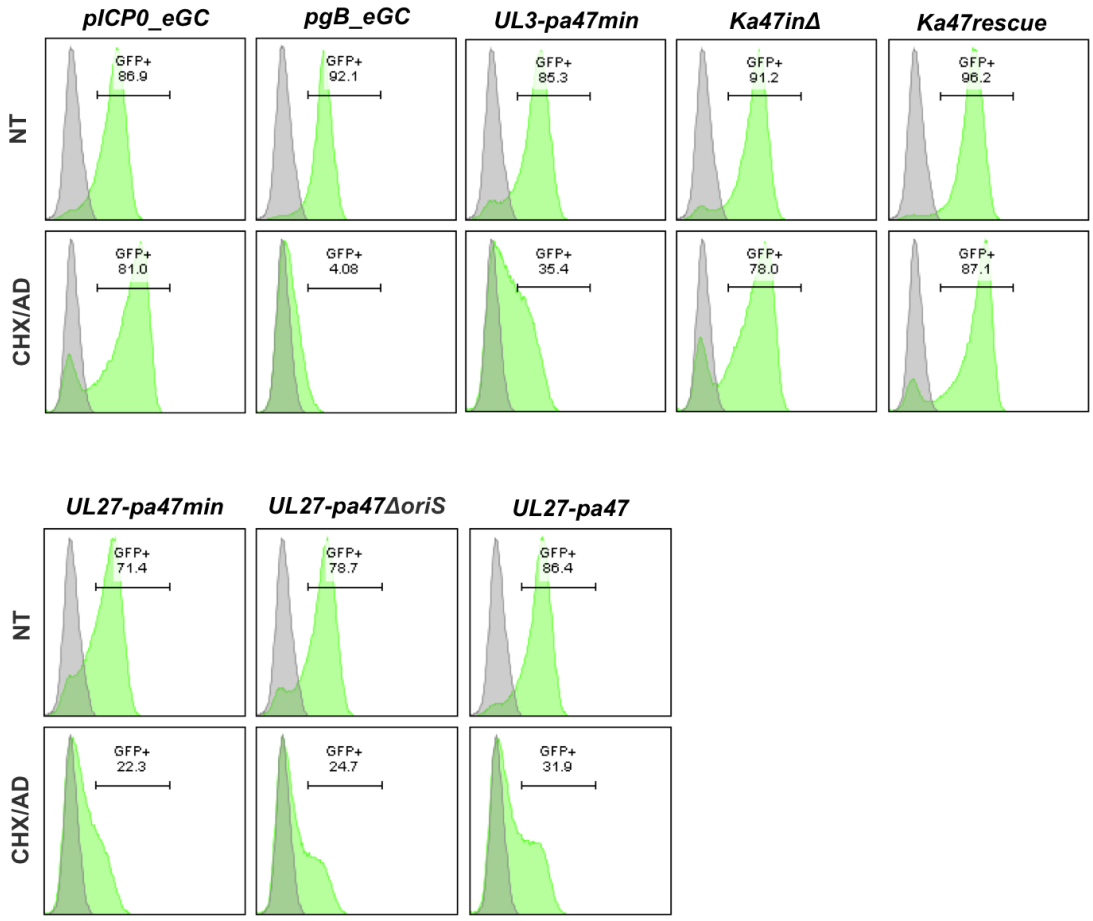

Figure 4.11 IE characteristics of the ICP47 promoter are unaltered by promoter location in the genome or the lack of oriS and 5′ UTR sequences. The promoter activity of each of the recombinant viruses under CHR (CHX/AD) or control (NT) conditions is shown. The histogram in grey represents the eGFP expression in cells infected with unmodified KOS, and the histogram in green represents the eGFP expression in cells infected with the recombinant virus. The viruses subjected to the CHR assay are indicated above each column.

4.2.6 Genomic loci may influence the activation of ICP47 promoter during latency

We hypothesised that difference in promoter activation after lytic infection might be a consequence of varying genomic locations of reporter gene insertion or promoter sequences. If the observed differences could be attributed to location, we would anticipate that the β-gal marked neurons would not accumulate during latency if we alter the position of the gene cassette in the viral genome. To test this possibility, we constructed recombinant HSV-1 UL27-pa47min, which contains the eGFP-Cre fusion gene under control of pa47min, inserted into the UL26-UL27 locus (see section 4.2.2). We infected ROSA26R mice with this virus and enumerated the number of β-gal producing neurons at various days after infection (Figure 4.2). Interestingly, we found that the number of marked neurons fell continuously and significantly from 5 to 20 days after infection and remained stable from 20 days onwards (Figure 4.12 A). Although the number of marked neurons did not increase beyond lytic infection, the number of DRG with marked neurons showed a slight, but not significant increase from 5 to 100 days after infection (Figure 4.12 B). When the modified ICP47 promoter, pa47min, was inserted into the UL3-UL4 locus, Cre marking of neurons continued to increase beyond lytic infection (Russell and Tscharke, 2016). Whereas when the same promoter was inserted into an alternate gene expression locus UL26-UL27, it did not promote neuronal marking beyond lytic phase. Two possible reasons for the current observation are: the UL3-UL4 region contains a regulatory element that permits gene expression during latency or conversely, the UL26-UL27 region and ICP47 locus include suppressor elements that block the gene expression during latency.

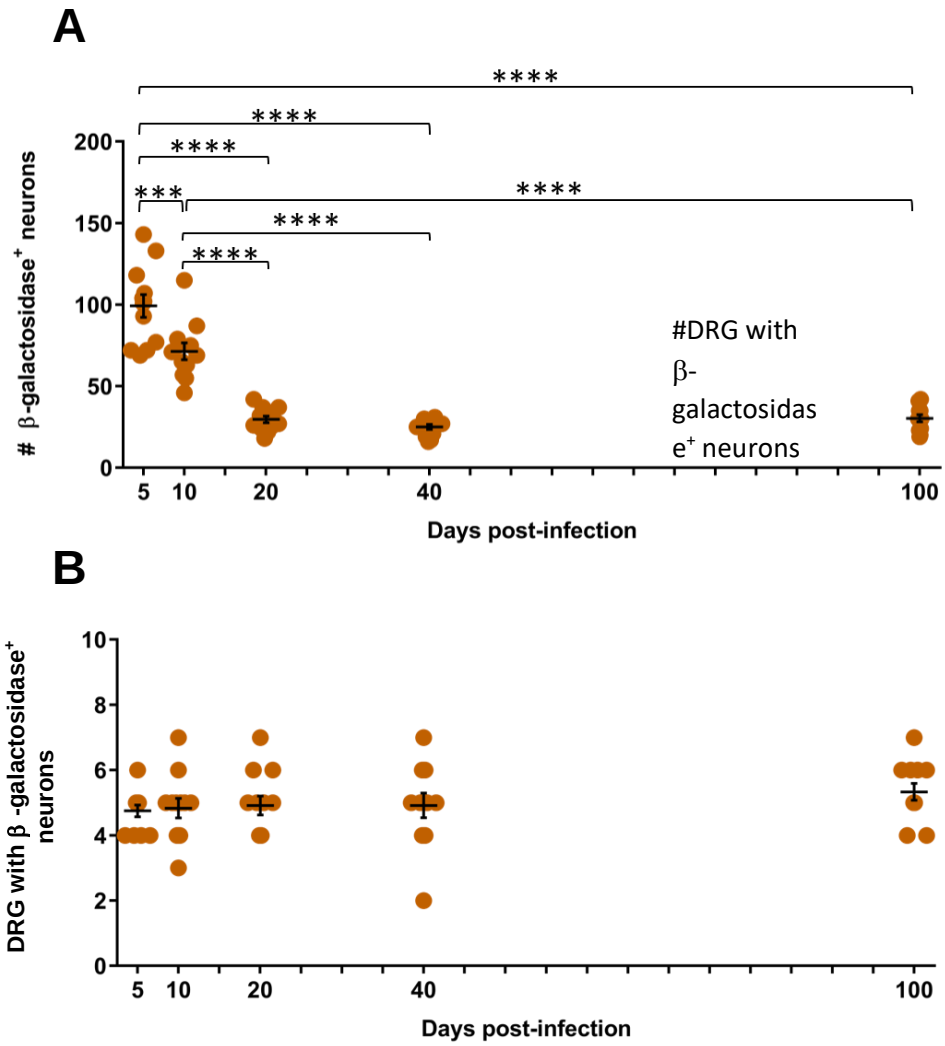

Figure 4.12 The modified ICP47 promoter, pa47min, is repressed beyond lytic infection in the UL26-UL27 locus. Groups of ROSA26R mice (n=12) were infected with HSV-1 UL27-pa47min and culled at 5, 10, 20, 40 and 100 days after infection. DRG from T5 to L1 were excised from each mouse, stained with X-Gal staining buffer, mounted intact and used for enumerating large blue cells that represent β-gal marked neurons. (A) The graph shows the number of β-gal positive cells per mouse at the indicated times post-infection. (B) The graph shows the number of DRG with at least one β-gal positive cell per mouse. (A&B) The results were pooled from three independent experiments each with at least two overlapping time points. The error bars represent mean ± SEM. The statistical significance was determined by comparing the mean at each time point to every other time point using one-way ANOVA with Bonferroni's multiple comparisons post-test (***p<0.001, ****p<0.0001).

4.2.7 The UL3-UL4 intergenic region is permissive of full-length ICP47 promoter activation

To obtain a better understanding of current observations related to ICP47 promoter activation during the latency establishment phase and latency itself, we infected ROSA26R mice with HSV-1 UL3-pa47 or UL3-pa47ΔoriS. As described earlier in section 4.2.3, these viruses express the eGFP-Cre fusion gene controlled by the ICP47 promoter that encompasses the minimal promoter and the downstream sequence until the translation initiation site. Infection of ROSA26R mice with these viruses resulted in an initial decrease in the number of β-gal producing neurons from days 5 to 10, followed by an upward trend from days 10 to 20 post-infection, however, the difference was not found to be statistically significant (Figure 4.13 and Figure 4.14). From 20 days after infection, the number of marked neurons continued to accumulate until the time of final examination (100 days). Comparison between the average numbers of β-gal marked neurons between 20 and 100 days after infection revealed a significant increase across the HSV-1 UL3-pa47 and UL3-pa47ΔoriS conditions. The number of neurons marked during lytic infection was comparable between all recombinants generated in this thesis in which the ICP47 promoter controlled Cre expression (Figure 4.15). However, neuronal marking was consistently documented during latency establishment phase (10 to 20 days) and latency (40 to 100 days) only when the reporter gene cassette was introduced into the region between the genes UL3 and UL4.

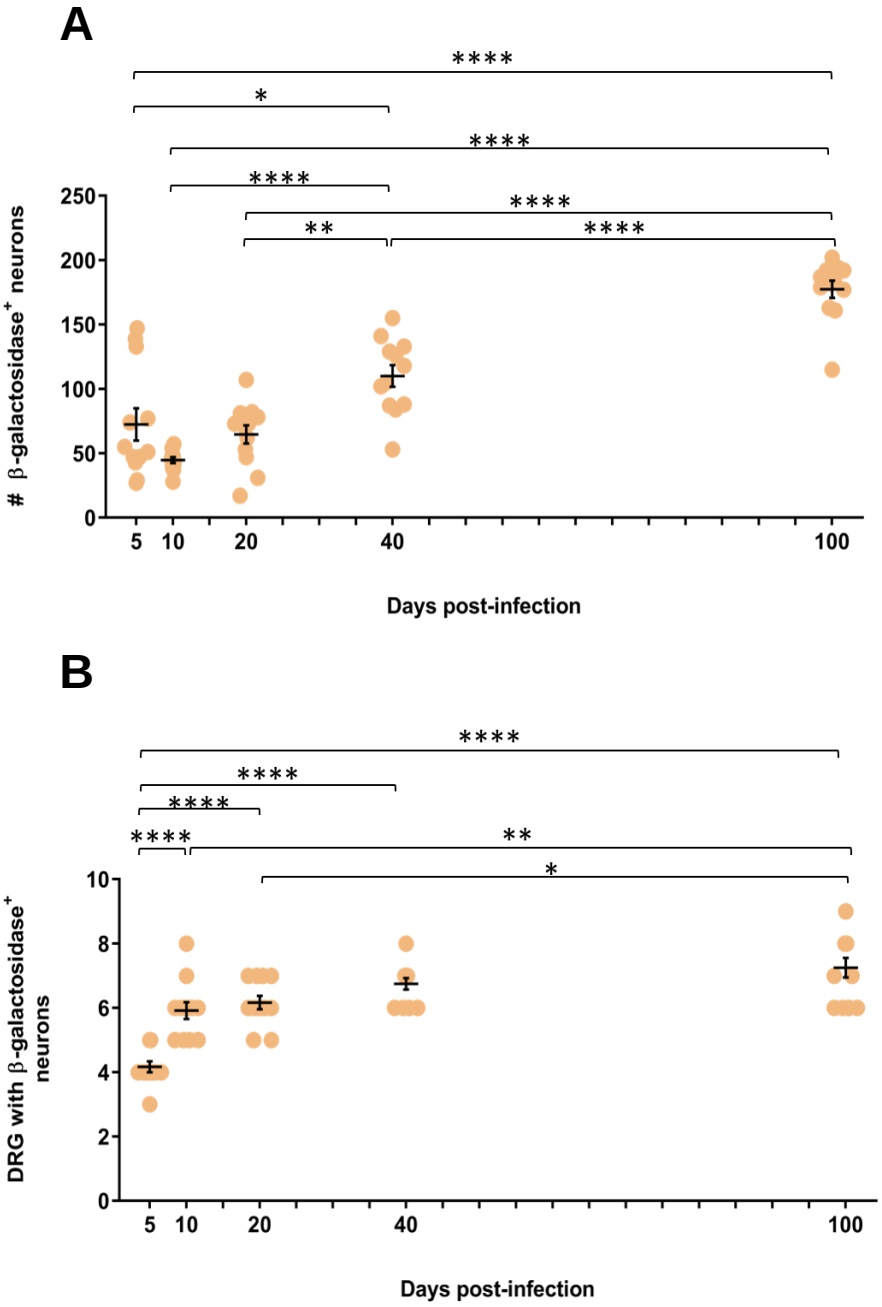

Figure 4.13 Use of the recombinant HSV-1 UL3-pa47 reveals that the UL3-UL4 intergenic region induces Cre marking of neurons during latency. Groups of ROSA26R mice were infected with HSV-1 UL3-pa47 on the flank. DRG from T5 to L1 were excised from each mouse on indicated days post-infection, stained with X-Gal, mounted intact and large blue cells were counted. The graphs show the number of β-gal positive cells per mouse (A) and the number of DRG with at least one β-gal positive cell per mouse (B). (A&B) Each symbol represents a mouse (n=12) and error bar shows mean ± SEM. The results were pooled from three independent experiments each with at least two overlapping time points. The means were compared at each time point and statistical significance was calculated using one-way ANOVA combined with Bonferroni's multiple comparisons post-test (*p<0.05, **p<0.01, ***p<0.001, ****p<0.0001).

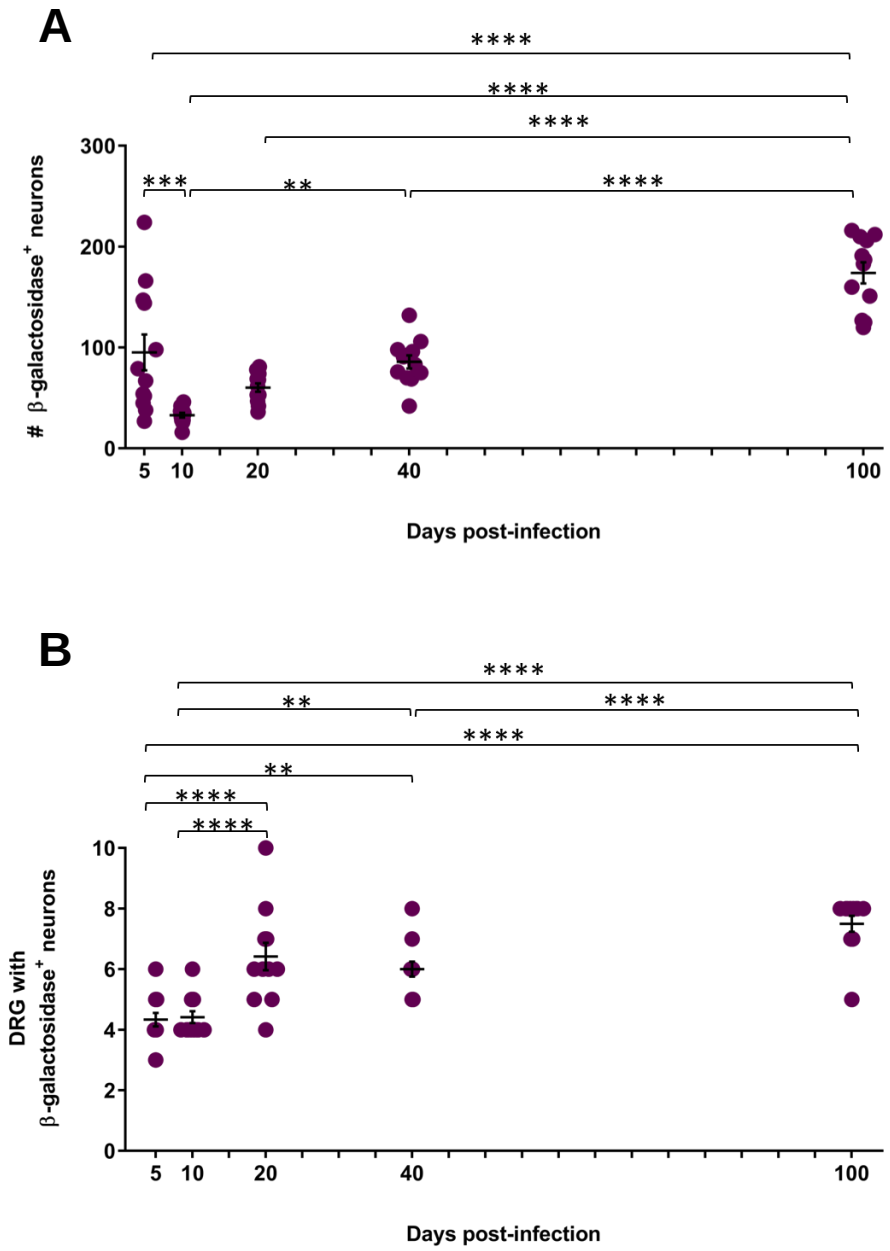

Figure 4.14 Recombinant HSV-1 UL3-pa47ΔoriS reveals that the UL3-UL4 intergenic region induces Cre marking of neurons during latency. Groups of ROSA26R mice were infected with HSV-1 UL3-pa47ΔoriS on the flank. DRG from T5 to L1 were excised from each mouse on 5, 10, 20, 40- and 100-days post-infection, stained with X-Gal, mounted intact and large blue cells were counted. The graphs show the number of β-gal positive cells per mouse (A) and the number of DRG with β-gal positive cells per mouse (B). Each symbol represents a mouse (n=12). The error bar shows mean ± SEM. The means were compared at each time point and statistical significance was calculated using one-way ANOVA combined with Bonferroni's multiple comparisons post-test (*p<0.05, **p<0.01, ***p<0.001, ****p<0.0001).

4.2.8 Summary of the Cre-marking data

The data from this chapter, summarised in Figure 4.15, suggest that changing the ectopic location from UL3-UL4 to UL26-UL27 altered the transcriptional behaviour of the ICP47 promoter. On the one hand, in the UL3-UL4 locus, ICP47 promoter induced Cre-mediated marking of new neurons beyond the lytic phase of infection. Additional neurons were marked regardless of whether the oriS, intron and 5′ UTR were present in the promoter. On the other hand, in the UL26-U27 locus, the minimal ICP47 promoter did not induce marking of further neurons beyond the lytic infection, instead, the number of marked neurons dropped from days 5 to 20 and remained unaltered beyond 20 days. Furthermore, the number of neurons marked at each time point by the UL27-pa47min virus was similar to that seen following infection with the recombinant viruses that expressed Cre from the ICP47 promoter at the native locus (Ka47inΔ and Ka47rescue). Together our data show that Cre marking of neurons beyond lytic infection is specific to the UL3-UL4 locus and suggests the regulatory elements present in the native ICP47 locus may not influence the accumulation of marked neurons. However, two major differences were noticed in marking between HSV-1 UL3-pa47min and HSV-1 UL3-pa47 or UL3-pa47ΔoriS. First, an inverse trend in marking was observed from 5 to 10 days after infection. Additionally, significantly more neurons were marked by pa47min compared to pa47 or pa47ΔoriS at UL3-UL4 locus beyond 10 days after infection. Whether the cis-acting elements in the full-length promoter play a role in the differential induction of Cre marking between these viruses is yet to be established.

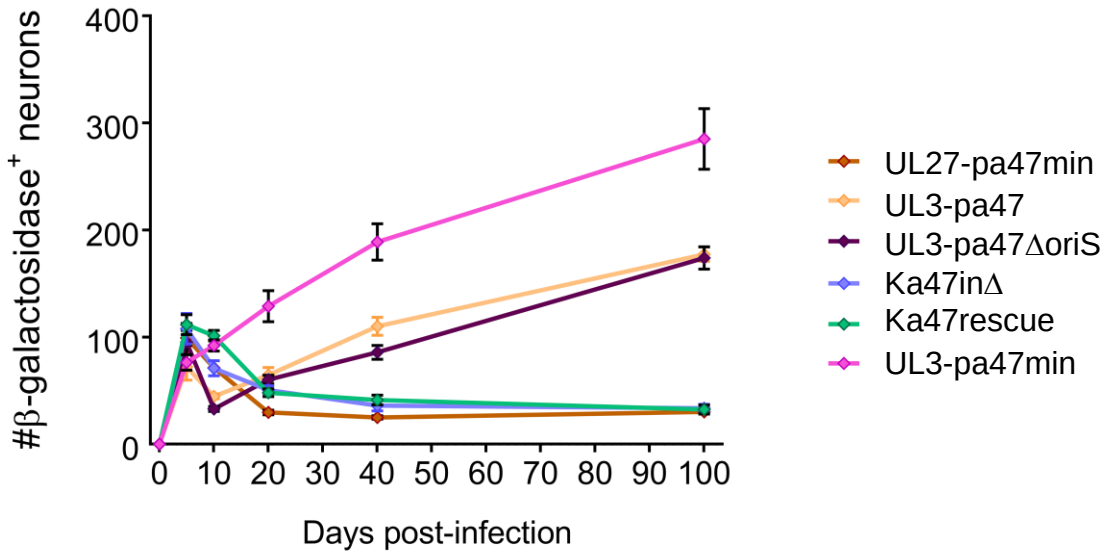

Figure 4.15 Summary of β-gal marking of neurons in ROSA26R mice. The summary graph illustrates the number of β-gal+ cells per mouse at different time points when infected with the indicated viruses. The symbols represent the averages of β-gal+ cells across all mice for each recombinant virus. The error bar shows mean ± SEM.

4.3 Discussion

In this chapter, we investigated the influence of *a)* potential regulatory elements in the ICP47 promoter and *b)* the location of gene expression on the promoter activation using the ROSA26R/Cre reporter mouse system. In a previous study, Proença and colleagues used this reporter mouse system to test lytic gene promoters representative of all kinetic classes (ICP0, ICP4, TK, gC, and VP16) by inserting reporter gene cassettes into US5 locus. At this position, none of the promoters induced detectable β-gal expression in previously unmarked neurons beyond 5 days (Proença et al., 2008, 2011). The results from this chapter demonstrate that ICP47 promoter was active beyond lytic infection when placed in the UL3-UL4 locus, however, placement at two other positions (ICP47 and UL26-UL27) resulted in no detectable promoter activity at this time. Given that ICP47 promoter activation was not detected in at least two alternate loci after 5 days in our study, and additionally no detectable activation was observed for other lytic promoters in the US5 locus during latency (Proença et al., 2008, 2011), the most obvious conclusion is that UL3-UL4 locus is more permissive for gene expression during latency. The ICP0 promoter was an exception, which, when allowed to drive Cre from UL3-UL4 locus, led to the number of marked neurons remaining stable after 20 days of infection (Russell and Tscharke, 2016). This finding indicates that the detectable level of promoter activation beyond lytic infection is not universal to all HSV-1 promoters in the UL3-UL4 locus.

From viral transcriptome analysis of acutely infected TG neurons, it can be seen that UL3 mRNA transcripts were produced but at a much lower level compared to the ICP47 transcripts (Harkness et al., 2014). Using an IE-gene deficient mutant to establish persistent infection in neurons, Harkness and colleagues showed that transcription of genes was more pronounced at the joint regions of long, short and repeat segments of the genome. The expression level of the genes UL1 to UL5 at the TRL/UL joint region was higher compared to most genes of the long segment of the genome, yet, several folds lower than ICP47 (Harkness et al., 2014). Indeed, ICP47 is one of the few genes that was transcribed abundantly in TG neuron culture (Harkness et al., 2014). Notably, ICP47 transcripts were also detected in neurons harbouring the latent viral genome (Ma et al., 2014). However, in our current study, detectable ICP47 promoter activation did not occur beyond the lytic infection when the gene cassette was introduced in the native ICP47 location or an ectopic location (UL26-UL27 locus). It is possible that Cre expression still occurred from these loci

but at a level below that is required to mediate the effective genetic recombination at loxP sites and subsequent β-gal expression. In that case, the UL3-UL4 locus is peculiar in its ability to impact the activity of ICP47 promoter in the latent HSV-1 genome. To our knowledge, the issue of position-dependent gene expression in HSV-1 has not been previously demonstrated *in vivo*.

The genes UL3 and UL4 are non-essential for virus replication in culture (Baines and Roizman, 1991). While UL3 and UL4 were shown to co-localise with ICP22 in the nucleus forming small dense nuclear bodies in cell culture (Jahedi et al., 1999; Xing et al., 2011; Zheng et al., 2011), the role of UL3 and UL4 in HSV-1 infection is currently unknown. Interestingly, the genes UL3 and UL4 are proximal to the LAT locus of the terminal repeat region of the HSV-1 genome (Stevens et al., 1987a). LATs are the most abundantly detectable transcripts during latency, expressed at least in one-third of the latently infected neurons at a given time (Stevens et al., 1987a; Mehta et al., 1995). The LAT transcription unit contains an upstream regulatory sequence comprising of a promoter and an enhancer element (Berthomme et al., 2000). In latent HSV-1 genomes, the LAT locus was shown to be enriched with histone H3 containing acetylated lysine residues (H3 K4, K9) and transcriptionally permissive dimethyl H3 K4 histones (Kubat et al., 2004). These data imply that the LAT region is transcriptionally active. The major LAT is transcribed anti-sense to ICP0 mRNA and these two genes exist as two copies, one located at IRL and the other copy at TRL segment of the genome (Spivack and Fraser, 1987; Stevens et al., 1987b). ICP27 (UL54) is located in the UL segment near the LAT locus in the IRL segment (McGeoch et al., 1988). Previous studies found that the IE genes, ICP0 and ICP27, bear acetylated histones in latently infected mouse DRG, although to a much lower extent than LAT region (Kubat et al., 2004). Similarly, in a rabbit model, latently infected TG showed transcriptionally permissive dimethyl H3 K4 histone marks not only on the LAT region but also to a lower extent on the ICP0 and ICP27 promoters (Giordani et al., 2008). Whether the acetylation extends from the LAT locus in the TRL region to the neighbouring genes (from UL1 to UL5) in the UL segment is unexplored. Given that the UL3-UL4 locus is near the LAT region, it is possible that the post-translational modification that supports active transcription is extended to the UL3-UL4 locus during latency, making it transcriptionally permissive. This would explain the observation of lytic gene promoter activation from the UL3-UL4 locus, particularly in ROSA26R mice where transient Cre expression is sufficient to mark the neurons with β-gal expression. Further analysis is

required to determine whether transcription permissive histone modifications of the LAT region influence gene expression from the UL3-UL4 locus and in that case whether other lytic genes near the LAT loci such as ICP0, ICP4, UL54, and UL3 are expressed during latency.

The LAT region is demarcated by the CTCCC boundary elements (CTRL1 and CTRL2) that bind CTCF proteins in latently infected neurons (Amelio et al., 2006). The binding of CTCF proteins to this region was shown to block enhancer activity from spreading to neighbouring genes (Amelio et al., 2006; Chen et al., 2007). Despite this enhancer blocking function, recent studies showed that CTCF has been associated with its ability to create chromatin loops and to mediate long-range genome interactions (Ohlsson et al., 2010; Kang et al., 2011; Tempera et al., 2011). CTCF-mediated chromatin looping and modulation of distal gene expression has been previously observed in Epstein-Barr virus (EBV) (Tempera et al., 2011; Chen et al., 2014). The HSV-1 genome is maintained as a circular episome in association with nucleosomes (Deshmane and Fraser, 1989) in which case the three-dimensional organisation of DNA may allow the LAT enhancer to regulate distal promoters leading to their activation. It is not known whether an interaction between the LAT enhancer and the promoter inserted into the UL3-UL4 locus occurs by chromatin reorganisation, however, currently, such a possibility cannot be excluded.

Future experiments could be designed to test if the native UL3 or UL4 promoters induce Cre marking during and after the establishment of latency. For example, simultaneous expression of UL3 and Cre by the same native promoter is possible by insertion of an internal ribosomal entry site (IRES) or by introducing a self-cleaving small peptide called 2A between the two genes (Hellen and Sarnow, 2001; Daniels et al., 2014; Ahier and Jarriault, 2014; Colussi et al., 2015). Whilst IRES allows translation of two open reading frames from one mRNA, the difference in expression level of genes inserted before and after IRES has been documented (Mizuguchi et al., 2000; Hennecke, 2001). This problem can be avoided by the use of 2A peptide. Introducing this small peptide sequence between two genes causes steric hindrance and ribosomal skipping during translation event, leading to co-expression of proteins at equal proportions (Szymczak et al., 2004; Ahier and Jarriault, 2014; Liu et al., 2017). Thus, a recombinant HSV-1 co-expressing Cre with UL3 or UL4 gene in a bi-cistronic manner in the native position would address if this region were prone to induce detectable Cre marking during latency. Because the gB and ICP6 promoters were

also active during latency in the UL3-UL4 locus, experiments could be conducted to determine if the promoters of gB and ICP6 at the native position are active during latency or whether their activation was specific to the UL3-UL4 locus. Such experiments may eventually lead to a broader understanding of lytic gene expression during latency. Given that ICP0 transcripts are detectable in latently infected neurons (Maillet et al., 2006), the lack of Cre marking by the ICP0 promoter in the UL3-UL4 locus could perhaps be due to the issue of sensitivity of the system. However, we cannot preclude the possibility that the ICP0 promoter carries a functional regulatory element that represses gene expression during and after the establishment of latency.

At the UL3-UL4 locus both the full-length and the minimal ICP47 promoter induced detectable β-gal in previously unmarked neurons during the establishment and maintenance of latency. However, the number of neurons marked by pa47 or pa47ΔoriS was considerably less compared to that of the neurons marked by pa47min from 10 days after infection (Figure 4.15). This reduction in a number of visibly marked neurons implies that regulatory elements of a suppressive nature might be present in pa47 and pa47ΔoriS. Interestingly, the ICP47 intron region contains a cluster of CTCT motifs called CTRS3, which were shown to be occupied by CTCF proteins during latency (Amelio et al., 2006; Washington et al., 2018). Previous reports have shown that the CTCF proteins recruit diverse transcription factors to exert transcription activation, repression or enhancer-blocking functions (Lutz et al., 2000; Chernukhin et al., 2007; Li et al., 2008). Consistent with this, a polycomb repressor complex (PRC) subunit called Suz12 was found to co-localise with CTCF at CTRS3 on latent viral genomes (Cliffe et al., 2013b; Washington et al., 2018). The five-subunit complex, PRC2 causes epigenetic modification of the target gene leading to transcriptional repression. When reactivation was induced in latently-infected mice, CTCF and Suz12 at CTSR3 were significantly reduced after 6 hours, most likely leading to transcription activation (Washington et al., 2018). This observation supports the idea that CTCF and PRC2 recruited through Suz12 may repress ICP47 gene expression during latency. Further, in the context of HCMV and MCMV infection, binding of CTCF with the intron of CMV major immediate early (MIE) gene was shown to cause repression of MIE gene (Martínez et al., 2014). The exact mechanism of transcriptional repression has not been established but it was suggested that CTCF may manipulate RNA polymerase II function in this case (Martínez et al., 2014). Since CTRS3 is also located on the ICP47 intron, a similar transcriptional dampening effect of the ICP47 gene is possible

during latency. This explains the differences in marking by the full-length and the intron-less promoters. However, CTCF may not bind efficiently to CTRS3 at the ectopic location, explaining why the promoters, pa47 and pa47ΔoriS, still marked neurons during latency. However, these hypotheses are yet to be empirically tested.

As demonstrated in this chapter, the local genomic environment in which a foreign gene is inserted can modulate gene expression. Similarly, a promoter taken out of the genomic context may act differentially compared to its functions at the native position. The data from the CHR assays support this hypothesis. Although inhibition of protein synthesis by CHX did not block ICP47 promoter activity at two ectopic locations, the level of reporter gene expression was considerably lower in these loci when compared to the native ICP47 promoter. This suggests that the regulation of ICP47 promoter activity is more complex at the native locus. However, it is not surprising considering the complexity of the position at which ICP47 is located in the genome and the number of regulatory elements present in this region.

Chapter 5
Investigation of inhibition of antigen presentation by ICP47 on human and mouse cells

5 Investigation of inhibition of antigen presentation by ICP47 on human and mouse cells

5.1 Introduction

In Chapter 3, the function of ICP47 was examined using a sensitive flow cytometry-based antigen presentation assay, where it became evident that ICP47 indeed inhibits antigen presentation in mouse cells. The *in vivo* data from chapter 3 showed that in a mouse model where the virus does not invade the CNS, removal of ICP47 did not affect the pathogenicity of the virus and its ability to establish or maintain latency. One possibility for the lack of phenotype is that perhaps the virus does not overcome $CD8^+$ T cell immunity because the viral determinants are not sufficiently blocked from the presentation. Hence, the removal of ICP47 would not significantly affect pathogenesis. As a result, the role of ICP47 *in vivo* remains inconclusive. It is unknown *a)* how much more efficient ICP47's inhibition of human TAP is compared to mouse TAP? *b)* whether the inhibition of TAP-mediated peptide translocation would affect HSV-1 infection in humans? and *c)* whether all $CD8^+$ T cell epitopes are equally inhibited?

Historically, the effect of ICP47 on the cell surface presentation of pMHC-I was addressed indirectly using cytotoxic T cell lysis assays, which measure the level of killing of target cells by activated HSV-1 specific $CD8^+$ T cells (Jugovic et al., 1998; Aubert et al., 2006). This method reveals differences in the $CD8^+$ T cell response against HSV-1 infected human and mouse cells (Jugovic et al., 1998), however, it is not a strictly quantitative assay. The threshold for lysis depends on the density of the $CD8^+$ T cell determinants on the cell surface and the quality of polyclonal or monoclonal $CD8^+$ T cell population used for the analysis. Our antigen presentation assay detected the differences in the level of K^b-SIINFEKL complex in the presence or absence of ICP47 on the surface of human and mouse cells. In mouse cells, the inhibition of antigen presentation was 44%, whereas in human cells presentation was reduced by 85% (see section 3.2.3 and Figure 3.8). However, this assay is based on relative quantification and it is limited in sensitivity by the 25D1.16 monoclonal antibody. Further, the assay is limited to a single epitope and although expressed by a virus, it has been engineered and is thus not a natural product of infection.

Thus, these assays may not provide the full picture of the effect of ICP47 on the HSV-1 immunopeptidome and on the presentation of individual HSV-1 peptides.

To overcome these limitations, in this chapter, we set out to determine the impact of ICP47 on human and mouse TAP by determining the absolute number of HSV-1 peptides presented on human and mouse cells using mass spectrometry. For this, endogenously derived MHC I bound HSV-1 peptides were first identified from infected mouse cells using a conventional mass spectrometry approach known as liquid chromatography-tandem mass spectrometry (LC-MS/MS) (see section 5.2.1.1 and Figure 5.2). Then, a subset of HSV-1 peptides presented on HSV-1 infected human and mouse cells were quantified by targeted MS (multiple reaction monitoring or MRM-MS) (see section 5.2.3 and Figure 5.15). With this, we aimed to measure the extent to which ICP47 hindered antigen presentation, which in turn would allow us to make a robust comparison between the human and mouse cells. The workflow of the MS-based experiments used for the quantification of HSV-1 peptides is summarised in Figure 5.1. This was a collaborative project with the Immunoproteomics laboratory led by Professor Purcell at the Department of Biochemistry and Molecular Biology (Monash University, Melbourne). Infection of cells was carried out at ANU (Canberra) and the subsequent experiments were carried out at Monash University under the guidance of Dr. Nathan Croft.

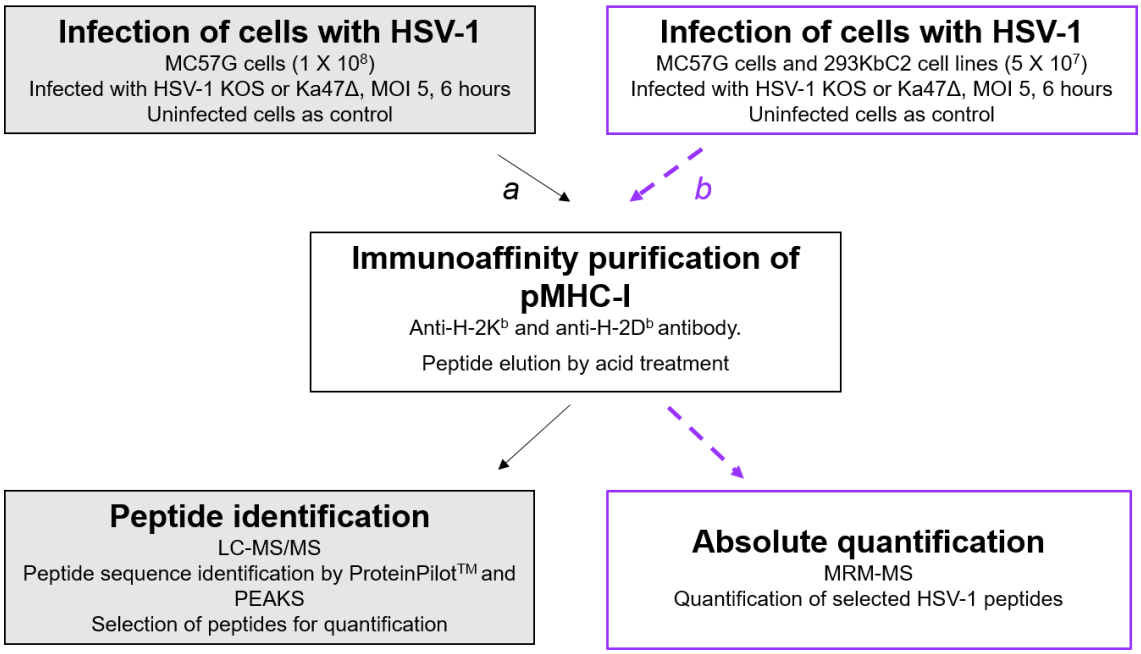

Figure 5.1 Workflow of MS-based experiments to quantify the naturally presented HSV-1 peptides on human and mouse cells after infection with wild-type HSV-1 (strain KOS) and ICP47 null mutant (HSV-1 Ka47Δ). Broadly, the first step is to identify HSV-1 peptides naturally processed and presented on infected mouse (MC57G) cells using mass spectrometry (a). The next step is to perform absolute quantification of selected HSV-1 peptides using targeted mass spectrometry (b).

5.2 Results

5.2.1 Identification of novel HSV-1 peptides using mass spectrometry

The first objective of this chapter was to identify naturally presented HSV-1 peptides during infection. In a previous study, St Leger and colleagues suggested 376 potential $CD8^+$ T cell epitopes in HSV-1. Of these predicted epitopes, only 19 peptides were recognised by $CD8^+$ T cells (St Leger et al., 2011). It is possible that many HSV-1 epitopes on infected cells were missed by this study due to the highly stringent peptide selection process. For instance, they only considered peptides of 8 amino acids long for H-$2K^b$ (K^b), peptides comprising 9 amino acids for H-$2D^b$ (D^b) and a high cut-off was set for selection of peptides based on MHC I binding affinity. Moreover, they did not test whether all 376 predicted epitopes were naturally presented on HSV-1 infected cells. Considering these limitations and to allow for a more extensive examination of the effect of ICP47 on antigen presentation, we chose to identify the diverse peptides that are naturally presented on HSV-1 infected cells. The strategy used for peptide identification, the quality of the immunopeptidome data, relationship between the HSV-1 peptides and their corresponding source proteins, and immunogenicity of the peptide identifications are presented in detail in the following sections.

5.2.1.1 Peptide identification strategy

Figure 5.2 summarises the workflow for the MS-based experiment used to identify the repertoire of MHC I bound HSV-1 peptides on mouse cells. The MC57G cell line was chosen for the discovery of MHC I bound peptides. Infecting MC57G cells with recombinant HSV-1 expressing eGFP at 5 pfu/cell for 6 hours yielded a maximal infection rate of about 95% as demonstrated using flow cytometry. These conditions were adopted to obtain optimal infection of cells for all mass spectrometry experiments. Overall, the peptide elution was performed on three biological replicates. MHC I bound peptide complexes were purified from MC57G cells infected with HSV-1 KOS or Ka47Δ using monoclonal antibody clone Y3 (anti-H-$2K^b$) or 28-14-8S (anti-H-$2D^b$) immobilised on protein A sepharose resin. Uninfected cells were analysed in parallel as controls and are referred to as "mock-treated cells" from here on. To reduce the complexity of the peptides

and to increase the detection of low abundance peptides, the peptides were separated by high-performance liquid chromatography (HPLC) into multiple fractions based on relative hydrophobicity. The fractions were then analysed using HPLC coupled to a Q Exactive™ Plus (Thermo) mass spectrometer (LC-MS/MS). The resulting mass spectra were searched against a custom reference database of murine (*Mus musculus*) and HSV-1 proteomes using ProteinPilot™ (SCIEX) and PEAKS (Bioinformatics Solutions Inc.) software. The HSV-1 protein database included a theoretical six-frame translation of HSV-1 KOS, as well as the annotated protein sequence of HSV-1 strain KOS (GenBank accession JQ673480), all appended to the UniProt reference proteome for *Mus musculus*. The resulting peptide sequence matches were subjected to a 5% false discovery rate. This methodology is robust and previously used for successful identification of a large number of mouse MHC I restricted vaccinia virus-derived peptides (Croft et al., In press)

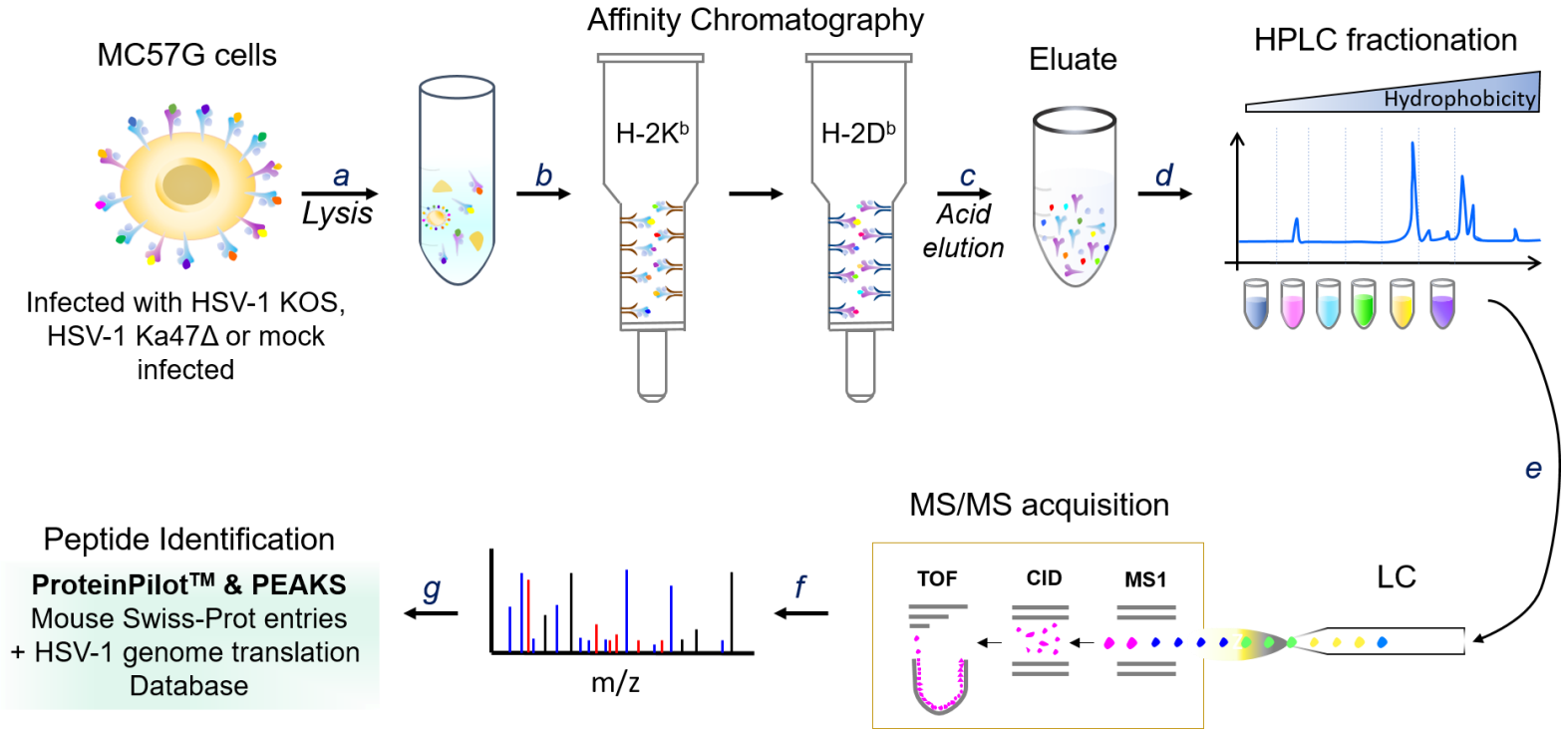

Figure 5.2 Schematic of MS-based identification of the HSV-1 immunopeptidome. Following large-scale expansion and infection of cells with HSV-1, cell pellets were lysed (a) and pMHC-I complexes purified by immunoprecipitation using affinity columns (b). Subsequently, the pMHC-I complexes were dissociated by acid elution (c) and peptides, MHC I heavy chain and β-2-microglobulin were separated based on hydrophobicity by HPLC using a C_{18} column (d). Fractions of interest were analysed by LC-MS/MS (e). In this untargeted discovery phase, all eluting peptides are scanned for their intact m/z (mass over charge) and during each cycle of the instrument, the most intense precursor ions are subjected to fragmentation by collision-induced dissociation (CID). For identification of peptide sequences, the resulting mass spectra (f) are searched by the algorithms of ProteinPilot and PEAKS software, utilising a customised reference database combining both the mouse and HSV-1 proteomes (g).

5.2.1.2 General characteristics of HSV-1 immunopeptidome from MC57G cells

A diverse set of host-derived peptides (n = 2,030) was identified from samples that were mock-treated, infected with wild-type HSV-1 (strain KOS) or with ICP47 null mutant (HSV-1 Ka47Δ) (Figure 5.3 A). Host peptides overlapped by 33% between mock-treated and HSV-1 infected samples. When HSV-1 infected samples were considered, the host peptides overlapped from 19% to 26% between any two replicates infected with wild-type HSV-1 and 26% to 29% overlap between any two replicates infected with ICP47 null mutant virus (Figure 5.3 B&C). While the majority of the peptides identified in each eluate were self-peptides, many distinct HSV-1 derived peptides were also identified (Figure 5.3 A). As expected, HSV-1 peptides were found exclusively in the virus-infected samples and not in the mock-treated samples. Collectively, 75 unique peptides of viral origin were identified from the triplicate samples infected with HSV-1 KOS or HSV-1 Ka47Δ. However, only a minimal overlap of peptide identification was observed between the replicates (Figure 5.3 D & E). Table A-1 in the Appendix lists all the HSV-1 peptides identified in this study and their corresponding source proteins.

Among the total HSV-1 peptides identified, 44 were exclusively eluted from K^b column and 25 were eluted only from D^b column. Six peptides ($UL5_{312-321}$, $UL50_{353-371}$, $UL40_{279-287}$, $UL26_{613-621}$, $UL23_{115-128}$, $UL19_{482-495}$) were eluted from both the K^b and the D^b columns. Based on the MHC I binding prediction, the peptides $UL5_{312-321}$, $UL40_{279-287}$ and $UL26_{613-621}$ showed a strong affinity to D^b. The peptides $UL50_{353-371}$, $UL23_{115-128}$ and $UL19_{482-495}$ have poor predicted binding affinity for both alleles, suggesting promiscuous MHC I binding. Four peptides, $gB_{498-505}$, $RRI_{822-829}$, $ICP8_{171-178}$, and $UL40_{279-287}$, from our peptide dataset were also previously described by other studies (Salvucci et al., 1995; St Leger et al., 2011; Wallace et al., 1999). The other 15 peptides discovered by St Leger et al. (2011) were not identified in our study.

Overall, the length distribution of peptides eluted from K^b and D^b columns were similar between the mouse (Figure 5.4 A) and HSV-1 -derived peptides (Figure 5.5 A). The K^b bound peptides peaked at 8 amino acids and D^b bound peptides peaked at 9 amino acids for both the mouse and the HSV-1 derived peptides. This observation is consistent with predictions from previous structural studies (Falk et al., 1991; Young et al., 1994). Further, peptides of up to 19 amino acid residues were found, however, peptides more than 13 amino acids long were relatively rare.

Falk and colleagues using crystal structure of MHC I molecules found that important anchor residues for H-2 allomorphs are at position 5 (p5) and at the carboxy-terminus (pΩ) of the peptides (Falk et al., 1991). We used WebLogo 3 (Crooks et al., 2004) to analyse the amino acid composition of the mouse and the HSV-1 peptides discovered in our study (Figure 5.4 B&C and Figure 5.5 B&C). The results from this analysis showed that in K^b bound octameric peptides, phenylalanine or tyrosine residues (F/Y) at the p5 anchor position and lysine or valine (L/V) at position p8 were enriched (Figure 5.4 B and Figure 5.5 B). Of D^b bound nonameric peptides, the asparagine residue (N) is enriched at the p5 position and Leucine (L) at the p9 position, which are typical to the D^b binders (Figure 5.4 C and Figure 5.5 C). In HSV-1 peptide set, the p5 position of D^b binders is also occupied by other amino acids such as serine (S), glycine (G), histidine (H), leucine (L) and threonine (T), which could be attributed to smaller sample size (n=12). Together, these data suggest that the host and the HSV-1 peptides identified in this study fit the expected characteristics of K^b and D^b binders and support the quality of the workflow used here to identify MHC ligands.

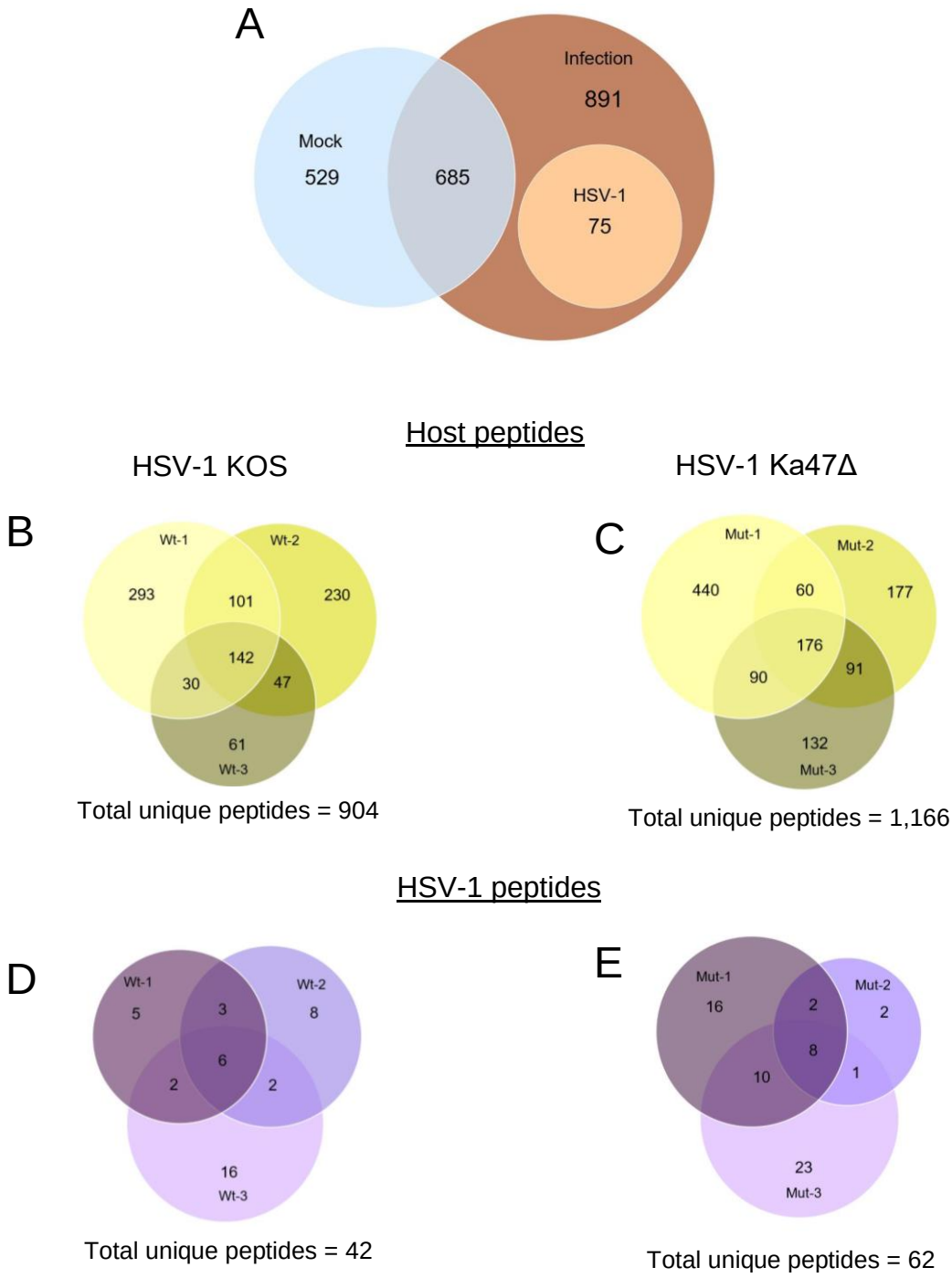

Figure 5.3 Overview of MS identified host and HSV-1 peptides. (A) Proportional venn diagram depicting the overlap of peptides identified across three mock-treated (blue) and HSV-1 infected samples (brown). The HSV-1 derived peptide subset distinctly found in infected samples is shown as light-brown circle. (B) & (C) Venn diagram depicting the overlap of mouse peptides in the three samples infected with HSV-1 KOS represented as Wt-1, Wt-2 and Wt-3 and samples infected with HSV-1 Ka47Δ represented as mut-1, mut-2 and mut-3. (D) & (E) shows the unique and overlapping HSV-1 peptides between three biological replicates. The sample identification is shown inside each circle. The number inside the circles shows the number of peptides identified in each subset.

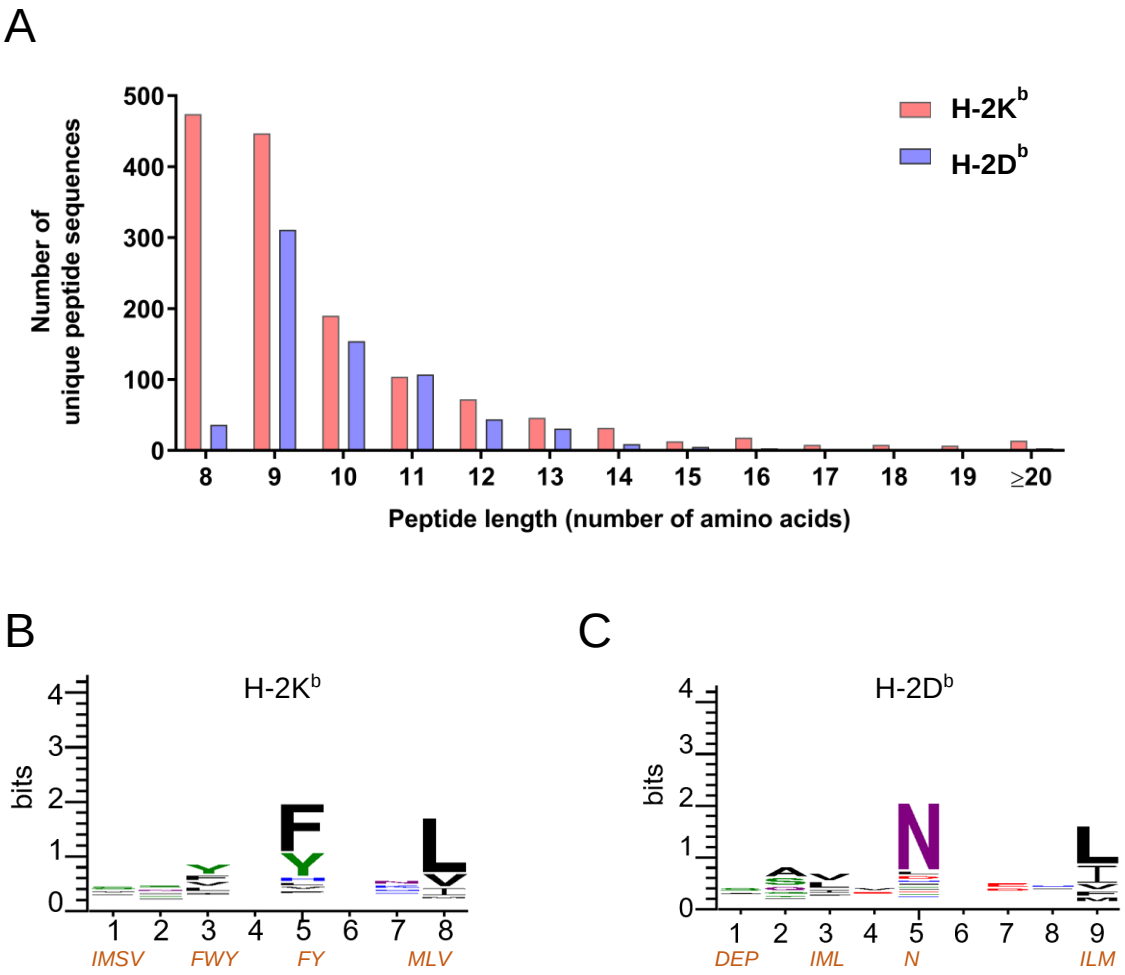

Figure 5.4 Overall characteristics of host immunopeptidome. Shown are pooled host peptide data from mock-treated, wild-type HSV-1 infected or ICP47 null mutant infected samples. (A) Length distribution of the host immunopeptidome is shown in the bar graph. (B) & (C) shows WebLogo 3 plots (Crooks et al., 2004) containing the amino acid composition of octameric peptides (n=474) eluted from K^b columns and nonameric peptides (n=311) eluted from D^b columns, respectively. The position of amino acids is shown in the x-axis. Known anchor residues for K^b and D^b haplotypes at various positions are listed below x-axis of each graph (information obtained from IEDB website). The overall height of the bar is proportional to the degree of sequence conservation at that position and the height of each amino acid is proportional to the frequency at which it occurs. The polar residues are indicated in green, neutral in purple, basic in blue, acidic in red and hydrophobic amino acids in black.

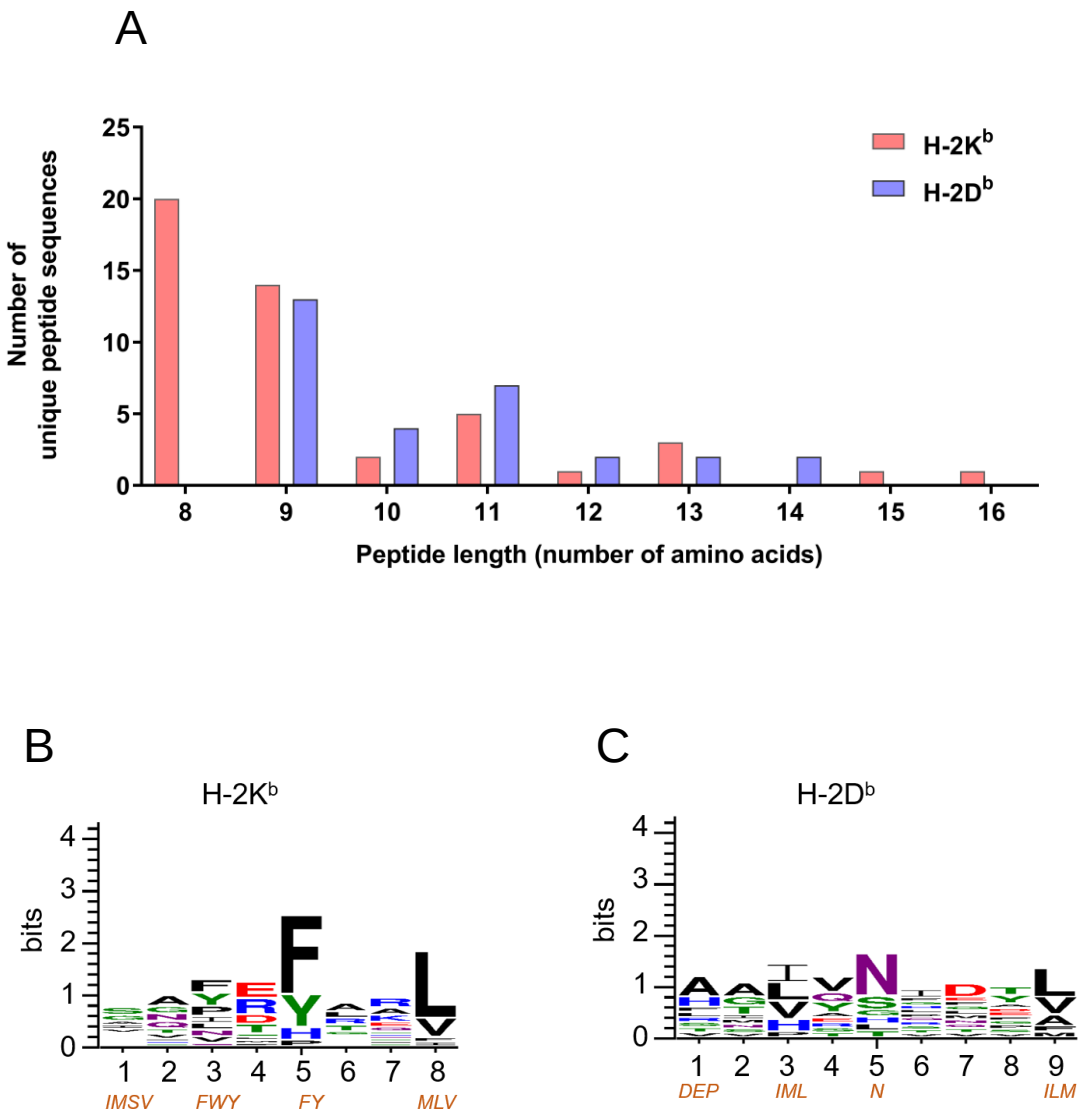

Figure 5.5 Overall characteristics of HSV-1 immunopeptidome. (A) Peptide length distribution of the K^b and D^b immunopeptidome of HSV-1 from all infected samples. (B) & (C) shows WebLogo 3 plots (Crooks et al., 2004) containing the amino acid composition of octameric peptides (n=20) eluted from K^b columns and nonameric peptides (n=12) eluted from D^b columns, respectively. The position of amino acids is shown in the x-axis. Known anchor residues for K^b and D^b haplotypes at various positions are listed below each graph, respectively (information obtained from the IEDB website). The overall height of the bar is proportional to the degree of sequence conservation at that position and the height of each amino acid is proportional to the frequency at which it occurs. The polar residues are indicated in green, neutral in purple, basic in blue, acidic in red and hydrophobic amino acids in black.

5.2.1.3 Source proteins of HSV-1 peptides

The 75 HSV-1 derived peptides identified in our study are derived from 31 different proteins, which are distributed along the HSV-1 genome (Figure 5.6 and Figure 5.7 A). These source proteins comprise 43% of the 72 HSV-1 proteins included in the HSV-1 database used to search the MS/MS spectra. For 35.4% of source proteins, a single peptide was presented, however, nearly 46% of the peptides were derived from just seven proteins, which includes UL5, UL19, UL25, UL26, UL29, UL39 and US8 (Figure 5.7 A&B). This is in agreement with previous observations, which revealed that only a small proportion of self-proteome (4.8% by Hickman et al., 2003 and 13% by Hoof et al., 2012) to be represented by more than one peptide. Unequal distribution of $CD8^+$ T cell determinants has also been noted for other viruses (Oseroff et al., 2008; Ternette et al., 2016; Croft et al., In press). For instance, a study conducted by Osseroff et al. (2008) showed that VACV epitopes represent only 50% of the viral proteins, of which, only six proteins give rise to five or more epitopes each. Several factors have been suggested to be responsible for determining which proteins are sampled for antigen-processing and MHC I mediated presentation. Some of these factors include mRNA level, the rate of translation, protein abundance and protein length (Reits et al., 2000; Khan et al., 2001; Fortier et al., 2008; Croft et al., 2013; Bassani-Sternberg et al., 2015). These factors are not independent but are related to each other (Hoof et al., 2012). For example, Hoof and colleagues (2012) noted an inverse correlation between protein length and protein abundance. They reasoned that smaller proteins have a greater chance of being represented in the immunopeptidome as they are supposedly translated at a higher rate (Hoof et al., 2012). In our study, we observed that the smallest source proteins, ICP47 with 88 amino acids, yielded three peptides, while the largest protein UL36 with 3100 amino acids resulted in a single peptide (Figure 5.7 A&C). However, overall the number of peptides derived from each protein was not significantly correlated to the length of the protein (Figure 5.7 C).

Previous studies showed that the presentation of VACV epitopes coincides with the onset of protein synthesis (Croft et al., 2013). In our study, to test whether the timing of protein synthesis affects the sampling of HSV-1 proteome, we analysed the distribution of HSV-1 peptides across various temporal classes of gene expression. The results showed that 60% (3 out of 5) of immediate early proteins, 50% (9 out of 18) of early proteins, 40% (12 out of 30) leaky late and 42% (7 out of 19) true late proteins are represented in the peptide set (Figure 5.8).

An explanation for the slightly, but not statistically significantly, low representation of late proteins in our peptide set is provided by a seminal study reported recently by Kulej and colleagues (2017) in which they performed a global proteome analysis in HSV-1 infected human foreskin fibroblast cells using mass spectrometry. They found that the IE proteins could be abundantly detected after 3 hours and early proteins after 6 hours of infection (Kulej et al., 2017a). Over 80% of the late proteins could be detected at 3 hours, however, the copy numbers of those proteins peaked only 9-12 hours after infection. Therefore, the infection time in our study may not be sufficient for the sampling of some late proteins. Acquiring proteomics data from our sample set would help analyse the correlation between the synthesis of late proteins and the immunopeptidome.

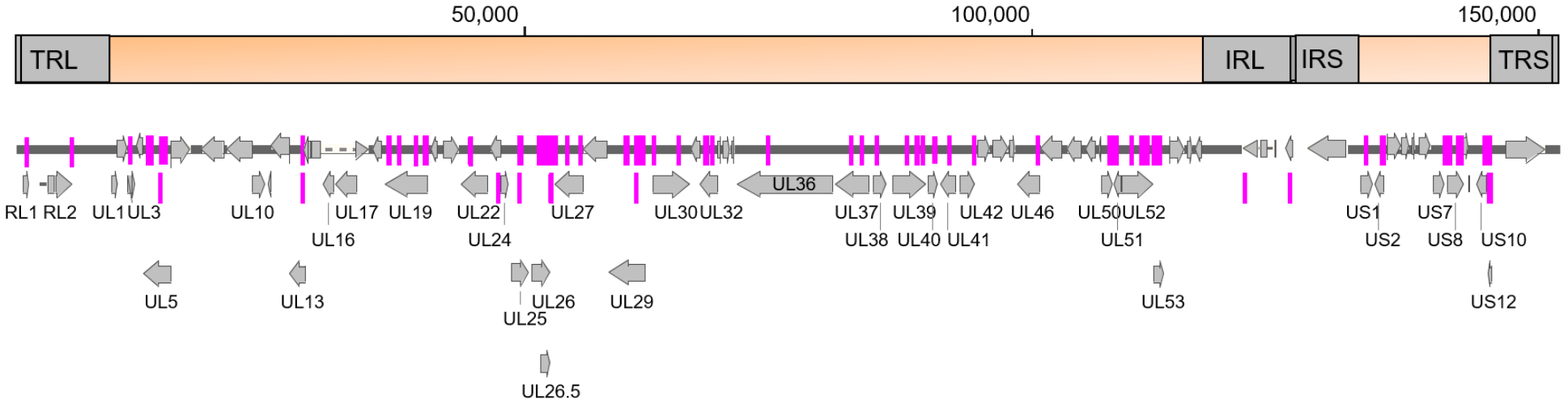

Figure 5.6 Schematic location of the naturally processed and presented HSV-1 derived peptides in the viral genome. The top figure shows the overall schematic of the HSV-1 genome. The bottom stack shows the relative position and orientation of HSV-1 coding sequences, which are depicted as grey arrows. The gene symbols are indicated below the grey arrows for reference. The pink lines indicate the position of LC-MS/MS identified HSV-1 peptides. The image was generated using SnapGene® Viewer Version 3.3.4.

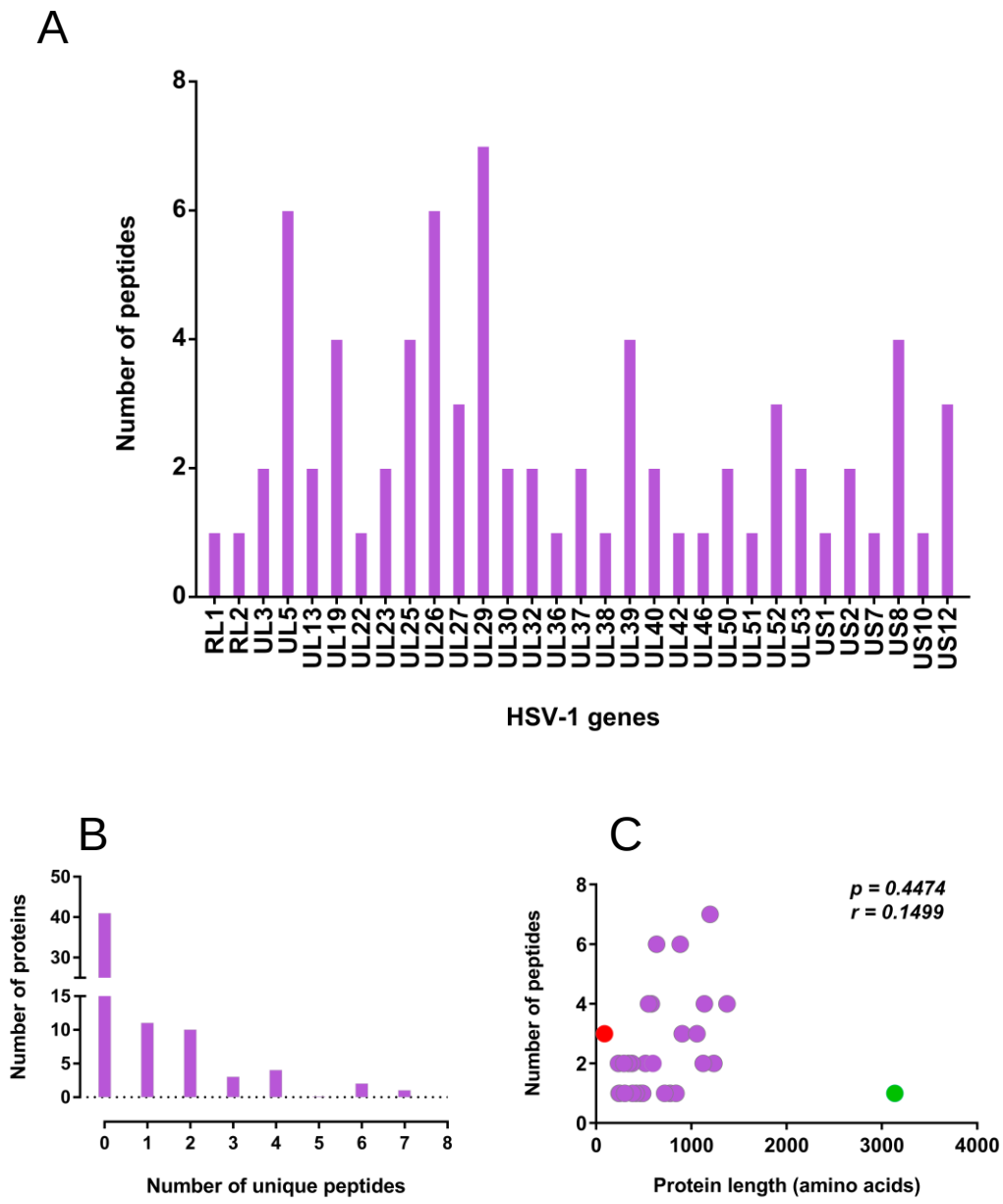

Figure 5.7 Analysis of the relationship between source protein and HSV-1 immunopeptidome. (A) The number of distinct peptides from a given source protein was enumerated and graphed. Gene symbols of all the sampled proteins are indicated in the x-axis. (B) The bar graph shows the grouping of source proteins based on a number of unique peptide sequences. (C) The association between the length of the source protein and the number of peptides derived from that protein is depicted as a scatter plot. The symbol in red represents the correlation for ICP47 protein (the shortest protein) and the symbol in green represents UL36 protein (the longest protein). Pearson's correlation coefficient (r) and p values are shown.

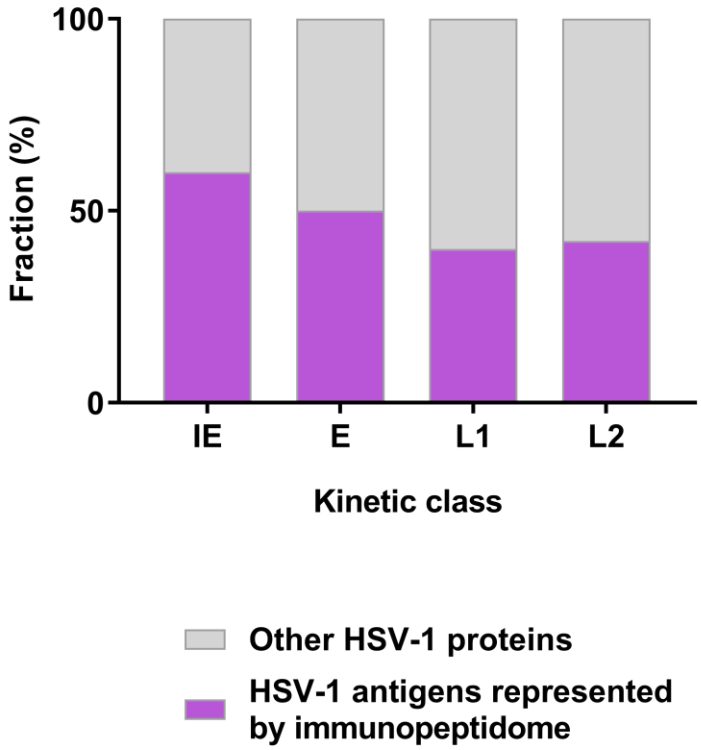

Figure 5.8 Distribution of source proteins based on the kinetic class of gene expression. After the infection of cells, HSV-1 genes express in an orderly fashion starting with immediate early (IE) genes followed by early (E) genes, then leaky late (L1) and true late (L2) genes. The graph shows the fraction of source proteins that fall under each kinetic class relative to the total HSV-1 proteins of that class.

5.2.1.4 Defining the immunogenicity of the novel HSV-1 peptides

The immunogenicity of the HSV-1 peptides identified in this study was tested in mice using the intracellular cytokine staining (ICS) assay (see materials and methods section 2.3.10.4) (Flesch et al., 2012). The peptides of eight to thirteen amino acids long identified using ProteinPilot™ program (46 peptides) were biochemically synthesised (GL Biochem (Shangai) Ltd.) and used for the analysis. To test these peptides, C57BL/6 mice were infected with HSV-1 KOS and after seven days, the splenocytes from these mice were stimulated *in vitro* using the synthetic peptides. Subsequently, the number of $CD8^+$ T cells that could be restimulated with each of these peptides was enumerated by staining for intracellular IFNγ.

Figure 5.9 shows the immunogenicity of all the peptides that triggered the $CD8^+$ T cell response in more than one mouse. When the size of the response to a peptide is above the average of three times the standard deviation of negative controls in at least two of the eight mice tested, then the peptide was considered as an immunogenic peptide. Based on these criteria, an HSV-1 specific $CD8^+$ T cell response was documented for a total of 11 peptides (of 46 peptides tested). The immunodominant peptide $gB_{498\text{-}505}$ derived from glycoprotein B showed the largest response in all eight mice tested. Previously identified epitopes $ICP8_{171\text{-}178}$, $RRI_{822\text{-}829}$ and $UL40_{279\text{-}287}$, which also came up in our MS-based immunopeptidome analysis, showed a smaller response compared with the size of response reported by by St Leger and colleagues (2011). This is intriguing because the HSV-1 strain, mouse strain and the method used to determine the $CD8^+$ T cell response are similar between the two studies. However, this observation is not peculiar to the current study because others in our laboratory have previously found similar differences (Spiering and Tscharke, unpublished). This suggests that the difference in outcome could be due to inter-laboratory variability, including mouse sub-strain and perhaps microbiota differences. The remaining 7 epitopes $UL40_{198\text{-}206}$, $UL39_{451\text{-}461}$, $UL39_{805\text{-}815}$, $UL39_{956\text{-}964}$, $UL37_{600\text{-}607}$, $UL29_{605\text{-}613}$ and $UL5_{126\text{-}133}$ are newly identified in this study. Even though immediate early proteins were sampled in the peptidomic dataset, interestingly, only peptides derived from the proteins that belong to the early and the late kinetic classes were found to be immunogenic.

A strong correlation has been suggested between the affinity with which a peptide bind to the MHC I and the immunogenicity of that peptide (Sette et al., 1994). Traditionally, the affinity between a peptide and MHC I is calculated by an inhibition assay in which the

peptide concentration required to cause 50% inhibition of the binding of a standard peptide is measured (IC_{50}) (Sette et al., 1994). However, several prediction algorithms are also available. These are based on artificial neural networks (ANN) or the stabilised matrix method (SMM) in both cases informed by the sequences of large sets of known MHC I - binding peptides and $CD8^+$ T cell epitopes (Nielsen et al., 2003; Peters and Sette, 2005). These algorithms allow *in silico* prediction of affinity between a given peptide and an MHC I allomorph. These predicted values are well correlated with measured values for a large number of viral peptides (Croft et al., In press). The peptide binding affinity of the HSV-1 peptides discovered in this study was predicted using ANN based algorithm at the Immune Epitope Database (IEDB) website (Nielsen et al., 2003). The predicted IC_{50} of peptides in our set ranged from 2.2 nM to nearly 50,000 nM (Figure 5.10 A). Interestingly, immunogenic HSV-1 peptides show a significantly higher binding affinity compared to the non-immunogenic ones (Figure 5.10 A). Previous studies suggested that IC_{50} of 500 nM is a reasonable threshold for predicting potential MHC I restricted immunogenic peptides (Sette et al., 1994; Paul et al., 2013). More than 80% of the $CD8^+$ T cell epitopes identified in our study have a predicted IC_{50} of less than 500 nM. The remaining two epitopes $UL39_{451-461}$ and $UL39_{805-815}$ show a low predicted binding affinity ($IC_{50} > 500$ nM). Similarly, not all strong binders induced a $CD8^+$ T cell response. When the relationship between the predicted MHC I binding affinity and the immunogenicity was analysed, no significant correlation was found (Figure 5.10 B). These data confirm previous findings that MHC I binding is a requirement for recognition by $CD8^+$ T cells but it is not the only determinant of immunogenicity (Harndahl et al., 2012; Gilchuk et al., 2015). Of note, there is a significant association between the peptide length and the predicted IC_{50} (Figure 5.10 C). It appears that longer peptides (>10 amino acids) have significantly higher predicted IC_{50} and therefore lower binding affinity. Given that the peptides were detected by MS, they must bind MHC I with adequate affinity for presentation. Therefore, we speculate that the *in-silico* analyses perform better for peptides of typical length for a given MHC I but are less able to predict the affinity of longer peptides.

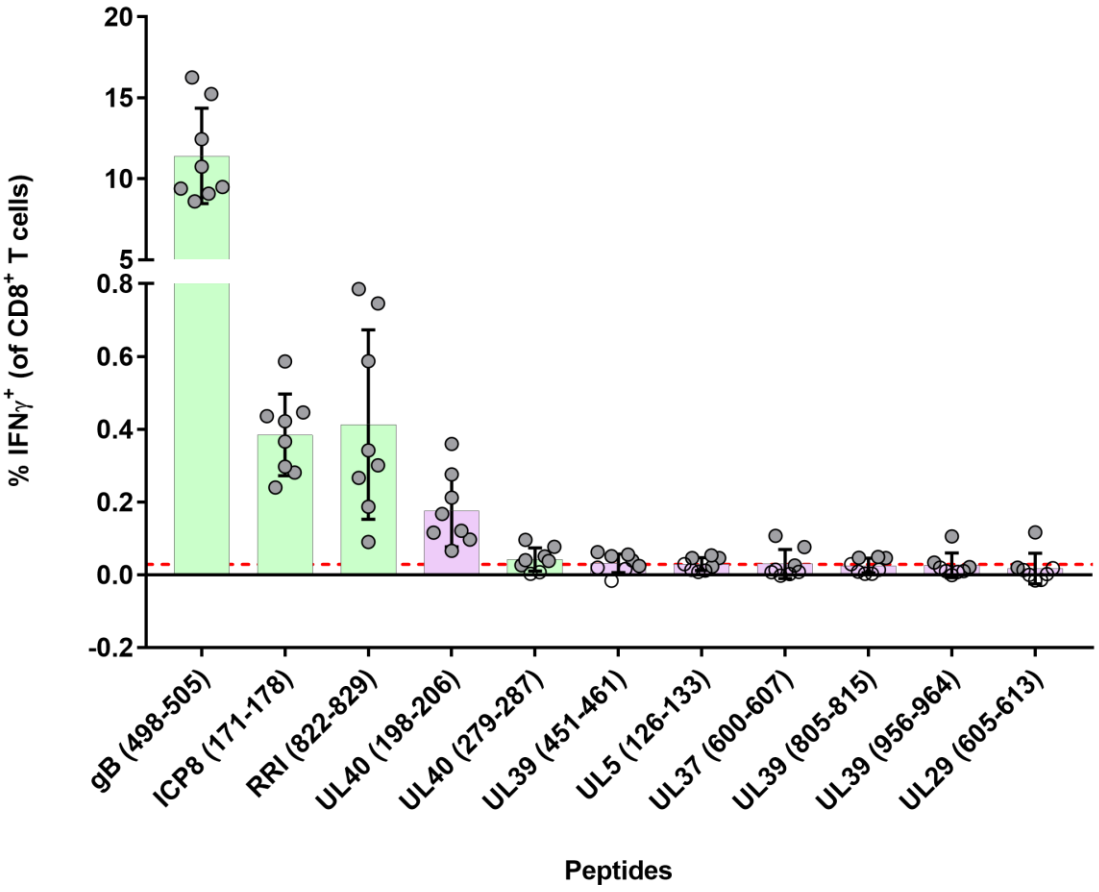

Figure 5.9 CD8$^+$ T cell response to identified HSV-1 peptides. The magnitude of HSV-1 peptide-specific CD8$^+$ T cell responses, as measured by the ability to make IFNγ using *in vitro* restimulation assay is shown. The assay was conducted using splenocytes from HSV-1 infected mice 7 days after infection. Only the peptides that resulted in an immunogenic response in more than one mouse are shown. The dashed red line represents the average of 3 times the standard deviation (SD) of negative controls across 8 mice. Each symbol represents a mouse. Each closed circle shows a mouse when immunogenicity was detected above the threshold, which is 3 × SD above the average of negative controls. The error bars show mean ± SD. The bars filled in green indicate the previously known epitopes (Salvucci et al., 1995; Wallace et al., 1999; St Leger et al., 2011) and the bars in pink show the epitopes identified in this study. I acknowledge Ms. Grace Patricia for contributing to the generation of the immunogenicity data.

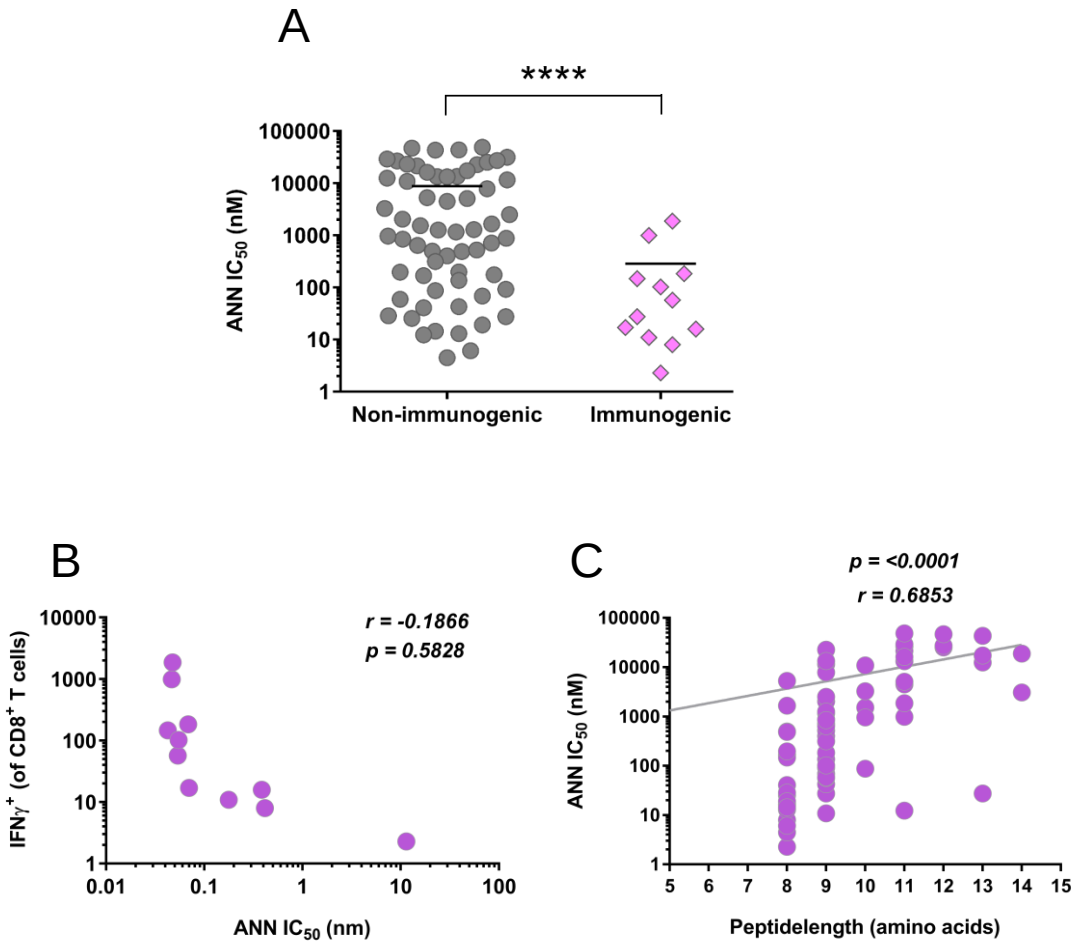

Figure 5.10 Predicted binding affinity of HSV-1 derived peptides. (A) The MHC I binding affinity (IC_{50}) of each peptide naturally presented by HSV-1 infected cells was predicted using the artificial neural network (ANN)-based alignment algorithm. The scatter plot shows the IC_{50} value of the non-immunogenic and immunogenic HSV-1 peptides identified in this study. The horizontal line represents the mean. The mean IC_{50} values of non-immunogenic and immunogenic peptides were compared using unpaired t-test with Welch's correction. Asterisks show that the means are significantly different ($p<0.0001$). (B) The relationship between the proportion of peptide-specific $CD8^+$ T cells and the predicted MHC I binding affinity score (IC_{50}) is shown. (C) The relationship between the peptide length and the predicted MHC I binding affinity score (IC_{50}) is shown. (B & C) Spearman linear correlation coefficient (*r*) and (*p*) value are indicated in the figure.

5.2.2 The effect of ICP47 on the overall characteristics of the immunopeptidome

The impact of ICP47 on the peptides identified from samples infected with HSV-1 KOS and HSV-1 Ka47Δ were analysed. Of all host and HSV-1 peptides identified in this study, 35% and 41% were commonly found in samples infected with HSV-1 KOS and HSV-1 Ka47Δ, respectively (Figure 5.11 A and Figure 5.12 A). Of the host-derived peptides, 24% were uniquely found in samples infected with HSV-1 KOS and 41% in samples infected with HSV-1 Ka47Δ (Figure 5.11 A). A similar proportion of unique HSV-1 peptides were detected in different sample types. Only 20% of the total HSV-1 peptides identified by MS were found exclusively in samples infected by HSV-1 KOS, but 39% of the peptides were exclusively found in samples infected by HSV-1 Ka47Δ (Figure 5.12 A). Together, these data suggest that ICP47 affects the repertoire of host- and HSV-1-derived pMHC-I on the cell surface. Furthermore, a proportion of 26% and 43% of the unique host-derived K^b-bound peptides were detected in HSV-1 KOS and Ka47Δ samples, respectively (Figure 5.11 B). Consistent to K^b peptides, relatively more host-derived D^b bound peptides were exclusively found in HSV-1 Ka47Δ samples (29%) compared to samples infected with the wild-type virus (22%) (Figure 5.11 C). Of the total K^b bound HSV-1 peptides, 23%, and 35% were found uniquely from wild-type and HSV-1 Ka47Δ infected samples, respectively (Figure 5.12 B). Similarly, 16% and 41% of the D^b bound peptides were derived from the wild-type and Ka47Δ infected samples, respectively (Figure 5.12 C). Thus, when the peptides were sub-divided based on the MHC I allomorphs, an increased repertoire was observed for both allomorphs in the absence of ICP47.

Analyses were next performed to check whether various characteristics of peptides affect the difference in the number of peptides identified between the two viruses. We investigated whether the distribution of peptide length is similar between HSV-1 KOS and Ka47Δ peptide sets. A majority of the peptides from the two peptide sets were found to have canonical length i.e., 8 amino acids for K^b binders and 9 residues for D^b binders (Figure 5.13 A and B). Further, neither the host peptides nor the HSV-1 peptides showed a significant difference in the distribution of peptides across different lengths between the peptide sets (Figure 5.13 A&B).

It has been shown that TAP selects peptides for translocation based on the amino acid composition of peptides (Momburg et al., 1994; Powis et al., 1992, 1996). While the amino-

and carboxy-terminal amino acid residues are critical for binding to TAP, the residues in between contributed less to the binding (Peters et al., 2003). To analyse the TAP dependency of peptides that are found in wild-type and Ka47Δ samples, a prediction matrix (Burgevin et al., 2008) was used to assess the contribution of each peptide residue towards the affinity to mouse TAP. TAP score was calculated for the host and HSV-1 peptides by considering the first three amino-terminal and the carboxy-terminal residue of each peptide. Our analysis showed that TAP binding affinity of the peptides does not vary significantly between the peptides identified from HSV-1 KOS and HSV-1 Ka47Δ samples, for both the host (Figure 5.14 A) and the HSV-1 peptides (Figure 5.14 B).

An analysis was performed to test whether the peptides identified from the two sample types showed a difference in MHC I binding affinity. Peptides with a range of IC_{50} values representing strong binders to non-binders were identified in both the peptide sets and the MHC I affinity was comparable between KOS-peptides and Ka47Δ-peptides (Figure 5.14 C). Further, the kinetic class of proteins appears to have no role in the sampling of peptides in the presence or absence of ICP47 (Figure 5.14 D).

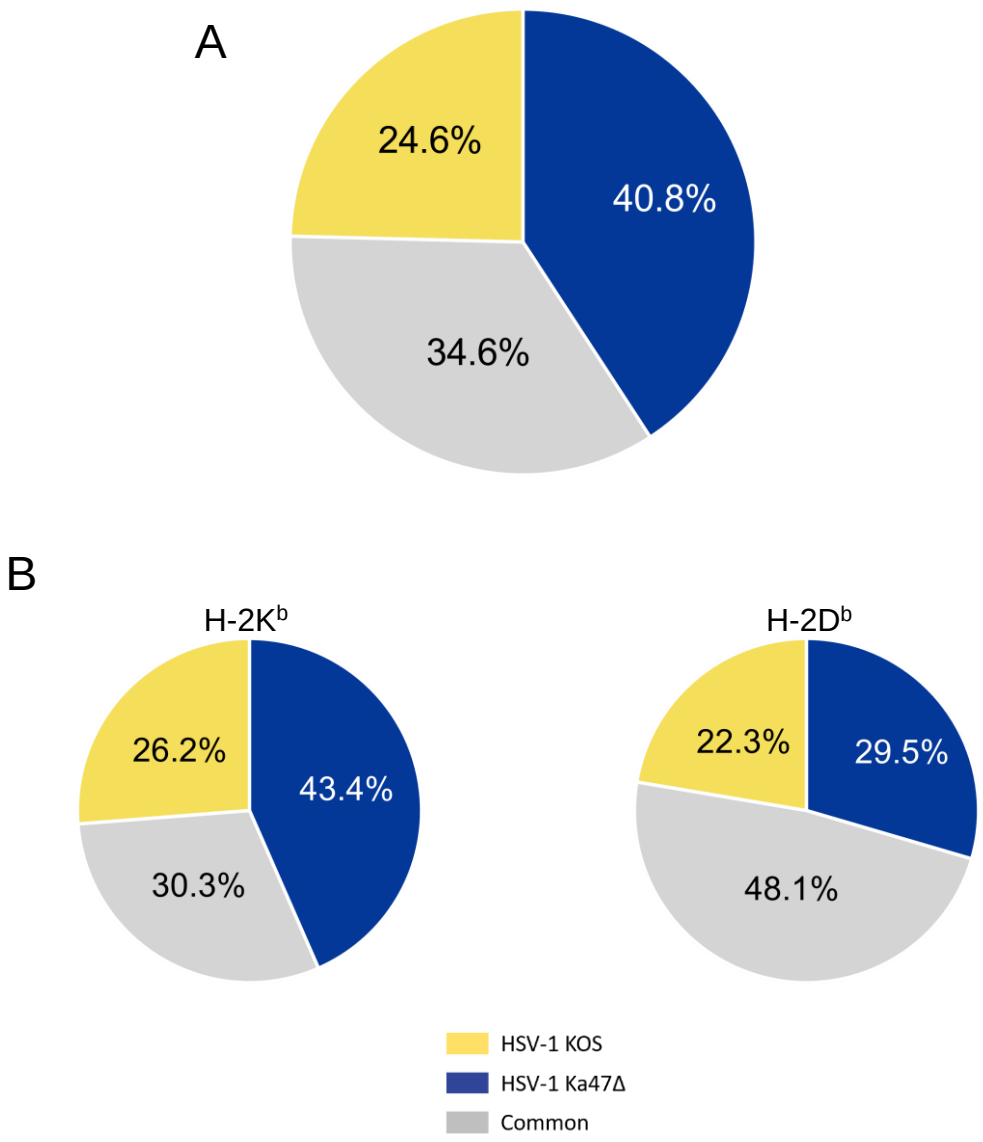

Figure 5.11 More host-derived MHC I-bound peptides were identified on cells infected with HSV-1 Ka47Δ compared to cells infected with HSV-1 KOS. (A) Venn diagram showing proportion of host-derived peptides identified exclusively in the HSV-1 KOS infected samples, in HSV-1 Ka47Δ infected samples and the peptides commonly found in both sample types. (B) The proportion of K^b (left side) or D^b-bound (right side) host-peptides exclusively found in HSV-1 KOS or HSV-1 Ka47Δ infected samples and those commonly identified between the two infected sample types are shown in the pie charts. The number of peptides identified in each subset is denoted as a percentage of total host-peptides bound to the corresponding MHC I allomorph.

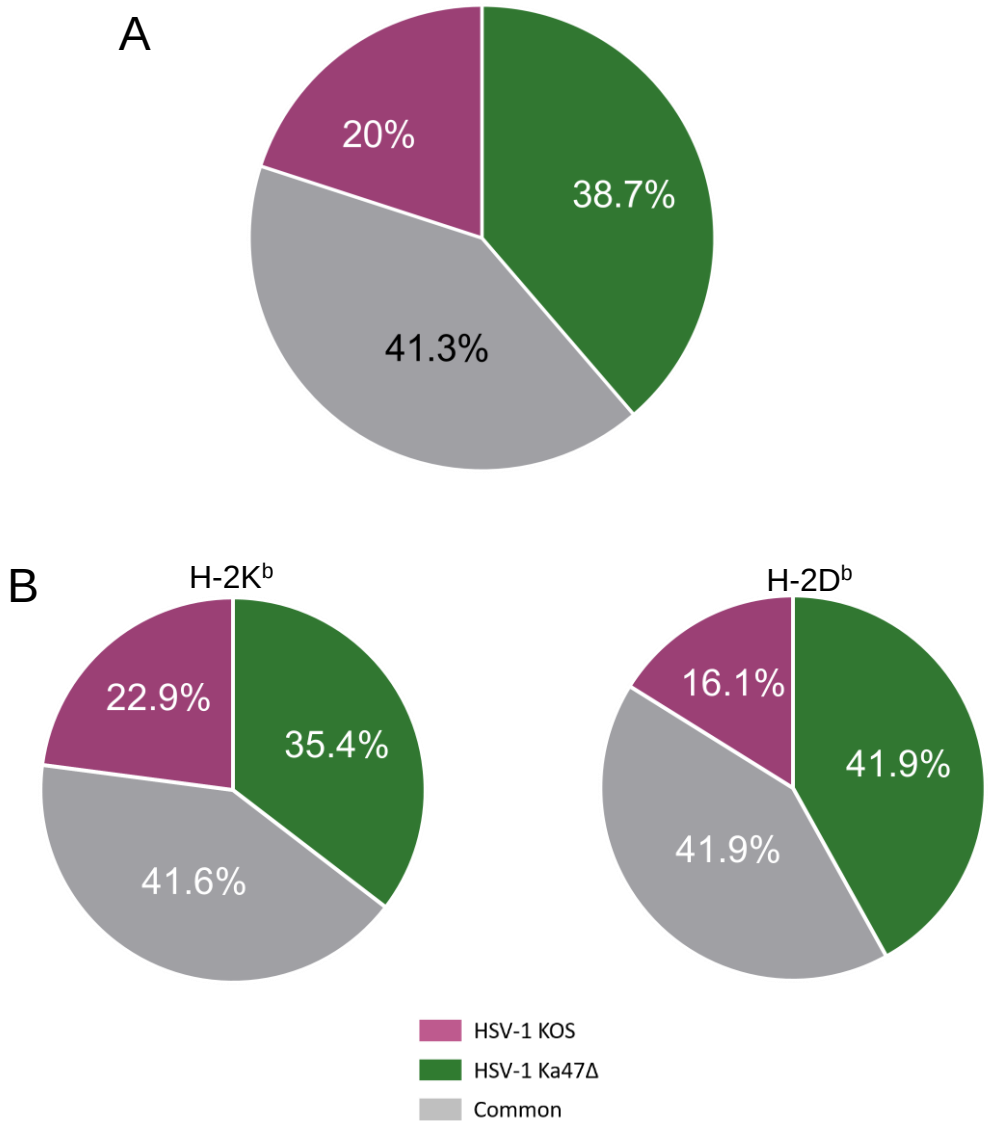

Figure 5.12 More HSV-1 derived MHC I-bound peptides were identified on cells infected with Ka47Δ than with HSV-1 KOS. (A) The proportional Venn diagram shows the number of HSV-1-peptides identified exclusively in the HSV-1 KOS or HSV-1 Ka47Δ virus-infected samples and the subset of peptides common between the samples. (B) The proportion of K^b-bound (left side) and D^b-bound (right side) HSV-1 peptides identified in samples infected with HSV-1 KOS, infected with HSV-1 Ka47Δ or common to the two infected sample types are shown in the pie charts. The number of peptides identified in each subset is denoted as a percentage of total host-peptides bound to the corresponding MHC I allomorph.

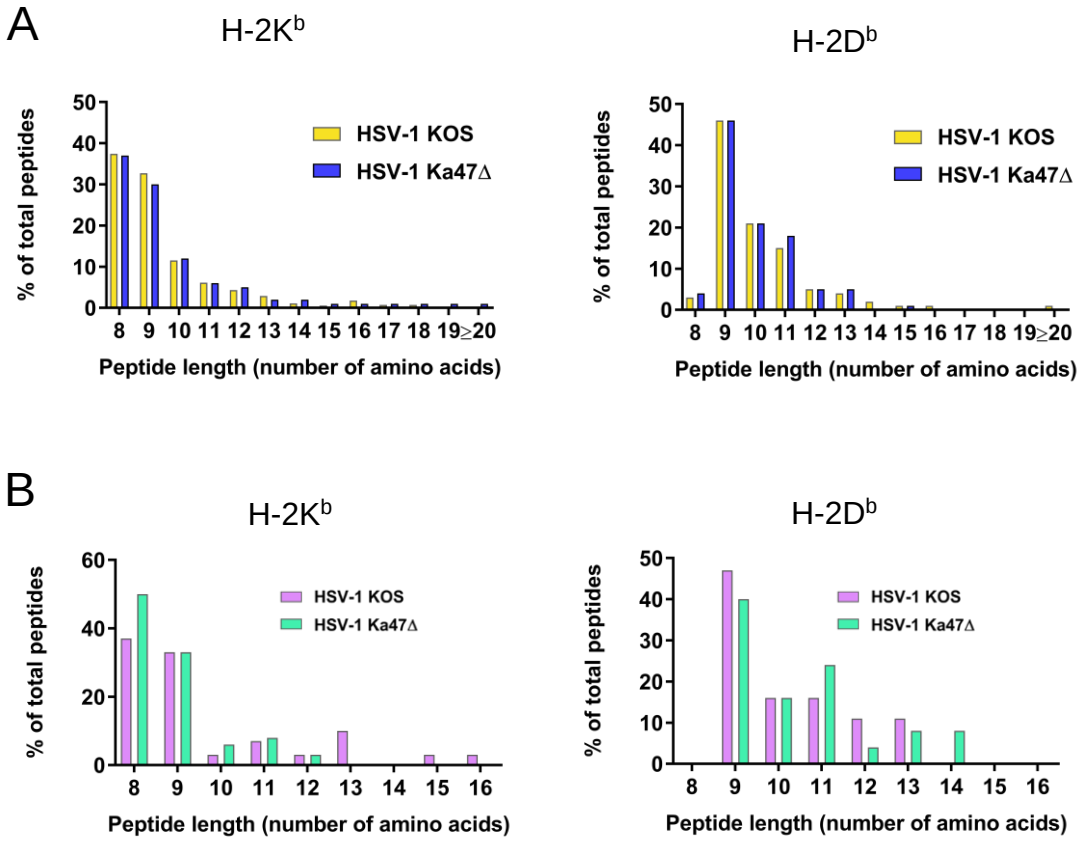

Figure 5.13 Length distributions of the MHC I -bound peptides detected in HSV-1 KOS or Ka47Δ infected samples. (A) The number of host-peptides distributed across the different length of peptides is shown for HSV-1 KOS or Ka47Δ infected samples. (B) Similarly, all HSV-1-derived peptides identified in HSV-1 KOS or Ka47Δ infected samples were grouped based on the number of amino acid residues. (A&B) The graphs on the left side denote K^b-bound peptides and the graphs on the right represent D^b bound peptides. The distribution of peptides with different amino acid residues was compared between the peptides derived from cells infected with HSV-1 KOS and cells infected with HSV-1 Ka47Δ using two-way ANOVA Sidak's multiple comparisons test. The differences are not statistically significant across any peptide length.

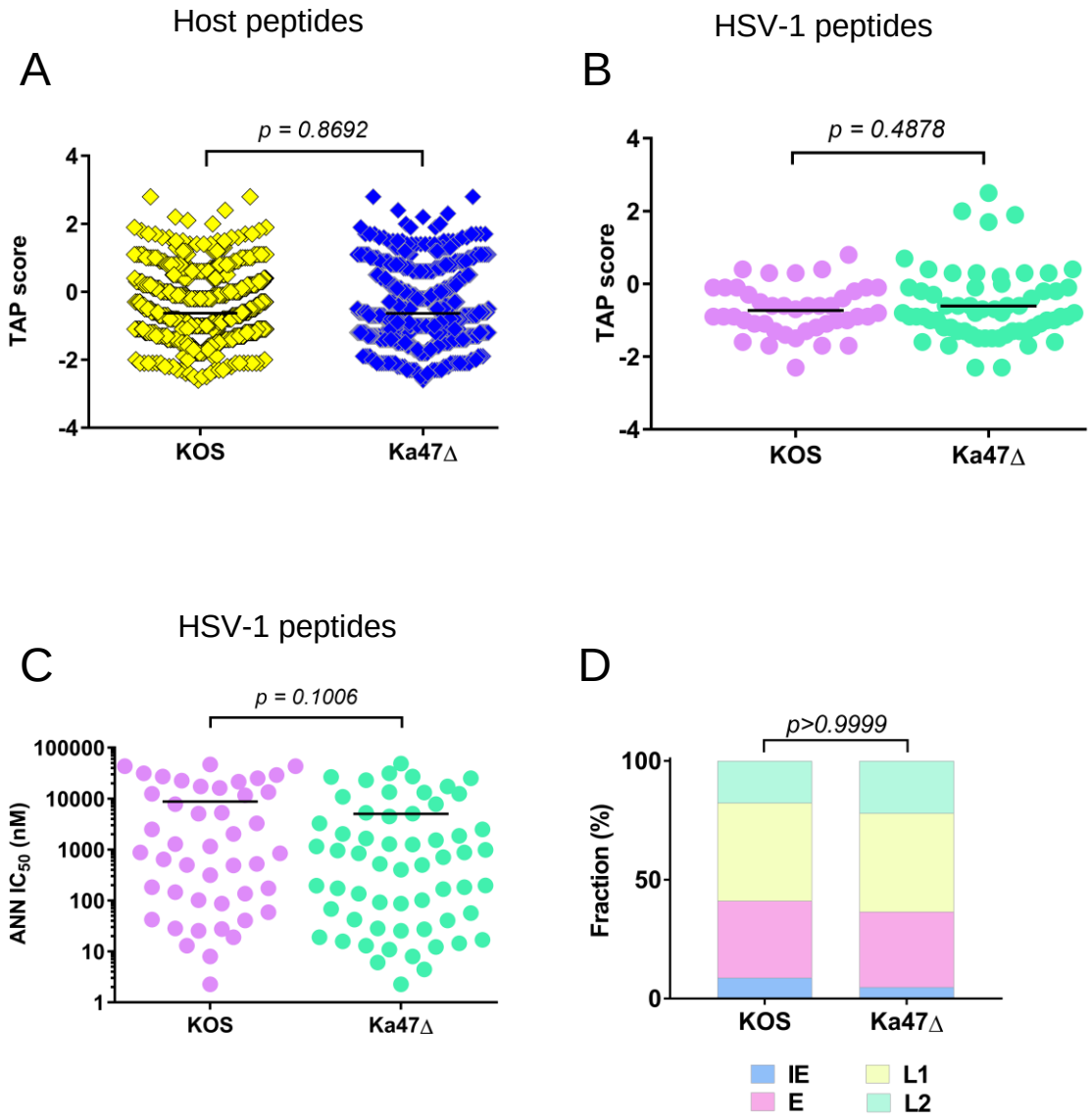

Figure 5.14 Characterisation of immunopeptidome in mouse cells as a function of TAP inhibition by ICP47. (A) and (B) The TAP score was calculated by considering the three N-terminal residues and the C-terminal residue of MHC I bound peptides as described by Burgevin et al. (2008). According to the prediction matrix, smaller the score, higher the affinity towards TAP. The scatter plot shows the predicted TAP binding affinity of the host-derived peptides (A) and HSV-1-derived peptides (B) that were identified in HSV-1 KOS or Ka47Δ infected samples. (A) and (B) Each symbol represents a peptide and the horizontal lines represent mean. The *p* values were calculated using the unpaired *t*-test. (C) Scatter plot shows the predicted binding affinity (IC_{50}) of HSV-1 peptides from different samples. ANN algorithm was used to calculate the IC_{50} values. Each symbol represents a peptide and horizontal line represents mean. The *p*-value was calculated using the unpaired *t*-test. (D) Distribution of source proteins across the kinetic classes for peptides found in cells infected with HSV-1 KOS and Ka47Δ peptides. The *p*-value was calculated using two-way ANOVA.

5.2.3 MS strategy for absolute quantification of MHC I bound HSV-1 derived peptides

The prime objective of this chapter was to estimate the efficiency by which ICP47 inhibits human and mouse TAP. Therefore, we employed a highly sensitive technique called MRM-MS for absolute quantification of a subset of HSV-1 peptides naturally presented on infected cells (Figure 5.15). A key aspect of MRM-MS is that the user programs the MS to focus on selected peptide ions with particular target values. MRM is an experiment performed on an LC coupled triple quadrupole MS instrument. The eluted fractions from the LC are introduced into the MS instrument by electrospray ionisation (Figure 5.15 A). The first quadrupole (Q1) filters peptide ions based on the mass to charge ratio (m/z) and allows only peptide ions of interest (as programmed), to pass to the next quadrupole. In the second quadrupole (Q2), the peptide ion is fragmented by a process called collision-induced dissociation (CID) (Figure 5.15 B). The fragmented product ions with a specific m/z values are again selected in the third quadrupole (Q3) and ultimately recorded by a detector. The predefined pairs of a given peptide ion in first quadruple and a corresponding product ion in the third quadruple is called an MRM transition. The main task during MRM-MS assay development is to select the transitions for the peptides of interest in order to optimise selectivity and sensitivity. The specificity of the transitions from precursor to product ion makes this technique more sensitive and allows targeted detection of even poorly abundant peptides within a complex sample. In conjunction with isotopic standards, this method can be used reliably to quantify multiple peptides with a sensitivity of one copy per cell (Croft et al., 2013).

5.2.3.1 Peptide selection and optimisation of MRM assay

A range of peptides with different binding affinities, immunogenicity and abundance were chosen for quantification. These included 15 K^b-restricted peptides from our peptide discovery dataset and two immunogenic peptides, RR1 (982-989) and ICP8 (876-883), identified by St Leger et al. (2011), which were not identified during our discovery experiments. Each of the chosen peptides was synthesised to incorporate a single isotopic (heavy) amino acid for use as standards. The newly synthesised labelled peptides for absolute quantification, commonly referred to as "AQUA peptides" (Gerber et al., 2003), are identical in sequence and thus, chemically identical to their native counterpart. However, the AQUA peptides can be easily distinguished by mass spectrometry due to the 7-10 Da (residue dependent) mass shift (Desiderio and Kai, 1983; Gerber et al., 2003).

The newly synthesised AQUA peptides were initially used for optimising the MRM assay conditions. In order to obtain high-resolution data on each peptide, its dominant precursor m/z and the nature of its fragmentation, a mixture of all peptides from Table 5.2 were analysed on a TripleTOF® 6600 system. Although this system is not a triple quadrupole, it uses the same collision cell as the QTRAP® 6500 LC-MS/MS system used for MRM-based quantification. This means that fragmentation information can be directly translated for quantification using QTRAP® 6500. Dominant Q1 precursors were selected, and the top five product ions were selected for each AQUA peptide. These were built into the transition list, which was then used to optimise collision energy and assess retention time. Then, the transitions of heavy peptides were used to generate a list of corresponding transitions for the native sequences (Lange et al., 2008). Table 5.1 and Table 5.2 detail the list of peptides for MRM, including information for all heavy and light sequences, the resultant mass shift, the dominant precursor m/z used and the selected transitions and optimal collision energy. Prior to the implementation of the method, ten-fold dilutions, ranging from 5 amoles to 500 fmoles, of the total AQUA peptide mixture were subjected to MRM-MS analysis in order to test the linearity and sensitivity of the optimised MRM assay. As shown in Figure 5.16, most peptides were measurable down to 50 amoles and the detection is linear over 50 amoles to 500 fmoles. Of the 17 AQUA peptides, two peptides ($UL5_{300\text{-}307}$ and $UL25_{304\text{-}311}$) were not detected by MRM analysis. It is likely that these two peptides did not undergo optimal separation by LC due to hydrophobicity, hence excluded from further analysis.

5.2.4 Detection of endogenous peptides in infected samples

MC57G or 293KbC2 cells (5×10^7) were infected with HSV-1 KOS or HSV-1 Ka47Δ for 6 hours. Mock-infected cells were used as a control. The experiment was conducted in triplicates. The cells were snap frozen and then treated with mild lysis buffer followed by affinity purification of pMHC-I complexes. Until this point, the experimental steps are similar to that of the peptide discovery process shown in Figure 5.2. Then, a mixture of each AQUA peptide (Table 5.1; 50 fmoles per peptide) was spiked into the eluted pMHC-I complex followed by pre-fractionation using HPLC (Figure 5.15 A). The addition of AQUA peptides to the pMHC-I eluate provides for the losses during sample handling, thus, enabling precise quantification of peptides. Each of the fractions containing peptides was subjected to LC-MRM-MS analysis. The previously developed MRM assay (Section 5.2.3.1 and Table 5.2) was used to simultaneously quantitate the 15 selected peptides in each

sample. Representative MRM transition peaks of $gB_{498-505}$ are shown in Figure 5.17. The areas under the curve of each of the selected transitions were combined to obtain a sum peak area. The peptide abundance was calculated using the formula noted in the materials and methods chapter (Section 2.3.12.9).

The native peptides were detected in the infected samples but not in the mock-treated samples. A total of 15 native peptides could be detected in the MC57G samples. Although detected at low level in two KOS-infected and two Ka47Δ-infected MC57G samples, the native peptide $UL40_{279-287}$ (AAIENYVRF) was not detected in any of the 293KbC2 samples. Given that 293KbC2 cells display relatively low-level MHC I on their surface (Figure 3.4 A), it is possible that $UL40_{279-287}$ is presented below detection level in 293KbC2 samples. This peptide was eliminated from further analysis only from 293KbC2 samples. Thus, in total, 14 peptides were detected in the 293KbC2 samples. Further, some peptides were not detected in some replicates during the analysis. For instance, $ICP8_{171-178}$ (INNTFLHL) and $UL5_{126-133}$ (AQNMYAKL) were detected in only one of the replicates in 293KbC2 samples (infected with HSV-1 Ka47Δ) (Figure 5.19). However, this same peptide was found, in low abundance, in all six MC57G samples (Figure 5.19). Additionally, $UL5_{126-133}$ was found in one replicate of KOS infected and two replicates of Ka47Δ infected MC57G samples (Figure 5.19). It is likely that in 293KbC2 cells these peptides were presented at levels close to the limit of detection of the instrument, and so were not found consistently in all replicates. Similarly, MRM transitions for the immunodominant peptide $gB_{498-505}$ were present in all six MC57G samples (Figure 5.17 and Figure 5.18) and three replicates of 293KbC2 infected with Ka47Δ, whereas it was either not detected or detected at a very low level in 293KbC2 cells infected with wild-type virus (Figure 5.17 and Figure 5.19). Peptides found in more than one replicate in each cell type were included for further analysis and an arbitrary value of 0.01 was added to all peptides to allow statistical testing despite some missing values. Because the peptides analysed in this study were detected from 50 amoles (Figure 5.16) and given that there were 5×10^7 viable cells in each sample, the limit of detection across our peptide set was determined to be 0.6 copies/cell. A value of 0.01 copies/cell is well below the limit of detection and therefore, not expected to skew the statistical analysis.

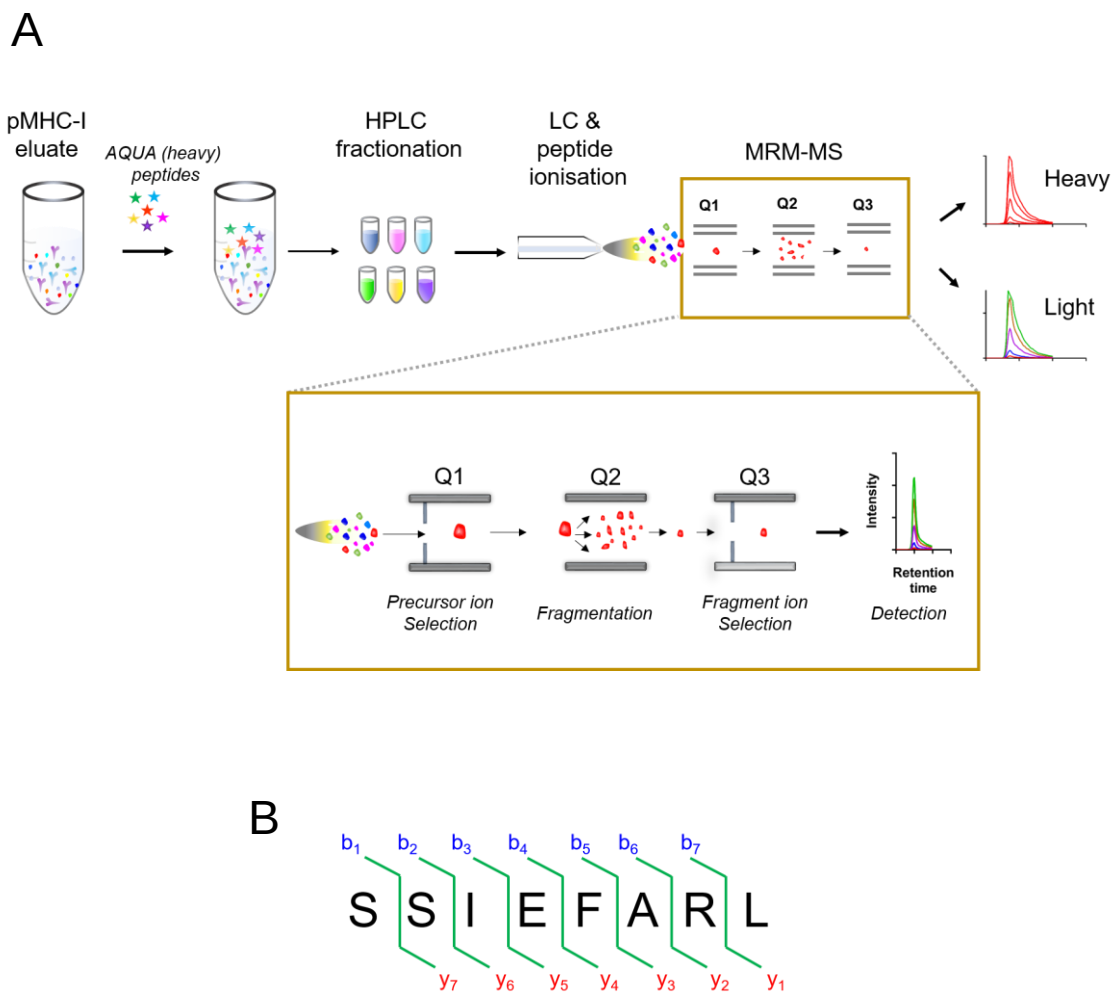

Figure 5.15 Schematic representation of the targeted MRM MS method of peptide quantification. (A) MHC I bound peptides eluted from the immunoaffinity column are mixed with isotopically labelled standard AQUA peptides followed by pre-fractionation using RP-HPLC. The peptide fractions are then loaded on the triple quadrupole mass spectrometer coupled to LC. Here, the peptides undergo further separation by the LC and ionisation by electrospray. User-defined precursor ions are filtered in the first quadruple and the selected precursor ion is fragmented in the second quadruple upon collision with an inert gas. The fragmented ions are selected for detection in the third quadrupole. Precise quantification of endogenous peptides is achieved by comparing the signal intensities of the unlabelled endogenous (light) peptides and the corresponding isotopically labelled AQUA (heavy) peptides. (B) Nomenclature of peptide fragmentation by MS. The example precursor peptide "SSIEFARL", which when fragmented would result in major product ions referred to as "b" ions when they retain N-terminal amino acids and "y" ions when they retain C-terminal amino acid. The number of amino acids retained in the product ion is shown as a subscript.

Table 5.1. List of heavy peptides used in MRM analysis.

Peptide	Peptide sequence	Isotope labelling	M.W shift	Epitope	MS detection
RR1$_{982-989}$	**F**APLFTNL	F (13C9 15N)	10	Yes[#]	−
ICP8$_{876-883}$	GAIN**F**INL	F (13C9 15N)	10	Yes[#]	−
RRI$_{822-829}$	QT**F**DFGRL	F (13C9 15N)	10	Yes[#]	+
ICP8$_{171-178}$	INNT**F**LHL	F (13C9 15N)	10	Yes[#]	+
gB$_{498-505}$	SSIEFA**R**L	R (13C6 15N4)	10	Yes[#]	+
UL40$_{198-206}$	IAYL**R**TNNL	R (13C6 15N4)	10	Yes	+
UL37$_{600-607}$	TQI**R**FPAL	R (13C6 15N4)	10	Yes	+
UL5$_{126-133}$	**A**QNMY**A**KL	A (13C3 15N)*2	8	Yes	+
UL39 $_{451-461}$	VALD**F**GLTERL	F (13C9 15N)	10	Yes	+
UL40$_{279-287}$	AAIENYV**R**F	F (13C6 15N4)	10	Yes[#]	+++
UL51$_{155-163}$	AIAE**R**ALGL	R (13C6 15N4)	10	No	+++
US1$_{198-205}$	INQL**F**RVL	F (13C9 15N)	10	No	+++
UL26$_{361-370}$	V**A**YGPHG**A**GL	A (13C3 15N)*2	8	No	+++
UL5$_{300-307}$	ST**F**EHQKL	F (13C9 15N)	10	No	+++
UL5$_{729-736}$	MGYTYT**R**V	R (13C6 15N4)	10	No	+
ICP0$_{748-755}$	GALDF**R**SL	R (13C6 15N4)	10	No	+++
UL25$_{304-311}$	G**R**YEHGAL	R (13C6 15N4)	10	No	+++

Red font bold - the isotopically labelled amino acid residue
M.W. is the abbreviation of molecular weight.
[#]previously published epitopes (Salvucci et al., 1995; Wallace et al., 1999; St Leger et al., 2011)
Yes - The peptide is immunogenic in mice
No - The peptide is non-immunogenic in mice
Minus symbol (−) points to the peptides not identified by MS
Plus symbol (+) points to the peptides identified by MS
+++ denotes that the peptide was frequently detected by MS

Table 5.2 MRM transitions of HSV-1 derived peptides

Peptide	*Heavy*		*Light*		Dwell time (ms)	Optimum collision energy
	Q1 m/z (charge)	Q3 m/z (ion)	Q1 m/z (charge)	Q3 m/z (ion)		
$RR1_{982-989}$	466.7689	783.4253 (b7-H2O)	461.7553	773.3981 (b7-H2O)	10	17.5
		669.3824 (b6-H2O)		659.3552 (b6-H2O)	10	17.5
		441.2496 (PLFT-H2O)		441.2496 (PLFT-H2O)	10	25.5
		358.2125 (PLF)		358.2125 (PLF)	10	29.5
		229.14 (b2)		219.1128 (b2)	10	21.5
$ICP8_{876-883}$	436.2587	740.4155 (b7)	431.2451	730.3883 (b7)	10	12.2
		496.2619 (b5-NH3)		486.2347 (b5-NH3)	10	20.2
		385.2299 (INF)		375.2027 (INF)	10	24.2
		272.1458 (NF)		262.1186 (NF)	10	28.2
		243.1921 (FI-28)		233.1648 (FI-28)	10	32.2
$RR1_{822-829}$	497.2645	865.4632 (y7)	492.2509	855.4359 (y7)	10	26.9
		764.4155 (y6)		754.3883 (y6)	10	26.9
		607.3198 (y5)		607.3198 (y5)	10	26.9
		345.2245 (y3)		345.2245 (y3)	10	30.9
		231.1557 (TF-28)		221.1285 (TF-28)	10	30.9
$ICP8_{171-178}$	491.2827	868.4741 (y7)	486.2691	858.4468 (y7)	10	22.6
		754.4311 (y6)		744.4039 (y6)	10	22.6
		640.3882 (y5)		630.361 (y5)	10	22.6
		269.1608 (y2)		269.1608 (y2)	10	30.6
		251.1503 (LH)		251.1503 (LH)	10	34.6

Peptide	*Heavy*		*Light*		Dwell time (ms)	Optimum collision energy
	Q1 m/z (charge)	**Q3 m/z (ion)**	**Q1 m/z (charge)**	**Q3 m/z (ion)**		
$gB_{498-505}$	466.7574	845.4755 (y7)	461.7533	835.4672 (y7)	10	21.5
		758.4435 (y6)		748.4352 (y6)	10	21.5
		645.3594 (y5)		635.3511 (y5)	10	21.5
		627.3488 (y5-H2O)		617.3406 (y5-H2O)	10	29.5
		516.3168 (y4)		506.3085 (y4)	10	25.5
$UL51_{155-163}$	462.281	735.4387 (b7)	457.2769	725.4304 (b7)	10	17.3
		707.4438 (a7)		697.4355 (a7)	10	29.3
		668.3965 (y6)		658.3883 (y6)	10	25.3
		650.386 (y6-H2O)		640.3777 (y6-H2O)	10	25.3
		539.3539 (y5)		529.3457 (y5)	10	21.3
$US1_{198-205}$	506.822	899.5526 (y7)	501.8084	889.5254 (y7)	10	27.3
		785.5097 (y6)		775.4825 (y6)	10	23.3
		657.4511 (y5)		647.4239 (y5)	10	23.3
		544.3671 (y4)		534.3398 (y5)	10	27.3
		228.1343 (b2)		228.1343 (b2)	10	23.3
$UL26_{361-370}$	475.2527	850.4297 (y9)	471.2456	842.4155 (y9)	10	25.9
		775.3855 (y8)		771.3784 (y8)	10	21.9
		612.3222 (y7)		608.3151 (y7)	10	21.9
		388.1964 (y8+2)		386.1928 (y8+2)	10	21.9
		136.0757 (Y)		136.0757 (Y)	10	33.9
$UL5_{300-307}$	500.2698	850.4271 (b7-H2O)	495.2562	840.3999 (b7-H2O)	10	31
		811.4526 (y6)		801.4254 (y6)	10	23

Peptide	*Heavy*		*Light*		Dwell time (ms)	Optimum collision energy
	Q1 m/z (charge)	**Q3 m/z (ion)**	**Q1 m/z (charge)**	**Q3 m/z (ion)**		
		740.3427 (b6)		730.3155 (b6)	10	27
		680.358 (FEHQK)		670.3307 (FEHQK)	10	27
		552.263 (FEHQ)		542.2358 (FEHQ)	10	31
UL40 $_{279-287}$	546.7892	950.497 (y7)	541.7851	940.4887 (y7)	10	25.1
		837.4129 (y6)		827.4046 (y6)	10	25.1
		708.3703 (y5)		698.362 (y5)	10	25.1
		594.3274 (y4)		584.3191 (y4)	10	25.1
		431.264 (y3)		421.2558 (y3)	10	25.1
$UL40_{198-206}$	544.3103	974.5293 (y8)	539.6357	964.5211 (y8)	10	24.9
		957.5028 (y8-NH3)		947.4945 (y8-NH3)	10	24.9
		903.4922 (y7)		893.4839 (y7)	10	28.9
		740.4289 (y6)		730.4206 (y6)	10	28.9
		627.3448 (y5)		617.3365 (y5)	10	24.9
$UL37_{600-607}$	478.2836	824.4653 (b7)	473.2795	814.457 (b7)	10	22
		726.4536 (y6)		716.4454 (y6)	10	22
		656.3754 (b5)		646.3671 (b5)	10	26
		613.3696 (y5)		603.3613 (y5)	10	22
		509.307 (b4)		499.2987 (b4)	10	38
$UL5_{126-133}$	473.7489	743.3878 (y6)	469.7418	739.3807 (y6)	10	21.8
		498.2503 (MYAK)		494.2432 (MYAK)	10	21.8
		409.154 (NMY)		409.154 (NMY)	10	33.8
		335.2411 (y3)		331.234 (y3)	10	29.8

Peptide	*Heavy*		*Light*		Dwell time (ms)	Optimum collision energy
	Q1 m/z (charge)	Q3 m/z (ion)	Q1 m/z (charge)	Q3 m/z (ion)		
		260.1969 (y2)		260.1969 (y2)	10	33.8
$UL39_{451-461}$	622.3591	960.5214 (y8)	617.3455	950.4942 (y8)	10	32.4
		845.4945 (y7)		835.4672 (y7)	10	36.4
		688.3988 (y6)		688.3988 (y6)	10	36.4
		518.2933 (y4)		518.2933 (y4)	10	32.4
		423.2509 (y7+2)		418.2373 (y7+2)	10	28.4
$UL5_{729-736}$	500.7434	869.4391 (y7)	495.7393	859.4308 (y7)	10	23
		812.4176 (y6)		802.4094 (y6)	10	23
		649.3543 (y5)		639.3461 (y5)	10	27
		548.3066 (y4)		538.2984 (y4)	10	23
		385.2433 (y3)		375.235 (y3)	10	23
$ICP0_{748-755}$	444.7443	760.4227 (y6)	439.7402	750.4145 (y6)	10	20.6
		647.3387 (y5)		637.3304 (y5)	10	20.6
		532.3117 (y4)		522.3035 (y4)	10	24.6
		419.2289 (ALDF-28)		419.2289 (ALDF-28)	10	36.6
		314.1851 (FR)		304.1768 (FR)	10	36.6
$UL25_{304-311}$	456.7317	799.3721 (b7+H2O)	451.7276	789.3638 (b7+H2O)	10	25.1
		710.3244 (b6)		700.3161 (b6)	10	21.1
		653.303 (b5)		643.2947 (b5)	10	25.1
		516.244 (b4)		506.2358 (b4)	10	37.1
		391.1844 (b7+2)		386.1803 (b7+2)	10	25.1

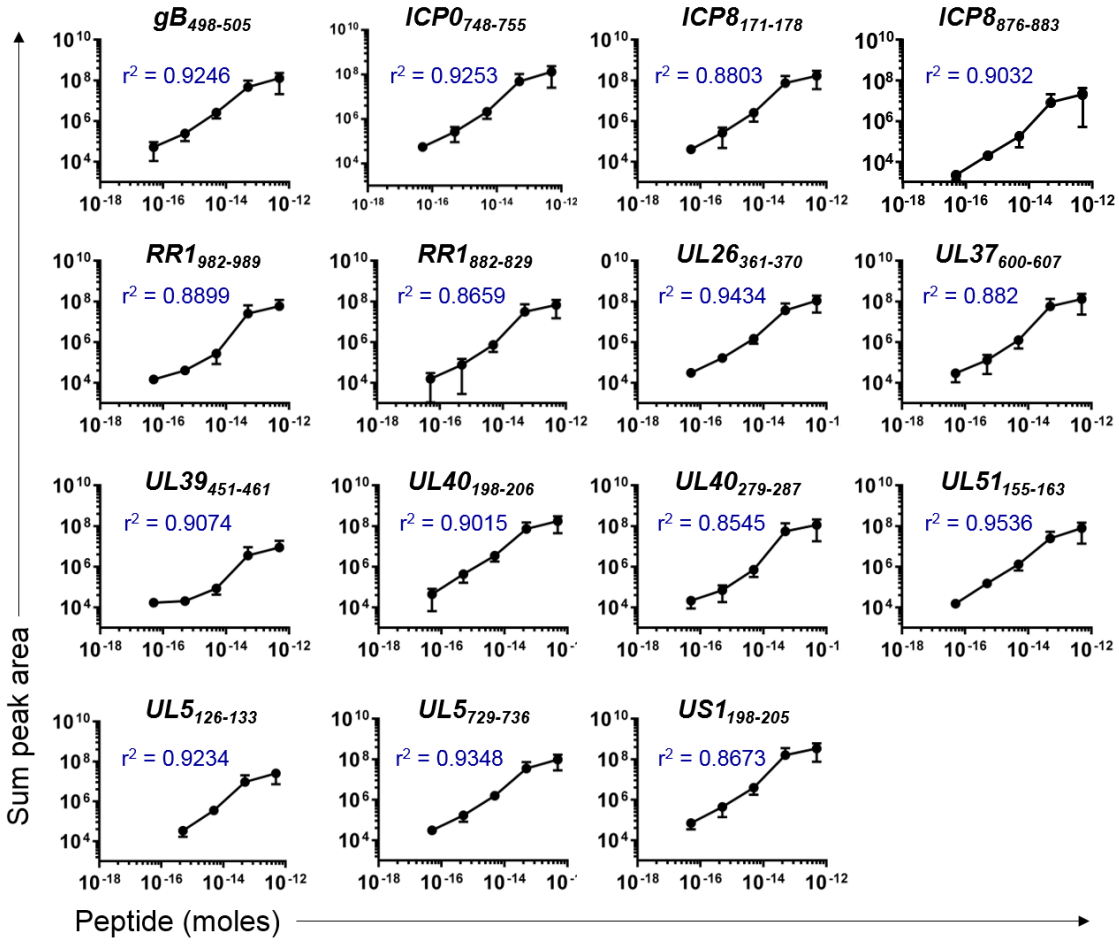

Figure 5.16 Assessment of MRM limit of detection and quantification of each HSV-1 AQUA peptide. The AQUA peptides were diluted across a ten-fold series (5 amoles to 500 fmoles) and subsequently detected by MRM, with data showing the sum peak area of the total transitions for each peptide. Peptide quantity from 50 amoles (or 5×10^{-17} moles) could be detected for most peptides. Each data point represents mean ± SD. The goodness of fit (r^2) value derived from the linear regression curve is shown for each peptide.

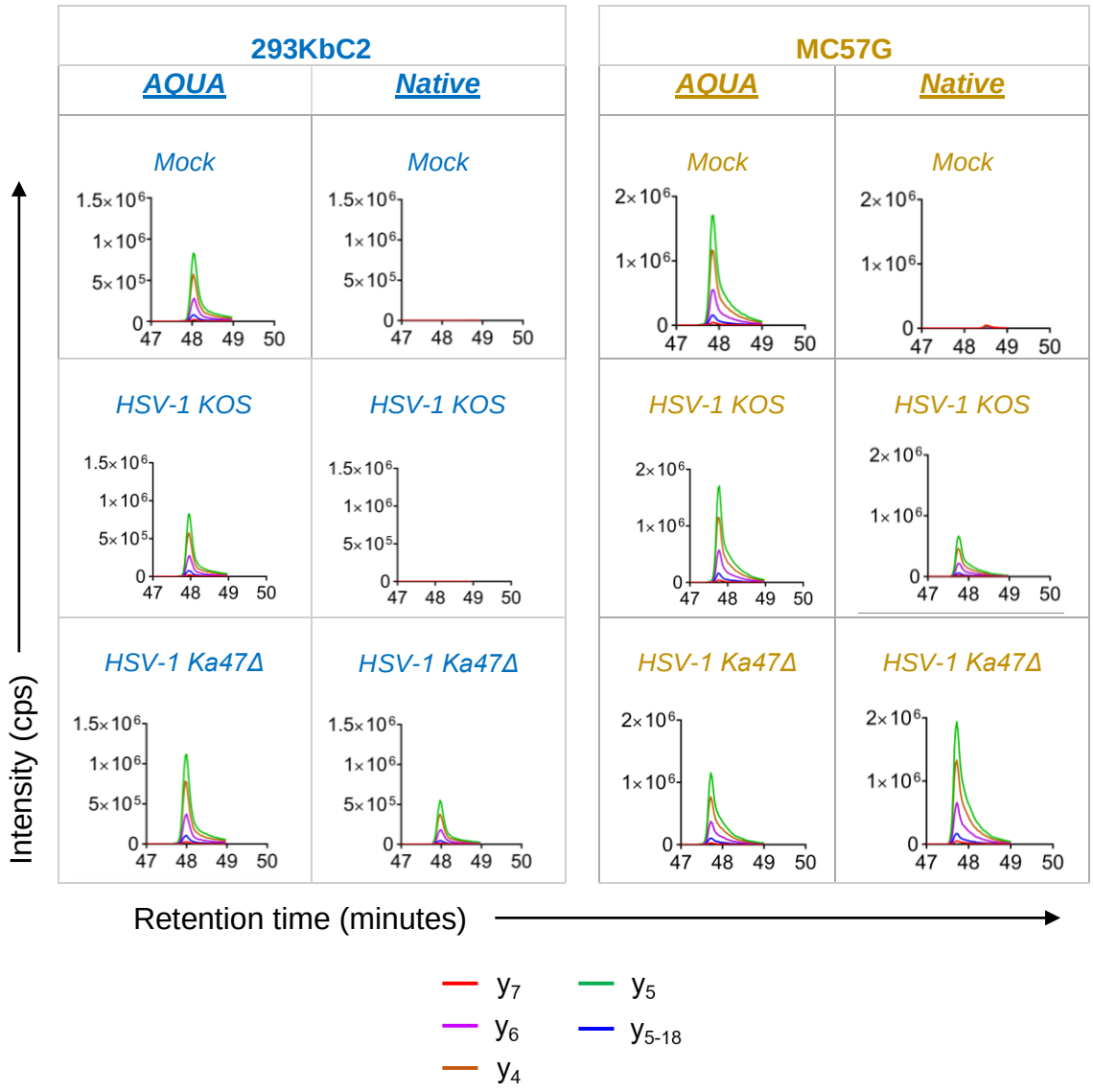

Figure 5.17 Detection of HSV-1 gB$_{498-505}$ (SSIEFARL) in 293KbC2 and MC57G cells. Shown are the MRM transitions (y_7, y_6, y_5, y_{5-18} and y_4) for the peptide gB$_{498-505}$ in the mock-treated cells and the cells infected with HSV-1 KOS or HSV-1 Ka47Δ. The left panel shows the transitions in 293KbC2 samples and the right panel shows transition peaks in MC57G samples. Results for AQUA and native peptide are shown in each panel for comparison. MRM transitions of AQUA peptides were detected in all samples. The results for the native peptide in mock-treated 293KbC2, mock-treated MC57G and HSV-1 KOS infected 293KbC2 samples were at background levels.

5.2.5 Quantification of endogenous HSV-1 peptides revealed the difference in ICP47 function between human and mouse cells

5.2.5.1 Overview of quantification of HSV-1 peptides

A total of 15 peptides were detectable in HSV-1 KOS and Ka47Δ infected MC57G samples. In 293KbC2 samples, only 9 peptides were above the detection limit in HSV-1 KOS infected cells and 14 peptides were above the detection limit in Ka47Δ infected cells. However, only 12 peptides detected in Ka47Δ infected 293KbC2 cells were considered for further analysis due to reduced frequency of detection (refer to section 5.2.4). When detected, the peptides spanned a range of 0.9 to 6014 copies/cell in MC57G (Figure 5.18) compared to 0.6 to 1491.6 copies/cell in 293KbC2 cell line (Figure 5.19). In MC57G cells, the average number of peptide molecules varied from 2 molecules to 4350 molecules per cell across peptides in the absence of ICP47 (Figure 5.20 A). Relative to MC57G cells, the average peptide abundance was significantly less ($p<0.0001$) in 293KbC2 cells infected with Ka47Δ (Figure 5.20 C), ranging from nearly 4 to 1500 copies/cell (Figure 5.20 B). This observation is reflective of the previously observed relatively low cell surface MHC I observed in 293KbC2 cells compared to MC57G cells (Figure 3.4 A). The quantification of K^b bound HSV-1 peptides revealed that the removal of ICP47 significantly increased the overall abundance of the peptides presented on MC57G cells (**Figure 5.20** A) and 293KbC2 cells (Figure 5.20 B). This observation is in line with the previous finding (chapter 3, section 3.2.3) that demonstrated the ability of ICP47 to significantly hinder antigen presentation both in MC57G cells and in 293KbC2 cells. When the average peptide copies/cell was compared between the two cell lines infected with wild-type HSV-1, there was a significantly lower number of peptides in 293KbC2 cells compared to MC57G cells (Figure 5.20 D). This finding is consistent with the data presented in Chapter 3 (Figure 3.8). Together, these data suggest that the difference in copy number of peptides between 293KbC2 and MC57G cells infected with HSV-1 KOS is largely due to the difference in efficiency at which ICP47 inhibit antigen presentation between the two cell lines.

5.2.5.2 ICP47 severely impairs antigen presentation in human cells

Analysis of the effect of ICP47 was performed at peptide level by comparing the peptide abundance between samples infected with HSV-1 KOS and HSV-1 Ka47Δ as paired samples in the same experiment (Figure 5.18 and Figure 5.19). Of the 15 K^b peptides examined in MC57G cells, we found a clear reduction in peptide copies for at least nine peptides in all three experiments infected with HSV-1 KOS compared to those infected

with HSV-1 Ka47Δ. The nine peptides include $gB_{498-505}$, $ICP8_{171-178}$, $ICP8_{876-883}$, $RR1_{982-989}$, $RR1_{822-829}$, $UL39_{451-461}$, $UL40_{198-206}$, $US1_{198-205}$ and $UL40_{279-287}$ (Figure 5.18). Three peptides, $UL5_{126-133}$, $UL5_{729-736}$ and $UL37_{600-607}$, showed diminished presentation in the presence of ICP47 in two experiments. In this case, the third pair was below the limit of sensitivity of the instrument. While the peptides $ICP0_{748-755}$ and $UL51_{155-163}$ were detected in all samples, the copy number was reduced in one experiment and increased in the other two experiments in HSV-1 KOS infected samples compared to samples infected with HSV-1 Ka47Δ. Another peptide, $UL26_{361-370}$ showed increased copy number in HSV-1 KOS infected samples compared to Ka47Δ infected samples in all three experiments. Of note, $UL26_{361-370}$ was detected at low abundance, with copy number ranging from 0.9 to 4 copies/cell across all samples (Figure 5.18). These data show that the presentation of peptides, $ICP0_{748-755}$, $UL51_{155-163}$ and $UL26_{361-370}$, are not affected majorly by ICP47 in mouse cells compared to other peptides tested in this study.

With 293KbC2 cell line, of the 14 peptides detected, 9 peptides including, $gB_{498-505}$, $ICP8_{876-883}$, $RR1_{982-989}$, $RR1_{822-829}$, $UL26_{361-370}$, $UL40_{198-206}$, $UL51_{155-163}$, $UL5_{729-736}$, and $US1_{198-205}$, were found to have reduced copy number in the presence of ICP47 in all three experiments (Figure 5.19). For three peptides, $ICP0_{748-755}$, $UL37_{600-607}$ and $UL39_{451-461}$, quantification was observed only in 2 experiments and for peptides, $ICP8_{171-178}$ and $UL5_{126-133}$, quantification was possible in only one experiment. However, in all cases where a peptide was detectable in a sample infected with HSV-1 Ka47Δ, there was a reduction in the number of molecules presented on the wild-type HSV-1 infected sample.

There are several observations that confirm the difference in efficiency at which ICP47 affect antigen presentation in MC57G and 293KbC2 cells. Notably, the peptides $gB_{498-505}$, $ICP8_{876-883}$, $RR1_{822-829}$, and $UL39_{451-461}$ are immunogenic (Figure 5.9) (St Leger et al., 2011) and are presented at high abundance (100 to 10000 copies/cell) in the absence of ICP47, consistently in MC57G and 293KbC2 cells (Figure 5.18 and Figure 5.19). However, in wild-type HSV-1 infected MC57G cells, these immunogenic peptides are still presented at high copy numbers, whereas, a steep decline in abundance was observed for 293KbC2 samples infected with the wild-type virus. Furthermore, in the presence of ICP47, 293KbC2 samples showed peptide abundance at an average of 10 molecules or less for all 14 peptides analysed (Figure 5.19 and Figure 5.21 A). Lack of direct correlation between the peptide copies presented between the KOS-infected and Ka47Δ-infected 293KbC2

cells (Figure 5.21 A) suggests that ICP47 severely impairs antigen presentation regardless of the maximum presenting capacity of a peptide in the absence of ICP47. Although the fold inhibition was variable across peptides in 293KbC2 cells, there was over ten-fold reduction in presentation of over 50% of the peptides (Figure 5.21 C). In comparison to 293KbC2 cells, the inhibition of presentation by ICP47 is significantly less pronounced for MC57G cells, being just within a 5-fold range across all peptides (Figure 5.21 B&C). The effect of ICP47, although diminished in mouse cells, retains a similar effect across the peptides (Figure 5.21 C). Together, these results suggest that ICP47 impairs antigen presentation severely in human cells but only modestly in mouse cells, according to the two cell lines tested here.

5.2.5.3 Level of inhibition of antigen presentation is variable between peptides

On the one hand, the peptides, $gB_{498\text{-}505}$, $UL37_{600\text{-}607}$, $UL39_{451\text{-}461}$, $UL40_{198\text{-}206}$, and $UL5_{729\text{-}736}$, are inhibited from presentation to near the detection limit by ICP47 in 293KbC2 samples (Figure 5.19). While on the other, the peptides $ICP0_{748\text{-}755}$, $RR1_{982\text{-}989}$, $UL26_{361\text{-}370}$, and $US1_{198\text{-}205}$ are not inhibited to the same extent by ICP47 (Figure 5.19). These data suggest that ICP47 blocks certain peptides highly efficiently from translocation, while other peptides are not fully inhibited (Figure 5.21 C). The variability in the level of inhibition could be due to translocation of at least some peptides directly to ER independent of TAP (Norbury et al., 2001) or an intrinsic feature of the peptide that may help to overcome TAP inhibition by ICP47. This theory is further supported by the significant association observed between the two cell lines with regard to the number of peptides presented in the absence of ICP47 and the level of inhibition of antigen presentation by ICP47 (Figure 5.22 A&B). These results demonstrate that each peptide is influenced in a similar manner in both cell lines and therefore, the variation observed in both the abundance of peptides and inhibition by ICP47 is unlikely to be an artefact of a particular cell line. Hence, some of the factors that might explain the variability in inhibition by ICP47 across peptides are explored in the following sections.

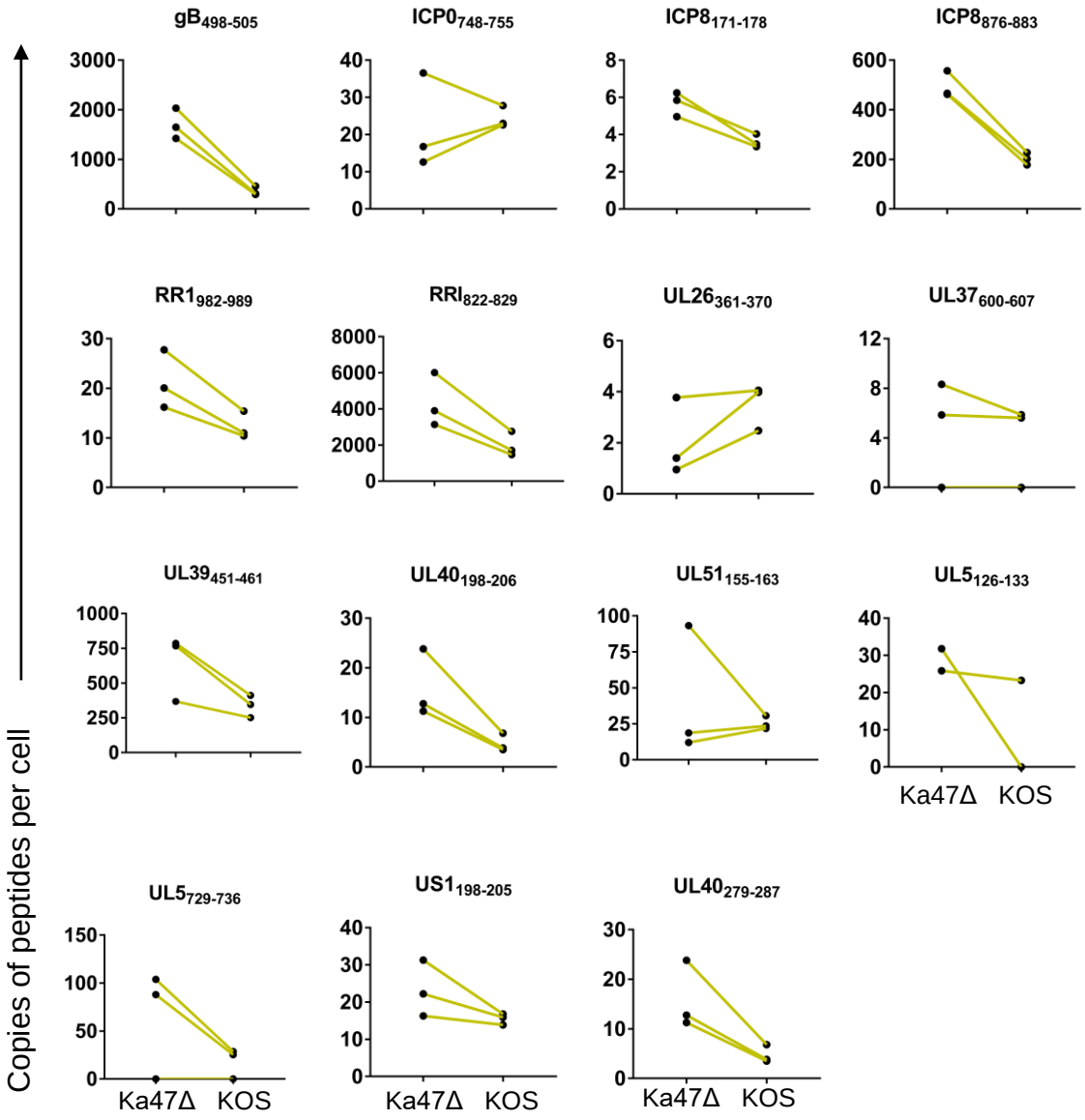

Figure 5.18 Quantification of K^b-bound HSV-1 peptides on MC57G cells. For each peptide, the average copy number of peptide per cell was calculated from each sample. The graphs show the copies of peptide per cell in each replicate sample, which is either infected with Ka47Δ or with KOS. The trend line connecting the paired samples for each peptide indicates the increase or decrease in peptide abundance in the absence (HSV-1 Ka47Δ) or presence of ICP47 (HSV-1 KOS) in an experiment.

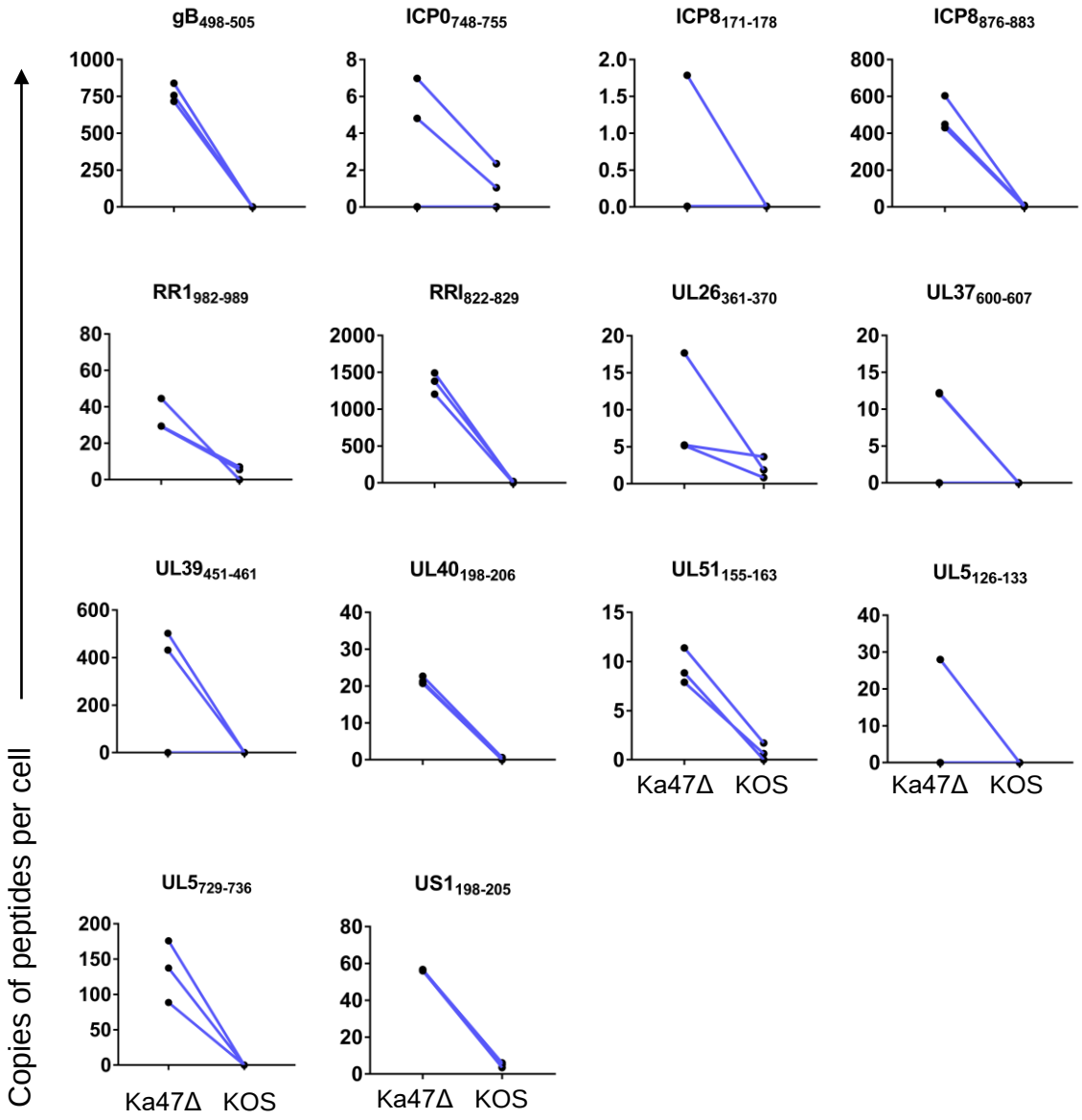

Figure 5.19 Quantification of K^b-bound HSV-1 peptides on 293KbC2 cells. The abundance of selected HSV-1 peptides presented on 293KbC2 cells infected with HSV-1 Ka47Δ or KOS was quantified using MRM-MS. The graphs show the copies/cell for the various peptides in every replicate sample. Each symbol represents a sample. The trend line connecting the paired samples for each peptide indicates the increase or decrease in peptide abundance in the absence (HSV-1 Ka47Δ) or presence of ICP47 (HSV-1 KOS).

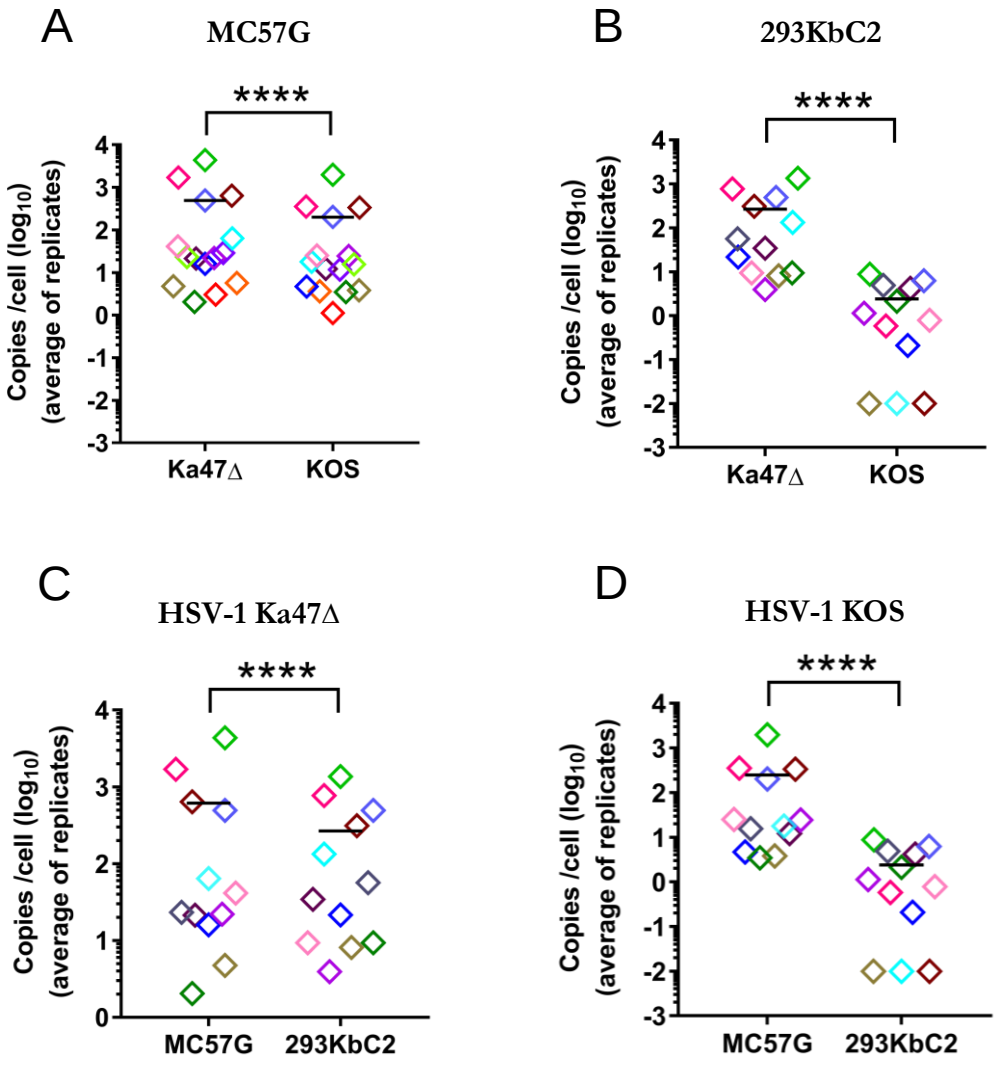

Figure 5.20 Overall effect of ICP47 on peptide abundance in MC57G and 293KbC2 cells. (A) Summary of average peptide copies/cell quantified in MC57G cells infected with HSV-1 Ka47Δ or HSV-1 KOS. (B) Summary of average peptide copies/cell quantified in 293KbC2 cells infected with HSV-1 Ka47Δ or HSV-1 KOS. (C) Comparison of peptide abundance between MC57G and 293KbC2 cells in the absence of ICP47. (D) Comparison of peptide abundance between the two cell lines infected with wild-type HSV-1. (A, B, C & D) The graphs show log_{10} transformed values. Each symbol represents a peptide and the peptides are colour coded for comparison between sample types. The horizontal line represents mean. The statistical significance was calculated using two-way ANOVA. ****$p<0.0001$.

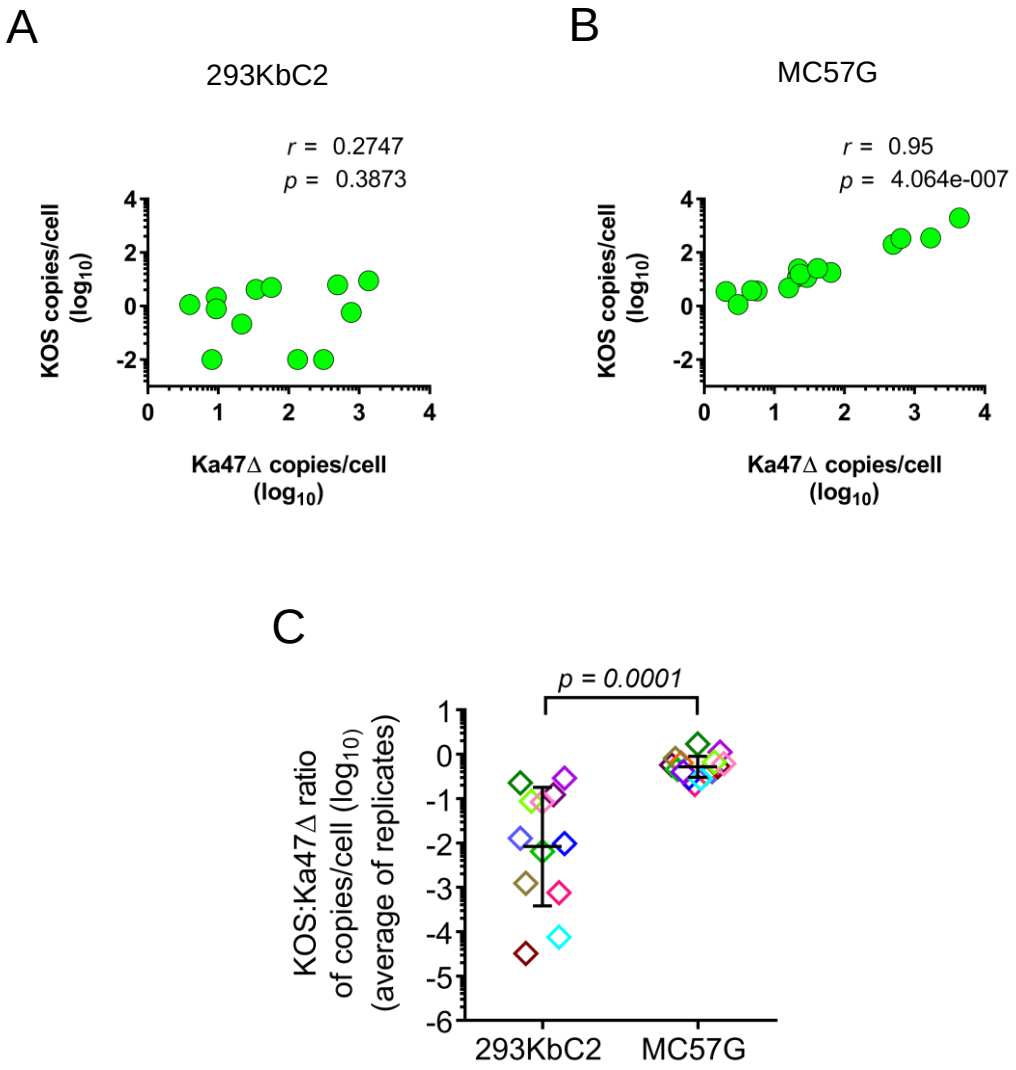

Figure 5.21 ICP47 severely impairs antigen presentation in 293KbC2 cells. (A) Analysis of correlation of the peptide copy number between KOS –infected and Ka47Δ –infected 293KbC2 cells. (B) Analysis of correlation of the peptide copy number between KOS –infected and Ka47Δ –infected MC57G cells. (A&B) The average copy number of peptides determined in three independent experiments was used for correlation analysis. The statistical significance was determined using the Spearman rank correlation. The correlation coefficient *(r)* and *p*-value are shown. (C) The $\log_{10}$ ratio of an average number of peptide molecules detected on cells infected with HSV-1 KOS and on cells infected with HSV-1 Ka47Δ is shown for 293KbC2 and MC57G cell lines. Each symbol represents a peptide. The peptides are colour coded for comparison between sample types. The error bars represent geometric mean ± SD. Statistical significance (p=0.0001) was calculated using two-way ANOVA.

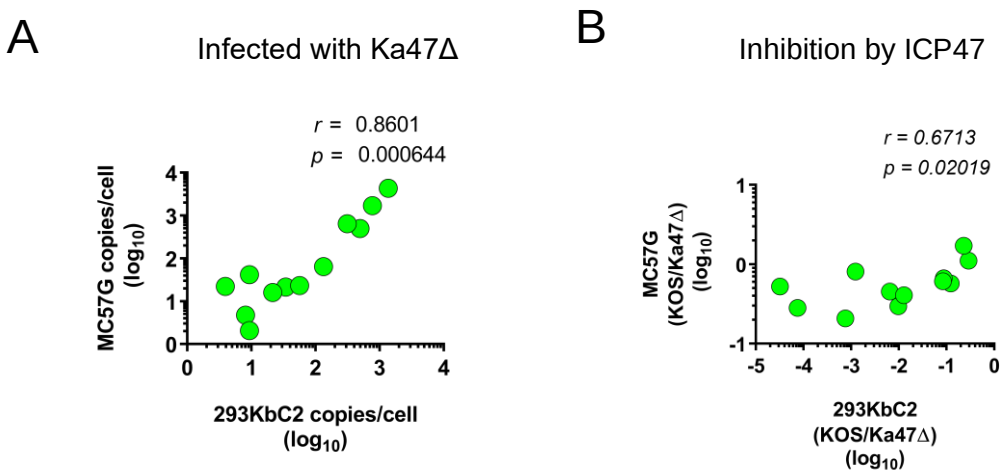

Figure 5.22 The abundance in the absence of ICP47 and level of inhibition of presentation of peptides by ICP47 show a significant correlation between 293KbC2 and MC57G cell lines. (A) The relationship between human and mouse cell lines in copies of peptides per cell. For analysis, the average copy number of peptides found in samples infected with Ka47Δ was used. (B) The relationship between human and mouse cell lines in the level of inhibition of peptides by ICP47 is shown. The correlation analysis was performed using the $\log_{10}$ ratio of average peptide copies between cells infected with HSV-1 KOS and HSV-1 Ka47Δ. (A&B) The statistical significance was determined using the Spearman rank correlation. The correlation coefficient *(r)* and *p*-value are shown.

5.2.6 Analysis of factors influencing the variability in peptide abundance and ICP47 mediated inhibition of antigen presentation

5.2.6.1 Association with ER-targeting signal sequence

Alternative processing and presentation pathways occur in conjunction to the classical TAP mediated MHC I peptide presentation (Hammond et al., 1993; Snyder et al., 1997; Wölfel et al., 2000; Lautscham et al., 2003). A proportion of peptides that are translocated independently of TAP are derived from precursors containing ER-targeting signal sequences (Henderson et al., 1992; Wei and Cresswell, 1992). Signal sequences are composed of polar amino- and carboxy-termini flanking a small hydrophobic core sequence (Martoglio and Dobberstein, 1998). Signal sequence embedded peptide precursors including newly synthesised proteins are targeted to the ER membrane where the signal peptidase liberates the carboxy-terminus and the resultant peptide is further processed by signal peptide peptidases (Oliveira et al., 2013). Some peptide fragments resulting from this process are loaded onto MHC I in the ER. In our study, the source proteins of the quantified HSV-1 peptides were analysed for an embedded signal sequence using SignalP 4.1 server (Petersen et al., 2011). This program predicts the occurrence of signal sequence and the signal peptidase recognition site in the source protein. The prediction analysis showed that none of the source proteins of the specified peptides was predicted to contain a signal peptide sequence. However, it is possible that those peptides less responsive to ICP47 inhibition might use another unknown pathway whereby the peptides are loaded independently of the TAP.

5.2.6.2 Hydropathicity of peptides

Another possible explanation for the observed differences in the degree of inhibition of peptide transport by ICP47 was explored. In this context, a previous study demonstrated a relationship between the hydrophobicity of peptides and TAP-independent presentation (Lautscham et al., 2001). Using an EBV model, Lautscham et al. (2001) showed that the most hydrophobic epitopes were TAP-independent and suggested that high hydrophobicity is required and is sufficient for TAP-independent translocation of peptides to the ER. We tested the correlation between inhibition of peptide presentation and hydrophobicity of peptides. Further, since hydrophobicity may also affect the number of peptides transported, we analysed the relationship between hydrophobicity and abundance of peptides.

The hydropathicity of the quantified peptides was calculated based on the Hopp-Woods hydropathy score (Hopp and Woods, 1981). Peptides with smaller hydropathy score are considered to be more hydrophobic (Hopp and Woods, 1981). The hydropathicity of our peptides ranges from 0.1 to -1.0 (Table 5.3). Among the peptides that were highly inhibited in all three experiments, $gB_{498-505}$, $RR1_{822-829,}$ and $UL39_{451-461}$ have a relatively larger hydropathy score (-0.1 to 0) indicating that these peptides are relatively less hydrophobic (Table 5.3). However, for $ICP8_{876-883,}$ whose presentation was inhibited nearly 70-fold by ICP47, the total hydropathy score of -0.8 shows that this peptide might be relatively more hydrophobic. Similarly, for the peptides that are not subjected to absolute inhibition, a poor correlation to hydrophobicity was observed. For instance, when the peptides $ICP0_{748-755}$ and $ICP8_{171-178}$ that are relatively less inhibited by ICP47 are considered, the former is less hydrophobic (hydropathy score -0.03) whereas the latter shows a large negative hydropathy score (-0.9) (Table 5.3). Overall, there was no significant correlation between the hydropathicity and ICP47 mediated TAP inhibition in the two cell lines (Figure 5.23 A) indicating that hydrophobicity is unlikely to explain the variable sensitivity of the peptides to inhibition of presentation by ICP47.

5.2.6.3 TAP binding specificity

The proteasomes and other cytosolic peptidases produce peptides that range in length from 2 to 25 amino acids (Nussbaum et al., 1998). From this peptide pool, TAP transports peptides based on length and the amino acid composition (Momburg et al., 1994; van Endert et al., 1994; Koopmann et al., 1996; Uebel et al., 1997). Peptides of lengths 8 to 16 amino acids are preferred, however, peptides as long as 40 amino acids are also transported to a lesser extent (van Endert et al., 1994; Koopmann et al., 1996). Peptides longer than the optimum size are processed in the ER lumen before loading onto MHC I (Serwold et al., 2002). Interestingly, the selection of peptides differs between human and mouse TAP (Momburg et al., 1994; Schumacher, 1994; van Endert, 1995; Burgevin et al., 2008). While mouse TAP prefers peptides with hydrophobic amino acids at the C-terminal end, human TAP selects peptides based on the amino acids at the first three N-terminal residues and the C-terminal residue (Uebel et al., 1997; Burgevin et al., 2008). Moreover, previous studies have demonstrated that the binding affinity to TAP is directly proportional to the transport and presentation of peptides (van Endert, 1995; Gubler et al., 1998).

Therefore, we tested whether the efficiency at which ICP47 inhibits antigen presentation correlates with the TAP binding affinity. The binding affinity of our peptide set towards human and mouse TAP was determined based on the prediction matrix developed by Burgevin et al., 2008 (Table 5.3). According to this matrix, the lower the score the higher the affinity of a peptide towards TAP. The analyses revealed a moderate but not statistically significant positive correlation (293KbC2, r = 0.5477, p = 0.069; MC57G, r = 0.4829, p = 0.070) between the level of inhibition of peptides and TAP score (Figure 5.23 B). This result suggests that peptides with higher predicted TAP binding affinity are likely to be more inhibited by ICP47 from the presentation on MHC I. Data from more peptides and empirical measurement of binding affinity is required to support this possibility.

5.2.6.4 Peptide abundance

Peptides that have high affinity towards TAP might be transported in high numbers into the ER. Further, as previously shown in Figure 5.18 and Figure 5.19, peptides are presented at varying abundance in the absence of ICP47. Therefore, it is plausible that peptide abundance might influence the level of inhibition of presentation. Our analysis showed that there is an apparent inverse correlation between peptide abundance and the level of inhibition but it did not reach statistical significance (293KbC2, r = -0.5664, p = 0.05905; MC57G, r = -0.4607, p = 0.08607) (Figure 5.23 C). It is possible that the borderline correlation is simply due to a bigger window to measure the drop-in peptide number in case of high abundance peptides, especially considering our arbitrary value of 0.01 copies per cell added to all samples.

5.2.6.5 MHC I binding affinity and immunogenicity

The peptides pre-selected by TAP are transported to the ER for selection by MHC I. The selection of peptides by K^b is relatively more stringent compared to TAP (Fremont et al., 1992; Molano et al., 1998). In theory, it is unlikely that MHC I binding affinity would contribute to the differences in the level of peptide inhibition by ICP47. However, because the inhibition of TAP function results in increased retention of MHC I in ER (Townsend and Bodmer, 1989), it is possible that peptides with lower binding affinity to MHC I could be presented. Further, it is established that the higher the affinity of a peptide to MHC I, the more likely the pMHC-I is translocated to the surface and stably presented (Feltkamp et al., 1994; Sette et al., 1994; Assarsson et al., 2007). In case of limited peptide availability, even peptides with lower binding affinity might have a chance of being presented.

Therefore, we tested if there is a relationship between the differential inhibition of peptides by ICP47 and the predicted MHC I binding affinity or the immunogenicity of each peptide. The results showed that neither the binding affinity to MHC I (Table 5.3) (Figure 5.23 D) nor the immunogenicity appears to correlate with the peptide inhibition by ICP47 (Table 5.3) (Figure 5.23 E).

5.2.6.6 Influence of timing of gene expression

At transcript level, ICP47 could be observed as early as 1 hour after infection and retained in the infected fibroblast cells for at least 24 hours (Harkness et al., 2014). Based on the above data, we expected that ICP47 would have a similar effect on peptides derived from proteins of all four kinetic classes. Therefore, the temporal relationship between the presentation of various HSV-1 peptides and ICP47 mediated inhibition of antigen presentation was analysed (Figure 5.24). In both the cell lines, IE peptides appear to be slightly less inhibited compared to the E and L peptides (Figure 5.24 A&C), however, with a small sample size (n = 2) it is not possible to reach a definitive conclusion. Statistical comparison amongst the peptides grouped based on temporal gene expression shows that there was no significant difference in the inhibition of peptides between the kinetic classes (Figure 5.24 B&D). Further, there is substantial variability in the inhibition level within E class, particularly in 293KbC2 cells, suggesting that even if expression time plays a role it cannot entirely explain the variability observed in peptide inhibition across all peptides.

Table 5.3 Characteristics of K^b associated HSV-1 peptides

Peptide	Hydropathicity[a]	*TAP score*[b]		Affinity to MHC I [c] (IC50 nm)	% IFNγ (of $CD8^+$) cells[d]	Ratio KOS:Ka47Δ (of average copies/cell)	
		Human	*Mouse*			*293KbC2 (human)*	*MC57G (mouse)*
$gB_{498-505}$	0	-1	-1.3	2.29	11.4133	0.000752	0.20850725
$RR1_{982-989}$	-1.033333333	0	0.4	7.04	0.59145	0.122243	0.5744735
$RR1_{822-829}$	-0.111111111	-0.7	-1.3	7.99	0.41329	0.006464	0.45489471
$ICP8_{171-178}$	-0.933333333	0.3	-0.2	15.86	0.38454	-	0.63794576
$UL40_{198-206}$	-0.52	-1.3	-1.3	10.91	0.17704	0.009742	0.29638844
$ICP8_{876-883}$	-0.888888889	-0.7	-1.1	36.94	0.07478	0.0127	0.40840901
$UL37_{600-607}$	-0.422222222	-1.2	-1.3	17.03	0.06994	0.001232	0.80989466
$ICP0_{748-755}$	-0.033333333	-0.4	-0.6	498.68	0.05481	0.28894	1.11253151
$UL39_{451-461}$	-0.108333333	-1.5	-1.4	990.73	0.04666667	0.000032	0.37160359
$UL5_{126-133}$	-0.333333333	-1.1	-0.9	147.11	0.04242	-	0.52472487
$UL5_{729-736}$	-0.577777778	-0.6	-0.8	4.47	0.04	0.000075	0.40388286
$US1_{198-205}$	-0.666666667	0.0	-0.1	25.5	0	0.087033122	0.28175463
$UL26_{361-370}$	-0.645454545	-0.7	-0.7	87.33	0	0.227404567	0.66713888
$UL51_{155-163}$	-0.09	-1.3	-1.0	2036.19	0	0.083648693	1.71431281
$UL40_{279-287}$	-0.29	-2.2	-2.3	175.28	0.054805556	-	0.61231385

[a]The hydropathy score was alculated using the method of Hopp and Woods, 1981.

[b]The TAP score was calculated based on the prediction matrix developed by Burgevin et al., 2008.

[c]MHC I binding affinity was predicted using ANN based algorithm at the Immune Epitope Database (IEDB) website (Nielsen et al., 2003)

[d]The immunogenicity of peptides in mice was determined as described in section 5.2.1.4.

Figure 5.23 Analysis of factors influencing peptide inhibition by ICP47. Spearman correlation coefficients were generated to test the correlation of level the inhibition of antigen presentation by ICP47 with (A) the Hopp-Woods hydropathy score, (B) TAP score, (C) abundance of peptides, (D) MHC I binding affinity, and (E) immunogenicity of peptides. Analysis for 293KbC2 cells is shown on the left panel (n=12 peptides) and for MC57G cells is shown on the right panel (n=15 peptides). The Spearman correlation coefficient (*r*) and *p* values are shown for each analysis.

	293KbC2 (left)	**MC57G** (right)
A	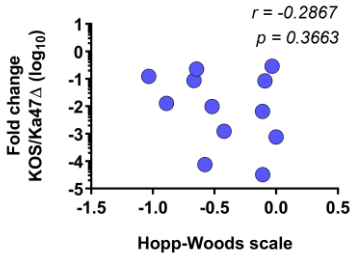	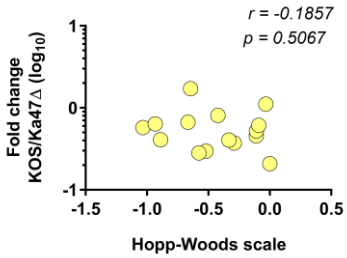
B	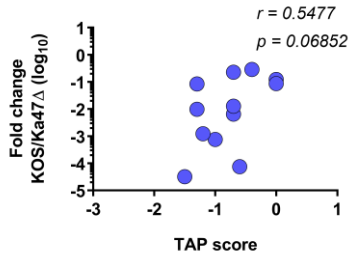	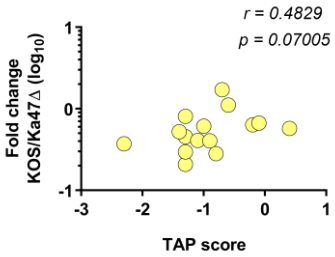
C	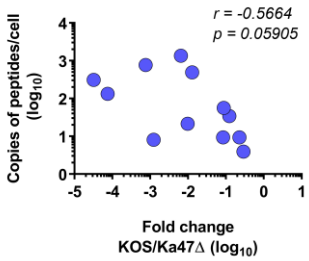	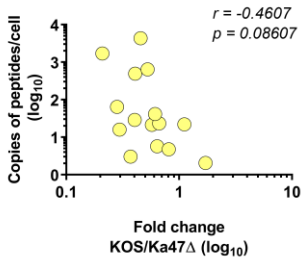
D	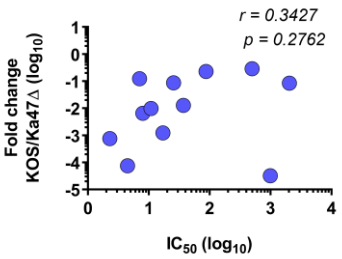	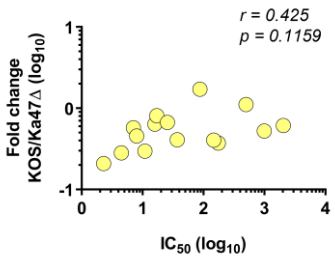
E	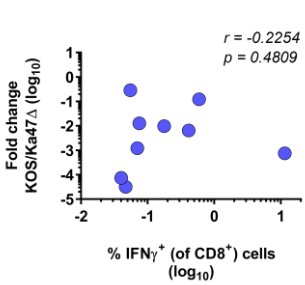	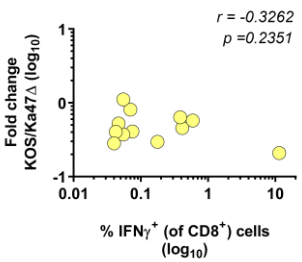

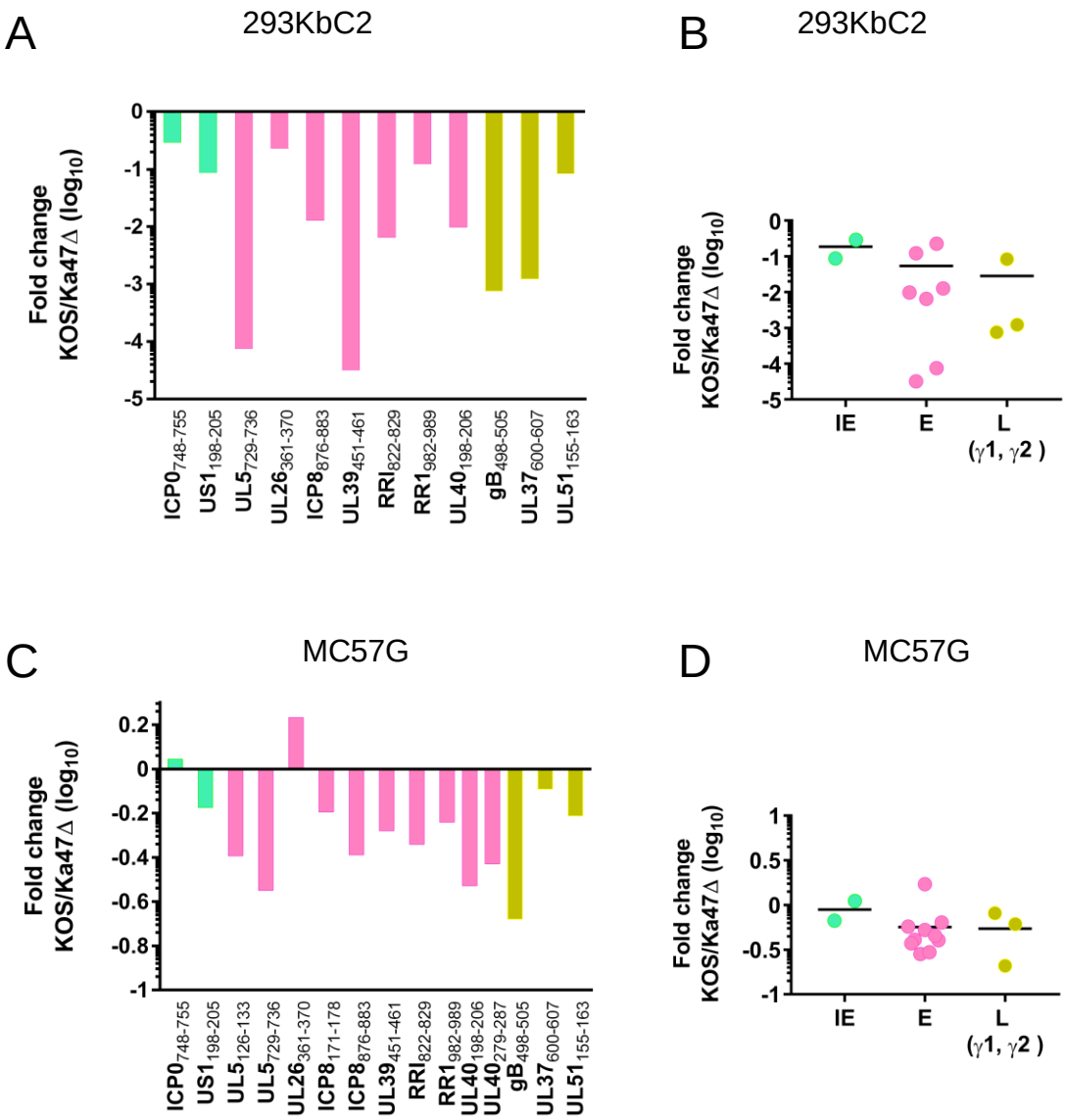

Figure 5.24 Impact of ICP47 on antigen presentation is not influenced by the expression kinetics of the source protein. Inhibition of presentation of K^b specific HSV-1 peptides is shown for 293KbC2 cells (A) and MC57G cells (C). The graph plotted shows the $\log_{10}$ ratio of the average copies/cell (n=3) in samples infected with HSV-1 KOS and in samples infected with HSV-1 Ka47Δ. Based on the expression of the source proteins, the peptides are classified as IE (green), E (pink) and L (yellow) class. Here, the genes expressed under early-late (γ1) and true-late (γ2) kinetics are grouped commonly as L. B & D shows the comparison of peptide inhibition among peptides from IE, E and L proteins. The differences between groups were not statistically significant based on the Kruskal-Wallis test by ranks and Dunn's multiple comparison tests.

5.3 Discussion

This chapter identified naturally presented HSV-1 peptides on infected MC57G cells using LC-MS/MS analysis. Seventy-five HSV-1 peptides were identified across six replicates of infected samples. This is the first report that lists the MHC I-bound peptides that are directly identified on HSV-1 infected cells. We tested forty-six MS identified HSV-1 peptides for $CD8^+$ T cell immunogenicity where, one-quarter of the peptides were found to be immunogenic, of which, 63% were newly discovered epitopes. For the remaining three-quarters of the peptides presented on infected cells, no response was detected. This finding is in concordance with recent MS based immunopeptidomics studies, which indicated that despite the presentation of diverse pathogen-derived peptides on infected cells, $CD8^+$ T cells recognise only a subset of these peptides during the *in vivo* infection (Johnson et al., 2009; Gilchuk et al., 2013; Ternette et al., 2016). However, Croft and colleagues found more than 80% of the VACV peptides identified by LC-MS/MS were immunogenic, which is substantially a large proportion of epitopes compared to HSV-1 epitopes identified in this study (Croft et al., In press). There are several possibilities that could explain the discordance between the current study and the VACV data. First, it is possible that not all peptides identified by the database search algorithm ProteinPilot™ software will be true (Kapp and Schütz, 2007). Manual validation of our peptide set by comparing the mass spectra of endogenous peptides with that of the synthetic peptides can be used to rule out the possibility of false peptide identification. Second, cross-presentation is considered as the major $CD8^+$ T cell-priming pathway during HSV-1 infection. While the peptide identification was performed using infected cells *in vitro*, these are unlikely to be a good model for a cross-presenting APC in mice. Finally, the detection limit of the ICS assay cannot be excluded from being responsible for the lack of immunogenic response to these peptides (Flesch et al., 2012). Nonetheless, this study has contributed to the finding of multiple novel immunogenic HSV-1 peptides in mice.

A distinctly larger repertoire of peptides was identified from mouse cells infected with Ka47Δ compared to the wild-type virus. These data support other findings that ICP47 inhibits mouse TAP and reduces peptide presentation (Chapter 3). However, the absolute quantification data, the limited peptide overlap amongst the replicates (see **Figure 5.3**) and the limited overlap with peptides detected by St Leger and colleagues (2011) suggest that the depth of sampling was a factor in peptide identification. For instance, some peptides

found exclusively in MC57G samples infected with just one virus, either wild-type virus or Ka47Δ, were detected in both sample types by the targeted MRM MS. Another observation is that two of the immunogenic peptides ($RR1_{982-989}$ & $ICP8_{876-883}$) discovered using a prediction algorithm by St Leger and colleagues (2011) but not found by our MS discovery run, were then detected using MRM MS in the MC57G samples. The LC-MS/MS method used for discovery was programmed such that if many peptides with similar m/z appear in an MS1 scan, then only the most abundant peptides are sampled and the less-abundant ones are often missed (Zhang et al., 2013). Further, a previously fragmented abundant peptide is excluded from repeated fragmentation for a specific time allowing identification of a broad range of sequences (Yates et al., 2009). Thus, the stochastic sampling of MS/MS presumably has lead to inconsistency in the identification of medium to low abundance peptides between replicates. This also explains why not all HSV-1 epitopes identified so far were detected by our method. By contrast, targeted MRM-MS focuses only on a small set of peptides with user-defined m/z values for precursor and fragment ions, which increases the reproducibility and sensitivity of detection. Therefore, a possible explanation for our observation is that the removal of ICP47 may have allowed the identification of some peptides, which might otherwise be presented below the detection limit of the current LC-MS/MS workflow. Therefore, the smaller peptide identifications in KOS-infected samples is likely to be due to the effect of ICP47 on the number of peptides transported by mouse TAP.

The major significance of this work lies in the provision of direct experimental evidence that demonstrates the highly efficient blockade of the human TAP by ICP47. Of the 14 peptides detected by MRM MS, eight peptides were significantly inhibited from presentation in 293KbC2 cells by ICP47. Notably, the immunodominant peptide $gB_{498-505}$ and the subdominant peptides $UL5_{729-736}$, $UL37_{600-607}$, $UL39_{451-461,}$ and $UL40_{198-206}$ are inhibited to below or close to the detection limit of the MRM-MS method, in all three replicates. Furthermore, all fourteen peptides were invariably detected at an average of fewer than 10 copies per cell in 293KbC2 cells infected by wild-type HSV-1 reflecting the effectiveness of ICP47 in blocking human TAP. The removal of ICP47 significantly improved the presentation of these peptides. This implies that the low copy number found in wild-type HSV-1 infected samples is due to the interference of TAP mediated translocation of peptides by ICP47 instead of 293KbC2 cells being inherently poor at

antigen presentation. To our knowledge, this is the first study to quantify the effect of a viral inhibitor of antigen presentation in human and mouse cells.

Even though the overall abundance of peptides was significantly improved in the absence of ICP47, in MC57G cells the peptide copy number was not as markedly diminished by ICP47 compared to 293KbC2 cells. For instance, $gB_{498-505}$ was inhibited by nearly 5-fold, but still presented at an abundance of about 350 copies on average per cell in the wild-type HSV-1 infected MC57G samples. In comparison, on 293KbC2 cells, $gB_{498-505}$ was presented at an average of about 0.6 copies/cell, when infected by wild-type virus and 770 copies/cell, when infected by ICP47 null mutant. This explains, in significant part, why the removal of ICP47 did not affect any of the parameters of HSV-1 infection in our mouse model (Chapter 3). However, this conclusion comes with the caveat that the copies of immunogenic peptides presented on HSV-1 infected mouse primary skin epithelial cells or neurons have not been analysed and whether ICP47 affects antigen presentation in these primary mouse cells remains to be tested. Although direct evidence is lacking, an earlier *in vivo* study using a flank infection model showed that $CD8^+$ T cells are sufficient to protect RAG-$1^{-/-}$ mice that lack both B cells and T cells from HSV-1 disease. Infection of RAG-$1^{-/-}$ mice with strain KOS resulted in neurological symptoms and death, whereas transfer of activated $gB_{498-505}$ specific $CD8^+$ T cells abolished virus replication in DRG and reduced the skin lesion to a rate similar to that of immunocompetent C57BL/6 mice (van Lint et al., 2004a). This indirect evidence shows that in mice, antigen presentation is not adequately inhibited by ICP47 and $CD8^+$ T cells can provide effective control of the virus.

With respect to a mechanistic explanation for the differences in ICP47's degree of inhibition, although human and mouse TAP are homologous with more than 80% sequence similarity (Yewdell et al., 1993), the amino acid residues that interact with ICP47 are not identical between the two species (Oldham et al., 2016b). A recent structural analysis shows that ICP47 interacts with the inner surface of TAP1 via amino acid residues of TMD4 and TAP2 interacts via TMD2, 3 and 6. While threonine (T) residue at position 425 of human TAP2 (TMD6) form close contact with phenylalanine and tyrosine residues at position 11 and 22 of ICP47 (Oldham et al., 2016b), substitution of this T425 residue by alanine was shown to reduce the inhibitory function of ICP47 (Galocha et al., 1997). In mouse TAP2, the polar residue asparagine (N) replaces threonine at position 425. Based on the finding by Galocha et al. (1997), this T425N substitution is believed to disrupt the

interaction between mouse TAP and ICP47 (Galocha et al., 1997; Oldham et al., 2016a). The mechanistic changes associated with this substitution on peptide translocation upon ICP47 binding are not known. However, our peptide quantification data suggests that it does not entirely eliminate the interaction between ICP47 and mouse TAP but may explain the degree to which ICP47 can diminish peptide translocation by TAP.

An unexpected finding from our data is that not every peptide was inhibited to the same extent. All quantified peptides were inhibited to less than 10 copies per 293KbC2 cell, however, some peptides were inhibited up to four-fold while others were inhibited over 100-fold. The differential inhibition across peptides did not appear to significantly correlate with the hydrophobicity of peptides, TAP binding affinity, peptide abundance, MHC I binding affinity or immunogenicity. There is evidence to suggest that peptides can use TAP-independent mechanisms for presentation on MHC I (Lautscham et al., 2003; Weinzierl et al., 2007; Tey and Khanna, 2012a; Vigneron et al., 2018). Our analysis showed that the less inhibited peptides were not derived from signal sequences for direct entry into the ER. In line with this, Weinzierl and colleagues (2008) showed that not all peptides presented independently of TAP are associated with a signal sequence. Additionally, some of these TAP-independent peptides have low predicted MHC I binding affinity. They reasoned that in case of low supply of peptides to ER due to TAP deficiency, MHC I molecules are less stringent in their peptide selection and presentation (Weinzierl et al., 2008). This might explain the lack of correlation between MHC I binding affinity and the level of inhibition observed in our study. Currently, the pathway by which the less inhibited peptides are transported to the ER for presentation is not known. It is also a possibility that these peptides are generated and loaded on MHC I in a vesicular compartment (Gromme et al., 1999; Tey and Khanna, 2012b; Vigneron et al., 2018). While cytotoxicity assays had suggested a complete shutdown of presentation by ICP47, our data demonstrate that when close to the limit of detection most peptides were still presented, albeit at extremely low levels.

In summary, using cutting-edge mass spectrometry techniques, we quantified the effect of ICP47 on antigen presentation in human and mouse cell lines. An initial peptide identification MS method allowed us to discover 75 HSV-1 peptides naturally presented on infected mouse fibroblast cells. A subset of the HSV-1 immunopeptidome derived from the newly discovered set in this study and those previously found by others was then

chosen for absolute quantification using MRM MS. Using MRM multiplexing analysis, we successfully quantified 15 and 14 peptides in HSV-1 infected MC57G and 293KbC2 cells, respectively. The peptide quantification study allowed us to make two major observations. First, ICP47 inhibits mouse TAP mediated antigen presentation by up to five-fold, supporting our previous data. Second, human TAP is severely impaired in transporting peptides for MHC I mediated presentation in the presence of ICP47. This study is the first to directly quantify the unprecedented blockade on antigen presentation caused by ICP47 during HSV-1 infection in human cells.

Chapter 6
Discussion

6 Discussion

HSV-1, like other herpes viruses, has evolved extensive mechanisms to subvert host defence mechanisms, including, but not limited to, the generation of numerous immune evasion proteins. The work outlined in this thesis focuses on one such protein, ICP47, the prototypic TAP inhibitor that blocks peptide transport into ER lumen and subsequent loading onto MHC I molecules in humans. However, outside the context of human cells, ICP47 has been shown to a) elicit no detectable inhibition of MHC I in mouse cell lines, b) no or low binding to mouse TAP and c) poor inhibition of peptides transport via mouse TAP in biochemical assays (Ahn et al., 1996; Tomazin et al., 1996; Jugovic et al., 1998; Tomazin et al., 1998). In stark contrast to these *in vitro* findings, *in vivo* studies using mouse models demonstrated a significant role for ICP47 in CNS infection (Goldsmith et al., 1998; Burgos et al., 2006). The authors suggested that ICP47 has the capacity to prevent the recognition of infected neurons by $CD8^+$ T cells; supported by the observation that infected mice develop lethal encephalitis as virus spreads to the CNS. These results raise concerns about the extrapolation of *in vitro* findings to *in vivo* situations. Furthermore, the discordance between these settings has remained unresolved for almost two decades, serving as a roadblock in understanding the importance of ICP47 during natural HSV infection.

Recent studies have indicated that ICP47 is expressed from as early as 1 to 8 hours post-infection both in a human embryonic lung fibroblast cell line and in primary mouse trigeminal neurons (Harkness et al., 2014). In another study, the ICP47 protein was found in abundance for as long as 15 hours after infection of human foreskin fibroblast cells (Kulej et al., 2017b). Besides its clear presence during acute infection, ICP47 transcripts were also found in a fraction of latently infected neurons (Ma et al., 2014), and a reporter gene driven by the ICP47 promoter expressed in a subset of latently infected neurons (Russell and Tscharke, 2016). These studies suggest that ICP47 might be relevant to other aspects of HSV-1 infection, for instance, latency and reactivation, in addition to its suspected role in infection of the CNS in mice. This prompted us to re-examine the functional significance of ICP47 with the overall aim of bridging the knowledge gap between the previous *in vitro* and *in vivo* studies.

Chapter 3 focused on this broad aim. A set of ICP47 null mutants and appropriate control viruses were constructed on the genetic background of HSV-1 strain KOS. Using these

new sets of viruses, we investigated the function of ICP47 in different stages of the HSV life cycle in mice. First, using a flow cytometry-based antigen presentation assay, we determined that ICP47 is functional in mouse cells, but inhibits peptide presentation significantly more efficiently in human cells. Despite this, ICP47 was shown not to affect *a)* viral replication in the skin and DRG during acute infection, *b)* the HSV-1-specific $CD8^+$ T cell response, *c)* the establishment of latency and maintenance of latency, *d)* the spread of the virus to distal DRG not directly innervating the infection site and *e)* the reactivation efficiency of the virus in mice. To further address the contradictory *in vitro* and *in vivo* data, the experiments discussed in Chapter 5 were performed. Here, we took a mass spectrometry approach to quantify HSV-1-derived peptides presented on infected human (293KbC2) and mouse (MC57G) cells. Using this approach, we found that ICP47 severely impairs antigen presentation in humans with detection of fewer than 10 molecules of most peptides. By contrast, on mouse cells, although significantly reduced, a considerable number of peptides were still presented in cells infected with ICP47 expressing virus. Immunological studies have previously suggested that $CD8^+$ T cells are highly sensitive, and, that at least under specific *in vitro* conditions, recognition of a few pMHC-I complexes is sufficient to trigger a response (Sykulev et al., 1996). Therefore, the modest effect of ICP47 on antigen presentation in mice may mean that the virus-specific $CD8^+$ T cells function effectively against infected cells similar to the condition in which there is no inhibitor present. This could explain the data from earlier *in vitro* studies as to why the HSV-1 infected mouse fibroblast cells were prone to specific lysis by $CD8^+$ T cells, while the human fibroblast cells were not killed (Jugovic et al., 1998). In accordance with these data, in our *in vivo* model, removal of ICP47 affected neither acute HSV-1 infection nor its latency. Thus, the data from this study clarifies the difference between the human and mouse cells with respect to $CD8^+$ T cell evasion at the molecular level. This study highlights need for a better model for understanding the consequence of immune evasion and antigen presentation during HSV-1 infection in humans.

Mouse models of HSV infection have provided important insight into the immunobiology of HSV diseases. Many of the phenomenon involving $CD8^+$ T cells observed in mouse models also occur in humans. For example, cross-presentation is established as the major pathway involved in the priming of $CD8^+$ T cells during HSV-1 infection of mice (Allan et al., 2003, 2006; Bedoui et al., 2009; Whitney et al., 2017). In accordance with this, emerging evidence suggests that similar phenomena may occur in humans whereby dermal DCs

uptake antigens from epidermal LCs, which serve as the source of epitopes for priming $CD8^+$ T cells (Bosnjak et al., 2005b; Kim et al., 2015). Both in the human cadaveric specimens and the mouse models, it was similarly found that HSV-specific $CD8^+$ T cells *a)* infiltrate the infected mucocutaneous site and ganglia (Koelle et al., 1994b; Liu et al., 1996; Koelle et al., 1998; Araki-Sasaki et al., 2006; Verjans et al., 2007; Zhu et al., 2007, 2013b; van Velzen et al., 2013a), *b)* establish a local effector memory population at the initial infection site (Zhu et al., 2013b; Zaid et al., 2014), *c)* reside in ganglia next to the neurons harbouring HSV-1 genome and *d)* have the capacity to suppress reactivation through the secretion of IFNγ and other non-cytolytic factors (Khanna et al., 2003a; Verjans et al., 2007). Thus, there is no doubt that mouse models are indispensable to HSV research and useful in untangling the intricacies of the immunological response to infection. However, our current study suggests that the evolutionary reason for the emergence of the $CD8^+$ T cell evasion molecule ICP47 cannot be possibly explored using the existing mouse models.

6.1 When does ICP47 function during HSV-1 infection in humans?

The co-evolution of HSV and humans for thousands of years has caused viral existence to depend on two main processes; firstly, infecting the host and establishing latency, and, subsequently, spreading to a new host. Immune evasion genes, such as ICP47, may help in both of these processes.

Based on animal model studies, it is well recognised that latency establishment occurs prior to mounting an adaptive immune response (Simmons and Nash, 1984; van Lint et al., 2004b; Wakim et al., 2008). However, clearance of infectious virus is correlated with the appearance of $CD8^+$ T cells at infection sites (Simmons and Tscharke, 1992; Koelle et al., 1998; Speck and Simmons, 1998; Coles et al., 2002; van Lint et al., 2004b; Dobbs et al., 2005). Perhaps, in humans, during acute HSV infection, ICP47 mediated $CD8^+$ T cell evasion may allow the virus to disseminate in the infected epithelial tissue and assist in the establishment of a larger latent pool of virus. Data from this thesis and previous *in vitro* studies suggests that it is not possible to test the above hypothesis using the current murine models due to the inefficient functioning of ICP47 (Ahn et al., 1996; Jugovic et al., 1998; Tomazin et al., 1996, 1998).

ICP47 may also drive transmission of HSV-1 through the human population by facilitating viral reactivation in latently infected ganglia. In humans that are seropositive for HSV-1 or

HSV-2 and in possession of an intact immune system, the virus spontaneously reactivates with frequent shedding episodes (Wald et al., 1997; Phipps et al., 2011; Tronstein et al., 2011; Ramchandani et al., 2016). The duration of the episode varies from a few hours to several days (Johnston and Corey, 2016). Likewise, there is a profound heterogeneity in the amount of virus found in epithelia between successive episodes (Wald et al., 1997, 2000). For instance, during HSV-2 reactivation episodes, infiltrates of $CD8^+$ T cells were found not only at sites of genital ulceration during recurrent genital herpes but also in intact epithelium during asymptomatic shedding (Zhu et al., 2007, 2013b). Schiffer and colleagues (2013) used mathematical modelling to analyse the influence of $CD8^+$ T cells in the complex episodic nature of HSV-2 reactivation. These models show that density and spatial distribution of $CD8^+$ T cells are factors which contribute to the differential containment of the reactivating virus, demonstrating that with high $CD8^+$ T cell density the incidence of genital ulceration is low (Schiffer and Corey, 2013; Schiffer et al., 2009, 2018). Such detailed studies have yet to be conducted for HSV-1, however, frequent oral shedding observed in seropositive individuals suggests that a similar immune landscape may exist during recurrent HSV-1 infections. These studies point to the functional significance of $CD8^+$ T cells in protection against recurrent disease. Furthermore, they imply that MHC I-mediated antigen presentation and recognition of infected cells occur at the level of mucosal epithelium. We speculate that ICP47 does not completely protect the infectious virus from elimination by $CD8^+$ T cells, it may increase the duration of shedding episodes, consequently increasing the chance of viral dissemination.

At the neuronal level, direct observations of reactivation in human ganglia are not possible due to lack of access to such tissues. However, frequent viral shedding in the genital tract or oral mucosa suggests that complete sets of viral proteins are synthesised in at least some neurons during latency, which subsequently lead to viral DNA replication, transport of virion components via axons and release of assembled virions at the peripheral site (Wald et al., 1997; Phipps et al., 2011; Tronstein et al., 2011; Ramchandani et al., 2016). Furthermore, permanent retention of activated HSV-1-specific effector memory $CD8^+$ T cells within the trigeminal ganglia reflected the frequent stimuli received from cognate pMHC-I complexes expressed on latently infected neurons (Verjans et al., 2007; van Velzen et al., 2013a). Despite substantial viral activity and presence of functional virus specific $CD8^+$ T cells in ganglia, these $CD8^+$ T cells appeared to be unable to entirely contain recurrent viral shedding. Results from chapter 5 provide a possible explanation for

this occurrence. Our results showed that ICP47 is able to block antigen presentation almost completely in human cells. Thus, if ICP47 is expressed even in a few neurons in which the virus attempts to reactivate, evasion of those neurons from $CD8^+$ T cell recognition can lead to virion production and emergence at the mucosal epithelium.

However, there appears to be a fine balance between reactivation and long-term persistence of the virus. A reactivation episode only lasts for a short time, from 2 to 12 hours in case of asymptomatic shedding and a few days for symptomatic shedding (Mark et al., 2008). One possible explanation for virus clearance during recurrent infection is that $CD8^+$ T cells recognise HSV-1 peptides presented via TAP-independent pathways. In Chapter 5, we found that although ICP47 blocks peptide presentation almost entirely in human cells, the level of inhibition was variable across peptides. This suggests that the peptides that are relatively less inhibited by ICP47 might use alternate peptide presentation pathways in addition to the TAP-mediated presentation pathway.

Two non-classical antigen presentation pathways have been described so far, both of which include transport via the trans-Golgi network and endosomal pathways. An endopeptidase furin, that is normally involved in the maturation of secreted proteins in trans-Golgi network (Thomas, 2002), is capable of generating peptides that can bind to MHC I (Gil-Torregrosa et al., 1998; Lu et al., 2004; Medina et al., 2009). Furin cleaves a protein or a polypeptide C-terminally to substrate recognition motifs Arg-X-X-Lys and Arg-X-Lys or Arg-Arg (Hosaka et al., 1991). While further trimming of the cleavage product by exopeptidases is necessary for loading on to MHC I (Gil-Torregrosa et al., 1998), currently little information is available on this process. Furthermore, TAP is essential for a functional conventional peptide-loading complex (Owen and Pease, 1999; Momburg and Tan, 2002), in which case how these peptides are loaded onto MHC I in this secretory-route is still unclear. Nevertheless, furin-mediated secretory antigen-processing pathways have been shown to co-exist with the conventional TAP-mediated pathway (Medina et al., 2009). The peptides can also be generated by the lytic proteases in vacuolar compartments, such as endosomes (Gromme et al., 1999). These peptides may encounter endosomally-located MHC I molecules recycled from the cell surface, which are subsequently assembled and transported to the cell surface for presentation to $CD8^+$ T cells. A melanoma vaccine epitope $pMEL_{209\text{-}217}$ was recently shown to be potentially presented via the endosomal pathway on TAP-deficient cells at levels recognised by $CD8^+$ T cells (Vigneron et al., 2018).

Similarly, the vacuolar pathway has been shown to mediate presentation of an endogenously derived epitope from HCMV protein UL138 (Tey and Khanna, 2012b). In addition to these pathways, peptides that associate with ER-targeting signal sequences (Anderson et al., 1991; Bacik et al., 1994) or that are highly hydrophobic in nature (Lautscham et al., 2003) can enter the ER without the assistance of TAP. These are loaded on to MHC I molecules by the conventional PLC.

Although alternate antigen presentation pathways exist, the lack of components dedicated to antigen processing and presentation in the vacuolar and secretory routes explain the rarity of these peptides. In concordance with this, peptides not affected by ICP47 have been shown to be presented at low abundances, irrespective of the presence of ICP47. Based on our data in Chapter 5, it is possible that TAP-independent HSV-1 peptides are generated in the human population. Particularly, several variants of human MHC I (HLA) show different levels of TAP dependency in humans. For example, peptide presentation by HLA-1 A2, -A23, -B7, -B8, -B35, -B57 and -B4405 molecules can load peptides independent of TAP (Henderson et al., 1992; Wei and Cresswell, 1992; Neisig et al., 1996; de la Salle et al., 1997; Geng et al., 2018). Whereas TAP is essential for loading of HLA-A1, -A3, -A11, -A24, -B15, -B27, and -B4402 (Grandea et al., 1995; de la Salle et al., 1997; Zernich, 2004; Thammavongsa et al., 2006; Hillen et al., 2008). Moreover, several TAP-independent self-peptides were identified in TAP-deficient cell lines using mass-spectrometric approaches (Weinzierl et al., 2008; Lorente et al., 2013). $CD8^+$ T cells may effectively control infection when there are a sufficient number of TAP-independent immunogenic peptides displayed on the infected cells. Therefore, identification of TAP-independent HSV-1 peptides in the human population that can elicit an immune response would help to understand if the host immune system has alternate ways to strike back and clear HSV-1 infection.

6.2 Does ICP47 block reactivation in mice?

For HSV to reactivate and emerge in peripheral tissues, there are several potential hurdles to overcome, including chromatin re-organisation of the latent episome, sufficient levels of gene expression, synthesis of viral proteins, DNA replication, transport of virion components via axons to nerve endings, assembly and release of virus particles to the periphery, and infection of epithelial cells. However, in mice, low levels of lytic mRNA can be detected in neurons harbouring the latent HSV-1 genome (Deatly et al., 1987; Gordon

et al., 1988; Kramer and Coen, 1995; Maillet et al., 2006; Ma et al., 2014). Curiously, this is accompanied by the detection of viral proteins in neurons during latency (Feldman et al., 2002b). Collectively, these studies suggest that in mice, the virus is capable of overcoming some of the early hurdles of reactivation, yet unable to generate infectious virion particles. It could potentially be due to the biphasic nature of HSV-1 reactivation (Kim et al., 2012a). Reactivation begins with the transient reversal of gene silencing and simultaneous transcription of genes from all three kinetic classes. VP16, synthesised during phase I, is believed to elevate the lytic transcript levels in phase II, leading to reactivation of the virus (Kim et al., 2012a). It is possible that the presentation of viral antigens, via MHC I molecules, occurs at phase I, and leaves cells exposed to $CD8^+$ T cell detection. At least two potential mechanisms have been described that are employed by $CD8^+$ T cells to curtail reactivation in the early phase. Firstly, IFNγ was shown to dampen the transcription of lytic genes and reduce early viral replication (Liu et al., 1996, 2001; Decman et al., 2005). Secondly, granzyme B, released by $CD8^+$ T cells, promotes degradation of ICP4, which is a transcriptional trans-activator of early and late genes (Knickelbein et al., 2008). This may explain, at least in part, why infectious virus is seldom observed in mice after the establishment of latency.

In our mouse model, a similar efficiency of reactivation between wild-type HSV-1 and ICP47 null virus was observed. In contrast, upon incorporation of genes, MCMV m152 or HCMV US11, encoding potent inhibitors of antigen presentation into HSV-1, there was enhanced capacity for reactivation upon UV exposure of the latently-infected mice (Orr et al., 2007). Together these results support the idea that in mice, reactivation of the wild-type virus is impeded at an early stage, due to the incomplete functioning of ICP47. Conceivably, in humans ICP47-mediated blocking of antigen presentation allows the virus to evade detection, thus providing the opportunity for subsequent reactivation. Previous *in vitro* studies demonstrated that ICP47 is less effective in blocking rabbit TAP (Jugovic et al., 1998). However, in experimentally infected rabbits spontaneous reactivation and peripheral shedding is frequent (Laibson and Kibrick, 1969; Berman and Hill, 1985; Hill et al., 1986, 1987, 1997, 2012). This suggests that there are other factors, viral or host, which may also contribute to reactivation.

6.3 Alternate models for evaluating the function of ICP47

Searching for an alternate *in vivo* model in which ICP47 is fully functional is necessary to better understand the host-viral interaction with respect to $CD8^+$ T cell immunity. The study by Jugovic et al. (1998) showed that the fibroblast cells from pigs, dogs or non-human primates, such as owl monkeys and chimpanzees, were resistant to lysis by virus-specific $CD8^+$ T cells after infection with HSV-1. While they may be suitable animal models for investigating how ICP47 influences HSV infection, they have not been explored extensively in HSV research and possess a number of ethical and practical pitfalls. Another potential candidate, Rhesus Macaques, could be useful in the HSV context, as they are already used for studying genital herpes and manifest clinical symptoms similar to humans (Crostarosa et al., 2009; Fan et al., 2017). However, the availability of such animal resources and the associated technical difficulties limit their use. An immortalised cell line HD10.6 derived from human dorsal root ganglia was recently established as an *in vitro* model for HSV-1 latency and reactivation (Raymon et al., 1999; Thellman et al., 2017). Such *in vitro* models could potentially be useful to elucidate the function of ICP47 during latency and reactivation. However, as this simplified cell culture system lacks essential immunological components and the supporting environment of an intact ganglion, the physiological relevance of the results derived would still require *in vivo* validation.

Mouse models can be enlightening due to extensive information provided on host-virus interactions and the current wealth of tools available for dissecting the mouse immune response. However, the effect of ICP47 on the function of human TAP is far more profound compared to mouse TAP. Previously, it has been shown that ICP47 interacts only with TAP (Hill et al., 1995). TAP1 and TAP2 can be substituted interchangeably between mice and humans without the loss of function of these proteins (Yewdell et al., 1993; Seliger et al., 1998; Ritz et al., 2001). Thus, differences observed in ICP47 functioning between mice and humans are likely due to sequence discrepancies in TAP1 and TAP2 protein sequences, which share a homology of 74% and 84%, respectively, between the two species. Therefore, a genetically humanised mouse model, where the mouse TAP1/2 is functionally replaced by human TAP1/2 would be ideal to study the impact of ICP47 during the acute infection, latency and reactivation. Such a model is currently being generated in our laboratory (Tscharke et al., Unpublished). Future experiments can focus

on defining the outcome of ICP47 and human TAP interaction using the recombinant viruses generated in the current study and the humanised TAP mice.

The efficiency of inhibition of antigen presentation by ICP47 could be determined by infection of primary fibroblasts derived from the humanised TAP mice and quantifying HSV-1 derived peptides using mass spectrometry. If the human TAP in these transgenic mice functions as expected, the efficiency of TAP inhibition by ICP47 should be similar to that seen in the results observed in chapter 5 for 293KbC2 cells. Humanised TAP mice could also be used as a robust model to determine the effect of ICP47 on HSV-1 pathogenesis. If ICP47 blocks the visibility of infected cells from $CD8^+$ T cells during acute infection, it might be reflected as a delay in resolution of lesion induced by flank infection or perhaps, as a delay in clearance of infectious virus in appropriate tissues or both. Further, in this model the contribution of ICP47 in the establishment of latency can be determined by quantifying the latent genome load. Humanised TAP mice could potentially be used to determine the role of $CD8^+$ T cells in blocking HSV-1 reactivation. This could be accomplished by measuring infectious virus in *ex vivo* cultured DRG isolated from latently infected mice or by using *in vivo* reactivation methods described by others. Humanised TAP mice crossed on to the ROSA26R mice would allow detection of even subtle differences in the ability of HSV-1 (expressing Cre recombinase) to spread and express genes when it is able to block TAP expression with the same efficiency as in human cells. Furthermore, transgenic humanised mice in possession of human HLA molecules have already been generated by others (Kievits et al., 1987; Ureta-Vidal et al., 1999; Cheuk et al., 2002) and are beginning to contribute to HSV research (Dervillez et al., 2013; Srivastava et al., 2015). Therefore, a mouse model that expresses human TAP in addition to various HLA I alleles could enable the discovery of novel TAP-independent epitopes, and providing a more faithful preclinical environment to investigate new therapeutics.

6.4 Redundancy in immune system

The evolutionary significance of various herpesvirus immunomodulatory proteins has been extensively explored, however, no definitive *in vivo* function has been assigned to many of those that interfere with antigen presentation (Yewdell et al., 1993; Verweij et al., 2015). Lack of suitable *in vivo* models is often responsible for this impediment. One exception to this is MCMV, which has the advantage of being studied in its natural host. MCMV encodes three proteins that interfere with different stages of antigen processing and

presentation, causing a significant down-modulation of surface MHC I *in vitro* (Pinto and Hill, 2005). However, in mouse models, deletion of all three immune evasion genes from MCMV did not have a biologically significant impact on viral fitness (Gold et al., 2004). This observation supplements data from patients who have defective antigen presentation pathways. For instance, humans with defects in TAP1, TAP2 or both, develop normal levels of functional $CD4^+$ T cells, but have significantly less surface MHC I and reduced numbers of $CD8^+$ T cells (Donato et al., 1995; de la Salle et al., 1994, 1999, 2002; Johnston and Corey, 2016; Law-Ping-Man et al., 2018). Furthermore, in TAP-deficient individuals the number of γδ T cells was enhanced, whilst levels of B cells, NK cells and NKT cells were comparable to individuals with functional TAP (Moins-Teisserenc et al., 1999; Gadola et al., 2000). TAP-deficient patients often develop recurrent bacterial lung infections leading to a condition known as bronchiectasis. Another manifestation of TAP deficiency is the development of skin ulcers on the face, arms and legs. However, TAP-deficient patients can fight viral infections as efficiently as healthy individuals (de la Salle et al., 1994; Donato et al., 1995; Moins-Teisserenc et al., 1999; Law-Ping-Man et al., 2018). The data suggest it is possible that other immune cells contribute to protection against viral infections. A previous report by de la Salle and colleagues (1997) showed that in TAP-deficient patients, $CD8^+$ T cells, although present in low numbers, retain a broad repertoire of TCRs. This observation was further supported by the discovery of EBV-specific $CD8^+$ T cells in TAP-deficient patients and EBV-specific TAP-independent epitopes throughout the human population (de la Salle et al., 1997; Lautscham et al., 2001, 2003). Collectively, these observations suggest that the redundant function of other immune cells, TAP-independent antigen presentation and the function of residual $CD8^+$ T cells may provide effective anti-viral immunity in humans with defective TAP. Thus, in other populations, where the immune system is intact, ICP47 may not have a significant biological impact due to the redundant immune cell function. However, ICP47 might significantly enhance the virulence in immunocompromised individuals. It might also increase shedding and therefore transmission in a manner that is subclinical, as noted above, providing selective pressure to keep this gene in the HSV genome.

6.5 Location in HSV-1 genome plays a major role in gene expression

In Chapter 3, by focussing on the impact of ICP47 expression during latency using the ROSA26R/Cre reporter mouse system, we uncovered that the activity of the ICP47 promoter *in vivo* was strikingly different in its native location compared to an ectopic location. We probed this further in Chapter 4 by generating new recombinant viruses. The results from these chapters collectively showed that the activity of an HSV-1 lytic promoter is different at different locations and gene expression depends on the type of promoter and the genomic position.

The phenomenon by which the local genomic region influences the expression of the inserted gene is called "position effect". It has been described in various organisms from yeast to humans, and diverse mechanisms have been demonstrated to cause this effect (Baker, 1968; Kleinjan and van Heyningen, 1998, 2005; De and Babu, 2010). This includes, but is not limited to, the loss or gain of essential *cis*-regulatory elements, juxtaposition of the gene with an enhancer element of another gene, chromatin architecture, epigenetic regulation, post-translational modification of histones or association of non-histone proteins, such as polycomb group proteins (Kleinjan and van Heyningen, 2005; De and Babu, 2010; Tchasovnikarova et al., 2015; Kellum and Schedl, 1991). Akhtar and colleagues developed a high throughput method for parallel monitoring of reporters inserted at different locations of the mouse genome. The study demonstrated that an enhancer has the potential to influence gene expression with an average distance of 20 Kbp. In addition, at distinct genomic locations, gene expression can differ by 1000 fold (Akhtar et al., 2013). In a similar high throughput study, latent HIV genomes were found to integrate further away from enhancers in host genome compared to the non-latent HIV genomes, which highlights the chromosomal context for the regulation of HIV latency (Chen et al., 2017). Position dependent gene expression has been found even in simple prokaryotic genomes, such as bacteria and fungi (Zhao and Peeters, 2003; Bryant et al., 2014; Sauer et al., 2016; Bilyk et al., 2017). Although this phenomenon has not yet been explicitly investigated in HSV-1, it has been described in other viruses such as coronavirus, hepatitis C virus and vaccinia virus (Coupar et al., 2000; Haan et al., 2003; Jopling et al., 2008). Typically, the HSV genome exists in the host nucleus as an autonomous circular episome (Strang and Stow, 2005). Previous studies have found that during the active lytic state, nucleosome deposition preferentially occurred at specific sites in the HSV-1 genome (Kent et al., 2004;

Lacasse and Schang, 2010; Oh et al., 2015). However, in neurons, the latent HSV-1 genome is associated with regularly spaced nucleosomes and utilises host epigenetic repression to restrict viral gene expression (Efstathiou et al., 1986b; Mellerick and Fraser', 1987; Deshmane and Fraser, 1989). Other than viral factors, the regulatory mechanisms that influence the expression of host genes are also applicable to HSV-1. Hence, it is plausible that the location dependent gene expression that we observed in our study is due to the position effect. A thorough genome-wide analysis of gene expression at various loci during lytic and latent infection is necessary to draw a definitive conclusion.

6.6 Conclusion

Most experimental models are not without inadequacies or unexpected features. ICP47 in this thesis highlights two specific shortcomings: a) species-specific effects on viral genes and b) position-specific effects on viral gene expression. The work presented in this thesis showed that ICP47 is not an effective immunomodulator in a mouse model where HSV is confined to the peripheral nervous system. This may be attributed to an insufficient blockade of mouse TAP as compared to the human equivalent. Further, the data presented here demonstrated that the same gene expressed from different loci within the HSV-1 genome had significant effect of insertion site and suggest that the local genomic context is critical for HSV-1 gene expression. Due to these features, we suggest future models attempt to more faithfully recapitulate ICP47-mediated HSV-1 pathogenesis in humans. Overall, these limitations can be considered hurdles to research, but alternatively as opportunity for deeper understanding of virus biology.

References

Abbas, A.K., Murphy, K.M., and Sher, A. (1996). Functional diversity of helper T lymphocytes. Nature *383*, 787–793.

Ace, C.I., McKee, T.A., Ryan, J.M., Cameron, J.M., and Preston, C.M. (1989). Construction and characterization of a herpes simplex virus type 1 mutant unable to transinduce immediate-early gene expression. J. Virol. *63*, 2260–2269.

Ackerman, A.L., Kyritsis, C., Tampe, R., and Cresswell, P. (2003). Early phagosomes in dendritic cells form a cellular compartment sufficient for cross presentation of exogenous antigens. Proc. Natl. Acad. Sci. *100*, 12889–12894.

Ahier, A., and Jarriault, S. (2014). Simultaneous expression of multiple proteins under a single promoter in Caenorhabditis elegans via a versatile 2A-based toolkit. Genetics *196*, 605–613.

Ahmad, A., Sharif-Askari, E., Fawaz, L., and Menezes, J. (2000). Innate immune response of the human host to exposure with herpes simplex virus type 1: In vitro control of the virus infection by enhanced natural killer activity via interleukin-15 induction. J. Virol. *74*, 7196–7203.

Ahmed, R., and Gray, D. (1996). Immunological memory and protective immunity: understanding their relation. Science *272*, 54–60.

Ahmed, M., Lock, M., Miller, C.G., and Fraser, N.W. (2002). Regions of the herpes simplex virus type 1 latency-associated transcript that protect cells from apoptosis in vitro and protect neuronal cells in vivo. J. Virol. *76*, 717–729.

Ahn, K., Meyer, T.H., Uebel, S., Sempé, P., Djaballah, H., Yang, Y., Peterson, P.A., Früh, K., and Tampé, R. (1996). Molecular mechanism and species specificity of TAP inhibition by herpes simplex virus ICP47. EMBO J. *15*, 3247–3255.

Ahn, K., Gruhler, A., Galocha, B., Jones, T.R., Wiertz, E.J.H.J., Ploegh, H.L., Peterson, P.A., Yang, Y., and Früh, K. (1997). The ER-luminal domain of the HCMV glycoprotein US6 inhibits peptide translocation by TAP. Immunity *6*, 613–621.

Aisenbrey, C., Sizun, C., Koch, J., Herget, M., Abele, R., Bechinger, B., and Tampé, R. (2006). Structure and dynamics of membrane-associated ICP47, a viral Inhibitor of the MHC I antigen-processing machinery. J. Biol. Chem. *281*, 30365–30372.

Akhtar, W., de Jong, J., Pindyurin, A.V., Pagie, L., Meuleman, W., de Ridder, J., Berns, A., Wessels, L.F.A., van Lohuizen, M., and van Steensel, B. (2013). Chromatin position effects assayed by thousands of reporters integrated in parallel. Cell *154*, 914–927.

Allan, R.S., Smith, C.M., Belz, G.T., Lint, A.L. van, Wakim, L.M., Heath, W.R., and Carbone, F.R. (2003). Epidermal viral immunity induced by CD8α+ dendritic cells but not by langerhans cells. Science *301*, 1925–1928.

Allan, R.S., Waithman, J., Bedoui, S., Jones, C.M., Villadangos, J.A., Zhan, Y., Lew, A.M., Shortman, K., Heath, W.R., and Carbone, F.R. (2006). Migratory dendritic cells transfer

antigen to a lymph node-resident dendritic cell population for efficient CTL priming. Immunity *25*, 153–162.

Amelio, A.L., McAnany, P.K., and Bloom, D.C. (2006). A chromatin insulator-like element in the herpes simplex virus type 1 latency-associated transcript region binds CCCTC-binding factor and displays enhancer-blocking and silencing activities. J. Virol. *80*, 2358–2368.

Anderson, B.J. (2003). The epidemiology and clinical analysis of several outbreaks of herpes gladiatorum. Med. Sci. Sports Exerc. *35*, 1809–1814.

Anderson, K., Cresswell, P., Gammon, M., Hermes, J., Williamson, A., and Zweerink, H. (1991). Endogenously synthesized peptide with an endoplasmic reticulum signal sequence sensitizes antigen processing mutant cells to class I-restricted cell-mediated lysis. J. Exp. Med. *174*, 489–492.

von Andrian, U.H., and Mackay, C.R. (2000). T-Cell Function and Migration — Two Sides of the Same Coin. N. Engl. J. Med. *343*, 1020–1034.

Anikeeva, N., Somersalo, K., Sims, T.N., Thomas, V.K., Dustin, M.L., and Sykulev, Y. (2005). Distinct role of lymphocyte function-associated antigen-1 in mediating effective cytolytic activity by cytotoxic T lymphocytes. Proc. Natl. Acad. Sci. U. S. A. *102*, 6437–6442.

Apcher, S., Daskalogianni, C., Lejeune, F., Manoury, B., Imhoos, G., Heslop, L., and Fahraeus, R. (2011). Major source of antigenic peptides for the MHC class I pathway is produced during the pioneer round of mRNA translation. Proc. Natl. Acad. Sci. *108*, 11572–11577.

Araki-Sasaki, K., Tanaka, T., Ebisuno, Y., Kanda, H., Umemoto, E., Hayashi, K., and Miyasaka, M. (2006). Dynamic expression of chemokines and the infiltration of inflammatory cells in the HSV-infected cornea and its associated tissues. Ocul. Immunol. Inflamm. *14*, 257–266.

Arbusow, V., Derfuss, T., Held, K., Himmelein, S., Strupp, M., Gurkov, R., Brandt, T., and Theil, D. (2010). Latency of herpes simplex virus type-1 in human geniculate and vestibular ganglia is associated with infiltration of CD8+ T cells. J. Med. Virol. *82*, 1917–1920.

Ariotti, S., Beltman, J.B., Chodaczek, G., Hoekstra, M.E., van Beek, A.E., Gomez-Eerland, R., Ritsma, L., van Rheenen, J., Maree, A.F.M., Zal, T., et al. (2012). Tissue-resident memory CD8+ T cells continuously patrol skin epithelia to quickly recognize local antigen. Proc. Natl. Acad. Sci. *109*, 19739–19744.

Ariotti, S., Hogenbirk, M.A., Dijkgraaf, F.E., Visser, L.L., Hoekstra, M.E., Song, J.-Y., Jacobs, H., Haanen, J.B., and Schumacher, T.N. (2014). Skin-resident memory CD8+ T cells trigger a state of tissue-wide pathogen alert. Science *346*, 101–105.

Arthur, J.L., Scarpini, C.G., Connor, V., Lachmann, R.H., Tolkovsky, A.M., and Efstathiou, S. (2001). Herpes simplex virus type 1 promoter activity during latency establishment, maintenance, and reactivation in primary dorsal root neurons in vitro. J. Virol. *75*, 3885–3895.

Asano, M., Toda, M., Sakaguchi, N., and Sakaguchi, S. (1996). Autoimmune disease as a consequence of developmental abnormality of a T cell subpopulation. J. Exp. Med. *184*, 387–396.

Assarsson, E., Sidney, J., Oseroff, C., Pasquetto, V., Bui, H.-H., Frahm, N., Brander, C., Peters, B., Grey, H., and Sette, A. (2007). A quantitative analysis of the variables affecting the repertoire of T cell specificities recognized after vaccinia virus infection. J. Immunol. Baltim. Md 1950 *178*, 7890–7901.

Aye, M.M., Kasai, T., Tashiro, Y., Xing, H.Q., Shirahama, H., Mitsuda, M., Suetsugu, T., Tanaka, K., Osame, M., and Izumo, S. (2009). CD8 positive T-cell infiltration in the dentate nucleus of paraneoplastic cerebellar degeneration. J. Neuroimmunol. *208*, 136–140.

Babbe, H., Roers, A., Waisman, A., Lassmann, H., Goebels, N., Hohlfeld, R., Friese, M., Schröder, R., Deckert, M., Schmidt, S., et al. (2000). Clonal expansions of CD8(+) T cells dominate the T cell infiltrate in active multiple sclerosis lesions as shown by micromanipulation and single cell polymerase chain reaction. J. Exp. Med. *192*, 393–404.

Babbitt, B.P., Allen, P.M., Matsueda, G., Haber, E., and Unanue, E.R. (2005). Binding of immunogenic peptides to Ia histocompatibility molecules. 1985. J. Immunol. Baltim. Md 1950 *175*, 4163–4165.

Babu, J.S., Thomas, J., Kanangat, S., Morrison, L.A., Knipe, D.M., and Rouse, B.T. (1996). Viral replication is required for induction of ocular immunopathology by herpes simplex virus. J. Virol. *70*, 101–107.

Bacik, I., Cox, J.H., Anderson, R., Yewdell, J.W., and Bennink, J.R. (1994). TAP (transporter associated with antigen processing)-independent presentation of endogenously synthesized peptides is enhanced by endoplasmic reticulum insertion sequences located at the amino- but not carboxyl-terminus of the peptide. J. Immunol. Baltim. Md 1950 *152*, 381–387.

Baines, J.D., and Roizman, B. (1991). The open reading frames UL3, UL4, UL10, and UL16 are dispensable for the replication of herpes simplex virus 1 in cell culture. J. Virol. *65*, 938–944.

Baker, W.K. (1968). Position-effect variegation. Adv. Genet. *14*, 133–169.

Balliet, J.W., Kushnir, A.S., and Schaffer, P.A. (2007). Construction and characterization of a herpes simplex virus type I recombinant expressing green fluorescent protein: Acute phase replication and reactivation in mice. Virology *361*, 372–383.

Banchereau, J., and Steinman, R.M. (1998). Dendritic cells and the control of immunity. Nature *392*, 245.

Barbosa, J.A., Santos-Aguado, J., Mentzer, S.J., Strominger, J.L., Burakoff, S.J., and Biro, P.A. (1987). Site-directed mutagenesis of class I HLA genes. Role of glycosylation in surface expression and functional recognition. J. Exp. Med. *166*, 1329–1350.

Barker, C.F., and Billingham, R.E. (1977). Immunologically privileged sites. Adv. Immunol. *25*, 1–54.

Barklie, C.J., Watson, R.J., and Wilkie, N.M. (1977). Temporal regulation of herpes simplex virus type 1 transcription: location of transcripts on the viral genome. Cell *12*, 275–285.

Barry, M., and Bleackley, R.C. (2002). Cytotoxic T lymphocytes: all roads lead to death. Nat. Rev. Immunol. *2*, 401–409.

Bassani-Sternberg, M., Pletscher-Frankild, S., Jensen, L.J., and Mann, M. (2015). Mass spectrometry of human leukocyte antigen class I peptidomes reveals strong effects of protein abundance and turnover on antigen presentation. Mol. Cell. Proteomics MCP *14*, 658–673.

Basta, S., and Alatery, A. (2007). The cross-priming pathway: a portrait of an intricate immune system. Scand. J. Immunol. *65*, 311–319.

Batterson, W., and Roizman, B. (1983). Characterization of the herpes simplex virion-associated factor responsible for the induction of alpha genes. J. Virol. *46*, 371–377.

Becker, T.M., Kodsi, R., Bailey, P., Lee, F., Levandowski, R., and Nahmias, A.J. (1988). Grappling with herpes: herpes gladiatorum. Am. J. Sports Med. *16*, 665–669.

Beckmann, A.M., and Wilce, P.A. (1997). Egr transcription factors in the nervous system. Neurochem. Int. *31*, 477–510.

Bedadala, G., Chen, F., Figliozzi, R., Balish, M., and Hsia, V. (2014). Construction and characterization of recombinant HSV-1 expressing Early Growth Response-1. ISRN Virol. *2014*, 1–7.

Bedadala, G.R., Pinnoji, R.C., and Hsia, S.-C.V. (2007). Early Growth Response gene 1 (Egr-1) regulates HSV-1 ICP4 and ICP22 gene expression. Cell Res. *17*, 546–555.

Bedadala, G.R., Palem, J.R., Graham, L., Hill, J.M., McFerrin, H.E., and Hsia, S.-C. (2011). Lytic HSV-1 infection induces the multifunctional transcription factor Early Growth Response-1 (EGR-1) in rabbit corneal cells. Virol. J. *8*, 262.

Bedoui, S., Whitney, P.G., Waithman, J., Eidsmo, L., Wakim, L., Caminschi, I., Allan, R.S., Wojtasiak, M., Shortman, K., Carbone, F.R., et al. (2009). Cross-presentation of viral and self antigens by skin-derived $CD103^+$ dendritic cells. Nat. Immunol. *10*, 488.

Beinert, D., Neumann, L., Uebel, S., and Tampé, R. (1997). Structure of the Viral TAP-Inhibitor ICP47 Induced by Membrane Association. Biochemistry *36*, 4694–4700.

Beland, J.L., Sobel, R.A., Adler, H., Del-Pan, N.C., and Rimm, I.J. (1999). B cell-deficient mice have increased susceptibility to HSV-1 encephalomyelitis and mortality. J. Neuroimmunol. *94*, 122–126.

Benencia, F., and Courreges, M.C. (1999). Nitric oxide and macrophage antiviral extrinsic activity. Immunology *98*, 363–370.

Beninga, J., Rock, K.L., and Goldberg, A.L. (1998). Interferon-gamma can stimulate post-proteasomal trimming of the N terminus of an antigenic peptide by inducing leucine aminopeptidase. J. Biol. Chem. *273*, 18734–18742.

Bennett, D.L., Michael, G.J., Ramachandran, N., Munson, J.B., Averill, S., Yan, Q., McMahon, S.B., and Priestley, J.V. (1998). A distinct subgroup of small DRG cells express GDNF receptor components and GDNF is protective for these neurons after nerve injury. J. Neurosci. Off. J. Soc. Neurosci. *18*, 3059–3072.

Berger, C., Xuereb, S., Johnson, D.C., Watanabe, K.S., Kiem, H.-P., Greenberg, P.D., and Riddell, S.R. (2000). Expression of herpes simplex virus ICP47 and human cytomegalovirus us11 prevents recognition of transgene products by CD8+ cytotoxic T lymphocytes. J. Virol. *74*, 4465–4473.

Bergström, T., Alestig, K., Svennerholm, B., Horal, P., Sköldenberg, B., and Vahlne, A. (1990). Neurovirulence of herpes simplex virus types 1 and 2 isolates in diseases of the central nervous system. Eur. J. Clin. Microbiol. Infect. Dis. *9*, 751–757.

Berman, E.J., and Hill, J.M. (1985). Spontaneous ocular shedding of HSV-1 in latently infected rabbits. Invest. Ophthalmol. Vis. Sci. *26*, 587–590.

Berthomme, H., Lokensgard, J., Yang, L., Margolis, T., and Feldman, L.T. (2000). Evidence for a bidirectional element located downstream from the herpes simplex virus type 1 latency-associated promoter that increases its activity during latency. J. Virol. *74*, 3613–3622.

Bertke, A.S., Swanson, S.M., Chen, J., Imai, Y., Kinchington, P.R., and Margolis, T.P. (2011). A5-positive primary sensory neurons are nonpermissive for productive infection with herpes simplex virus 1 in vitro. J. Virol. *85*, 6669–6677.

Bevan, M.J. (1977). In a radiation chimaera, host H-2 antigens determine immune responsiveness of donor cytotoxic cells. Nature *269*, 417–418.

Bilyk, B., Horbal, L., and Luzhetskyy, A. (2017). Chromosomal position effect influences the heterologous expression of genes and biosynthetic gene clusters in Streptomyces albus J1074. Microb. Cell Factories *16*.

Biron, C.A. (1997). Activation and function of natural killer cell responses during viral infections. Curr. Opin. Immunol. *9*, 24–34.

Biron, C.A., Sonnenfeld, G., and Welsh, R.M. (1984). Interferon induces natural killer cell blastogenesis in vivo. J. Leukoc. Biol. *35*, 31–37.

Biron, C.A., Byron, K.S., and Sullivan, J.L. (1989). Severe herpesvirus infections in an adolescent without natural killer cells. N. Engl. J. Med. *320*, 1731–1735.

Blees, A., Januliene, D., Hofmann, T., Koller, N., Schmidt, C., Trowitzsch, S., Moeller, A., and Tampé, R. (2017). Structure of the human MHC-I peptide-loading complex. Nature.

Bloom, D.C. (2004). HSV LAT AND NEURONAL SURVIVAL. Int. Rev. Immunol. *23*, 187–198.

Blum, J.S., Wearsch, P.A., and Cresswell, P. (2013). Pathways of antigen processing. Annu. Rev. Immunol. *31*, 443–473.

Blyth, W.A., Hill, T.J., Field, H.J., and Harbour, D.A. (1976). Reactivation of herpes simplex virus infection by ultraviolet light and possible involvement of prostaglandins. J. Gen. Virol. *33*, 547–550.

Blyth, W.A., Harbour, D.A., and Hill, T.J. (1984). Pathogenesis of zosteriform spread of herpes simplex virus in the mouse. J. Gen. Virol. *65*, 1477–1486.

Bolovan, C.A., Sawtell, N.M., and Thompson, R.L. (1994). ICP34.5 mutants of herpes simplex virus type 1 strain 17syn+ are attenuated for neurovirulence in mice and for replication in confluent primary mouse embryo cell cultures. J. Virol. *68*, 48–55.

Bosnjak, L., Miranda-Saksena, M., Koelle, D.M., Boadle, R.A., Jones, C.A., and Cunningham, A.L. (2005a). Herpes simplex virus infection of human dendritic cells induces apoptosis and allows cross-presentation via uninfected dendritic cells. J. Immunol. *174*, 2220–2227.

Bosnjak, L., Miranda-Saksena, M., Koelle, D.M., Boadle, R.A., Jones, C.A., and Cunningham, A.L. (2005b). Herpes simplex virus infection of human dendritic cells induces apoptosis and allows cross-presentation via uninfected dendritic cells. J. Immunol. *174*, 2220–2227.

Boucher, A., Herrmann, J.L., Morand, P., Buzelé, R., Crabol, Y., Stahl, J.P., and Mailles, A. (2017). Epidemiology of infectious encephalitis causes in 2016. Médecine Mal. Infect. *47*, 221–235.

Bowen, C.D., Renner, D.W., Shreve, J.T., Tafuri, Y., Payne, K.M., Dix, R.D., Kinchington, P.R., Gatherer, D., and Szpara, M.L. (2016). Viral forensic genomics reveals the relatedness of classic herpes simplex virus strains KOS, KOS63, and KOS79. Virology *492*, 179–186.

Brady, R.C., and Bernstein, D.I. (2004). Treatment of herpes simplex virus infections. Antiviral Res. *61*, 73–81.

Branco, F.J., and Fraser, N.W. (2005). Herpes simplex virus type 1 latency-associated transcript expression protects trigeminal ganglion neurons from apoptosis. J. Virol. *79*, 9019–9025.

Bravo, F.J., Bourne, N., Harrison, C.J., Mani, C., Stanberry, L.R., Myers, M.G., and Bernstein, D.I. (1996). Effect of antibody alone and combined with acyclovir on neonatal herpes simplex virus infection in guinea pigs. J. Infect. Dis. *173*, 1–6.

Breitfeld, D., Ohl, L., Kremmer, E., Ellwart, J., Sallusto, F., Lipp, M., and Förster, R. (2000). Follicular B helper T cells express CXC chemokine receptor 5, localize to B cell follicles, and support immunoglobulin production. J. Exp. Med. *192*, 1545–1552.

Brown, Z.A., Benedetti, J., Ashley, R., Burchett, S., Selke, S., Berry, S., Vontver, L.A., and Corey, L. (1991). Neonatal herpes simplex virus infection in relation to asymptomatic maternal infection at the time of labor. N. Engl. J. Med. *324*, 1247–1252.

Brown, Z.A., Selke, S., Zeh, J., Kopelman, J., Maslow, A., Ashley, R.L., Watts, D.H., Berry, S., Herd, M., and Corey, L. (1997). The acquisition of herpes simplex virus during pregnancy. N. Engl. J. Med. *337*, 509–515.

Bryant, J.A., Sellars, L.E., Busby, S.J.W., and Lee, D.J. (2014). Chromosome position effects on gene expression in Escherichia coli K-12. Nucleic Acids Res. *42*, 11383–11392.

Burgevin, A., Saveanu, L., Kim, Y., Barilleau, É., Kotturi, M., Sette, A., van Endert, P., and Peters, B. (2008). A Detailed Analysis of the Murine TAP Transporter Substrate Specificity. PLoS ONE *3*, e2402.

Burgos, J.S., Serrano-Saiz, E., Sastre, I., and Valdivieso, F. (2006). ICP47 mediates viral neuroinvasiveness by induction of TAP protein following intravenous inoculation of herpes simplex virus type 1 in mice. J. Neurovirol. *12*, 420–427.

Camarena, V., Kobayashi, M., Kim, J.Y., Roehm, P., Perez, R., Gardner, J., Wilson, A.C., Mohr, I., and Chao, M.V. (2010). Nature and duration of growth factor signaling through receptor tyrosine kinases regulates HSV-1 latency in neurons. Cell Host Microbe *8*, 320–330.

Cameron, J.M., McDougall, I., Marsden, H.S., Preston, V.G., Ryan, D.M., and Subak-Sharpe, J.H. (1988). Ribonucleotide reductase encoded by herpes simplex virus is a determinant of the pathogenicity of the virus in mice and a valid antiviral target. J. Gen. Virol. *69*, 2607–2612.

Campbell, M.E., Palfreyman, J.W., and Preston, C.M. (1984). Identification of herpes simplex virus DNA sequences which encode a trans-acting polypeptide responsible for stimulation of immediate early transcription. J. Mol. Biol. *180*, 1–19.

Cantin, E., Tanamachi, B., and Openshaw, H. (1999). Role for gamma interferon in control of herpes simplex virus type 1 reactivation. J. Virol. *73*, 3418–3423.

Cantin, E.M., Hinton, D.R., Chen, J., and Openshaw, H. (1995). Gamma interferon expression during acute and latent nervous system infection by herpes simplex virus type 1. J. Virol. *69*, 4898–4905.

Cavallero, S., Huot, N., Francelle, L., Lomonte, P., Naas, T., and Labetoulle, M. (2014). Biological features of herpes simplex virus type 1 latency in mice according to experimental conditions and type of neurones. Invest. Ophthalmol. Vis. Sci. *55*, 7761–7774.

Cereghini, S., and Yaniv, M. (1984). Assembly of transfected DNA into chromatin: structural changes in the origin-promoter-enhancer region upon replication. EMBO J. *3*, 1243–1253.

Cerundolo, V., Kelly, A., Elliott, T., Trowsdale, J., and Townsend, A. (1995). Genes encoded in the major histocompatibility complex affecting the generation of peptides for TAP transport. Eur. J. Immunol. *25*, 554–562.

Cheeran, M.C.-J., Gekker, G., Hu, S., Palmquist, J.M., and Lokensgard, J.R. (2005). T cell–mediated restriction of intracerebral murine cytomegalovirus infection displays dependence upon perforin but not interferon-γ. J. Neurovirol. *11*, 274–280.

Chen, H.-C., Martinez, J.P., Zorita, E., Meyerhans, A., and Filion, G.J. (2017). Position effects influence HIV latency reversal. Nat. Struct. Mol. Biol. *24*, 47–54.

Chen, H.-S., Martin, K.A., Lu, F., Lupey, L.N., Mueller, J.M., Lieberman, P.M., and Tempera, I. (2014). Epigenetic deregulation of the LMP1/LMP2 locus of Epstein-Barr virus by mutation of a single CTCF-cohesin binding site. J. Virol. *88*, 1703–1713.

Chen, Q., Lin, L., Smith, S., Huang, J., Berger, S.L., and Zhou, J. (2007). CTCF-dependent chromatin boundary element between the latency-associated transcript and ICP0 promoters in the herpes simplex virus type 1 genome. J. Virol. *81*, 5192–5201.

Chen, S.H., Kramer, M.F., Schaffer, P.A., and Coen, D.M. (1997). A viral function represses accumulation of transcripts from productive-cycle genes in mouse ganglia latently infected with herpes simplex virus. J. Virol. *71*, 5878–5884.

Chen, S.-H., Yao, H.-W., Chen, I.-T., Shieh, B., Li, C., and Chen, S.-H. (2008). Suppression of transcription factor early growth response 1 reduces herpes simplex virus lethality in mice. J. Clin. Invest. *118*, 3470–3477.

Chen, Y., Sidney, J., Southwood, S., Cox, A.L., Sakaguchi, K., Henderson, R.A., Appella, E., Hunt, D.F., Sette, A., and Engelhard, V.H. (1994). Naturally processed peptides longer than nine amino acid residues bind to the class I MHC molecule HLA-A2.1 with high affinity and in different conformations. J. Immunol. Baltim. Md 1950 *152*, 2874–2881.

Cheng, H., Tumpey, T.M., Staats, H.F., van Rooijen, N., Oakes, J.E., and Lausch, R.N. (2000). Role of macrophages in restricting herpes simplex virus type 1 growth after ocular infection. Invest. Ophthalmol. Vis. Sci. *41*, 1402–1409.

Chentoufi, A.A., Kritzer, E., Tran, M.V., Dasgupta, G., Lim, C.H., Yu, D.C., Afifi, R.E., Jiang, X., Carpenter, D., Osorio, N., et al. (2011). The Herpes Simplex Virus 1 Latency-Associated Transcript Promotes Functional Exhaustion of Virus-Specific CD8+ T Cells in Latently Infected Trigeminal Ganglia: a Novel Immune Evasion Mechanism. J. Virol. *85*, 9127–9138.

Chernukhin, I., Shamsuddin, S., Kang, S.Y., Bergstrom, R., Kwon, Y.-W., Yu, W., Whitehead, J., Mukhopadhyay, R., Docquier, F., Farrar, D., et al. (2007). CTCF interacts with and recruits the largest subunit of RNA Polymerase II to CTCF target sites genome-wide. Mol. Cell. Biol. *27*, 1631–1648.

Cheuk, E., D'Souza, C., Hu, N., Liu, Y., Lang, H., and Chamberlain, J.W. (2002). Human MHC class I transgenic mice deficient for H2 class I expression facilitate identification and characterization of new HLA class I-restricted viral T cell epitopes. J. Immunol. Baltim. Md 1950 *169*, 5571–5580.

Chevalier, G., Suberbielle, E., Monnet, C., Duplan, V., Martin-Blondel, G., Farrugia, F., Masson, G.L., Liblau, R., and Gonzalez-Dunia, D. (2011). Neurons are MHC class I-dependent targets for CD8 T cells upon neurotropic viral infection. PLOS Pathog. *7*, e1002393.

Chisholm, S.E., Howard, K., Gómez, M.V., and Reyburn, H.T. (2007). Expression of ICP0 is sufficient to trigger natural killer cell recognition of herpes simplex virus–infected cells by natural cytotoxicity receptors. J. Infect. Dis. *195*, 1160–1168.

Chiu, Y.-H., MacMillan, J.B., and Chen, Z.J. (2009). RNA polymerase III detects cytosolic DNA and induces type I interferons through the RIG-I pathway. Cell *138*, 576–591.

Cho, S.J., Kang, M.J., Homer, R.J., Kang, H.R., Zhang, X., Lee, P.J., Elias, J.A., and Lee, C.G. (2006). Role of Early Growth Response-1 (Egr-1) in interleukin-13-induced inflammation and remodeling. J. Biol. Chem. *281*, 8161–8168.

Ciechanover, A. (1998). The ubiquitin-proteasome pathway: on protein death and cell life. EMBO J. *17*, 7151–7160.

Cliffe, A.R., Garber, D.A., and Knipe, D.M. (2009). Transcription of the herpes simplex virus latency-associated transcript promotes the formation of facultative heterochromatin on lytic promoters. J. Virol. *83*, 8182–8190.

Cliffe, A.R., Coen, D.M., and Knipe, D.M. (2013a). Kinetics of facultative heterochromatin and polycomb group protein association with the herpes simplex viral genome during establishment of latent infection. MBio *4*, e00590-12.

Cliffe, A.R., Coen, D.M., and Knipe, D.M. (2013b). Kinetics of facultative heterochromatin and polycomb group protein association with the herpes simplex viral genome during establishment of latent infection. MBio *4*.

Cliffe, A.R., Arbuckle, J.H., Vogel, J.L., Geden, M.J., Rothbart, S.B., Cusack, C.L., Strahl, B.D., Kristie, T.M., and Deshmukh, M. (2015). Neuronal stress pathway mediating a histone methyl/phospho switch is required for herpes simplex virus reactivation. Cell Host Microbe *18*, 649–658.

Cocchi, F., Menotti, L., Mirandola, P., Lopez, M., and Campadelli-Fiume, G. (1998). The ectodomain of a novel member of the immunoglobulin subfamily related to the poliovirus receptor has the attributes of a bona fide receptor for herpes simplex virus types 1 and 2 in human cells. J. Virol. *72*, 9992–10002.

Coles, R.M., Mueller, S.N., Heath, W.R., Carbone, F.R., and Brooks, A.G. (2002). Progression of armed CTL from draining lymph node to spleen shortly after localized infection with herpes simplex virus 1. J. Immunol. *168*, 834–838.

Colussi, T.M., Costantino, D.A., Zhu, J., Donohue, J.P., Korostelev, A.A., Jaafar, Z.A., Plank, T.-D.M., Noller, H.F., and Kieft, J.S. (2015). Initiation of translation in bacteria by a structured eukaryotic IRES RNA. Nature *519*, 110–113.

Cong, L., Ran, F.A., Cox, D., Lin, S., Barretto, R., Habib, N., Hsu, P.D., Wu, X., Jiang, W., Marraffini, L.A., et al. (2013). Multiplex genome engineering using CRISPR/Cas systems. Science *339*, 819–823.

Conrady, C.D., Drevets, D.A., and Carr, D.J.J. (2010). Herpes simplex type I (HSV-1) infection of the nervous system: Is an immune response a good thing? J. Neuroimmunol. *220*, 1–9.

Cook, M.L., and Stevens, J.G. (1973a). Pathogenesis of herpetic neuritis and ganglionitis in mice: evidence for intra-axonal transport of infection. Infect. Immun. *7*, 272–288.

Cook, M.L., and Stevens, J.G. (1973b). Pathogenesis of herpetic neuritis and ganglionitis in mice: evidence for intra-axonal transport of infection. Infect. Immun. *7*, 272–288.

Cook, M.L., Bastone, V.B., and Stevens, J.G. (1974). Evidence that neurons harbor latent herpes simplex virus. Infect. Immun. *9*, 946–951.

Corey, L., Langenberg, A.G.M., Ashley, R., Sekulovich, R.E., Izu, A.E., Douglas, Jr, J.M., Handsfield, H.H., Warren, T., Marr, L., Tyring, S., et al. (1999). Recombinant Glycoprotein Vaccine for the Prevention of Genital HSV-2 Infection: Two Randomized Controlled Trials. JAMA *282*.

Corey, L., Wald, A., Celum, C.L., and Quinn, T.C. (2004). The effects of herpes simplex virus-2 on HIV-1 acquisition and transmission: a review of two overlapping epidemics.

Corriveau, R.A., Huh, G.S., and Shatz, C.J. (1998). Regulation of class I MHC gene expression in the developing and mature CNS by neural activity. Neuron *21*, 505–520.

Coupar, B.E.H., Oke, P.G., and Andrew, M.E. (2000). Insertion sites for recombinant vaccinia virus construction: effects on expression of a foreign protein. J. Gen. Virol. *81*, 431–439.

Cresswell, P., Bangia, N., Dick, T., and Diedrich, G. (1999). The nature of the MHC class I peptide loading complex. Immunol. Rev. *172*, 21–28.

Cresswell, P., Ackerman, A.L., Giodini, A., Peaper, D.R., and Wearsch, P.A. (2005). Mechanisms of MHC class I-restricted antigen processing and cross-presentation. Immunol. Rev. *207*, 145–157.

Croft, N.P., Smith, S.A., Sidney, J., Peters, B., Faridi, P., Witney, M., Sebastian, P., Flesch, I., Heading, S., Sette, A., et al. (In press). Most viral peptides displayed by class I MHC on infected cells are immunogenic. PNAS.

Croft, N.P., Smith, S.A., Wong, Y.C., Tan, C.T., Dudek, N.L., Flesch, I.E.A., Lin, L.C.W., Tscharke, D.C., and Purcell, A.W. (2013). Kinetics of antigen expression and epitope presentation during virus infection. PLoS Pathog. *9*, e1003129.

Crostarosa, F., Aravantinou, M., Akpogheneta, O.J., Jasny, E., Shaw, A., Kenney, J., Piatak, M., Lifson, J.D., Teitelbaum, A., Hu, L., et al. (2009). A macaque model to study vaginal HSV-2/immunodeficiency virus co-infection and the impact of hsv-2 on microbicide efficacy. PLoS ONE *4*, e8060.

Cunningham, A.L., Taylor, R., Taylor, J., Marks, C., Shaw, J., and Mindel, A. (2006). Prevalence of infection with herpes simplex virus types 1 and 2 in Australia: a nationwide population based survey. Sex. Transm. Infect. *82*, 164–168.

Daniels, R.W., Rossano, A.J., Macleod, G.T., and Ganetzky, B. (2014). Expression of multiple transgenes from a single construct using viral 2A peptides in Drosophila. PLoS ONE *9*, e100637.

Darougar, S., Wishart, M.S., and Viswalingam, N.D. (1985). Epidemiological and clinical features of primary herpes simplex virus ocular infection. Br. J. Ophthalmol. *69*, 2–6.

Davido, D.J., and Leib, D.A. (1996). Role of cis-acting sequences of the ICPO promoter of herpes simplex virus type 1 in viral pathogenesis, latency and reactivation. J. Gen. Virol. *77*, 1853–1863.

Davison, A.J. (2010). Herpesvirus systematics. Vet. Microbiol. *143*, 52–69.

De, S., and Babu, M.M. (2010). Genomic neighbourhood and the regulation of gene expression. Curr. Opin. Cell Biol. *22*, 326–333.

Deatly, A.M., Spivack, J.G., Lavi, E., and Fraser, N.W. (1987). RNA from an immediate early region of the type 1 herpes simplex virus genome is present in the trigeminal ganglia of latently infected mice. Proc. Natl. Acad. Sci. U. S. A. *84*, 3204–3208.

Decman, V., Kinchington, P.R., Harvey, S.A.K., and Hendricks, R.L. (2005). Gamma interferon can block herpes simplex virus type 1 reactivation from latency, even in the presence of late gene expression. J. Virol. *79*, 10339–10347.

Degli-Esposti, M.A., Leaver, A.L., Christiansen, F.T., Witt, C.S., Abraham, L.J., and Dawkins, R.L. (1992). Ancestral haplotypes: conserved population MHC haplotypes. Hum. Immunol. *34*, 242–252.

Dervillez, X., Qureshi, H., Chentoufi, A.A., Khan, A.A., Kritzer, E., Yu, D.C., Diaz, O.R., Gottimukkala, C., Kalantari, M., Villacres, M.C., et al. (2013). Asymptomatic HLA-A*02:01-restricted epitopes from herpes simplex virus glycoprotein B preferentially recall polyfunctional CD8+ T cells from seropositive asymptomatic individuals and protect HLA transgenic mice against ocular herpes. J. Immunol. Baltim. Md 1950 *191*, 5124–5138.

Deshmane, S.L., and Fraser, N.W. (1989). During latency, herpes simplex virus type 1 DNA is associated with nucleosomes in a chromatin structure. J. Virol. *63*, 943–947.

Deshpande, S., Zheng, M., Lee, S., Banerjee, K., Gangappa, S., Kumaraguru, U., and Rouse, B.T. (2001). Bystander activation involving T lymphocytes in herpetic stromal keratitis. J. Immunol. *167*, 2902–2910.

Desiderio, D.M., and Kai, M. (1983). Preparation of stable isotope-incorporated peptide internal standards for field desorption mass spectrometry quantification of peptides in biologic tissue. Biol. Mass Spectrom. *10*, 471–479.

Diefenbach, A., and Raulet, D.H. (2001). Strategies for target cell recognition by natural killer cells. Immunol. Rev. *181*, 170–184.

Dix, R.D., McKendall, R.R., and Baringer, J.R. (1983). Comparative neurovirulence of herpes simplex virus type 1 strains after peripheral or intracerebral inoculation of BALB/c mice. Infect. Immun. *40*, 103–112.

Dobbs, M.E., Strasser, J.E., Chu, C.-F., Chalk, C., and Milligan, G.N. (2005). Clearance of herpes simplex virus type 2 by CD8+ T cells requires gamma interferon and either perforin- or Fas-mediated cytolytic mechanisms. J. Virol. *79*, 14546–14554.

Donaghy, H., Bosnjak, L., Harman, A.N., Marsden, V., Tyring, S.K., Meng, T.-C., and Cunningham, A.L. (2009). Role for plasmacytoid dendritic cells in the immune control of recurrent human herpes simplex virus infection. J. Virol. *83*, 1952–1961.

Donato, L., de la Salle, H., Hanau, D., Tongio, M.M., Oswald, M., Vandevenne, A., and Geisert, J. (1995). Association of HLA class I antigen deficiency related to a TAP2 gene mutation with familial bronchiectasis. J. Pediatr. *127*, 895–900.

Du, T., Zhou, G., and Roizman, B. (2011). HSV-1 gene expression from reactivated ganglia is disordered and concurrent with suppression of latency-associated transcript and miRNAs. Proc. Natl. Acad. Sci. *108*, 18820–18824.

Du, T., Han, Z., Zhou, G., and Roizman, B. (2015). Patterns of accumulation of miRNAs encoded by herpes simplex virus during productive infection, latency, and on reactivation. Proc. Natl. Acad. Sci. *112*, E49–E55.

Dudek, N.L., Croft, N.P., Schittenhelm, R.B., Ramarathinam, S.H., and Purcell, A.W. (2016). A systems approach to understand antigen presentation and the immune response. In Proteomics in Systems Biology, J. Reinders, ed. (New York, NY: Springer New York), pp. 189–209.

Dudley, K.L., Bourne, N., and Milligan, G.N. (2000). Immune protection against HSV-2 in B-cell-deficient mice. Virology *270*, 454–463.

Dustin, M.L. (1987). Purified lymphocyte function-associated antigen 3 binds to CD2 and mediates T lymphocyte adhesion. J. Exp. Med. *165*, 677–692.

Dustin, M.L., Bromley, S.K., Kan, Z., Peterson, D.A., and Unanue, E.R. (1997). Antigen receptor engagement delivers a stop signal to migrating T lymphocytes. Proc. Natl. Acad. Sci. U. S. A. *94*, 3909–3913.

Easterfield, A.J., Austen, B.M., and Westwood, O.M. (2001). Inhibition of antigen transport by expression of infected cell peptide 47 (ICP47) prevents cell surface expression of HLA in choriocarcinoma cell lines. J. Reprod. Immunol. *50*, 19–40.

Efstathiou, S., and Preston, C.M. (2005). Towards an understanding of the molecular basis of herpes simplex virus latency. Virus Res. *111*, 108–119.

Efstathiou, S., Minson, A.C., Field, H.J., Anderson, J.R., and Wildy, P. (1986a). Detection of herpes simplex virus-specific DNA sequences in latently infected mice and in humans. J. Virol. *57*, 446–455.

Efstathiou, S., Minson, A.C., Field, H.J., Anderson, J.R., and Wildy, P. (1986b). Detection of herpes simplex virus-specific DNA sequences in latently infected mice and in humans. J. Virol. *57*, 446–455.

Efstathiou, S., Kemp, S., Darby, G., and Minson, A.C. (1989). The Role of Herpes Simplex Virus Type 1 Thymidine Kinase in Pathogenesis. J. Gen. Virol. *70*, 869–879.

Elias, P., and Lehman, I.R. (1988). Interaction of origin binding protein with an origin of replication of herpes simplex virus 1. Proc. Natl. Acad. Sci. U. S. A. *85*, 2959–2963.

Elias, P., Gustafsson, C.M., and Hammarsten, O. (1990). The origin binding protein of herpes simplex virus 1 binds cooperatively to the viral origin of replication oris. J. Biol. Chem. *265*, 17167–17173.

Ellison, A.R., Yang, L., Voytek, C., and Margolis, T.P. (2000). Establishment of latent herpes simplex virus type 1 infection in resistant, sensitive, and immunodeficient mouse strains. Virology *268*, 17–28.

Elmer, B.M., and McAllister, A.K. (2012). Major histocompatibility complex class I proteins in brain development and plasticity. Trends Neurosci. *35*, 660–670.

van Endert, P.M. (1995). The peptide-binding motif for the human transporter associated with antigen processing. J. Exp. Med. *182*, 1883–1895.

van Endert, P.M., Tampé, R., Meyer, T.H., Tisch, R., Bach, J.F., and McDevitt, H.O. (1994). A sequential model for peptide binding and transport by the transporters associated with antigen processing. Immunity *1*, 491–500.

Ertel, M.K., Cammarata, A.L., Hron, R.J., and Neumann, D.M. (2012). CTCF occupation of the herpes simplex virus 1 genome is disrupted at early times postreactivation in a transcription-dependent manner. J. Virol. *86*, 12741–12759.

Escher, C., Reiter, L., MacLean, B., Ossola, R., Herzog, F., Chilton, J., MacCoss, M.J., and Rinner, O. (2012). Using iRT, a normalized retention time for more targeted measurement of peptides. PROTEOMICS *12*, 1111–1121.

Esiri, M.M. (1982). Herpes simplex encephalitis. J. Neurol. Sci. *54*, 209–226.

Esiri, M.M., and Tomlinson, A.H. (1984). Herpes simplex encephalitis. J. Neurol. Sci. *64*, 213–217.

Falk, K., Rötzschke, O., Stevanović, S., Jung, G., and Rammensee, H.G. (1991). Allele-specific motifs revealed by sequencing of self-peptides eluted from MHC molecules. Nature *351*, 290–296.

Fan, S., Cai, H., Xu, X., Feng, M., Wang, L., Liao, Y., Zhang, Y., He, Z., Yang, F., Yu, W., et al. (2017). The characteristics of herpes simplex virus type 1 infection in rhesus macaques and the associated pathological features. Viruses *9*, 26.

Fan, Z., Beresford, P.J., Oh, D.Y., Zhang, D., and Lieberman, J. (2003). Tumor suppressor NM23-H1 is a granzyme A-activated DNase during CTL-mediated apoptosis, and the nucleosome assembly protein SET is its inhibitor. Cell *112*, 659–672.

Farooq, A.V., and Shukla, D. (2012). Herpes simplex epithelial and stromal keratitis: an epidemiologic update. Surv. Ophthalmol. *57*, 448–462.

Feldman, L.T., Ellison, A.R., Voytek, C.C., Yang, L., Krause, P., and Margolis, T.P. (2002a). Spontaneous molecular reactivation of herpes simplex virus type 1 latency in mice. Proc. Natl. Acad. Sci. U. S. A. *99*, 978–983.

Feldman, L.T., Ellison, A.R., Voytek, C.C., Yang, L., Krause, P., and Margolis, T.P. (2002b). Spontaneous molecular reactivation of herpes simplex virus type 1 latency in mice. Proc. Natl. Acad. Sci. *99*, 978–983.

Feltkamp, M.C., Vierboom, M.P., Kast, W.M., and Melief, C.J. (1994). Efficient MHC class I-peptide binding is required but does not ensure MHC class I-restricted immunogenicity. Mol. Immunol. *31*, 1391–1401.

Ferlazzo, G., Pack, M., Thomas, D., Paludan, C., Schmid, D., Strowig, T., Bougras, G., Muller, W.A., Moretta, L., and Munz, C. (2004). Distinct roles of IL-12 and IL-15 in human natural killer cell activation by dendritic cells from secondary lymphoid organs. Proc. Natl. Acad. Sci. *101*, 16606–16611.

Fillet, A.-M. (2002). Prophylaxis of herpesvirus infections in immunocompetent and immunocompromised older patients. Drugs Aging *19*, 343–354.

Fischer, M.A., Tscharke, D.C., Donohue, K.B., Truckenmiller, M.E., and Norbury, C.C. (2007). Reduction of vector gene expression increases foreign antigen-specific CD8+ T-cell priming. J. Gen. Virol. *88*, 2378–2386.

Fisman, D.N., Lipsitch, M., HOOK III, E.W., and Goldie, S.J. (2002). Projection of the future dimensions and costs of the genital herpes simplex type 2 epidemic in the United States. Sex. Transm. Dis. *29*, 608–622.

Flesch, I.E.A., Hollett, N.A., Wong, Y.C., and Tscharke, D.C. (2012). Linear fidelity in quantification of anti-viral CD8+ T cells. PLoS ONE *7*.

Fortier, M.-H., Caron, É., Hardy, M.-P., Voisin, G., Lemieux, S., Perreault, C., and Thibault, P. (2008). The MHC class I peptide repertoire is molded by the transcriptome. J. Exp. Med. *205*, 595–610.

Frank, G.M., Lepisto, A.J., Freeman, M.L., Sheridan, B.S., Cherpes, T.L., and Hendricks, R.L. (2010). Early CD4(+) T cell help prevents partial CD8(+) T cell exhaustion and promotes maintenance of herpes simplex virus 1 latency. J. Immunol. Baltim. Md 1950 *184*, 277–286.

Frank, G.M., Buela, K.-A.G., Maker, D.M., Harvey, S.A.K., and Hendricks, R.L. (2012). Early responding dendritic cells direct the local NK response to control herpes simplex virus 1 infection within the cornea. J. Immunol. *188*, 1350–1359.

Freeman, M.L., Sheridan, B.S., Bonneau, R.H., and Hendricks, R.L. (2007a). Psychological Stress Compromises CD8+ T Cell Control of Latent Herpes Simplex Virus Type 1 Infections. J. Immunol. *179*, 322–328.

Freeman, M.L., Sheridan, B.S., Bonneau, R.H., and Hendricks, R.L. (2007b). Psychological stress compromises CD8+ T cell control of latent herpes simplex virus type 1 infections. J. Immunol. Baltim. Md 1950 *179*, 322–328.

Fremont, D.H., Matsumura, M., Stura, E.A., Peterson, P.A., and Wilson, I.A. (1992). Crystal structures of two viral peptides in complex with murine MHC class I H-2Kb. Science *257*, 919–927.

Früh, K., Ahn, K., Djaballah, H., Sempé, P., van Endert, P.M., Tampé, R., Peterson, P.A., and Yang, Y. (1995). A viral inhibitor of peptide transporters for antigen presentation. Nature *375*, 415–418.

Fu, J., Jiang, C., Wang, J., Zhao, F., Ma, T., Shi, R., Zhao, Y., and Zhang, X. (2017). Epidemiology of varicella in Haidian district, Beijing, China—2007–2015. Vaccine *35*, 2365–2371.

Gadola, S.D., Moins-Teisserenc, H.T., Trowsdale, J., Gross, W.L., and Cerundolo, V. (2000). TAP deficiency syndrome. Clin. Exp. Immunol. *121*, 173–178.

Gaffney, D.F., McLauchlan, J., Whitton, J.L., and Barklie, C.J. (1985). A modular system for the assay of transcription regulatory signals: the sequence TAATGARAT is required for herpes simplex virus immediate early gene activation. Nucleic Acids Res. *13*, 7847–7863.

Galocha, B., Hill, A., Barnett, B.C., Dolan, A., Raimondi, A., Cook, R.F., Brunner, J., McGeoch, D.J., and Ploegh, H.L. (1997). The active site of ICP47, a herpes simplex virus–encoded inhibitor of the major histocompatibility complex (MHC)-encoded peptide transporter associated with antigen processing (TAP), maps to the NH2-terminal 35 residues. J. Exp. Med. *185*, 1565–1572.

Gangappa, S., Deshpande, S.P., and Rouse, B.T. (1999). Bystander activation of CD4+ T cells can represent an exclusive means of immunopathology in a virus infection. Eur. J. Immunol. *29*, 3674–3682.

Garber, D.A., Schaffer, P.A., and Knipe, D.M. (1997). A LAT-associated function reduces productive-cycle gene expression during acute infection of murine sensory neurons with herpes simplex virus type 1. J. Virol. *71*, 5885–5893.

Garboczi, D.N., Ghosh, P., Utz, U., Fan, Q.R., Biddison, W.E., and Wiley, D.C. (2010). Structure of the complex between human T-cell receptor, viral peptide and HLA-A2. Nature. 1996. 384: 134-141. J. Immunol. Baltim. Md 1950 *185*, 6394–6401.

Garrett, T.P., Saper, M.A., Bjorkman, P.J., Strominger, J.L., and Wiley, D.C. (1989). Specificity pockets for the side chains of peptide antigens in HLA-Aw68. Nature *342*, 692–696.

Gebhardt, T., Wakim, L.M., Eidsmo, L., Reading, P.C., Heath, W.R., and Carbone, F.R. (2009). Memory T cells in nonlymphoid tissue that provide enhanced local immunity during infection with herpes simplex virus. Nat. Immunol. *10*, 524–530.

Gebhardt, T., Whitney, P.G., Zaid, A., Mackay, L.K., Brooks, A.G., Heath, W.R., Carbone, F.R., and Mueller, S.N. (2011). Different patterns of peripheral migration by memory CD4+ and CD8+ T cells. Nature *477*, 216–219.

Gelman, I.H., and Silverstein, S. (1987). Herpes simplex virus immediate-early promoters are responsive to virus and cell trans-acting factors. J. Virol. *61*, 2286–2296.

Geng, J., Zaitouna, A.J., and Raghavan, M. (2018). Selected HLA-B allotypes are resistant to inhibition or deficiency of the transporter associated with antigen processing (TAP). PLOS Pathog. *14*, e1007171.

Gerber, S.A., Rush, J., Stemman, O., Kirschner, M.W., and Gygi, S.P. (2003). Absolute quantification of proteins and phosphoproteins from cell lysates by tandem MS. Proc. Natl. Acad. Sci. *100*, 6940–6945.

Ghiasi, H., Cai, S., Perng, G.C., Nesburn, A.B., and Wechsler, S.L. (2000). Both CD4+ and CD8+ T cells are involved in protection against HSV-1 induced corneal scarring. Br. J. Ophthalmol. *84*, 408–412.

Gilchuk, P., Hill, T.M., Wilson, J.T., and Joyce, S. (2015). Discovering protective CD8 T cell epitopes—no single immunologic property predicts it! Curr. Opin. Immunol. *34*, 43–51.

Gil-Torregrosa, B.C., Raúl Castaño, A., and Del Val, M. (1998). Major histocompatibility complex class I viral antigen processing in the secretory pathway defined by the trans-Golgi network protease furin. J. Exp. Med. *188*, 1105–1116.

Giordani, N.V., Neumann, D.M., Kwiatkowski, D.L., Bhattacharjee, P.S., McAnany, P.K., Hill, J.M., and Bloom, D.C. (2008). During herpes simplex virus type 1 infection of rabbits, the ability to express the latency-associated transcript increases latent-phase transcription of lytic genes. J. Virol. *82*, 6056–6060.

Goel, N., Mao, H., Rong, Q., Docherty, J.J., Zimmerman, D., and Rosenthal, K.S. (2002). The ability of an HSV strain to initiate zosteriform spread correlates with its neuroinvasive disease potential. Arch. Virol. *147*, 763–773.

Gold, M.C., Munks, M.W., Wagner, M., McMahon, C.W., Kelly, A., Kavanagh, D.G., Slifka, M.K., Koszinowski, U.H., Raulet, D.H., and Hill, A.B. (2004). Murine cytomegalovirus interference with antigen presentation has little effect on the size or the effector memory phenotype of the CD8 T cell response. J. Immunol. *172*, 6944–6953.

Goldberg, A.L., and Rock, K.L. (1992). Proteolysis, proteasomes and antigen presentation. Nature *357*, 375–379.

Goldsmith, K., Chen, W., Johnson, D.C., and Hendricks, R.L. (1998). Infected cell protein (ICP) 47 enhances herpes simplex virus neurovirulence by blocking the CD8+ T cell response. J. Exp. Med. *187*, 341–348.

Goodpasture, E.W. (1925). The axis-cylinders of peripheral nerves as portals of entry to the central nervous system for the virus of herpes simplex in experimentally infected rabbits. Am. J. Pathol. *1*, 11-28.5.

Goodpasture, E.W., and Teague, O. (1923). Transmission of the virus of herpes febrilis along nerves in experimentally infected rabbits. J. Med. Res. *44*, 139-184.7.

Gordon, Y.J., Simon, P.L., and Armstrong, J.A. (1984). Neurovirulence of an herpes simplex type 1 thymidine kinase negative mutant determined by virus biochemical defect and host immune system in mice. Brief report. Arch. Virol. *80*, 225–229.

Gordon, Y.J., Johnson, B., Romanowski, E., and Araullo-Cruz, T. (1988). RNA complementary to herpes simplex virus type 1 ICP0 gene demonstrated in neurons of human trigeminal ganglia. J. Virol. *62*, 1832–1835.

Grandea, A.G., Spies, T., Androlewicz, M.J., Athwal, R.S., and Geraghty, D.E. (1995). Dependence of peptide binding by MHC class I molecules on their interaction with TAP. Science *270*, 105–108.

Gray, E.E., Winship, D., Snyder, J.M., Child, S.J., Geballe, A.P., and Stetson, D.B. (2016). The AIM2-like receptors are dispensable for the interferon response to intracellular DNA. Immunity *45*, 255–266.

Greco, A., Simonin, D., Diaz, J.J., Barjhoux, L., Kindbeiter, K., Madjar, J.J., and Massé, T. (1994). The DNA sequence coding for the 5' untranslated region of herpes simplex virus type 1 ICP22 mRNA mediates a high level of gene expression. J. Gen. Virol. *75 (Pt 7)*, 1693–1702.

Greenberg, M.S. (1996). Herpesvirus infections. Dent. Clin. North Am. *40*, 359–368.

Gromme, M., Uytdehaag, F.G.C.M., Janssen, H., Calafat, J., van Binnendijk, R.S., Kenter, M.J.H., Tulp, A., Verwoerd, D., and Neefjes, J. (1999). Recycling MHC class I molecules and endosomal peptide loading. Proc. Natl. Acad. Sci. *96*, 10326–10331.

Grune, T., Merker, K., Sandig, G., and Davies, K.J.A. (2003). Selective degradation of oxidatively modified protein substrates by the proteasome. Biochem. Biophys. Res. Commun. *305*, 709–718.

Gubler, B., Daniel, S., Armandola, E.A., Hammer, J., Caillat-Zucman, S., Endert, P.M. van, and U, I. (1998). Substrate selection by transporters associated with antigen processing occurs during peptide binding to TAP. Mol. Immunol. *35*, 427–433.

Guermonprez, P., Saveanu, L., Kleijmeer, M., Davoust, J., van Endert, P., and Amigorena, S. (2003). ER–phagosome fusion defines an MHC class I cross-presentation compartment in dendritic cells. Nature *425*, 397–402.

Guidotti, L.G., Ishikawa, T., Hobbs, M.V., Matzke, B., Schreiber, R., and Chisari, F.V. (1996). Intracellular inactivation of the hepatitis B virus by cytotoxic T lymphocytes. Immunity *4*, 25–36.

Guo, H., Omoto, S., Harris, P.A., Finger, J.N., Bertin, J., Gough, P.J., Kaiser, W.J., and Mocarski, E.S. (2015). Herpes Simplex Virus Suppresses Necroptosis in Human Cells. Cell Host Microbe *17*, 243–251.

Guo, H.-C., Jardetzky, T.S., Garrettt, T.P.J., Lane, W.S., Strominger, J.L., and Wiley, D.C. (1992). Different length peptides bind to HLA-Aw68 similarly at their ends but bulge out in the middle. Nature *360*, 364–366.

Haan, C.A.M. de, Genne, L. van, Stoop, J.N., Volders, H., and Rottier, P.J.M. (2003). Coronaviruses as vectors: position dependence of foreign gene expression. J. Virol. *77*, 11312–11323.

Hafezi, W., Lorentzen, E.U., Eing, B.R., Müller, M., King, N.J.C., Klupp, B., Mettenleiter, T.C., and Kühn, J.E. (2012). Entry of herpes simplex virus type 1 (HSV-1) into the distal axons of trigeminal neurons favors the onset of nonproductive, silent infection. PLOS Pathog *8*, e1002679.

Hagmann, M., Georgiev, O., Schaffner, W., and Douville, P. (1995). Transcription factors interacting with herpes simplex virus α gene promoters in sensory neurons. Nucleic Acids Res. *23*, 4978–4985.

Halford, W.P., and Schaffer, P.A. (2001). ICP0 is required for efficient reactivation of herpes simplex virus type 1 from neuronal latency. J. Virol. *75*, 3240–3249.

Halford, W.P., Gebhardt, B.M., and Carr, D.J. (1996). Mechanisms of herpes simplex virus type 1 reactivation. J. Virol. *70*, 5051–5060.

Hammond, S.A., Bollinger, R.C., Tobery, T.W., and Silliciano, R.F. (1993). Transporter-independent processing of HIV-1 envelope protein for recognition by CD8+ T cells. Nature *364*, 158–161.

Harkness, J.M., Kader, M., and DeLuca, N.A. (2014). Transcription of the herpes simplex virus 1 genome during productive and quiescent infection of neuronal and nonneuronal cells. J. Virol. *88*, 6847–6861.

Harndahl, M., Rasmussen, M., Roder, G., Pedersen, I.D., Sørensen, M., Nielsen, M., and Buus, S. (2012). Peptide-MHC class I stability is a better predictor than peptide affinity of CTL immunogenicity. Eur. J. Immunol. *42*, 1405–1416.

Harty, J.T., Tvinnereim, A.R., and White, D.W. (2000). CD8+ T cell effector mechanisms in resistance to infection. Annu. Rev. Immunol. *18*, 275–308.

Hashimoto, M., Kamphorst, A.O., Im, S.J., Kissick, H.T., Pillai, R.N., Ramalingam, S.S., Araki, K., and Ahmed, R. (2018). CD8 T Cell Exhaustion in Chronic Infection and Cancer: Opportunities for Interventions. Annu. Rev. Med. *69*, 301–318.

Heath, W.R., and Carbone, F.R. (2001). Cross-presentation in viral immunity and self-tolerance. Nat. Rev. Immunol. *1*, 126–134.

Hellen, C.U., and Sarnow, P. (2001). Internal ribosome entry sites in eukaryotic mRNA molecules. Genes Dev. *15*, 1593–1612.

Henderson, G., Peng, W., Jin, L., Perng, G.-C., Nesburn, A., Wechsler, S., and Jones, C. (2002). Regulation of caspase 8- and caspase 9-induced apoptosis by the herpes simplex virus type 1 latency-associated transcript. J. Neurovirol. *8*, 103–111.

Henderson, R., Michel, H., Sakaguchi, K., Shabanowitz, J., Appella, E., Hunt, D., and Engelhard, V. (1992). HLA-A2.1-associated peptides from a mutant cell line: a second pathway of antigen presentation. Science *255*, 1264–1266.

Hennecke, M. (2001). Composition and arrangement of genes define the strength of IRES-driven translation in bicistronic mRNAs. Nucleic Acids Res. *29*, 3327–3334.

Henry, C.J., Ornelles, D.A., Mitchell, L.M., Brzoza-Lewis, K.L., and Hiltbold, E.M. (2008). IL-12 produced by dendritic cells augments CD8+ T cell activation through the production of the chemokines CCL1 and CCL17. J. Immunol. Baltim. Md 1950 *181*, 8576–8584.

Herbring, V., Bäucker, A., Trowitzsch, S., and Tampé, R. (2016). A dual inhibition mechanism of herpesviral ICP47 arresting a conformationally thermostable TAP complex. Sci. Rep. *6*, 36907.

Hernandez, T.R., Dutch, R.E., Lehman, I.R., Gustafsson, C., and Elias, P. (1991). Mutations in a herpes simplex virus type 1 origin that inhibit interaction with origin-binding protein also inhibit DNA replication. J. Virol. *65*, 1649–1652.

Herrera, F.J., and Triezenberg, S.J. (2004). VP16-dependent association of chromatin-modifying coactivators and underrepresentation of histones at immediate-early gene promoters during herpes simplex virus infection. J. Virol. *78*, 9689–9696.

Hill, A., Jugovic, P., York, L., Russ, G., Bennink, J., Yewdell, J., Ploegh, H., and Johnson, D. (1995). Herpes simplex virus turns off the TAP to evade host immunity. Nature *375*, 411–415.

Hill, J.M., Dudley, J.B., Shimomura, Y., and Kaufman, H.E. (1986). Quantitation and kinetics of induced HSV-1 ocular shedding. Curr. Eye Res. *5*, 241–246.

Hill, J.M., Field, M.A.R., and Haruta, Y. (1987). Strain specificity of spontaneous and adrenergically induced HSV-1 ocular reactivation in latently infected rabbits. Curr. Eye Res. *6*, 91–97.

Hill, J.M., Sedarati, F., Javier, R.T., Wagner, E.K., and Stevens, J.G. (1990). Herpes simplex virus latent phase transcription facilitates in vivo reactivation. Virology *174*, 117–125.

Hill, J.M., Garza, H.H., Helmy, M.F., Cook, S.D., Osborne, P.A., Johnson, E.M., Thompson, H.W., Green, L.C., O'Callaghan, R.J., and Gebhardt, B.M. (1997). Nerve growth factor antibody stimulates reactivation of ocular herpes simplex virus type 1 in latently infected rabbits. J. Neurovirol. *3*, 206–211.

Hill, J.M., Nolan, N.M., McFerrin, H.E., Clement, C., Foster, T.P., Halford, W.P., Kousoulas, K.G., Lukiw, W.J., Thompson, H.W., Stern, E.M., et al. (2012). HSV-1 latent rabbits shed viral DNA into their saliva. Virol. J. *9*, 221.

Hill, T.J., Blyth, W.A., and Harbour, D.A. (1978). Trauma to the skin causes recurrence of herpes simplex in the mouse. J. Gen. Virol. *39*, 21–28.

Hillen, N., Mester, G., Lemmel, C., Weinzierl, A.O., Müller, M., Wernet, D., Hennenlotter, J., Stenzl, A., Rammensee, H.-G., and Stevanović, S. (2008). Essential differences in ligand presentation and T cell epitope recognition among HLA molecules of the HLA-B44 supertype. Eur. J. Immunol. *38*, 2993–3003.

Himmelein, S., St Leger, A.J., Knickelbein, J.E., Rowe, A., Freeman, M.L., and Hendricks, R.L. (2011). Circulating herpes simplex type 1 (HSV-1)-specific CD8+ T cells do not access HSV-1 latently infected trigeminal ganglia. Herpesviridae *2*, 5.

Hirsch, M.S., Zisman, B., and Allison, A.C. (1970). Macrophages and age-dependent resistance to Herpes simplex virus in mice. J. Immunol. Baltim. Md 1950 *104*, 1160–1165.

Hjalmarsson, A., Blomqvist, P., and Sköldenberg, B. (2007). Herpes simplex encephalitis in Sweden, 1990-2001: incidence, morbidity, and mortality. Clin. Infect. Dis. Off. Publ. Infect. Dis. Soc. Am. *45*, 875–880.

Hogan, T., Kadolsky, U., Tung, S., Seddon, B., and Yates, A. (2014). Spatial heterogeneity and peptide availability determine CTL killing efficiency in vivo. PLoS Comput. Biol. *10*, e1003805.

Honess, R.W., and Roizman, B. (1974). Regulation of herpesvirus macromolecular synthesis I. Cascade regulation of the synthesis of three groups of viral proteins. J. Virol. *14*, 8–19.

Honess, R.W., and Roizman, B. (1975). Regulation of herpesvirus macromolecular synthesis: sequential transition of polypeptide synthesis requires functional viral polypeptides. Proc. Natl. Acad. Sci. *72*, 1276–1280.

Hoof, I., van Baarle, D., Hildebrand, W.H., and Keşmir, C. (2012). Proteome sampling by the HLA class I antigen processing pathway. PLoS Comput. Biol. *8*, e1002517.

Hopp, T.P., and Woods, K.R. (1981). Prediction of protein antigenic determinants from amino acid sequences. Proc. Natl. Acad. Sci. U. S. A. *78*, 3824–3828.

Horton, R., Gibson, R., Coggill, P., Miretti, M., Allcock, R.J., Almeida, J., Forbes, S., Gilbert, J.G.R., Halls, K., Harrow, J.L., et al. (2008). Variation analysis and gene annotation of eight MHC haplotypes: The MHC Haplotype Project. Immunogenetics *60*, 1–18.

Hosaka, M., Nagahama, M., Kim, W.S., Watanabe, T., Hatsuzawa, K., Ikemizu, J., Murakami, K., and Nakayama, K. (1991). Arg-X-Lys/Arg-Arg motif as a signal for precursor cleavage catalyzed by furin within the constitutive secretory pathway. J. Biol. Chem. *266*, 12127–12130.

Hoshino, Y., Pesnicak, L., Cohen, J.I., and Straus, S.E. (2007). Rates of reactivation of latent herpes simplex virus from mouse trigeminal ganglia ex vivo correlate directly with viral load and inversely with number of infiltrating CD8+ T cells. J. Virol. *81*, 8157–8164.

Hosken, N., McGowan, P., Meier, A., Koelle, D.M., Sleath, P., Wagener, F., Elliott, M., Grabstein, K., Posavad, C., and Corey, L. (2006). Diversity of the CD8+ T-cell response to herpes simplex virus type 2 proteins among persons with genital herpes. J. Virol. *80*, 5509–5515.

Hsia, S. (2013). Induction of transcription factor early growth response protein 1 during HSV-1 infection promotes viral replication in corneal cells. Br. Microbiol. Res. J. *3*, 706–723.

Huang, A.Y., Bruce, A.T., Pardoll, D.M., and Levitsky, H.I. (1996). In vivo cross-priming of MHC class I–restricted antigens requires the TAP transporter. Immunity *4*, 349–355.

Huang, W., Xie, P., Xu, M., Li, P., and Zao, G. (2011). The influence of stress factors on the reactivation of latent herpes simplex virus type 1 in infected mice. Cell Biochem. Biophys. *61*, 115–122.

Huang, Z., Wu, S.-Q., Liang, Y., Zhou, X., Chen, W., Li, L., Wu, J., Zhuang, Q., Chen, C., Li, J., et al. (2015). RIP1/RIP3 Binding to HSV-1 ICP6 Initiates Necroptosis to Restrict Virus Propagation in Mice. Cell Host Microbe *17*, 229–242.

Huard, B., and Früh, K. (2000). A role for MHC class I down-regulation in NK cell lysis of herpes virus-infected cells. Eur. J. Immunol. *30*, 509–515.

Huh, G.S., Boulanger, L.M., Du, H., Riquelme, P.A., Brotz, T.M., and Shatz, C.J. (2000). Functional requirement for class I MHC in CNS development and plasticity. Science *290*, 2155–2159.

Iijima, N., Linehan, M.M., Zamora, M., Butkus, D., Dunn, R., Kehry, M.R., Laufer, T.M., and Iwasaki, A. (2008). Dendritic cells and B cells maximize mucosal Th1 memory response to herpes simplex virus. J. Exp. Med. *205*, 3041–3052.

Irmler, M., Hertig, S., MacDonald, H.R., Sadoul, R., Becherer, J.D., Proudfoot, A., Solari, R., and Tschopp, J. (1995). Granzyme A is an interleukin 1 beta-converting enzyme. J. Exp. Med. *181*, 1917–1922.

Jacob, J., Kelsoe, G., Rajewsky, K., and Weiss, U. (1991). Intraclonal generation of antibody mutants in germinal centres. Nature *354*, 389–392.

Jahedi, S., Markovitz, N.S., Filatov, F., and Roizman, B. (1999). Colocalization of the herpes simplex virus 1 UL4 protein with infected cell protein 22 in small, dense nuclear structures formed prior to onset of DNA synthesis. J. Virol. *73*, 5132–5138.

Janeway, C.A. (1989). Approaching the Asymptote? Evolution and Revolution in Immunology. Cold Spring Harb. Symp. Quant. Biol. *54*, 1–13.

Janßen, L., Ramnarayan, V.R., Aboelmagd, M., Iliopoulou, M., Hein, Z., Majoul, I., Fritzsche, S., Halenius, A., and Springer, S. (2016). The murine cytomegalovirus immunoevasin gp40 binds MHC class I molecules to retain them in the early secretory pathway. J. Cell Sci. *129*, 219–227.

Javier, R.T., Stevens, J.G., Dissette, V.B., and Wagner, E.K. (1988). A herpes simplex virus transcript abundant in latently infected neurons is dispensable for establishment of the latent state. Virology *166*, 254–257.

Jeon, S., Leger, A.J.S., Cherpes, T.L., Sheridan, B.S., and Hendricks, R.L. (2013). PD-L1/B7-H1 Regulates the Survival but Not the Function of CD8+ T Cells in Herpes Simplex Virus Type 1 Latently Infected Trigeminal Ganglia. J. Immunol. *190*, 6277–6286.

Jerome, K.R., Fox, R., Chen, Z., Sears, A.E., Lee, H. y, and Corey, L. (1999). Herpes simplex virus inhibits apoptosis through the action of two genes, Us5 and Us3. J. Virol. *73*, 8950–8957.

Jiang, X., Chentoufi, A.A., Hsiang, C., Carpenter, D., Osorio, N., BenMohamed, L., Fraser, N.W., Jones, C., and Wechsler, S.L. (2011). The herpes simplex virus type 1 latency-associated transcript can protect neuron-derived C1300 and Neuro2A cells from granzyme B-induced apoptosis and CD8 T-cell killing. J. Virol. *85*, 2325–2332.

Jiang, Y., Yin, X., Stuart, P.M., and Leib, D.A. (2015). Dendritic cell autophagy contributes to herpes simplex virus-driven stromal keratitis and immunopathology. MBio *6*, e01426-15.

Jiang, Y., Patel, C.D., Manivanh, R., North, B., Backes, I.M., Posner, D.A., Gilli, F., Pachner, A.R., Nguyen, L.N., and Leib, D.A. (2017). Maternal antiviral immunoglobulin accumulates in neural tissue of neonates to prevent hsv neurological disease. MBio *8*, e00678-17.

Jin, H., Ma, Y., Prabhakar, B.S., Feng, Z., Valyi-Nagy, T., Yan, Z., Verpooten, D., Zhang, C., Cao, Y., and He, B. (2009). The γ134.5 protein of herpes simplex virus 1 is required to interfere with dendritic cell maturation during productive infection. J. Virol. *83*, 4984–4994.

Jin, X., Qin, Q., Chen, W., and Qu, J. (2007). Expression of toll-like receptors in the healthy and herpes simplex virus-infected cornea. Cornea *26*, 847–852.

Jirmo, A.C., Nagel, C.-H., Bohnen, C., Sodeik, B., and Behrens, G.M.N. (2009). Contribution of direct and cross-presentation to CTL immunity against herpes simplex virus 1. J. Immunol. *182*, 283–292.

Joffre, O.P., Segura, E., Savina, A., and Amigorena, S. (2012). Cross-presentation by dendritic cells. Nat. Rev. Immunol. *12*, 557–569.

Johnson, A.J., Chu, C.-F., and Milligan, G.N. (2008a). Effector CD4+ T-Cell involvement in clearance of infectious herpes simplex virus type 1 from sensory ganglia and spinal cords. J. Virol. *82*, 9678–9688.

Johnson, D.C., Frame, M.C., Ligas, M.W., Cross, A.M., and Stow, N.D. (1988). Herpes simplex virus immunoglobulin G Fc receptor activity depends on a complex of two viral glycoproteins, gE and gI. J. Virol. *62*, 1347–1354.

Johnson, K.E., Song, B., and Knipe, D.M. (2008b). Role for herpes simplex virus 1 ICP27 in the inhibition of type I interferon signaling. Virology *374*, 487–494.

Johnston, C., and Corey, L. (2016). Current concepts for genital herpes simplex virus infection: diagnostics and pathogenesis of genital tract shedding. Clin. Microbiol. Rev. *29*, 149–161.

Jones, K.A., and Tjian, R. (1985). Sp1 binds to promoter sequences and activates herpes simplex virus "immediate-early" gene transcription in vitro. Nature *317*, 179–182.

Jopling, C.L., Schütz, S., and Sarnow, P. (2008). Position-dependent function for a tandem microrna mir-122-binding site located in the hepatitis C virus RNA genome. Cell Host Microbe *4*, 77–85.

Jouan, Y., Grammatico-Guillon, L., Espitalier, F., Cazals, X., François, P., and Guillon, A. (2015). Long-term outcome of severe herpes simplex encephalitis: a population-based observational study. Crit. Care *19*, 345.

Jugovic, P., Hill, A.M., Tomazin, R., Ploegh, H., and Johnson, D.C. (1998). Inhibition of major histocompatibility complex class I antigen presentation in pig and primate cells by herpes simplex virus type 1 and 2 ICP47. J. Virol. *72*, 5076–5084.

Jurak, I., Kramer, M.F., Mellor, J.C., van Lint, A.L., Roth, F.P., Knipe, D.M., and Coen, D.M. (2010). Numerous conserved and divergent microRNAs expressed by herpes simplex viruses 1 and 2. J. Virol. *84*, 4659–4672.

Kameyama, T., Sujaku, C., Yamamoto, S., Hwang, C.B., and Shillitoe, E.J. (1988). Shedding of herpes simplex virus type 1 into saliva. J. Oral Pathol. *17*, 478–481.

Kang, H., Wiedmer, A., Yuan, Y., Robertson, E., and Lieberman, P.M. (2011). Coordination of KSHV latent and lytic gene control by CTCF-Cohesin mediated chromosome conformation. PLoS Pathog. *7*, e1002140.

Kapoor, A.K., Nash, A.A., Wildy, P., Phelan, J., McLean, C.S., and Field, H.J. (1982). Pathogenesis of herpes simplex virus in congenitally athymic mice: the relative roles of cell-mediated and humoral immunity. J. Gen. Virol. *60*, 225–233.

Kapp, E., and Schütz, F. (2007). Overview of tandem mass spectrometry (MS/MS) database search algorithms. In Current Protocols in Protein Science, J.E. Coligan, B.M. Dunn, D.W. Speicher, and P.T. Wingfield, eds. (Hoboken, NJ, USA: John Wiley & Sons, Inc.), pp. 25.2.1-25.2.19.

Kärre, K., Ljunggren, H.G., Piontek, G., and Kiessling, R. (1986). Selective rejection of H-2-deficient lymphoma variants suggests alternative immune defence strategy. Nature *319*, 675–678.

Kassim, S.H., Rajasagi, N.K., Ritz, B.W., Pruett, S.B., Gardner, E.M., Chervenak, R., and Jennings, S.R. (2009). Dendritic cells are required for optimal activation of natural killer functions following primary infection with herpes simplex virus type 1. J. Virol. *83*, 3175–3186.

Kastrukoff, L., Hamada, T., Schumacher, U., Long, C., Doherty, P.C., and Koprowski, H. (1982). Central nervous system infection and immune response in mice inoculated into the lip with herpes simplex virus type 1. J. Neuroimmunol. *2*, 295–305.

Kastrukoff, L.F., Lau, A.S., Takei, F., Smyth, M.J., Jones, C.M., Clarke, S.R.M., and Carbone, F.R. (2010). Redundancy in the immune system restricts the spread of HSV-1 in the central nervous system (CNS) of C57BL/6 mice. Virology *400*, 248–258.

Kastrukoff, L.F., Lau, A.S., and Thomas, E.E. (2012a). The effect of mouse strain on herpes simplex virus type 1 (HSV-1) infection of the central nervous system (CNS). Herpesviridae *3*, 4.

Kastrukoff, L.F., Lau, A.S., and Thomas, E.E. (2012b). The effect of mouse strain on herpes simplex virus type 1 (HSV-1) infection of the central nervous system (CNS). Herpesviridae *3*, 4.

Kastrukoff, L.F., Lau, A.S., Takei, F., Carbone, F.R., and Scalzo, A.A. (2015). A NK complex-linked locus restricts the spread of herpes simplex virus type 1 in the brains of C57BL/6 mice. Immunol. Cell Biol.

Kaufman, H.E., Azcuy, A.M., Varnell, E.D., Sloop, G.D., Thompson, H.W., and Hill, J.M. (2005). HSV-1 DNA in tears and saliva of normal adults. Invest. Ophthalmol. Vis. Sci. *46*, 241–247.

Kawai, T., and Akira, S. (2009). The roles of TLRs, RLRs and NLRs in pathogen recognition. Int. Immunol. *21*, 317–337.

Kellum, R., and Schedl, P. (1991). A position-effect assay for boundaries of higher order chromosomal domains. Trends Cell Biol. *1*, 11.

Kent, J.R., Zeng, P.-Y., Atanasiu, D., Gardner, J., Fraser, N.W., and Berger, S.L. (2004). During lytic infection herpes simplex virus type 1 is associated with histones bearing modifications that correlate with active transcription. J. Virol. *78*, 10178–10186.

Kern, E.R., Richards, J.T., and Overall, J.C. (1986). Acyclovir treatment of disseminated herpes simplex virus type 2 infection in weanling mice: alteration of mortality and pathogenesis. Antiviral Res. *6*, 189–195.

Khan, S., de Giuli, R., Schmidtke, G., Bruns, M., Buchmeier, M., van den Broek, M., and Groettrup, M. (2001). Cutting edge: neosynthesis is required for the presentation of a T cell epitope from a long-lived viral protein. J. Immunol. *167*, 4801–4804.

Khanna, K.M., Bonneau, R.H., Kinchington, P.R., and Hendricks, R.L. (2003a). Herpes simplex virus-specific memory CD8+ T cells are selectively activated and retained in latently infected sensory ganglia. Immunity *18*, 593–603.

Khanna, K.M., Bonneau, R.H., Kinchington, P.R., and Hendricks, R.L. (2003b). Herpes simplex virus-specific memory CD8+ T cells are selectively activated and retained in latently infected sensory ganglia. Immunity *18*, 593–603.

Kievits, F., Ivanyi, P., Krimpenfort, P., Berns, A., and Ploegh, H.L. (1987). HLA-restricted recognition of viral antigens in HLA transgenic mice. Nature *329*, 447–449.

Kim, J.Y., Mandarino, A., Chao, M.V., Mohr, I., and Wilson, A.C. (2012a). Transient reversal of episome silencing precedes VP16-dependent transcription during reactivation of latent HSV-1 in neurons. PLoS Pathog *8*, e1002540.

Kim, M., Osborne, N.R., Zeng, W., Donaghy, H., McKinnon, K., Jackson, D.C., and Cunningham, A.L. (2012b). Herpes simplex virus antigens directly activate NK cells via TLR2, thus facilitating their presentation to CD4 T lymphocytes. J. Immunol. *188*, 4158–4170.

Kim, M., Truong, N.R., James, V., Bosnjak, L., Sandgren, K.J., Harman, A.N., Nasr, N., Bertram, K.M., Olbourne, N., Sawleshwarkar, S., et al. (2015). Relay of herpes simplex virus between Langerhans cells and dermal dendritic cells in human skin. PLoS Pathog. *11*, e1004812.

Kimberlin, D.W. (2004). Neonatal herpes simplex infection. Clin. Microbiol. Rev. *17*, 1–13.

Kimura, T., and Griffin, D.E. (2000). The role of CD8(+) T cells and major histocompatibility complex class I expression in the central nervous system of mice infected with neurovirulent Sindbis virus. J. Virol. *74*, 6117–6125.

Kleinjan, D.A., and van Heyningen, V. (2005). Long-range control of gene expression: emerging mechanisms and disruption in disease. Am. J. Hum. Genet. *76*, 8–32.

Kleinjan, D.J., and van Heyningen, V. (1998). Position effect in human genetic disease. Hum. Mol. Genet. *7*, 1611–1618.

Knickelbein, J.E., Khanna, K.M., Yee, M.B., Baty, C.J., Kinchington, P.R., and Hendricks, R.L. (2008). Noncytotoxic lytic granule-mediated CD8+ T cell inhibition of HSV-1 reactivation from neuronal latency. Science *322*, 268–271.

Kobayashi, M., Wilson, A.C., Chao, M.V., and Mohr, I. (2012). Control of viral latency in neurons by axonal mTOR signaling and the 4E-BP translation repressor. Genes Dev. *26*, 1527–1532.

Kobiler, O., Lipman, Y., Therkelsen, K., Daubechies, I., and Enquist, L.W. (2010). Herpesviruses carrying a Brainbow cassette reveal replication and expression of limited numbers of incoming genomes. Nat. Commun. *1*.

Kodukula, P., Liu, T., Rooijen, N.V., Jager, M.J., and Hendricks, R.L. (1999). Macrophage control of herpes simplex virus type 1 replication in the peripheral nervous system. J. Immunol. *162*, 2895–2905.

Koelle, D.M. (2000). Herpes simplex virus: the importance of asymptomatic shedding. J. Antimicrob. Chemother. *45*, 1–8.

Koelle, D.M., Corey, L., Burke, R.L., Eisenberg, R.J., Cohen, G.H., Pichyangkura, R., and Triezenberg, S.J. (1994a). Antigenic specificities of human CD4+ T-cell clones recovered from recurrent genital herpes simplex virus type 2 lesions. J. Virol. *68*, 2803–2810.

Koelle, D.M., Abbo, H., Peck, A., Ziegweid, K., and Corey, L. (1994b). Direct recovery of herpes simplex virus (HSV)-specific T lymphocyte clones from recurrent genital HSV-2 lesions. J. Infect. Dis. *169*, 956–961.

Koelle, D.M., Posavad, C.M., Barnum, G.R., Johnson, M.L., Frank, J.M., and Corey, L. (1998). Clearance of HSV-2 from recurrent genital lesions correlates with infiltration of HSV-specific cytotoxic T lymphocytes. J. Clin. Invest. *101*, 1500–1508.

Kollias, C.M., Huneke, R.B., Wigdahl, B., and Jennings, S.R. (2015a). Animal models of herpes simplex virus immunity and pathogenesis. J. Neurovirol. *21*, 8–23.

Kollias, C.M., Huneke, R.B., Wigdahl, B., and Jennings, S.R. (2015b). Animal models of herpes simplex virus immunity and pathogenesis. J. Neurovirol. *21*, 8–23.

Koopmann, J.-O., Post, M., Neefjes, J.J., Hämmerling, G.J., and Momburg, F. (1996). Translocation of long peptides by transporters associated with antigen processing (TAP). Eur. J. Immunol. *26*, 1720–1728.

Kramer, M.F., and Coen, D.M. (1995). Quantification of transcripts from the ICP4 and thymidine kinase genes in mouse ganglia latently infected with herpes simplex virus. J. Virol. *69*, 1389–1399.

Kramer, T., and Enquist, L.W. (2013). Directional spread of alphaherpesviruses in the nervous system. Viruses *5*, 678–707.

Kramer, M.F., Chen, S.H., Knipe, D.M., and Coen, D.M. (1998). Accumulation of viral transcripts and DNA during establishment of latency by herpes simplex virus. J. Virol. *72*, 1177–1185.

Kristie, T.M., Vogel, J.L., and Sears, A.E. (1999). Nuclear localization of the C1 factor (host cell factor) in sensory neurons correlates with reactivation of herpes simplex virus from latency. Proc. Natl. Acad. Sci. U. S. A. *96*, 1229–1233.

Krug, A., Luker, G.D., Barchet, W., Leib, D.A., Akira, S., and Colonna, M. (2004). Herpes simplex virus type 1 activates murine natural interferon-producing cells through toll-like receptor 9. Blood *103*, 1433–1437.

Kubat, N.J., Amelio, A.L., Giordani, N.V., and Bloom, D.C. (2004). The herpes simplex virus type 1 latency-asociated transcript (LAT) enhancer/rcr is hyperacetylated during latency independently of LAT transcription. J. Virol. *78*, 12508–12518.

Kuklin, N.A., Daheshia, M., Chun, S., and Rouse, B.T. (1998). Role of mucosal immunity in herpes simplex virus infection. J. Immunol. Baltim. Md 1950 *160*, 5998–6003.

Kulej, K., Avgousti, D.C., Sidoli, S., Herrmann, C., Fera, A.N.D., Kim, E.T., Garcia, B.A., and Weitzman, M.D. (2017a). Time-resolved global and chromatin proteomics during herpes simplex virus (HSV-1) infection. Mol. Cell. Proteomics mcp.M116.065987.

Kulej, K., Avgousti, D.C., Sidoli, S., Herrmann, C., Della Fera, A.N., Kim, E.T., Garcia, B.A., and Weitzman, M.D. (2017b). Time-resolved global and chromatin proteomics during herpes simplex virus type 1 (HSV-1) infection. Mol. Cell. Proteomics *16*, S92–S107.

Kurachi, R., Daikoku, T., Tsurumi, T., Maeno, K., Nishiyama, Y., and Kurata, T. (1993). The pathogenicity of a US3 protein kinase-deficient mutant of herpes simplex virus type 2 in mice. Arch. Virol. *133*, 259–273.

Kurt-Jones, E.A., Chan, M., Zhou, S., Wang, J., Reed, G., Bronson, R., Arnold, M.M., Knipe, D.M., and Finberg, R.W. (2004). Herpes simplex virus 1 interaction with Toll-like receptor 2 contributes to lethal encephalitis. Proc. Natl. Acad. Sci. U. S. A. *101*, 1315–1320.

Kwiatkowski, D.L., Thompson, H.W., and Bloom, D.C. (2009). The polycomb group protein bmi1 binds to the herpes simplex virus 1 latent genome and maintains repressive histone marks during latency. J. Virol. *83*, 8173–8181.

Lacasse, J.J., and Schang, L.M. (2010). During lytic infections, herpes simplex virus type 1 DNA is in complexes with the properties of unstable nucleosomes. J. Virol. *84*, 1920–1933.

Lachmann, R.H., Sadarangani, M., Atkinson, H.R., and Efstathiou, S. (1999). An analysis of herpes simplex virus gene expression during latency establishment and reactivation. J. Gen. Virol. *80*, 1271–1282.

Lafaille, F.G., Pessach, I.M., Zhang, S.-Y., Ciancanelli, M.J., Herman, M., Abhyankar, A., Ying, S.-W., Keros, S., Goldstein, P.A., Mostoslavsky, G., et al. (2012). Impaired intrinsic immunity to HSV-1 in human iPSC-derived TLR3-deficient CNS cells. Nature *491*, 769–773.

Lafferty, W.E., Coombs, R.W., Benedetti, J., Critchlow, C., and Corey, L. (1987). Recurrences after oral and genital herpes simplex virus infection. Influence of site of infection and viral type. N. Engl. J. Med. *316*, 1444–1449.

Laibson, P.R., and Kibrick, S. (1969). Recurrence of herpes simplex virus in rabbit eyes: results of a three-year study. Invest. Ophthalmol. *8*, 346–350.

Lairson, D.R., Begley, C.E., Reynolds, T.F., and Wilhelmus, K.R. (2003). Prevention of herpes simplex virus eye disease: a cost-effectiveness analysis. Arch. Ophthalmol. *121*, 108–112.

Lampson, L.A. (1995). Interpreting MHC class I expression and class I/class II reciprocity in the CNS: reconciling divergent findings. Microsc. Res. Tech. *32*, 267–285.

Lang, A., and Nikolich-Zugich, J. (2005). Development and migration of protective CD8+ T cells into the nervous system following ocular herpes simplex virus-1 infection. J. Immunol. Baltim. Md 1950 *174*, 2919–2925.

Lange, V., Picotti, P., Domon, B., and Aebersold, R. (2008). Selected reaction monitoring for quantitative proteomics: a tutorial. Mol. Syst. Biol. *4*, 222.

Latchman, D.S. (1999). Regulation of DNA virus transcription by cellular POU family transcription factors. Rev. Med. Virol. *9*, 31–38.

Lautscham, G., Mayrhofer, S., Taylor, G., Haigh, T., Leese, A., Rickinson, A., and Blake, N. (2001). Processing of a multiple membrane spanning Epstein-Barr virus protein for CD8 + T cell recognition reveals a proteasome-dependent, transporter associated with antigen processing–independent pathway. J. Exp. Med. *194*, 1053–1068.

Lautscham, G., Rickinson, A., and Blake, N. (2003). TAP-independent antigen presentation on MHC class I molecules: lessons from Epstein–Barr virus. Microbes Infect. *5*, 291–299.

Lawlor, D.A., Zemmour, J., Ennis, P.D., and Parham, P. (1990). Evolution of class-I MHC genes and proteins: from natural selection to thymic selection. Annu. Rev. Immunol. *8*, 23–63.

Law-Ping-Man, S., Toutain, F., Rieux-Laucat, F., Picard, C., Kammerer-Jacquet, S., Magérus-Chatinet, A., Dupuy, A., and Adamski, H. (2018). Chronic granulomatous skin lesions leading to a diagnosis of TAP1 deficiency syndrome. Pediatr. Dermatol.

LeBien, T.W., and Tedder, T.F. (2008). B lymphocytes: how they develop and function. Blood *112*, 1570–1580.

Lee, S.S., and Lehman, I.R. (1997). Unwinding of the box I element of a herpes simplex virus type 1 origin by a complex of the viral origin binding protein, single-strand DNA binding protein, and single-stranded DNA. Proc. Natl. Acad. Sci. U. S. A. *94*, 2838–2842.

Lee, H.K., Zamora, M., Linehan, M.M., Iijima, N., Gonzalez, D., Haberman, A., and Iwasaki, A. (2009). Differential roles of migratory and resident DCs in T cell priming after mucosal or skin HSV-1 infection. J. Exp. Med. *206*, 359–370.

Lee, P.Y., Park, B.C., Chi, S.W., Bae, K.-H., Kim, S., Cho, S., Kang, S., Kim, J.-H., and Park, S.G. (2016). Histone H4 is cleaved by granzyme A during staurosporine-induced cell death in B-lymphoid Raji cells. BMB Rep. *49*, 560–565.

Leger, A.J.S., and Hendricks, R.L. (2011). CD8+ T cells patrol HSV-1-infected trigeminal ganglia and prevent viral reactivation. J. Neurovirol. *17*, 528–534.

Lehnert, E., and Tampé, R. (2017). Structure and dynamics of antigenic peptides in complex with TAP. Front. Immunol. *8*.

Leib, D.A., Bogard, C.L., Kosz-Vnenchak, M., Hicks, K.A., Coen, D.M., Knipe, D.M., and Schaffer, P.A. (1989). A deletion mutant of the latency-associated transcript of herpes simplex virus type 1 reactivates from the latent state with reduced frequency. J. Virol. *63*, 2893–2900.

Leib, D.A., Harrison, T.E., Laslo, K.M., Machalek, M.A., Moorman, N.J., and Virgin, H.W. (1999). Interferons regulate the phenotype of wild-type and mutant herpes simplex viruses in vivo. J. Exp. Med. *189*, 663–672.

Li, T., Hu, J.-F., Qiu, X., Ling, J., Chen, H., Wang, S., Hou, A., Vu, T.H., and Hoffman, A.R. (2008). CTCF regulates allelic expression of Igf2 by orchestrating a promoter-polycomb repressive complex 2 intrachromosomal loop. Mol. Cell. Biol. *28*, 6473–6482.

Liepe, J., Marino, F., Sidney, J., Jeko, A., Bunting, D.E., Sette, A., Kloetzel, P.M., Stumpf, M.P.H., Heck, A.J.R., and Mishto, M. (2016). A large fraction of HLA class I ligands are proteasome-generated spliced peptides. Science *354*, 354–358.

Lima, G.K., Zolini, G.P., Mansur, D.S., Freire Lima, B.H., Wischhoff, U., Astigarraga, R.G., Dias, M.F., das Graças Almeida Silva, M., Béla, S.R., do Valle Antonelli, L.R., et al. (2010). Toll-like receptor (TLR) 2 and TLR9 expressed in trigeminal ganglia are critical to viral control during herpes simplex virus 1 infection. Am. J. Pathol. *177*, 2433–2445.

Lin, R., Noyce, R.S., Collins, S.E., Everett, R.D., and Mossman, K.L. (2004). The Herpes Simplex Virus ICP0 RING Finger Domain Inhibits IRF3- and IRF7-Mediated Activation of Interferon-Stimulated Genes. J. Virol. *78*, 1675–1684.

van Lint, A.L., Ayers, M., Brooks, A.G., Coles, R.M., Heath, W.R., and Carbone, F.R. (2004a). Herpes simplex virus-specific CD8+ T cells can clear established lytic infections from skin and nerves and can partially limit the early spread of virus after cutaneous inoculation. J. Immunol. *172*, 392–397.

van Lint, A.L., Ayers, M., Brooks, A.G., Coles, R.M., Heath, W.R., and Carbone, F.R. (2004b). Herpes simplex virus-specific CD8+ T cells can clear established lytic infections from skin and nerves and can partially limit the early spread of virus after cutaneous inoculation. J. Immunol. *172*, 392–397.

van Lint, A.L., Kleinert, L., Clarke, S.R.M., Stock, A., Heath, W.R., and Carbone, F.R. (2005). Latent infection with herpes simplex virus is associated with ongoing CD8+ T-cell stimulation by parenchymal cells within sensory ganglia. J. Virol. *79*, 14843–14851.

van Lint, A.L., Murawski, M.R., Goodbody, R.E., Severa, M., Fitzgerald, K.A., Finberg, R.W., Knipe, D.M., and Kurt-Jones, E.A. (2010). Herpes simplex virus immediate-early ICP0 protein inhibits Toll-like receptor 2-dependent inflammatory responses and NF-kappaB signaling. J. Virol. *84*, 10802–10811.

Liu, T., Tang, Q., and Hendricks, R.L. (1996). Inflammatory infiltration of the trigeminal ganglion after herpes simplex virus type 1 corneal infection. J. Virol. *70*, 264–271.

Liu, T., Khanna, K.M., Chen, X., Fink, D.J., and Hendricks, R.L. (2000). CD8+ T cells can block herpes simplex virus type 1 (HSV-1) reactivation from latency in sensory neurons. J. Exp. Med. *191*, 1459–1466.

Liu, T., Khanna, K.M., Carriere, B.N., and Hendricks, R.L. (2001). Gamma interferon can prevent herpes simplex virus type 1 reactivation from latency in sensory neurons. J. Virol. *75*, 11178–11184.

Liu, Z., Chen, O., Wall, J.B.J., Zheng, M., Zhou, Y., Wang, L., Ruth Vaseghi, H., Qian, L., and Liu, J. (2017). Systematic comparison of 2A peptides for cloning multi-genes in a polycistronic vector. Sci. Rep. *7*.

Ljunggren, H.-G., Stam, N.J., Öhlén, C., Neefjes, J.J., Höglund, P., Heemels, M.-T., Bastin, J., Schumacher, T.N.M., Townsend, A., Kärre, K., et al. (1990). Empty MHC class I molecules come out in the cold. Nature *346*, 476–480.

Looker, K.J., Magaret, A.S., May, M.T., Turner, K.M.E., Vickerman, P., Gottlieb, S.L., and Newman, L.M. (2015a). Global and regional estimates of prevalent and incident herpes simplex virus type 1 infections in 2012. PLOS ONE *10*, e0140765.

Looker, K.J., Magaret, A.S., Turner, K.M.E., Vickerman, P., Gottlieb, S.L., and Newman, L.M. (2015b). Global estimates of prevalent and incident herpes simplex virus type 2 infections in 2012. PLOS ONE *10*, e114989.

Looker, K.J., Magaret, A.S., May, M.T., Turner, K.M.E., Vickerman, P., Newman, L.M., and Gottlieb, S.L. (2017). First estimates of the global and regional incidence of neonatal herpes infection. Lancet Glob. Health.

Lopez, C., and Dudas, G. (1979). Replication of herpes simplex virus type 1 in macrophages from resistant and susceptible mice. Infect. Immun. *23*, 432–437.

Lopez, C., Kirkpatrick, D., Read, S.E., Fitzgerald, P.A., Pitt, J., Pahwa, S., Ching, C.Y., and Smithwick, E.M. (1983). Correlation between low natural killing of fibroblasts infected with herpes simplex virus type 1 and susceptibility to herpesvirus infections. J. Infect. Dis. *147*, 1030–1035.

Lorente, E., Infantes, S., Barnea, E., Beer, I., Barriga, A., García-Medel, N., Lasala, F., Jiménez, M., Admon, A., and López, D. (2013). Diversity of natural self-derived ligands presented by different HLA class I molecules in transporter antigen processing-deficient cells. PLoS ONE *8*, e59118.

Lowin, B., Hahne, M., Mattmann, C., and Tschopp, J. (1994). Cytolytic T-cell cytotoxicity is mediated through perforin and Fas lytic pathways. Nature *370*, 650–652.

Lu, J., Higashimoto, Y., Appella, E., and Celis, E. (2004). Multiepitope trojan antigen peptide vaccines for the induction of antitumor CTL and Th immune responses. J. Immunol. *172*, 4575–4582.

Lubinski, J.M., Lazear, H.M., Awasthi, S., Wang, F., and Friedman, H.M. (2011). The herpes simplex virus 1 IgG Fc receptor blocks antibody-mediated complement activation and antibody-dependent cellular cytotoxicity in vivo. J. Virol. *85*, 3239–3249.

Lucinda, N., Figueiredo, M.M., Pessoa, N.L., Santos, B.S.Á. da S., Lima, G.K., Freitas, A.M., Machado, A.M.V., Kroon, E.G., Antonelli, L.R. do V., and Campos, M.A. (2017). Dendritic cells, macrophages, NK and CD8+ T lymphocytes play pivotal roles in

controlling HSV-1 in the trigeminal ganglia by producing IL1-beta, iNOS and granzyme B. Virol. J. *14*.

Lund, J., Sato, A., Akira, S., Medzhitov, R., and Iwasaki, A. (2003). Toll-like receptor 9-mediated recognition of Herpes simplex virus-2 by plasmacytoid dendritic cells. J. Exp. Med. *198*, 513–520.

Lundberg, P., Ramakrishna, C., Brown, J., Tyszka, J.M., Hamamura, M., Hinton, D.R., Kovats, S., Nalcioglu, O., Weinberg, K., Openshaw, H., et al. (2008). The immune response to herpes simplex virus type 1 infection in susceptible mice is a major cause of central nervous system pathology resulting in fatal encephalitis. J. Virol. *82*, 7078–7088.

Lutz, M., Burke, L.J., Barreto, G., Goeman, F., Greb, H., Arnold, R., Schultheiss, H., Brehm, A., Kouzarides, T., Lobanenkov, V., et al. (2000). Transcriptional repression by the insulator protein CTCF involves histone deacetylases. Nucleic Acids Res. *28*, 1707–1713.

Ma, J.Z., Russell, T.A., Spelman, T., Carbone, F.R., and Tscharke, D.C. (2014). Lytic gene expression is frequent in HSV-1 latent infection and correlates with the engagement of a cell-intrinsic transcriptional response. PLoS Pathog. *10*, e1004237.

Mackay, L.K., Wakim, L., van Vliet, C.J., Jones, C.M., Mueller, S.N., Bannard, O., Fearon, D.T., Heath, W.R., and Carbone, F.R. (2012). Maintenance of T cell function in the face of chronic antigen stimulation and repeated reactivation for a latent virus infection. J. Immunol. *188*, 2173–2178.

Mackem, S., and Roizman, B. (1982). Structural features of the herpes simplex virus alpha gene 4, 0, and 27 promoter-regulatory sequences which confer alpha regulation on chimeric thymidine kinase genes. J. Virol. *44*, 939–949.

MacLean, B., Tomazela, D.M., Abbatiello, S.E., Zhang, S., Whiteaker, J.R., Paulovich, A.G., Carr, S.A., and MacCoss, M.J. (2010). Effect of collision energy optimization on the measurement of peptides by selected reaction monitoring (SRM) mass spectrometry. Anal. Chem. *82*, 10116–10124.

MacNamara, K.C., Chua, M.M., Nelson, P.T., Shen, H., and Weiss, S.R. (2005). Increased epitope-specific cd8+ t cells prevent murine coronavirus spread to the spinal cord and subsequent demyelination. J. Virol. *79*, 3370–3381.

Madden, D.R. (1995). The three-dimensional structure of peptide-MHC complexes. Annu. Rev. Immunol. *13*, 587–622.

Mailles, A., Stahl, J.-P., and Steering Committee and Investigators Group (2009). Infectious encephalitis in France in 2007: a national prospective study. Clin. Infect. Dis. Off. Publ. Infect. Dis. Soc. Am. *49*, 1838–1847.

Maillet, S., Naas, T., Crepin, S., Roque-Afonso, A.-M., Lafay, F., Efstathiou, S., and Labetoulle, M. (2006). Herpes simplex virus type 1 latently infected neurons differentially express latency-associated and ICP0 transcripts. J. Virol. *80*, 9310–9321.

Mak, T.W., and Jett, B.D. (2014). The major histocompatibility complex. In Primer to The Immune Response, (Philadelphia, PA), pp. 143–159.

Makhov, A.M., Lee, S.S.-K., Lehman, I.R., and Griffith, J.D. (2003). Origin-specific unwinding of herpes simplex virus 1 DNA by the viral UL9 and ICP8 proteins: Visualization of a specific preunwinding complex. Proc. Natl. Acad. Sci. *100*, 898–903.

Manickan, E., and Rouse, B.T. (1995). Roles of different T-cell subsets in control of herpes simplex virus infection determined by using T-cell-deficient mouse-models. J. Virol. *69*, 8178–8179.

Manickan, E., Rouse, R.J., Yu, Z., Wire, W.S., and Rouse, B.T. (1995). Genetic immunization against herpes simplex virus. Protection is mediated by CD4+ T lymphocytes. J. Immunol. Baltim. Md 1950 *155*, 259–265.

Margolis, T.P., Sedarati, F., Dobson, A.T., Feldman, L.T., and Stevens, J.G. (1992). Pathways of viral gene expression during acute neuronal infection with HSV-1. Virology *189*, 150–160.

Margolis, T.P., Imai, Y., Yang, L., Vallas, V., and Krause, P.R. (2007). Herpes Simplex Virus Type 2 (HSV-2) Establishes Latent Infection in a Different Population of Ganglionic Neurons than HSV-1: Role of Latency-Associated Transcripts. J. Virol. *81*, 1872–1878.

Mark, K.E., Wald, A., Magaret, A.S., Selke, S., Olin, L., Huang, M., and Corey, L. (2008). Rapidly cleared episodes of herpes simplex virus reactivation in immunocompetent adults. J. Infect. Dis. *198*, 1141–1149.

Martin, D.W., Deb, S.P., Klauer, J.S., and Deb, S. (1991). Analysis of the herpes simplex virus type 1 OriS sequence: mapping of functional domains. J. Virol. *65*, 4359–4369.

Martínez, F.P., Cruz, R., Lu, F., Plasschaert, R., Deng, Z., Rivera-Molina, Y.A., Bartolomei, M.S., Lieberman, P.M., and Tang, Q. (2014). CTCF binding to the first intron of the Major Immediate Early (MIE) gene of human cytomegalovirus (HCMV) negatively regulates MIE gene expression and HCMV replication. J. Virol. *88*, 7389–7401.

Martoglio, B., and Dobberstein, B. (1998). Signal sequences: more than just greasy peptides. Trends Cell Biol. *8*, 410–415.

Masopust, D. (2001). Preferential localization of effector memory cells in nonlymphoid tissue. Science *291*, 2413–2417.

Matschulla, T., Berry, R., Gerke, C., Döring, M., Busch, J., Paijo, J., Kalinke, U., Momburg, F., Hengel, H., and Halenius, A. (2017). A highly conserved sequence of the viral TAP inhibitor ICP47 is required for freezing of the peptide transport cycle. Sci. Rep. *7*, 2933.

Matsumura, M., Fremont, D.H., Peterson, P.A., and Wilson, I.A. (1992). Emerging principles for the recognition of peptide antigens by MHC class I molecules. Science *257*, 927–934.

McCarthy, M.K., and Weinberg, J.B. (2015). The immunoproteasome and viral infection: a complex regulator of inflammation. Front. Microbiol. *6*.

McClelland, R.S., Wang, C.C., Overbaugh, J., Richardson, B.A., Corey, L., Ashley, R.L., Mandaliya, K., Ndinya-Achola, J., Bwayo, J.J., and Kreiss, J.K. (2002). Association between cervical shedding of herpes simplex virus and HIV-1. Aids *16*, 2425–2430.

McClements, W.L., Armstrong, M.E., Keys, R.D., and Liu, M.A. (1997). The prophylactic effect of immunization with DNA encoding herpes simplex virus glycoproteins on HSV-induced disease in guinea pigs. Vaccine *15*, 857–860.

McGeoch, D.J., Dolan, A., Donald, S., and Rixon, F.J. (1985). Sequence determination and genetic content of the short unique region in the genome of herpes simplex virus type 1. J. Mol. Biol. *181*, 1–13.

McGeoch, D.J., Dolan, A., Donald, S., and Brauer, D.H. (1986). Complete DNA sequence of the short repeat region in the genome of herpes simplex virus type 1. Nucleic Acids Res. *14*, 1727–1745.

McGeoch, D.J., Dalrymple, M.A., Davison, A.J., Dolan, A., Frame, M.C., McNab, D., Perry, L.J., Scott, J.E., and Taylor, P. (1988). The complete DNA sequence of the long unique region in the genome of herpes simplex virus type 1. J. Gen. Virol. *69 (Pt 7)*, 1531–1574.

McHeyzer-Williams, L.J., and McHeyzer-Williams, M.G. (2005). Antigen-specific memory B cell development. Annu. Rev. Immunol. *23*, 487–513.

Medina, F., Ramos, M., Iborra, S., de Leon, P., Rodriguez-Castro, M., and Del Val, M. (2009). Furin-processed antigens targeted to the secretory route elicit functional TAP1-/-CD8+ T lymphocytes in vivo. J. Immunol. *183*, 4639–4647.

Medzhitov, R. (2007). Recognition of microorganisms and activation of the immune response. Nature *449*, 819–826.

Mehta, A., Maggioncalda, J., Bagasra, O., Thikkavarapu, S., Saikumari, P., Valyi-Nagy, T., Fraser, N.W., and Block, T.M. (1995). In situ DNA PCR and RNA hybridization detection of herpes simplex virus sequences in trigeminal ganglia of latently infected mice. Virology *206*, 633–640.

Meignier, B., Longnecker, R., Mavromara-Nazos, P., Sears, A.E., and Roizman, B. (1988). Virulence of and establishment of latency by genetically engineered deletion mutants of herpes simplex virus I. Virology *162*, 251–254.

Melchjorsen, J., Pedersen, F.S., Mogensen, S.C., and Paludan, S.R. (2002). Herpes simplex virus selectively induces expression of the CC Chemokine RANTES/CCL5 in macrophages through a mechanism dependent on PKR and ICP0. J. Virol. *76*, 2780–2788.

Melchjorsen, J., Sirén, J., Julkunen, I., Paludan, S.R., and Matikainen, S. (2006). Induction of cytokine expression by herpes simplex virus in human monocyte-derived macrophages and dendritic cells is dependent on virus replication and is counteracted by ICP27 targeting NF-kappaB and IRF-3. J. Gen. Virol. *87*, 1099–1108.

Melchjorsen, J., Rintahaka, J., Søby, S., Horan, K.A., Poltajainen, A., Østergaard, L., Paludan, S.R., and Matikainen, S. (2010). Early Innate Recognition of Herpes Simplex Virus in Human Primary Macrophages Is Mediated via the MDA5/MAVS-Dependent and MDA5/MAVS/RNA Polymerase III-Independent Pathways. J. Virol. *84*, 11350–11358.

Mellerick, D.M., and Fraser', N.W. (1987). Physical state of the latent herpes simplex virus genome in a mouse model system: Evidence suggesting an episomal state. Virology *158*, 265–275.

Menendez, C.M., and Carr, D.J.J. (2017). Herpes simplex virus-1 infects the olfactory bulb shortly following ocular infection and exhibits a long-term inflammatory profile in the form of effector and HSV-1-specific T cells. J. Neuroinflammation *14*, 124.

Menotti, L., Casadio, R., Bertucci, C., Lopez, M., and Campadelli-Fiume, G. (2002). Substitution in the murine nectin1 receptor of a single conserved amino acid at a position distal from the herpes simplex virus gD binding site confers high-affinity binding to gD. J. Virol. *76*, 5463–5471.

Metcalf, J.F., and Michaelis, B.A. (1984). Herpetic keratitis in inbred mice. Invest. Ophthalmol. Vis. Sci. *25*, 1222–1225.

Metkar, S.S., Wang, B., Ebbs, M.L., Kim, J.H., Lee, Y.J., Raja, S.M., and Froelich, C.J. (2003). Granzyme B activates procaspase-3 which signals a mitochondrial amplification loop for maximal apoptosis. J. Cell Biol. *160*, 875–885.

Mikloska, Z., Kesson, A.M., Penfold, M.E., and Cunningham, A.L. (1996). Herpes simplex virus protein targets for CD4 and CD8 lymphocyte cytotoxicity in cultured epidermal keratinocytes treated with interferon-gamma. J. Infect. Dis. *173*, 7–17.

Miller, C.S., Danaher, R.J., and Jacob, R.J. (1998). Molecular aspects of herpes simplex virus I latency, reactivation, and recurrence. Crit. Rev. Oral Biol. Med. *9*, 541–562.

Milligan, G.N., Meador, M.G., Chu, C.-F., Young, C.G., Martin, T.L., and Bourne, N. (2005). Long-term presence of virus-specific plasma cells in sensory ganglia and spinal cord following intravaginal inoculation of herpes simplex virus type 2. J. Virol. *79*, 11537–11540.

Minagawa, H., Sakuma, S., Mohri, S., Mori, R., and Watanabe, T. (1988). Herpes simplex virus type 1 infection in mice with severe combined immunodeficiency (SCID). Arch. Virol. *103*, 73–82.

Mitchell, G.F., and Miller, J.F. (1968). Cell to cell interaction in the immune response. II. The source of hemolysin-forming cells in irradiated mice given bone marrow and thymus or thoracic duct lymphocytes. J. Exp. Med. *128*, 821–837.

Miyagawa, Y., Marino, P., Verlengia, G., Uchida, H., Goins, W.F., Yokota, S., Geller, D.A., Yoshida, O., Mester, J., Cohen, J.B., et al. (2015). Herpes simplex viral-vector design for efficient transduction of nonneuronal cells without cytotoxicity. Proc. Natl. Acad. Sci. *112*, E1632–E1641.

Mizuguchi, H., Xu, Z., Ishii-Watabe, A., Uchida, E., and Hayakawa, T. (2000). IRES-dependent second gene expression is significantly lower than cap-dependent first gene expression in a bicistronic vector. Mol. Ther. *1*, 376–382.

Mo, X.Y., Cascio, P., Lemerise, K., Goldberg, A.L., and Rock, K. (1999). Distinct proteolytic processes generate the C and N termini of MHC class I-binding peptides. J. Immunol. Baltim. Md 1950 *163*, 5851–5859.

Moins-Teisserenc, H.T., Gadola, S.D., Cella, M., Dunbar, P.R., Exley, A., Blake, N., Baycal, C., Lambert, J., Bigliardi, P., Willemsen, M., et al. (1999). Association of a syndrome resembling Wegener's granulomatosis with low surface expression of HLA class-I molecules. The Lancet *354*, 1598–1603.

Molano, A., Erdjument-Bromage, H., Fremont, D.H., Messaoudi, I., Tempst, P., and Nikolić-Zugić, J. (1998). Peptide selection by an MHC H-2Kb class I molecule devoid of the central anchor ("C") pocket. J. Immunol. Baltim. Md 1950 *160*, 2815–2823.

Momburg, F., and Tan, P. (2002). Tapasin-the keystone of the loading complex optimizing peptide binding by MHC class I molecules in the endoplasmic reticulum. Mol. Immunol. *39*, 217–233.

Momburg, F., Roelse, J., Howard, J.C., Butcher, G.W., Hämmerling, G.J., and Neefjes, J.J. (1994). Selectivity of MHC-encoded peptide transporters from human, mouse and rat. Nature *367*, 648–651.

Morahan, P.S., Morse, S.S., and McGeorge, M.G. (1980). Macrophage extrinsic antiviral activity during herpes simplex virus infection. J. Gen. Virol. *46*, 291–300.

Morimoto, T., Arii, J., Akashi, H., and Kawaguchi, Y. (2009). Identification of multiple sites suitable for insertion of foreign genes in herpes simplex virus genomes. Microbiol. Immunol. *53*, 155–161.

Mørk, N., Kofod-Olsen, E., Sørensen, K.B., Bach, E., Ørntoft, T.F., Østergaard, L., Paludan, S.R., Christiansen, M., and Mogensen, T.H. (2015). Mutations in the TLR3 signaling pathway and beyond in adult patients with herpes simplex encephalitis. Genes Immun. *16*, 552–566.

Mott, K., Brick, D.J., van Rooijen, N., and Ghiasi, H. (2007). Macrophages are important determinants of acute ocular HSV-1 infection in immunized mice. Investig. Opthalmology Vis. Sci. *48*, 5605.

Mott, K.R., Gate, D., Matundan, H.H., Ghiasi, Y.N., Town, T., and Ghiasi, H. (2016). CD8+ T cells play a bystander role in HSV-1 latently infected mice. J. Virol.

Mueller, S.N., and Mackay, L.K. (2016). Tissue-resident memory T cells: local specialists in immune defence. Nat. Rev. Immunol. *16*, 79–89.

Mueller, S.N., Jones, C.M., Smith, C.M., Heath, W.R., and Carbone, F.R. (2002). Rapid Cytotoxic T Lymphocyte Activation Occurs in the Draining Lymph Nodes After Cutaneous Herpes Simplex Virus Infection as a Result of Early Antigen Presentation and Not the Presence of Virus. J. Exp. Med. *195*, 651–656.

Murchie, M.-J., and Mcgeoch, D.J. (1982). DNA sequence analysis of an immediate-early gene region of the herpes simplex virus type 1 genome (Map Coordinates 0.950 to 0.978). J. Gen. Virol. *62*, 1–15.

Nagafuchi, S., Oda, H., Mori, R., and Taniguchi, T. (1979). Mechanism of Acquired Resistance to Herpes Simplex Virus Infection as Studied in Nude Mice. J. Gen. Virol. *44*, 715–723.

Nahmias, A.J., Lee, F.K., and Beckman-Nahmias, S. (1990). Sero-epidemiological and -sociological patterns of herpes simplex virus infection in the world. Scand. J. Infect. Dis. Suppl. *69*, 19–36.

Nailwal, H., and Chan, F.K.-M. (2019). Necroptosis in anti-viral inflammation. Cell Death Differ. *26*, 4–13.

Nakanishi, Y., Lu, B., Gerard, C., and Iwasaki, A. (2009). CD8+ T lymphocyte mobilization to virus-infected tissue requires CD4+ T-cell help. Nature *462*, 510–513.

Nandakumar, S., Woolard, S.N., Yuan, D., Rouse, B.T., and Kumaraguru, U. (2008). Natural killer cells as novel helpers in anti-herpes simplex virus immune response. J. Virol. *82*, 10820–10831.

Nash, A.A., Jayasuriya, A., Phelan, J., Cobbold, S.P., Waldmann, H., and Prospero, T. (1987). Different roles for L3T4+ and Lyt 2+ T cell subsets in the control of an acute herpes simplex virus infection of the skin and nervous system. J. Gen. Virol. *68 (Pt 3)*, 825–833.

Neefjes, J., Jongsma, M.L.M., Paul, P., and Bakke, O. (2011). Towards a systems understanding of MHC class I and MHC class II antigen presentation. Nat. Rev. Immunol.

Neisig, A., Wubbolts, R., Zang, X., Melief, C., and Neefjes, J. (1996). Allele-specific differences in the interaction of MHC class I molecules with transporters associated with antigen processing. J. Immunol. Baltim. Md 1950 *156*, 3196–3206.

Neumann, H., Cavalié, A., Jenne, D.E., and Wekerle, H. (1995). Induction of MHC class I genes in neurons. Science *269*, 549–552.

Neumann, L., Kraas, W., Uebel, S., Jung, G., and Tampé, R. (1997). The active domain of the herpes simplex virus protein ICP47: a potent inhibitor of the transporter associated with antigen processing. J. Mol. Biol. *272*, 484–492.

Nguyen-Huynh, A.T., and Schaffer, P.A. (1998). Cellular transcription factors enhance herpes simplex virus type 1 oriS-dependent DNA replication. J. Virol. *72*, 3635–3645.

Nielsen, M., Lundegaard, C., Worning, P., Lauemøller, S.L., Lamberth, K., Buus, S., Brunak, S., and Lund, O. (2003). Reliable prediction of T-cell epitopes using neural networks with novel sequence representations. Protein Sci. Publ. Protein Soc. *12*, 1007–1017.

Nishiyama, Y., Kurachi, R., Daikoku, T., and Umene, K. (1993). The US 9, 10, 11, and 12 genes of herpes simplex virus type 1 are of no importance for its neurovirulence and latency in mice. Virology *194*, 419–423.

Noisakran, S., Halford, W.P., Veress, L., and Carr, D.J. (1998). Role of the hypothalamic pituitary adrenal axis and IL-6 in stress-induced reactivation of latent herpes simplex virus type 1. J. Immunol. Baltim. Md 1950 *160*, 5441–5447.

Norbury, C.C., Hewlett, L.J., Prescott, A.R., Shastri, N., and Watts, C. (1995). Class I MHC presentation of exogenous soluble antigen via macropinocytosis in bone marrow macrophages. Immunity *3*, 783–791.

Norbury, C.C., Princiotta, M.F., Bacik, I., Brutkiewicz, R.R., Wood, P., Elliott, T., Bennink, J.R., and Yewdell, J.W. (2001). Multiple antigen-specific processing pathways for activating naive CD8+ T cells in vivo. J. Immunol. Baltim. Md 1950 *166*, 4355–4362.

Norgren, R.B., McLean, J.H., Bubel, H.C., Wander, A., Bernstein, D.I., and Lehman, M.N. (1992). Anterograde transport of HSV-1 and HSV-2 in the visual system. Brain Res. Bull. *28*, 393–399.

Nossal, G.J., Cunningham, A., Mitchell, G.F., and Miller, J.F. (1968). Cell to cell interaction in the immune response. 3. Chromosomal marker analysis of single antibody-forming cells in reconstituted, irradiated, or thymectomized mice. J. Exp. Med. *128*, 839–853.

Nussbaum, A.K., Dick, T.P., Keilholz, W., Schirle, M., Stevanovic, S., Dietz, K., Heinemeyer, W., Groll, M., Wolf, D.H., Huber, R., et al. (1998). Cleavage motifs of the yeast 20S proteasome subunits deduced from digests of enolase 1. Proc. Natl. Acad. Sci. *95*, 12504–12509.

O'Garra, A. (1998). Cytokines induce the development of functionally heterogeneous t helper cell subsets. Immunity *8*, 275–283.

Oh, J., Sanders, I.F., Chen, E.Z., Li, H., Tobias, J.W., Isett, R.B., Penubarthi, S., Sun, H., Baldwin, D.A., and Fraser, N.W. (2015). Genome Wide Nucleosome Mapping for HSV-1 Shows Nucleosomes Are Deposited at Preferred Positions during Lytic Infection. PLOS ONE *10*, e0117471.

O'Hare, P. (1993). The virion transactivator of herpes simplex virus. Semin. Virol. *4*, 145–155.

Ohlsson, R., Lobanenkov, V., and Klenova, E. (2010). Does CTCF mediate between nuclear organization and gene expression? BioEssays *32*, 37–50.

Oldham, M.L., Hite, R.K., Steffen, A.M., Damko, E., Li, Z., Walz, T., and Chen, J. (2016a). A mechanism of viral immune evasion revealed by cryo-EM analysis of the TAP transporter. Nature *529*, 537–540.

Oldham, M.L., Grigorieff, N., and Chen, J. (2016b). Structure of the transporter associated with antigen processing trapped by herpes simplex virus. ELife *5*.

Oliveira, C.C., Querido, B., Sluijter, M., de Groot, A.F., van der Zee, R., Rabelink, M.J.W.E., Hoeben, R.C., Ossendorp, F., van der Burg, S.H., and van Hall, T. (2013). New Role of Signal Peptide Peptidase To Liberate C-Terminal Peptides for MHC Class I Presentation. J. Immunol. *191*, 4020–4028.

Orr, M.T., Edelmann, K.H., Vieira, J., Corey, L., Raulet, D.H., and Wilson, C.B. (2005). Inhibition of MHC class I is a virulence factor in herpes simplex virus infection of mice. PLoS Pathog *1*, e7.

Orr, M.T., Mathis, M.A., Lagunoff, M., Sacks, J.A., and Wilson, C.B. (2007). CD8 T cell control of HSV reactivation from latency is abrogated by viral inhibition of MHC class I. Cell Host Microbe *2*, 172–180.

Ortmann, B., Copeman, J., Lehner, P.J., Sadasivan, B., Herberg, J.A., Grandea, A.G., Riddell, S.R., Tampé, R., Spies, T., Trowsdale, J., et al. (1997). A critical role for tapasin in the assembly and function of multimeric MHC class I-TAP complexes. Science *277*, 1306–1309.

Oseroff, C., Peters, B., Pasquetto, V., Moutaftsi, M., Sidney, J., Panchanathan, V., Tscharke, D.C., Maillere, B., Grey, H., and Sette, A. (2008). Dissociation between epitope hierarchy and immunoprevalence in CD8 responses to vaccinia virus western reserve. J. Immunol. Baltim. Md 1950 *180*, 7193–7202.

Owen, B.A., and Pease, L.R. (1999). TAP association influences the conformation of nascent MHC class I molecules. J. Immunol. Baltim. Md 1950 *162*, 4677–4684.

Oxman, M.N., Levin, M.J., Johnson, G.R., Schmader, K.E., Straus, S.E., Gelb, L.D., Arbeit, R.D., Simberkoff, M.S., Gershon, A.A., Davis, L.E., et al. (2005). A vaccine to prevent herpes zoster and postherpetic neuralgia in older adults. N. Engl. J. Med. *352*, 2271–2284.

Ozato, K., Hansen, T.H., and Sachs, D.H. (1980). Monoclonal antibodies to mouse MHC antigens. II. Antibodies to the H-2Ld antigen, the products of a third polymorphic locus of the mouse major histocompatibility complex. J. Immunol. Baltim. Md 1950 *125*, 2473–2477.

Paladino, P., and Mossman, K.L. (2009). Mechanisms Employed by Herpes Simplex Virus 1 to Inhibit the Interferon Response. J. Interferon Cytokine Res. *29*, 599–608.

Pamer, E., and Cresswell, P. (1998). Mechanisms of MHC class I-restricted antigen processing. Annu. Rev. Immunol. *16*, 323–358.

Pan, D., Flores, O., Umbach, J.L., Pesola, J.M., Bentley, P., Rosato, P.C., Leib, D.A., Cullen, B.R., and Coen, D.M. (2014). A neuron-specific host microrna targets herpes simplex virus-1 ICP0 expression and promotes latency. Cell Host Microbe *15*, 446–456.

Paul, S., Weiskopf, D., Angelo, M.A., Sidney, J., Peters, B., and Sette, A. (2013). HLA Class I Alleles Are Associated with Peptide-Binding Repertoires of Different Size, Affinity, and Immunogenicity. J. Immunol. *191*, 5831–5839.

Penfold, M.E., Armati, P., and Cunningham, A.L. (1994). Axonal transport of herpes simplex virions to epidermal cells: evidence for a specialized mode of virus transport and assembly. Proc. Natl. Acad. Sci. *91*, 6529–6533.

Pereira, R.A., and Simmons, A. (1999). Cell surface expression of H2 antigens on primary sensory neurons in response to acute but not latent herpes simplex virus infection in vivo. J. Virol. *73*, 6484–6489.

Pereira, R.A., Tscharke, D.C., and Simmons, A. (1994). Upregulation of class I major histocompatibility complex gene expression in primary sensory neurons, satellite cells, and Schwann cells of mice in response to acute but not latent herpes simplex virus infection in vivo. J. Exp. Med. *180*, 841–850.

Pereira, R.A., Simon, M.M., and Simmons, A. (2000). Granzyme A, a noncytolytic component of CD8+ cell granules, restricts the spread of herpes simplex virus in the peripheral nervous systems of experimentally infected mice. J. Virol. *74*, 1029–1032.

Peri, P., Mattila, R.K., Kantola, H., Broberg, E., Karttunen, H.S., Waris, M., Vuorinen, T., and Hukkanen, V. (2008). Herpes simplex virus type 1 Us3 gene deletion influences toll-like receptor responses in cultured monocytic cells. Virol. J. *5*, 140.

Perng, G. (2000). Virus-Induced Neuronal Apoptosis Blocked by the Herpes Simplex Virus Latency-Associated Transcript. Science *287*, 1500–1503.

Perng, G.C., Dunkel, E.C., Geary, P.A., Slanina, S.M., Ghiasi, H., Kaiwar, R., Nesburn, A.B., and Wechsler, S.L. (1994a). The latency-associated transcript gene of herpes simplex virus type 1 (HSV-1) is required for efficient in vivo spontaneous reactivation of HSV-1 from latency. J. Virol. *68*, 8045–8055.

Perng, G.C., Dunkel, E.C., Geary, P.A., Slanina, S.M., Ghiasi, H., Kaiwar, R., Nesburn, A.B., and Wechsler, S.L. (1994b). The latency-associated transcript gene of herpes simplex virus type 1 (HSV-1) is required for efficient in vivo spontaneous reactivation of HSV-1 from latency. J. Virol. *68*, 8045–8055.

Perry, L.J., and McGeoch, D.J. (1988). The DNA sequences of the long repeat region and adjoining parts of the long unique region in the genome of herpes simplex virus type 1. J. Gen. Virol. *69 (Pt 11)*, 2831–2846.

Peters, B., Bulik, S., Tampe, R., Van Endert, P.M., and Holzhütter, H.-G. (2003). Identifying MHC class I epitopes by predicting the TAP transport efficiency of epitope precursors. J. Immunol. Baltim. Md 1950 *171*, 1741–1749.

Petersen, T.N., Brunak, S., von Heijne, G., and Nielsen, H. (2011). SignalP 4.0: discriminating signal peptides from transmembrane regions. Nat. Methods *8*, 785–786.

Petrie, H.T. (1995). T cell receptor gene recombination patterns and mechanisms: cell death, rescue, and T cell production. J. Exp. Med. *182*, 121–127.

Phipps, W., Saracino, M., Magaret, A., Selke, S., Remington, M., Huang, M.-L., Warren, T., Casper, C., Corey, L., and Wald, A. (2011). Persistent genital herpes simplex virus-2 shedding years following the first clinical episode. J. Infect. Dis. *203*, 180–187.

Piedade, D., and Azevedo-Pereira, J.M. (2016). The role of micrornas in the pathogenesis of herpesvirus infection. Viruses *8*, 156.

Pietra, G., Semino, C., Cagnoni, F., Boni, L., Cangemi, G., Frumento, G., and Melioli, G. (2000). Natural killer cells lyse autologous herpes simplex virus infected targets using cytolytic mechanisms distributed clonotypically. J. Med. Virol. *62*, 354–363.

Pinto, A.K., and Hill, A.B. (2005). Viral interference with antigen presentation to CD8+ T cells: lessons from cytomegalovirus. Viral Immunol. *18*, 434–444.

Portaro, F.C., Gomes, M.D., Cabrera, A., Fernandes, B.L., Silva, C.L., Ferro, E.S., Juliano, L., and de Camargo, A.C. (1999). Thimet oligopeptidase and the stability of MHC class I epitopes in macrophage cytosol. Biochem. Biophys. Res. Commun. *255*, 596–601.

Posavad, C.M., Koelle, D.M., Shaughnessy, M.F., and Corey, L. (1997). Severe genital herpes infections in HIV-infected individuals with impaired herpes simplex virus-specific CD8+ cytotoxic T lymphocyte responses. Proc. Natl. Acad. Sci. *94*, 10289–10294.

Posavad, C.M., Huang, M.L., Barcy, S., Koelle, D.M., and Corey, L. (2000). Long term persistence of herpes simplex virus-specific CD8+ CTL in persons with frequently recurring genital herpes. J. Immunol. Baltim. Md 1950 *165*, 1146–1152.

Post, L.E., Mackem, S., and Roizman, B. (1981). Regulation of alpha genes of herpes simplex virus: expression of chimeric genes produced by fusion of thymidine kinase with alpha gene promoters. Cell *24*, 555–565.

Powis, S.J., Deverson, E.V., Coadweil, W.J., Ciruela, A., Huskisson, N.S., Smith, H., Butcher, G.W., and Howard, J.C. (1992). Effect of polymorphism of an MHC-linked transporter on the peptides assembled in a class I molecule. Nature *357*, 211–215.

Powis, S.J., Young, L.L., Joly, E., Barker, P.J., Richardson, L., Brandt, R.P., Melief, C.J., Howard, J.C., and Butcher, G.W. (1996). The rat cim effect: TAP allele-dependent changes in a class I MHC anchor motif and evidence against C-terminal trimming of peptides in the ER. Immunity *4*, 159–165.

Preston, C.M., Frame, M.C., and Campbell, M.E.M. (1988). A complex formed between cell components and an HSV structural polypeptide binds to a viral immediate early gene regulatory DNA sequence. Cell *52*, 425–434.

Price, R.W., and Schmitz, J. (1978). Reactivation of latent herpes simplex virus infection of the autonomic nervous system by postganglionic neurectomy. Infect. Immun. *19*, 523–532.

Proença, J.T., Coleman, H.M., Connor, V., Winton, D.J., and Efstathiou, S. (2008). A historical analysis of herpes simplex virus promoter activation in vivo reveals distinct populations of latently infected neurones. J. Gen. Virol. *89*, 2965–2974.

Proença, J.T., Coleman, H.M., Nicoll, M.P., Connor, V., Preston, C.M., Arthur, J., and Efstathiou, S. (2011). An investigation of herpes simplex virus promoter activity compatible with latency establishment reveals VP16-independent activation of immediate-early promoters in sensory neurones. J. Gen. Virol. *92*, 2575–2585.

Proença, J.T., Nelson, D., Nicoll, M.P., Connor, V., and Efstathiou, S. (2016). Analyses of herpes simplex virus type 1 latency and reactivation at the single cell level using fluorescent reporter mice. J. Gen. Virol. *97*, 767–777.

Purbhoo, M.A., Irvine, D.J., Huppa, J.B., and Davis, M.M. (2004). T cell killing does not require the formation of a stable mature immunological synapse. Nat. Immunol. *5*, 524–530.

Radosevich, T.J., Seregina, T., and Link, C.J. (2003). Effective suppression of class I major histocompatibility complex expression by the US11 or ICP47 genes can be limited by cell type or interferon-gamma exposure. Hum. Gene Ther. *14*, 1765–1775.

Rajasagi, N.K., Kassim, S.H., Kollias, C.M., Zhao, X., Chervenak, R., and Jennings, S.R. (2009). CD4+ T Cells Are Required for the Priming of CD8+ T Cells following Infection with Herpes Simplex Virus Type 1. J. Virol. *83*, 5256–5268.

Rajcáni, J., Andrea, V., and Ingeborg, R. (2004). Peculiarities of herpes simplex virus (HSV) transcription: an overview. Virus Genes *28*, 293–310.

Ramchandani, M., Kong, M., Tronstein, E., Selke, S., Mikhaylova, A., Magaret, A., Huang, M.-L., Johnston, C., Corey, L., and Wald, A. (2016). Herpes simplex virus type 1 shedding in tears and nasal and oral mucosa of healthy adults. Sex. Transm. Dis. *43*, 756–760.

Ramirez, M.C., and Sigal, L.J. (2002). Macrophages and dendritic cells use the cytosolic pathway to rapidly cross-present antigen from live, vaccinia-infected cells. J. Immunol. Baltim. Md 1950 *169*, 6733–6742.

Ran, F.A., Hsu, P.D., Wright, J., Agarwala, V., Scott, D.A., and Zhang, F. (2013). Genome engineering using the CRISPR-Cas9 system. Nat. Protoc. *8*, 2281–2308.

Raymon, H.K., Thode, S., Zhou, J., Friedman, G.C., Pardinas, J.R., Barrere, C., Johnson, R.M., and Sah, D.W. (1999). Immortalized human dorsal root ganglion cells differentiate into neurons with nociceptive properties. J. Neurosci. Off. J. Soc. Neurosci. *19*, 5420–5428.

Redwine, J.M., Buchmeier, M.J., and Evans, C.F. (2001). In vivo expression of major histocompatibility complex molecules on oligodendrocytes and neurons during viral infection. Am. J. Pathol. *159*, 1219–1224.

Reinhardt, R.L., Khoruts, A., Merica, R., Zell, T., and Jenkins, M.K. (2001). Visualizing the generation of memory CD4 T cells in the whole body. Nature *410*, 101–105.

Reinherz, E.L., Tan, K., Tang, L., Kern, P., Liu, J., Xiong, Y., Hussey, R.E., Smolyar, A., Hare, B., Zhang, R., et al. (1999). The crystal structure of a T cell receptor in complex with peptide and MHC class II. Science *286*, 1913–1921.

Reits, E.A.J., Vos, J.C., Grommé, M., and Neefjes, J. (2000). The major substrates for TAP in vivo are derived from newly synthesized proteins. Nature *404*, 774–778.

Ritz, U., Momburg, F., Pircher, H.-P., Strand, D., Huber, C., and Seliger, B. (2001). Identification of sequences in the human peptide transporter subunit TAP1 required for transporter associated with antigen processing (TAP) function. Int. Immunol. *13*, 31–41.

Rock, K.L., and Goldberg, A.L. (1999). Degradation of cell proteins and the generation of MHC class I-presented peptides. Annu. Rev. Immunol. *17*, 739–779.

Rock, K.L., and Shen, L. (2005). Cross-presentation: underlying mechanisms and role in immune surveillance. Immunol. Rev. *207*, 166–183.

Roitt, I.M., Greaves, M.F., Torrigiani, G., Brostoff, J., and Playfair, J.H. (1969). The cellular basis of immunological responses. A synthesis of some current views. Lancet Lond. Engl. *2*, 367–371.

Roizman, B. (2011). The Checkpoints of Viral Gene Expression in Productive and Latent Infection: the Role of the HDAC/CoREST/LSD1/REST Repressor Complex. J. Virol. *85*, 7474–7482.

Roizman, B., Kristie, T., McKnight, J.L., Michael, N., Mavromara-Nazos, P., and Spector, D. (1988). The trans-activation of herpes simplex virus gene expression: comparison of two factors and their cis sites. Biochimie *70*, 1031–1043.

Rowe, A.M., St. Leger, A.J., Jeon, S., Dhaliwal, D.K., Knickelbein, J.E., and Hendricks, R.L. (2013). Herpes keratitis. Prog. Retin. Eye Res. *32*, 88–101.

Rudolph, M.G., Stanfield, R.L., and Wilson, I.A. (2006). How TCRs bind MHCs, peptides, and coreceptors. Annu. Rev. Immunol. *24*, 419–466.

Russell, T.A. (2015). Herpes Simplex Virus type 1 lytic viral gene expression during the establishment and maintenance of latency.

Russell, W.C. (1962). A sensitive and precise plaque assay for herpes virus. Nature *195*, 1028–1029.

Russell, T.A., and Tscharke, D.C. (2016). Lytic promoters express protein during herpes simplex virus latency. PLOS Pathog *12*, e1005729.

Russell, T.A., Stefanovic, T., and Tscharke, D.C. (2015). Engineering herpes simplex viruses by infection-transfection methods including recombination site targeting by CRISPR/Cas9 nucleases. J. Virol. Methods *213*, 18–25.

Ryan, S.O., and Cobb, B.A. (2012). Roles for major histocompatibility complex glycosylation in immune function. Semin. Immunopathol. *34*, 425–441.

Ryser, J.E., and Vassalli, P. (1974). Mouse bone marrow lymphocytes and their differentiation. J. Immunol. Baltim. Md 1950 *113*, 719–728.

Sadasivan, B., Lehner, P.J., Ortmann, B., Spies, T., and Cresswell, P. (1996). Roles for calreticulin and a novel glycoprotein, tapasin, in the interaction of MHC class I molecules with TAP. Immunity *5*, 103–114.

Sadowski, I., Ma, J., Triezenberg, S., and Ptashne, M. (1988). GAL4-VP16 is an unusually potent transcriptional activator. Nature *335*, 563–564.

Sakaguchi, S., Sakaguchi, N., Asano, M., Itoh, M., and Toda, M. (1995). Immunologic self-tolerance maintained by activated T cells expressing IL-2 receptor alpha-chains (CD25). Breakdown of a single mechanism of self-tolerance causes various autoimmune diseases. J. Immunol. Baltim. Md 1950 *155*, 1151–1164.

de la Salle, H., Hanau, D., Fricker, D., Urlacher, A., Kelly, A., Salamero, J., Powis, S.H., Donato, L., Bausinger, H., and Laforet, M. (1994). Homozygous human TAP peptide transporter mutation in HLA class I deficiency. Science *265*, 237–241.

de la Salle, H., Houssaint, E., Peyrat, M.A., Arnold, D., Salamero, J., Pinczon, D., Stevanovic, S., Bausinger, H., Fricker, D., Gomard, E., et al. (1997). Human peptide transporter deficiency: importance of HLA-B in the presentation of TAP-independent EBV antigens. J. Immunol. Baltim. Md 1950 *158*, 4555–4563.

de la Salle, H., Zimmer, J., Fricker, D., Angenieux, C., Cazenave, J.-P., Okubo, M., Maeda, H., Plebani, A., Tongio, M.-M., Dormoy, A., et al. (1999). HLA class I deficiencies due to mutations in subunit 1 of the peptide transporter TAP1. J. Clin. Invest. *103*, R9–R13.

de la Salle, H., Saulquin, X., Mansour, I., Klaymé, S., Fricker, D., Zimmer, J., Cazenave, J.-P., Hanau, D., Bonneville, M., Houssaint, E., et al. (2002). Asymptomatic deficiency in the peptide transporter associated to antigen processing (TAP). Clin. Exp. Immunol. *128*, 525–531.

Sallusto, F., Lenig, D., Förster, R., Lipp, M., and Lanzavecchia, A. (1999). Two subsets of memory T lymphocytes with distinct homing potentials and effector functions. Nature *401*, 708–712.

Salvucci, L.A., Bonneau, R.H., and Tevethia, S.S. (1995). Polymorphism within the herpes simplex virus (HSV) ribonucleotide reductase large subunit (ICP6) confers type specificity for recognition by HSV type 1-specific cytotoxic T lymphocytes. J. Virol. *69*, 1122–1131.

Sato, A., and Iwasaki, A. (2004). Induction of antiviral immunity requires Toll-like receptor signaling in both stromal and dendritic cell compartments. Proc. Natl. Acad. Sci. U. S. A. *101*, 16274–16279.

Sato, A., Linehan, M.M., and Iwasaki, A. (2006). Dual recognition of herpes simplex viruses by TLR2 and TLR9 in dendritic cells. Proc. Natl. Acad. Sci. U. S. A. *103*, 17343–17348.

Sauer, C., Syvertsson, S., Bohorquez, L.C., Cruz, R., Harwood, C.R., van Rij, T., and Hamoen, L.W. (2016). Effect of genome position on heterologous gene expression in Bacillus subtilis : An unbiased analysis. ACS Synth. Biol. *5*, 942–947.

Sawtell, N.M. (1997). Comprehensive quantification of herpes simplex virus latency at the single-cell level. J. Virol. *71*, 5423–5431.

Sawtell, N.M., and Thompson, R.L. (1992). Rapid in vivo reactivation of herpes simplex virus in latently infected murine ganglionic neurons after transient hyperthermia. J. Virol. *66*, 2150–2156.

Sawtell, N.M., and Thompson, R.L. (2004). Comparison of herpes simplex virus reactivation in ganglia in vivo and in explants demonstrates quantitative and qualitative differences. J. Virol. *78*, 7784–7794.

Schaerli, P., Willimann, K., Lang, A.B., Lipp, M., Loetscher, P., and Moser, B. (2000). CXC chemokine receptor 5 expression defines follicular homing T cells with B cell helper function. J. Exp. Med. *192*, 1553–1562.

Schiffer, J.T., and Corey, L. (2013). Rapid host immune response and viral dynamics in herpes simplex virus-2 infection. Nat. Med. *19*, 280–288.

Schiffer, J.T., Abu-Raddad, L., Mark, K.E., Zhu, J., Selke, S., Magaret, A., Wald, A., and Corey, L. (2009). Frequent release of low amounts of herpes simplex virus from neurons: Results of a mathematical model. Sci. Transl. Med. *1*, 7ra16-7ra16.

Schiffer, J.T., Abu-Raddad, L., Mark, K.E., Zhu, J., Selke, S., Koelle, D.M., Wald, A., and Corey, L. (2010). Mucosal host immune response predicts the severity and duration of herpes simplex virus-2 genital tract shedding episodes. Proc. Natl. Acad. Sci. *107*, 18973–18978.

Schiffer, J.T., Swan, D.A., Roychoudhury, P., Lund, J.M., Prlic, M., Zhu, J., Wald, A., and Corey, L. (2018). A Fixed Spatial Structure of CD8+ T Cells in Tissue during Chronic HSV-2 Infection. J. Immunol. *201*, 1522–1535.

Schilling, B., Rardin, M.J., MacLean, B.X., Zawadzka, A.M., Frewen, B.E., Cusack, M.P., Sorensen, D.J., Bereman, M.S., Jing, E., Wu, C.C., et al. (2012). Platform-independent and

label-free quantitation of proteomic data using MS1 extracted ion chromatograms in skyline: Application to protein acetylation and phosphorylation. Mol. Cell. Proteomics *11*, 202–214.

Schmitt, L., and Tampé, R. (2002). Structure and mechanism of ABC transporters. Curr. Opin. Struct. Biol. *12*, 754–760.

Schneider, K., Wronka-Edwards, L., Leggett-Embrey, M., Walker, E., Sun, P., Ondov, B., Wyman, T.H., Rosovitz, M.J., Bohn, S.S., Burans, J., et al. (2015). Psoralen inactivation of viruses: A process for the safe manipulation of viral antigen and nucleic acid. Viruses *7*, 5875–5888.

Schölz, C., and Tampé, R. (2005). The intracellular antigen transport machinery TAP in adaptive immunity and virus escape mechanisms. J. Bioenerg. Biomembr. *37*, 509–515.

Schumacher, T.N. (1994). Peptide length and sequence specificity of the mouse TAP1/TAP2 translocator. J. Exp. Med. *179*, 533–540.

Sciammas, R., Kodukula, P., Tang, Q., Hendricks, R.L., and Bluestone, J.A. (1997). T cell receptor–γ/δ cells protect mice from herpes simplex virus type 1–induced lethal encephalitis. J. Exp. Med. *185*, 1969–1975.

Scieux, C. (1997). [Herpes simplex virus and macrophages]. Pathol. Biol. (Paris) *45*, 159–164.

Scott, D.A., Coulter, W.A., and Lamey, P.-J. (1997). Oral shedding of herpes simplex virus type 1: a review. J. Oral Pathol. Med. *26*, 441–447.

Seliger, B., Harders, C., Lohmann, S., Momburg, F., Urlinger, S., Tampé, R., and Huber, C. (1998). Down-regulation of the MHC class I antigen-processing machinery after oncogenic transformation of murine fibroblasts. Eur. J. Immunol. *28*, 122–133.

Selling, B., and Kibrick, S. (1964). An outbreak of herpes simplex among wrestlers (Herpes gladiatorum). N. Engl. J. Med. *270*, 979–982.

Serwold, T., Gonzalez, F., Kim, J., Jacob, R., and Shastri, N. (2002). ERAAP customizes peptides for MHC class I molecules in the endoplasmic reticulum. Nature *419*, 480–483.

Sette, A., Vitiello, A., Reherman, B., Fowler, P., Nayersina, R., Kast, W.M., Melief, C.J., Oseroff, C., Yuan, L., Ruppert, J., et al. (1994). The relationship between class I binding affinity and immunogenicity of potential cytotoxic T cell epitopes. J. Immunol. Baltim. Md 1950 *153*, 5586–5592.

Seward, J., and Jumaan, A. (2007). VSV: persistence in the population (Cambridge University Press).

Seward, J.F., Watson, B.M., Peterson, C.L., Mascola, L., Pelosi, J.W., Zhang, J.X., Maupin, T.J., Goldman, G.S., Tabony, L.J., Brodovicz, K.G., et al. (2002). Varicella disease after introduction of varicella vaccine in the United States, 1995-2000. JAMA *287*, 606–611.

Shen, Z., Reznikoff, G., Dranoff, G., and Rock, K.L. (1997). Cloned dendritic cells can present exogenous antigens on both MHC class I and class II molecules. J. Immunol. Baltim. Md 1950 *158*, 2723–2730.

Sheridan, B.S., Cherpes, T.L., Urban, J., Kalinski, P., and Hendricks, R.L. (2009). Reevaluating the CD8 T-cell response to herpes simplex virus type 1: Involvement of CD8 T cells reactive to subdominant epitopes. J. Virol. *83*, 2237–2245.

Sheridan, S.L., Quinn, H.E., Hull, B.P., Ware, R.S., Grimwood, K., and Lambert, S.B. (2017). Impact and effectiveness of childhood varicella vaccine program in Queensland, Australia. Vaccine *35*, 3490–3497.

Sherwood, C.A., Eastham, A., Lee, L.W., Risler, J., Mirzaei, H., Falkner, J.A., and Martin, D.B. (2009). Rapid optimization of MRM-MS instrument parameters by subtle alteration of precursor and product m/z targets. J. Proteome Res. *8*, 3746–3751.

Shimeld, C. (1995). Immune cell infiltration and persistence in the mouse trigeminal ganglion after infection of the cornea with herpes simplex virus type 1. J. Neuroimmunol. *61*, 7–16.

Shimeld, C., Hill, T.J., Blyth, W.A., and Easty, D.L. (1990a). Passive immunization protects the mouse eye from damage after herpes simplex virus infection by limiting spread of virus in the nervous system. J. Gen. Virol. *71 (Pt 3)*, 681–687.

Shimeld, C., Hill, T.J., Blyth, W.A., and Easty, D.L. (1990b). Reactivation of latent infection and induction of recurrent herpetic eye disease in mice. J. Gen. Virol. *71 (Pt 2)*, 397–404.

Shimeld, C., Whiteland, J.L., Williams, N.A., Easty, D.L., and Hill, T.J. (1996a). Reactivation of herpes simplex virus type 1 in the mouse trigeminal ganglion: an in vivo study of virus antigen and immune cell infiltration. J. Gen. Virol. *77*, 2583–2590.

Shimeld, C., Whiteland, J.L., Nicholls, S.M., Easty, D.L., and Hill, T.J. (1996b). Immune cell infiltration in corneas of mice with recurrent herpes simplex virus disease. J. Gen. Virol. *77*, 977–985.

Shrestha, B., and Diamond, M.S. (2004). Role of CD8+ T cells in control of West Nile virus infection. J. Virol. *78*, 8312–8321.

Shrestha, B., Samuel, M.A., and Diamond, M.S. (2006). CD8+ T cells require perforin to clear West Nile virus from infected neurons. J. Virol. *80*, 119–129.

Simmons, A. (1989). H-2-linked genes influence the severity of herpes simplex virus infection of the peripheral nervous system. J. Exp. Med. *169*, 1503–1507.

Simmons, A. (2002). Clinical manifestations and treatment considerations of herpes simplex virus infection. J. Infect. Dis. *186 Suppl 1*, S71-77.

Simmons, D.L. (1995). The role of ICAM expression in immunity and disease. Cancer Surv. *24*, 141–155.

Simmons, A., and La Vista, A.B. (1989). Neural infection in mice after cutaneous inoculation with HSV-1 is under complex host genetic control. Virus Res. *13*, 263–270.

Simmons, A., and Nash, A.A. (1984). Zosteriform spread of herpes simplex virus as a model of recrudescence and its use to investigate the role of immune cells in prevention of recurrent disease. J. Virol. *52*, 816–821.

Simmons, A., and Nash, A.A. (1985). Role of antibody in primary and recurrent herpes simplex virus infection. J. Virol. *53*, 944–948.

Simmons, A., and Tscharke, D.C. (1992). Anti-CD8 impairs clearance of herpes simplex virus from the nervous system: implications for the fate of virally infected neurons. J. Exp. Med. *175*, 1337–1344.

Simmons, A., Tscharke, D., and Speck, P. (1992a). The role of immune mechanisms in control of herpes simplex virus infection of the peripheral nervous system. Curr. Top. Microbiol. Immunol. *179*, 31–56.

Simmons, A., Slobedman, B., Speck, P., Arthur, J., and Efstathiou, S. (1992b). Two patterns of persistence of herpes simplex virus DNA sequences in the nervous systems of latently infected mice. J. Gen. Virol. *73*, 1287–1291.

Slifka, M.K., Rodriguez, F., and Whitton, J.L. (1999). Rapid on/off cycling of cytokine production by virus-specific CD8+ T cells. Nature *401*, 76–79.

Sloan, D.D., Han, J.-Y., Sandifer, T.K., Stewart, M., Hinz, A.J., Yoon, M., Johnson, D.C., Spear, P.G., and Jerome, K.R. (2006). Inhibition of TCR signaling by herpes simplex virus. J. Immunol. Baltim. Md 1950 *176*, 1825–1833.

Smiley, J.R. (2004). Herpes simplex virus virion host shutoff protein: Immune evasion mediated by a viral RNase? J. Virol. *78*, 1063–1068.

Smith, C.M., Wilson, N.S., Waithman, J., Villadangos, J.A., Carbone, F.R., Heath, W.R., and Belz, G.T. (2004). Cognate CD4(+) T cell licensing of dendritic cells in CD8(+) T cell immunity. Nat. Immunol. *5*, 1143–1148.

Smith, P.M., Wolcott, R.M., Chervenak, R., and Jennings, S.R. (1994). Control of acute cutaneous herpes simplex virus infection: T cell-mediated viral clearance is dependent upon interferon-gamma (IFN-gamma). Virology *202*, 76–88.

Smith-Garvin, J.E., Koretzky, G.A., and Jordan, M.S. (2009). T cell activation. Annu. Rev. Immunol. *27*, 591–619.

Smyth, M.J., Cretney, E., Kelly, J.M., Westwood, J.A., Street, S.E.A., Yagita, H., Takeda, K., Dommelen, S.L.H. van, Degli-Esposti, M.A., and Hayakawa, Y. (2005). Activation of NK cell cytotoxicity. Mol. Immunol. *42*, 501–510.

Snyder, H.L., Bačík, I., Bennink, J.R., Kearns, G., Behrens, T.W., Bächi, T., Orlowski, M., and Yewdell, J.W. (1997). Two Novel Routes of Transporter Associated with Antigen Processing (TAP)-independent Major Histocompatibility Complex Class I Antigen Processing. J. Exp. Med. *186*, 1087–1098.

Soriano, P. (1999). Generalized lacZ expression with the ROSA26 Cre reporter strain. Nat. Genet. *21*, 70–71.

Speck, P., and Simmons, A. (1998). Precipitous clearance of herpes simplex virus antigens from the peripheral nervous systems of experimentally infected C57BL/10 mice. J. Gen. Virol. *79*, 561–564.

Speck, P.G., and Simmons, A. (1991). Divergent molecular pathways of productive and latent infection with a virulent strain of herpes simplex virus type 1. J. Virol. *65*, 4001–4005.

Spiliotis, E.T., Manley, H., Osorio, M., Zúñiga, M.C., and Edidin, M. (2000). Selective export of MHC class I molecules from the ER after their dissociation from TAP. Immunity *13*, 841–851.

Spivack, J.G., and Fraser, N.W. (1987). Detection of herpes simplex virus type 1 transcripts during latent infection in mice. J. Virol. *61*, 3841–3847.

Spivack, J.G., Woods, G.M., and Fraser, N.W. (1991). Identification of a novel latency-specific splice donor signal within the herpes simplex virus type 1 2.0-kilobase latency-associated transcript (LAT): translation inhibition of LAT open reading frames by the intron within the 2.0-kilobase LAT. J. Virol. *65*, 6800–6810.

Sprecher, E., and Becker, Y. (1987). Herpes simplex virus type 1 pathogenicity in footpad and ear skin of mice depends on Langerhans cell density, mouse genetics, and virus strain. J. Virol. *61*, 2515–2522.

Sprecher, E., and Becker, Y. (1989). Langerhans cell density and activity in mouse skin and lymph nodes affect herpes simplex type 1 (HSV-1) pathogenicity. Arch. Virol. *107*, 191–205.

Spruance, S.L. (1984). Pathogenesis of herpes simplex labialis: excretion of virus in the oral cavity. J. Clin. Microbiol. *19*, 675–679.

Srivastava, R., Khan, A.A., Spencer, D., Vahed, H., Lopes, P.P., Thai, N.T.U., Wang, C., Pham, T.T., Huang, J., Scarfone, V.M., et al. (2015). HLA-A02:01–restricted epitopes identified from the herpes simplex virus tegument protein VP11/12 preferentially recall polyfunctional effector memory CD8+ T cells from seropositive asymptomatic individuals and protect humanized HLA-A*02:01 transgenic mice against ocular herpes. J. Immunol. *194*, 2232–2248.

St Leger, A.J., Peters, B., Sidney, J., Sette, A., and Hendricks, R.L. (2011). Defining the herpes simplex virus-specific CD8+ T cell repertoire in C57BL/6 mice. J. Immunol. *186*, 3927–3933.

St Leger, A.J., Jeon, S., and Hendricks, R.L. (2013). Broadening the repertoire of functional herpes simplex virus type 1-specific CD8+ T cells reduces viral reactivation from latency in sensory ganglia. J. Immunol. Baltim. Md 1950 *191*, 2258–2265.

Stanberry, L.R., Cunningham, A.L., Mindel, A., Scott, L.L., Spruance, S.L., Aoki, F.Y., and Lacey, C.J. (2000). Prospects for control of herpes simplex virus disease through immunization. Clin. Infect. Dis. *30*, 549–566.

Staunton, D.E., Dustin, M.L., and Springer, T.A. (1989). Functional cloning of ICAM-2, a cell adhesion ligand for LFA-1 homologous to ICAM-1. Nature *339*, 61–64.

Steiner, I., Spivack, J.G., Lirette, R.P., Brown, S.M., MacLean, A.R., Subak-Sharpe, J.H., and Fraser, N.W. (1989). Herpes simplex virus type 1 latency-associated transcripts are evidently not essential for latent infection. EMBO J. *8*, 505–511.

Steiner, I., Spivack, J.G., Deshmane, S.L., Ace, C.I., Preston, C.M., and Fraser, N.W. (1990). A herpes simplex virus type 1 mutant containing a nontransinducing Vmw65 protein establishes latent infection in vivo in the absence of viral replication and reactivates efficiently from explanted trigeminal ganglia. J. Virol. *64*, 1630–1638.

Stetson, D.B., and Medzhitov, R. (2006). Type I interferons in host defense. Immunity *25*, 373–381.

Stevens, J.G., and Cook, M.L. (1971a). Restriction of herpes simplex virus by macrophages an analysis of the cell-virus interaction. J. Exp. Med. *133*, 19–38.

Stevens, J.G., and Cook, M.L. (1971b). Latent herpes simplex virus in spinal ganglia of mice. Science *173*, 843–845.

Stevens, J., Wagner, E., Devi-Rao, G., Cook, M., and Feldman, L. (1987a). RNA complementary to a herpesvirus alpha gene mRNA is prominent in latently infected neurons. Science *235*, 1056–1059.

Stevens, J.G., Wagner, E.K., Devi-Rao, G.B., Cook, M.L., and Feldman, L.T. (1987b). RNA complementary to a herpesvirus alpha gene mRNA is prominent in latently infected neurons. Science *235*, 1056–1059.

Stoopler, E.T., Pinto, A., DeRossi, S.S., and Sollecito, T.P. (2003). Herpes simplex and varicella-zoster infections: clinical and laboratory diagnosis. Gen. Dent. *51*, 281–286; quiz 287.

Storkus, W.J., Howell, D.N., Salter, R.D., Dawson, J.R., and Cresswell, P. (1987). NK susceptibility varies inversely with target cell class I HLA antigen expression. J. Immunol. Baltim. Md 1950 *138*, 1657–1659.

Stow, N.D. (1982). Localization of an origin of DNA replication within the TRS/IRS repeated region of the herpes simplex virus type 1 genome. EMBO J. *1*, 863–867.

Strang, B.L., and Stow, N.D. (2005). Circularization of the herpes simplex virus type 1 genome upon lytic infection. J. Virol. *79*, 12487–12494.

Stulting, R.D., Kindle, J.C., and Nahmias, A.J. (1985). Patterns of herpes simplex keratitis in inbred mice. Invest. Ophthalmol. Vis. Sci. *26*, 1360–1367.

Su, C., and Zheng, C. (2017). Herpes simplex virus 1 abrogates the cGAS/STING-mediated cytosolic dna-sensing pathway via its virion host shutoff protein, UL41. J. Virol. *91*.

Su, R.-C., and Miller, R.G. (2001). Stability of surface H-2Kb, H-2Db, and peptide-receptive H-2Kb on splenocytes. J. Immunol. *167*, 4869–4877.

Su, C., Zhan, G., and Zheng, C. (2016). Evasion of host antiviral innate immunity by HSV-1, an update. Virol. J. *13*, 38.

Summers, B.C., and Leib, D.A. (2002). Herpes simplex virus type 1 origins of DNA replication play no role in the regulation of flanking promoters. J. Virol. *76*, 7020–7029.

Sykulev, Y., Joo, M., Vturina, I., Tsomides, T.J., and Eisen, H.N. (1996). Evidence that a single peptide–MHC complex on a target cell can elicit a cytolytic T cell response. Immunity *4*, 565–571.

Szymczak, A.L., Workman, C.J., Wang, Y., Vignali, K.M., Dilioglou, S., Vanin, E.F., and Vignali, D.A.A. (2004). Correction of multi-gene deficiency in vivo using a single "self-cleaving" 2A peptide–based retroviral vector. Nat. Biotechnol. *22*, 589–594.

Takaoka, A., Wang, Z., Choi, M.K., Yanai, H., Negishi, H., Ban, T., Lu, Y., Miyagishi, M., Kodama, T., Honda, K., et al. (2007). DAI (DLM-1/ZBP1) is a cytosolic DNA sensor and an activator of innate immune response. Nat. Lond. *448*, 501–505.

Tal-Singer, R., Lasner, T.M., Podrzucki, W., Skokotas, A., Leary, J.J., Berger, S.L., and Fraser, N.W. (1997). Gene expression during reactivation of herpes simplex virus type 1 from latency in the peripheral nervous system is different from that during lytic infection of tissue cultures. J. Virol. *71*, 5268–5276.

Tal-Singer, R., Pichyangkura, R., Chung, E., Lasner, T.M., Randazzo, B.P., Trojanowski, J.Q., Fraser, N.W., and Triezenberg, S.J. (1999). The Transcriptional Activation Domain of VP16 Is Required for Efficient Infection and Establishment of Latency by HSV-1 in the Murine Peripheral and Central Nervous Systems. Virology *259*, 20–33.

Tanaka, M., Kagawa, H., Yamanashi, Y., Sata, T., and Kawaguchi, Y. (2003). Construction of an excisable bacterial artificial chromosome containing a full-length infectious clone of herpes simplex virus type 1: viruses reconstituted from the clone exhibit wild-type properties in vitro and in vivo. J. Virol. *77*, 1382–1391.

Tanaka, M., Kodaira, H., Nishiyama, Y., Sata, T., and Kawaguchi, Y. (2004). Construction of recombinant herpes simplex virus type I expressing green fluorescent protein without loss of any viral genes. Microbes Infect. *6*, 485–493.

Tang, S., Bertke, A.S., Patel, A., Wang, K., Cohen, J.I., and Krause, P.R. (2008). An acutely and latently expressed herpes simplex virus 2 viral microRNA inhibits expression of ICP34.5, a viral neurovirulence factor. Proc. Natl. Acad. Sci. U. S. A. *105*, 10931–10936.

Tang, S., Patel, A., and Krause, P.R. (2009). Novel less-abundant viral microRNAs encoded by herpes simplex virus 2 latency-associated transcript and their roles in regulating ICP34.5 and ICP0 mRNAs. J. Virol. *83*, 1433–1442.

Tatarowicz, W.A., Martin, C.E., Pekosz, A.S., Madden, S.L., Rauscher, F.J., Chiang, S.Y., Beerman, T.A., and Fraser, N.W. (1997). Repression of the HSV-1 latency-associated transcript (LAT) promoter by the early growth response (EGR) proteins: involvement of a binding site immediately downstream of the TATA box. J. Neurovirol. *3*, 212–224.

Taylor, J.M., Lin, E., Susmarski, N., Yoon, M., Zago, A., Ware, C.F., Pfeffer, K., Miyoshi, J., Takai, Y., and Spear, P.G. (2007). Alternative entry receptors for herpes simplex virus and their roles in disease. Cell Host Microbe *2*, 19–28.

Tchasovnikarova, I.A., Timms, R.T., Matheson, N.J., Wals, K., Antrobus, R., Gottgens, B., Dougan, G., Dawson, M.A., and Lehner, P.J. (2015). Epigenetic silencing by the HUSH complex mediates position-effect variegation in human cells. Science *348*, 1481–1485.

Tempera, I., Klichinsky, M., and Lieberman, P.M. (2011). EBV latency types adopt alternative chromatin conformations. PLoS Pathog. *7*, e1002180.

Ternette, N., Yang, H., Partridge, T., Llano, A., Cedeño, S., Fischer, R., Charles, P.D., Dudek, N.L., Mothe, B., Crespo, M., et al. (2016). Defining the HLA class I-associated viral antigen repertoire from HIV-1-infected human cells: Antigen processing. Eur. J. Immunol. *46*, 60–69.

Tey, S.-K., and Khanna, R. (2012a). Host immune system strikes back: Autophagy-mediated antigen presentation bypasses viral blockade of the classic MHC class I processing pathway. Autophagy *8*, 1839–1841.

Tey, S.-K., and Khanna, R. (2012b). Autophagy mediates transporter associated with antigen processing-independent presentation of viral epitopes through MHC class I pathway. Blood *120*, 994–1004.

Thaiss, C.A., Semmling, V., Franken, L., Wagner, H., and Kurts, C. (2011). Chemokines: A new dendritic cell signal for T cell activation. Front. Immunol. *2*.

Thammavongsa, V., Raghuraman, G., Filzen, T.M., Collins, K.L., and Raghavan, M. (2006). HLA-B44 polymorphisms at position 116 of the heavy chain influence TAP complex binding via an effect on peptide occupancy. J. Immunol. Baltim. Md 1950 *177*, 3150–3161.

Thapa, M., Welner, R.S., Pelayo, R., and Carr, D.J.J. (2008). CXCL9 and CXCL10 expression are critical for control of genital herpes simplex virus type 2 infection through mobilization of HSV-specific CTL and NK cells to the nervous system. J. Immunol. Baltim. Md 1950 *180*, 1098–1106.

Theil, D., Derfuss, T., Paripovic, I., Herberger, S., Meinl, E., Schueler, O., Strupp, M., Arbusow, V., and Brandt, T. (2003). Latent herpesvirus infection in human trigeminal ganglia causes chronic immune response. Am. J. Pathol. *163*, 2179–2184.

Thellman, N.M., Botting, C., Madaj, Z., and Triezenberg, S.J. (2017). An immortalized human dorsal root ganglia cell line provides a novel context to study herpes simplex virus type-1 latency and reactivation. J. Virol. JVI.00080-17.

Thomas, G. (2002). Furin at the cutting edge: from protein traffic to embryogenesis and disease. Nat. Rev. Mol. Cell Biol. *3*, 753–766.

Thomas, J., Gangappa, S., Kanangat, S., and Rouse, B.T. (1997). On the essential involvement of neutrophils in the immunopathologic disease: herpetic stromal keratitis. J. Immunol. *158*, 1383–1391.

Thompson, R.L., and Sawtell, N.M. (2006). Evidence that the herpes simplex virus type 1 ICP0 protein does not initiate reactivation from latency in vivo. J. Virol. *80*, 10919–10930.

Thompson, R.L., Cook, M.L., Devi-Rao, G.B., Wagner, E.K., and Stevens, J.G. (1986). Functional and molecular analyses of the avirulent wild-type herpes simplex virus type 1 strain KOS. J. Virol. *58*, 203–211.

Thompson, R.L., Preston, C.M., and Sawtell, N.M. (2009). De novo synthesis of VP16 coordinates the exit from HSV latency in vivo. PLoS Pathog. *5*, e1000352.

Ting, J.P.-Y., Lovering, R.C., Alnemri, E.S., Bertin, J., Boss, J.M., Davis, B.K., Flavell, R.A., Girardin, S.E., Godzik, A., Harton, J.A., et al. (2008). The NLR gene family: a standard nomenclature. Immunity *28*, 285–287.

Tomazin, R., Hill, A.B., Jugovic, P., York, I., van Endert, P., Ploegh, H.L., Andrews, D.W., and Johnson, D.C. (1996). Stable binding of the herpes simplex virus ICP47 protein to the peptide binding site of TAP. EMBO J. *15*, 3256–3266.

Tomazin, R., van Schoot, N.E.G., Goldsmith, K., Jugovic, P., Sempé, P., Früh, K., and Johnson, D.C. (1998). Herpes simplex virus type 2 ICP47 inhibits human TAP but not mouse TAP. J. Virol. *72*, 2560–2563.

Tony, H.P., and Parker, D.C. (1985). Major histocompatibility complex-restricted, polyclonal B cell responses resulting from helper T cell recognition of antiimmunoglobulin presented by small B lymphocytes. J. Exp. Med. *161*, 223–241.

Townsend, A., and Bodmer, H. (1989). Antigen recognition by class I-restricted T lymphocytes. Annu. Rev. Immunol. *7*, 601–624.

Townsend, A., and Trowsdale, J. (1993). The transporters associated with antigen presentation. Semin. Cell Biol. *4*, 53–61.

Townsend, A., Öhlén, C., Bastin, J., Ljunggren, H.-G., Foster, L., and Kärre, K. (1989). Association of class I major histocompatibility heavy and light chains induced by viral peptides. Nature *340*, 443–448.

Trapani, J.A. (2001). Granzymes: a family of lymphocyte granule serine proteases. Genome Biol. *2*, REVIEWS3014.

Trapani, J.A., and Smyth, M.J. (2002). Functional significance of the perforin/granzyme cell death pathway. Nat. Rev. Immunol. Lond. *2*, 735–747.

Treat, B.R., Bidula, S.M., Ramachandran, S., St Leger, A.J., Hendricks, R.L., and Kinchington, P.R. (2017). Influence of an immunodominant herpes simplex virus type 1 CD8+ T cell epitope on the target hierarchy and function of subdominant CD8+ T cells. PLOS Pathog. *13*, e1006732.

Triezenberg, S.J., LaMarco, K.L., and McKnight, S.L. (1988). Evidence of DNA: protein interactions that mediate HSV-1 immediate early gene activation by VP16. Genes Amp Dev. *2*, 730–742.

Tronstein, E., Johnston, C., Huang, M.-L., Selke, S., Magaret, A., Warren, T., Corey, L., and Wald, A. (2011). Genital shedding of herpes simplex virus among symptomatic and asymptomatic persons with HSV-2 infection. JAMA *305*, 1441–1449.

Trung, N.H.D., Phuong, T.L.T., Wolbers, M., Minh, H.N.V., Thanh, V.N., Van, M.P., Thieu, N.T.V., Van, T.L., Song, D.T., Thi, P.L., et al. (2012). Aetiologies of central nervous system infection in Viet Nam: A prospective provincial hospital-based descriptive surveillance study. PLOS ONE *7*, e37825.

Tscharke, D.C., Karupiah, G., Zhou, J., Palmore, T., Irvine, K.R., Haeryfar, S.M.M., Williams, S., Sidney, J., Sette, A., Bennink, J.R., et al. (2005). Identification of poxvirus

CD8+ T cell determinants to enable rational design and characterization of smallpox vaccines. J. Exp. Med. *201*, 95–104.

Tullo, A.B., Shimeld, C., Blyth, W.A., Hill, T.J., and Easty, D.L. (1982). Spread of virus and distribution of latent infection following ocular herpes simplex in the non-immune and immune mouse. J. Gen. Virol. *63*, 95–101.

Tyler, C.M., and Boulanger, L.M. (2014). New roles for MHC class I immune molecules in the healthy and diseased nervous system. In ELS, John Wiley & Sons Ltd, ed. (Chichester, UK: John Wiley & Sons, Ltd), p.

Tynan, F.E., Borg, N.A., Miles, J.J., Beddoe, T., El-Hassen, D., Silins, S.L., van Zuylen, W.J.M., Purcell, A.W., Kjer-Nielsen, L., McCluskey, J., et al. (2005). High resolution structures of highly bulged viral epitopes bound to major histocompatibility complex class I. Implications for T-cell receptor engagement and T-cell immunodominance. J. Biol. Chem. *280*, 23900–23909.

Uebel, S., Kraas, W., Kienle, S., Wiesmuller, K.-H., Jung, G., and Tampe, R. (1997). Recognition principle of the TAP transporter disclosed by combinatorial peptide libraries. Proc. Natl. Acad. Sci. *94*, 8976–8981.

Umbach, J.L., Kramer, M.F., Jurak, I., Karnowski, H.W., Coen, D.M., and Cullen, B.R. (2008). MicroRNAs expressed by herpes simplex virus 1 during latent infection regulate viral mRNAs. Nature *454*, 780–783.

Unanue, E.R. (1984). Antigen-presenting function of the macrophage. Annu. Rev. Immunol. *2*, 395–428.

Urban, R.G., Chicz, R.M., Lane, W.S., Strominger, J.L., Rehm, A., Kenter, M.J., UytdeHaag, F.G., Ploegh, H., Uchanska-Ziegler, B., and Ziegler, A. (1994). A subset of HLA-B27 molecules contains peptides much longer than nonamers. Proc. Natl. Acad. Sci. U. S. A. *91*, 1534–1538.

Ureta-Vidal, A., Firat, H., Pérarnau, B., and Lemonnier, F.A. (1999). Phenotypical and functional characterization of the CD8+ T cell repertoire of HLA-A2.1 transgenic, H-2KbnullDbnull double knockout mice. J. Immunol. Baltim. Md 1950 *163*, 2555–2560.

Utley, T.F., Ogden, J.A., Gibb, A., McGrath, N., and Anderson, N.E. (1997). The long-term neuropsychological outcome of herpes simplex encephalitis in a series of unselected survivors. Neuropsychiatry. Neuropsychol. Behav. Neurol. *10*, 180–189.

Valitutti, S., Müller, S., Cella, M., Padovan, E., and Lanzavecchia, A. (1995). Serial triggering of many T-cell receptors by a few peptide–MHC complexes. Nature *375*, 148–151.

Varadkar, S., Bien, C.G., Kruse, C.A., Jensen, F.E., Bauer, J., Pardo, C.A., Vincent, A., Mathern, G.W., and Cross, J.H. (2014). Rasmussen's encephalitis: clinical features, pathobiology, and treatment advances. Lancet Neurol. *13*, 195–205.

van Velzen, M., Jing, L., Osterhaus, A.D.M.E., Sette, A., Koelle, D.M., and Verjans, G.M.G.M. (2013a). Local CD4 and CD8 T-cell reactivity to HSV-1 antigens documents

broad viral protein expression and immune competence in latently infected human trigeminal ganglia. PLoS Pathog *9*, e1003547.

van Velzen, M., Jing, L., Osterhaus, A.D.M.E., Sette, A., Koelle, D.M., and Verjans, G.M.G.M. (2013b). Local CD4 and CD8 T-cell reactivity to HSV-1 antigens documents broad viral protein expression and immune competence in latently infected human trigeminal ganglia. PLoS Pathog. *9*, e1003547.

Verjans, G.M.G.M., Hintzen, R.Q., Dun, J.M. van, Poot, A., Milikan, J.C., Laman, J.D., Langerak, A.W., Kinchington, P.R., and Osterhaus, A.D.M.E. (2007). Selective retention of herpes simplex virus-specific T cells in latently infected human trigeminal ganglia. Proc. Natl. Acad. Sci. *104*, 3496–3501.

Verweij, M.C., Horst, D., Griffin, B.D., Luteijn, R.D., Davison, A.J., Ressing, M.E., and Wiertz, E.J.H.J. (2015). Viral inhibition of the transporter associated with antigen processing (TAP): A striking example of functional convergent evolution. PLOS Pathog. *11*, e1004743.

Vigneron, N., Stroobant, V., Chapiro, J., Ooms, A., Degiovanni, G., Morel, S., van der Bruggen, P., Boon, T., and Van den Eynde, B.J. (2004). An antigenic peptide produced by peptide splicing in the proteasome. Science *304*, 587–590.

Vigneron, N., Ferrari, V., Van den Eynde, B.J., Cresswell, P., and Leonhardt, R.M. (2018). Cytosolic processing governs TAP-independent presentation of a critical melanoma antigen. J. Immunol. ji1701479.

Virolle, T., Krones-Herzig, A., Baron, V., De Gregorio, G., Adamson, E.D., and Mercola, D. (2003). Egr1 promotes growth and survival of prostate cancer cells: Identification of novel Egr1 target genes. J. Biol. Chem. *278*, 11802–11810.

Wadsworth, S., Jacob, R.J., and Roizman, B. (1975). Anatomy of herpes simplex virus DNA. II. Size, composition, and arrangement of inverted terminal repetitions. J. Virol. *15*, 1487–1497.

Wagner, E.K., and Bloom, D.C. (1997). Experimental investigation of herpes simplex virus latency. Clin. Microbiol. Rev. *10*, 419–443.

Wakim, L.M., Jones, C.M., Gebhardt, T., Preston, C.M., and Carbone, F.R. (2008). CD8+ T-cell attenuation of cutaneous herpes simplex virus infection reduces the average viral copy number of the ensuing latent infection. Immunol. Cell Biol. *86*, 666–675.

Wald, A., Corey, L., Cone, R., Hobson, A., Davis, G., and Zeh, J. (1997). Frequent genital herpes simplex virus 2 shedding in immunocompetent women. Effect of acyclovir treatment. J. Clin. Invest. *99*, 1092–1097.

Wald, A., Zeh, J., Selke, S., Warren, T., Ryncarz, A.J., Ashley, R., Krieger, J.N., and Corey, L. (2000). Reactivation of genital herpes simplex virus type 2 infection in asymptomatic seropositive persons. N. Engl. J. Med. *342*, 844–850.

Wallace, M.E., Keating, R., Heath, W.R., and Carbone, F.R. (1999). The cytotoxic T-cell response to herpes simplex virus type 1 infection of C57BL/6 mice is almost entirely directed against a single immunodominant determinant. J. Virol. *73*, 7619–7626.

Wallach, D., Fellous, M., and Revel, M. (1982). Preferential effect of gamma interferon on the synthesis of HLA antigens and their mRNAs in human cells. Nature *299*, 833–836.

Walz, J., Erdmann, A., Kania, M., Typke, D., Koster, A.J., and Baumeister, W. (1998). Proteasome structure revealed by three-dimensional electron microscopy. J. Struct. Biol. *121*, 19–29.

Walz, M.A., Price, R.W., and Notkins, A.L. (1974). Latent ganglionic infection with herpes simplex virus types 1 and 2: Viral reactivation in vivo after neurectomy. Science *184*, 1185–1187.

Walz, M.A., Yamamoto, H., and Notkins, A.L. (1976). Immunological response restricts number of cells in sensory ganglia infected with herpes simplex virus. Nature *264*, 554–556.

Wang, H., Davido, D.J., and Morrison, L.A. (2013a). HSV-1 strain McKrae is more neuroinvasive than HSV-1 KOS after corneal or vaginal inoculation in mice. Virus Res. *173*, 436–440.

Wang, H., Davido, D.J., and Morrison, L.A. (2013b). HSV-1 strain McKrae is more neuroinvasive than HSV-1 KOS after corneal or vaginal inoculation in mice. Virus Res. *173*, 436–440.

Wang, K., Goodman, K.N., Li, D.Y., Raffeld, M., Chavez, M., and Cohen, J.I. (2016). A herpes simplex virus 2 (HSV-2) gD mutant impaired for neural tropism is superior to an HSV-2 gD subunit vaccine to protect animals from challenge with HSV-2. J. Virol. *90*, 562–574.

Wang, Q.-Y., Zhou, C., Johnson, K.E., Colgrove, R.C., Coen, D.M., and Knipe, D.M. (2005a). Herpesviral latency-associated transcript gene promotes assembly of heterochromatin on viral lytic-gene promoters in latent infection. Proc. Natl. Acad. Sci. U. S. A. *102*, 16055–16059.

Wang, Q.-Y., Zhou, C., Johnson, K.E., Colgrove, R.C., Coen, D.M., and Knipe, D.M. (2005b). Herpesviral latency-associated transcript gene promotes assembly of heterochromatin on viral lytic-gene promoters in latent infection. Proc. Natl. Acad. Sci. U. S. A. *102*, 16055–16059.

Wang, X., Li, Y., Liu, S., Yu, X., Li, L., Shi, C., He, W., Li, J., Xu, L., Hu, Z., et al. (2014). Direct activation of RIP3/MLKL-dependent necrosis by herpes simplex virus 1 (HSV-1) protein ICP6 triggers host antiviral defense. Proc. Natl. Acad. Sci. *111*, 15438–15443.

Washington, S.D., Musarrat, F., Ertel, M.K., Backes, G.L., and Neumann, D.M. (2018). CTCF binding sites in the herpes simplex virus 1 genome display site-specific CTCF occupation, protein recruitment, and insulator function. J. Virol. *92*, e00156-18.

Watson, Z.L., Washington, S.D., Phelan, D.M., Lewin, A.S., Tuli, S.S., Schultz, G.S., Neumann, D.M., and Bloom, D.C. (2018). In Vivo Knockdown of the Herpes Simplex Virus 1 Latency-Associated Transcript Reduces Reactivation from Latency. J. Virol. *92*.

Watts, C. (1997). Capture and processing of exogenous antigens for presentation on MHC molecules. Annu. Rev. Immunol. *15*, 821–850.

Wei, M.L., and Cresswell, P. (1992). HLA-A2 molecules in an antigen-processing mutant cell contain signal sequence-derived peptides. Nature *356*, 443–446.

Weinzierl, A.O., Lemmel, C., Schoor, O., Müller, M., Krüger, T., Wernet, D., Hennenlotter, J., Stenzl, A., Klingel, K., Rammensee, H.-G., et al. (2007). Distorted Relation between mRNA Copy Number and Corresponding Major Histocompatibility Complex Ligand Density on the Cell Surface. Mol. Cell. Proteomics *6*, 102–113.

Weinzierl, A.O., Rudolf, D., Hillen, N., Tenzer, S., van Endert, P., Schild, H., Rammensee, H.-G., and Stevanović, S. (2008). Features of TAP-independent MHC class I ligands revealed by quantitative mass spectrometry. Eur. J. Immunol. *38*, 1503–1510.

Wherry, E.J. (2011). T cell exhaustion. Nat. Immunol. *12*, 492–499.

Whitley, R.J. (2006). Herpes simplex encephalitis: Adolescents and adults. Antiviral Res. *71*, 141–148.

Whitley, R.J., and Roizman, B. (2001). Herpes simplex virus infections. The Lancet *357*, 1513–1518.

Whitley, R.J., Kimberlin, D.W., and Roizman, B. (1998). Herpes Simplex Viruses. Clin. Infect. Dis. *26*, 541–553.

Whitney, P.G., Makhlouf, C., MacLeod, B., Ma, J.Z., Gressier, E., Greyer, M., Hochheiser, K., Bachem, A., Zaid, A., Voehringer, D., et al. (2017). Effective priming of HSV-specific CD8+ T cells in vivo does not require infected dendritic cells. J. Virol.

Wiertz, E.J., Jones, T.R., Sun, L., Bogyo, M., Geuze, H.J., and Ploegh, H.L. (1996). The human cytomegalovirus US11 gene product dislocates MHC class I heavy chains from the endoplasmic reticulum to the cytosol. Cell *84*, 769–779.

Wilcox, C.L., and Johnson, E.M. (1987). Nerve growth factor deprivation results in the reactivation of latent herpes simplex virus in vitro. J. Virol. *61*, 2311–2315.

Wilson, A.C., and Mohr, I. (2012a). A cultured affair: HSV latency and reactivation in neurons. Trends Microbiol. *20*, 604–611.

Wilson, A.C., and Mohr, I. (2012b). A cultured affair: HSV latency and reactivation in neurons. Trends Microbiol. *20*, 604–611.

Wilson, E.B., and Livingstone, A.M. (2008). Cutting Edge: CD4+ T cell-derived IL-2 is essential for help-dependent primary CD8+ T cell responses. J. Immunol. *181*, 7445–7448.

Wölfel, C., Drexler, I., Van Pel, A., Thres, T., Leister, N., Herr, W., Sutter, G., Huber, C., and Wölfel, T. (2000). Transporter (TAP)- and proteasome-independent presentation of a melanoma-associated tyrosinase epitope. Int. J. Cancer *88*, 432–438.

Wollenberg, A., Zoch, C., Wetzel, S., Plewig, G., and Przybilla, B. (2003). Predisposing factors and clinical features of eczema herpeticum: a retrospective analysis of 100 cases. J. Am. Acad. Dermatol. *49*, 198–205.

Wong, S.W., and Schaffer, P.A. (1991). Elements in the transcriptional regulatory region flanking herpes simplex virus type 1 oriS stimulate origin function. J. Virol. *65*, 2601–2611.

Wucherpfennig, K.W. (2010). The first structures of T cell receptors bound to peptide-MHC. J. Immunol. Baltim. Md 1950 *185*, 6391–6393.

Wysocka, J., and Herr, W. (2003). The herpes simplex virus VP16-induced complex: the makings of a regulatory switch. Trends Biochem. Sci. *28*, 294–304.

Xing, J., Wang, S., Lin, F., Pan, W., Hu, C.-D., and Zheng, C. (2011). Comprehensive characterization of interaction complexes of herpes simplex virus type 1 ICP22, UL3, UL4, and UL20.5. J. Virol. *85*, 1881–1886.

Yang, L., Voytek, C.C., and Margolis, T.P. (2000). Immunohistochemical Analysis of Primary Sensory Neurons Latently Infected with Herpes Simplex Virus Type 1. J. Virol. *74*, 209–217.

Yao, H.-W., Chen, S.-H., Li, C., Tung, Y.-Y., and Chen, S.-H. (2012). Suppression of transcription factor early growth response 1 reduces herpes simplex virus 1-induced corneal disease in mice. J. Virol. *86*, 8559–8567.

Yates, J.R., Ruse, C.I., and Nakorchevsky, A. (2009). Proteomics by Mass Spectrometry: Approaches, Advances, and Applications. Annu. Rev. Biomed. Eng. *11*, 49–79.

Yeager, A.S., Arvin, A.M., Urbani, L.J., and Kemp, J.A. (1980). Relationship of antibody to outcome in neonatal herpes simplex virus infections. Infect. Immun. *29*, 532–538.

Yewdell, J.W. (2007). Plumbing the sources of endogenous MHC class I peptide ligands. Curr. Opin. Immunol. *19*, 79–86.

Yewdell, J.W. (2011). DRiPs solidify: progress in understanding endogenous MHC class I antigen processing. Trends Immunol. *32*, 548–558.

Yewdell, J.W., Esquivel, F., Arnold, D., Spies, T., Eisenlohr, L.C., and Bennink, J.R. (1993). Presentation of numerous viral peptides to mouse major histocompatibility complex (MHC) class I-restricted T lymphocytes is mediated by the human MHC-encoded transporter or by a hybrid mouse-human transporter. J. Exp. Med. *177*, 1785–1790.

Yoneyama, M., and Fujita, T. (2008). Structural mechanism of RNA recognition by the RIG-I-like receptors. Immunity *29*, 178–181.

York, I.A., Roop, C., Andrews, D.W., Riddell, S.R., Graham, F.L., and Johnson, D.C. (1994). A cytosolic herpes simplex virus protein inhibits antigen presentation to CD8+ T lymphocytes. Cell *77*, 525–535.

Young, A.C., Zhang, W., Sacchettini, J.C., and Nathenson, S.G. (1994). The three-dimensional structure of H-2Db at 2.4 A resolution: implications for antigen-determinant selection. Cell *76*, 39–50.

Yu, J., Baron, V., Mercola, D., Mustelin, T., and Adamson, E.D. (2007). A network of p73, p53 and Egr1 is required for efficient apoptosis in tumor cells. Cell Death Differ. *14*, 436–446.

Zaid, A., Mackay, L.K., Rahimpour, A., Braun, A., Veldhoen, M., Carbone, F.R., Manton, J.H., Heath, W.R., and Mueller, S.N. (2014). Persistence of skin-resident memory T cells within an epidermal niche. Proc. Natl. Acad. Sci. *111*, 5307–5312.

Zarafonetis, C.J.D., and Smadel, J.E. (1944). Fatal herpes simplex encephalitis in man. Am. J. Pathol. *20*, 429–445.

Zawatzky, R., Gresser, I., DeMaeyer, E., and Kirchner, H. (1982). The role of interferon in the resistance of CS7BL/6 mice to various doses of herpes simplex virus type 1. J. Infect. Dis. *146*, 405–410.

Zernich, D. (2004). Natural HLA class I polymorphism controls the pathway of antigen presentation and susceptibility to viral evasion. J. Exp. Med. *200*, 13–24.

Zhang, B., Chan, Y.K., Lu, B., Diamond, M.S., and Klein, R.S. (2008). CXCR3 mediates region-specific antiviral T cell trafficking within the central nervous system during West Nile virus encephalitis. J. Immunol. Baltim. Md 1950 *180*, 2641–2649.

Zhang, D., Pasternack, M.S., Beresford, P.J., Wagner, L., Greenberg, A.H., and Lieberman, J. (2001). Induction of rapid histone degradation by the cytotoxic T lymphocyte protease Granzyme A. J. Biol. Chem. *276*, 3683–3690.

Zhang, Y., Fonslow, B.R., Shan, B., Baek, M.-C., and Yates, J.R. (2013). Protein analysis by shotgun/bottom-up proteomics. Chem. Rev. *113*, 2343–2394.

Zhao, H., and Peeters, B.P.H. (2003). Recombinant Newcastle disease virus as a viral vector: effect of genomic location of foreign gene on gene expression and virus replication. J. Gen. Virol. *84*, 781–788.

Zheng, C., Lin, F., Wang, S., and Xing, J. (2011). A novel virus-encoded nucleocytoplasmic shuttling protein: The UL3 protein of herpes simplex virus type 1. J. Virol. Methods *177*, 206–210.

Zhou, Y., Ye, L., Wan, Q., Zhou, L., Wang, X., Li, J., Hu, S., Zhou, D., and Ho, W. (2009). Activation of Toll-like receptors inhibits herpes simplex virus-1 infection of human neuronal cells. J. Neurosci. Res. *87*, 2916–2925.

Zhu, J., and Paul, W.E. (2008). CD4 T cells: fates, functions, and faults. Blood *112*, 1557–1569.

Zhu, J., Koelle, D.M., Cao, J., Vazquez, J., Huang, M.L., Hladik, F., Wald, A., and Corey, L. (2007). Virus-specific CD8+ T cells accumulate near sensory nerve endings in genital skin during subclinical HSV-2 reactivation. J. Exp. Med. *204*, 595–603.

Zhu, J., Peng, T., Johnston, C., Phasouk, K., Kask, A.S., Klock, A., Jin, L., Diem, K., Koelle, D.M., Wald, A., et al. (2013a). Immune surveillance by CD8αα+ skin-resident T cells in human herpes virus infection. Nature *497*, 494–497.

Zhu, J., Peng, T., Johnston, C., Phasouk, K., Kask, A.S., Klock, A., Jin, L., Diem, K., Koelle, D.M., Wald, A., et al. (2013b). Immune surveillance by CD8αα+ skin-resident T cells in human herpes virus infection. Nature *497*, 494–497.

Ziegler, H., Muranyi, W., Burgert, H.G., Kremmer, E., and Koszinowski, U.H. (2000). The luminal part of the murine cytomegalovirus glycoprotein gp40 catalyzes the retention of MHC class I molecules. EMBO J. *19*, 870–881.

Zinkernagel, R.M. (1982). Differentiation of T cells: thymic selection of specificity for self. Prog. Clin. Biol. Res. *85 Pt A*, 427–434.

Appendix

Table A - 1 MHC I bound HSV-1 derived peptides eluted from virus infected MC57G cells

Gene symbol (peptide position)	*Peptide sequences*	*MHC I allele (H-2)*	*$MHC I binding affinity ($IC_{50}$)*	*Kinetic class*	*Samples found in*	*#Immunogenicity*		*Gene / Source protein*
						%IFNγ$^+$ (of CD8$^+$) cells	*Number of mice positive*	
$RRI_{822-829}$	*QTFDFGRL	K^b	7.99	E	3 × KOS, 3 × Ka47Δ	0.41	8	UL39 (RR1) Ribonucleoside-diphosphate reductase large subunit
$US1_{198-205}$	INQLFRVL	K^b	25.5	IE	3 × KOS, 3 × Ka47Δ	0	0	US1 (ICP22) Transcriptional regulator
$gB_{498-505}$	*SSIEFARL	K^b	2.29	L1	3 × KOS, 3 × Ka47Δ	11.41	8 out of 8	UL27 (gB) Envelope glycoprotein B
$UL40_{279-287}$	*AAIENYVRF	K^b/D^b	102.2 (D^b), 175.28 (K^b)	E	3 × KOS, 3 × Ka47Δ	0.05	6 out of 8	UL40 Ribonucleoside-diphosphate reductase small subunit
$UL26_{613-621}$	AAHVDVDTA	K^b/D^b	848.39 (D^b), 31503 (K^b)	L1	3 × KOS, 3 × Ka47Δ	0	0	UL26 Capsid scaffolding protein
$US8_{99-110}$	YAPPAPSATGGL	D^b	27331	L1	3 × KOS, 2 × Ka47Δ	0	0	US8 Envelope glycoprotein E

Gene symbol (peptide position)	***Peptide sequences***	***MHC I allele (H-2)***	***[$] MHC I binding affinity (IC_{50})***	***Kinetic class***	***Samples found in***	***[#] Immunogenicity***		***Gene / Source protein***
						%IFNγ$^+$ (of CD8$^+$) cells	***Number of mice positive***	
$UL26_{483-495}$	GAVTSLQQELAHM	K^b/D^b	12483 (D^b), 12854 (K^b)	L1	2 × KOS, 3 × Ka47Δ	0	0	UL26 Capsid scaffolding protein
$UL29_{605-613}$	TIITNREAL	D^b	183.45	E	2 × KOS, 2 × Ka47Δ	0.07	2 out of 8	UL29 Major DNA-binding protein
$UL26_{331-339}$	ASHYNQLVA	D^b	879.48	L1	2 × KOS, 2 × Ka47Δ	0	0	UL26 Capsid scaffolding protein
$UL51_{155-163}$	AIAERALGL	K^b	2036.19	L1	2 × KOS, 2 × Ka47Δ	0	0	UL51 Tegument protein UL51
$RL1_{136-144}$	VTAEHLARL	K^b	42.65	L1	1 × KOS, 3 × Ka47Δ	NA	NA	RL1 (ICP34.5) Neurovirulence factor
$UL26_{361-370}$	VAYGPHGAGL	K^b	87.33	L1	2 × KOS, 2 × Ka47Δ	0	0	UL26 Capsid scaffolding protein
$US8_{349-358}$	ASPQHSGLYL	K^b/D^b	5475 (K^b), 1529 (D^b)	L1	1 × KOS, 2 × Ka47Δ	0	0	US8 Envelope glycoprotein E
$UL3_{101-109}$	FMVSSIDEL	D^b	68.64	L2	3 × Ka47Δ	NA	NA	UL3 Nuclear phosphoprotein
$UL5_{300-307}$	STFEHQKL	K^b	40.75	E	1 × KOS, 2 × Ka47Δ	0	0	UL5 DNA replication helicase

Gene symbol (peptide position)	***Peptide sequences***	***MHC I allele (H-2)***	***[$]MHC I binding affinity (IC_{50})***	***Kinetic class***	***Samples found in***	***[#]Immunogenicity***		***Gene / Source protein***
						%IFNγ$^+$ (of CD8$^+$) cells	***Number of mice positive***	
$UL5_{213-221}$	AALERTLGL	K^b	524.28	E	1 × KOS, 2 × Ka47Δ	NA	NA	UL5 DNA replication helicase
$US7_{372-383}$	PTTSTPTPPLLV	K^b	25189.24	L1	1 × KOS, 2 × Ka47Δ	NA	NA	UL7 Envelope glycoprotein I
$US2_{49-56}$	VVVRPANL	K^b	28.56	L2	1 × KOS, 2 × Ka47Δ	0	0	US2
$UL29_{324-332}$	LALESIVSM	D^b	1259.36	E	2 × Ka47Δ	NA	NA	UL29 Major DNA-binding protein
$US12_{41-51}$	RTAVHDPERPL	D^b	16284.92	IE	2 × KOS	0	0	US12 (ICP47) TAP transporter inhibitor
$UL19_{947-955}$	HTIQNGDYF	D^b	59.08	L1	2 × KOS	NA	NA	UL19 Major capsid protein
$MCP_{1251-1263}$	SYGDLLYNGAYHL	D^b	12483.37	L1	1 × KOS, 1 × Ka47Δ	0	0	UL19 Major capsid protein
$UL25_{255-263}$	RAPVTFGDL	D^b	7839.28	L2	1 × KOS, 1 × Ka47Δ	0	0	UL25 Capsid vertex component 2
$US2_{3-11}$	VVVVNVMTL	D^b	92.37	L2	2 × Ka47Δ	NA	NA	US2

Gene symbol (peptide position)	*Peptide sequences*	*MHC I allele (H-2)*	*[$]MHC I binding affinity (IC_{50})*	*Kinetic class*	*Samples found in*	*[#]Immunogenicity*		*Gene / Source protein*
						%IFNγ$^+$ (of CD8$^+$) cells	*Number of mice positive*	
$UL25_{338-346}$	STHVNPDGV	D^b	1285.35	L2	1 × KOS, 1 × Ka47Δ	NA	NA	UL25 Capsid vertex component 2
$UL38_{99-109}$	AALIGSPRHHL	D^b	13479.26	L2	1 × KOS, 1 × Ka47Δ	0	0	UL38 Triplex capsid protein 1
$UL53_{5-15}$	RSLQHLSTVVL	D^b	5080.85	L2	1 × KOS, 1 × Ka47Δ	NA	NA	UL53 Envelope glycoprotein K
$UL5_{610-617}$	RAFDFKQL	K^b	19.15	E	1 × KOS, 1 × Ka47Δ	NA	NA	UL5 DNA replication helicase
$ICP0_{748-755}$	GALDFRSL	K^b	498.68	IE	1 × KOS, 1 × Ka47Δ	0	0	RL2 (ICP0) Ubiquitin E3 ligase
$UL25_{304-311}$	GRYEHGAL	K^b	5291.01	L2	1 × KOS, 1 × Ka47Δ	0	0	UL25 Capsid vertex component 2
$UL32_{384-391}$	VAPRFAQF	K^b	13.02	L2	1 × KOS, 1 × Ka47Δ	0	0	UL32 Packaging protein
$UL36_{2139-2147}$	SSPEHIYTF	K^b	1161.84	L2	1 × KOS, 1 × Ka47Δ	0.03	1 out of 8	UL36 Large tegument protein deneddylase

Gene symbol (peptide position)	***Peptide sequences***	***MHC I allele (H-2)***	***[$]MHC I binding affinity (IC_{50})***	***Kinetic class***	***Samples found in***	***[#]Immunogenicity***		***Gene / Source protein***
						%IFNγ$^+$ (of CD8$^+$) cells	***Number of mice positive***	
$UL22_{562-570}$	TNADLRTAL	K^b	2507	L2	1 × KOS, 1 × Ka47Δ	0	0	UL22 Envelope glycoprotein H
$UL50_{353-371}$	DAEAPPSERGTGG FGSTGI	K^b/D^b	NA	E	1 × KOS, 1 × Ka47Δ	NA	NA	UL50 Deoxyuridine 5'-triphosphate nucleotidohydrolase
$UL39_{956-964}$	HGLRNSQFV	D^b	56.9	E	1 × Ka47Δ	0.05	3 out of 8	UL39 Ribonucleoside-diphosphate reductase large subunit
$UL52_{655-663}$	AAVQLLFPA	D^b	641.65	E	1 × KOS	NA	NA	UL52 DNA primase
$UL13_{114-123}$	TAPPSSPSHI	D^b	10876.3	E	1 × Ka47Δ	0	0	UL13 Tegument serine/threonine protein kinase
$UL39_{805-815}$	SGVCNLGSVNL	D^b	1866.7	E	1 × Ka47Δ	0.05	3 out of 8	UL39 Ribonucleoside-diphosphate reductase large subunit
$UL29_{104-114}$	DPSTQAPNLTR	D^b	48793.25	E	1 × Ka47Δ	0	0	UL29 Major DNA-binding protein
$UL23_{115-128}$	EDAAVVMTSAQIT	D^b	3072.46	E	1 × Ka47Δ	NA	NA	UL23

Gene symbol (peptide position)	*Peptide sequences*	*MHC I allele (H-2)*	*[$] MHC I binding affinity (IC_{50})*	*Kinetic class*	*Samples found in*	*[#] Immunogenicity*		*Gene / Source protein*
						%IFNγ$^+$ (of CD8$^+$) cells	*Number of mice positive*	
	M							Thymidine kinase
$UL26_{237-245}$	AGIAGHTYL	D^b	314.78	L1	1 × KOS	NA	NA	UL26 Capsid scaffolding protein
$UL26_{611-621}$	SSAAHVDVDTA	D^b	13285.1	L1	1 × Ka47Δ	0	0	UL26 Capsid scaffolding protein
$UL27_{55-66}$	APPALGAAPTGD	D^b	46885.06	L1	1 × KOS	0.04	1 out of 8	UL27 Envelope glycoprotein B
$UL19_{482-495}$	EAANPYGAYVAAP A	D^b	38438.89	L1	1 × Ka47Δ	NA	NA	UL19 Major capsid protein
$UL25_{255-264}$	RAPVTFGDLL	D^b	3276.16	L2	1 × Ka47Δ	0.04	1 out of 8	UL25 Capsid vertex component 2
$UL3_{44-54}$	GAALASPAQPL	D^b	4493.89	L2	1 × Ka47Δ	0	0	UL3 Nuclear phosphoprotein
$UL5_{729-736}$	MGYTYTRV	K^b	4.47	E	1 × Ka47Δ	0.04	1 out of 8	UL5 DNA replication helicase
$ICP8_{171-178}$	*INNTFLHL	K^b	15.86	E	1 × Ka47Δ	0.38	8 out of 8	UL29 (ICP8) Major DNA-binding protein I

Gene symbol (peptide position)	*Peptide sequences*	*MHC I allele (H-2)*	*[$]MHC I binding affinity (IC_{50})*	*Kinetic class*	*Samples found in*	*[#]Immunogenicity*		*Gene / Source protein*
						%IFNγ$^+$ (of CD8$^+$) cells	*Number of mice positive*	
$UL5_{126-133}$	AQNMYAKL	K^b	147.11	E	1 × KOS	0.042	4 out of 8	UL5 DNA replication helicase
$UL30_{816-823}$	SVYGFTGV	K^b	6.11	E	1 × Ka47Δ	NA	NA	UL30 DNA polymerase catalytic subunit
$UL40_{198-206}$	IAYLRTNNL	K^b	10.91	E	1 × Ka47Δ	0.18	8 out of 8	UL40 Ribonucleoside-diphosphate reductase small subunit
$UL29_{639-647}$	RNFKFRDGL	K^b	27.41	E	1 × Ka47Δ	0	0	UL29 Major DNA-binding protein
$UL52_{292-300}$	TSFAAITRF	K^b	403.45	E	1 × Ka47Δ	0	0	UL52 DNA primase
$UL50_{277-285}$	PGHVCAFFV	K^b	22627.87	E	1 × KOS	0	0	UL50 Deoxyuridine 5'-triphosphate nucleotidohydrolase
$UL13_{118-126}$	SSPSHILTL	K^b	136.13	L1	1 × Ka47Δ	NA	NA	UL13 Tegument serine/threonine protein kinase

Gene symbol (peptide position)	*Peptide sequences*	*MHC I allele (H-2)*	*[$] MHC I binding affinity (IC_{50})*	*Kinetic class*	*Samples found in*	*[#] Immunogenicity*		*Gene / Source protein*
						%IFNγ$^+$ (of CD8$^+$) cells	*Number of mice positive*	
$UL42_{467-475}$	ASPGAFSAF	K^b	711.63	E	1 × Ka47Δ	NA	NA	UL42 DNA polymerase processivity factor
$UL29_{93-103}$	SVYVFHGGRHL	K^b	12.31	E	1 × Ka47Δ	0	0	UL29 Major DNA-binding protein
$UL39_{451-461}$	VALDFGLTERL	K^b	990.73	E	1 × Ka47Δ	0.05	5 out of 8	UL39 Ribonucleoside-diphosphate reductase large subunit
$UL30_{27-39}$	AGPRGAGPGPPPC	K^b	43341.72	E	1 × KOS	0	0	UL30 DNA polymerase catalytic subunit
$UL29_{93-105}$	SVYVFHGGRHLDP	K^b	27.62	E	1 × KOS	NA	NA	UL29 Major DNA-binding protein
UL23	CNLPPGWSRPTSPPQ	K^b	NA	E	1 × KOS	NA	NA	UL23 Thymidine kinase
$UL52_{835-850}$	PACGRLLPVFVIPPAC	K^b	NA	E	1 × KOS	NA	NA	UL52 DNA primase
$US12_{44-52}$	VHDPERPLL	K^b	11599.26	IE	1 × KOS	0	0	US12 (ICP47) TAP transporter inhibitor

Gene symbol (peptide position)	***Peptide sequences***	***MHC I allele (H-2)***	***[$] MHC I binding affinity (IC_{50})***	***Kinetic class***	***Samples found in***	***[#] Immunogenicity***		***Gene / Source protein***
						%IFNγ$^+$ (of CD8$^+$) cells	***Number of mice positive***	
$US12_{73-85}$	RTGGTVTDSPRNP	K^b	43598.04	IE	1 × KOS	NA	NA	US12 (ICP47) TAP transporter inhibitor
$UL37_{600-607}$	TQIRFPAL	K^b	17.03	L1	1 × Ka47Δ	0.07	3 out of 8	UL37 Inner tegument protein
$UL37_{233-240}$	EGLRFLAL	K^b	489.74	L1	1 × KOS	0.041	1 out of 8	UL37 Inner tegument protein
$US8_{459-466}$	KGPTYIRV	K^b	196.95	L1	1 × Ka47Δ	NA	NA	US8 Envelope glycoprotein E
$US10_{54-61}$	GNPEYREL	K^b	1659.04	L1	1 × Ka47Δ	NA	NA	US10 Virion protein
$UL19_{66-73}$	SLVRFLEL	K^b	198.85	L1	1 × Ka47Δ	NA	NA	UL19 Major capsid protein
$US8_{12-22}$	GVCVVSCLAVT	K^b	26655.16	L1	1 × Ka47Δ	0	0	US8 Envelope glycoprotein E
$UL27_{867-877}$	GTSALLSAKVT	K^b	21523.39	L1	1 × KOS	0.037	1 out of 8	UL27 Envelope glycoprotein B
$UL46_{45-55}$	EGLLSAAVGAL	K^b	29150.54	L1	1 × KOS	NA	NA	UL46 Tegument protein

Gene symbol (peptide position)	*Peptide sequences*	*MHC I allele (H-2)*	*[$] MHC I binding affinity (IC_{50})*	*Kinetic class*	*Samples found in*	*[#] Immunogenicity*		*Gene / Source protein*
						%IFNγ$^+$ (of CD8$^+$) cells	*Number of mice positive*	
$UL53_{175-182}$	LQYPYTKI	K^b	168.03	L1	1 × Ka47Δ	0	0	UL53 Envelope glycoprotein K
$UL32_{171-178}$	AAFEFVYV	K^b	14.46	L2	1 × Ka47Δ	NA	NA	UL32 Packaging protein
$UL5_{312-321}$	RQSENVLTYL	Kb/Db	963.74 (Db), 23102 (Kb)	E	1 × Ka47Δ	NA	NA	UL5 DNA replication helicase

*Previously found by St Leger et al., 2011

[$]MHC I binding affinity was predicted using ANN 4.0 algorithm from IEDB analysis resource. For peptides comprising more than 14 amino acids, it is not possible to obtain IC_{50} value, hence denoted NA.

[#]Immunogenicity of 46 peptides were tested in eight C57BL/6 mice. The peptides for which the immunogenicity was not tested is denoted as NA.

Figure A-1 HSV-1 genome sequence showing the *cis*-acting regulatory elements in the ICP47 promoter region. The grey arrows show the location and orientation of region coding for ICP47, US11 and US10. The yellow arrow indicates the location and orientation of the minimal promoter required for ICP47 expression. The minimum oriS site of 62 bp is shown as a white box. The three red arrows in the oriS site indicate the box I, box II and box III to which the OBP bind. The green box shows the intron that is located 5′ to the ICP47 coding region and 3′ to the promoter. The blue box shows the TATA box and the blue arrow show the VP16 inducing complex binding motif (TAATGARAT). The pink arrows represent the sp1 binding motifs, which span the ICP47 promoter. Located within intron, indicated as blue arrows, are the reiterated Egr1 binding motifs. NFIII-binding site is indicated as dark red line situated 5′ to the ICP47 promoter.


5′
ATGCGATAAAATCTGTTTGTAAAATTTATTAAGGGTACAAATTGCCC
144,000
3′
TACGCTATTTTAGACAAACATTTTAAATAATTCCCATGTTTAACGGG
US10
TAGCACAGGGGTGGGGTTAGGGCCGGGTCCCCACACCCAAACGCACCAAACAGATGCAGGCAGTGGGTCGAGTACAGCCCCGCGTACGAACACGTCGATGCGTGTGTCAGACAGCACCAG
144,120
ATCGTGTCCCCACCCCAATCCCGGCCCAGGGGTGTGGGTTTGCGTGGTTTGTCTACGTCCGTCACCCAGCTCATGTCGGGGCGCATGCTTGTGCAGCTACGCACACAGTCTGTCGTGGTC
US10
AAAGCACAGGCCATCAACAGGTCGTGCATGTGTCGGTGGGTTTGGACGCGGGGGGCCATGGTGGTGATAAAGTTAATGGCCGCCGTCCGCCAGGGCCACAGGGGCGACGTCTCTTGGTTG
144,240
TTTCGTGTCCGGTAGTTGTCCAGCACGTACACAGCCACCCAAACCTGCGCCCCCCGGTACCACCACTATTTCAATTACCGGCGGCAGGCGGTCCCGGTGTCCCCGCTGCAGAGAACCAAC
US10
GCCCGGAGCCACTGGGTGTGGACCAGCCGCGCGTGGCGGCCCAACATGGCCCCTGTAGCCGGGGGCGGGGGATCGCGCACGTTTGCAGCGCACATGCGAGACACCTCGACCACGGTTCGA
144,360
CGGGCCTCGGTGACCCACACCTGGTCGGCGCGCACCGCCGGGTTGTACCGGGGACATCGGCCCCCGCCCCCTAGCGCGTGCAAACGTCGCGTGTACGCTCTGTGGAGCTGGTGCCAAGCT
US10
Sp1 binding site
AAGAAGGCCCGGTGGTCCGCGGGCAACATCACCAGGTGCGCAAGCGCCCGGGCGTCCAGAGGGTAGAGCCCTGAGTCATCCGAGGTTGGCTCATCGCCCGGGTCTTGCCGCAAGTGCGTG
144,480
TTCTTCCGGGCCACCAGGCGCCCGTTGTAGTGGTCCACGCGTTCGCGGGCCCGCAGGTCTCCCATCTCGGGACTCAGTAGGCTCCAACCGAGTAGCGGGCCCAGAACGGCGTTCACGCAC
US10


TGGGTTGGGCTTCCGGTGGGCGGGACGCGAACCGCGGTGTGGATCCCGACGCGGGCCCGAGCGTATGCTCCATCTTGTGGGGAGAAGGGGTCTGGGCTCGCCAGGGGGGCATACTTGCCC
144,600
ACCCAACCCGAAGGCCACCCGCCCTGCGCTTGGCGCCACACCTAGGGCTGCGCCCGGGCTCGCATACGAGGTAGAACACCCCTCTTCCCCAGACCCGAGCGGTCCCCCCGTATGAACGGG
US10
Sp1 binding site
GGGCTATACAGACCCGCGAGCCGTACGTGGTTCGCGGGGGGTGCGTGGGGTCCGGGGCTCCCTGGGAGACCGGGGTTGTCGTGGATCCCTGGGGTCACGCGGTACCCTGGGGTCTCTGGG
144,720
CCCGATATGTCTGGGCGCTCGGCATGCACCAAGCGCCCCCCACGCACCCCAGGCCCCGAGGGACCCTCTGGCCCCAACAGCACCTAGGGACCCCAGTGCGCCATGGGACCCCAGAGACCC
US10
US11
AGCTCGCGGTACTCTGGGTTCCCTAGGTTCTCGGGGTGGTCGCGGAACCCGGGGCTCCCGGGGAACACGCGGTGTCCTGGGGATTGTTGGCGGTCGGACGGCTTCAGATGGCTTCGAGAT
144,840
TCGAGCGCCATGAGACCCAAGGGATCCAAGAGCCCCACCAGCGCCTTGGGCCCCGAGGGCCCCTTGTGCGCCACAGGACCCCTAACAACCGCCAGCCTGCCGAAGTCTACCGAAGCTCTA
US10
US11
CGTAGTGTCCGCACCGACTCGTAGTAGACCCGAATCTCCACATTGCCCCGCCGCTTGATCATTATCACCCCGTTGCGGGGGTCCGGAGATCATGCGCGGGTGTCCTCGAGGTGCGTGAAC
144,960
GCATCACAGGCGTGGCTGAGCATCATCTGGGCTTAGAGGTGTAACGGGGCGGCGAACTAGTAATAGTGGGGCAACGCCCCCAGGCCTCTAGTACGCGCCCACAGGAGCTCCACGCACTTG
US10
US11


ACCTCTGGGGTGCATGCCGGCGGACGGCACGCCTTTTAAGTAAACATCTGGGTCGCCCGGCCCAACTGGGGCCGGGGGTTGGGTCTGGCTCATCTCGAGAGACACGGGGGGGAACCACCC
145,080
TGGAGACCCCACGTACGGCCGCCTGCCGTGCGGAAAATTCATTTGTAGACCCAGCGGGCCGGGTTGACCCCGGCCCCCAACCCAGACCGAGTAGAGCTCTCTGTGCCCCCCCTTGGTGGG
US11
TATA signal
TCCGCCCAGAGACTCGGGTGATGGTCGTACCCGGGACTCAACGGGTTACCGGATTACGGGGACTGTCGGTCACGGTCCCGCCGGTTCTTCGATGTGCCACACCCAAGGATGCGTTGGGGG
145,200
AGGCGGGTCTCTGAGCCCACTACCAGCATGGGCCCTGAGTTGCCCAATGGCCTAATGCCCCTGACAGCCAGTGCCAGGGCGGCCAAGAAGCTACACGGTGTGGGTTCCTACGCAACCCCC
ICP47
CGATTTCGGGCAGCAGCCCGGGAGAGCGCAGCAGGGGACGCTCCGGGTCGTGCACGGCGGTTCTGGCCGCCTCCCGGTCCTCACGCCCCCTTTTATTGATCTCATCGCGTACGTCGGCGT
145,320
GCTAAAGCCCGTCGTCGGGCCCTCTCGCGTCGTCCCCTGCGAGGCCCAGCACGTGCCGCCAAGACCGGCGGAGGGCCAGGAGTGCGGGGGAAAATAACTAGAGTAGCGCATGCAGCCGCA
ICP47
ACGTCCTGGGCCCAACCCGCATGTTGTCCAGGAAGGTGTCCGCCATTTCCAGGGCCCACGACATGCTTTTCCCCCCGACGAGCAGGAAGCGGTCCACGCAACGGTCGCCGCCGGTCGCCT
145,440
TGCAGGACCCGGGTTGGGCGTACAACAGGTCCTTCCACAGGCGGTAAAGGTCCCGGGTGCTGTACGAAAAGGGGGGCTGCTCGTCCTTCGCCAGGTGCGTTGCCAGCGGCGGCCAGCGGA
ICP47
CGACGAGGGCGTTCCTCCTGCGGGAAGGCACGAACGCGGGTGAGCCCCCTCCTCCGCCCCCGCGTCCCCCCTCCTCCGCCCCCGCGTCCCCCCTCCTCCGCCCCCGCGTCCCCCCTCCTC
145,560
GCTGCTCCCGCAAGGAGGACGCCCTTCCGTGCTTGCGCCCACTCGGGGGAGGAGGCGGGGGCGCAGGGGGGAGGAGGCGGGGGCGCAGGGGGGAGGAGGCGGGGGCGCAGGGGGGAGGAG
IE68
Egr1 binding site
Egr1 binding site
Egr1 binding site

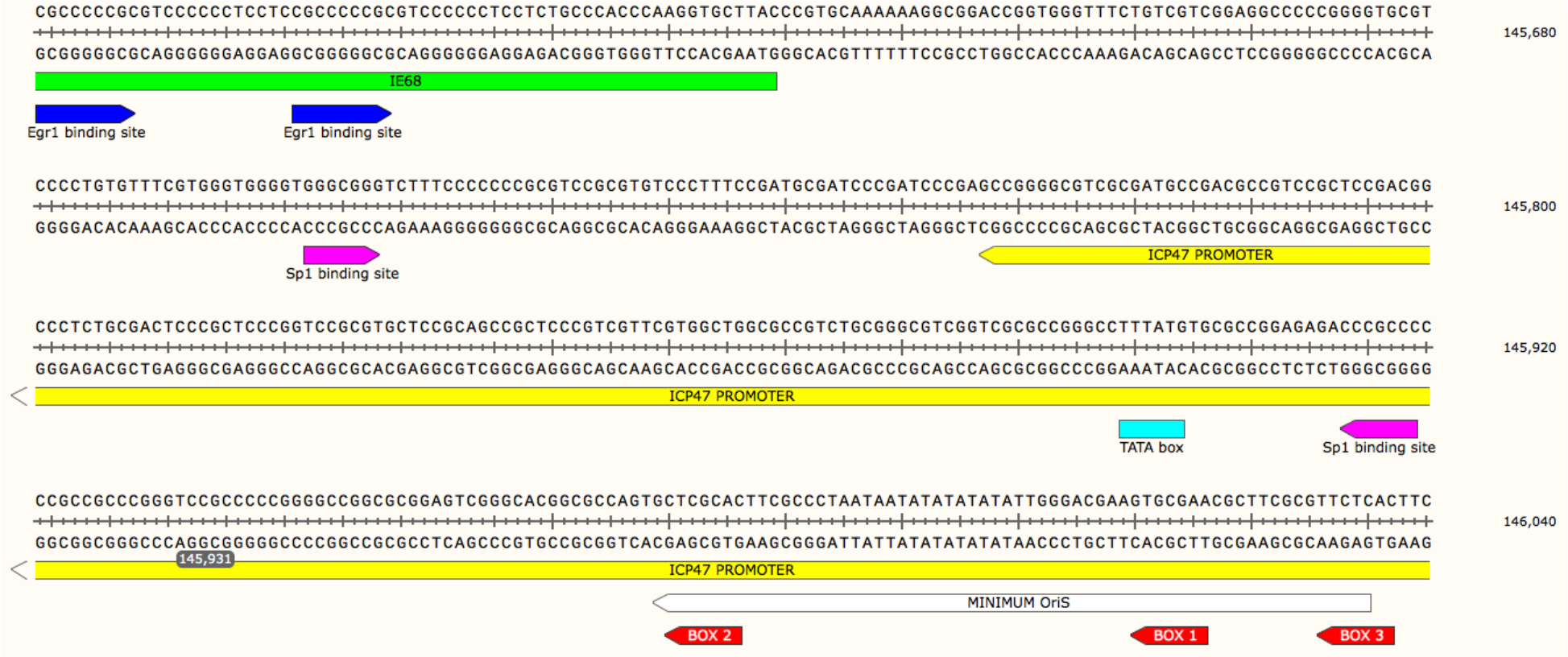
CGCCCCCGCGTCCCCCCTCCTCCGCCCCCGCGTCCCCCCTCCTCTGCCCACCCAAGGTGCTTACCCGTGCAAAAAAGGCGGACCGGTGGGTTTCTGTCGTCGGAGGCCCCCGGGGTGCGT
GCGGGGGCGCAGGGGGGAGGAGGCGGGGGCGCAGGGGGGAGGAGACGGGTGGGTTCCACGAATGGGCACGTTTTTTCCGCCTGGCCACCCAAAGACAGCAGCCTCCGGGGGCCCCACGCA
145,680
IE68
Egr1 binding site
Egr1 binding site
CCCCTGTGTTTCGTGGGTGGGGTGGGCGGGTCTTTCCCCCCCGCGTCCGCGTGTCCCTTTCCGATGCGATCCCGATCCCGAGCCGGGGCGTCGCGATGCCGACGCCGTCCGCTCCGACGG
GGGGACACAAAGCACCCACCCCACCCGCCCAGAAAGGGGGGGCGCAGGCGCACAGGGAAAGGCTACGCTAGGGCTAGGGCTCGGCCCCGCAGCGCTACGGCTGCGGCAGGCGAGGCTGCC
145,800
Sp1 binding site
ICP47 PROMOTER
CCCTCTGCGACTCCCGCTCCCGGTCCGCGTGCTCCGCAGCCGCTCCCGTCGTTCGTGGCTGGCGCCGTCTGCGGGCGTCGGTCGCGCCGGGCCTTTATGTGCGCCGGAGAGACCCGCCCC
GGGAGACGCTGAGGGCGAGGGCCAGGCGCACGAGGCGTCGGCGAGGGCAGCAAGCACCGACCGCGGCAGACGCCCGCAGCCAGCGCGGCCCGGAAATACACGCGGCCTCTCTGGGCGGGG
145,920
ICP47 PROMOTER
TATA box
Sp1 binding site
CCGCCGCCCGGGTCCGCCCCCGGGGCCGGCGCGGAGTCGGGCACGGCGCCAGTGCTCGCACTTCGCCCTAATAATATATATATATTGGGACGAAGTGCGAACGCTTCGCGTTCTCACTTC
GGCGGCGGGCCCAGGCGGGGGCCCCGGCCGCGCCTCAGCCCGTGCCGCGGTCACGAGCGTGAAGCGGGATTATTATATATATATAACCCTGCTTCACGCTTGCGAAGCGCAAGAGTGAAG
146,040
145,931
ICP47 PROMOTER
MINIMUM OriS
BOX 2
BOX 1
BOX 3


TTTTACCCGGCGGCCCCGCCCCCTTGGGGCGGTCCCGCCCGCCGGCCAATGGGGGGGCGGCAAGGCGGGCGGCCCAAGGGCCGCCCGCCGTCCCGTTGGTCCCGGCGTCCGGCGGGCGGG
AAAATGGGCCGCCGGGGCGGGGGAACCCCGCCAGGGCGGGCGGCCGGTTACCCCCCCGCCGTTCCGCCCGCCGGGTTCCCGGCGGGCGGCAGGGCAACCAGGGCCGCAGGCCGCCCGCCC
146,160
ICP47 PROMOTER
Sp1 binding site
Sp1 binding site
Sp1 binding site
ACCGGGGGCCCGGGGACGGCCAACGGGCGCGCGGGGCTCGTATCTCATTACCGCCGAACCGGGAAGTCGGGGCCCGGGCCCCGCCCCCTGCCCGTTCCTCGTTAGCATGCGGAACGGAAG
TGGCCCCCGGGCCCCTGCCGGTTGCCCGCGCGCCCCGAGCATAGAGTAATGGCGGCTTGGCCCTTCAGCCCCGGGCCCGGGGCGGGGGACGGGCAAGGAGCAATCGTACGCCTTGCCTTC
146,280
ICP47 PROMOTER
TAATGARAT
Sp1 binding site
NF-III-binding site
CGGAAACCGCCGGATCGGGCGGTAATGAGATGCCATGCGGGGCGGGGCGCGGACCCACCCGCCCTCGCGCCCCGTCCATGGCAGATGGCGCGGATGGGCGGGGCCGGGGGTTCGACCAAC
GCCTTTGGCGGCCTAGCCCGCCATTACTCTACGGTACGCCCCGCCCCGCGCCTGGGTGGGCGGGAGCGCGGGGCAGGTACCGTCTACCGCGCCTACCCGCCCCGGCCCCCAAGCTGGTTG
146,400
TAATGARAT
Sp1 binding site
Sp1 binding site
Sp1 binding site
GGGCCGCGGCCACGGGCCCCCGGCGTGCCGGCGTCGGGGCGGGGTCGTGCATAATGGAATTCCGTTCGGGGTGGGCCCGCCGGGGGGCGGGGGGCCGGCGGCCTCCGCTGCTCCTCCTTC
CCCGGCGCCGGTGCCCGGGGGCCGCACGGCCGCAGCCCCGCCCCAGCACGTATTACCTTAAGGCAAGCCCCACCCGGGCGGCCCCCCGCCCCCCGGCCGCCGGAGGCGACGAGGAGGAAG
146,520
Sp1 binding site
Sp1 binding site
146,532
CCGCCGGCCCCTGGGACTATATGAGCCCGAGGACGCCCCGATCGTCCACACGGAGCGCGGCTGCCGACACGGATCCACGACCCGACGCGGGACCGCCAGAGACAGACCGTCAGACGCTCG
GGCGGCCGGGGACCCTGATATACTCGGGCTCCTGCGGGGCTAGCAGGTGTGCCTCGCGCCGACGGCTGTGCCTAGGTGCTGGGCTGCGCCCTGGCGGTCTCTGTCTGGCAGTCTGCGAGC
146,640


CCGCGCCGGGACGCCGATACGCGGACGAAGCGCGGGAGGGGGATCGGCCGTCCCTGTCCTTTTTCCCCACCCAAGCATCGACCGGTCCGCGCTAGTTCCGCGTCGACGGCGGGGGTCGTC
146,760
GGCGCGGCCCTGCGGCTATGCGCCTGCTTCGCGCCCTCCCCCTAGCCGGCAGGGACAGGAAAAAGGGGTGGGTTCGTAGCTGGCCAGGCGCGATCAAGGCGCAGCTGCCGCCCCCAGCAG
GGGGTCCGTGGGTCTCGCCCCCTCCCCCCATCGAGAGTCCGTAGGTGACCTACCGTGCTACGTCCGCCGTCGCAGCCGTATCCCCGGAGGATCGCCCCGCATCGGCGATGGCGTCGGAGA
146,880
CCCCAGGCACCCAGAGCGGGGGAGGGGGGTAGCTCTCAGGCATCCACTGGATGGCACGATGCAGGCGGCAGCGTCGGCATAGGGGCCTCCTAGCGGGGCGTAGCCGCTACCGCAGCCTCT
ACAAGCAGCGCCCCGGCTCCCCGGGCCCCACCGACGGGCCGCCGCCCACCCCGAGCCCAGACCGCGACGAGCGGGGGGCCCTCGGGTGGGGCGCGGAGACGGAGGAGGGCGGGGACGACC
147,000
TGTTCGTCGCGGGGCCGAGGGGCCCGGGGTGGCTGCCCGGCGGCGGGTGGGGCTCGGGTCTGGCGCTGCTCGCCCCCCGGGAGCCCACCCCGCGCCTCTGCCTCCTCCCGCCCCTGCTGG
Sp1 binding site
CCGACCACGACCCCGACCACCCCCACGACCTCGACGACGCCCGGCGGGACGGGAGGGCCCCCGCGGCGGGCACCGACGCCGGCGAGGACGCCGGGGACGCCGTCTCGTCGCGACAGCTGG
147,120
GGCTGGTGCTGGGGCTGGTGGGGGTGCTGGAGCTGCTGCGGGCCGCCCTGCCCTCCCGGGGGCGCCGCCCGTGGCTGCGGCCGCTCCTGCGGCCCCTGCGGCAGAGCAGCGCTGTCGACC
147,129
CTCTGCTGGCCTCCATGGTAGAGGAGGCCGTCCGGACGATCCCGACGCCCGACCCCGCGGCCTCGCCGCCCCGGACCCCCGCCTTTCTAGCCGACGACGATGACGGGGACGAGTACGACG
147,240
GAGACGACCGGAGGTACCATCTCCTCCGGCAGGCCTGCTAGGGCTGCGGGCTGGGGCGCCGGAGCGGCGGGGCCTGGGGGCGGAAAGATCGGCTGCTGCTACTGCCCCTGCTCATGCTGC
ACGCAGCCGACGCCGCCGGCGACCGGGCCCCGGCCCGGGGCCGCGAACGGGAGGCCCCGCTACGCGGCGCGTATCCGGACCCCACGGACCGCCTGTCGCCGCGCCCGCCGGCCCAGCCGC
147,360
TGCGTCGGCTGCGGCGGCCGCTGGCCCGGGGCCGGGCCCCGGCGCTTGCCCTCCGGGGCGATGCGCCGCGCATAGGCCTGGGGTGCCTGGCGGACAGCGGCGCGGGCGGCCGGGTCGGCG
CGCGGAGACGTCGTCACGGCCGGCGGCGGCCATCGGCGTCATCGACCTCGTCGGACTCCGGGTCCTCGTCCTCGTCGTCCGCATCCTCTTCGTCCTCGTCGTCCGACGAGGACGAGGACG
147,480
GCGCCTCTGCAGCAGTGCCGGCCGCCGCCGGTAGCCGCAGTAGCTGGAGCAGCCTGAGGCCCAGGAGCAGGAGCAGCAGGCGTAGGAGAAGCAGGAGCAGCAGGCTGCTCCTGCTCCTGC


ACGACGGCAACGACGCGGCCGACCACGCACGCGAGGCGCGGGCCGTCGGGCGGGGTCCGTCGAGCGCGGCGCCGGAAGCCCCCGGGCGGACGCCGCCCCCGCCCGGGCCACCCCCCCTCT
147,600
TGCTGCCGTTGCTGCGCCGGCTGGTGCGTGCGCTCCGCGCCCGGCAGCCCGCCCCAGGCAGCTCGCGCCGCGGCCTTCGGGGGCCCGCCTGCGGCGGGGGCGGGCCCGGTGGGGGGGAGA
Sp1 binding site
Sp1 binding site
CCGAGGCCGCGCCCAAGCCCCGGGCGGCGGCGAGGACCCCCGCGGCCTCCGCGGGCCGCATCGAGCGCCGCCGGGCCCGCGCGGCGGTGGCCGGCCGCGACGCCACGGGCCGCTTCACGG
147,720
GGCTCCGGCGCGGGTTCGGGGCCCGCCGCCGCTCCTGGGGGCGCCGGAGGCGCCCGGCGTAGCTCGCGGCGGCCCGGGCGCGCCGCCACCGGCCGGCGCTGCGGTGCCCGGCGAAGTGCC
CCGGGCAGCCCCGGCGGGTCGAGCTGGACGCCGACGCGGCCTCCGGCGCCTTCTACGCGCGCTATCGCGACGGGTACGTCAGCGGGGAGCCGTGGCCCGGCGCCGGGCCCCCGCCCCCGG
147,840
GGCCCGTCGGGGCCGCCCAGCTCGACCTGCGGCTGCGCCGGAGGCCGCGGAAGATGCGCGCGATAGCGCTGCCCATGCAGTCGCCCCTCGGCACCGGGCCGCGGCCCGGGGGCGGGGGCC
Sp1 binding site
Sp1 binding site
GGCGGGTGCTGTACGGCGGCCTGGGCGACAGCCGCCCGGGCCTCTGGGGGGCGCCCGAGGCGGAGGAGGCGCGACGCCGGTTCGAGGCCTCGGGCGCCCCGGCGGCCGTGTGGGCGCCCG
147,960
CCGCCCACGACATGCCGCCGGACCCGCTGTCGGCGGGCCCGGAGACCCCCCGCGGGCTCCGCCTCCTCCGCGCTGCGGCCAAGCTCCGGAGCCCGCGGGGCCGCCGGCACACCCGCGGGC
Sp1 binding site
AGCTGGGCGACGCCGCGCAGCAGTACGCCCTGATCACGCGGCTGCTGTAC 3′
148,010
TCGACCCGCTGCGGCGCGTCGTCATGCGGGACTAGTGCGCCGACGACATG 5′
P